NEW APPROACHES AGAINST DRUG-RESISTANT *M. TUBERCULOSIS*

EDITED BY: Maria Rosalia Pasca, Yossef Av-Gay and Giorgia Mori
PUBLISHED IN: Frontiers in Microbiology

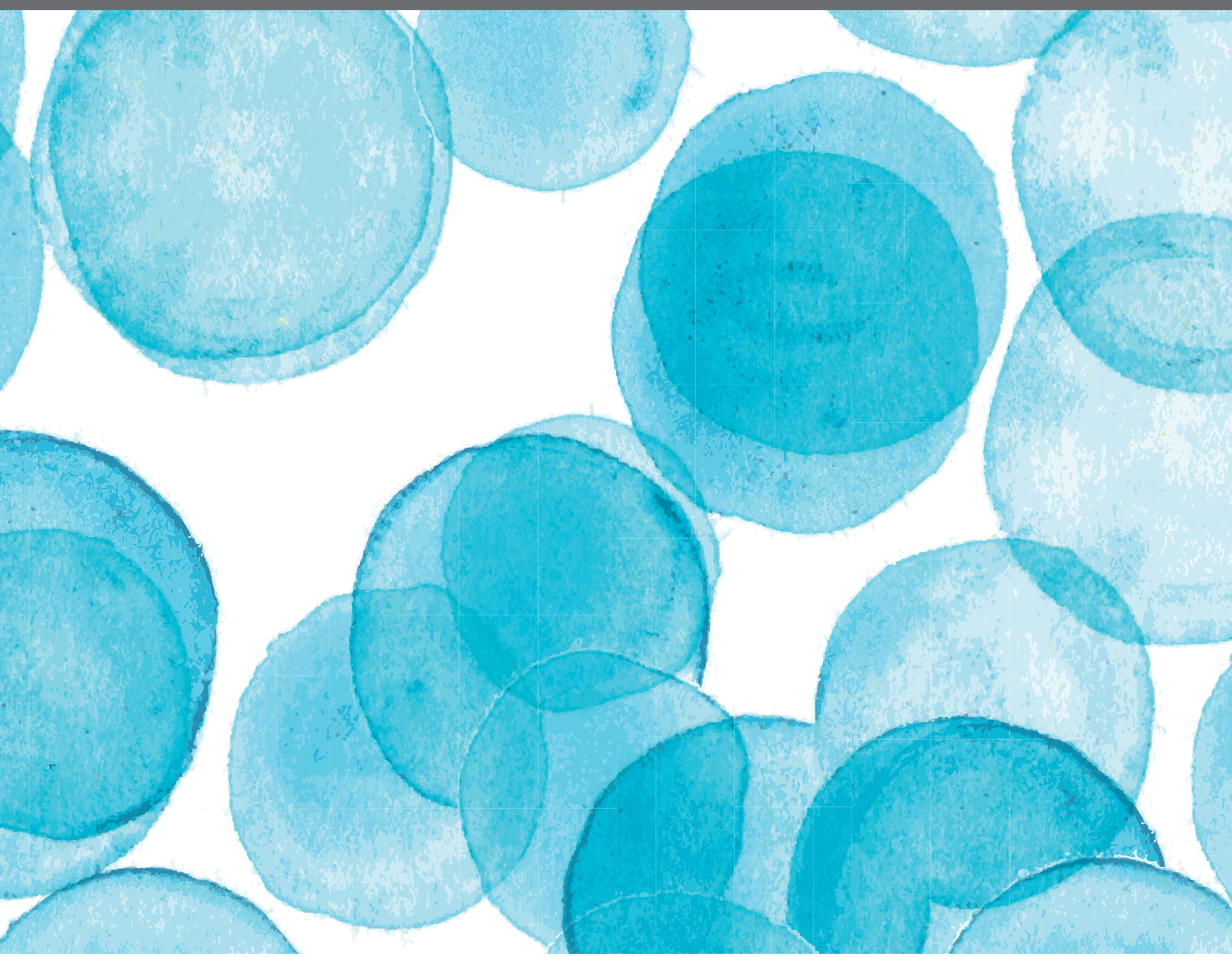

frontiers Research Topics

frontiers

ISSN 1664-8714
ISBN 978-2-88966-869-4
DOI 10.3389/978-2-88966-869-4

About Frontiers

Frontiers is more than just an open-access publisher of scholarly articles: it is a pioneering approach to the world of academia, radically improving the way scholarly research is managed. The grand vision of Frontiers is a world where all people have an equal opportunity to seek, share and generate knowledge. Frontiers provides immediate and permanent online open access to all its publications, but this alone is not enough to realize our grand goals.

Frontiers Journal Series

The Frontiers Journal Series is a multi-tier and interdisciplinary set of open-access, online journals, promising a paradigm shift from the current review, selection and dissemination processes in academic publishing. All Frontiers journals are driven by researchers for researchers; therefore, they constitute a service to the scholarly community. At the same time, the Frontiers Journal Series operates on a revolutionary invention, the tiered publishing system, initially addressing specific communities of scholars, and gradually climbing up to broader public understanding, thus serving the interests of the lay society, too.

Dedication to Quality

Each Frontiers article is a landmark of the highest quality, thanks to genuinely collaborative interactions between authors and review editors, who include some of the world's best academicians. Research must be certified by peers before entering a stream of knowledge that may eventually reach the public - and shape society; therefore, Frontiers only applies the most rigorous and unbiased reviews.
Frontiers revolutionizes research publishing by freely delivering the most outstanding research, evaluated with no bias from both the academic and social point of view. By applying the most advanced information technologies, Frontiers is catapulting scholarly publishing into a new generation.

What are Frontiers Research Topics?

Frontiers Research Topics are very popular trademarks of the Frontiers Journals Series: they are collections of at least ten articles, all centered on a particular subject. With their unique mix of varied contributions from Original Research to Review Articles, Frontiers Research Topics unify the most influential researchers, the latest key findings and historical advances in a hot research area! Find out more on how to host your own Frontiers Research Topic or contribute to one as an author by contacting the Frontiers Editorial Office: frontiersin.org/about/contact

NEW APPROACHES AGAINST DRUG-RESISTANT *M. TUBERCULOSIS*

Topic Editors:
Maria Rosalia Pasca, University of Pavia, Italy
Yossef Av-Gay, University of British Columbia, Canada
Giorgia Mori, The University of Queensland, Australia

Citation: Pasca, M. R., Av-Gay, Y., Mori, G., eds. (2021). New Approaches Against Drug-Resistant *M. tuberculosis*. Lausanne: Frontiers Media SA. doi: 10.3389/978-2-88966-869-4

Table of Contents

05 ***Editorial: New Approaches Against Drug-Resistant* M. tuberculosis**
Yossef Av-Gay, Giorgia Mori and Maria Rosalia Pasca

08 ***Ultra-Short Antimicrobial Peptoids Show Propensity for Membrane Activity Against Multi-Drug Resistant* Mycobacterium tuberculosis**
Jasmeet Singh Khara, Biljana Mojsoska, Devika Mukherjee, Paul R. Langford, Brian D. Robertson, Håvard Jenssen, Pui Lai Rachel Ee and Sandra M. Newton

19 ***Involvement of Transcription Elongation Factor GreA in* Mycobacterium *Viability, Antibiotic Susceptibility, and Intracellular Fitness***
Siyuan Feng, Yan Liu, Wanfei Liang, Mohamed Abd El-Gawad El-Sayed Ahmed, Zihan Zhao, Cong Shen, Adam P. Roberts, Lujie Liang, Liya Liao, Zhijuan Zhong, Zhaowang Guo, Yongqiang Yang, Xin Wen, Hongtao Chen and Guo-bao Tian

34 ***Antimycobacterial Effect of Selenium Nanoparticles on* Mycobacterium tuberculosis**
Hector Estevez, Ainhoa Palacios, David Gil, Juan Anguita, Maria Vallet-Regi, Blanca González, Rafael Prados-Rosales and Jose L. Luque-Garcia

40 ***Two Novel* katG *Mutations Conferring Isoniazid Resistance in* Mycobacterium tuberculosis**
Li-Yu Hsu, Li-Yin Lai, Pei-Fang Hsieh, Tzu-Lung Lin, Wan-Hsuan Lin, Hsing-Yuan Tasi, Wei-Ting Lee, Ruwen Jou and Jin-Town Wang

46 ***New Conjugated Compound T5 Epidioxy-Sterol-ANB Inhibits the Growth of* Mycobacterium tuberculosis *Affecting the Cholesterol and Folate Pathways***
Andres Baena, Emanuel Vasco, Manuel Pastrana, Juan F. Alzate, Luis F. Barrera and Alejandro Martínez

58 **In vitro *Study of Bedaquiline Resistance in* Mycobacterium tuberculosis *Multi-Drug Resistant Clinical Isolates***
Giulia Degiacomi, José Camilla Sammartino, Virginia Sinigiani, Paola Marra, Alice Urbani and Maria Rosalia Pasca

66 ***High-Content Screening of Eukaryotic Kinase Inhibitors Identify CHK2 Inhibitor Activity Against* Mycobacterium tuberculosis**
Tirosh Shapira, Leah Rankine-Wilson, Joseph D. Chao, Virginia Pichler, Celine Rens, Tom Pfeifer and Yossef Av-Gay

77 ***A Glutamine Insertion at Codon 432 of RpoB Confers Rifampicin Resistance in* Mycobacterium tuberculosis**
Li-Yin Lai, Li-Yu Hsu, Shang-Hui Weng, Shuo-En Chung, Hui-En Ke, Tzu-Lung Lin, Pei-Fang Hsieh, Wei-Ting Lee, Hsing-Yuan Tsai, Wan-Hsuan Lin, Ruwen Jou and Jin-Town Wang

84 ***Search for Antimicrobial Activity Among Fifty-Two Natural and Synthetic Compounds Identifies Anthraquinone and Polyacetylene Classes That Inhibit* Mycobacterium tuberculosis**
Luiz A. E. Pollo, Erlon F. Martin, Vanessa R. Machado, Daire Cantillon, Leticia Muraro Wildner, Maria Luiza Bazzo, Simon J. Waddell, Maique W. Biavatti and Louis P. Sandjo

95 ***Unbiased Identification of Angiogenin as an Endogenous Antimicrobial Protein With Activity Against Virulent* Mycobacterium tuberculosis**
Reiner Noschka, Fabian Gerbl, Florian Löffler, Jan Kubis, Armando A. Rodríguez, Daniel Mayer, Mark Grieshober, Armin Holch, Martina Raasholm Wolf-Georg Forssmann, Barbara Spellerberg, Sebastian Wiese, Gilbert Weidinger, Ludger Ständker and Steffen Stenger

108 ***Protein Kinase R Restricts the Intracellular Survival of* Mycobacterium tuberculosis *by Promoting Selective Autophagy***
Robin Smyth, Stefania Berton, Nusrah Rajabalee, Therese Chan and Jim Sun

126 ***The Prospective Synergy of Antitubercular Drugs With NAD Biosynthesis Inhibitors***
Kyle H. Rohde and Leonardo Sorci

135 ***Early Drug Development and Evaluation of Putative Antitubercular Compounds in the Omics Era***
Alina Minias, Lidia Żukowska, Ewelina Lechowicz, Filip Gąsior, Agnieszka Knast, Sabina Podlewska, Daria Zygała and Jarosław Dziadek

frontiers in Microbiology

EDITORIAL
published: 15 April 2021
doi: 10.3389/fmicb.2021.681420

Editorial: New Approaches Against Drug-Resistant *M. tuberculosis*

Yossef Av-Gay[1]*, *Giorgia Mori*[2]* and *Maria Rosalia Pasca*[3]*

[1] Departments of Medicine and Microbiology & Immunology, The University of British Columbia, Vancouver, BC, Canada,
[2] The University of Queensland Diamantina Institute, The University of Queensland, Woolloongabba, QLD, Australia,
[3] Department of Biology and Biotechnology "Lazzaro Spallanzani", University of Pavia, Pavia, Italy

Keywords: tuberculosis, host directed therapy, drug discovery, antimicrobial resistance, drug targets, anti-tubercular drugs

Editorial on the Research Topic

New Approaches Against Drug-Resistant *M. tuberculosis*

OPEN ACCESS

Edited by:
Thomas Dick,
Center for Discovery and Innovation, Hackensack Meridian Health, United States

Reviewed by:
Marco Pieroni,
University of Parma, Italy

***Correspondence:**
Yossef Av-Gay
yossi@mail.ubc.ca
Giorgia Mori
g.mori@uq.edu.au
Maria Rosalia Pasca
mariarosalia.pasca@unipv.it

Specialty section:
This article was submitted to Antimicrobials, Resistance and Chemotherapy, a section of the journal Frontiers in Microbiology

Received: *16 March 2021*
Accepted: *24 March 2021*
Published: *15 April 2021*

Citation:
Av-Gay Y, Mori G and Pasca MR (2021) Editorial: New Approaches Against Drug-Resistant M. tuberculosis. Front. Microbiol. 12:681420. doi: 10.3389/fmicb.2021.681420

Tuberculosis (TB) is the most devastating infectious disease worldwide, killing 1.4 million people each year (World Health Organization [WHO], 2020). Treatment regimens are lengthy and cause considerable adverse effects, leading to poor patient compliance, as well as high costs and economic burden worldwide. Moreover, resistance to newly approved antimicrobials for TB develops quickly (Bloemberg et al., 2015; Zimenkov et al., 2017). This, together with the widespread occurrence of *Mycobacterium tuberculosis* (*Mtb*) drug-resistant strains, necessitates discovery of novel and innovative drugs that will shorten the duration of TB treatments and/or be less toxic to the human host.

Our Research Topic entitled "New approaches against drug-resistant *Mtb*" called for original research papers and reviews describing novel approaches for drug discovery, target identification and mechanisms of drug resistance. The response we have received was exciting resulting in 13 articles with more than 30,000 views.

Our collection includes an exciting review describing drug development in our era where modern -omic technologies, such as DNA and RNA sequencing, proteomics, and genetic manipulation of organisms, facilitate the drug discovery process for TB treatment. These methods enable us to better understand mechanisms of action of antibiotics and allow the evaluation of new drug candidates using mathematical modeling and modern computational analysis for the drug discovery process.

Mtb, the causative agent of TB, infects, survives, and replicates intracellularly within alveolar macrophages. *Mtb* utilizes numerous strategies to avoid host defense mechanisms and preys on the host cell response to establish infection (Hmama et al., 2015). A novel drug discovery approach termed Host Directed Therapy (HDT), was proposed recently to overcome drug resistance (Zumla et al., 2016; Parish, 2020). Since HDTs do not target *Mtb* directly but rather assist the host in fighting infection, they would have reduced chances of generating resistance.

A series of publications within our Collection explore this new and exciting approach to TB drug development.

Shapira et al. screened a library of human kinase inhibitors and identified several compounds that are active in an intracellular model of TB infection. A specific checkpoint inhibitor showed promising activity and CHK2 inhibition by RNAi phenocopied the intracellular inhibitory effect of the drug.

Smyth et al. showed that Protein Kinase R (PKR) is a human host cell sensor that function in the

cellular response to mycobacterial infection. They demonstrated that the over-expression of PKR enhanced anti-mycobacterial activity of macrophages and it is mediated by selective autophagy and by the inhibition of autophagolysosome maturation which limit *Mtb* replication, suggesting that PKR can be considered for HDT development.

Screening of compound libraries is a valuable tool in drug discovery; Pollo et al. tested a library of 52 natural and synthetic compounds for activity against *Mtb* growth and identified the natural products isobavachalcone and isoneorautenol, and a synthetic chromene as active at low micromolar concentrations.

Noschka et al., screened a library of antimicrobial peptides generated from hemo-filtrate identifying Angiogenin as the only active compound against *Mtb* growth. They confirmed its activity using the synthetic Angiogenin. They derived the small peptide fragment Angie1, which is active against intracellular and extracellular *Mtb* growth, as well as they tested that it is not toxic for zebrafish embryos.

Khara et al. assessed the anti-mycobacterial potency of three novel synthetic anti-microbial peptoides against *Mtb* growth and showed that BM2 peptoid kills mycobacteria both *in vitro* and intracellularly. More importantly, it significantly reduced bacterial load in the lungs of infected mice.

The effect of novel and alternative compounds was also described in our collection; selenium nanoparticles (by Estevez et al.) and epidioxy-sterol analogs (Baena et al. In particular, Estevez et al. demonstrated that the selenium nanoparticles are active against both *Mtb* and *Mycobacterium smegmatis* growth by targeting their cell envelope. This finding opens new perspectives because this type of nanoparticles is characterized by a low toxicity.

Baena et al. tested the activity of 15 epidioxy-sterol analogs against *Mtb* both *in vitro* and *ex vivo*. T5 epidioxy-sterol-ANB was effective against *Mtb in vitro* only inside macrophages. Furthermore, it was showed that it is active also in a *Mtb* infected murine model. By transcriptomics analysis of *Mtb* infected macrophages after T5 epidioxy-sterol-ANB treatment, a significant down-regulation of enzymes involved in the cholesterol and folic acid pathways was discovered.

Study of the mechanism of resistance and mode of action of drugs used in TB treatment as well as identification of novel resistance mutations are extremely important for our understanding of this topic and for the development of novel approaches to fight these emerging *Mtb* drug-resistant strains.

Isoniazid (INH) and rifampicin (RIF) are two first-line drugs which are extensively used in TB therapy (Lange et al., 2019). Several SNPs conferring drug resistance have already known for both compounds, but it is mandatory to continue to search for new ones.

Hsu et al. identified two novel mutations (W341R and L398P) in the known drug activator KatG conferring INH resistance. Interestingly, they showed that these two polymorphisms are responsible for INH resistance by complementation and by the construction of two mutants harboring the same mutations.

Lai et al. demonstrated that a specific insertion in the *rpoB* gene confers RIF resistance, by the construction of a *Mtb* mutant harboring the same mutation.

Unfortunately, several *Mtb* clinical isolates resistant to new compounds used in TB therapy, such as bedaquiline (BDQ), have already spreaded worldwide (Bloemberg et al., 2015; Zimenkov et al., 2017). To better understand this phenomenon, Degiacomi et al. generated *Mtb* mutants resistant to BDQ starting from two MDR clinical isolates, miming what happens in clinical setting. These new BDQ resistant mutants harbored mutations in both *atpE* gene, coding for the target, and *Rv0678*, which encodes the repressor of MmpL5 efflux pump. The growth curves of BDQ resistant mutants were also evaluated. It was shown that *Rv0678* mutations could give an advantage in the growth rate, explaining the spread of BDQ resistance among *Mtb* clinical isolates also prior to BDQ treatment.

Further findings in the study of new TB drug targets and in the characterization of the existing ones are present in our collection.

In order to characterize GreA as new drug target, Feng et al. isolated *Mycobacterium smegmatis* and *Mtb* mutants and showed that knock-down *greA* mutant resulted in growth retardation in *Mtb* and it is essential for its survival under heat shock stress. Furthermore, these mutants are more susceptible to vancomycin and RIF. By RNA-seq, they showed the role of GreA in the metabolic regulation of mycobacteria.

Rohde and Sorci evaluated the possible synergy of NAD biosynthesis inhibitors with some antitubercular drugs for drug combination. In fact, several prodrugs require a NAD biosynthesis enzyme to be activated, such as INH, ethionamide, and delamanid.

This unique collection of articles in our Research Topic gives new insights into the characterization drug resistance mechanisms in *Mtb* as well as provides novel strategies to fight this notorious pathogen.

We would like to thank the reviewers for their comments that improved our manuscripts, and the authors for their excellent contributions.

Finally, we hope that this Collection would stimulate open discussions about this topic and new researches which will assist the scientific and pharmaceutical communities in finding promising weapons against TB.

AUTHOR CONTRIBUTIONS

All authors listed have made a substantial, direct and intellectual contribution to the work, and approved it for publication.

FUNDING

This research was supported by the Italian Ministry of Education, University and Research (MIUR): Dipartimenti di Eccellenza Program (2018–2022)—Department of Biology and Biotechnology Lazzaro Spallanzani, University of Pavia to MP, and the TB Veterans Association to YA-G.

ACKNOWLEDGMENTS

We are grateful to all the authors and reviewers for their contributions to this Research Topic.

REFERENCES

Bloemberg, G. V., Keller, P. M., Stucki, D., Trauner, A., Borrell, S., Latshang, T., et al. (2015). Acquired resistance to bedaquiline and delamanid in therapy for tuberculosis. *N. Engl. J. Med*. 373, 1986–1988. doi: 10.1056/NEJMc1505196

Hmama, Z., Pena-Diaz, S., Joseph, S., and Av-Gay, Y. (2015). Immunoevasion and immunosuppression of the macrophage by Mycobacterium tuberculosis. *Immunol. Rev*. 264, 220–232. doi: 10.1111/imr.12268

Lange, C., Dheda, K., Chesov, D., Mandalakas, A. M., Udwadia, Z., Horsburgh, C. R., et al. (2019). Management of drug-resistant tuberculosis. *Lancet*. 394, 953–966. doi: 10.1016/S0140-6736(19)31882-3

Parish, T. (2020). In vitro drug discovery models for *Mycobacterium tuberculosis* relevant for host infection. *Expert Opin. Drug Discov*. 15, 349–358. doi: 10.1080/17460441.2020.1707801

World Health Organization [WHO] (2020). Global Tuberculosis Report. Available online at: https://www.who.int/publications/i/item/9789240013131 (accessed October 15, 2020).

Zimenkov, D. V., Nosova, E. Y., Kulagina, E. V., Antonova, O. V., Arslanbaeva, L. R., Isakova, A. I., et al. (2017). Examination of bedaquiline- and linezolid-resistant *Mycobacterium tuberculosis* isolates from the Moscow region. *J. Antimicrob. Chemother*. 72(7):1901–1906. doi: 10.1093/jac/dkx094

Zumla, A., Rao, M., Wallis, R. S., Kaufmann, S. H., Rustomjee, R., Mwaba, P., et al. (2016). Host-directed therapies for infectious diseases: current status, recent progress, and future prospects. *Lancet Infect. Dis*. 16, e47–63. doi: 10.1016/S1473-3099(16)00078-5

Conflict of Interest: The authors declare that the research was conducted in the absence of any commercial or financial relationships that could be construed as a potential conflict of interest.

frontiers in Microbiology

ORIGINAL RESEARCH
published: 17 March 2020
doi: 10.3389/fmicb.2020.00417

Ultra-Short Antimicrobial Peptoids Show Propensity for Membrane Activity Against Multi-Drug Resistant *Mycobacterium tuberculosis*

Jasmeet Singh Khara[1,2†], Biljana Mojsoska[3†], Devika Mukherjee[1†], Paul R. Langford[2], Brian D. Robertson[4], Håvard Jenssen[3], Pui Lai Rachel Ee[1] and Sandra M. Newton[2*]*

[1] Department of Pharmacy, National University of Singapore, Singapore, Singapore, [2] Section of Paediatric Infectious Disease, Department of Infectious Disease, Imperial College London, London, United Kingdom, [3] Department of Science and Environment, Roskilde University, Roskilde, Denmark, [4] MRC Centre for Molecular Bacteriology and Infection, Department of Infectious Disease, Imperial College London, London, United Kingdom

OPEN ACCESS

Edited by:
Maria Rosalia Pasca, University of Pavia, Italy

Reviewed by:
Neeraj Dhar, Swiss Federal Institute of Technology in Lausanne, Switzerland
Annelise Emily Barron, Stanford University, United States

***Correspondence:**
Pui Lai Rachel Ee
phaeplr@nus.edu.sg
Sandra M. Newton
s.newton@imperial.ac.uk

† These authors have contributed equally to this work

Specialty section:
This article was submitted to Antimicrobials, Resistance and Chemotherapy, a section of the journal Frontiers in Microbiology

Received: *27 November 2019*
Accepted: *27 February 2020*
Published: *17 March 2020*

Citation:
Khara JS, Mojsoska B, Mukherjee D, Langford PR, Robertson BD, Jenssen H, Ee PLR and Newton SM (2020) Ultra-Short Antimicrobial Peptoids Show Propensity for Membrane Activity Against Multi-Drug Resistant Mycobacterium tuberculosis. Front. Microbiol. 11:417. doi: 10.3389/fmicb.2020.00417

Tuberculosis (TB) results in both morbidity and mortality on a global scale. With drug resistance on the increase, there is an urgent need to develop novel anti-mycobacterials. Thus, we assessed the anti-mycobacterial potency of three novel synthetic peptoids against drug-susceptible and multi-drug resistant (MDR) *Mycobacterium tuberculosis in vitro* using Minimum Inhibitory Concentration, killing efficacy and intracellular growth inhibition assays, and *in vivo* against mycobacteria infected BALB/c mice. In addition, we verified cell selectivity using mammalian cells to assess peptoid toxicity. The mechanism of action was determined using flow cytometric analysis, and microfluidic live-cell imaging with time-lapse microscopy and uptake of propidium iodide. Peptoid BM 2 demonstrated anti-mycobacterial activity against both drug sensitive and MDR *M. tuberculosis* together with an acceptable toxicity profile that showed selectivity between bacterial and mammalian membranes. The peptoid was able to efficiently kill mycobacteria both *in vitro* and intracellularly in murine RAW 264.7 macrophages, and significantly reduced bacterial load in the lungs of infected mice. Flow cytometric and time lapse fluorescence microscopy indicate mycobacterial membrane damage as the likely mechanism of action. These data demonstrate that peptoids are a novel class of antimicrobial which warrant further investigation and development as therapeutics against TB.

Keywords: tuberculosis, peptoids, drug resistant, membrane, anti-mycobacterial, *Mycobacterium tuberculosis*

INTRODUCTION

Tuberculosis (TB), caused by *Mycobacterium tuberculosis*, is the leading cause of death among infectious diseases according to the World Health Organization (WHO). In 2017, 10 million people were diagnosed with TB, while 1.6 million cases result in death (WHO, 2018). In addition, there were 446,000 cases of multi-drug resistant TB (MDR TB) and 558,000 cases were resistant to rifampicin alone, the standard first-line anti-mycobacterial. The shortfalls associated with the

current TB therapy are the long duration of treatment leading to non-adherence to the regimen and the emergence of drug resistant strains, and failure to completely cure cases of MDR or extensively drug resistant (XDR) TB (Mukherjee et al., 2016). This problem is compounded by the rise in drug resistance and the concomitant decrease in available drugs. With only Bedaquiline and Delamanid approved in the last few years (Esposito et al., 2015), there is an urgent and unmet need for the development of novel anti-mycobacterial agents against drug resistant TB to stop the global epidemic.

Antimicrobial peptides (AMPs) are short, amphipathic, cationic molecules. They have been widely studied as most bacteria, including mycobacteria, have an extremely low propensity to develop resistance against them due to their non-specific mode of action (Gordon et al., 2005; Zhang and Gallo, 2016; Katarzyna and Małgorzata, 2017; Kang et al., 2017). Their main mode of action is to act by lysing or disrupting the bacterial membrane, although some AMPs are able to pass through the lipid bilayer without permeabilization and exhibit intracellular effects such as inhibition of cell wall, nucleic acid and protein synthesis (Haney et al., 2017). Their broad spectrum of activity against a wide range of microorganisms and rapid mode of action combined with the low proclivity for resistance development makes them an attractive choice for therapeutics against drug resistant organisms (Ghosh et al., 2014). However AMPs have various drawbacks, including their sensitivity to enzymatic degradation (Miller et al., 1994), low bioavailability and the high costs of synthesis (Gordon et al., 2005; Khara et al., 2016). These shortcomings make the translation of AMPs as therapeutics for drug resistant infections from bench to bedside a challenging undertaking.

To overcome the disadvantages of AMPs, oligo-N-substituted glycines (peptoids) are a good alternative (Czyzewski et al., 2016). Peptoids are sequence-specific peptidomimetics (Simon et al., 1992) with a peptide backbone but differ from AMPs in that the side chains are attached to the amide nitrogen instead of the α-carbon (Godballe et al., 2011); thus, there are no known proteases that will recognize and degrade the peptoid structure making them more stable. Furthermore, any chemical group which can be used as a primary amine can be incorporated in to a peptoid via submonomer synthesis thus giving rise to a much larger library of compounds with greater variation in side chains for development than is possible by modifying conventional AMPs. Interest in peptoids has increased over the past few years due to their antimicrobial activity against a broad spectrum of pathogens, non-specific mode of action, decreased susceptibility to enzymatic degradation, stability to heat and the relative ease of synthesis (Godballe et al., 2011; Mojsoska et al., 2017). Peptoids have been shown to act via disruption of bacterial membranes and have increased membrane permeability when compared to peptides, or by interacting with intracellular targets such as bacterial DNA (Miller et al., 1994; Mojsoska et al., 2017). Thus, peptoids have great potential to be developed into novel therapeutic adjuncts to existing drug regimens for TB.

Structure-activity relationship studies (SAR) reveal that tuning the structure of peptoids is an important key process when designing potent antimicrobials. For example, Mojsoska et al. (2015) designed a library of short linear cationic and hydrophobic peptoids with modifications to study the effect of hydrophobicity on peptoid activity and cytotoxicity whilst maintaining a constant charge. They found that higher hydrophobicity resulted in greater potency against *Staphylococcus aureus* but not against *Escherichia coli* or *Pseudomonas aeruginosa in vitro*. They also showed that the introduction of aromatic residues resulted in the loss of selectivity between bacterial and mammalian membranes. Other studies on antimicrobial peptoids against Gram positive and Gram negative bacteria have shown promising results (Bremner et al., 2010; Ghosh et al., 2014; Bolt et al., 2017). With regards to the anti-tubercular activity of peptoids, there has been only one study by Kapoor et al. that demonstrated potency against *M. tuberculosis* exerted by short lipophilic (Ntridec) peptoids compared to peptoids with shorter or no lipophilic tail attached. They evaluated the efficacy and cytotoxicity of their peptoids but did not shed any light on the mechanism of action of these compounds (Kapoor et al., 2011).

In this study we used a whole cell screening approach to determine whether peptoids can be a good alternative to AMPs to tackle the global epidemic caused by TB. Peptoids were designed with repeating monomeric units mimicking three amino acids (*N*lys, *N*spe, *N*he) to study the effect of chain length on peptoid activity against *M. tuberculosis*. Peptoids mimic the best features of AMPs, i.e., hydrophobicity, cationic nature and amphipathicity while overcoming their disadvantage of being susceptible to protease degradation (Bolt et al., 2017). Thus, by incorporating these characteristics into our design we could begin to determine the influence of positively charged, hydrophobic and aromatic chiral residues on the biological activity of the peptoids. We evaluated the *in vitro* anti-mycobacterial activity of the peptoids against both drug sensitive and MDR mycobacteria using the broth microdilution method. We examined the cytotoxicity against the murine macrophage cell line, RAW267.4, and evaluated the selectivity index (SI) for the peptoids. Furthermore, we assessed the killing efficacy in broth and mycobacteria infected macrophages as *M. tuberculosis* is primarily an intracellular pathogen. As some AMPs can modulate the host immune response (Dawson and Scott, 2012), we also evaluated the ability of the peptoids to activate macrophages. The mechanism of action of peptoids against MDR *M. tuberculosis* was studied using flow cytometric analysis and time lapse microscopy with propidium iodide (PI) uptake. Finally, we evaluated the *in vivo* efficacy of our lead peptoid, BM 2, *in vivo* using BALB/c mice.

MATERIALS AND METHODS

Ethics

All animal procedures were performed under the license issued by the UK Home Office (PPL/708653) and in accordance with the Animal Scientific Procedures Act of 1986. BALB/c mice (Charles River Ltd, United Kingdom) were maintained in biosafety Containment Level (CL)-3 facilities according to institutional protocols.

Media and Reagents

Dulbecco's Modified Eagle Medium (DMEM), Phosphate Buffered Saline (PBS), rifampicin, moxifloxacin, dimethyl sulfoxide (DMSO), Tween 80, glycerol, PI, HPLC-grade water, Triton X-100 and lipopolysaccharide (LPS) from *Escherichia coli* 0111:B4 were obtained from Sigma-Aldrich (St Louis, MO, United States). Fetal Bovine Serum (FBS) was obtained from Labtech International (Sussex, United Kingdom). Middlebrook 7H9 broth, Middlebrook 7H11 agar, BBL Middlebrook Albumin Dextrose Catalase (ADC) supplement and Oleic Acid, Albumin, Dextrose, Catalase (OADC) were purchased from BD (Sparks, MD, United States). MTT [3-(4,5-dimethylthiazol-2-yl)-2,5-diphenyltetrazolium bromide] was from Duchefa Biochemie (Haarlem, Netherlands). The Griess Reagent System was from Promega (Madison, WI, United States).

Peptoid Synthesis

The peptoids were synthesized by submonomeric solid phase synthesis as described by Mojsoska et al. (2015). Briefly, peptoid sequences were synthesized using an automated (Intavis, ResPep SL Bioanalytical Instruments AG) synthesizer on Rink amide MBHA resin on a 15 μM scale. Peptoids were cleaved from the resin in a trifluoroacetic acid (TFA)-water-triisopropylsilane (95:2.5:2.5) solution for 30–60 min and purified (>95%) using reverse-phase HPLC on a C_{18} column (10 μm, 250 × 10 mm; Higgins Analytical, Inc.) with an acetonitrile-water gradient (0.1% TFA). Upon purification, no TFA adducts were observed. The analytical purity and correct mass were verified using an analytical Dionex UltiMate 3000 reverse-phase UPLC (Thermo Scientific™) with a C_{18} (100 Å, 100 × 2.1 mm; Kinetex) and electronspray ionization mass spectrometry (Finnigan LTQ). The mass spectra of the peptoids are shown in **Supplementary Figure S1** and **Supplementary Table S1**.

Mycobacterial Strains and Growth Conditions

M. tuberculosis H37Rv was obtained from the ATCC (United States). MDR clinical isolate, *M. tuberculosis* CSU87, resistant to rifampicin, isoniazid, ethambutol, streptomycin and kanamycin, and *Mycobacterium bovis* BCG *lux* (BCG) were gifts from Dr. Diane Ordway, Colorado State University and Professor Douglas Young, Imperial College London, respectively. Liquid cultures were grown in Middlebrook 7H9 broth, supplemented with 0.05% Tween 80, 0.2% glycerol and 10% ADC, to mid-log phase at 37°C in a shaking incubator (180 rpm) (Khara et al., 2016). Mycobacterial colonies were grown on Middlebrook 7H11 agar supplemented with 0.5% glycerol and 10% OADC. BCG were grown in broth or on agar, supplemented with hygromycin (50 mg/L) as a selection marker.

Growth Inhibition and Minimum Inhibitory Concentration (MIC) Assays

The anti-mycobacterial activities of the peptoids were assessed using the standard broth microdilution method. Mid-log-phase bacterial cultures were diluted to 10^6 colony forming units (CFU)/mL and 100 μL was added to twofold serial dilutions of the compounds in a 96-well plate. Following incubation at 37°C in a shaking incubator for 7 days, optical density (OD_{595}) was measured. The lowest concentration with no bacterial growth was defined as the MIC, determined visually and by spectrophotometric measurements using the iMark™ Microplate Absorbance Reader (Bio-Rad Laboratories, Hertfordshire, United Kingdom) (Khara et al., 2014, 2016).

In vitro Killing Efficacy

Peptoid BM 2 was evaluated for its bactericidal activity against H37Rv and CSU87 by serially diluting with broth to give concentrations of 4 (0.5 × MIC), 8 (1 × MIC), 16 (2 × MIC) and 32 mg/L (4 × MIC) for H37Rv and 2 (0.5 × MIC), 4 (1 × MIC), 8 (2 × MIC), 16 mg/L (4 × MIC) for CSU87. Bacterial culture (100 μL), corresponding to an inoculum size of 10^6 CFU/mL, was added to an equal volume of peptoid and incubated shaking for 7 days at 37°C. Samples were plated on agar and CFU were enumerated (Khara et al., 2016).

Cell Culture and Cytotoxicity

Peptoids were assessed for cytotoxic effects on the mouse macrophage cell line (RAW 264.7) by the 3-(4,5-dimethylthiazol-2-yl)-2,5-diphenytetrazolium bromide (MTT) cell viability assay. Cells were maintained in DMEM supplemented with 10% FBS and cultured at 37°C in 5% CO_2. Cells were seeded in 96-well plates (1×10^4 cells per well) and incubated for 24 h before treating with concentrations of peptoids, up to 64 mg/L, for 24 h. Next, the medium was replaced with DMEM and MTT solution (5 mg/L) and incubated at 37°C for 4 h. Formazan crystals were dissolved in DMSO and OD was measured spectrophotometrically at 595 nm in a VersaMax Tunable microplate reader (Molecular Devices, Sunnyvale, CA, United States). Cell viability was determined relative to untreated controls and expressed as (A_{595} of treated sample)/(A_{595} of control) × 100% (Khara et al., 2016).

To determine peptoid selectivity for activity against bacterial over mammalian cells, the selectivity index (SI) was calculated as the ratio between the IC_{50} (concentration that inhibits 50% of metabolic activity of RAW 264.7 cells) and MIC.

Nitric Oxide (NO) Production by Peptoid-Treated Macrophages

To evaluate the stimulation of macrophages, RAW 264.7 cells were seeded at 4×10^4 per well in microtiter plates and incubated at 37°C in 5% CO_2 for 24 h. Cells were then treated with fresh medium containing peptoids (doubling concentrations ranging 2–64 mg/L) for 24 h. The production of NO was estimated using nitrite as a surrogate and measuring nitrite concentrations in supernatants using the Griess reagent (0.1% *N*-1-napthylethylenediamine dihydrochloride, 1% sulfanilamide and 5% phosphoric acid). The absorbance was measured at 540 nm and nitrite concentrations were determined using standard curves generated with $NaNO_2$ solutions. Macrophages stimulated with LPS (0.0001 mg/L) served as positive controls,

while unstimulated macrophages served as negative controls (Khara et al., 2016).

Intracellular Anti-mycobacterial Activity

The intracellular activity of peptoid BM 2 was assessed against H37Rv and CSU87 as described previously (Wilkinson et al., 1999). Briefly, RAW 264.7 cells were plated in to 96-well microtiter plates at a final concentration of 4×10^4 cells per well and incubated for 24 h. Bacterial cultures were washed, resuspended in DMEM and added at a final concentration of 4×10^5 CFU per well to achieve a multiplicity of infection (MOI) of 10:1. Plates were incubated at 37°C and 5% CO_2 for 4 h and cells were washed with pre-warmed DMEM thrice to remove extracellular bacteria. BM 2, suspended in DMEM, was tested in triplicate at 4, 8, 16, 32 mg/L corresponding to 0.5 ×, 1 ×, 2 ×, 4 × MIC for H37Rv and 1 ×, 2 ×, 4 ×, 8 × MIC for CSU87. Macrophages were then lysed with sterile water, and the samples plated on agar at time 0 and 4 days for CFU determination (Wilkinson et al., 1999; Khara et al., 2016).

Flow Cytometric Analysis of Membrane Permeabilization

To determine whether BM 2 was membrane active, the integrity of the mycobacterial membrane was evaluated using PI treated cells via flow cytometry. Briefly, H37Rv and CSU87 were washed, resuspended to give a cell density of 10^8 CFU/mL, and then incubated in the presence of the peptoids (4 × MIC) for 3 h. Next, cells were treated with 20 mg/L of the membrane impermeable dye, PI, by incubating the cultures for 30 min at 4°C, followed by washing to remove unbound dye. Flow cytometric analysis was performed using a CyAnTM ADP Analyzer (Becton Dickinson, San Jose, CA, United States). Rifampicin and moxifloxacin (4 × MIC), served as negative controls.

Microfluidic Live-Cell Imaging With Time-Lapse Fluorescence Microscopy

Live-cell imaging was performed using the automated CellASIC ONIX Microfluidic Platform with CellASIC ONIX B04A-03 Microfluidic Bacteria Plates (EMD Millipore Corporation, Hayward, CA, United States) using BCG due to the housing of the platform being in a CL-2 laboratory. BCG cultures were diluted with broth to 10^7 CFU/mL and 100 μL was added to each cell inlet wells. BM 2 was serially diluted with broth (4 × MIC) and added with PI (10 mg/L) to the inlet wells (total volume 350 μL). The microfluidic plate was vacuum-sealed to the F84 manifold and the CellASIC ONIX FG Software initiated. Loading and washing of un-trapped bacterial cells was carried out according to the manufacturer's protocol. Peptoid was perfused into culture chambers at the recommended pressure of 2 psi for 3 h at 37°C. Negative controls included bacteria with medium and PI alone. Phase-contrast and fluorescent images of bacteria were captured with a 63 × oil-immersion objective lens every 10-min using a Zeiss Axiovert 200M inverted microscope (Carl Zeiss Inc.) (Khara et al., 2016). Microscopy was performed in the Facility for Imaging by Light Microscopy (FILM) at Imperial College London.

In vivo Evaluation of BM 2 in BALB/c Mice

To evaluate the efficacy of BM 2 *in vivo*, thirteen, 6 to 8-week-old female BALB/c mice infected with H37Rv were used (control group, $n = 5$, plus 3 mice to check bacterial numbers at day 1 post-infection; Treatment BM 2 group $n = 5$). Animals were randomly assigned to 5 per Tecniplast Isocage with *ad libitum* food and water. Mice were infected with 1×10^3 CFU/mouse (35 μL volume) via the intranasal route under isoflurane anesthesia. The following day, 3 mice were culled, the lungs were removed and plated onto agar to determine the inoculum. Animals were monitored daily and weighed on day 7 and on day 15 before treatment began. Treatment of BM 2 was initiated 14 days post-infection as six intra-tracheal doses (5 mg/kg) administered under isoflurane anesthesia on alternate days over 2 weeks. On day 28, the mice were culled by a Schedule 1 method, lungs removed and homogenized, and then plated on to agar for CFU enumeration (Tenland et al., 2018; Tenland et al., 2019). No adverse effects with BM 2 were observed.

RESULTS

Peptoid Design Strategy

As peptides are known to be cationic, amphipathic and hydrophobic in nature, peptoids which are non-natural peptidomimetics, would likely need the same characteristics to exhibit antimicrobial properties (Chongsiriwatana et al., 2008; Mojsoska et al., 2015, 2017). Thus, three peptoids (BM 1, BM 2, and BM 3) were designed to study the effect of chain length, charge, and hydrophobicity on antimicrobial activity. Each peptoid contains three residues, *N*lys, *N*he and *N*spe which comprise one monomeric subunit (**Figure 1A**). BM 1 has a single monomeric unit (three residues), BM 2 has two repeating monomeric units (six residues) and BM 3 has three repeating monomeric units (nine residues) (**Figure 1B**). The *N*lys residue contributes to increasing the net positive charge of the peptoid, *N*he and *N*spe both contribute to the overall hydrophobicity and *N*spe is aromatic and chiral in nature, while *N*he is less frequently used in peptoid design. These hydrophobic elements were chosen to enhance the anti-TB activity through increasing the interaction with the hydrophobic membrane of *M. tuberculosis*.

In vitro Anti-mycobacterial Activity and Killing Efficacy

The peptoids were assessed for their ability to inhibit the growth *in vitro* of BCG, and drug sensitive and resistant H37Rv and CSU87 *M. tuberculosis* strains respectively, using MIC assays. BM 2 was the most potent against BCG (2–4 mg/L), H37Rv (8 mg/L), and CSU87 (4 mg/L). BM 1 did not display anti-mycobacterial activity against H37Rv or CSU87 at the highest concentration tested (**Table 1**). MIC was also tested for Gram positive and Gram negative bacteria namely methicillin-sensitive *Staphylococcus aureus* (MSSA), methicillin-resistant *Staphylococcus aureus* (MRSA), *P. aeruginosa, E. coli* and non-tuberculous mycobacteria *Mycobacterium abscessus*

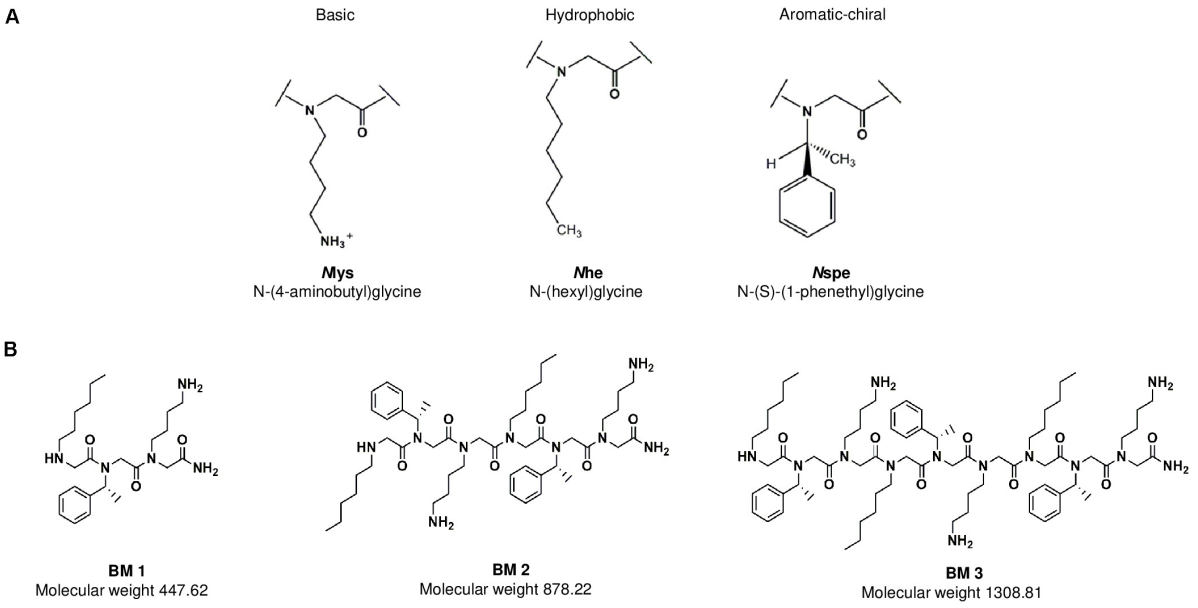

FIGURE 1 | (A) The three residues *N*lys, *N*spe, and *N*he comprise one monomeric subunit. These subunits were used to design the three peptoids BM 1, BM 2 and BM 3. **(B)** BM 1 has one monomeric unit (three residues), BM 2 has two repeating monomers (six residues), and BM 3 has three repeating monomers (nine residues).

TABLE 1 | Minimum inhibitory concentrations (MICs) and selectivity indices (SIs) of various peptoids against *M. bovis* BCG, the laboratory strain *M. tuberculosis* H37Rv and the MDR clinical isolate *M. tuberculosis* CSU87.

Peptoid	MIC[a] (mg/L)			GM[b]	IC_{50}[c]	SI[d]	MW[e]	miLogP[f]	R_t (min)[g]
	BCG	H37Rv	CSU87						
BM 1	16–32	>64	>64	–	>64	n.d	447.6	0.93	8.02
BM 2	2–4	8	4	6.3	>64	>10	878.2	2.74	11.51
BM 3	4–8	16	16	16	32	2	1308.8	4.54	13.05

[a]MIC results are representative of three independent experiments. [b]The geometric mean (GM) of the MICs against the three mycobacterial strains tested. [c]Cytotoxicity is represented by IC_{50} values, defined as the concentration that inhibits 50% of the metabolic activity of RAW 264.7 macrophage cell line. [d]Selectivity index (SI) is determined as follows: (IC_{50}/GM). [e]Molecular weight (g/mol). [f]miLogP (octanol/water partition coefficient) calculated with Molinspiration. [g]Analytical retention times (Rt) estimated on a reverse phase C_{18} Kinetex 100 × 2.1 mm 100 Å column, 60°C run on a 15–65% acetonitrile gradient over 20 min.

and *Mycobacterium avium* but no inhibition was observed (data not shown).

Further, we tested the bactericidal activity of BM 2 (0.5 ×, 1 ×, 2 ×, and 4 × MIC) against H37Rv and CSU87 for 7 days by CFU enumeration (**Figure 2**). BM 2 resulted in >99.9% killing of H37Rv at 2 × and 4 × MIC (16 and 32 mg/L), while >99% and 99.9% killing was achieved against CSU87 at 2 × and 4 × MIC (8 and 16 mg/L) respectively, highlighting its bactericidal activity. In comparison rifampicin reduced the bacterial burden by ≥99% at 4 × MIC (0.03 mg/L) after 6 days of treatment as shown by Steenwinkel et al. (2010).

Cytotoxicity and Cell Selectivity

Peptoids were evaluated for cytotoxicity against RAW 264.7 cells over 24 h in line with our previous work (Khara et al., 2016). BM 1 and BM 2 did not show cytotoxicity at 64 mg/L, while BM 3 showed a 50% reduction in cell viability at 32 mg/L (**Figure 3A**). The SI of BM 2 and BM 3 was >10 and 2, respectively, but undetermined for BM 1 as it did not have an MIC (**Table 1**). Hence BM 2 possessed good selectivity for bacterial over mammalian cells.

To establish whether the peptoids stimulate macrophages, production of NO from RAW 264.7 macrophages in the presence of a range of doubling concentrations of peptoids (2 – 64 mg/L) was determined. There was no production of NO from macrophages treated with the peptoids compared to stimulation with the control, LPS (**Figure 3B**), indicating that these peptoids are unlikely to have any macrophage stimulating activity over the concentration range tested.

Intracellular Anti-mycobacterial Activity

Intracellular anti-mycobacterial activity was evaluated for the most active peptoid, BM 2 (4, 8, 16, and 32 mg/L), using murine RAW 264.7 macrophages infected with H37Rv and CSU87 for 4 days (**Figure 4**). Treatment with all concentrations of the peptoid resulted in a similar reduction in mycobacterial burden compared to the untreated control at day 4 (1.8×10^5 CFU/mL for H37Rv and 6.87×10^5 CFU/mL for CSU87) for both

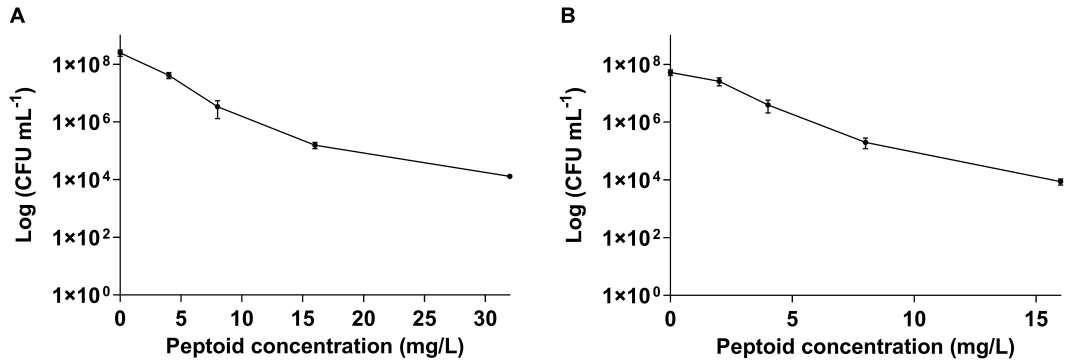

FIGURE 2 | Killing efficiency of peptoid BM 2 against **(A)** drug sensitive *M. tuberculosis* H37Rv and **(B)** multi-drug resistant *M. tuberculosis* CSU87 following treatment for 7 days at concentrations of 4 (0.5 × MIC), 8 (1 × MIC), 16 (2 × MIC), and 32 mg/L (4 × MIC) for H37Rv and 2 (0.5 × MIC), 4 (1 × MIC), 8 (2 × MIC), 16 mg/L (4 × MIC) for CSU87. BM 2 resulted in >99.9% killing of H37Rv at 2 × and 4 × MIC, while >99% and 99.9% killing was achieved against CSU87 at 2 × and 4 × MIC respectively. Data are expressed as mean and standard deviation for three independent experiments.

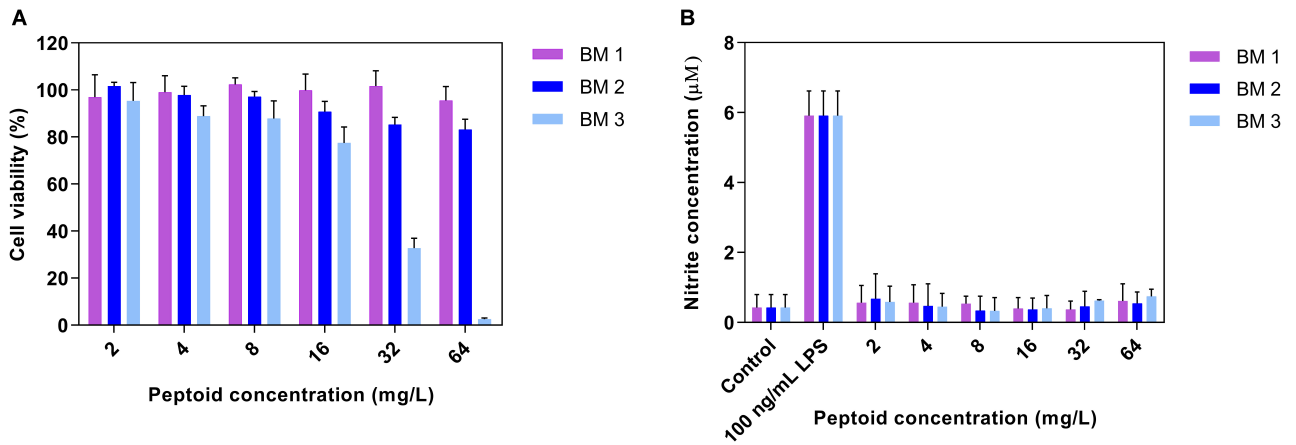

FIGURE 3 | (A) Cytotoxicity profiles of peptoids (BM 1, BM 2, and BM 3) and **(B)** the ability of peptoids to promote nitric oxide (NO) production in unstimulated RAW 264.7 mouse macrophage cells following 24 h treatment. Peptoids BM 1 and BM 2 displayed cell viabilities in excess of 80% at 64 mg/L, while the peptoids did not induce NO production as compared to cells stimulated with 0.0001 mg/L lipopolysaccharide (LPS) as the positive control. Control refers to cells treated with media and BM 1-3 alone while LPS treated refers to cells treated with LPS and peptoid BM 1-3. Data are expressed as mean and standard deviation for two independent experiments performed in triplicate.

M. tuberculosis strains as determined by CFU counts. BM 2 reduced H37Rv bacterial burden in a dose dependent manner, with a 22% reduction at a concentration as low as 0.5 × MIC (4 mg/L) to 1.36 × 10^5 CFU/mL, and a 51% reduction at a concentration of 4 × MIC (32 mg/L) to 8.75 × 10^4 CFU/mL. A very similar reduction at each concentration was achieved against CSU87 with a 32% reduction at 1 × MIC (4 mg/L) to 4.67 × 10^5 CFU/mL ($p < 0.05$) and a 56% reduction at a concentration of 8 × MIC (32 mg/L) to 2.96 × 10^5 CFU/mL ($p < 0.0001$).

Mechanism of Action Studies: Membrane Permeabilization

The results from the flow cytometry, showing the proportion of mycobacterial cells fluorescently stained by PI following a 3 h treatment (4 × MIC) with the peptoids or standard anti-mycobacterial drugs (negative controls, rifampicin and moxifloxacin for H37Rv and CSU87, respectively), demonstrate a similar trend for both H37Rv (**Figure 5A**) and CSU87 (**Figure 5B**). For H37Rv treated with rifampicin, there was negligible uptake of PI by mycobacteria (4.5%) (**Figure 5Aii**) similar to medium alone (**Figure 5Ai**). As expected, the activity of BM 1 was similar to negative controls for H37Rv and CSU87 as this peptoid did not show inhibitory activity in MIC assays, possibly due to its hydrophilic nature (**Figures 5Aiii,Biii**). BM 2 resulted in a relatively small shift in fluorescence compared to controls (7.12% positive PI cells) (**Figure 5Aiv**). BM 3 resulted in a significant shift in fluorescence (31.4% positive PI cells), indicative of its membrane permeabilizing activity which could be explained on the basis of its high hydrophobicity which results in this molecule being cytotoxic in nature against both bacterial and mammalian cells (**Figure 5Av**). CSU87, treated with moxifloxacin (**Figure 5Bii**) showed PI uptake similar to that of the control

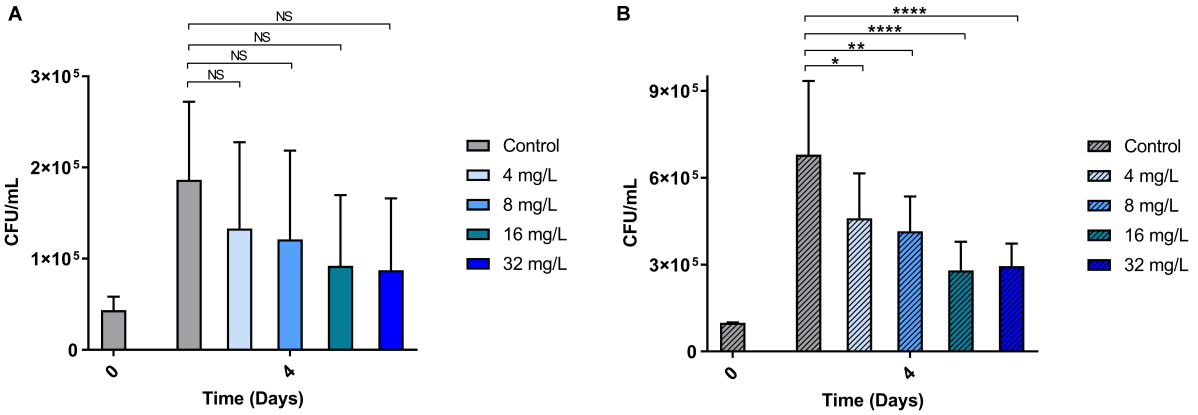

FIGURE 4 | The ability of BM 2 to reduce intracellular bacterial burden (measured as CFU counts) of *M. tuberculosis* H37Rv **(A)** and MDR clinical isolate CSU87 **(B)** after 4 days of treatment. There was a significant reduction in the bacterial burden (between 22 and 56%) for both strains with all concentrations of BM 2 (4, 8, 16, 32 mg/L) compared to the untreated controls as evidenced by the reduction in CFU. The percentage reduction was similar for both H37Rv and CSU87 at each concentration. Data are expressed as mean and standard deviation for two independent experiments. One-way ANOVA followed by Bonferroni's *post hoc* test was applied for the determination of significant differences where $^{*}p < 0.05$, $^{**}p < 0.01$, $^{****}p < 0.0001$, not significant (NS).

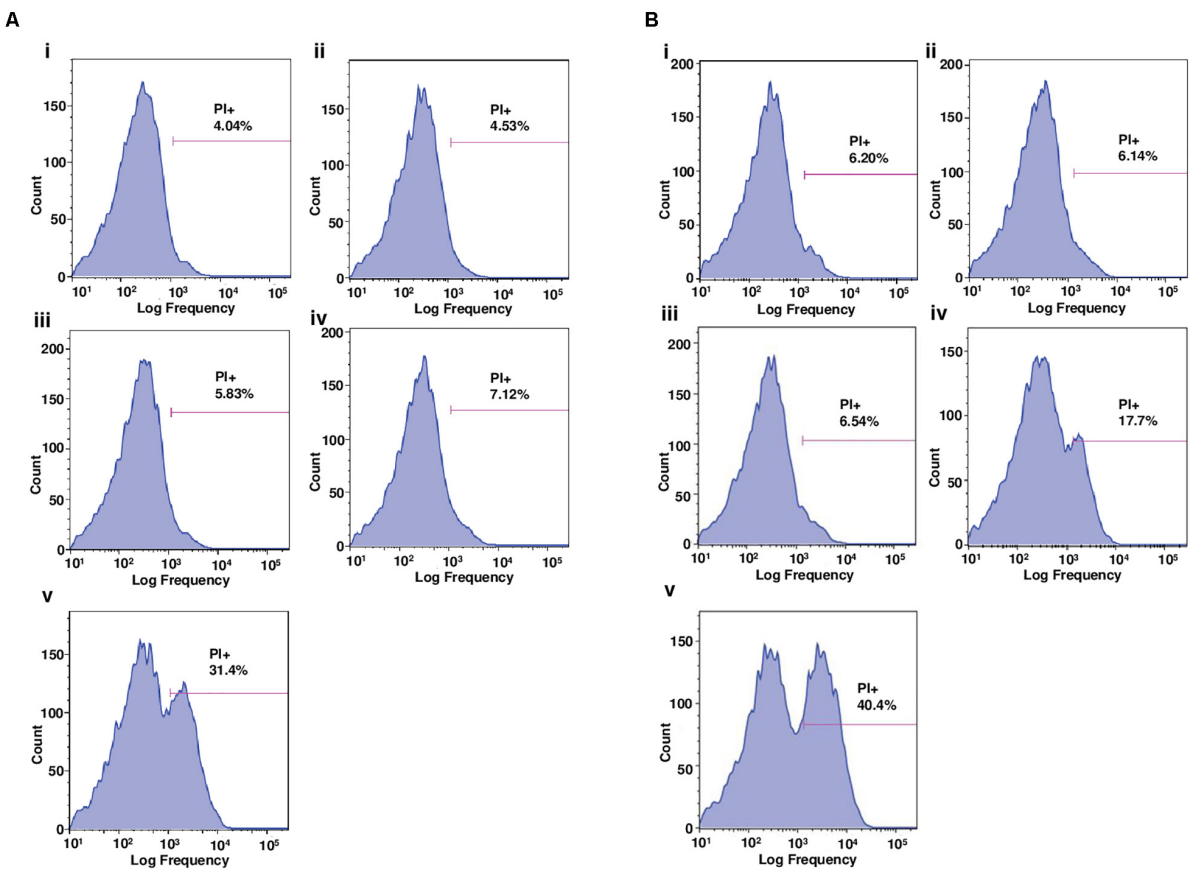

FIGURE 5 | (A) Flow cytometric analysis of the proportion of *M. tuberculosis* H37Rv cells positively stained by the membrane-impermeable dye, propidium iodide (PI), following 3 h treatment with **(i)** media, **(ii)** rifampicin, **(iii)** BM 1, **(iv)** BM 2, and **(v)** BM 3. Drug treatments were performed at 4 × MIC concentration (64 mg/L). BM1 treated cells demonstrated negligible uptake of PI similar to the negative controls (media and rifampicin). BM 2 induced a slight uptake of PI and BM 3 induced significant uptake suggestive of membrane permeabilizing mechanisms of action. **(B)** Flow cytometric analysis of the proportion of *M. tuberculosis* CSU87 cells positively stained by PI, following 3 h treatment with **(i)** media, **(ii)** moxifloxacin, **(iii)** BM 1, **(iv)** BM 2, and **(v)** BM 3. Drug treatments were performed at 4 × MIC (32 mg/L) concentration. As expected BM1 treatment resulted in negligible uptake of PI similar to the negative controls (media and moxifloxacin). BM 2 and BM 3 both induced significant uptake of PI suggestive of membrane permeabilizing mechanisms of action. Data are representative from one of three independent runs.

(media only) (**Figure 5Bi**). Both BM 2 and BM 3 caused a shift in fluorescence (17.7 and 40.4% positive PI cells, respectively) and hence it is likely that they both permeabilize the membrane (**Figures 5Biv,v**).

The time-lapse fluorescence microscopy images of BCG (used for safety reasons) (**Figure 6**), exposed to peptoid BM 2 at 4 × MIC (64 mg/L) for 3 h in the presence of PI, also correlated with the flow cytometry data. Fluorescence staining of bacterial cells demonstrated entry of PI into the cells within 60 min of exposure to BM 2, indicative of membrane disruption induced by this peptoid.

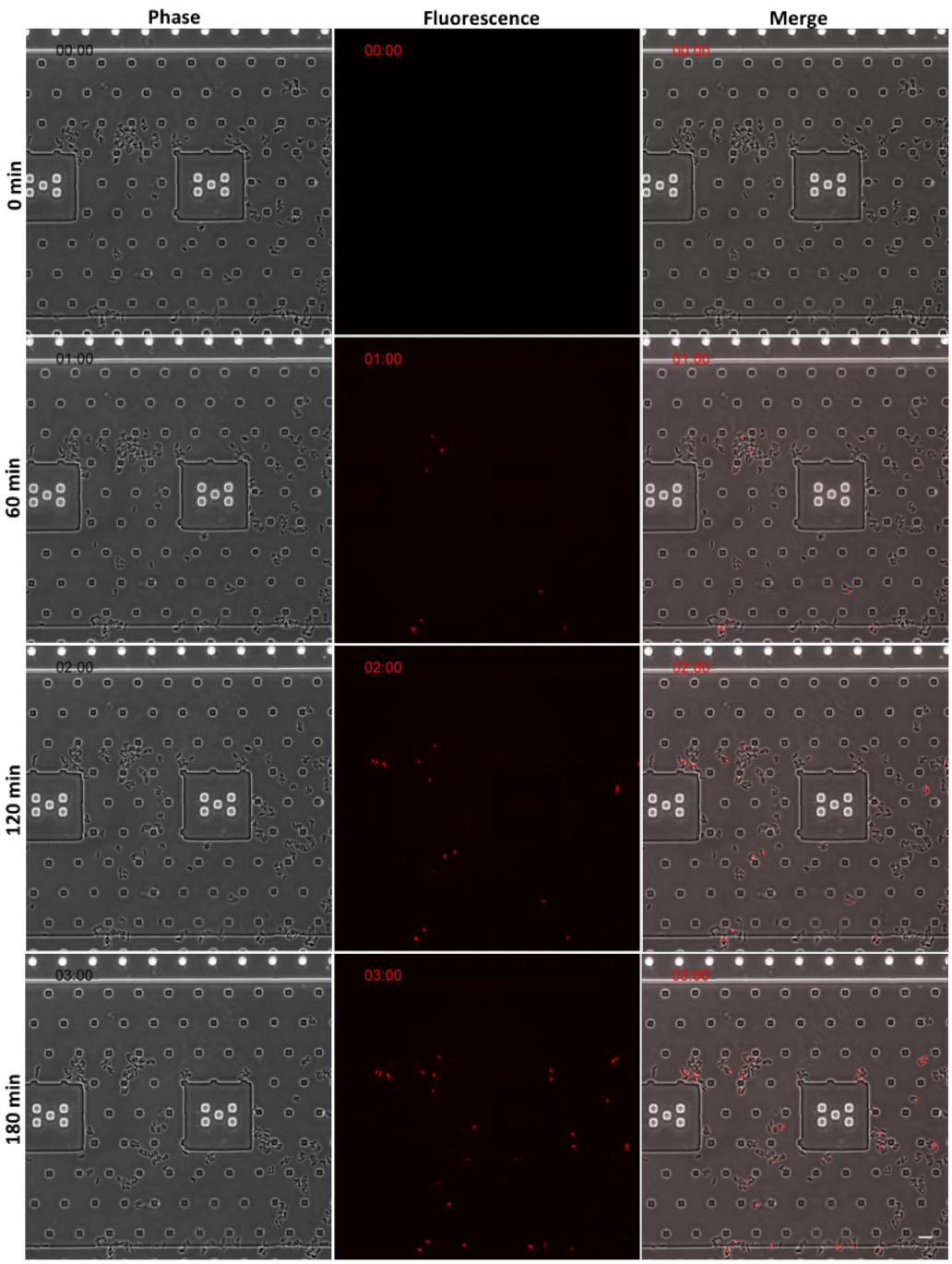

FIGURE 6 | Time-lapse fluorescence microscopy images of BCG (for safety reasons) following 3 h treatment with peptoid BM 2 at 4 × MIC (32 mg/L) in the presence of the membrane-impermeable dye, propidium iodide (PI). Peptoid-mediated membrane disruption promoted uptake of PI into bacterial cells. Images are presented from one representative experiment. Scale bar = 10 μm.

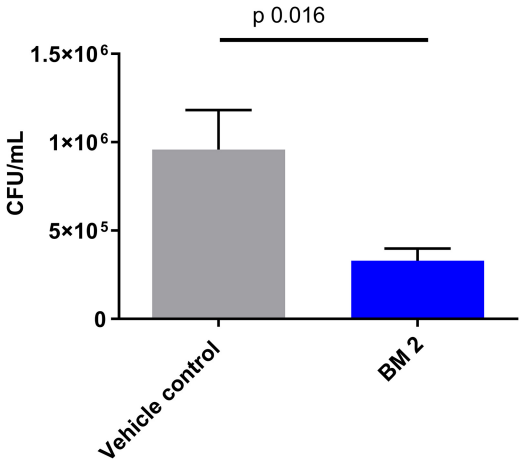

FIGURE 7 | CFU in the lungs of BALB/c mice infected intra-nasally with *M. tuberculosis* H37Rv and treated with six doses of peptoid BM 2 (5 mg/kg per dose) over a 2 weeks period via the intra-tracheal route. The CFU in the lungs of the mice showed a significant reduction in the bacterial load ($p = 0.016$) following treatment with BM 2 compared to the untreated control group. Data is representative of five mice for each group. Mann–Whitney test was applied to determine statistical differences between the two groups.

In vivo Efficacy of BM 2

The *in vivo* efficacy of BM 2 was evaluated in BALB/c mice infected with H37Rv compared to an untreated control group. CFU were estimated in the lung to determine if infection had been established, and whether the peptoid was able to reduce the bacterial burden. At day 1 post-infection, the average infecting dose was 300 CFU/lung ($n = 3$ mice). At 14 days post- peptoid challenge, the CFU counts from the lungs of five mice/group were significantly reduced from 9.5×10^5 in the control group to 3.3×10^5 in the treatment group (~0.6 log, $p = 0.016$) (**Figure 7**). As the lung is the primary affected organ in TB, and the peptoid reduced the bacterial load in the organ after only a short treatment period of 2 weeks, we conclude that BM 2 is efficacious *in vivo*.

DISCUSSION

The mycobacterial envelope is predominantly hydrophobic with a high composition of exceptionally long chain fatty acids known as mycolic acids, and serves as an effective barrier to most broad-spectrum antibiotics. On the other hand, compounds with hydrophobic lipid-like side chains gain easier access by temporarily dissolving in the lipid bilayer of *M. tuberculosis* (Machado et al., 2018). Based on this premise, ultrashort oligo-N-substituted glycines with three monomeric repeating units were synthesized to study the influence of charge (*N*lys), aromaticity and chirality (*N*spe), and hydrophobicity (*N*he), on the potency of the compounds. In comparison to what was reported by Kapoor et al. (2011), where anti-tubercular peptoids were short 4mers with long 13 carbon chains (H-Ntridec-*N*lys-*N*spe-*N*spe-*N*lys-NH_2), this series of peptoids were ultrashort trimer, dimer and monomer used to investigate chain length and anti-tubercular potency. In addition, preliminary mechanistic evaluations were carried out to delineate their mechanism of action vis-à-vis AMPs.

We employed the whole cell phenotypic screening approach which has been shown to be superior to the target-based approach as evidenced by the discoveries of Bedaquiline and Delamanid (Koul et al., 2011; Laughon and Nacy, 2017). All the peptoids exhibited specificity toward members of the *M. tuberculosis* complex as shown by the lack of activity against Gram positive, negative and non-tuberculous mycobacteria. Among those tested, BM 2 and BM 3 have a net charge of +2 and +3, contributed by the *N*lys residues and believed to be sufficient for initial electrostatic interaction with bacteria. BM 2 and BM 3 also displayed increased hydrophobicity through *N*spe and *N*he groups, providing superior affinity hence anti-mycobacterial activity as compared to the relatively hydrophilic BM 1. Importantly, intracellular bactericidal activity against a drug sensitive and an MDR strain of *M. tuberculosis,* was shown, validating their potential as drugs against intracellular pathogens (Machado et al., 2018). Nonetheless, although BM 3 demonstrated good anti-mycobacterial activity, it displayed reduced selectivity as shown by its increased cytotoxicity to macrophages. This is much to our expectation as reports have already highlighted the balance of hydrophobicity with biocompatibility (Bolt et al., 2017). Both BM 1 and BM 2, on the other hand, demonstrated very little cytotoxic activity (<20%).

AMPs are bactericidal mainly due to their pore forming and membrane disruptive effects resulting in the leakage of cytoplasmic contents out of the bacteria, causing lysis and death (Hancock and Sahl, 2006; Devocelle, 2012). To study the mechanism involved in the bactericidal activity of BM 2 against both H37Rv and CSU87, we investigated the ability of the peptoid to permeabilize or disrupt the mycobacterial membrane in comparison to BM 3, BM 1 and standard anti-mycobacterial drugs. We used flow cytometry, and microfluidics and time lapse microscopy in the presence of PI, a fluorescent DNA intercalating dye that does not penetrate intact bacterial cells; thus it is excluded from live cells and only cells with a damaged membrane are stained (Lin et al., 2009). Bacterial cell fluorescence provides evidence of the membrane-permeabilizing activity of a drug, resulting from the loss of membrane integrity, which allows intracellular diffusion and binding of PI to DNA. The difference in the membrane permeabilizing activity of BM 2 between *M. tuberculosis* strains, may be accounted for by differences in the cell walls, as a consequence of differences in strain origin. Another possibility is that the peptoid may have a non-membrane permeabilizing mode of action. However, we have shown that BM 2 demonstrated bactericidal activity at 2 × MIC against *M. tuberculosis*, with >99% reduction in CFU after 7 days of treatment. Taken together, these findings suggest that the bactericidal activity of BM 2 may partly be mediated by disrupting the structural integrity of the mycobacterial membrane, but other mechanisms may be involved.

BM 2 demonstrated efficacy in the acute model of tuberculosis. Over a period of 2 weeks, treatment with BM 2 reduced the

bacterial load in the lungs of the mice. Based on these results future experiments for testing efficacy over a longer duration at different dosages along with pharmacokinetic studies will establish the value of this peptoid as a therapeutic lead candidate.

In summary, this study has shown that peptoids are a promising group of molecules with selective anti-tubercular activity against drug sensitive and MDR *M. tuberculosis*. The selectivity toward bacterial rather than mammalian membranes can be modulated using SAR. The dimer BM 2 showed direct bactericidal activity *in vitro* and efficiently killed drug resistant bacteria at 2 × MIC. It did not activate macrophages, as evidenced by the inability to produce NO, implying that it does not modulate the immune response but rather interacts directly with the bacteria resulting in its bactericidal action on the intracellular bacteria. The mechanism of action is likely to be via disruption of the bacterial membrane as seen by the entry of PI into the mycobacteria. Additionally, BM 2 significantly reduces the bacterial load in the lungs of mice in the acute model of TB. Overall, we have demonstrated that peptoids display anti-mycobacterial activity and thus, in the future, have the potential to be developed into novel therapeutic adjuncts for TB alongside existing drug regimens.

DATA AVAILABILITY STATEMENT

The raw data supporting the conclusions of this article will be made available by the authors, without undue reservation, to any qualified researcher.

ETHICS STATEMENT

The animal study was reviewed and approved by the UK Home Office (PPL/708653) and all animal procedures were performed in accordance with the Animal Scientific Procedures Act of 1986.

AUTHOR CONTRIBUTIONS

JK and BM conducted the *in vitro* experiments. BR and SN conducted the *in vivo* experiments. DM analyzed the data. BM synthesized the peptoids. BM, JK, HJ, SN, PL, BR, and PE designed the experiments. DM, SN, and PE wrote the manuscript. All authors reviewed the manuscript.

FUNDING

This research was supported by the Singapore Ministry of Health's National Medical Research Council under its Individual Research Grant Scheme (NMRC/OFIRG/0026/2016 awarded to PE), the British Society for Antimicrobial Chemotherapy (BSAC GA2016-009P to BR, PL, and SN), the UK Medical Research Council award to the Centre for Molecular Bacteriology and Infection, Imperial College London (MR/P028225/1), the National University of Singapore President's Graduate Fellowship to JK. BM and HJ received funding from the Danish Council for Independent Research (#10-085287 and #4005-00029).

ACKNOWLEDGMENTS

We would like to acknowledge the Imperial College London FILM, Debora Keller, Stephen Rothery and David Gaboriau for providing microscopy support, and Izabela Glegola-Madejska for help with *in vivo* testing.

SUPPLEMENTARY MATERIAL

The Supplementary Material for this article can be found online at: https://www.frontiersin.org/articles/10.3389/fmicb.2020.00417/full#supplementary-material

REFERENCES

Bolt, H. L., Eggimann, G. A., Jahoda, C. A. B., Zuckermann, R. N., Sharples, G. J., and Cobb, S. L. (2017). Exploring the links between peptoid antibacterial activity and toxicity. *MedChemComm* 8, 886–896. doi: 10.1039/c6md00648e

Bremner, J. B., Keller, P. A., Pyne, S. G., Boyle, T. P., Brkic, Z., and Rhodes, D. I. (2010). Binaphthyl-based dicationic peptoids with therapeutic potential. *Angew. Chem. Int. Ed.* 49, 537–540. doi: 10.1002/anie.200904392

Chongsiriwatana, N. P., Patch, J. A., Czyzewski, A. M., Dohm, M. T., Ivankin, A., Gidalevitz, D., et al. (2008). Peptoids that mimic the structure, function, and mechanism of helical antimicrobial peptides. *Proc. Natl. Acad. Sci. U.S.A.* 105, 2794–2799. doi: 10.1073/pnas.0708254105

Czyzewski, A. M., Jenssen, H., Fjell, C. D., Waldbrook, M., Hancock, R. E. W., and Barron, A. E. (2016). In vivo, in vitro, and in silico characterization of peptoids as antimicrobialagents. *PLoS One* 11:e0135961. doi: 10.1371/journal.pone.0135961

Dawson, M. J., and Scott, R. W. (2012). New horizons for host defense peptides and lantibiotics. *Curr. Opin. Pharmacol.* 12, 545–550. doi: 10.1016/j.coph.2012.06.006

Devocelle, M. (2012). Targeted antimicrobial peptides. *Front. Immunol.* 3:309.

Esposito, S., Bianchini, S., and Blasi, F. (2015). Bedaquiline and delamanid in tuberculosis. *Expert Opin. Pharmacother.* 16, 2319–2330. doi: 10.1517/14656566.2015.1080240

Ghosh, C., Manjunath, G. B., Akkapeddi, P., Yarlagadda, V., Hoque, J., Uppu, D. S. S. M., et al. (2014). Small molecular antibacterial peptoid mimics: the simpler the better! *J. Med. Chem.* 57, 1428–1436. doi: 10.1021/jm401680a

Godballe, T., Nilsson, L. L., Petersen, P. D., and Jenssen, H. (2011). Antimicrobial β-peptides and α-peptoids. *Chem. Biol. Drug Design* 77, 107–116. doi: 10.1111/j.1747-0285.2010.01067.x

Gordon, Y. J., Romanowski, E. G., and Mcdermott, A. M. (2005). A review of antimicrobial peptides and their therapeutic potential as anti-infective drugs. *Curr. Eye Res.* 30, 505–515. doi: 10.1080/02713680590968637

Hancock, R. E. W., and Sahl, H.-G. (2006). Antimicrobial and host-defense peptides as new anti-infective therapeutic strategies. *Nat. Biotechnol.* 24:1551. doi: 10.1038/nbt1267

Haney, E. F., Mansour, S. C., and Hancock, R. E. W. (2017). "Antimicrobial peptides: an introduction," in *Antimicrobial Peptides: Methods and Protocols*, ed. P. R. Hansen (New York, NY: Springer New York).

Kang, H.-K., Kim, C., Seo, C. H., and Park, Y. (2017). The therapeutic applications of antimicrobial peptides (AMPs): a patent review. *J. Microbiol.* 55, 1–12. doi: 10.1007/s12275-017-6452-1

Kapoor, R., Eimerman, P. R., Hardy, J. W., Cirillo, J. D., Contag, C. H., and Barron, A. E. (2011). Efficacy of antimicrobial peptoids against *Mycobacterium tuberculosis*. *Antimicrob. Agents Chemother.* 55, 3058–3062. doi: 10.1128/AAC.01667-10

Katarzyna, E. G., and Małgorzata, D. (2017). Antimicrobial peptides under clinical trials. *Curr. Top. Med. Chem.* 17, 620–628. doi: 10.2174/1568026616666160713143331

Khara, J. S., Priestman, M., Uhía, I., Hamilton, M. S., Newton, S. M., Robertson, B. D., et al. (2016). Unnatural amino acid analogues of membrane-active helical peptides with anti-mycobacterial activity and improved stability. *J. Antimicrob. Chemother.* 71, 2181–2191. doi: 10.1093/jac/dkw107

Khara, J. S., Wang, Y., Ke, X.-Y., Liu, S., Yang, Y. Y., and Ee, P. L. R. (2014). Anti-mycobacterial activities of synthetic cationic α-helical peptides and their synergism with rifampicin. *Biomaterials* 35, 2032–2038. doi: 10.1016/j.biomaterials.2013.11.035

Koul, A., Arnoult, E., Lounis, N., Guillemont, J., and Andries, K. (2011). The challenge of new drug discovery for tuberculosis. *Nature* 469, 483–490. doi: 10.1038/nature09657

Laughon, B. E., and Nacy, C. A. (2017). Tuberculosis — drugs in the 2016 development pipeline. *Nat. Rev. Dis. Primers* 3:17015.

Lin, L. J. R., Liao, C. C., Chen, Y. R., and Chak, K. F. (2009). Induction of membrane permeability in *Escherichia coli* mediated by lysis protein of the ColE7 operon. *FEMS Microbiol. Lett.* 298, 85–92. doi: 10.1111/j.1574-6968.2009.01705.x

Machado, D., Girardini, M., Viveiros, M., and Pieroni, M. (2018). Challenging the drug-likeness dogma for new drug discovery in tuberculosis. *Front. Microbiol.* 9:1367. doi: 10.3389/fmicb.2018.01367

Miller, S. M., Simon, R. J., Ng, S., Zuckermann, R. N., Kerr, J. M., and Moos, W. H. (1994). Proteolytic studies of homologous peptide and N-substituted glycine peptoid oligomers. *Bioorg. Med. Chem. Lett.* 4, 2657–2662. doi: 10.1016/s0960-894x(01)80691-0

Mojsoska, B., Carretero, G., Larsen, S., Mateiu, R. V., and Jenssen, H. (2017). Peptoids successfully inhibit the growth of gram negative *E. coli* causing substantial membrane damage. *Sci. Rep.* 7, 42332–42332. doi: 10.1038/srep42332

Mojsoska, B., Zuckermann, R. N., and Jenssen, H. (2015). Structure-activity relationship study of novel peptoids that mimic the structure of antimicrobial peptides. *Antimicrob. Agents Chemother.* 59, 4112–4120. doi: 10.1128/AAC.00237-15

Mukherjee, D., Zou, H., Liu, S., Beuerman, R., and Dick, T. (2016). Membrane-targeting AM-0016 kills mycobacterial persisters and shows low propensity for resistance development. *Future Microbiol.* 11, 643–650. doi: 10.2217/fmb-2015-0015

Simon, R. J., Kania, R. S., Zuckermann, R. N., Huebner, V. D., Jewell, D. A., and Marlowe, C. K. (1992). Peptoids: a modular approach to drug discovery. *Proc. Natl. Acad. Sci. U.S.A.* 89, 9367–9371. doi: 10.1073/pnas.89.20.9367

Steenwinkel, J. E. M., de Knegt, G. J., and de Irma, A. J. M. (2010). Time-kill kinetics of anti-tuberculosis drugs, and emergence of resistance, in relation to metabolic activity of *Mycobacterium tuberculosis*. *J. Antimicrob. Chemother.* 65, 2582–2589. doi: 10.1093/jac/dkq374

Tenland, E., Krishnan, N., Rönnholm, A., Kalsum, S., Puthia, M., Mörgelinet, M., et al. (2018). A novel derivative of the fungal antimicrobial peptide plectasin is active against *Mycobacterium tuberculosis*. *Tuberculosis* 113, 231–238. doi: 10.1016/j.tube.2018.10.008

Tenland, E., Pochert, A., Krishnan, N., Rao, U. M., Kalsum, S., Braun, K., et al. (2019). Effective delivery of the anti-mycobacterial peptide NZX in mesoporous silica nanoparticles. *PLoS One* 14:e0212858. doi: 10.1371/journal.pone.0212858

WHO (2018). *Global Tuberculosis Health Report*. Geneva: WHO.

Wilkinson, R. J., Patel, P., Llewelyn, M. G., Davidson, R. N., and Toossi, Z. (1999). Influence of polymorphism in the genes for the interleukin (IL)-1 receptor antagonist and IL-1β on tuberculosis. *J. Exp. Med.* 189, 1863–1874. doi: 10.1084/jem.189.12.1863

Zhang, L.-J., and Gallo, R. L. (2016). Antimicrobial peptides. *Curr. Biol.* 26, R14–R19. doi: 10.1016/j.cub.2015.11.017

Conflict of Interest: The authors declare that the research was conducted in the absence of any commercial or financial relationships that could be construed as a potential conflict of interest.

frontiers in Microbiology

ORIGINAL RESEARCH
published: 23 March 2020
doi: 10.3389/fmicb.2020.00413

Involvement of Transcription Elongation Factor GreA in *Mycobacterium* Viability, Antibiotic Susceptibility, and Intracellular Fitness

Siyuan Feng[1,2†], Yan Liu[3†], Wanfei Liang[1,2], Mohamed Abd El-Gawad El-Sayed Ahmed[1,2,4], Zihan Zhao[1,2], Cong Shen[1,2], Adam P. Roberts[5,6], Lujie Liang[1,2], Liya Liao[3], Zhijuan Zhong[3], Zhaowang Guo[3], Yongqiang Yang[1,7], Xin Wen[1,2], Hongtao Chen[3‡] and Guo-bao Tian[1,2*‡]*

[1] Department of Microbiology, Zhongshan School of Medicine, Sun Yat-sen University, Guangzhou, China, [2] Key Laboratory of Tropical Diseases Control, Ministry of Education, Sun Yat-sen University, Guangzhou, China, [3] Clinical Laboratory, Fifth Affiliated Hospital, Sun Yat-sen University, Zhuhai, China, [4] Department of Microbiology and Immunology, Faculty of Pharmaceutical Sciences and Drug Manufacturing, Misr University for Science and Technology, Cairo, Egypt, [5] Department of Tropical Disease Biology, Liverpool School of Tropical Medicine, Liverpool, United Kingdom, [6] Centre for Drugs and Diagnostics, Liverpool School of Tropical Medicine, Liverpool, United Kingdom, [7] School of Pharmaceutical Sciences (Shenzhen), Sun Yat-sen University, Guangzhou, China

There is growing evidence that GreA aids adaptation to stressful environments in various bacteria. However, the functions of GreA among mycobacteria remain obscure. Here, we report on cellular consequences following deletion of *greA* gene in *Mycobacterium* spp. The *greA* mutant strain (Δ*greA*) was generated in *Mycobacterium smegmatis*, *Mycobacterium tuberculosis* (MTB) H37Ra, and *M. tuberculosis* H37Rv. Deletion of *greA* results in growth retardation and poor survival in response to adverse stress, besides rendering *M. tuberculosis* more susceptible to vancomycin and rifampicin. By using RNA-seq, we observe that disrupting *greA* results in the differential regulation of 195 genes in *M. smegmatis* with 167 being negatively regulated. Among these, KEGG pathways significantly enriched for differentially regulated genes included tryptophan metabolism, starch and sucrose metabolism, and carotenoid biosynthesis, supporting a role of GreA in the metabolic regulation of mycobacteria. Moreover, like *Escherichia coli* GreA, *M. smegmatis* GreA exhibits a series of conservative features, and the anti-backtracking activity of C-terminal domain is indispensable for the expression of *glgX*, a gene was down-regulated in the RNA-seq data. Interestingly, the decrease in the expression of *glgX* by CRISPR interference, resulted in reduced growth. Finally, intracellular fitness significantly declines due to loss of *greA*. Our data indicates that GreA is an important factor for the survival and resistance establishment in *Mycobacterium* spp. This study provides new insight into GreA as a potential target in multi-drug resistant TB treatment.

Keywords: *greA*, *Mycobacterium tuberculosis*, *Mycobacterium smegmatis*, bacterial fitness, antibiotic susceptibility

OPEN ACCESS

Edited by:
Yossef Av-Gay, The University of British Columbia, Canada

Reviewed by:
Jianping Xie, Southwest University, China
Hiroyuki Yamada, Japan Anti-tuberculosis Association, Japan

***Correspondence:**
Hongtao Chen
13926925941@139.com
Guo-Bao Tian
tiangb@mail.sysu.edu.cn

†These authors have contributed equally to this work

‡These authors share senior authorship

Specialty section:
This article was submitted to Antimicrobials, Resistance and Chemotherapy, a section of the journal Frontiers in Microbiology

Received: *02 January 2020*
Accepted: *27 February 2020*
Published: *23 March 2020*

Citation:
Feng S, Liu Y, Liang W, El-Sayed Ahmed MAE-G, Zhao Z, Shen C, Roberts AP, Liang L, Liao L, Zhong Z, Guo Z, Yang Y, Wen X, Chen H and Tian G (2020) Involvement of Transcription Elongation Factor GreA in Mycobacterium Viability, Antibiotic Susceptibility, and Intracellular Fitness. Front. Microbiol. 11:413. doi: 10.3389/fmicb.2020.00413

INTRODUCTION

Mycobacterium tuberculosis (MTB), the causative agent of tuberculosis (TB) has influenced human populations since ancient times. In 2018, *M. tuberculosis* caused seven million TB cases and was responsible for 1.5 million deaths worldwide (Harding, 2019). The administration of anti-TB drugs has led to the emergence of drug-resistant strains of MTB (Kumar et al., 2017) with approximately 5% of infections being caused by multidrug-resistant (MDR) strains globally (Wright et al., 2009). China has a high prevalence of drug-resistant TB and is the region with second largest number of MDR cases worldwide (Yang et al., 2017). Therefore, exploring the cause of MDR-TB will be pivotal within the implementation of effective public health strategies to reduce MDR-TB.

Transcription (the first step of gene expression) is fundamentally important to all life. Once RNA polymerase (RNAP) initiates the process of transcription, it is vital for the enzyme to carry out elongation and termination to ensure full-length RNA synthesis. Several transcription factors can bind to RNAP, modifying its properties by affecting transcription processivity and fidelity through modulating pausing, arrest, and termination (Tehranchi et al., 2010; Li et al., 2015). The transcript cleavage factor, GreA, interacts with the RNAP secondary channel and stimulates the intrinsic transcript cleavage activity of RNAP for the removal of the aberrant RNA 3′ ends. Therefore, polymerization activity can be restarted from the end of a cleaved RNA allowing transcription to resume (Komissarova and Kashlev, 1997).

Gre factors are widely distributed in prokaryotes. There is growing evidence that Gre factors participate in each step during the transcription process, including initiation, elongation, and fidelity (Yuzenkova et al., 2014; Traverse and Ochman, 2018). In addition, it has been reported that GreA is essential for the survival of bacteria under stress (Volker et al., 1994; Nogales et al., 2002). Moreover, GreA, which can facilitate RecBCD-mediated resection and inhibits RecA, plays an important role in impeding DNA break repair in *Escherichia coli* (Sivaramakrishnan et al., 2017), indicating a role for GreA in adapting to stressful environments.

The genome of *M. tuberculosis* contains a Gre-factor encoded by *rv1080c*. Recent *in vitro* experiments demonstrated that *Mycobacterium smegmatis* GreA exhibits chaperone-like activity (Joseph et al., 2019). It has been shown that *M. tuberculosis* GreA failed to rescue *E. coli* RNAP stalled elongation complexes (China et al., 2011). This suggested that the function of *M. tuberculosis* GreA is sufficiently different from the other well-studied bacterial GreA systems to warrant further investigation. Gumber et al. (2009) revealed that *greA* was found to be upregulated in anaerobic and acidic conditions in *Mycobacterium avium*. Moreover, further studies showed that *greA* was upregulated in *M. tuberculosis* following treatment with ofloxacin, moxifloxacin, and streptomycin (Sharma et al., 2010; Lata et al., 2015), indicating an important role for GreA in the environmental adaptation.

Here, we aimed to dissect the role of GreA and determine any influence on the fitness of mycobacteria. We revealed that GreA serves as a transcriptional factor that coordinates the expression of genes involved in metabolism in *M. smegmatis*. Our data suggests that GreA may be a novel target for adjunctive therapy.

MATERIALS AND METHODS

Ethics Statement

All animal experiments were performed in accordance with the National Institutes of Health Guide for the Care and Use of Laboratory Animals, and the experimental procedures were approved by the Ethics Committee of Zhongshan School of Medicine on Laboratory Animal Care (reference number: 2016-159), Sun Yat-sen University.

Animal Studies in C57BL/6 Mice

Female C57BL/6 mice were purchased from Animal Supply Center, Sun Yat-sen University. Mice were bred and maintained under specific pathogen-free conditions at the animal facility of the Sun Yat-sen University. Adult mice between 6–8 weeks of age were used, and infected mice were maintained under biosafety two conditions. Mice were infected with 1×10^7 colony-forming units (CFUs) of H37Ra, Δ*greA* and *comp*-Δ*greA*, through the intraperitoneal injection. Four mice from each group were sacrificed after 14- and 21- days post-infection, and the lung and spleen homogenates (prepared by homogenizing aseptically removed organs in 1 ml of sterile saline) were plated on 7H10 agar supplemented with 10% OADC (BD Biosciences), in triplicates. CFUs of *M. tuberculosis* were counted after 3-4 weeks of incubation at 37°C.

Bacterial Strains and Generation of *greA* Mutants

A mutant (Δ*greA*) strain of *M. tuberculosis* was constructed as described previously (Jain et al., 2014). For the deletion of *greA* in *M. tuberculosis* H37Rv, PCR was performed to synthesize fragments bearing the 1000 and 980 bps of flanking regions of endogenous *greA* of *M. tuberculosis*, resulting in a deletion of the gene (primer set Mtb *greA*-LL and Mtb *greA*-LR for the 5′ region and primer set Mtb *greA*-RL and Mtb *greA*-RR for the 3′ flanking region). Amplicons corresponding to upstream and downstream flanking regions were digested with *Van*91I and cloned into the *Van*91I digested p0004s plasmid that contains a hygromycin resistance cassette and the *sacB* gene to be able to select for sucrose sensitivity. This allelic exchange substrate was introduced into the *Pac*I site of phasmid phAE159 and electroporated into *M. smegmatis* mc2[1] 155 to obtain high titers of phage phAE159. Subsequently, the *M. tuberculosis* wild-type strain was incubated with high titers of the corresponding phage to create *greA* knockouts. Colonies that had deleted endogenous *greA* were selected on hygromycin-containing plates and verified for sucrose sensitivity. Since the H37Ra genome is highly similar to that of H37Rv with respect to gene content,

[1]https://www.ncbi.nlm.nih.gov/genbank/

similar experiments have been performed for generation of H37Ra mutant strain. For unmarking of the deletion mutations generated by the helper plasmid pYUB870 (SacB, tnpR, and KanR). After transformation by electroporation with pYUB870 and plating onto medium containing kanamycin, 5 kanamycin-resistance colonies were obtained and screened by steaking on 7H10 agar alone and on 7H10 agar with 50 μg/ml hygromycin. A hygromycin-sensitive clone was grown in liquid medium in the absence of antibiotic selection. Further confirmation of *res-hyg-sacB-res* cassette deletion was achieved by PCR analysis and sequencing.

For the construction of *M. smegmatis* Δ*greA* strain, an in-frame deletion of the gene was enabled using Xer site-specific recombination as previously described (van Kessel and Hatfull, 2007). Briefly, two DNA fragments, approximately 500 bp, flanking *greA* of *M. smegmatis* were acquired through PCR and cloned at the borders of the hygromycin excisable cassette. The resulting DNA fragment was purified and electroporated into the competent cells of *M. smegmatis* harboring pJV53 plasmid. The hygromycin-resistant colonies were grown for ten generations in the absence of hygromycin and kanamycin to allow excision of the hygromycin cassette and the loss of pJV53. Finally, unmarked Δ*greA* strain was confirmed by PCR and sequencing.

For the complementation strain of *M. smegmatis* (*comp*-Δ*greA*) and *M. tuberculosis* H37Ra (*comp*-Δ*greA*), *greA* from *M. smegmatis* strain and *greA* from *M. tuberculosis* H37Ra strain was cloned into a pMV306-P_{hsp60} plasmid, and then the recombinant plasmid pMV306-P_{hsp60}-*greA* was transformed into *M. smegmatis* Δ*greA* and *M. tuberculosis*Δ*greA* strains, resulting in *M. smegmatis comp*-Δ*greA* and *M. tuberculosis comp*-Δ*greA*, respectively. The *comp*-Δ*greA* strains were selected on Middlebrook 7H10 agar medium (complemented with 10% OADC) containing 30 μg/ml kanamycin.

The open reading frame (ORF) of *greA* fused with 2 × FLAG was amplified on a template of *M. smegmatis* mc^2 155 (WT) chromosomal DNA using primer pairs. The two single-point mutants of *greA* were generated using overlapping PCR. All of the *greA* variants were cloned into a pMV306-P_{hsp60} plasmid. The *glgX (MSMEG_3186)* gene included its native promoter were cloned into pSMT3-LxEGFP vector in order to perform flow cytometry experiment. As a result, all the plasmid constructs were confirmed via direct DNA sequencing and PCR assay.

Construction of CRISPR Interference (CRISPRi) Targeting Constructs in *M. smegmatis*

CRISPRi targeting constructs in *M. smegmatis* was performed as previously described (Singh et al., 2016). Briefly, we have designed oligos to target two sites in the *glgX* gene. The oligos were annealed to generate a double-stranded insert which was phosphorylated by T4 polynucleotide kinase and then ligated into the *Bbs*I digested pRH2521 to obtain pRH2521-sgRNA. pRH2521 containing sgRNA-targeting the genes of interest was transformed into *M. smegmatis* competent cells into which the *dcas9*-containing vector pRH2502 was previously introduced. Transformants were selected for hygromycin and kanamycin resistance. Addition of anhydrotetracycline (ATc) was repeated every 48 h to maintain induction of *dcas9* and sgRNA for experiments.

Antimicrobial Sensitivity Assays

Antimicrobial sensitivity assays for *M. tuberculosis* have been performed as previously described (Goodsmith et al., 2015). Mycobacteria strains were grown to early log phase and were diluted to an optical density of 0.02 in 7H9 media containing 0.05% Tween 80 and 10% OADC. Then the bacterial strains were exposed to two-fold dilutions of the following antimicrobials; rifampicin, vancomycin, bedaquiline, streptomycin, ofloxacin, isoniazid, Capreomycin, amikacin, and ethambutol (Sigma-Aldrich, United States). The minimum inhibitory concentrations (MICs) were recorded as the minimum concentrations at which the growth was inhibited by at least 90%, as compared to a control containing no antibiotic.

For *M. smegmatis*, the MICs at which no bacterial growth was observed were recorded after 3–5 days of incubation. For *M. tuberculosis*, MICs at which no bacterial growth was observed were recorded after approximately 2 weeks of incubation.

Growth Inhibition Test

Mycobacterium smegmatis had been grown to early log phase and was diluted to an optical density of 0.02 in 7H9 broth medium containing 10% OADC. Then, *M. smegmatis* culture was mixed with each antibiotic, at the final concentration to 1/100th the MIC, including streptomycin, and rifampicin. The OD_{600} value of the bacteria was monitored hourly.

Analysis of *in vitro* Response to Adverse Stress

Exponentially growing bacterial cultures (OD_{600} 0.4–0.6) were pelleted and washed three times with 7H9/Tween-80.

In *M. smegmatis*, for the low pH stress, the strains were washed twice in 7H9 acidified to pH 4.5 with HCl, supernatants were adjusted to an OD600 = 0.5, and CFU was determined after 24 h. For heat shock stresses, *M. smegmatis* strains were incubated at 48°C in a water bath for 6 h, CFUs were counted after 3∼4 days of incubation. For other stresses, *M. smegmatis* strains prepared as above were adjusted to OD600 = 0.5, and SDS, H_2O_2, or antibiotics were added, then the CFUs were determined after 24 h.

For *M. tuberculosis* H37Rv strains, the cells were treated only in 7H9 broth medium with 0.5% SDS and were incubated for 24 h. Then bacterial cells were diluted 10-fold and spotted on Middlebrook 7H10 agar media. While for *M. tuberculosis* H37Ra strain, the cells were resuspended in Middlebrook 7H9 broth under 0.5% SDS and were incubated for 8 h. The CFUs were counted after 4 weeks of incubation.

Synthesis of cDNA and RT-PCR

Equal amounts of bacteria of *M. smegmatis* strains, which were grown to logarithmic phase, were collected. Total RNA and

cDNA from *M. smegmatis* were extracted as previously described (Rustad et al., 2009). cDNA was prepared and amplified as previously described (Alland et al., 1998). Control reactions were performed using primers specific to *sigA* (Manganelli et al., 1999) (see **Supplementary Table S1**). PCR products were separated on 2% agarose gels. The mean intensity of each band was analyzed using ImageJ software. The relative expression was calculated by normalizing the intensity of the *glgX* band with that of the *sigA* band amplified with the same cDNA sample.

Cell Culture

Murine macrophage-like RAW264.7 cells (ATCC; TIB-71) were cultured on Dulbecco' s Modified Eagle Medium (DMEM) supplemented with 10% fetal bovine serum (FBS), 100 U/ml penicillin, and 100 μg/ml streptomycin (GIBCO, Invitrogen) with 5% CO_2 at 37°C.

Macrophage Infection Study

RAW264.7 cells were seeded at 3×10^5 cells/well in a 24-well plate and incubated for 18 h. Homogenized bacterial suspension at a multiplicity of infection (MOI) of 10, was transformed into adherent RAW264.7 cells. The extracellular bacteria were removed by washing three times with phosphate buffer saline (PBS) after incubation for 2 h. Cells were further incubated for 48 h with 5% CO_2. Then cell lysates were serially diluted 10-fold and spotted on 7H10-OADC agar. CFUs of *M. smegmatis* were counted after 3∼4 days of incubation at 37°C, while CFUs of *M. tuberculosis* were counted after 4 weeks days of incubation at 37°C.

Structural Modeling

The architecture of GreA in full length was modeled with Swiss-Model[2]. The GreA of *E. coli* [PDB: 1grj.1] has functioned as a structural template, and the ribbon structure was presented with the PyMol software.

RNA Preparation and RNA-Seq Analysis

Wild-type *M. smegmatis* mc^{2}155 as well as the *greA* deletion strain were grown to the log-phase (OD600, 0.4) in Middlebrook 7H9-ADC. Total RNA was prepared from wild-type and mutant strains using TRIzol reagent (Invitrogen), followed by DNase I treatment. Approximately 1-μg total RNA samples were treated by the Ribo-Zero rRNA removal procedure (Illumina) to enrichment for mRNA. Approximately 1 μg of RNA was used for library preparation using a ScriptSeq (v2) RNA-seq kit and high-throughput sequencing on an Illumina NextSeq platform. All raw sequence reads by RNA-Seq were initially pre-processed by Trimmomatic (v0.36) to trim the adaptor sequences and remove low-quality sequences. The remaining clean reads were mapped to the *M. smegmatis* mc^2 155 genomes using Tophat2. The alignment results were input into Cufflinks (v2.2.1). Unless otherwise stated, the unit of expression level in our analyses is FPKM. Cuffdiff (v2.2.1) was used to test for differential expression. We defined genes as differentially expressed using the following criteria: FPKM > 10 and FDR < 0.001. The data for visualization was generated by R (R Development Core Team, Vienna, Austria). The genome sequences and the annotations of *M. smegmatis* mc^2 155 were obtained from the GenBank[2]. We analyzed differences in the enrichment of Gene Ontology (GO) categories and KEGG pathways for the DEGs using the DAVID (v6.8) functional annotation analysis tool[3].

Chromatin Immunoprecipitation

ChIP was performed using log-phase (OD600, 0.4) liquid medium grown cultures of *M. smegmatis* strains producing GreA-FLAG. As a negative control, WT log-phase culture was used. The cells were fixed with 1% formaldehyde for 30 min, the reaction was quenched with 150 mM glycine for 15 min, and then the cells were washed three times with cold PBS (54,000 rpm, 5 min, 4°C) and frozen at −80°C. To prepare lysates, pellets were resuspended in FA-1 buffer (HEPES-KOH at 50 mM [pH 7.5], NaCl at 140 mM, EDTA at 1 mM, Triton X-100 at 1%, and protease inhibitor cocktail [Sigma-Aldrich]), disintegrated with silica beads (0.1 mm) for 45 min, and sonicated on ice using ten cycles of a 10-s pulse followed by a 50-s pause. The obtained lysates were centrifuged (5 min, 12,000 rpm, 4°C) and frozen at −80°C in 5% glycerol. For immunoprecipitation, 200 μg of total protein was incubated on a rotary shaker (Thermo Fisher Scientific, China Co., Ltd.) for 4 h at 4°C with a 15-μl packed-gel volume of anti-FLAG M2 magnetic beads (Sigma-Aldrich) and then washed twice with FA-1 buffer. Samples were processed in a final volume of 0.5 ml in two biological replicates, with input DNA controls (200 μg of total protein alone) included for each replicate. Samples were washed using a magnetic separator with sequential applications of FA-1 buffer, FA-2 buffer (HEPES-KOH at 50 mM [pH 7.5], NaCl at 500 mM, EDTA at 1 mM, Triton X-100 at 1%, and protease inhibitor cocktail), and Tris–EDTA buffer solution (TE) (Tris–HCl at 10 mM [pH 8.0], EDTA at 1 mM). Immunoprecipitated samples were de-cross-linked overnight in TE containing 1% SDS at 65°C and then digested with proteinase K (final concentration, 0.05 mg/ml) for 1.5 h at 55°C. The immunoprecipitated DNA was extracted using Cycle-Pure Kit (OMEGA Bio-tek, Inc.).

Library Construction and Illumina Sequencing

The library of DNA fragments was prepared using a QIAseq Ultralow Input library kit (Qiagen). Briefly, the protocol includes DNA end-repair, sequencing adapter ligation, cleanup, and PCR amplification. At the end of the procedure, quantification and quality evaluations were done using a NanoPhotometer® spectrophotometer (IMPLEN), a Qubit® 2.0 Fluorometer (Life Technologies), and a 2100 Bioanalyzer (Agilent). Second-generation sequencing was performed using a HiSeq 1500 sequencing platform (Illumina).

Analysis of CHIP-Seq Data

The obtained FASTQ files were filtered according to read quality, and adapter sequences were trimmed using the Trimmomatic

[2]https://swissmodel.expasy.org/repository/uniprot/A0R2X1

[3]https://david.ncifcrf.gov

software (Usadel Lab; Aachen University, Aachen, Germany). The filtered FASTQ files were mapped to the genome of *M. smegmatis* strain mc^2 155 (from GenBank) using the BWA v0.7.12 (Burrows-Wheeler aligner), and the Bwa mem algorithm was applied. The bam files were sorted and indexed. Then the bam files for the ChIP and input samples were subjected to MACS analysis (MACS2 software) for ChIP-Seq peak detection. Peak calling was performed without building a model using a shift size of 150 bp. The ChIP-Seq peaks were uploaded into the R environment as bed files, and the peaks were annotated ChIP-Seq data.

Statistical Analysis

Statistical analysis was performed using Prism (version 6.0c; GraphPad Software). Data were analyzed using the paired Student's *t*-test, and in the comparisons of data from three or more conditions, analysis of variance (ANOVA) was used. A *p*-value of 0.05 or less was considered significant.

RESULTS

Mutants for *greA* Caused a Delay in Mycobacterial Growth

To explore the function of *greA* in mycobacteria, we deleted the *greA* (*MSMEG_5263*) gene by allelic exchange facilitated via recombination in *M. smegmatis* mc^{2}155 which is widely used as a model to study non-pathogenic aspects of mycobacterial physiology. We have detected colonies of small sizes in the *greA* mutant strain compared with the parental strain (**Figure 1A**), it was observed that Δ*greA* strain grows slower than the wild-type *M. smegmatis* and the phenotypes that were complemented by expression of *greA* (*comp*-Δ*greA*) from *M. smegmatis* on the chromosome (**Figure 1B**). To confirm the phenotype of GreA in *M. tuberculosis* strain, we knocked out *greA* (*rv1080c*) in *M. tuberculosis* H37Rv and H37Ra by specialized transducing mycobacteriophages (**Supplementary Figure S1**). Following the observation that a growth defect was caused by *greA* deficiency in *M. smegmatis*, we found that colonies of small sizes were also observed in the Δ*greA* strain of H37Ra and H37Rv (**Figure 1A**) and a growth defect was detected in the Δ*greA* strain of H37Ra (**Figure 1C**). Our observation was consistent with a previous study (China et al., 2011).

Deletion of *greA* Increased the Sensitivity to Adverse Stress

It has been reported that GreA is essential for the survival of *E. coli* under stress conditions (Sharma and Chatterji, 2010). Herein, we investigated the role of GreA in the environmental adaptation of mycobacteria. The WT, Δ*greA*, and *comp*-Δ*greA* strains were treated with adverse stresses. When compared to parental bacteria and complement strain, the Δ*greA* strain was more sensitive to SDS, hydrogen peroxide, and starvation (**Figures 2A–C**). However, there were no differences in the survival rate of bacteria which were treated with low pH and heat shock (**Figures 2D,E**). In addition, we also found that the survivability of *M. tuberculosis* Δ*greA* mutant strain was significantly reduced compared to H37Rv strain upon the treatment with 0.5% SDS (**Figure 2F**) and a similar phenotype was also observed in *M. tuberculosis* H37Ra strain (**Figure 2G**). Moreover, the *greA* gene also complemented the phenotype of Δ*greA* in *M. tuberculosis* H37Ra (**Figure 2G**). These results indicated that mycobacteria GreA is required for adaptation to these stressful conditions.

Of note, the *greA* gene was found upregulated under stress with antibiotics in *M. tuberculosis* (Sharma et al., 2010; Lata et al., 2015). We speculated that Δ*greA* strain might be more susceptible to antibiotics. To test this hypothesis, we performed antibiotic susceptibility tests where, *M. smegmatis* WT, Δ*greA*, and *comp*-Δ*greA* strains were challenged with streptomycin, rifampicin, and bedaquiline. We found that Δ*greA* strain was more susceptible to the tested antibiotics compared with both parental and complemented bacteria (**Figures 2H–J**). Moreover, we also evaluated the susceptibility to antibiotics through the MIC test in *M. tuberculosis*, and we found that *M. tuberculosis*Δ*greA* strain showed increased susceptibility to rifampicin, bedaquiline, and vancomycin. Surprisingly, the MIC of the Δ*greA* strain decreased by 4-fold with rifampicin and by 8-fold with vancomycin compared with MTB H37Rv (**Table 1**), suggesting that *greA* plays an important role in the antibiotic susceptibility in mycobacteria.

In accordance with the observation that the *greA* mutant strain has an increase in the sensitivity to antibiotics, we found that the growth of Δ*greA* strain was more retarded despite at low antibiotic concentrations used when compared to WT and complemented strains (**Supplementary Figure S2**).

In vivo Transcription Analysis of GreA-Responsive Genes

Given our observations that inactivation of *greA* in *M. smegmatis* results in reduced survivability under stress, we next sought to identify the proteins being regulated by GreA. To understand how GreA may affect gene expression at the transcriptional level, we performed whole-transcriptome RNA-seq analyses. We found that disrupting *greA* resulted in the differential regulation of 195 genes in *M. smegmatis* during the exponential growth. Among these, 28 were positively regulated and 167 were negatively regulated (**Figure 3A** and **Supplementary Table S2**). Moreover, our findings for enriched KEGG pathways are summarized in **Figure 3B** and **Supplementary Table S3**. Three pathways were significantly overrepresented. Three genes are involved in tryptophan metabolism, and four genes are involved in starch and sucrose metabolism. Interestingly, the *glgX* gene, which encodes the debranching enzyme of the catabolic enzymes, was involved with starch and sucrose metabolism (Schneider et al., 2000). Chromosomal inactivation of *glgX* in *Corynebacterium glutamicum* led to slower growth (Seibold and Eikmanns, 2007), it is suggested that GreA mediated regulation of the growth might be partly associated with *glgX*. This outcome demonstrated that GreA has a profound

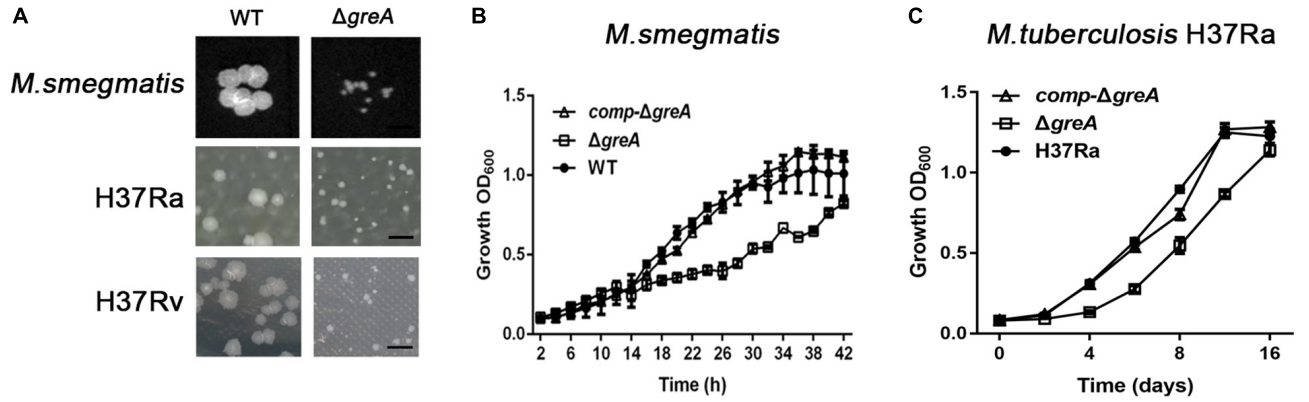

FIGURE 1 | Mutants for *greA* on growth, colonial morphology in mycobacteria. **(A)** The colony size of WT and Δ*greA* strains from *M. smegmatis,* H37Ra and H37Rv. The bar corresponds to 0.5 cm. The growth of WT, Δ*greA*, and *comp*-Δ*greA* strains from **(B)** *M. smegmatis* and **(C)** *M. tuberculosis* H37Ra in 7H9 broth. Bacteria were diluted to an initial OD_{600} of 0.02 and the OD_{600} was monitored at the designated time points. Data are shown as mean ± SEM of three independent experiments.

effect on cellular gene regulation, especially on metabolic associated genes. Collectively, these transcriptional changes are consistent with the scenario that *greA* gene expression is required for optimal growth of mycobacteria, whereas loss of *greA* results in slower growth and reduced tolerance to adverse environments.

Identification of GreA-Binding Sites Using ChIP-Seq

To examine whether GreA binds to specific chromosomal regions, we performed chromatin immunoprecipitation followed by deep sequencing (CHIP-seq) and then sought to verify the binding mode of GreA. CHIP-seq experiments were performed by using *M. smegmatis* strains producing GreA proteins fused with two repeats of the FLAG epitope ($FLAG_2$). GreA-$FLAG_2$-DNA nucleoprotein complexes fixed with formaldehyde in the log phase of growth were immunoprecipitated using magnetic beads. To exclude unspecific interactions with magnetic beads, we used a WT strain lacking the FLAG epitope as a negative control for our CHIP-seq experiments. Enriched regions were determined by comparison to the background noise level, which was estimated versus the input DNA of each ChIP-Seq replicate. Using the data obtained from this analysis, we established chromosomal binding maps for the analyzed proteins. The GreA-$FLAG_2$ binding sites were distributed evenly along the *M. smegmatis* (**Figure 4**). The identified GreA-$FLAG_2$ binding sites included 1005 CHIP-seq peaks that were confirmed in two biological replicates and absent in WT strain (**Supplementary Table S4**). Among the 1005 CHIP-seq peaks identified for GreA-$FLAG_2$, we observed that several binding sites were located downstream of the gene (∼0.7% of all ChIP-Seq peaks). However, GreA binding sites seemed to be more frequent within promoters (∼84.8% of all ChIP-Seq peaks), and ∼14.5% of all ChIP-Seq peaks were identified in gene bodies (**Supplementary Figure S3**). Notably, from the CHIP-seq dataset, we found that one of the peaks was located at the coding sequence of *glgX*, suggesting that GreA might regulate the transcription of *glgX*.

The Full Activity of the GreA Is Crucial in *M. smegmatis* Growth

It is known that *E. coli* GreA consists of two domains: an N-terminal extended coiled-coil domain (NTD, residues 1–75)

TABLE 1 | Changes of MICs of wild-type mycobacteria and Δ*greA* strains against different antimicrobial agents.

Mycobacteria strains	Minimum inhibitory concentrations (mg/L)								
	INH	RIF	EMB	SM	CPM	OFX	VAN	AMK	BDQ
H37Rv	0.0125	0.018	1	2.5	5.12	0.32	6.25	5.12	0.05
Δ*greA*-H37Rv	0.0125	0.0045	1	2.5	5.12	0.32	0.781	5.12	0.025
mc^2155	8	16	1	0.5	5	1	10	0.5	0.05
Δ*greA*-mc^2155	8	16	1	0.25	1.25	1	5	0.25	0.025
comp-Δ*greA*-mc^2155	8	16	1	0.5	5	1	10	0.5	0.05
H37Ra	0.0375	0.0015	1	0.1	5.12	0.32	3.125	5.12	0.02
Δ*greA*-H37Ra	0.0375	0.0002	0.5	0.1	5.12	0.32	0.781	5.12	0.01
comp-Δ*greA*-H37Ra	0.0375	0.0015	1	0.1	5.12	0.32	3.125	5.12	0.02

VAN, vancomycin; INH, isoniazid; RIF, rifampicin; EMB, ethambutol; OFX, ofloxacin; AMK, amikacin; SM, streptomycin; CPM, capreomycin; BDQ, bedaquiline.

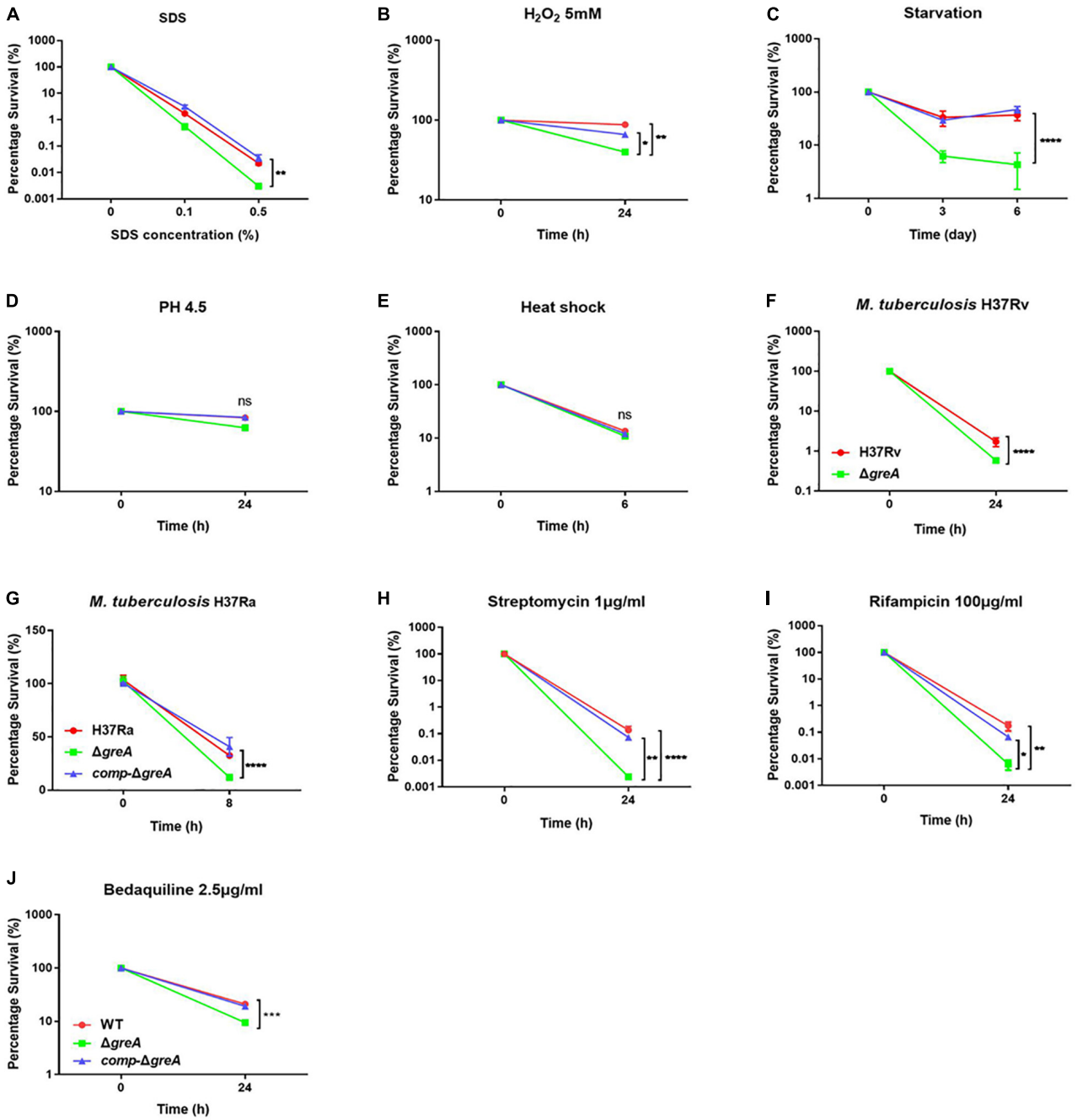

FIGURE 2 | GreA is required for resistance to adverse stress. **(A–E, H–J)** Survival of *M. smegmatis* strains during adverse stress. The strain symbols listed in the **(J)**. WT, Δ*greA* and *comp*-Δ*greA* strains were treated for at the indicated time with varying concentrations of SDS **(A)**, 5mM H_2O_2 **(B)**, PBS + 0.05% Tween 80 **(C)**, low pH (pH4.5) **(D)**, heat shock (48°C) **(E)**, 1 μg/ml of streptomycin **(H)**, 100 μg/ml of rifampicin **(I)**, or 2.5 μg/ml of bedaquiline **(J)**. After treatment, dilutions were plated on 7H10 and survival is expressed as a ratio of CFUs compared to untreated cultures. **(F)** *M. tuberculosis* H37Rv strains were spotted on the 7H10 plates after they were treated under 0.5% SDS for 24 h. **(G)** WT, Δ*greA*, and *comp*-Δ*greA* strains from *M. tuberculosis* H37Ra were subjected to 0.5% SDS for 8 h. CFU enumeration was performed after incubation for the indicated time. These experiments were performed three times with similar results. Data are shown as mean ± SEM of three independent experiments. $^*p < 0.05$, $^{**}p < 0.01$, $^{***}p < 0.001$, $^{****}p < 0.0001$, ns, $p \geq 0.05$.

and a C-terminal globular domain (CTD, residues 76–158) (Stebbins et al., 1995; Koulich et al., 1997). The NTD carries the structural determinants conferring the cleavage activity and, presumably, the anti-arrest and readthrough activities. The CTD participates in binding to RNAP (Koulich et al., 1998). Alignment of the mycobacterial GreA with *E. coli* GreA revealed the similar conserved features (**Figure 5A**). In addition, GreA from *M. smegmatis* is almost identical to that of *M. tuberculosis* GreA,

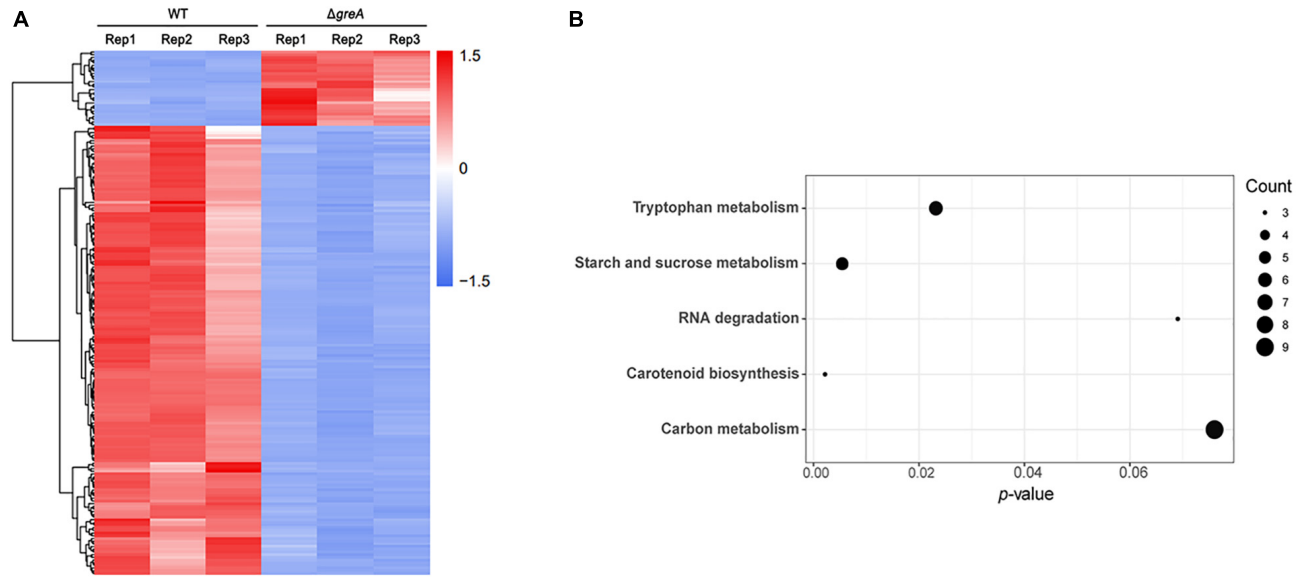

FIGURE 3 | Differentially regulated genes were identified between Δ*greA* strain and WT strain by RNA-seq. **(A)** Heat maps showing the expression profiles of genes upregulated or downregulated by deletion of the *greA* gene in *M smegmatis*. **(B)** Summary of the KEGG reference pathway results. Three biological replicates were tested.

FIGURE 4 | Heat maps of the distributions of GreA-FLAG binding sites in two biological replicates. Two biological replicates were tested.

indicating its similar function in mycobacteria. To gain further structural insight into the conserved domain of mycobacterial GreA, structural modeling by the Swiss-Model program was performed using *E. coli* GreA (PDB accession no. 1grj.1) as a structural template (**Figure 5B**). The ribbon structure of *M. smegmatis* GreA, together with *E. coli* GreA were generated with the PyMol software. Of note, structural comparison of the two GreA proteins illustrated that the coiled-coil domain and RNAP interaction of CTD constitute almost identical motifs (**Figure 5C**). To further explore their physiological role in the growth phenotype of GreA, we applied overlapping PCR to generate the following two single point mutations of GreA (D43N, S127E). As expected, the D43N and S127E mutations completely disrupted the optimal growth of *M. smegmatis* GreA (**Figure 5D**), the observation is in line with a previous *in vitro* study (China et al., 2011). Collectively, these observations strongly support the conclusion that the full activity of the GreA is required for *M. smegmatis* growth.

The *glgX* Gene Regulated by GreA Is Involved in the Optimal Growth of *M. smegmatis*

To extend our *in silico* finding, we performed genetic experiments to confirm the relationship between GreA and a candidate gene. We selected the candidate gene based on their down-regulation in the RNA-seq data, the enrichment in CHIP-seq data, and the potential role of their gene product in the growth phenotype. Taking these into consideration, we focused on the function of the *glgX* gene. To determine whether the reduced growth of *M. smegmatis greA* mutant strain was attributed to the decreased expression of *glgX*, we applied the mycobacterial CRISPRi for rapid validation. Initially, we introduced a plasmid encoding the gene of green fluorescent protein (GFP) fused with the *glgX* gene, including its native promoter, into both wild type and mutant *M. smegmatis* strains. Then we determined the mean fluorescence intensity of GFP by the flow cytometry. The mean fluorescence intensity of GFP was significantly decreased in Δ*greA* strain compared to WT strain (**Figure 6A**), confirming that disruption of *greA* was responsible for the reduced expression of *glgX*. Moreover, the silencing efficiency was measured by semi-quantitative RT-PCR that showed a ∼80% decrease in the expression of the *glgX* gene (**Figure 6B**). As expected, the decrease in the expression of *glgX*, resulted in reduced growth compared to the strain without induction of ATc (**Figures 6C,D**), indicating that loss of *greA* has led to a partial defect of growth by down-regulating *glgX*.

In *E. coli*, the residues D41 of the GreA protein are required to prevent the backtracking of paused complexes, thereby suppressing the transcriptional pauses (Vinella et al., 2012). Since the GreA protein of *E. coli* and *M. smegmatis* shares the residues

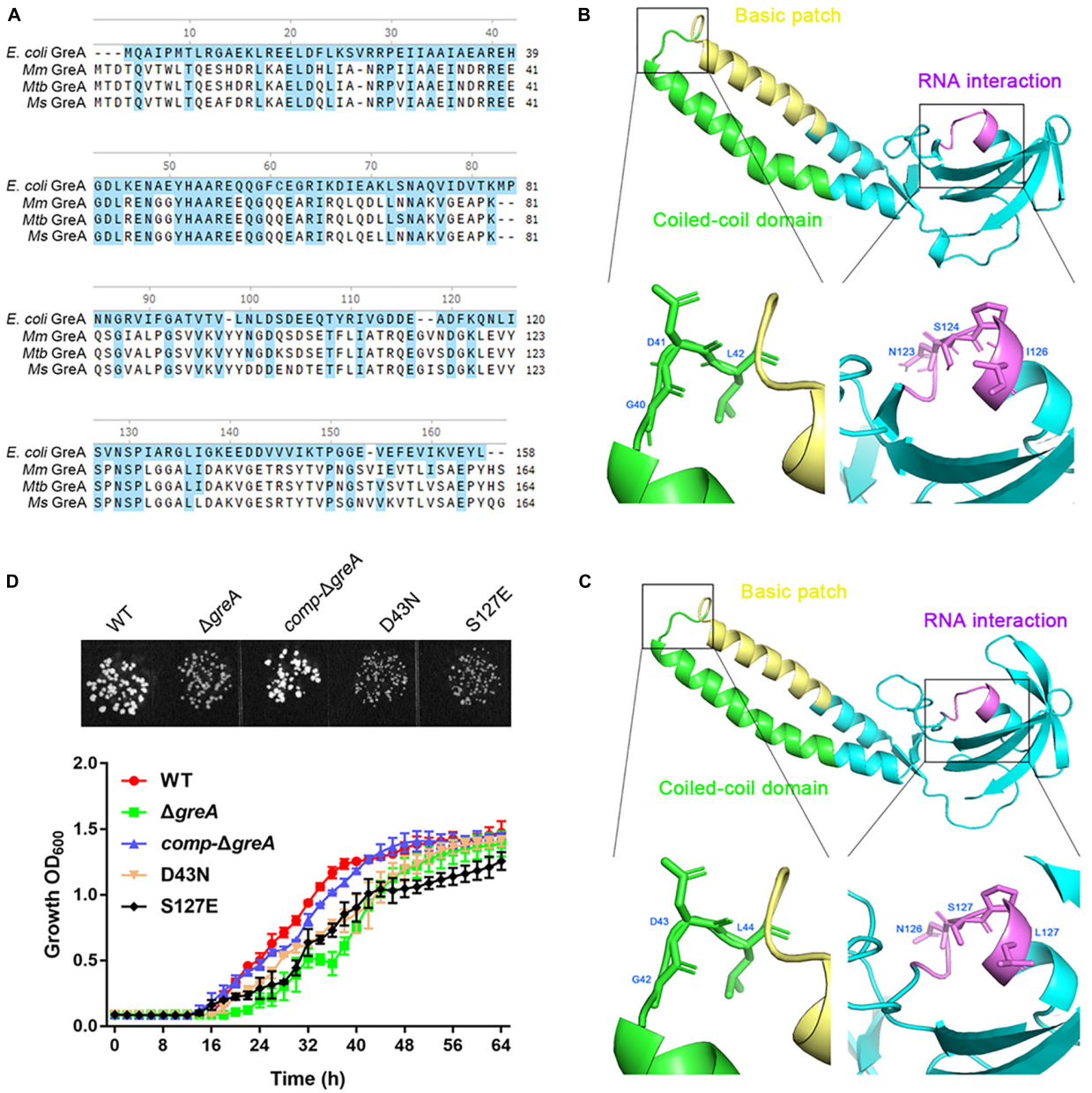

FIGURE 5 | Optimal growth of *M. smegmatis* is required for the full activity of the GreA. **(A)** Multiple sequence alignment of *E. coli* GreA (158 aa) with *M. smegmatis* GreA (164 aa), *M. tuberculosis* GreA (164 aa), and *M. marinum* (165 aa). The conservative residues of *E. coli* GreA **(B)** and *M. smegmatis* GreA **(C)**. PyMol is applied to generate the photographs of coiled-coil domain, basic patch, and RNAP interaction. **(D)** The growth of *M. smegmatis* strains harboring *greA* and/or its point mutants. Three biological replicates were tested. Data are shown as mean ± SEM of three independent experiments.

mentioned above, we determined if the anti-backtracking activity of GreA was associated with the regulation *glgX*. To achieve this, the transcriptional expression of *glgX* was detected in *M. smegmatis* strains. Interestingly, transcriptional expression of *glgX* was fully restored in *comp*-Δ*greA* strain. However, this has not been observed in the D43N strain and *greA* mutant strain (**Figure 6E**), indicating that the anti-backtracking activity of GreA is required for the transcriptional expression of the *glgX* gene.

Deletion of *greA* Attenuated the Intracellular Survivability

The persistence inside a host macrophage is a vital characteristic that distinguishes the pathogenic mycobacteria from non-pathogenic strains (Singh et al., 2008; Yaseen et al., 2015). RAW264.7 cells were infected with WT, Δ*greA* or complemented strains of *M. smegmatis*. The numbers of the surviving intracellular bacteria were assessed after 24 and 48 h post-infection. A significant reduction in the number of viable

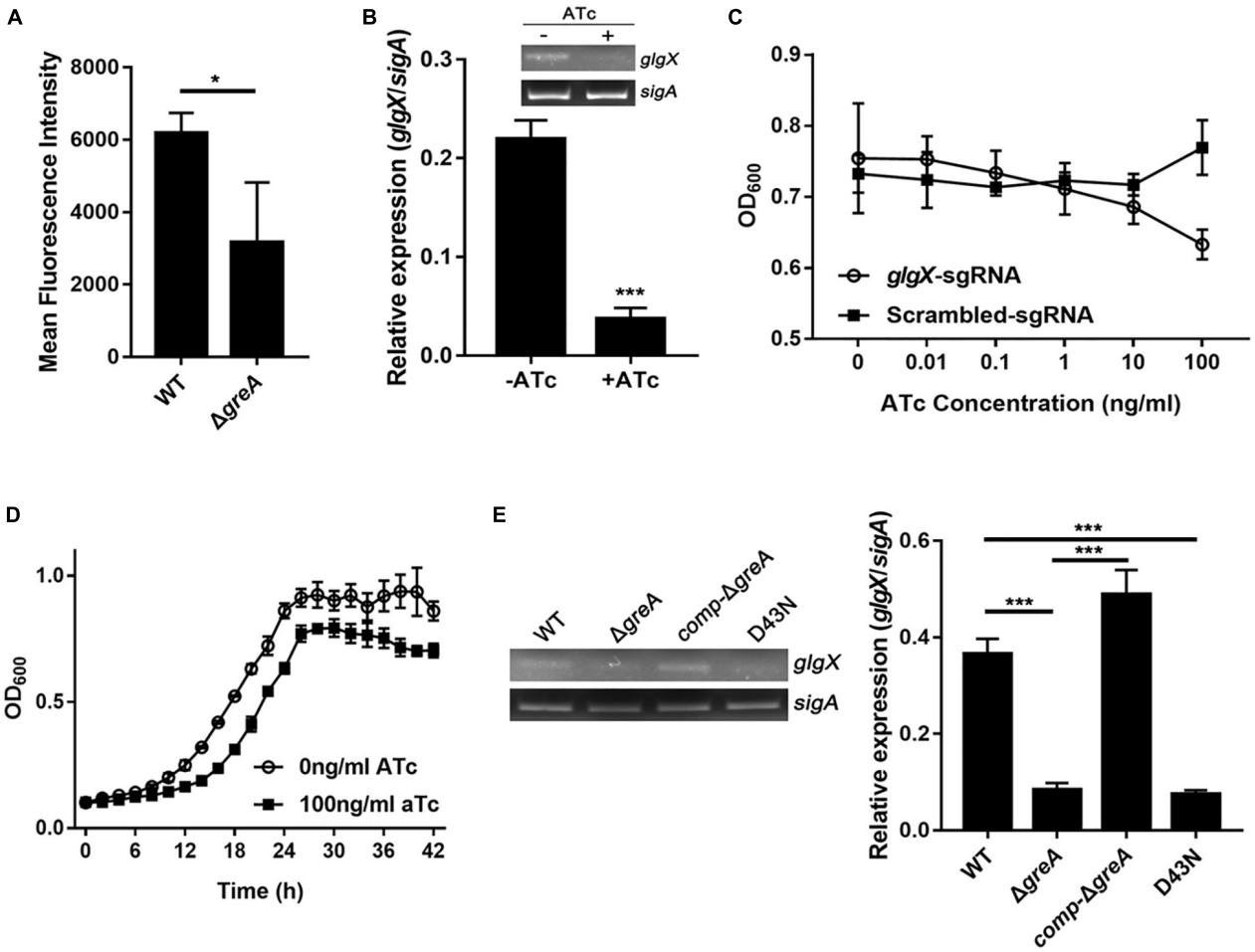

FIGURE 6 | The *glgX* gene regulated by GreA is involved in the optimal growth of *M. smegmatis*. **(A)** Bacteria was collected at logarithmic phase. The mean fluorescence intensity of GFP in the *M. smegmatis* strains harboring a plasmid encoding *gfp* fusion with the *glgX* gene including its native promoter. **(B)** Expression of *glgX* was determined by semi-quantitative RT-PCR with or without induction of ATc. **(C,D)** *In vitro* growth of culture with or without induction of ATc. **(E)** Results of semi-quantitative RT-PCR of glgX in *M. smegmatis* strains harboring *greA* and/or its point mutants. **(B,E)** The gel images shown are representative of three repeat experiments. The PCRs of *sigA* served as controls for normalization of the cDNAs. The relative expression of *glgX* versus that of *sigA* was quantitated using ImageJ. The bar graphs show the means of two independent experiments. The error bars indicate the standard errors of the means (SEM). Three biological replicates were tested. $^{*}p < 0.05$, $^{***}p < 0.001$.

intracellular mycobacteria was observed after 24 and 48 h in the Δ*greA* strain (**Figure 7A**). Moreover, the survivability of H37Rv and Δ*greA* strain was assessed by the detection of the bacterial CFUs inside the macrophage. We found that the survivability of *greA* mutant strain was significantly decreased in macrophages after 48 h when compared to the H37Rv strain (**Figure 7C**). In addition, the RAW264.7 cells were infected with WT, Δ*greA*, or complemented strains of *M. tuberculosis* H37Ra. In this case, no significant difference between H37Ra and Δ*greA* strain for intracellular survivability was observed at 48 h post-infection (**Figure 7B**). The findings lead us to suppose that this survival phenotype may be the result of the growth defect of *M. tuberculosis* lacking *greA*. It has been demonstrated that strain H37Ra is avirulent, and does not multiply in mice (Larson and Wicht, 1964). Thus, we believe that *in vivo* experiments may help to clarify this ambiguous phenomenon. To do this, mice were infected with WT, Δ*greA*, or complemented strains of *M. tuberculosis* H37Ra. After 14-days of infection, we observed a decrease of bacterial burden in mice infected with the H37Ra *greA* mutant strain (**Figure 7D**).

Overall, these results emphasize that GreA facilitates the intracellular survival of mycobacteria, and thus revealed its critical role in both an *in vitro* and an *in vivo* infection model.

DISCUSSION

GreA Is Essential for Sustaining Mycobacterial Growth and Environmental Adaptation

Few studies are available about the functional characteristics of GreA in *Mycobacterium* spp. A previous study showed

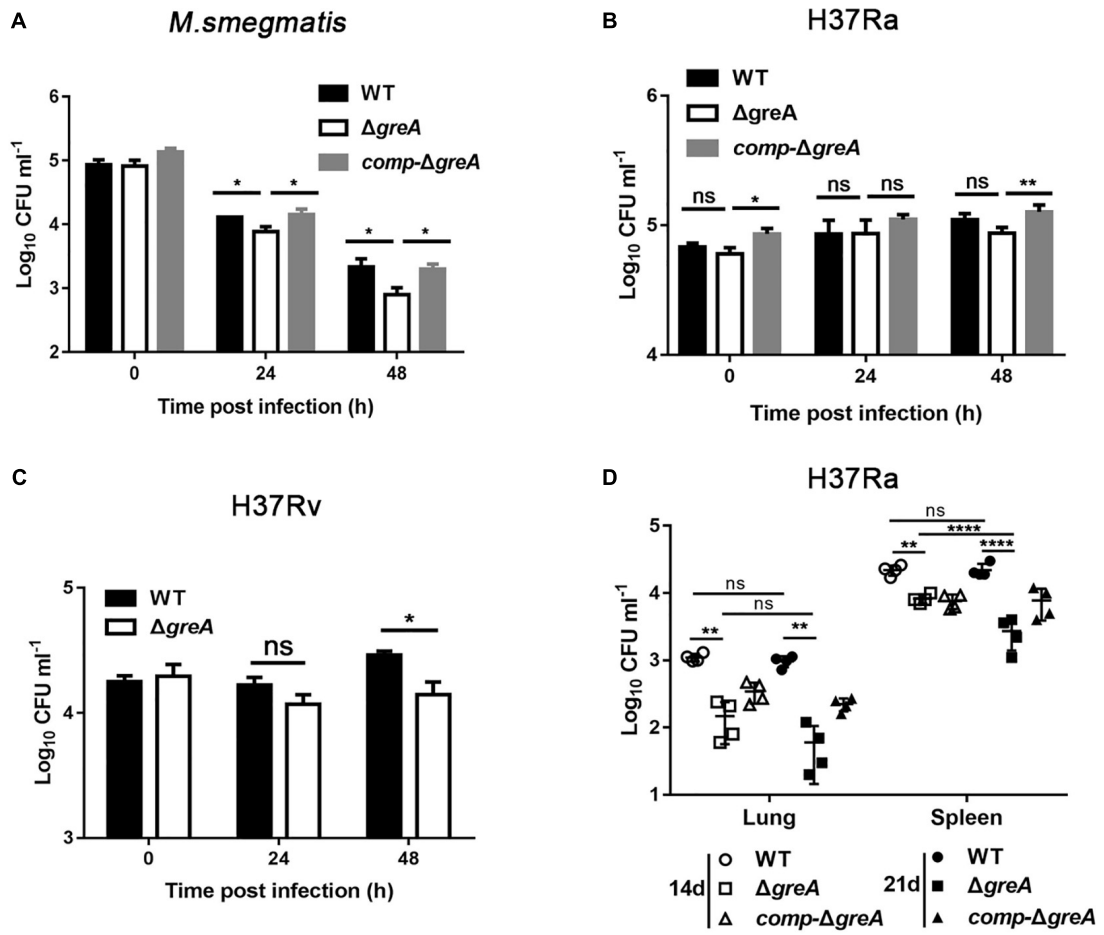

FIGURE 7 | Intracellular fitness of Δ*greA* mutant strain was evaluated *in vivo* and *in vitro*. RAW264.7 cells were seeded at 3×10^5 cells per well in 24-well culture plates. After adhesion, cells were infected with bacteria at MOI of 10. The extracellular bacteria were removed 2 h post infection by washing with PBS. The cells of *M. smegmatis* **(A)**, *M. tuberculosis* H37Ra **(B)**, and *M. tuberculosis* H37Rv **(C)** were further incubated for 24 and 48 h at 37°C. Then serially diluted (10-fold) cells lysates were spotted on a 7H10-OADC agar and cultured in 37°C. CFUs were counted after incubation for the indicated time for *M. smegmatis* and *M. tuberculosis*, respectively. **(D)** Mice were infected i.p. (1×10^7) with WT, Δ*greA*, or *comp*-Δ*greA* strains of *M. tuberculosis* H37Ra. The number of surviving bacilli by CFU counting at the indicated time. Data are shown as mean ± SEM of two independent experiments. $^*p < 0.05$, $^{**}p < 0.01$, $^{****}p < 0.0001$, ns, $p \geq 0.05$.

that knocking down of *greA* resulted in growth retardation in *M. tuberculosis* H37Ra (China et al., 2011). For example, the absence of *greA* in *S. pneumoniae* severely perturbed its growth (Yuzenkova et al., 2014). Regarding the universal role of Gre factors in prokaryotes, it is not surprising that deletion of *greA* in *M. tuberculosis* resulted in growth retardation.

It has been convincingly shown in several studies that GreA is required for the survival of bacteria under stress. For instance, Wei and colleagues found that the deletion of *greA* in *Sinorhizobium meliloti* results in sensitivity to salt stress (Wei et al., 2004). Another study revealed that overexpression of GreA provides the host cells with enhanced resistance to heat shock and oxidative stress in *E. coli* (Li et al., 2012). A very recent study has shown that similar with *E. coli* GreA, *M. smegmatis* GreA exhibits chaperone-like activity *in vitro*, which prevents heat-induced aggregation of substrate protein (Joseph et al., 2019). Intriguingly, it has been established that double-deletion of *greA* and *greB*, encoding a transcript cleavage factors function-similar to that of GreA, causes heat sensitivity, indicating that another Gre factor may partially complement the phenotype of *greA* mutant. Our data shows that GreA is dispensable for the survival of *M. tuberculosis* under heat shock stress. It seems to be that the phenotype, in part, may be complemented by another copy of *greA*, since there are two genes (*MSMEG_5263* and *MSMEG_6292*) encoding transcription elongation factor GreA in *M. smegmatis* (Mohan et al., 2015). Further experiments are required to address the role of MSMEG_6292 in *M. smegmatis*.

Moreover, the deletion of *greA* in *M. smegmatis* increased the susceptibility to bedaquiline, capreomycin, streptomycin, amikacin, and vancomycin (**Table 1**). Notably, our data has established that the growth defect of Δ*greA* strain was more obvious despite the low antibiotic concentrations used. This finding is crucial, as it provides the evidence to support that a GreA inhibitor might be able to enhance the efficacy of the current anti-TB drugs.

Transcription Regulation by the *M. smegmatis* Transcription Elongation Factor GreA

Here, we showed that 167 genes were down-regulated in the *M. smegmatis* lacking the *greA*, while only 28 genes were positively regulated. Most of the down-regulated genes were associated with metabolism, supporting the view that GreA optimizes mycobacterial growth and environmental adaptation by the regulation of metabolism. For example, *glgX*, a gene involved in starch and sucrose metabolism, was significantly down-regulated in *greA* mutant strain and the inactivation of *glgX* in *C. glutamicum* led to slower growth (Seibold and Eikmanns, 2007). It is suggested that GreA mediated regulation of the growth might be partly associated with *glgX*. In addition, *katG*, a gene encoded catalase-peroxidase-peroxynitritase, plays a role in the intracellular survival of the mycobacteria within macrophages and in protection against reactive oxygen and nitrogen intermediates produced by phagocytic cells (Milano et al., 2001; Pym et al., 2002; Sassetti et al., 2003). Given the down-regulation of *katG* in the *greA* mutant strain, this could explain the role of GreA in mediating the regulation of oxidation resistance.

GreA has an impact on the regulation of gene expression in *E. coli* (Roberts et al., 2008) and *S. pneumoniae* (Yuzenkova et al., 2014) by affecting the transcription elongation. In addition to the effect of GreA on transcription elongation, competition between GreA and DksA has been reported. DksA, an RNAP-binding transcription factor, binds to the secondary channel of RNAP and plays a vital role in controlling polyP activation, which is required for stress survival and virulence in diverse pathogenic microbes (Gray, 2019).

Moreover, GreA and DksA, have an opposite regulation of a subset of genes in *E. coli* (Vinella et al., 2012). These data suggest that GreA might have a global role in the regulation of genes expressed in a prokaryotic organism. From our CHIP-seq dataset, it was revealed that GreA is symmetrically distributed on the *M. smegmatis* chromosome. However, we were unable to identify discrete binding sites for GreA. Of note, there is no evidence that the Gre factors can bind with nucleic acids. Indeed, the Gre factors are proteins interacting with the RNAPs, this might suggest that GreA indirectly regulates the gene expression by interaction with the RNAP complex.

GreA consists of two domains; a C-terminal globular domain and an extended N-terminal coiled-coil domain. The NTD is responsible for the GreA induction of nucleolytic activity, while the CTD determines the binding of GreA to RNAP. Both domains are required for full functional activity of GreA (Koulich et al., 1998). We also confirmed that the full activity of the GreA is crucial in *M. smegmatis* growth. Of note, it has been reported that, another Gre homolog, Rv3788 binds near the secondary channel of RNAP to inhibit transcription. However, the factor did not show any transcript cleavage stimulatory activity (China et al., 2012). Furthermore, our data demonstrated that *glgX*, a gene involved in starch and sucrose metabolism, regulated by the anti-backtracking activity of GreA is required for the optimal growth of *M. smegmatis*. Recently, studies in *Salmonella enterica* serovar Typhimurium demonstrated that GreA-mediated rescue of backtracked paused complexes during transcription is crucial in promoting *hilD* expression through its 3′-UTR (Gaviria-Cantin et al., 2017). In addition, GreA enhanced expression of several *E. coli* RNAP promoters *in vitro* (Erie et al., 1993; Feng et al., 1994; Hsu et al., 1995; Maddalena et al., 2016). Given that GreA has a multitude of effects on transcription, initiation, and elongation (Stepanova et al., 2007; Vinella et al., 2012), this could explain our failure to identify the binding motif of GreA. Based on the present study, we suppose that the anti-backtracking activity GreA is involved in the regulation of gene expression in mycobacteria. It would be interesting in future studies to examine the regulation of GreA on gene expression *in vitro*.

It is known that GreA influences not only cellular invasion but also replication in *Francisella tularensis* subsp. *Novicida* (Cui et al., 2018) and *Salmonella typhimurium* (Gaviria-Cantin et al., 2017). Our data also revealed that *greA* deletion caused a slight reduction of intracellular fitness in *M. tuberculosis* H37Rv, suggesting that GreA is required for the maintenance of intracellular survival of *M. tuberculosis*. The use of a non-pathogenic species, *M. smegmatis*, may have been a limitation of the present study. Although there is some evidence that *M. smegmatis* has been used as a model to study the function of interesting gene of *M. tuberculosis* (Wang et al., 2015, 2017; Yaseen et al., 2015, 2018), *M. smegmatis* isn't closely related to *M. tuberculosis* in genetically. Very recently, based on the comprehensive phylogenomic analyses and comparative genomic studies, *M. smegmatis* categorized as a novel classification of Mycobacterium is distinguished as a different genus comparing to *M. tuberculosis*. (Gupta et al., 2019). It suggests that certain functions of GreA in pathogenic *M. tuberculosis* may be different from in *M. smegmatis*, especially with the virulence, since most experiments have been performed in *M. smegmatis*, instead of *M. tuberculosis* H37Rv. In a further study, we will provide evidence to elucidate the regulation role of GreA in pathogenic *M. tuberculosis*.

In conclusion, our study revealed that GreA plays an important role in mycobacterial biology where, the deletion of *greA* resulted in bacterial growth retardation, reduction of intracellular fitness, and more importantly from a clinical treatment point of view, improvement of antibiotic susceptibility. Overall, our results strongly suggest that GreA warrants being studied as a potential target for the development of MDR-TB inhibitor therapy.

DATA AVAILABILITY STATEMENT

The datasets for this study can be found in GEO, under accession number GSE143764: https://www.ncbi.nlm.nih.gov/geo/query/acc.cgi?acc=GSE143764.

ETHICS STATEMENT

All animal experiments were performed in accordance with the National Institutes of Health Guide for the Care and Use

of Laboratory Animals, and the experimental procedures were approved by the Ethics Committee of Zhongshan School of Medicine on Laboratory Animal Care (reference number: 2016-159), Sun Yat-sen University.

AUTHOR CONTRIBUTIONS

GT conceived the study and supervised global data analysis. HC and AR Provided advice in design and co-edited manuscript. SF and YL Designed and performed the experiments, analyzed the data, and co-wrote the manuscript. WL and ME-S performed the construction of deletion of Gre in mycobacteria. ZhZ and CS performed the intracellular fitness experiment. ZiZ and ZG designed and performed the RNAseq experiment. LuL and LiL performed the ChIPseq experiment. YY and XW contributed to data interpretation and wrote the manuscript. All authors read and approved the final manuscript.

FUNDING

This work has been supported by grants from National Natural Science Foundation of China (Grant Numbers 81830103 and 81722030), the Guangdong Natural Science Foundation (Grant Number 2017A030306012), National Science and Technology Key Projects for Major Infectious Diseases (2017ZX10302301), and the Science and Technology Planning Project of Guangdong (Grant Number 2016A020219002).

ACKNOWLEDGMENTS

We are grateful to Yaxin Chen of Sun Yat-sen University for data analysis.

SUPPLEMENTARY MATERIAL

The Supplementary Material for this article can be found online at: https://www.frontiersin.org/articles/10.3389/fmicb.2020.00413/full#supplementary-material

FIGURE S1 | Generation of *greA* gene replacement mutant. Schematic representation of the strategy used for the generation of *greA* gene replacement mutant and confirmation of *greA* disruption in *M. smegmatis* **(A)**, *M. tuberculosis* H37Rv **(B)**, and *M. tuberculosis* H37Ra **(C)**, respectively.

FIGURE S2 | Deletion of *greA* altered susceptibility of antibiotics in *M. smegmatis*. WT, Δ*greA* and *comp*-Δ*greA* strains were exposed to 7H9 medium in the absent (control) or present of different antibiotics at 1/100th the MIC. The initial OD_{600} was 0.02. The growth curves were monitored for 42 h. **(A)** Streptomycin (MIC = 0.005 mg/L) and **(B)** Rifampicin (MIC = 0.16 mg/L).

FIGURE S3 | Analysis of binding sites identified from the ChIP-seq experiments. **(A)** Histogram showing the frequency distribution of distances between GreA ChIP-seq peak centers and TSSs. **(B)** Chromosomal binding map of HupB-FLAG.

TABLE S1 | All primers and strains used in this study.

TABLE S2 | Transcriptome of the *M. smegmatis* wild type and the Δ*greA* mutant.

TABLE S3 | ChIP-seq of GreA: ChIP-seq binding sites.

TABLE S4 | Results of gene ontology analyses (DAVID; FDR < 0.05).

REFERENCES

Alland, D., Kramnik, I., Weisbrod, T. R., Otsubo, L., Cerny, R., Miller, L. P., et al. (1998). Identification of differentially expressed mRNA in prokaryotic organisms by customized amplification libraries (DECAL): the effect of isoniazid on gene expression in *Mycobacterium tuberculosis*. *Proc. Natl. Acad. Sci. U S A.* 95, 13227–13232. doi: 10.1073/pnas.95.22.13227

China, A., Mishra, S., and Nagaraja, V. (2011). A transcript cleavage factor of *Mycobacterium tuberculosis* important for its survival. *PLoS One* 6:e21941. doi: 10.1371/journal.pone.0021941

China, A., Mishra, S., Tare, P., and Nagaraja, V. (2012). Inhibition of *Mycobacterium tuberculosis* RNA polymerase by binding of a Gre factor homolog to the secondary channel. *J. Bacteriol.* 194, 1009–1017. doi: 10.1128/JB.06128-11

Cui, G. L., Wang, J., Qi, X. Y., and Su, J. L. (2018). Transcription elongation factor GreA plays a key role in cellular invasion and virulence of *Francisella tularensis* subsp *novicida*. *Sci. Rep.* 8:6895. doi: 10.1038/s41598-018-25271-5

Erie, D. A., Hajiseyedjavadi, O., Young, M. C., and von Hippel, P. H. (1993). Multiple RNA polymerase conformations and GreA: control of the fidelity of transcription. *Science* 262, 867–873. doi: 10.1126/science.8235608

Feng, G. H., Lee, D. N., Wang, D., Chan, C. L., and Landick, R. (1994). GreA-induced transcript cleavage in transcription complexes containing *Escherichia coli* RNA polymerase is controlled by multiple factors, including nascent transcript location and structure. *J. Biol. Chem.* 269, 22282–22294.

Gaviria-Cantin, T., El Mouali, Y., Le Guyon, S., Romling, U., and Balsalobre, C. (2017). Gre factors-mediated control of hilD transcription is essential for the invasion of epithelial cells by *Salmonella enterica* serovar Typhimurium. *PLoS Pathog.* 13:e1006312. doi: 10.1371/journal.ppat.1006312

Goodsmith, N., Guo, X. V., Vandal, O. H., Vaubourgeix, J., Wang, R., Botella, H., et al. (2015). Disruption of an *M. tuberculosis membrane protein causes a magnesium-dependent cell division defect and failure to persist in mice*. *PLoS Pathog.* 11:e1004645. doi: 10.1371/journal.ppat.1004645

Gray, M. J. (2019). Inorganic polyphosphate accumulation in *Escherichia coli* is regulated by DksA but not by (p)ppGpp. *J. Bacteriol.* 201, e664-18. doi: 10.1128/JB.00664-18

Gumber, S., Taylor, D. L., Marsh, I. B., and Whittington, R. J. (2009). Growth pattern and partial proteome of *Mycobacterium avium* subsp. *paratuberculosis during the stress response to hypoxia and nutrient starvation*. *Vet. Microbiol.* 133, 344–357. doi: 10.1016/j.vetmic.2008.07.021

Gupta, R. S., Lo, B., and Son, J. (2019). Phylogenomics and comparative genomic studies robustly support division of the genus *Mycobacterium* into an emended genus *Mycobacterium* and four novel genera. *Front. Microbiol.* 13:67. doi: 10.3389/fmicb.2018.00067

Harding, E. (2019). WHO global progress report on tuberculosis elimination. *Lancet Respir. Med.* 8:19. doi: 10.1016/s2213-2600(19)30418-7

Hsu, L. M., Vo, N. V., and Chamberlin, M. J. (1995). *Escherichia coli* transcript cleavage factors GreA and GreB stimulate promoter escape and gene expression in vivo and in vitro. *Proc. Natl. Acad. Sci. U S A.* 92, 11588–11592. doi: 10.1073/pnas.92.25.11588

Jain, P., Hsu, T., Arai, M., Biermann, K., Thaler, D. S., Nguyen, A., et al. (2014). Specialized transduction designed for precise high-throughput unmarked deletions in *Mycobacterium tuberculosis*. *MBio* 5, e1245–14. doi: 10.1128/mBio.01245-14

Joseph, A., Nagaraja, V., and Natesh, R. (2019). Mycobacterial transcript cleavage factor Gre, exhibits chaperone-like activity. *Biochim. Biophys. Acta. Proteins. Proteom.* 1867, 757–764. doi: 10.1016/j.bbapap.2019.05.008

Komissarova, N., and Kashlev, M. (1997). Transcriptional arrest: *Escherichia coli* RNA polymerase translocates backward, leaving the 3′ end of the RNA intact

and extruded. *Proc. Natl. Acad. Sci. U S A.* 94, 1755–1760. doi: 10.1073/pnas.94.5.1755

Koulich, D., Nikiforov, V., and Borukhov, S. (1998). Distinct functions of N and C-terminal domains of GreA, an *Escherichia coli* transcript cleavage factor. *J. Mol. Biol.* 276, 379–389. doi: 10.1006/jmbi.1997.1545

Koulich, D., Orlova, M., Malhotra, A., Sali, A., Darst, S. A., and Borukhov, S. (1997). Domain organization of *Escherichia coli* transcript cleavage factors GreA and GreB. *J. Biol. Chem.* 272, 7201–7210. doi: 10.1074/jbc.272.11.7201

Kumar, A., Saini, V., Kumar, A., Kaur, J., and Kaur, J. (2017). Modulation of trehalose dimycolate and immune system by Rv0774c protein enhanced the intracellular survival of *Mycobacterium smegmatis* in human macrophages cell line. *Front. Cell Infect. Microbiol.* 7:289. doi: 10.3389/fcimb.2017.00289

Larson, C. L., and Wicht, W. C. (1964). Infection of mice with *Mycobacterium tuberculosis*, strain H37Ra. *Am. Rev. Respir. Dis.* 90, 742–748.

Lata, M., Sharma, D., Kumar, B., Deo, N., Tiwari, P. K., Bisht, D., et al. (2015). Proteome analysis of ofloxacin and moxifloxacin induced *mycobacterium tuberculosis* isolates by proteomic approach. *Protein. Pept. Lett.* 22, 362–371. doi: 10.2174/0929866522666150209113708

Li, J., Overall, C. C., Johnson, R. C., Jones, M. B., McDermott, J. E., Heffron, F., et al. (2015). ChIP-Seq analysis of the sigmaE regulon of *Salmonella enterica* Serovar Typhimurium reveals new genes implicated in heat shock and oxidative stress response. *PLoS One* 10:e0138466. doi: 10.1371/journal.pone.0138466

Li, K., Jiang, T., Yu, B., Wang, L., Gao, C., Ma, C., et al. (2012). Transcription elongation factor GreA has functional chaperone activity. *PLoS One* 7:e47521. doi: 10.1371/journal.pone.0047521

Maddalena, L. L., Niederholtmeyer, H., Turtola, M., Swank, Z. N., Belogurov, G. A., and Maerkl, S. J. (2016). GreA and GreB enhance expression of *Escherichia coli* RNA Polymerase promoters in a reconstituted transcription-translation system. *ACS Synth. Biol.* 5, 929–935. doi: 10.1021/acssynbio.6b00017

Manganelli, R., Dubnau, E., Tyagi, S., Kramer, F. R., and Smith, I. (1999). Differential expression of 10 sigma factor genes in *Mycobacterium tuberculosis*. *Mol. Microbiol.* 31, 715–724. doi: 10.1046/j.1365-2958.1999.01212.x

Milano, A., Forti, F., Sala, C., Riccardi, G., and Ghisotti, D. (2001). Transcriptional regulation of furA and katG upon oxidative stress in *Mycobacterium smegmatis*. *J. Bacteriol.* 183, 6801–6806. doi: 10.1128/jb.183.23.6801-6806.2001

Mohan, A., Padiadpu, J., Baloni, P., and Chandra, N. (2015). Complete genome sequences of a *Mycobacterium smegmatis* laboratory strain (MC2 155) and isoniazid-resistant (4XR1/R2) mutant strains. *Genome Announc.* 3, e01520–14. doi: 10.1128/genomeA.01520-14

Nogales, J., Campos, R., BenAbdelkhalek, H., Olivares, J., Lluch, C., and Sanjuan, J. (2002). Rhizobium tropici genes involved in free-living salt tolerance are required for the establishment of efficient nitrogen-fixing symbiosis with Phaseolus vulgaris. *Mol. Plant Microbe. Interact.* 15, 225–232. doi: 10.1094/mpmi.2002.15.3.225

Pym, A. S., Saint-Joanis, B., and Cole, S. T. (2002). Effect of katG mutations on the virulence of *Mycobacterium tuberculosis* and the implication for transmission in humans. *Infect. Immun.* 70, 4955–4960. doi: 10.1128/iai.70.9.4955-4960.2002

Roberts, J. W., Shankar, S., and Filter, J. J. (2008). RNA polymerase elongation factors. *Annu. Rev. Microbiol.* 62, 211–233. doi: 10.1146/annurev.micro.61.080706.093422

Rustad, T. R., Roberts, D. M., Liao, R. P., and Sherman, D. R. (2009). Isolation of mycobacterial RNA. *Methods Mol. Biol.* 465, 13–21. doi: 10.1007/978-1-59745-207-6_2

Sassetti, C. M., Boyd, D. H., and Rubin, E. J. (2003). Genes required for mycobacterial growth defined by high density mutagenesis. *Mol. Microbiol.* 48, 77–84. doi: 10.1046/j.1365-2958.2003.03425.x

Schneider, D., Bruton, C. J., and Chater, K. F. (2000). Duplicated gene clusters suggest an interplay of glycogen and trehalose metabolism during sequential stages of aerial mycelium development in Streptomyces coelicolor A3(2). *Mol. Gen. Genet.* 263, 543–553. doi: 10.1007/s004380051200

Seibold, G. M., and Eikmanns, B. J. (2007). The *glgX* gene product of *Corynebacterium glutamicum* is required for glycogen degradation and for fast adaptation to hyperosmotic stress. *Microbiology* 153, 2212–2220. doi: 10.1099/mic.0.2006/005181-0

Sharma, P., Kumar, B., Singhal, N., Katoch, V. M., Venkatesan, K., Chauhan, D. S., et al. (2010). Streptomycin induced protein expression analysis in *Mycobacterium tuberculosis* by two-dimensional gel electrophoresis & mass spectrometry. *Indian J. Med. Res.* 132, 400–408.

Sharma, U. K., and Chatterji, D. (2010). Transcriptional switching in *Escherichia coli* during stress and starvation by modulation of sigma activity. *FEMS Microbiol. Rev.* 34, 646–657. doi: 10.1111/j.1574-6976.2010.00223.x

Singh, A. K., Carette, X., Potluri, L. P., Sharp, J. D., Xu, R., Prisic, S., et al. (2016). Investigating essential gene function in *Mycobacterium tuberculosis* using an efficient CRISPR interference system. *Nucl. Acid. Res.* 44:e143. doi: 10.1093/nar/gkw625

Singh, P. P., Parra, M., Cadieux, N., and Brennan, M. J. (2008). A comparative study of host response to three *Mycobacterium tuberculosis* PE_PGRS proteins. *Microbiology* 154(Pt 11), 3469–3479. doi: 10.1099/mic.0.2008/019968-0

Sivaramakrishnan, P., Sepulveda, L. A., Halliday, J. A., Liu, J., Nunez, M. A. B., Golding, I., et al. (2017). The transcription fidelity factor GreA impedes DNA break repair. *Nature* 550, 214–218. doi: 10.1038/nature23907

Stebbins, C. E., Borukhov, S., Orlova, M., Polyakov, A., Goldfarb, A., and Darst, S. A. (1995). Crystal structure of the GreA transcript cleavage factor from *Escherichia coli*. *Nature* 373, 636–640. doi: 10.1038/373636a0

Stepanova, E., Lee, J., Ozerova, M., Semenova, E., Datsenko, K., Wanner, B. L., et al. (2007). Analysis of promoter targets for *Escherichia coli* transcription elongation factor GreA in vivo and in vitro. *J. Bacteriol.* 189, 8772–8785. doi: 10.1128/jb.00911-07

Tehranchi, A. K., Blankschien, M. D., Zhang, Y., Halliday, J. A., Srivatsan, A., Peng, J., et al. (2010). The transcription factor DksA prevents conflicts between DNA replication and transcription machinery. *Cell* 141, 595–605. doi: 10.1016/j.cell.2010.03.036

Traverse, C. C., and Ochman, H. (2018). A genome-wide assay specifies only GreA as a transcription fidelity factor in *Escherichia coli*. *G3 (Bethesda)* 8, 2257–2264. doi: 10.1534/g3.118.200209

van Kessel, J. C., and Hatfull, G. F. (2007). Recombineering in *Mycobacterium tuberculosis*. *Nat. Methods* 4, 147–152. doi: 10.1038/nmeth996

Vinella, D., Potrykus, K., Murphy, H., and Cashel, M. (2012). Effects on growth by changes of the balance between GreA, GreB, and DksA suggest mutual competition and functional redundancy in *Escherichia coli*. *J. Bacteriol.* 194, 261–273. doi: 10.1128/JB.06238-11

Volker, U., Engelmann, S., Maul, B., Riethdorf, S., Volker, A., Schmid, R., et al. (1994). Analysis of the induction of general stress proteins of *Bacillus subtilis*. *Microbiology* 140(Pt 4), 741–752. doi: 10.1099/00221287-140-4-741

Wang, J., Ge, P. P., Qiang, L. H., Tian, F., Zhao, D. D., Chai, Q. Y., et al. (2017). The mycobacterial phosphatase PtpA regulates the expression of host genes and promotes cell proliferation. *Nat. Commun.* 8:244. doi: 10.1038/s41467-017-00279-z

Wang, J., Li, B. X., Ge, P. P., Li, J., Wang, Q., Gao, G. F., et al. (2015). *Mycobacterium tuberculosis* suppresses innate immunity by coopting the host ubiquitin system. *Nat. Immunol.* 16, 237–45. doi: 10.1038/ni.3096

Wei, W., Jiang, J., Li, X., Wang, L., and Yang, S. S. (2004). Isolation of salt-sensitive mutants from *Sinorhizobium meliloti* and characterization of genes involved in salt tolerance. *Lett. Appl. Microbiol.* 39, 278–283. doi: 10.1111/j.1472-765x.2004.01577.x

Wright, A., Zignol, M., Van Deun, A., Falzon, D., Gerdes, S. R., Feldman, K., et al. (2009). Epidemiology of antituberculosis drug resistance 2002-07: an updated analysis of the Global Project on Anti-Tuberculosis Drug Resistance Surveillance. *Lancet* 373, 1861–1873. doi: 10.1016/S0140-6736(09)60331-7

Yang, C., Luo, T., Shen, X., Wu, J., Gan, M., Xu, P., et al. (2017). Transmission of multidrug-resistant *Mycobacterium tuberculosis* in Shanghai, China: a retrospective observational study using whole-genome sequencing and epidemiological investigation. *Lancet Infect. Dis.* 17, 275–284. doi: 10.1016/S1473-3099(16)30418-2

Yaseen, I., Choudhury, M., Sritharan, M., and Khosla, S. (2018). Histone methyltransferase SUV39H1 participates in host defense by methylating mycobacterial histone-like protein HupB. *EMBO J.* 37, 183–200. doi: 10.15252/embj.201796918

Yaseen, I., Kaur, P., Nandicoori, V. K., and Khosla, S. (2015). Mycobacteria modulate host epigenetic machinery by Rv1988 methylation of a non-tail arginine of histone H3. *Nat. Commun.* 6:8922. doi: 10.1038/ncomms9922

Yuzenkova, Y., Gamba, P., Herber, M., Attaiech, L., Shafeeq, S., Kuipers, O. P., et al. (2014). Control of transcription elongation by GreA determines rate of gene expression in *Streptococcus pneumoniae*. *Nucleic Acids Res.* 42, 10987–10999. doi: 10.1093/nar/gku790

Conflict of Interest: The authors declare that the research was conducted in the absence of any commercial or financial relationships that could be construed as a potential conflict of interest.

frontiers in Microbiology

ORIGINAL RESEARCH
published: 28 April 2020
doi: 10.3389/fmicb.2020.00800

Antimycobacterial Effect of Selenium Nanoparticles on *Mycobacterium tuberculosis*

Hector Estevez[1†], Ainhoa Palacios[2†], David Gil[3], Juan Anguita[2,4], Maria Vallet-Regi[5,6], Blanca González[5,6], Rafael Prados-Rosales[7] and Jose L. Luque-Garcia[1]**

[1] Department of Analytical Chemistry, Faculty of Chemistry, Complutense University of Madrid, Madrid, Spain, [2] Inflammation and Macrophage Plasticity Lab, CIC bioGUNE, Derio, Spain, [3] Electron Microscopy Platform, CIC bioGUNE, Derio, Spain, [4] Ikerbasque, Basque Foundation for Science, Bilbao, Spain, [5] Department of Chemistry in Pharmaceutical Sciences, Faculty of Pharmacy, Instituto de Investigación Sanitaria Hospital 12 de Octubre (imas12), Complutense University of Madrid, Madrid, Spain, [6] Centro de Investigación Biomédica en Red de Bioingeniería, Biomateriales y Nanomedicina (CIBER-BBN), Madrid, Spain, [7] Department of Preventive Medicine and Public Health and Microbiology, Faculty of Medicine, Autonomous University of Madrid, Madrid, Spain

OPEN ACCESS

Edited by:
Giorgia Mori, The University of Queensland, Australia

Reviewed by:
Luisana Di Cristo, Italian Institute of Technology (IIT), Italy
Andrea Zille, University of Minho, Portugal

***Correspondence:**
Rafael Prados-Rosales
rafael.prados@uam.es
Jose L. Luque-Garcia
jlluque@ucm.es

† These authors have contributed equally to this work

Specialty section:
This article was submitted to Antimicrobials, Resistance and Chemotherapy, a section of the journal Frontiers in Microbiology

Received: *24 February 2020*
Accepted: *03 April 2020*
Published: *28 April 2020*

Citation:
Estevez H, Palacios A, Gil D, Anguita J, Vallet-Regi M, González B, Prados-Rosales R and Luque-Garcia JL (2020) Antimycobacterial Effect of Selenium Nanoparticles on Mycobacterium tuberculosis. Front. Microbiol. 11:800. doi: 10.3389/fmicb.2020.00800

Tuberculosis (TB) remains the leading cause of death from a single infection agent worldwide. In recent years, the occurrence of TB cases caused by drug-resistant strains has spread, and is expected to continue to grow. Therefore, the development of new alternative treatments to the use of antibiotics is highly important. In that sense, nanotechnology can play a very relevant role, due to the unique characteristics of nanoparticles. In fact, different types of nanoparticles have already been evaluated both as potential bactericides and as efficient drug delivery vehicles. In this work, the use of selenium nanoparticles (SeNPs) has been evaluated to inhibit the growth of two types of mycobacteria: *Mycobacterium smegmatis* (*Msm*) and *Mycobacterium tuberculosis* (*Mtb*). The results showed that SeNPs are able to inhibit the growth of both types of mycobacteria by damaging their cell envelope integrity. These results open a new opportunity for the use of this type of nanoparticles as antimycobacterial agents by themselves, or for the development of novel nanosystems that combine the action of these nanoparticles with other drugs.

Keywords: selenium nanoparticles, mycobacterium tuberculosis, antimycobacterial effect, *smegmatis*, cell wall damaging agents

INTRODUCTION

Tuberculosis (TB) is a chronic infectious disease transmitted aerially through droplets expelled by an infected person. The disease is caused by the slow-growing tubercle bacillus *Mycobacterium tuberculosis* (*Mtb*). TB is the leading cause of death due to infection worldwide, with approximately 1.4 million deceased in 2018 (World Health Organization [WHO], 2019) and estimates at 75 million people dying from TB over the next 35 years. In 2018 alone, new TB cases were estimated to be 10.4 million worldwide (World Health Organization [WHO], 2019). Currently, TB treatment requires a 6-month regimen of four first-line drugs, which are ineffective at treating infection with multidrug-resistant (MDR) *Mtb* strains. These strains are rapidly spreading worldwide (more than 480,000 cases reported last year according to the TB alliance) and could cost $16 trillion over the next 35 years. Since microbial resistance to antibiotics increases, there is a call for non-antibiotic

therapies that can fill the gaps for bactericidal purposes where antibiotics fail (Chandra Mohana et al., 2018). In the recent years, the combination of nanotechnology and biomedicine has proven to be promising for multiple purposes, including in bactericide applications (Jayawardana et al., 2015; Reshma et al., 2017; Vallet-Regí et al., 2019).

Nanoparticles are highly promising as antimicrobials, complementary to antibiotics, as they act by influencing the bacterial cell wall by direct contact without the need to be endocytosed (Herman and Herman, 2014; Wang et al., 2017). Their small size implies a greater surface-area-to-volume ratio than bulk material. Also, they may have optical or even magnetic properties (Baranwal et al., 2018). There is a great variety of nanoparticles in use as antimicrobials, such as metal, metal oxide or organic nanoparticles, involving multiple modes of action (Hoseinzadeh et al., 2017; Reshma et al., 2017; Khan et al., 2020). However, nanoparticles affect bacteria in two main lethal pathways, which can occur simultaneously: disruption of membrane potential and integrity, or production of reactive oxygen species (ROS) (Beyth et al., 2015).

Selenium nanoparticles (SeNPs) have already been suggested for multiple biomedical applications due to their antioxidant properties and differential behavior in comparison to other selenospecies (Estevez et al., 2014). Also, SeNPs have been shown to have antimicrobial activity against different types of bacteria (Huang et al., 2019). However, SeNPs have never been proven before to have an antimicrobial effect on *Mtb*.

Therefore, in this work, the mycobactericidal capacity of SeNPs has been evaluated on two types of mycobacteria, the fast-growing *Mycobacterium smegmatis* (*Msm*) and the slow-growing *Mtb*, finding an effective inhibition in the mycobacterial growth in a dose-dependent manner. A structural analysis of the mycobacteria subjected to the presence of the SeNPs has been performed by means of electron microscopy to analyze their effect on the cell envelope, showing that SeNPs interact directly with the mycobacteria membrane of *Mtb* and *Msm*, compromising their integrity and inducing extrusion of cytoplasmic material.

MATERIALS AND METHODS

Chemicals

Reagents for the synthesis of SeNPs: chitosan, bovine serum albumin, sodium selenite, ascorbic, and acetic acid were purchased from Sigma-Aldrich. Reagents for electron microscopy: glutaraldehyde, cacodylate and formaldehyde were purchased from Sigma. Uranyl formate was purchased from Electron Microscopy Sciences (Hatfield, PA, United States).

Synthesis of SeNPs

Chitosan-stabilized SeNPs (Ch-SeNPs) were synthesized following the procedure described by Bai et al. (2008). Briefly, 10 mL of an aqueous chitosan polysaccharide solution (0.5% w/v) were mixed with 7.5 mL of ascorbic acid 0.23 M and 5 mL of acetic acid 2.4 M. Then, 0.25 mL of sodium selenite 0.51 M were slowly added to the previous solution. SeNPs formation was recognized by observing the change of the solution from colorless to red as the reaction progressed. After the synthesis, the colloidal suspension was diluted to 50 mL with distilled water, resulting in final concentrations of 200 mg L^{-1} of Se and 0.1% of chitosan. Finally, the colloidal suspension was dialyzed for 2 h at room temperature in a ratio of 10 mL against 2 L of distilled water and using a 12 kDa of MWCO membrane.

For control experiments, BSA-SeNPs were also prepared following the same procedure but using an aqueous bovine serum albumin solution (0.5% w/v) instead of the chitosan solution.

Analytical Characterization of the Synthesized SeNPs

Transmission electron microscopy (TEM) was performed using a JEOL JEM 1400 instrument operated at 120 kV equipped with a CCD camera (KeenView Camera) and an energy dispersive X-ray spectroscopy (EDS) analyzer. Sample preparation was performed by placing one or two drops of the SeNPs colloidal suspension onto carbon-coated copper grids.

Electrophoretic mobility measurements of the materials suspended in water were used to calculate the zeta potential (ζ) values of the nanoparticles. Measurements were performed in a Zetasizer Nano ZS (Malvern Instruments Ltd., United Kingdom) equipped with a 633 nm "red" laser. The hydrodynamic size of nanoparticles was measured by dynamic light scattering (DLS) with the same Malvern instrument.

Bacterial Strains and Culture Conditions

Mycobacterium smegmatis mc^2155 (*Msm*) and *Mycobacterium tuberculosis* H37Rv (*Mtb*) strains (obtained from the ATCC) were grown in Middlebrook 7H9 medium supplemented with 10% (v/v) OADC supplement (NaCl 8.5 g/L, BSA fraction V 50 g/L, dextrose 20 g/L, 5% (v/v) oleic acid solution 1%, 40 mg/L catalase), 0.5% (v/v) glycerol and 0.05% Tyloxapol (v/v; Sigma). Cultures were grown at 37°C in static standing 25 cm^2 flasks with vented caps. *Msm*-Lux was generated by transforming *Msm* with the plasmid construct pMV306hsp + Lux (which contains the entire bacterial Lux operon cloned in a mycobacterial integrative expression vector) (Andreu et al., 2010).

Minimum Inhibitory Concentration (MIC) Assay

Minimum inhibitory concentration (MIC) assay was carried out in 96-well plates diluting exponentially growing *Msm* or *Mtb* at an initial density of 1×10^5 bacteria/mL in the presence of two-fold serial dilutions of Ch-SeNPs or BSA-SeNPs starting at 50 μg/mL and including one control sample with no NPs. Plates were incubated at 37°C for 7 days (*Msm*) or for 20 days (*Mtb*). Bacterial growth was monitored every day for *Msm* and every week for *Mtb* and was determined by measuring optical density at 570 nm. The assay was performed in triplicate. MIC values were selected as the minimum concentration able to suppress mycobacterial growth. Alternatively, *Msm*-lux was submitted to MIC assay and cell viability was assessed by measuring relative luminescence units (RLUs) at day 2. Correlation between colony

forming units (CFUs) was performed according to a previously performed *in vitro* RLUs vs. CFUs curve.

Transmission Electron Microscopy (TEM) (Negative Staining)

Mycobacterium smegmatis cells were fixed with 2% glutaraldehyde in 0.1 M cacodylate at room temperature for 2 h, and then incubated overnight in 4% formaldehyde, 1% glutaraldehyde, and 0.1% PBS. For negative staining of the samples, a drop of the fixed bacterial suspension was applied directly onto a glow-discharged EM grid (QUANTIFOIL. Formvar/Carbon. Cu 400 mesh grids). The sample was allowed to be adsorbed and then blotted with filter paper (Whatman grade No. 1). The grid was washed by touching the surface with two consecutive drops of 0.75% (w/v) uranyl formate, blotting each time, and stained for 1 min with one more drop of the same staining agent. Negative stained samples were examined in a JEOL JEM-1230 (accelerating voltage 100 kV) electron microscope, and images were recorded with a CCD camera ORIUS SC100 (4 × 2.7 k pixel).

Cryo-Electron Microscopy (Cryo-EM)

Mycobacterium smegmatis and *Mtb* cultures were fixed as above prior to vitrification. Grids were prepared following standard procedures and observed at liquid nitrogen temperatures in a JEM-2200FS/CR transmission electron microscope (JEOL Europe, Croissy-sur-Seine, France) operated at 200 kV. An in-column omega energy filter helped to record images with improved signal/noise ratio by zero-loss filtering. The energy selecting slit width was set at 9 eV. Digital images were recorded on an UltraScan4000 CCD camera under low-dose conditions at a magnification of 55,058 obtaining a final pixel size of 2.7 Å/pixel.

RESULTS

Synthesis and Characterization of SeNPs

Selenium nanoparticles were prepared via a redox system in the presence of a biomacromolecule as soft template to control the nucleation and growth of the inorganic nanoselenium. The chemical reduction of selenite with ascorbic acid in the presence of a polysaccharide such as chitosan as stabilizer and capping agent afforded red elemental selenium in colloidal state (Zhang et al., 2010). Based on our previous work, 0.1% of chitosan concentration was selected to prepare the SeNPs (Estevez et al., 2014). Under these conditions, the nanoparticles proved to be colloidally stable. Two months after their synthesis, no flocculated material was present, DLS measurements showed no displacement of the hydrodynamic size distribution and no significant differences in the shape or size of the SeNPs were observed by TEM.

Transmission electron microscopy images show well dispersed Ch-SeNPs that exhibit spherical morphology and homogeneous sizes of around 60–80 nm (**Figure 1A**). The energy dispersive spectroscopy analysis (**Figure 1B**) indicates a composition in selenium for the Ch-SeNPs, also being observed in the spectrum the signals for C and O from chitosan and the carbon coated copper grid.

The hydrodynamic size distribution of the Ch-SeNPs measured in the aqueous colloidal suspension (**Figure 1C**) is monomodal and reasonably narrow, with a maximum centered at 105.7 ± 2.5 nm of diameter, which is in concordance with the smaller size of the inorganic nanoparticle determined in the TEM study. The ζ-potential of the Ch-SeNPs in water is in the zone of colloidal stability with a value of +66.6 ± 4.7 mV. This highly positive value is due to the surface stabilization with chitosan, which possesses a equilibrium for the protonation of the amino groups in water. Therefore, chitosan allows the SeNPs to form stable colloidal suspensions due to both electrostatic as well as steric stabilization.

Antimycobacterial Activity of SeNPs

We evaluated the ability of SeNPs to inhibit the growth of two different species of mycobacteria: the fast-growing *Msm* and the slow-growing *Mtb*. SeNPs were found to be effective in inhibiting mycobacterial growth in a dose-dependent manner, showing MIC values of 0.400 μg/mL for *Msm* (**Supplementary Figure S1A**) and 0.195 μg/mL for *Mtb* (**Figure 2A**). To determine whether this inhibition was concomitant to bacterial cell death we generated a luciferase-expressing reporter strain of *Msm* (Msm-Lux) (Andreu et al., 2010). Correlation between relative fluorescence units (RLUs) and CFUs was previously determined (**Supplementary Figure S2A**) and used to calculate viable bacteria after treatment of *Msm*-Lux with SeNPs (**Supplementary Figure S2B**). We observed a reduction in CFUs as concentration of NPs increased, indicating the bactericidal effect of SeNPs. By this method MIC was similar to that of previously determined by measuring optical density.

To gain insight into the nature of the inhibitory effect of SeNPs, we performed ultrastructural analysis of *Msm* submitted to 0.400 μg/mL of SeNPs. Transmission electron micrographs of negative stained samples suggested that *Msm* exposed to SeNPs manifested reduced integrity of cell envelope leading to extrusion of cytoplasmic material, relative to untreated *Msm* (**Supplementary Figures S1B,C**). To capture the antimycobacterial effect of SeNPs in a close-to-native state, treated (0.195 μg/mL) and untreated *Msm* and *Mtb* cells were submitted to cryo-EM. This technique revealed more in detail the membrane damage, both in *Msm* (**Supplementary Figures S1D,E**) and *Mtb* (**Figures 2B–F**). In addition, SeNPs could be spotted in direct contact with the mycobacterial cell wall, suggesting a direct connection between the effect of SeNPs and the reduction of the integrity of the mycobacterial cell envelope.

DISCUSSION

The rapid spread of antibiotic-resistant *Mtb* strains makes it necessary to search for alternative treatments. In this sense, the use of nanoparticles with mycobactericidal potential could be especially interesting, since nanoparticles have a high surface area, which means that they contain a high number of active sites

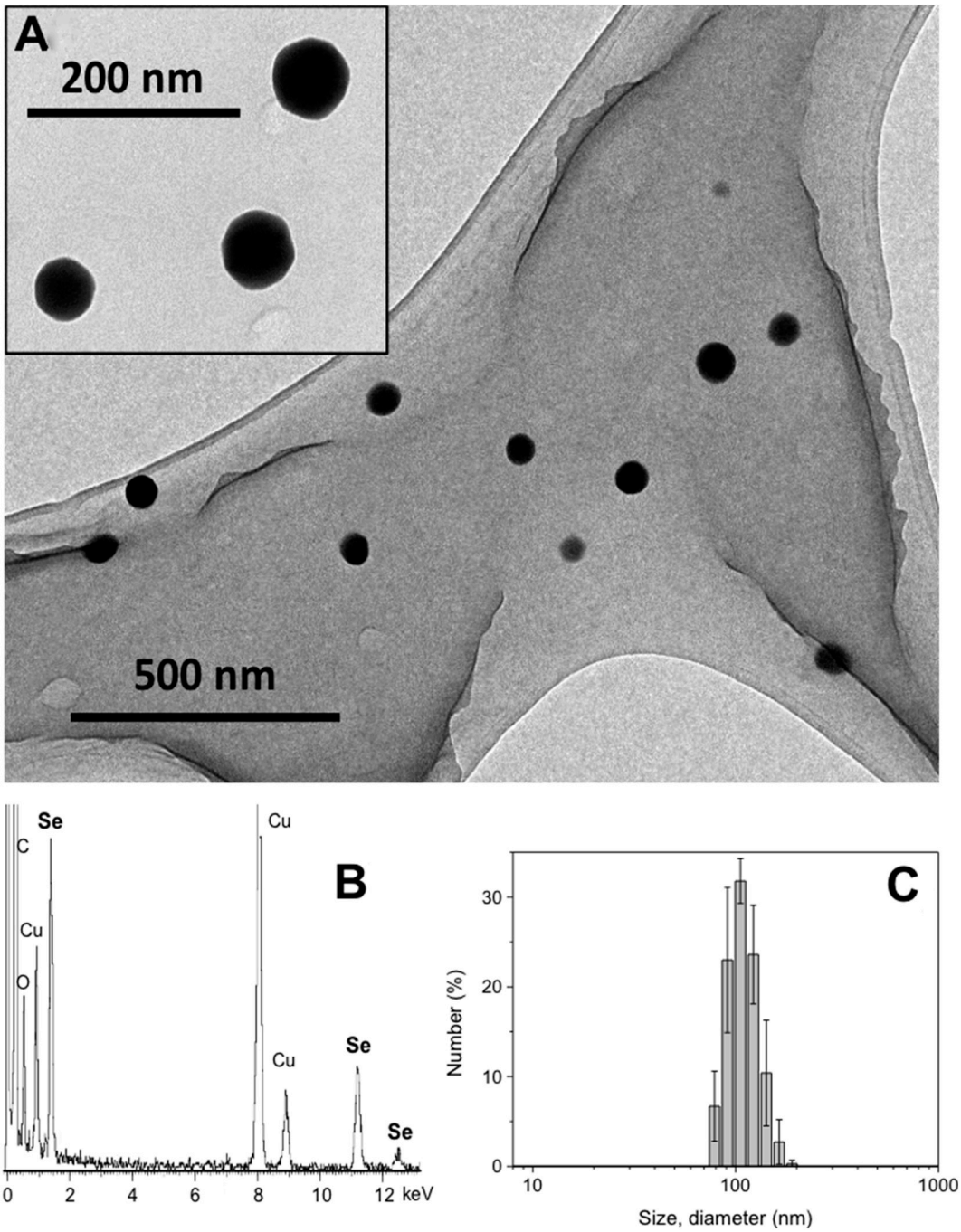

FIGURE 1 | Characterization of the synthesized SeNPs. **(A)** TEM images of a 200 mg L^{-1} suspension of Ch-SeNPs. **(B)** EDS spectrum of Ch-SeNPs. **(C)** Hydrodynamic size distribution of the Ch-SeNPs in aqueous colloidal suspension measured by dynamic light scattering.

to be able to interact with biological entities and, on the other hand, they have a high capacity to penetrate cells and tissues (Lu et al.; Singh et al., 2015).

Previous studies have used different types of nanoparticles, either as drug carriers (Lu et al., 2018) or as bactericidal agents themselves against TB. In the latter case, the mycobactericidal potential of different metallic nanoparticles such as Ag (Selim et al., 2018), AgO, AgZnO (Jafari et al., 2017) or Ga (Choi et al., 2017) nanoparticles, has been evaluated.

Among the different nanoparticles that are being used in biomedicine, Se nanoparticles are especially interesting because of their low toxicity. While Se has a narrow therapeutic window and the toxicity margins are very delicate, SeNPs possess remarkably reduced toxicity (Khurana et al., 2019)

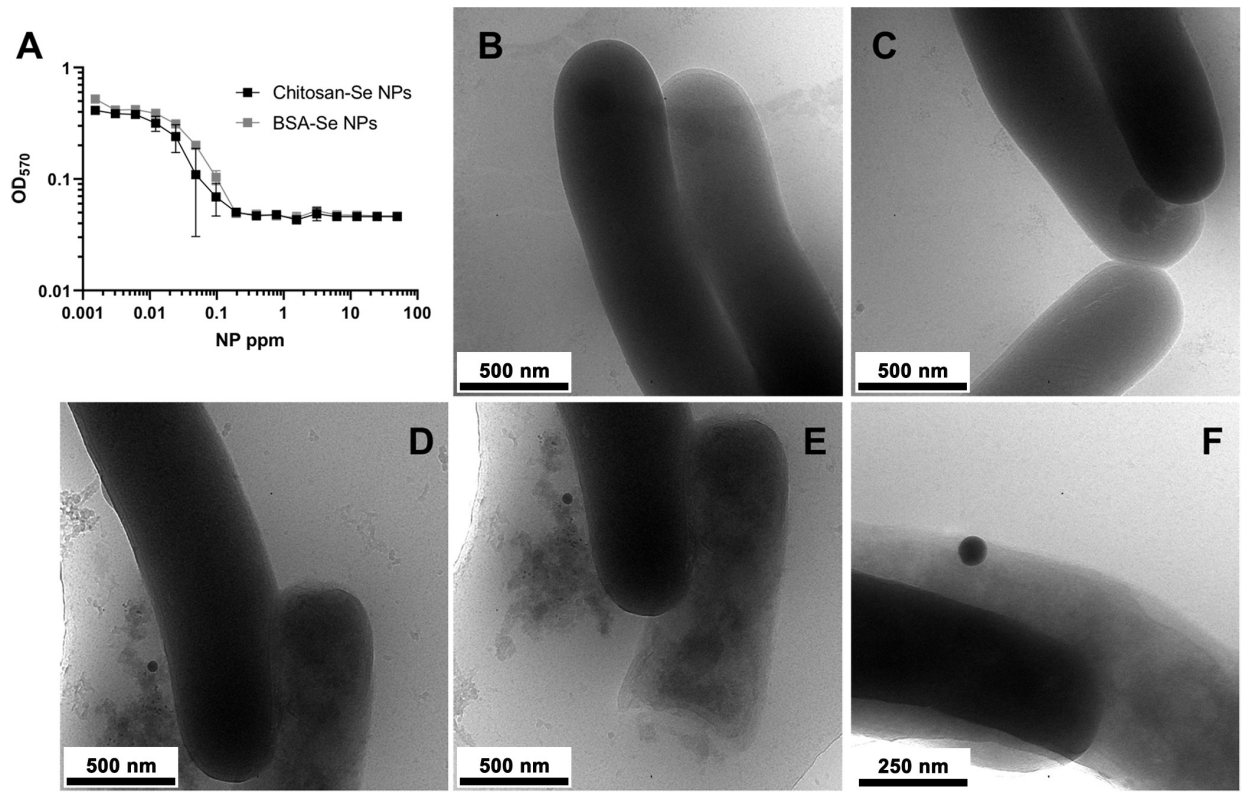

FIGURE 2 | Antimicrobial activity of SeNPs against *Mycobacterium tuberculosis*. **(A)** MIC assay testing the antibacterial activity of Ch-SeNPs and BSA-SeNPs after 20 days of treatment. **(B–E)** Ultrastructural analysis by cryo-EM of untreated *Mtb* cells **(B,C)** or *Mtb* cells treated with an inhibitory concentration (0.195 μg/mL) of SeNPs **(D–F)**.

and it has been proposed as a therapeutic agent for different applications without significant side effects (Hosnedlova et al., 2018). As a matter of fact, it has been demonstrated that SeNPs are less toxic than other inorganic and organic selenospecies (Estevez et al., 2014), showing unique properties such as their capacity for inducing cell cycle arrest (Lopez-Heras et al., 2014) without inducing a significant degree of apoptosis (Estevez et al., 2014). In addition, SeNPs have also been used as a bactericidal agent against *Staphylococcus aureus* (Tran and Webster, 2011) and their anti-biofilm capacity has been demonstrated against *S. aureus, Pseudomonas aeruginosa*, and *Proteus mirabilis* (Shakibaie et al., 2014). However, to date, the potential of Se nanoparticles against *Mtb* has not been evaluated.

In this study, the mycobactericidal capacity of SeNPs has been demonstrated against two types of mycobacteria, *Msm* and *Mtb*, with MIC values of 0.400 μg/mL and 0.195 μg/mL, respectively. Furthermore, to rule out an effect of the chitosan in the Ch-SeNPs bactericidal action, SeNPs stabilized with a protein such as bovine serum albumin (BSA-SeNPs) have been evaluated on *Mtb* showing an inhibition on the bacterial growth at similar concentrations than Ch-SeNPs (**Figure 2A**). Therefore, the mycobactericidal effect is due to the SeNPs themselves and not to the presence of the stabilizing agent chitosan. In agreement with the previously demonstrated bactericidal effect of SeNPs on unrelated bacterial pathogens, we have demonstrated that these NPs can also kill Mycobacteria. Furthermore, our analyses by TEM and cryo-EM have shown that SeNPs come into contact with the cell wall of *Mtb* and *Msm*, compromising their integrity and inducing extrusion of cytoplasmic material. These results open a new opportunity for the development of novel nanosystems with high antimycobacterial potential that, alone or in combination with antibiotics, could improve the treatment of multi-drug resistant TB strains.

DATA AVAILABILITY STATEMENT

The datasets generated for this study are available on request to the corresponding authors.

AUTHOR CONTRIBUTIONS

JL-G, RP-R, and BG designed the study, supervised the experimental work, analyzed and interpreted the data, and wrote the manuscript together with HE, AP, JA, and MV-R. HE, AP, and DG performed the experimental work.

FUNDING

This study was supported by the Ministerio de Economía y Competitividad (MINECO) grants: CTQ2017-85673-R (JL-G), SAF2016–77433-R (RP-R), RTI2018-096494-B-100 (JA) and the European Research Council ERC-2015-AdG (VERDI) Proposal No. 694160. CIBER is a public research consortium created by ISCIII whose actions are co-funded by the European Regional Development Fund. CIC bioGUNE thanks MINECO for the Severo Ochoa Excellence Accreditation (SEV-2016–0644). HE acknowledges Ministerio de Ciencia, Innovacion y Universidades from the Spanish Government for a predoctoral fellowship (PRE2018-084196). AP holds a fellowship form the Department of Education of the Basque Government (PRE_2018_1_0229).

SUPPLEMENTARY MATERIAL

The Supplementary Material for this article can be found online at: https://www.frontiersin.org/articles/10.3389/fmicb.2020.00800/full#supplementary-material

REFERENCES

Andreu, N., Zelmer, A., Fletcher, T., Elkington, P. T., Ward, T. H., Ripoll, J., et al. (2010). Optimisation of bioluminescent reporters for use with mycobacteria. *PLoS One* 5:e10777. doi: 10.1371/journal.pone.0010777

Bai, Y., Wang, Y., Zhou, Y., Li, W., and Zheng, W. (2008). Modification and modulation of saccharides on elemental selenium nanoparticles in liquid phase. *Mater. Lett.* 62, 2311–2314. doi: 10.1016/j.matlet.2007.11.098

Baranwal, A., Srivastava, A., Kumar, P., Bajpai, V. K., Maurya, P. K., and Chandra, P. (2018). Prospects of nanostructure materials and their composites as antimicrobial agents. *Front. Microbiol.* 9:422. doi: 10.3389/fmicb.2018.00422

Beyth, N., Houri-Haddad, Y., Domb, A., Khan, W., and Hazan, R. (2015). Alternative antimicrobial approach: nano-antimicrobial materials. *Evid. Based Complement. Alternat. Med.* 2015:246012.

Chandra Mohana, N., Yashavantha Rao, H. C., Rakshith, D., Mithun, P. R., Nuthan, B. R., and Satish, S. (2018). Omics based approach for biodiscovery of microbial natural products in antibiotic resistance era. *J. Genet. Eng. Biotechnol.* 1, 1–8. doi: 10.1016/j.jgeb.2018.01.006

Choi, S. R., Britigan, B. E., Moran, D. M., and Narayanasamy, P. (2017). Gallium nanoparticles facilitate phagosome maturation and inhibit growth of virulent *Mycobacterium tuberculosis* in macrophages. *PLoS One* 12:e0177987. doi: 10.1371/journal.pone.0177987

Estevez, H., Garcia-Lidon, J. C., Luque-García, J. L., and Cámara, C. (2014). Effects of chitosan-modified selenium nanoparticles on cell proliferation, apoptosis and cell cycle pattern in HepG2 cells: comparison with other selenospecies. *Colloids Surf. B Biointerfaces* 122, 184–193. doi: 10.1016/j.colsurfb.2014.06.062

Herman, A., and Herman, A. P. (2014). Nanoparticles as antimicrobial agents: their toxicity and mechanisms of action. *J. Nanosci. Nanotechnol.* 1, 946–957. doi: 10.1166/jnn.2014.9054

Hoseinzadeh, E., Makhdoumi, P., Taha, P., Hossini, H., Stelling, J., Kamal, M. A., et al. (2017). A review on nano-antimicrobials: metal nanoparticles, methods and mechanisms. *Curr. Drug Metab.* 18, 120–128. doi: 10.2174/1389200217666161201111146

Hosnedlova, B., Kepinska, M., Skalickova, S., Fernandez, C., Ruttkay-Nedecky, B., Peng, Q., et al. (2018). Nano-selenium and its nanomedicine applications: a critical review. *Int. J. Nanomedicine* 13, 2017–2018. doi: 10.2147/IJN.S157541

Huang, T., Holden, J. A., Heath, D. E., O'Brien-Simpson, N. M., and O'Connor, A. J. (2019). Engineering highly effective antimicrobial selenium nanoparticles through control of particle size. *Nanoscale* 11, 14937–14951. doi: 10.1039/c9nr04424h

Jafari, A., Mosavari, N., Movahedzadeh, F., Nodooshan, S. J., Safarkar, R., Moro, R., et al. (2017). Bactericidal impact of Ag, ZnO and mized AgZnO colloid nanoparticles on H37Rv *Mycobacterium tuberculosis* phagocytez by THP-1 cell lines. *Microb. Pathog.* 110, 335–344. doi: 10.1016/j.micpath.2017.07.010

Jayawardana, K. W., Jayawardana, H. S. N., Wijesundera, S. A., De Zoysa, T., Sundhoro, M., and Yan, M. (2015). Selective targeting of mycobacterium smegmatis with trehalose-functionalized nanoparticles. *Chem. Commun.* 51, 12028–12031. doi: 10.1039/c5cc04251h

Khan, F., Lee, J. W., Pham, D. T. N., Khan, M. M., Park, S. K., Shin, I. S., et al. (2020). Antibiofilm action of ZnO, SnO2 and CeO2 nanoparticles towards Gram-positive biofilm formin pathogenic bacteria. *Recent Pat. Nanotechnol.* doi: 10.2174/1872210514666200313121953 [Epub ahead of print].

Khurana, A., Tekula, S., Saifi, M. A., Venkatesh, P., and Godugu, C. (2019). Therapeutic applications of selenium nanoparticles. *Biomed. Phamacother.* 111, 802–812. doi: 10.1016/j.biopha.2018.12.146

Kumarasingam, K., Vincent, M., Mane, S. R., Shunmugam, R., Sivakumar, S., and Uma Devi, K. R. (2018). Enhancing antimycobacterial activity of isoniazid and rifampicin incorporated norbornene nanoparticles. *Int. J. Mycobacteriol.* 7, 84–88. doi: 10.4103/ijmy.ijmy_162_17

Lopez-Heras, I., Sanchez-Diaz, R., Anunciacao, D. S., Madrid, Y., Luque-Garcia, J. L., and Camara, C. (2014). Effect of chitosan-stabilized selenium nanoparticles on cell cycle arrest and invasiveness in hepatocarcinoma cells revealed by quantitative proteomics. *J. Nanomed. Nanotechnol.* 5:5.

Lu, T., Wu, Y., Zhao, C., Su, F., Liu, J., Ma, Z., et al. (2018). One-step fabrication and characterization of Fe3O4/HBPE-DDSA/INH nanoparticles with controlled drug release for treatment of tuberculosis. *Mater. Sci. Eng. C Mater. Biol. Appl.* 93, 838–845. doi: 10.1016/j.msec.2018.08.046

Reshma, V. G., Syama, S., Sruthi, S., Reshma, S. C., Remya, N. S., and Mohanan, P. V. (2017). Engineered nanoparticles with antimicrobial property. *Curr. Drug Metab.* 11, 1040–1054. doi: 10.2174/1389200218666170925122201

Selim, A., Elhaig, M. M., Taha, S. A., and Nasr, E. A. (2018). Antibacterial activity of silver nanoparticles agains field and reference strains of *Mycobacterium tuberculosis*, *Mycobacterium bovis* and multiple drug-resistant tuberculosis strains. *Rev. Sci. Tech.* 37, 823–830. doi: 10.20506/rst.37.3.2888

Shakibaie, M., Foroontanfar, H., Golkari, Y., Mohammadi-Khorsand, T., and Shakibaie, M. R. (2014). Anti-biofilm activity of biogenic selenium nanoparticles and selenium dioxide against clinical isolates of *Staphylococcus aureus*, *Pseudomonas aeruginosa*, and *Proteus mirabilis*. *J. Trace Elem. Med. Biol.* 29, 235–241. doi: 10.1016/j.jtemb.2014.07.020

Singh, R., Nawale, L. U., Arkile, M., Shedbalkar, U. U., Wadhwani, S. A., Sarkar, D., et al. (2015). Chemical and biological metal nanoparticles as antimycobacterial agents: a comparative study. *Int. J. Antimicrob. Agents* 46, 183–188. doi: 10.1016/j.ijantimicag.2015.03.014

Tran, P. A., and Webster, T. J. (2011). Selenium nanoparticles inhibit *Staphylococcus aureus* growth. *Int. J. Nanomed.* 6, 1553–1558.

Vallet-Regí, M., González, B., and Izquierdo-Barba, I. (2019). Nanomaterials as promising alternative in the infection treatment. *Int. J. Mol. Sci.* 20:3806. doi: 10.3390/ijms20153806

Wang, L., Hu, C., and Shao, L. (2017). The antimicrobial activity of nanoparticles: present situation and prospects for the future. *Inter. J. Nanomedicine* 12, 1227–1249. doi: 10.2147/IJN.S121956

World Health Organization [WHO] (2019). *Global Tuberculosis Report*. Geneva: World Health Organization.

Zhang, Y., Wang, J., and Zhang, L. (2010). Creation of highly stable selenium nanoparticles capped with hyperbranched polysaccharide in water. *Langmuir* 26, 17617–17623. doi: 10.1021/la1033959

Conflict of Interest: The authors declare that the research was conducted in the absence of any commercial or financial relationships that could be construed as a potential conflict of interest.

frontiers in Microbiology

ORIGINAL RESEARCH
published: 15 July 2020
doi: 10.3389/fmicb.2020.01644

Two Novel *katG* Mutations Conferring Isoniazid Resistance in *Mycobacterium tuberculosis*

*Li-Yu Hsu[1], Li-Yin Lai[1], Pei-Fang Hsieh[1], Tzu-Lung Lin[1], Wan-Hsuan Lin[2,3], Hsing-Yuan Tasi[2,3], Wei-Ting Lee[2,3], Ruwen Jou[2,3] and Jin-Town Wang[1,4]**

[1]Department of Microbiology, National Taiwan University College of Medicine, Taipei, Taiwan, [2]Tuberculosis Research Center, Taiwan Centers for Disease Control, Taipei, Taiwan, [3]Diagnostics and Vaccine Center, Taiwan Centers for Disease Control, Taipei, Taiwan, [4]Department of Internal Medicine, National Taiwan University Hospital, Taipei, Taiwan

Tuberculosis (TB), an infectious disease caused by *Mycobacterium tuberculosis*, is among the top 10 leading causes of death worldwide. The treatment course for TB is challenging; it requires antibiotic administration for at least 6 months, and bacterial drug resistance makes treatment even more difficult. Understanding the mechanisms of resistance is important for improving treatment. To investigate new mechanisms of isoniazid (INH) resistance, we obtained three INH-resistant (INH-R) *M. tuberculosis* clinical isolates collected by the Taiwan Centers for Disease Control (TCDC) and sequenced genes known to harbor INH resistance-conferring mutations. Then, the relationship between the mutations and INH resistance of these three INH-R isolates was investigated. Sequencing of the INH-R isolates identified three novel *katG* mutations resulting in R146P, W341R, and L398P KatG proteins, respectively. To investigate the correlation between the observed INH-R phenotypes of the clinical isolates and these *katG* mutations, wild-type *katG* from H37Rv was expressed on a plasmid (pMN437-*katG*) in the isolates, and their susceptibilities to INH were determined. The plasmid expressing H37Rv *katG* restored INH susceptibility in the two INH-R isolates encoding the W341R KatG and L398P KatG proteins. In contrast, no phenotypic change was observed in the KatG R146P isolate harboring pMN437-*katG*. H37Rv isogenic mutant with W341R KatG or L398P KatG was further generated. Both showed resistant to INH. In conclusion, W341R KatG and L398P KatG conferred resistance to INH in *M. tuberculosis*, whereas R146P KatG did not affect the INH susceptibility of *M. tuberculosis*.

Keywords: ***Mycobacterium tuberculosis*, drug resistance, isoniazid, mutation, *katG***

OPEN ACCESS

Edited by:
Giorgia Mori,
The University of Queensland, Australia

Reviewed by:
Diana Machado,
New University of Lisbon, Portugal
Daniela Fernandes Ramos,
Federal University of Rio Grande, Brazil

***Correspondence:**
Jin-Town Wang
wangjt@ntu.edu.tw

Specialty section:
This article was submitted to Antimicrobials, Resistance and Chemotherapy, a section of the journal Frontiers in Microbiology

Received: *29 April 2020*
Accepted: *24 June 2020*
Published: *15 July 2020*

Citation:
Hsu L-Y, Lai L-Y, Hsieh P-F, Lin T-L, Lin W-H, Tasi H-Y, Lee W-T, Jou R and Wang J-T (2020) Two Novel katG Mutations Conferring Isoniazid Resistance in Mycobacterium tuberculosis. Front. Microbiol. 11:1644. doi: 10.3389/fmicb.2020.01644

INTRODUCTION

According to the Global Tuberculosis Report published by the World Health Organization (WHO), tuberculosis (TB), the airborne infectious disease caused by *Mycobacterium tuberculosis* (Cambau and Drancourt, 2014), is one of the top 10 causes of death worldwide, and thus remains a major global public health problem (WHO, 2019). The emergence of drug-resistant TB has made the need for improvements in diagnostic accuracy and successful treatment even more urgent, as both are major challenges in TB control and key causes of its high mortality rate (Nguyen et al., 2019).

Since the 1940s, several drugs have been developed for the treatment of TB (Sotgiu et al., 2015; Kurz et al., 2016). These drugs can be classified as first-line anti-TB drugs, including the isoniazid (INH), rifampicin, pyrazinamide, and ethambutol, as well as other second-line drugs, which are used in cases of treatment failure (Rendon et al., 2016). The first-line anti-TB drug, INH, which was initially shown to have anti-TB activity in 1952 (Fox, 1952), is suitable for treatment when *M. tuberculosis* is replicating (Chakraborty and Rhee, 2015). INH is a prodrug that is activated by the catalase-peroxidase KatG. The metabolites produced then react with nicotinamide adenine dinucleotide (NAD^+), and binding of the INH-NAD adduct to the NADH-dependent enoyl-ACP reductase InhA. InhA inhibits mycolic acid formation and cell wall synthesis in *M. tuberculosis*, leading to cell death (Vilchèze and Jacobs, 2014; Chakraborty and Rhee, 2015; Islam et al., 2017).

Most INH-resistant (INH-R) strains harbor mutations in genes associated with cell wall synthesis, the *katG* gene (Somoskovi et al., 2001; Laurenzo and Mousa, 2011), the *inhA* gene and its promoter (Zhang et al., 1992; Nguyen et al., 2019), or the *oxyR-ahpC* region (Sreevatsan et al., 1997; Lempens et al., 2018). Articles suggest that *katG* deletion mutants have higher INH resistance than strains with mutations in *inhA* or its promoter (Somoskovi et al., 2001; Lempens et al., 2018). In addition, upregulation of INH inactivators or efflux pumps was involved in INH resistance (Vilchèze and Jacobs, 2014; Unissa et al., 2016).

In this work, three INH-R clinical isolates with minimum inhibitory concentrations (MICs) ≥64 mg/L were found to have novel *katG* mutations that were not previously reported to confer INH resistance. The aim of this study was to examine whether the amino acid changes encoded by the *katG* mutations in these high-level INH-R clinical isolates are determinants of INH resistance. We compared the INH susceptibility of these isolates to those of isolates expressing the H37Rv KatG protein, and then recreated these point mutations in H37Rv to confirm the relationship between the *katG* mutations and INH resistance.

MATERIALS AND METHODS

Ethics Statement

According to the Taiwan Communicable Disease Control Act, TB is one of the notifiable diseases, and specimen collection for laboratory testing is mandatory. This study did not require ethics approval, and participant consent was not required.

Bacterial Strains and Culture Conditions

The bacterial strains used in this study are listed in **Supplementary Table S1**. All the experiments for *M. tuberculosis* strains were carried out at a BSL-3 laboratory in National Taiwan University College of Medicine, Taiwan, following institutional biosafety procedures. The INH-R *M. tuberculosis* isolates identified by clinical TB laboratories of Taiwan were sent to the Reference laboratory of Mycobacteriology at the Taiwan Centers for Disease Control (TCDC) for confirmation. Reference strain *M. tuberculosis* H37Rv, H37Rv-derived isogenic mutants, and the clinical INH-R isolates were grown in Middlebrook 7H9 liquid medium (BD Difco, Sparks, MD, USA) containing 10% oleic acid/albumin/dextrose/catalase (OADC; BD Difco, Sparks, MD, USA), 0.5% glycerol, and 0.05% Tween-80 or Middlebrook 7H11 solid agar (BD Difco, Sparks, MD, USA) containing 10% OADC and 0.5% glycerol at 37°C. *Escherichia coli* DH10B, for plasmid construction, was grown in Luria-Bertani (LB) medium (Bio Basic, Toronto, Canada) at 37°C. The following were added to medium as needed for selection: 50 mg/L hygromycin (BioShop, Ontario, Canada), 100 mg/L X-gal, and 4% sucrose for *M. tuberculosis* and 100 mg/L hygromycin (BioShop, Ontario, Canada) for *E. coli*.

Screening and Sequencing of INH-R Clinical Isolates

The MIC of INH-R *M. tuberculosis* isolates was screened and determined using the Sensititre™ MYCOTB MIC Plate (Trek Diagnostic Systems, OH, USA) according to the manufacturer's instructions. The ranges of drug concentrations were 0.03–4 mg/L for INH. The bacterial solution was adjusted to turbidity at a McFarland standard of 0.5 and then added to the Sensititre™ MYCOTB MIC Plate before the plate was covered with the adhesive plastic seal. After incubation at 37°C for 14 or 21 days, the results were recorded using the Sensititre™ Vizion™ Digital MIC Viewing System.

The primers used to sequences *katG*, *inhA*, *oxyR*, and *aphC* are listed in **Supplementary Table S2**. The polymerase chain reaction (PCR) cycling conditions were previously described (Jou et al., 2019). The sequences of *katG* in INH-R strains CDC-A, CDC-B, and CDC-C had been submitted to NCBI (GenBank accession numbers: MT572851, MT572852, and MT572853).

KatG Expression Constructs

The primer and plasmids used in this study are listed in **Supplementary Tables S2**, **S3**. To express wild-type *katG* in the INH-R clinical strains, a *katG* expression plasmid, pMN437-*katG*, was generated by ligating the *katG* gene from *M. tuberculosis* H37Rv to pMN437 (Song et al., 2008; Steinhauer et al., 2010), which was linearized *via* reverse PCR to remove the *gfp* gene. The pMN437 and pMN437-*katG* plasmids were transformed into competent *M. tuberculosis* cells by electroporation at 2,500 V, 1,000 Ω, and 25 μF as previously described (Larsen et al., 2007).

Mutagenesis of *katG* in H37Rv

To replace the *katG* gene in H37Rv with the mutant genes in the INH-R clinical isolates, fragments of the mutated *katG* genes in clinical strains CDC-A and CDC-B were amplified and ligated into the pGOAL19 plasmid at the *Sca*I site. The primers used are listed in **Supplementary Table S2**. The pGOAL19 plasmid is a suicide plasmid that lacks a mycobacterial origin for plasmid replication (Parish and Stoker, 2000).

Nomenclature: TB, Tuberculosis; INH, Isoniazid; INH-R, INH-resistant; WHO, World Health Organization; NAD^+, Nicotinamide adenine dinucleotide; MICs, Minimum inhibitory concentrations; TCDC, Taiwan Centers for Disease Control; OADC, Oleic acid/albumin/dextrose/catalase; LB, Luria-Bertani; PCR, Polymerase chain reaction.

When the pGOAL19 recombinant plasmid (pGOAL19-*katG* W341R R463L or pGOAL19-*katG* L398P R463L) was transformed to the H37Rv strain, a two-step homologous recombination has *occurred* between the plasmid and the genome results in replacement of the H37Rv gene with the mutant gene. The H37Rv isogenic mutants were confirmed by PCR and sequencing.

INH Susceptibility Tests

To evaluate the effect of H37Rv KatG expression in INH-R isolates and the impact of KatG from the INH-R isolates in H37Rv isogenic mutants, the INH susceptibility was assessed by the agar dilution assay. Briefly, 5 μl of a 4×10^6 CFU/ml bacterial suspension (equivalent to 2×10^4 cfu) was spotted on Middlebrook 7H11 agar plates containing 10% OADC, 0.5% glycerol, and serial diluted INH (Sigma, St. Louis, MO, USA) concentrations of 0, 0.2, 1, 4, 16, and 64 mg/L and incubated at 37°C. The results were recorded after 3 weeks of incubation. Resistance was defined as colonies growing in the presence of the critical concentrations of 0.2 mg/L INH, according to the CLSI guidelines (Clinical and Laboratory Standards Institute, 2011). All reported MICs were represented from three independent experiments. For the H37Rv KatG expression, H37Rv/pMN437 was used as the control strain, and 50 mg/L hygromycin was added to the agar plates to maintain the transformed plasmids. To compare the INH susceptibility of KatG from the clinical isolates in H37Rv isogenic mutants, H37Rv was used as the control.

RESULTS

Three INH-R Clinical Isolates Harbor Novel Mutations in *katG*

Three INH-R strains, CDC-A, CDC-B, and CDC-C, were provided by TCDC. The MICs of the three INH-R isolates were all >4 mg/L, which were initially determined using the Sensititre™ MYCOTB MIC Plate. To identify the uncommon mutations that conferred INH resistance in these isolates, we sequenced the frequent INH resistance hotspots of *katG*, *inhA*, and *oxyR-aphC* regions. The results demonstrated that the three isolates were carried wild-type *inhA*, *oxyR*, and *aphC* genes and had mutations in the *katG* gene resulting in the following amino acid changes: W341R (TGG/CGG), L398P (CTG/CCG), and R146P (CGG/CCG), respectively. All of them also harbored the R463L (CGG/CTG) change in KatG, and this residue change has been confirmed earlier as a polymorphism (**Figure 1**). Then, we further confirm the INH susceptibilities of all three isolates and revealed those were >64 mg/L by the agar dilution assay (**Figure 2**). The results indicate that the three amino acid residues change in *katG* might result in INH resistance in our INH-R isolates.

H37Rv KatG-Complemented Clinical Strains Carrying W341R and L398P KatG Are More Susceptible to INH

To delineate the association of the W341R, L398P, and R146P KatG proteins with the INH resistance in the isolates CDC-A, CDC-B, and CDC-C, we expressed the KatG protein from H37Rv in these INH-R strains using pMN437-*katG*. To examine whether expression of H37Rv KatG could restore INH resistance, INH susceptibility tests were conducted (**Figure 3**). The results showed that CDC-A/pMN437-*katG* was more susceptible to INH (MIC <4 mg/L) than the CDC-A carrying an empty vector (CDC-A/pMN437; MIC >64 mg/L). CDC-B/pMN437-*katG* was INH sensitive (MIC <0.2 mg/L), whereas CDC-B/pMN437 was highly resistant (MIC >64 mg/L). In contrast, CDC-C/pMN437-*katG* showed no difference in INH susceptibility when compared with CDC-C/pMN437 (**Table 1**). Therefore, we concluded that KatG W341R and L398P are the resistance-conferring amino acid changes in strains CDC-A and CDC-B, respectively. In contrast, KatG R146P is not the determinant for INH resistance of the CDC-C strain.

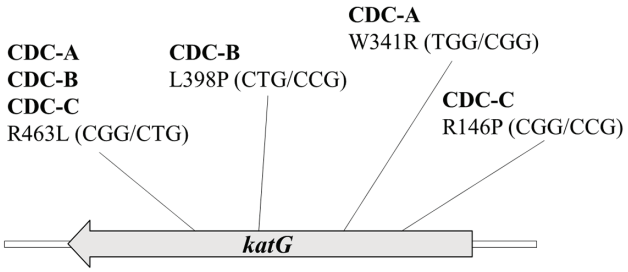

FIGURE 1 | The *katG* sequence results of three high INH resistance strains CDC-A, CDC-B, and CDC-C shows that all strains encode a mutation at R463L (CGG/CTG) and another mutation at W341R (TGG/CGG), L398P (CTG/ CCG), and R146P (CGG/CCG), respectively.

The W341R and L398P KatG Proteins Confer INH Resistance in *M. tuberculosis*

To directly confirm the contribution of the W341R and L398P KatG proteins on INH resistance, the *katG* gene of H37Rv was replaced with a segment of the DNA from the clinical isolates containing these *katG* mutations. The DNA sequencing of the H37Rv isogenic mutants H37Rv *katG* W341R and H37Rv *katG* L398P R463L showed that the *katG* of H37Rv was successfully substituted with the *katG* gene from CDC-A and CDC-B, respectively. The INH susceptibilities of the H37Rv isogenic mutants H37Rv *katG* W341R and H37Rv *katG* L398P R463L were measured by the agar dilution method (**Figure 2**), and revealed that, like CDC-A and CDC-B, both strains were resistant to the highest INH concentration tested (64 mg/L), indicating a MIC >64 mg/L and demonstrating that *katG* W341R and L398P confer INH resistance (**Table 2**).

DISCUSSIONS

INH is a first-line TB drug, and researchers have clarified various mechanisms of INH resistance by collecting INH-R strains and identifying the mutated genes. Studies have shown that 50–94% INH-R strains have at least one mutation in *katG*, 10–35% INH-R strains carry at least one mutation in the *inhA*

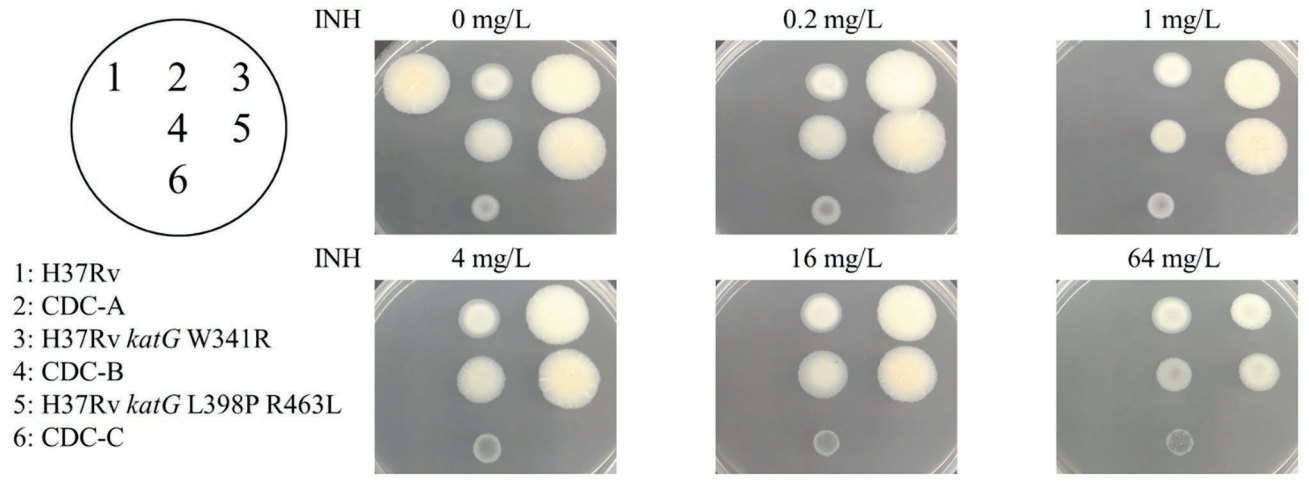

FIGURE 2 | INH susceptibility testing of the control (H37Rv, spot 1), clinical isolates [CDC-A (spot 2), CDC-B (spot 4), and CDC-C (spot 6)] and H37Rv isogenic mutants [H37Rv *katG* W341R (spot 3), and H37Rv *katG* L398P R463L (spot 5)].

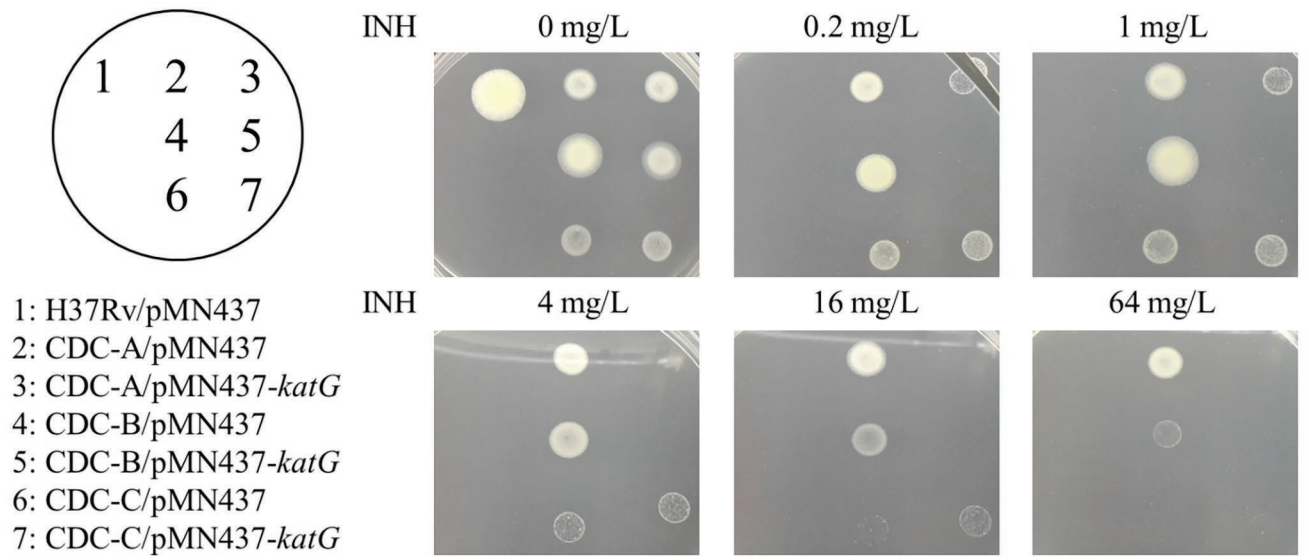

FIGURE 3 | Complementation of INH resistance in the clinical isolates. INH susceptibility testing of the control H37Rv carrying the empty vector pMN437 (H37Rv/pMN437, spot 1); clinical isolate control strains carrying the empty vector pMN437 [CDC-A/pMN437 (spot 2), CDC-B/pMN437 (spot 4), and CDC-C/pMN437 (spot 6)]; and clinical isolates carrying wild-type *katG* expression plasmid [CDC-A/pMN437-*katG* (spot 3), CDC-B/pMN437-*katG* (spot 5), and CDC-C/pMN437-*katG* (spot 7)].

promoter, and 10–40% INH-R strains carry at least one mutation in *oxyR-ahpC* region (Li et al., 2015). The *katG* 315 mutation, which leads to high-level INH resistance and the *inhA*-15 mutation, which leads to low-level INH resistance, are two of the most common mutations (Yao et al., 2010; Zenteno-Cuevas et al., 2019). However, mutations in the *oxyR-ahpC* region have not yet been recorded to confer INH resistance directly (Kandler et al., 2018). Studies reported that the expression level of alkylhydroperoxidase (AhpC) was different in INH-R strains with mutations in *katG*, indicating that AhpC were compensated for the loss of KatG activity and restored the anti-oxidative stress capacity (Ng et al., 2004; Nieto et al., 2016).

In this study, the KatG sequences of isolates CDC-A, CDC-B, and CDC-C revealed that each had a mutation at R463L (CGG/CTG) and had another mutation, which have not been previously reported as INH resistance-conferring mutations at W341R (TGG/CGG), L398P (CTG/CCG), and R146P (CGG/CCG), respectively. KatG R463L, was previously identified as a polymorphism, which is irrelevant to INH resistance (Johnsson et al., 1997; Ramaswamy et al., 2003; Lempens et al., 2018), and an epidemiological marker for Beijing strains (Tsolaki et al., 2005).

There are three studies, which had mentioned the mutations at KatG W341 in INH-R *M. tuberculosis*. A genetic analysis by next-generation sequencing performed in Ukraine.

TABLE 1 | INH sensitivity test results for *Mycobacterium tuberculosis* clinical isolates with and without H37Rv KatG expression plasmid.

Strains	INH MIC (mg/L)	Susceptibility
H37Rv/pMN437	<0.2	Sensitive
CDC-A/pMN437	>64	Resistant
CDC-A/pMN437-*katG*	≦4(>1)	Resistant
CDC-B/pMN437	>64	Resistant
CDC-B/pMN437-*katG*	<0.2	Sensitive
CDC-C/pMN437	>64	Resistant
CDC-C/pMN437-*katG*	>64	Resistant

INH, isoniazid; MIC, minimum inhibitory concentration.

TABLE 2 | Drug susceptibility testing of clinical isolates and H37Rv isogenic mutants harboring mutant *katG*.

Strains	INH MIC (mg/L)	Susceptibility
H37Rv	<0.2	Sensitive
H37Rv *katG* W341R	>64	Resistant
H37Rv *katG* L398P R463L	>64	Resistant
CDC-A	>64	Resistant
CDC-B	>64	Resistant

INH, isoniazid; MIC, minimum inhibitory concentration.

Daum et al. found a poly-resistant strain of *M. tuberculosis* containing the amino acid substitutions W341R and R463L in KatG (Daum et al., 2018), which are the same amino acid changes as strain CDC-A. A strain with MIC >1 mg/L found to have mutations at W341G and R463L by DNA sequencing (Brossier et al., 2006); and a group in Brazil found a strain with an INH MIC >32 mg/L harbors KatG W341S (Cardoso et al., 2004). In this study, the MIC of INH for H37Rv *katG* W341R confirmed that W341R is the INH resistance determinant in *M. tuberculosis*. Therefore, we concluded that amino acid residue 341 of KatG could be crucial for INH resistance in *M. tuberculosis*.

The INH resistance of strain CDC-C could not be reversed by expression of H37Rv KatG. Therefore, we concluded that the mechanism underlying INH resistance in the CDC-C strain may involve another INH-associated gene than those studied or other non-explored resistance mechanism.

The mutagenesis system described here could be adapted in future studies of drug resistance mechanisms in *M. tuberculosis* to establish a more reliable genetic diagnosis. Once the resistance-conferring mutation is identified, clinical institutions could shorten the time for drug susceptibility testing to facilitate the control and treatment of drug-resistant *M. tuberculosis*.

DATA AVAILABILITY STATEMENT

The original contributions presented in the study are included in the article/**Supplementary Material**, and further inquiries can be directed to the corresponding author.

AUTHOR CONTRIBUTIONS

J-TW performed experiment conception and design. W-HL, H-YT, W-TL, and RJ performed clinical strains analysis. L-YH and L-YL performed investigation. L-YH, L-YL, T-LL, and P-FH performed data analysis. L-YH, P-FH, and J-TW wrote manuscript. All authors contributed to the article and approved the submitted version.

FUNDING

This work was supported by grants from the Ministry of Science and Technology, the Excellent Translational Medicine Research Projects of National Taiwan University College of Medicine and National Taiwan University Hospital, the Liver Disease Prevention and Treatment Research Foundation of Taiwan, Taiwan Centers for Disease Control, and the "Center of Precision Medicine" from The Featured Areas Research Center Program within the framework of the Higher Education Sprout Project by the Ministry of Education (MOE).

SUPPLEMENTARY MATERIAL

The Supplementary Material for this article can be found online at: https://www.frontiersin.org/articles/10.3389/fmicb.2020.01644/full#supplementary-material.

REFERENCES

Brossier, F., Veziris, N., Truffot-Pernot, C., Jarlier, V., and Sougakoff, W. (2006). Performance of the genotype MTBDR line probe assay for detection of resistance to rifampin and isoniazid in strains of *Mycobacterium tuberculosis* with low- and high-level resistance. *J. Clin. Microbiol.* 44, 3659–3664. doi: 10.1128/JCM.01054-06

Cambau, E., and Drancourt, M. (2014). Steps towards the discovery of *Mycobacterium tuberculosis* by Robert Koch, 1882. *Clin. Microbiol. Infect.* 20, 196–201. doi: 10.1111/1469-0691.12555

Cardoso, R. F., Cooksey, R. C., Morlock, G. P., Barco, P., Cecon, L., Forestiero, F., et al. (2004). Screening and characterization of mutations in isoniazid-resistant *Mycobacterium tuberculosis* isolates obtained in Brazil. *Antimicrob. Agents Chemother.* 48, 3373–3381. doi: 10.1128/AAC.48.9.3373-3381.2004

Chakraborty, S., and Rhee, K. Y. (2015). Tuberculosis drug development: history and evolution of the mechanism-based paradigm. *Cold Spring Harb. Perspect. Med.* 5:a021147. doi: 10.1101/cshperspect.a021147

Clinical and Laboratory Standards Institute (2011). *CLSI document M24-A2*. Wayne: Clinical and Laboratory Standards Institute.

Daum, L. T., Konstantynovska, O. S., Solodiankin, O. S., Liashenko, O. O., Poteiko, P. I., Bolotin, V. I., et al. (2018). Next-generation sequencing for characterizing drug resistance-conferring *Mycobacterium tuberculosis* genes from clinical isolates in the Ukraine. *J. Clin. Microbiol.* 56, e00009–e00018. doi: 10.1128/JCM.00009-18

Fox, H. H. (1952). The chemical approach to the control of tuberculosis. *Science* 116, 129–134. doi: 10.1126/science.116.3006.129

Islam, M. M., Hameed, H. M. A., Mugweru, J., Chhotaray, C., Wang, C., Tan, Y., et al. (2017). Drug resistance mechanisms and novel drug targets for tuberculosis therapy. *J. Genet. Genomics* 44, 21–37. doi: 10.1016/j.jgg.2016.10.002

Johnsson, K., Froland, W. A., and Schultz, P. G. (1997). Overexpression, purification, and characterization of the catalase-peroxidase KatG from *Mycobacterium tuberculosis*. *J. Biol. Chem.* 272, 2834–2840. doi: 10.1074/jbc.272.5.2834

Jou, R., Lee, W. T., Kulagina, E. V., Weng, J. Y., Isakova, A. I., Lin, W. H., et al. (2019). Redefining MDR-TB: comparison of *Mycobacterium tuberculosis* clinical isolates from Russia and Taiwan. *Infect. Genet. Evol.* 72, 141–146. doi: 10.1016/j.meegid.2018.12.031

Kandler, J. L., Mercante, A. D., Dalton, T. L., Ezewudo, M. N., Cowan, L. S., Burns, S. P., et al. (2018). Validation of novel *Mycobacterium tuberculosis* isoniazid resistance mutations not detectable by common molecular tests. *Antimicrob. Agents Chemother.* 62, e00974–e01018. doi: 10.1128/AAC.00974-18

Kurz, S. G., Furin, J. J., and Bark, C. M. (2016). Drug-resistant tuberculosis: challenges and progress. *Infect. Dis. Clin. North Am.* 30, 509–522. doi: 10.1016/j.idc.2016.02.010

Larsen, M. H., Biermann, K., Tandberg, S., Hsu, T., and Jacobs, W. R. Jr. (2007). Genetic manipulation of *Mycobacterium tuberculosis*. *Curr. Protoc. Microbiol.* Chapter 10, Unit 10A.2. doi: 10.1002/9780471729259.mc10a02s6

Laurenzo, D., and Mousa, S. A. (2011). Mechanisms of drug resistance in *Mycobacterium tuberculosis* and current status of rapid molecular diagnostic testing. *Acta Trop.* 119, 5–10. doi: 10.1016/j.actatropica.2011.04.008

Lempens, P., Meehan, C. J., Vandelannoote, K., Fissette, K., De Rijk, P., Van Deun, A., et al. (2018). Isoniazid resistance levels of *Mycobacterium tuberculosis* can largely be predicted by high-confidence resistance-conferring mutations. *Sci. Rep.* 8:3246. doi: 10.1038/s41598-018-21378-x

Li, G., Zhang, J., Guo, Q., Jiang, Y., Wei, J., Zhao, L. -L., et al. (2015). Efflux pump gene expression in multidrug-resistant *Mycobacterium tuberculosis* clinical isolates. *PLoS One* 10:e0119013. doi: 10.1371/journal.pone.0119013

Ng, V. H., Cox, J. S., Sousa, A. O., Macmicking, J. D., and Mckinney, J. D. (2004). Role of KatG catalase-peroxidase in mycobacterial pathogenesis: countering the phagocyte oxidative burst. *Mol. Microbiol.* 52, 1291–1302. doi: 10.1111/j.1365-2958.2004.04078.x

Nguyen, T. N. A., Anton-Le Berre, V., Bañuls, A. -L., and Nguyen, T. V. A. (2019). Molecular diagnosis of drug-resistant tuberculosis; a literature review. *Front. Microbiol.* 10:794. doi: 10.3389/fmicb.2019.00794

Nieto, R. L. M., Mehaffy, C., Creissen, E., Troudt, J., Troy, A., Bielefeldt-Ohmann, H., et al. (2016). Virulence of *Mycobacterium tuberculosis* after acquisition of isoniazid resistance: individual nature of katG mutants and the possible role of AhpC. *PLoS One* 11:e0166807. doi: 10.1371/journal.pone.0166807

Parish, T., and Stoker, N. G. (2000). Use of a flexible cassette method to generate a double unmarked *Mycobacterium tuberculosis* tlyA plcABC mutant by gene replacement. *Microbiology* 146, 1969–1975. doi: 10.1099/00221287-146-8-1969

Ramaswamy, S. V., Reich, R., Dou, S. J., Jasperse, L., Pan, X., Wanger, A., et al. (2003). Single nucleotide polymorphisms in genes associated with isoniazid resistance in *Mycobacterium tuberculosis*. *Antimicrob. Agents Chemother.* 47, 1241–1250. doi: 10.1128/AAC.47.4.1241-1250.2003

Rendon, A., Tiberi, S., Scardigli, A., D'ambrosio, L., Centis, R., Caminero, J. A., et al. (2016). Classification of drugs to treat multidrug-resistant tuberculosis (MDR-TB): evidence and perspectives. *J. Thorac. Dis.* 8, 2666–2671. doi: 10.21037/jtd.2016.10.14

Somoskovi, A., Parsons, L. M., and Salfinger, M. (2001). The molecular basis of resistance to isoniazid, rifampin, and pyrazinamide in *Mycobacterium tuberculosis*. *Respir. Res.* 2, 164–168. doi: 10.1186/rr54

Song, H., Sandie, R., Wang, Y., Andrade-Navarro, M. A., and Niederweis, M. (2008). Identification of outer membrane proteins of *Mycobacterium tuberculosis*. *Tuberculosis* 88, 526–544. doi: 10.1016/j.tube.2008.02.004

Sotgiu, G., Centis, R., D'ambrosio, L., and Migliori, G. B. (2015). Tuberculosis treatment and drug regimens. *Cold Spring Harb. Perspect. Med.* 5:a017822. doi: 10.1101/cshperspect.a017822

Sreevatsan, S., Pan, X., Zhang, Y., Deretic, V., and Musser, J. M. (1997). Analysis of the oxyR-ahpC region in isoniazid-resistant and -susceptible *Mycobacterium tuberculosis* complex organisms recovered from diseased humans and animals in diverse localities. *Antimicrob. Agents Chemother.* 41, 600–606. doi: 10.1128/AAC.41.3.600

Steinhauer, K., Eschenbacher, I., Radischat, N., Detsch, C., Niederweis, M., and Goroncy-Bermes, P. (2010). Rapid evaluation of the mycobactericidal efficacy of disinfectants in the quantitative carrier test EN 14563 by using fluorescent *Mycobacterium terrae*. *Appl. Environ. Microbiol.* 76, 546–554. doi: 10.1128/AEM.01660-09

Tsolaki, A. G., Gagneux, S., Pym, A. S., Goguet De La Salmoniere, Y. -O. L., Kreiswirth, B. N., Van Soolingen, D., et al. (2005). Genomic deletions classify the Beijing/W strains as a distinct genetic lineage of *Mycobacterium tuberculosis*. *J. Clin. Microbiol.* 43, 3185–3191. doi: 10.1128/JCM.43.7.3185-3191.2005

Unissa, A. N., Subbian, S., Hanna, L. E., and Selvakumar, N. (2016). Overview on mechanisms of isoniazid action and resistance in *Mycobacterium tuberculosis*. *Infect. Genet. Evol.* 45, 474–492. doi: 10.1016/j.meegid.2016.09.004

Vilchèze, C., and Jacobs, W. R. Jr. (2014). Resistance to isoniazid and ethionamide in *Mycobacterium tuberculosis*: genes, mutations, and causalities. *Microbiol. Spectr.* 2. doi: 10.1128/microbiolspec.MGM2-0014-2013

WHO (2019). *Global tuberculosis report 2019*. World Health Organization.

Yao, C., Zhu, T., Li, Y., Zhang, L., Zhang, B., Huang, J., et al. (2010). Detection of rpoB, katG and inhA gene mutations in *Mycobacterium tuberculosis* clinical isolates from Chongqing as determined by microarray. *Clin. Microbiol. Infect.* 16, 1639–1643. doi: 10.1111/j.1469-0691.2010.03267.x

Zenteno-Cuevas, R., Cuevas-Cordoba, B., and Parissi-Crivelli, A. (2019). rpoB, katG and inhA mutations in multi-drug resistant strains of *Mycobacterium tuberculosis* clinical isolates from Southeast Mexico. *Enferm. Infecc. Microbiol. Clin.* 37, 307–313. doi: 10.1016/j.eimc.2018.09.002

Zhang, Y., Heym, B., Allen, B., Young, D., and Cole, S. (1992). The catalase-peroxidase gene and isoniazid resistance of *Mycobacterium tuberculosis*. *Nature* 358, 591–593. doi: 10.1038/358591a0

Conflict of Interest: The authors declare that the research was conducted in the absence of any commercial or financial relationships that could be construed as a potential conflict of interest.

frontiers in Microbiology

ORIGINAL RESEARCH
published: 10 September 2020
doi: 10.3389/fmicb.2020.537935

New Conjugated Compound T5 Epidioxy-Sterol-ANB Inhibits the Growth of *Mycobacterium tuberculosis* Affecting the Cholesterol and Folate Pathways

Andres Baena[1], Emanuel Vasco[1], Manuel Pastrana[2], Juan F. Alzate[3,4], Luis F. Barrera[1] and Alejandro Martínez[2]*

[1] Grupo de Inmunología Celular e Inmunogenética, Facultad de Medicina, Universidad de Antioquia, Medellín, Colombia, [2] Grupo de Productos Naturales Marinos, Facultad de Ciencias Farmacéuticas y Alimentarias, Universidad de Antioquia, Medellín, Colombia, [3] Grupo de Parasitología, Facultad de Medicina, Universidad de Antioquia, Medellín, Colombia, [4] Centro Nacional de Secuenciación Genómica, Facultad de Medicina, Universidad de Antioquia, Medellín, Colombia

OPEN ACCESS

Edited by:
Maria Rosalia Pasca, University of Pavia, Italy

Reviewed by:
Vikram Saini, All India Institute of Medical Sciences, India
Evgeniya V. Nazarova, Genentech, United States

***Correspondence:**
Andres Baena
andres.baenag@udea.edu.co

Specialty section:
This article was submitted to Antimicrobials, Resistance and Chemotherapy, a section of the journal Frontiers in Microbiology

Received: *25 February 2020*
Accepted: *13 August 2020*
Published: *10 September 2020*

Citation:
Baena A, Vasco E, Pastrana M, Alzate JF, Barrera LF and Martínez A (2020) New Conjugated Compound T5 Epidioxy-Sterol-ANB Inhibits the Growth of Mycobacterium tuberculosis Affecting the Cholesterol and Folate Pathways. Front. Microbiol. 11:537935. doi: 10.3389/fmicb.2020.537935

The upsurge and persistence of drug resistant strains of *Mycobacterium tuberculosis* (Mtb) is an important limitant to the battery of drugs available for the elimination of tuberculosis (TB). To avoid future scarcity of antibiotics against Mtb, it is important to discover new effective anti-mycobacterial agents. In this study, we present data from a series of experiments to determine *in vitro* and *in vivo* anti-mycobacterial activity of a library of epidioxy-sterol analogs. We test 15 compounds for their ability to reduce the viability of Mtb. We found that one compound called T5 epidioxy-sterol-ANB display significant potency against Mtb *in vitro* specifically inside macrophages but without effectivity in axenic cultures. A viability assay confirms that this T5 compound is less toxic for macrophages *in vitro* as compared to the current Mtb drug Rifampicin at higher concentrations. We use a transcriptomic analysis of Mtb inside macrophages after T5 epidioxy-sterol-ANB treatment, and we found a significant down-regulation of enzymes involved in the cholesterol and folic acid pathways. *In vivo*, significant differences were found in the lungs and spleen CFUs of Mtb infected mice treated with the T5 epidioxy-sterol-ANB as compared with the untreated control group, which provides additional evidence of the effectivity of the T5 compound. Altogether these results confirm the potential of this T5 epidioxy-sterol-ANB compound against Mtb.

Keywords: antimicobacterial, macrophages, cholesterol pathway, folic acid pathway, *Mycobacterium tuberculosis*

INTRODUCTION

Tuberculosis (TB), produced by *Mycobacterium tuberculosis* (Mtb), is the primary cause of death worldwide due to an infectious agent (McShane, 2019). In 2018, TB killed 1.5 million people, and 10 million were infected in the same year (World Health Organization [WHO], 2018). The worldwide prevalence of TB is sustained by the continuing HIV-AIDS pandemic, widespread antibiotic multi-drug-resistant (MDR) strains, and extensively drug-resistant (XDR) strains and poverty. Also, more

than half of a million cases of rifampicin resistant TB were reported annually, with nearly 78% of those cases being MDR-TB. In addition, WHO statistics reported that about 1 in 3 deaths of TB are due to antimicrobial resistance (World Health Organization [WHO], 2018).

TB requires treatment with a combination of drugs; four anti-TB drugs taken for 6 months are required for the most drug-sensitive forms of TB (Lange et al., 2019). Treatment for MDR-TB and XDR-TB has been demonstrated to be lengthy and complicated; usually for XDR-TB patients the treatment consists of a combination of at least eight drugs, in some cases involving daily injections, for 18 months or even longer (Pontali et al., 2019). In 2019, the US Food and Drug Administration (FDA) approved the new BPaL regimen containing the drugs pretomanid, bedaquiline, and linezolid (Burki, 2019). In the Nix-TB trial in South Africa, this drug combination cured within just 6 months up to 90% of XDR tuberculosis with 5 pills a day (Nunn et al., 2019).

The development of new antibiotics by the pharmaceutical industry had mostly been stuck due to economic and regulatory hurdles (Spellberg, 2014; Anonymous., 2019). When new drugs against infectious diseases are used, the emergence of resistance is almost inevitable. Though bacterial evolution is unpredictable, the timeline for the development of resistance is uncertain. Different mechanisms have been associated with antibiotic resistance that includes mutations in genes targeted by antibiotics, the degradation or modification of antibiotics by the bacteria, the overexpression of efflux pumps to reduce the uptake of antibiotics, and alterations of the cell wall by osmoregulation in the phagosome (Larrouy-Maumus et al., 2016; Gygli et al., 2017; Laws et al., 2019). Intracellular persistence within macrophages is an essential feature of Mtb pathogenesis (Baena and Porcelli, 2009; Queval et al., 2017). When Mtb is inside macrophages it normally replicates in phagosomes, which are believed to be a restricted and stressful environment (Ehrt and Schnappinger, 2009; Bussi and Gutierrez, 2019). To be able to replicate in this closed environment, Mtb utilizes particular metabolic pathways to obtain host-derived nutrients (Lopez-Agudelo et al., 2017; Baena et al., 2019; Mashabela et al., 2019). A variety of transcriptional profiling studies in macrophages have indicated that lipid metabolism and cholesterol are important for Mtb survival (Aguilar-Ayala et al., 2017; Zimmermann et al., 2017; Baena et al., 2019; Lee et al., 2019). Additionally, genes involved in cholesterol utilization, gluconeogenesis, or the methyl citrate cycle (MCC) are required for full Mtb virulence during infection; mutants in some genes along these metabolic pathways fail to establish infection in macrophages (Joshi et al., 2006; Pandey and Sassetti, 2008; Miner et al., 2009; Russell, 2011; Griffin et al., 2012; Lopez-Agudelo et al., 2017; Fieweger et al., 2019). Based on this information, the central carbon metabolic pathways of Mtb are thought to be potential targets for TB drug discovery. An important study showed a structurally diverse set of compounds that target the Mtb cholesterol pathway that causes growth restriction of the bacteria inside macrophages but not in axenic cultures in the absence of cholesterol (VanderVen et al., 2015).

In summary, it is vital to unveil new drugs to treat TB that inhibit new biological targets and pathways. Identifying small molecules that are capable of inhibiting specific enzymatic targets in Mtb using target-based screens is still challenging. In this report we used a chemical library screen to identify new compounds that inhibit Mtb replication during infection inside macrophages, which allow us to identify the T5 epidioxy-sterol-ANB compound with a good anti-mycobacterial activity. The T5 compound is the result of the conjugation of the 4-nitrobenzoic acid (ANB) and the 5α,8α-epidioxy-3β-cholesterol. Although there are a few reports in the literature showing some activity of these molecules, none of them have been used *in vivo* in animal models for tuberculosis (Cateni et al., 2007; Giampaglia et al., 2007). Here we show *in vivo* activity and a metabolic effect of this T5 compound that suggest that it may inhibit simultaneously the cholesterol degradation and folic acid synthesis pathways in Mtb.

MATERIALS AND METHODS

Bacteria and Plasmid

H37Rv was grown at 120 rpm in a shaker at 37°C in a square bottle containing 10 ml of 7H9 (Difco, Sparks, MD. United States) supplemented with 10% of oleic acid-albumin-dextrose-catalase (OADC) (Becton Dickinson Microbiology Systems, NJ, United States), 0.5% Glycerol (Sigma, Saint Louis, MO, United States), and 0.05% Tyloxapol (Sigma, Saint Louis, MO, United States), to an optical density of 0.5 at $OD_{600\ nm}$. H37Rv-pMV261.kan-GFP was grown in the presence of 50 μg/ml of kanamycin. The pMV261.kan-GFP is a multicopy plasmid under the control of the hsp60 that expresses GFP.

Compound Library Synthesis

Syntheses of the 5 epidioxy steryl esters were done in two steps. The first step is the synthesis of the compound 1, 5α,8α-epidioxy-3β-cholesterol, by the photochemical reaction of 7-dehydrocholesterol with oxygen mediated by eosine like *photosensitizer* (Feng et al., 2007). In this reaction the endoperoxide group was formed in positions C-5 and C-8 in a [4 + 2] cycloaddition reaction. The aromatic esters were done by the Steglich methodology with compound 1 using DCC and DMAP in $CHCl_3$ with different aromatic acids (Farshori et al., 2010) (**Supplementary Figure S1**).

NMR of Compound T5

The NMR experiments were obtained in CDCl3 using a Bruker spectrometer AVANCE III NMR operating at 600 MHz for 1H and 150 MHz for 13C.

^{1}H NMR (600 MHz, Chloroform-d) δ 9.22 (d, J = 2.1 Hz, 1H), 9.14 (d, J = 2.2 Hz, 2H), 6.56 (d, J = 8.5 Hz, 1H), 6.29 (d, J = 8.5 Hz, 1H), 5.36 (q, J = 11.2, 5.1 Hz, 1H), 2.31 (ddd, J = 13.6, 5.6, 1.7 Hz, 1H), 2.26 (dd, J = 13.6, 11.6 Hz, 1H), 2.16 – 2.07 (m, 2H), 2.05 – 1.98 (m, 1H), 1.98 – 1.89 (m, 1H), 1.85 – 1.74 (m, 2H), 1.65 (m, J = 11.6, 9.0, 8.1, 2.5 Hz, 1H), 1.61 – 1.49 (m, 4H), 1.49 – 1.39 (m, 1H), 1.41 – 1.36 (m, 1H), 1.39 – 1.30 (m, 2H), 1.30 – 1.17 (m, 3H), 1.14 (s, 2H), 1.19 – 1.07 (m, 2H), 1.06 – 0.98 (m, 1H), 0.98 (s, 3H), 0.91 (d, J = 6.5 Hz, 3H), 0.87 (dd, J = 6.7, 2.9 Hz, 7H), 0.85 (s, 3H), 0.82 (s, 3H).

^{13}C NMR (151 MHz, Chloroform-d) δ 148.61, 134.70, 131.24, 129.45, 122.29, 81.75, 79.62, 72.74, 56.39, 51.47, 50.97, 44.77, 39.42, 39.35, 36.99, 35.93, 35.22, 34.27, 33.13, 28.24, 27.99, 26.30, 23.78, 23.42, 22.81, 22.55, 20.60, 18.57, 18.12, 12.65.

Cell Viability Assay

The AMJ2-C8 macrophages were infected at an MOI of 10:1. Cell viability was determined by fluorescence microscopy. After 48 hrs of treatment with the compound library, the treated cells were stained with Acridine Orange (AO) and Propidium Iodide (PI) in PBS (4 mg/ml). AO is excited at wavelengths near 502 nanometers (nm) when intercalated with dsDNA, emitting a green fluorescence with wavelengths of approximately 525 nm. AO stains acidic compartments such as lysosomes, where it becomes sequestered and protonated in live cells. Within this low lysosomal pH, the vesicles emit red fluorescence when loaded with the dye. When cells have an affected plasma membrane integrity, the PI is permeable and emits red fluorescence in the nucleus once it is intercalated with the DNA, which is excited at wavelengths of approximately 535 nm and fluoresces in the spectrum of 617 nm. Thus, cell viability could be assessed by the differential uptake of both dyes. The method for the cell viability quantification is showed in **Supplementary Figure S4**.

MTT Assay

The MTT (3-[4,5-dimethylthiazol-2-yl]-2,5 diphenyl tetrazolium bromide) assay is founded on the conversion of MTT into formazan crystals by viable bacteria, which determines succinate dehydrogenase activity. The MTT assay was carried out as described before (Mshana et al., 1998). Briefly, in a 96 well plate we put 5×10^7 bacteria (H37Rv) with 40 μL of culture medium into each well, and then each compound was added at different concentrations diluted with DMSO. We performed three independent experiments for each compound concentration. The plates were incubated at 37°C for 48 h. The compound MTT (Sigma, St. Louis, MO, United States) was dissolved in PBS (pH 7.2) to get a final concentration of 5 mg/ml. Following, 10 μL of the MTT solution was added to each well in the plate and incubated for 4 h at 37°C. Finally, 50 μL of a lysing buffer (20% sodium dodecyl sulfate in 50% *N1N*-dimethylformamide [pH 4.7]) was added to each well, and the plates were incubated overnight. The absorbance was measured with a spectrophotometer at a wavelength of 570 nm. The H37Rv bacteria was grown as described above in the bacteria and plasmid section. CFU counts of H37Rv axenic culture after 48 h of treatment with the T5 and Rifampicin compounds were determined in 7H10 agar plates.

Macrophage Cell Lines and Mtb Infection

The AMJ2-C8 murine alveolar macrophage cell line was obtained as a gift from Steven A. Porcelli at the Albert Einstein College of Medicine. The cells were grown in DMEM supplemented with 10% FBS, 1X Pen/strep, 0.05 mM of 2-mercaptoethanol, and 1X NEAA.

The THP-1 cell line was obtained from ATCC (TIB-202) and maintained in sterile RPMI-1640 medium supplemented with 10% FBS, 1X Pen/strep, 0.05 mM of 2-mercaptoethanol, and 1X NEAA. For differentiation 2×10^6 THP-1 cells were seeded per well in a 6-well plate and differentiated to macrophages for 48 h, in the presence of 100 ng/ml PMA (162 nM). After a resting period of 24 h, macrophages were then infected with Mtb H37Rv for 4 h at a multiplicity of infection (MOI) of 10:1, and incubated for 4 and 20 h (RNA-seq experiments) and also for 48 h (CFUs experiments in the presence of the T5 and rifampicin compounds), at 37°C with 5% CO_2. To measure the survival of the cell-associated Mtb-H37Rv, THP-1 cells were lysed in 1.5 mL of distilled water with 1% SDS to collect the intracellular bacteria. The lysates were serially diluted in 7H9 broth, plated on 7H10 agar plates, and incubated for 3 weeks at 37°C. Colony counting was then performed in triplicate.

In vivo Experiment With the T5 Compound

Female wild type Balb/C mice (6–8 weeks of age) were used in the experiment and maintained under a sterile BSL3 facility. Four mice per group were infected with 2×10^5 bacteria intra peritoneal (i.p) in 200 μL of PBS with 0.05% Tween 80. The amount of bacteria during the challenge was verified by plating the inoculum on 7H10 plates. After 4 days of infection, the mice were treated with the T5 compound or the vehicle. The mice received 550 μg/200 μL of T5 compound daily by i.p injection (25 mg/Kg). On day 32, the mice were sacrificed, and the lungs and spleens were smashed and plated in 7H10 media plates. After 24 days, the CFUs were estimated. All experiments were performed in accordance with the Ethics Committee for Animal Experiments (CEEA) of the University of Antioquia.

RNA Extraction

The Mtb infected THP-1 cells were lysed at 4°C by adding 1 ml of RLT buffer (RNeasy Plus mini kit, QIAGEN, Hilden, Germany). We maintained the lysates frozen in liquid nitrogen for 15 s and then the lysates were homogenized for 20 s with a tissue tearor homogenizer (Biospec, Bartlesville, OK, United States; model 985–370 at 5,000 rpm). The homogenization procedure was repeated two times with an intermediate incubation of 1 min on ice. Next, the lysates were transferred to an Eppendorf 1.5-ml tube where they were disrupted using bead beating (Bead beater Instrument; applying six cycles of 30 s at maximum speed with cooling on ice between the different cycles) using high impact zirconium-silica beads (BenchmarkScientific, Bartlesville, OK, United States). Following this, the samples were centrifuged at 10,000 rpm for 10 min at 4°C. Finally, we used the aqueous phase to extract the total RNA with the Qiagen RNeasy plus mini kit, which includes the DNA retention column according to the manufacturer's instructions. We performed three independent experiments for each condition, and the extracted RNA was pooled for its related replicates. The RNA Integrity Number (RIN) was determined by a Bioanalyzer 2000 instrument; values for all the samples were between 8.1 and 8.6.

RNA-seq

RNA-seq libraries were sequenced using an Illumina platform (Macrogen, South Korea). The libraries for the RNA-seq were

generated using the TruSeq®RNA-Sample-Preparation Kitv2 following the manufacturer instructions (Illumina, Inc., San Diego, CA, United States). Briefly, the sequencing library is prepared by random fragmentation of the RNA sample, followed by 5′ and 3′ adapter ligation. The libraries started with double-stranded cDNA synthesized from RNA with insert sizes from 300–500 bp that are used for paired-end sequencing. Blunt-end DNA fragments are produced using a combination of fill-in reactions and exonuclease activity. An 'A'- base is then added to the blunt ends of each strand, preparing them for ligation to the sequencing adapters. Each adapter contains a 'T'-base overhang on 3′-end providing a complementary overhang for ligating the adapter to the A-tailed fragmented DNA. These newly redesigned adapters contain the full complement of sequencing primer hybridization sites for single, paired-end, and multiplexed reads. rRNA from macrophages and bacteria was depleted (Illumina Ribo-Zero Gold rRNA Removal Kit -Epidemiology), and sequencing was performed (TrueSeq, stranded, paired-end reads of 100 bp). The "clean" read dataset (clean reads refer to reads that passes the process of adapter removal, low quality bases removal at both ends [<Q30] and that after this two process the reads retain a minimum length of 70 bases) was used in order to map to the reference genome of the H37Rv strain of Mtb (AL123456_update130713), using the software BOWTIE2 with the default settings. We converted the SAM file to BAM, and then we sorted and indexed the reads using SAMTOOLS. Reads counts assigned to each gene present in the reference Mtb strain were done by means of the HTSEQ script with the stranded option. Next, we used the R package EDGER for the differential expression analysis, following the directions of the software authors for the different RNA-seq experiments. We stablished the coefficient of biological variation to 0.3, due to the lack of library replicates. The results of the EDGER analysis were printed as graphs and tables. The RNA-seq transcriptomic data was deposited in https://www.ncbi.nlm.nih.gov/bioproject: DMSO 4 h, BaenaRNA1_1.fastq.gz (SRR11195990); DMSO

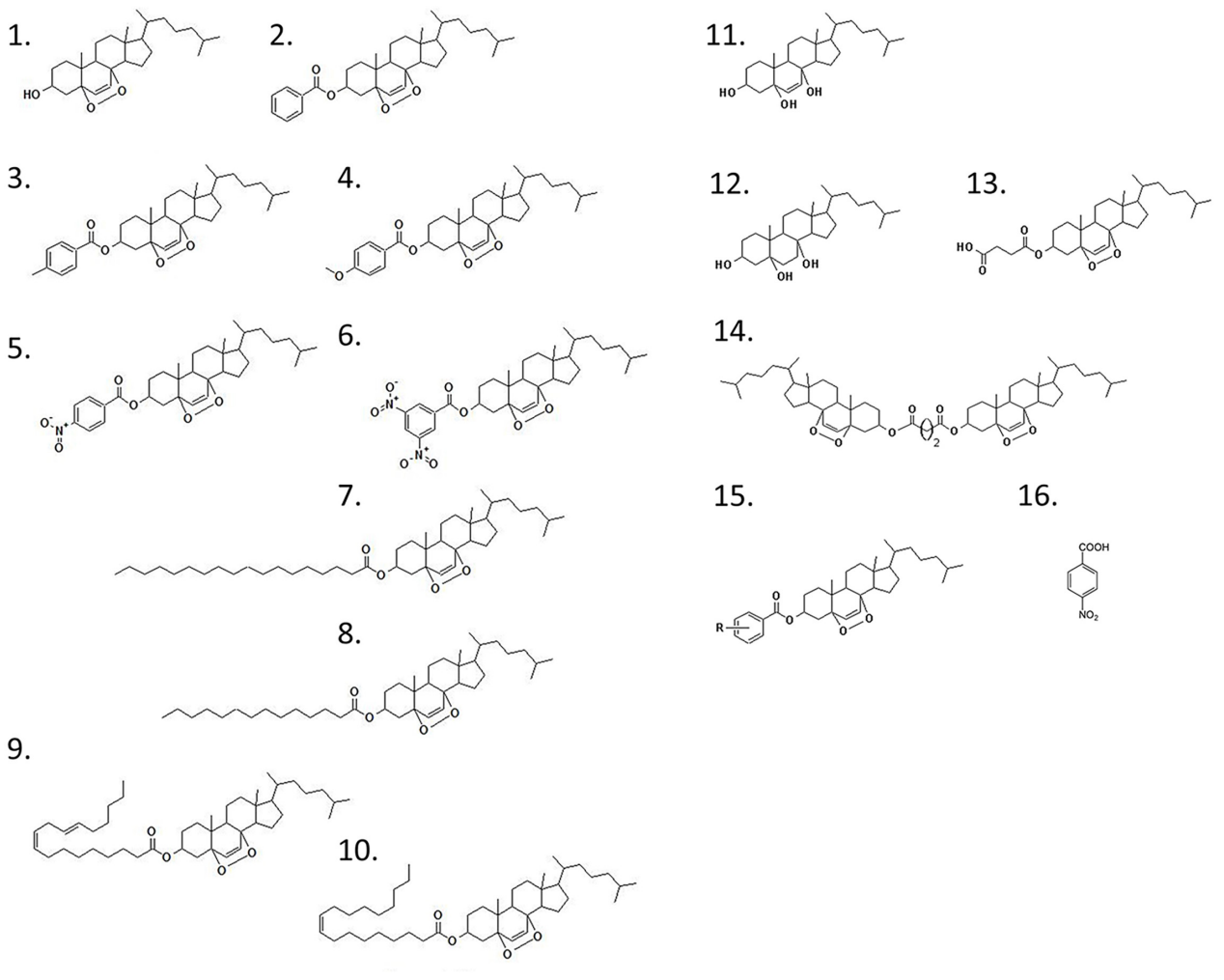

FIGURE 1 | Chemical structure of the epidioxy-sterol analogs. This compound library started with the compound 1 (T1) that corresponded to a 5α,8α-epidioxy-3β-cholesterol. The other compounds are called after the addition of a second (R) group from which we have generated the compounds 1–15 that in this paper we called T1–T15. The compound 16 is the 4-nitrobenzoic acid (ANB).

20 hrs, BaenaRNA3_1.fastq.gz (SRR11195989); T5 4 h, BaenaRNA2_1.fastq.gz (SRR11195988); and T5 20 h, BaenaRNA4_1.fastq.gz (SRR11195987).

RESULTS

The T5 Compound Has Anti-mycobacterial Activity

Previous reports have shown that epidioxy-sterols-like compounds have activity against Mtb (Saludes et al., 2002; Cateni et al., 2007; Duarte et al., 2007; Zhou et al., 2015). Thus, we decided to evaluate the activity of a unique library of 15 epidioxy-sterol analog conjugated compounds against this bacterium (**Figure 1**). For this purpose, we implemented an assay using H37Rv containing a plasmid that expresses GFP under a constitutive promoter. In this assay, Mtb replicates in the THP-1 macrophages and constitutively produces GFP. In the presence of an anti-mycobacterial compound GFP fluorescent signal is quenched in a concentration-dependent manner, as we observed with the positive control drug Rifampicin (**Figures 2A,B**). A similar strategy was previously used in the discovery of novel inhibitors of cholesterol degradation pathway in Mtb (VanderVen et al., 2015). The only compound that showed good activity in the infected THP-1 macrophages was the T5 compound, evidenced in the low IC_{50} of 0.116 μg/mL (0.2 μM) although 6.7 times higher than rifampicin that showed an IC_{50} of 0.024 μg/mL (0.03 μM) (**Figures 2C,D**). As we mentioned above, this T5 compound is the result of conjugation of the compound T1 and ANB. In contrast to T5, the compound T1 and ANB showed very low activity against Mtb (**Figures 2C,D**). Similar results were obtained by using the murine alveolar macrophage cell line AMJ2-C8 (data not showed). To confirm this result, we evaluate the Mtb viability

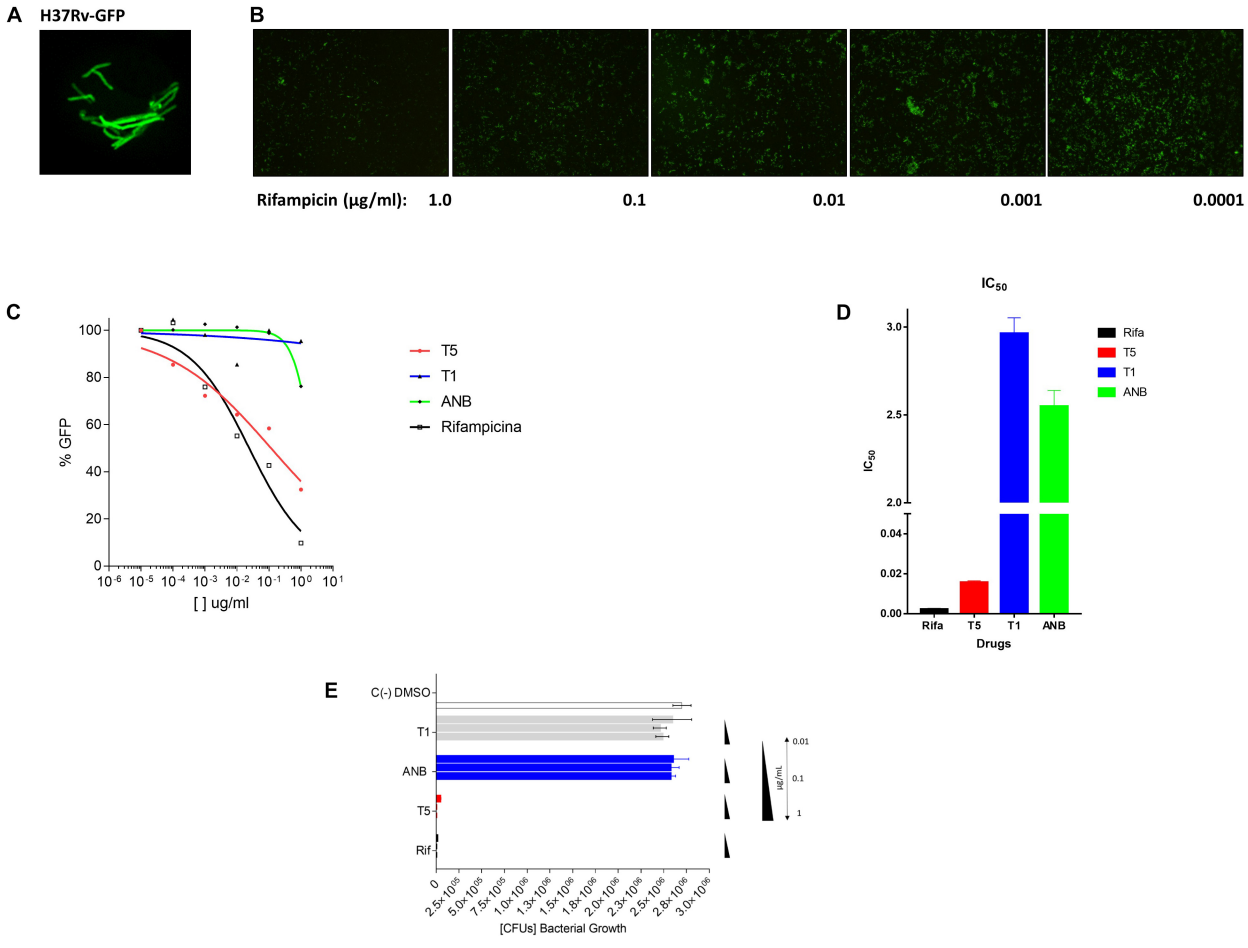

FIGURE 2 | Inhibitory assay for the selection of compound analogs with activity against Mtb. **(A)** The Mtb bacteria H37Rv expressing the plasmid pMV261-GFP. **(B)** Inhibitory effect of Rifampicin (48 h) in the expression of GFP after the Mtb infection (4 h) of the THP-1 macrophage cell line. The panel shows 5 concentrations of the rifampicin compound. **(C)** Inhibitory GFP curves for the compound T5 relative to the compound T1, ANB, and the control compound rifampicin after 48 h of treatment post-infection. **(D)** Inhibitory concentration 50 (IC_{50}) calculated based on the inhibitory curves. **(E)** The colony forming units (CFUs) that resulted after the lysis of the infected THP-1 cell line. The molecular weight (g/mol) of the compounds is as follow: T1 (416.6), T5 (565.7), ANB (167.11), and rifampicin (822.94). The equivalent molar concentration to the μg/mL used in the assays (1, 0.1, 0.01, 0.001, and 0.0001) for the different compound are: T1 (2.4, 0.24 μM, 24, 2.4, and 0.24 nM), T5 (1.7, 0.17 μM, 17, 1.7, and 0.17 nM), ANB (6, 0.6 μM, 60, 6, and 0.6 nM), and for rifampicin (1.2, 0.12 μM, 12, 1.2, and 0.12 nM).

by lysing the macrophages and plating the recovered bacteria and counted CFUs. The data shows undetectable CFUs at as low as 0.1 μg/ml, which is comparable to the treatment of Rifampicin (**Figure 2E** and **Supplementary Figure S2**). Thus, both the sterol ring and the ANB together in the T5 compound are required for effective anti-mycobacterial activity. We next analyzed the effectivity of the library compounds against an axenic Mtb culture. While the ANB compound has an anti-mycobacterial activity, the T5 compound did not show any significant activity under this experimental condition (**Figures 3A,B**). We confirmed this result with the CFU measurement in which rifampicin is able to reduce the bacterial numbers significantly but the result with the T5 compound is similar to the negative control (**Figure 3C**). The ANB also known as 4-nitrobenzoic acid was previously shown to have anti-mycobacterial activity against Mtb in axenic cultures in the diagnostic setting, but there is no data showing if the compound is effective inside macrophages (Giampaglia et al., 2007). Thus, we have a T5 compound with effective anti-mycobacterial activity inside macrophages but with no activity against extracellular bacteria. This could suggest that a particular processing condition inside the macrophage (e.g., activating

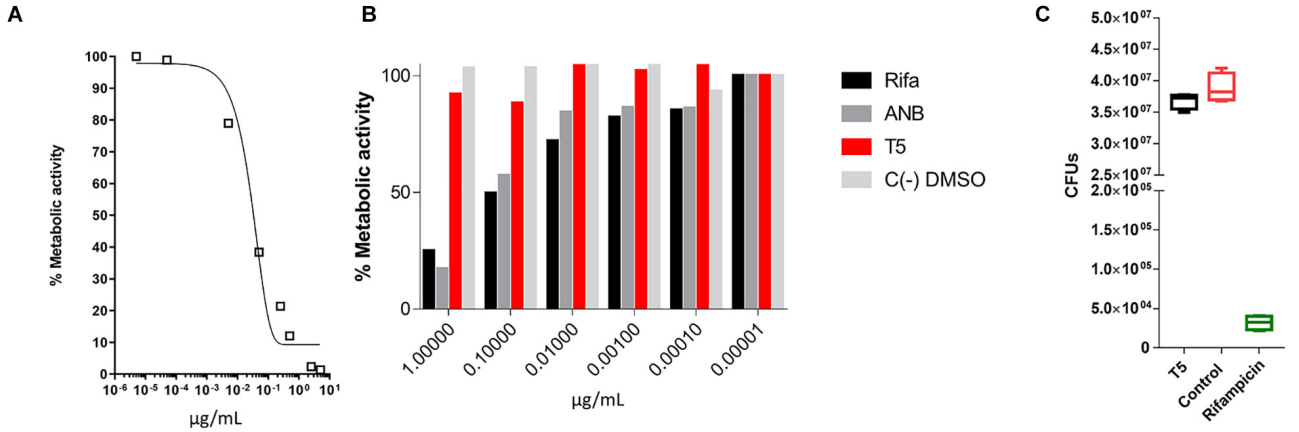

FIGURE 3 | MTT assay to evaluate the inhibitory capacity of the T5 compound against an axenic culture of Mtb. **(A)** Evaluation of the% metabolic activity of the control compound rifampicin by the MTT assay *in vitro* for 48 h, against an axenic culture of Mtb. **(B)** Determination of the % metabolic activity based on the MTT assay of the T5 compound relative to the control compounds ANB and rifampicin at different concentrations. **(C)** CFU counts of H37Rv axenic culture after 48 h of treatment with the T5 and Rifampicin compounds. The optical density values (OD) obtained in the MTT assay were converted to percentage of metabolic activity relative to the DMSO control treatment which represent 100% of metabolic activity.

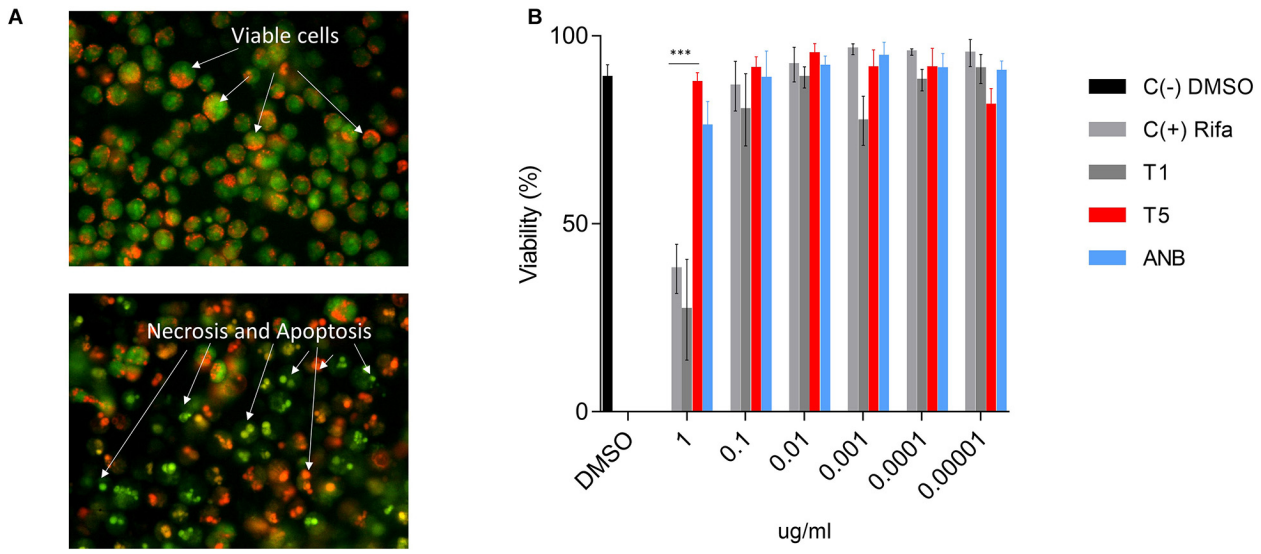

FIGURE 4 | Cytotoxicity assay for T5 compound in the AMJ2-C8 cell line. **(A)** A representation of healthy and viable cells (no treatment) and cells treated with a high concentration of rifampicin (1 μg/mL). The cells were stained with acridine orange (AO) and propidium iodide (PI). **(B)** Viability (%) of the AM cell line after 48 h treatment with the T5 compound relative to the control compounds T1, ANB, and Rifampicin. ***p-value < 0.0001. We are showing data of a representative experiment from four independent ones.

enzymes) may be required to transform the T5 compound in order to work against Mtb.

The T5 Compound Has Low Cell Toxicity at Higher Concentrations

Cytotoxicity of the T5 compound was tested using the AMJ2-C8 macrophage cell line by staining the cells with AO and PI (**Figure 4A**). We used a range of concentrations (0.0001, 0.001, 0.01, 0.1, and 1 μg/ml) of the T5 as well as for T1 and ANB compounds, Rifampicin and DMSO, as the positive negative controls respectively. We found that while the T1 and Rifampicin are highly toxic at the higher concentration of 1 μg/mL, the T5 compound showed low cytotoxicity at the same concentration (**Figure 4B**). This is an interesting result because it is expected that any new candidate compound has low toxicity, which could be associated with fewer side effects for future experiments such as the experimentation in animal models.

The Transcriptome of Infected THP-1 Cells Treated With the T5 Compound

In order to precisely define the genes in Mtb and in the THP-1 macrophages, which are affected by the T5 compound, we performed a dual transcriptome by RNA-seq. The macrophages were infected for 4 and 20 h and then the total RNA was extracted and sequenced (methods section, **Supplementary Figure S3**). Using $\log_2FC > 2.0$, $\log_2FC < -2.0$, and a p-value < 0.05 as

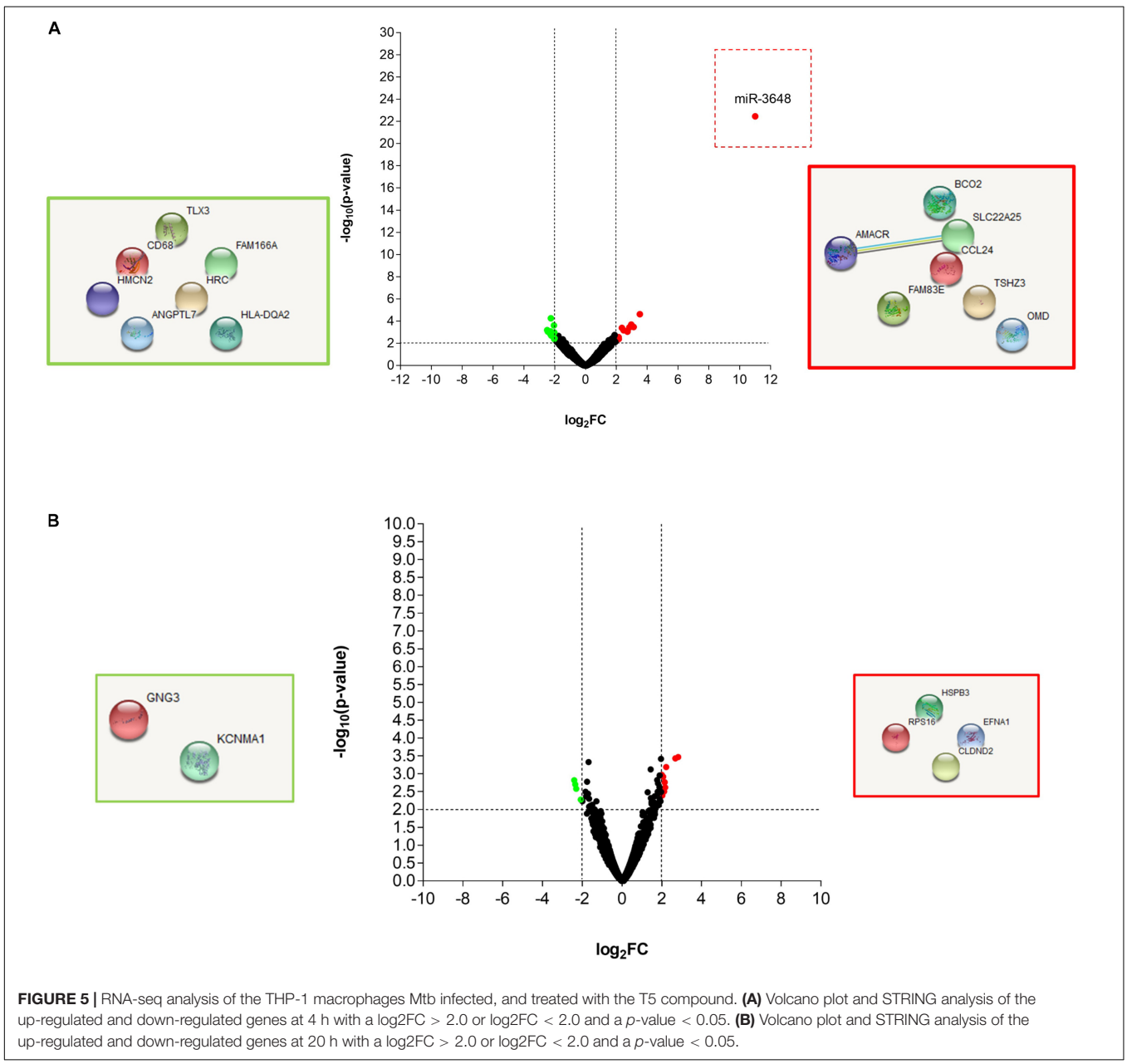

FIGURE 5 | RNA-seq analysis of the THP-1 macrophages Mtb infected, and treated with the T5 compound. **(A)** Volcano plot and STRING analysis of the up-regulated and down-regulated genes at 4 h with a log2FC > 2.0 or log2FC < 2.0 and a *p*-value < 0.05. **(B)** Volcano plot and STRING analysis of the up-regulated and down-regulated genes at 20 h with a log2FC > 2.0 or log2FC < 2.0 and a *p*-value < 0.05.

selection criteria for differentially expressed genes, we found that macrophages expressed very few genes up-regulated and down-regulated in response to the T5 compound either at 4 or 20 h post-treatment (**Figures 5A,B**). The most noticeable up-regulated gene at 4 h was miR-3648 with a $\log_2$FC > 10 (**Figure 5A**). This gene was shown to be involved in the negative regulation of the adenomatous polyposis coli 2 (*APC2*) that is expressed in different cell lines and is a tumor suppressor gene (Rashid et al., 2017). Thus, the reduced levels of *APC2* may result in an increased expression of the Wnt/β-catenin signaling pathway genes, and promotes cell proliferation. Another interesting up-regulated gene is the BCO2 that encodes for a β-carotene-9′, 10′-oxygenase 2 (**Figure 5A**). The increased expression of BCO2 may confer and increase survival since its knockdown causes an increment in apoptosis due to its protective role to oxidative stress (Ref: Lei woo, Exp Biol Med [Maywood], 2016). Also, we have the up-regulation of the EFNA1 gene that codes for the Ephrin A1 protein, which is a member of the A-type ephrin family and has been implicated as a negative inductor of apoptosis (Ref: Spencer Alford, Cancer Cell Int. 2010). The up-regulation of the genes miR-3648, BCO2, and EFNA1 by the T5 compound could be associated with its lower cytotoxicity.

Transcriptome of Mtb Treated With the T5 Compound Affects the Cholesterol and Folic Acid Pathways

While the transcriptome of the macrophage remained mostly unaffected by the treatment of the T5 compound, the Mtb transcriptome showed a significant number of up-regulated and down-regulated genes (**Figures 6A,B**). To find out which were the most affected pathways in Mtb under the treatment of the T5 compound, we used the Mtb pathway/genome from the BioCyc database collection[1] (version 23.1). Using this approach, we found a significant down-regulation of enzymes involved in the cholesterol and folic acid pathways like the para-aminobenzoate synthase (pabB) (**Figures 7A,B**). In addition, we found a significant up-regulation of the ammonium-transport integral protein (*Amt*), which is important for detoxification of the bacteria from the accumulation of ammonia (**Figure 7C**).

The Compound T5 Reduces the Mtb CFUs in the Mouse Model

To validate the anti-mycobacterial activity of the T5 compound, we did a pilot *in vivo* experiment using Balb/C mice. In this experiment we observed that the T5 compound cause a significant 2–3 fold reduction of the Mtb CFUs in the lungs as well as in the spleen of the treated mice, as compared to the control vehicle treated group (**Figures 8A,B**). We did not observe significant differences in weight of the animals at the end of the treatment and 15 days post-infection between the T5 treated mice and the control group (**Figure 8C**). In summary, these findings suggest that this T5 compound is not only active *in vitro* but also *in vivo*.

DISCUSSION

One difficulty in TB drug discovery arises from a limited knowledge of the physiological environment and growth

[1]https://biocyc.org/organism-summary?object=MTBH37RV

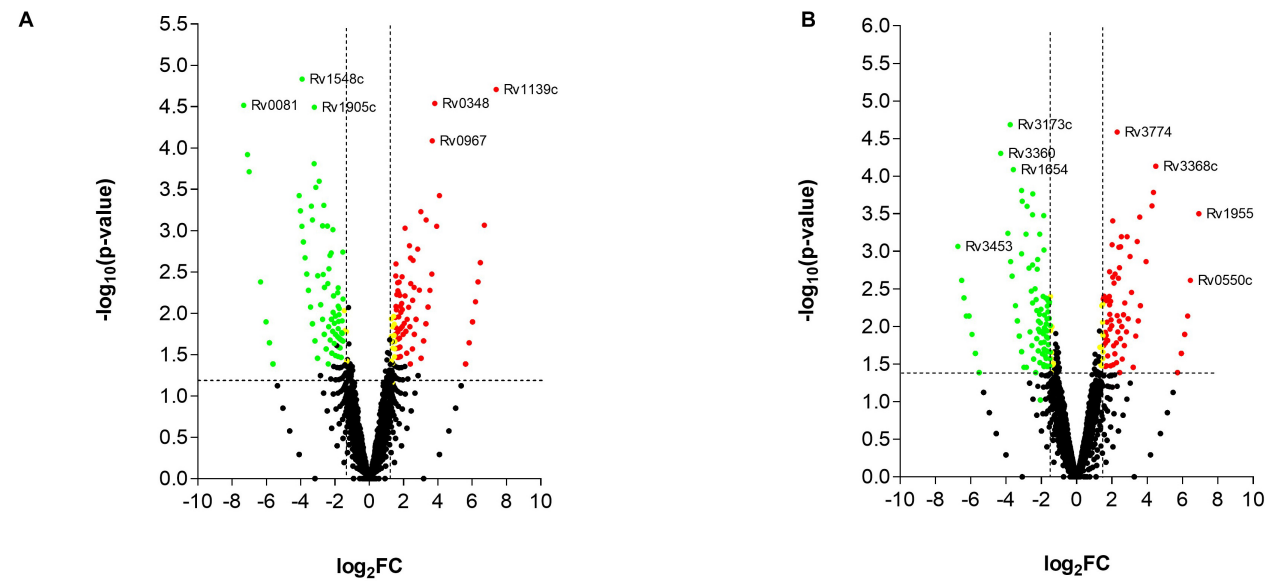

FIGURE 6 | RNA-seq analysis of Mtb after the treatment with the T5 compound. **(A)** Volcano plot analysis of the up-regulated and down-regulated genes at 4 h with a log2FC > 2.0 or log2FC < 2.0 and a *p*-value < 0.05. **(B)** Volcano plot analysis of the up-regulated and down-regulated genes at 20 h with a log2FC > 2.0 or log2FC < 2.0 and a *p*-value < 0.05.

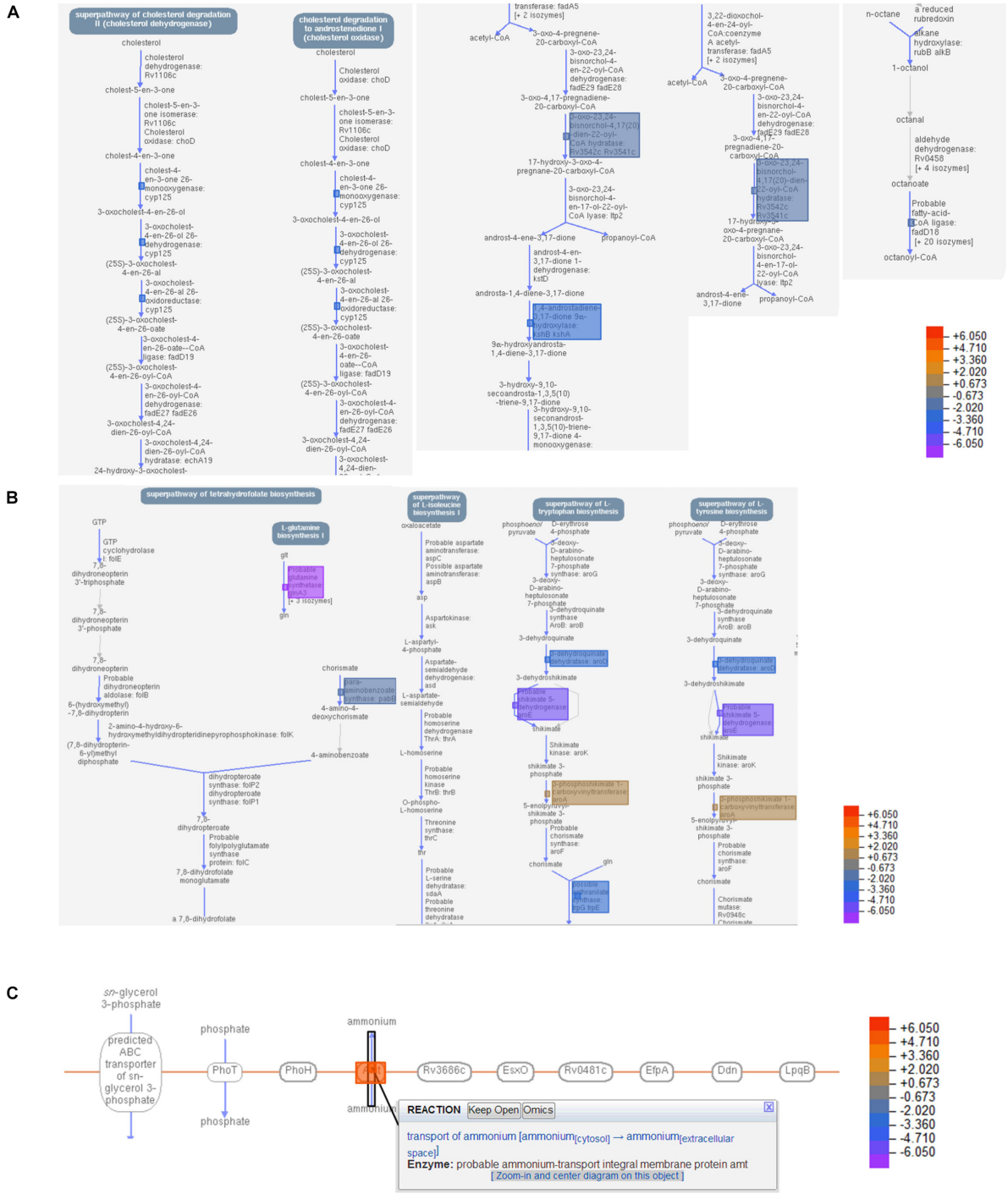

FIGURE 7 | T5 compound affect the cholesterol and folic acid pathways in Mtb. **(A)** Shows the main enzymes and reactions of the cholesterol degradation pathway in Mtb that were significantly affected by the treatment of the T5 compound using the BioCyc database Collection (https://biocyc.org/organism-summary?object=MTBH37RV, version 23.1). **(B)** Shows the main enzymes and reactions of the folic acid synthesis pathway that were significantly affected by the treatment of the T5 compound using the BioCyc database. **(C)** Shows the up-regulation of the ammonium-transport integral protein (Amt) in response to the treatment with the T5 compound using the BioCyc database. The data in **(A,B)** are from the 4 h and in **(C)** from 20 h transcriptome.

conditions that Mtb experienced during infection. A rising in drug-resistant TB is a major impediment to successfully deal with this disease. The WHO recognizes antimicrobial resistance as one of the most demanding global threats to cure TB. Drug resistance is probably a consequence of overuse of antibiotics in the treatment of humans or lack of adherence

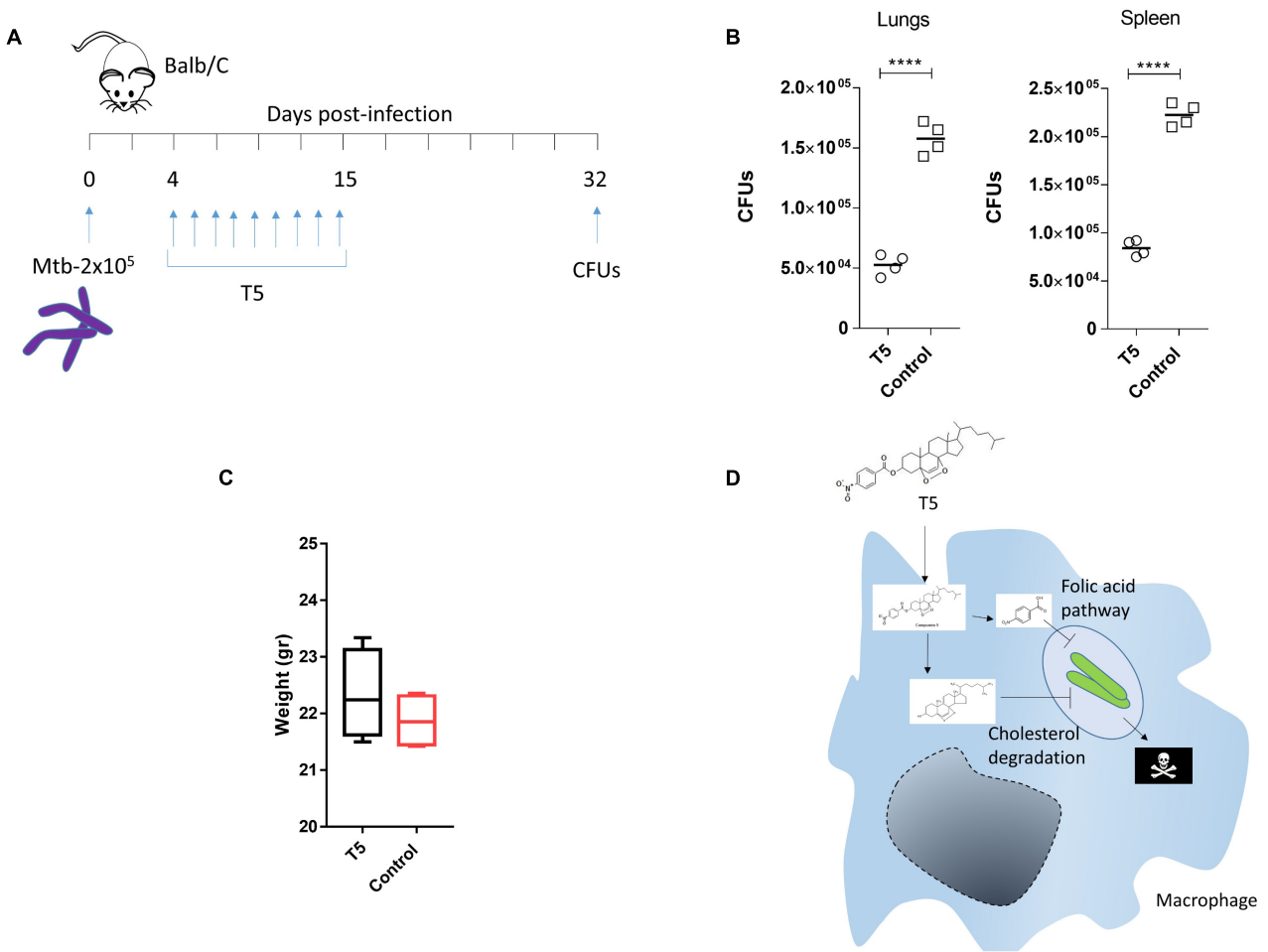

FIGURE 8 | The T5 compound has anti-mycobacteral activity *in vivo*. **(A)** The diagram shows the treatment scheme for the T5 compound and the CFU determination time points. Four mice per group were infected with 2 × 10^5 bacteria intra peritoneal (i.p) in 200 μL of PBS with 0.05% Tween 80. **(B)** Quantification of the CFUs in spleen and lungs of the T5 treated Balb/C mice after 32 days. **(C)** Body weight of Balb/C mice at the end of drug treatment 15 days post-infection. **(D)** Diagram showing a model of the possible mechanism of action of the T5 compound against Mtb. Unpaired *t*-test ****p-value < 0.0001. Representative of two independent experiments.

to the treatment. When a new antibiotic is introduced, it can have great results for a period of time, but then the bacteria gradually adapt and the antibiotic becomes less effective. This is why we need to maintain a constant search for new effective antibiotics that target different pathways in an organism like Mtb.

Our results define the activity of a new compound called T5, which has anti-mycobacterial activity against Mtb, specifically when the bacteria locate inside the macrophages, but surprisingly not in the extracellular environment. We hypothesize that this T5 compound may have a combinatorial effect in which the conjugation may help their entry into cells, likely due to the requirement of Mtb to utilize cholesterol. Once inside of the bacteria, an enzymatic reaction, probably mediated by a macrophage specific esterase, could release the ANB part from the T1 compound, and then the ANB may interfere with the enzymes of the folic acid pathway. In addition, the released T1 part of the T5 compound may simultaneously affect the enzymes of the cholesterol degradation pathways (**Figure 8D**).

Even though anti-folate drugs have been very successful as anticancer and antimicrobial agents, they are poorly effective in the TB therapy (Minato et al., 2015a; Hajian et al., 2019). The ineffectiveness of these type of drugs is probably due to the lack of permeability to them in Mtb (Nixon et al., 2014). Moreover, anti-folates have a past history of use in TB therapy especially through the use of the drug para-aminosalicylic-acid (PAS) that worked as a bacteriostatic anti-tubercular agent. Finding a compound that is both permeable and effective to inhibit this folate pathway would be highly desirable. On the other hand, the cholesterol catabolic pathway is an important therapeutic target in Mtb in which many of its genes are involved in pathogenesis. This has been demonstrated by the mutation or deletion of these genes and the attenuation of the bacteria. The cholesterol catabolic pathway in Mtb is accomplished in two major lanes, first by the degradation of the aliphatic side chain and second by the

degradation of the sterol A-D rings. A compound that could disrupt the two major steps in the degradation of cholesterol in Mtb could be a great finding.

It is important to mention that spontaneous resistance to the ANB part of the T5 compound, which is similar to the PAS compound, could emerge via multiple mechanisms that include limited bio-activation within the folate synthesis pathway, efflux pumps, specific mutations like in the *pabB* gene, and an insufficient accumulation within the bacilli (Minato et al., 2015a). We do not have information about spontaneous drug-resistant mutation for the epidioxy-sterol-T1 part of the molecule. However, it is interesting that a compound like the T5 compound that acts over different metabolic pathways is less likely to encounter resistance in the same bacteria, which could be advantageous for this compound in the fight against Mtb.

The up-regulation of the ammonium transporter could be a consequence of the nitro group present in the ANB part of the T5 compound. This ANB could behave similarly to a nitroimidazole compound releasing nitric oxide (NO) and converted into ammonium by the bacteria, which has to be shuttled out to avoid toxicity. The activity that we observed for the T5 compound *in vivo* is significant but not as effective if we compared the results with drugs like Rifampicin; however, we know that the T5 compound is highly hydrophobic and may require a better vehicle in order to obtain more effective results in future animal experiments.

CONCLUSION

We found a new compound called T5 with a good anti-mycobacterial activity *in vivo* and *in vitro* which may be functioning as a simultaneous inhibitor of the folate and cholesterol pathways.

DATA AVAILABILITY STATEMENT

The RNA-seq transcriptomic data was deposited in https://www.ncbi.nlm.nih.gov/bioproject: DMSO 4 h, BaenaRNA1_1.fastq.gz (SRR11195990); DMSO 20 h, BaenaRNA3_1.fastq.gz (SRR11195989); T5 4 h, BaenaRNA2_1.fastq.gz (SRR11195988); and T5 20 h, BaenaRNA4_1.fastq.gz (SRR11195987).

ETHICS STATEMENT

The animal study was reviewed and approved by the animal ethics committee of the Universidad de Antioquia.

AUTHOR CONTRIBUTIONS

AB, JA, AM, and LB conceived and designed the experiments. AB, EV, and MP performed the experiments. AB, JA, MP, and EV analyzed the data. AB, LB, MP, JA, and AM wrote and revised the manuscript. All the authors read and approved the manuscript.

FUNDING

We want to acknowledge our funding source CODI Universidad de Antioquia 2015-6726.

ACKNOWLEDGMENTS

We would like to acknowledge "Estrategia de Sostenibilidad" Universidad de Antioquia.

SUPPLEMENTARY MATERIAL

The Supplementary Material for this article can be found online at: https://www.frontiersin.org/articles/10.3389/fmicb.2020.537935/full#supplementary-material

FIGURE S1 | Compound library and T5 NMR. **(A)** Reaction to produce the T5 compound. **(B)** ^{1}H NMR spectrum of compound T5. **(C)** ^{13}C NMR spectrum of compound T5. **(D)** ^{1}H- ^{13}C HMBC 2D NMR correlation spectroscopy of compound T5. **(E)** ^{1}H- ^{13}C HMBC 2D NMR correlation spectroscopy of compound T5. **(F)** Inhibitory GFP curves for the compounds T2–T4 and T6–T15 after 48 h of treatment post-infection.

FIGURE S2 | CFUs of the Mtb after the THP-1 macrophage lysis. The THP-1 macrophages were lysed and 5 μl of bacteria were plated for each dilution in 7H10 media for 23 days. The plates were divided in 4 quadrants and labeled clockwise with the dilution (Undiluted [1], 10^{-1}, 10^{-2}, 10^{-3}), starting with upper left quadrant.

FIGURE S3 | RNA quality of the samples used for the RNA-seq. **(A)** Agarose gel showing the integrity of the ribosomal RNA bands. **(B)** RNA integrity number (RIN) obtained for each sample. **(C)** Showing the bio-analyzer electropherograms for each sample.

FIGURE S4 | Cell viability assay quantification. **(A)** The cell death phenotypes encountered after the treatment with the different compounds. **(B)** Example of the cell death quantification procedure that we have used to generate the viability data in **Figure 4B**.

TABLE S1 | THP-1 Macrophage transcriptome.

TABLE S2 | Mtb-H37Rv transcriptome.

REFERENCES

Aguilar-Ayala, D. A., Tilleman, L., Van Nieuwerburgh, F., Deforce, D., Palomino, J. C., Vandamme, P., et al. (2017). The transcriptome of *Mycobacterium tuberculosis* in a lipid-rich dormancy model through RNAseq analysis. *Sci. Rep.* 7:17665.

Anonymous. (2019). Antibiotic susceptibility diagnostics for the future. *Nat. Microbiol.* 4:1603. doi: 10.1038/s41564-019-0577-4

Baena, A., Cabarcas, F., Alvarez-Eraso, K. L. F., Isaza, J. P., Alzate, J. F., Barrera, L. F., et al. (2019). Differential determinants of virulence in two *Mycobacterium tuberculosis* colombian clinical isolates of the LAM09 family. *Virulence* 10, 695–710. doi: 10.1080/21505594.2019.1642045

Baena, A., and Porcelli, S. A. (2009). Evasion and subversion of antigen presentation by *Mycobacterium tuberculosis*. *Tissue Antigens* 74, 189–204. doi: 10.1111/j.1399-0039.2009.01301.x

Burki, T. (2019). BPaL approved for multidrug-resistant tuberculosis. *Lancet Infect. Dis.* 19, 1063–1064. doi: 10.1016/s1473-3099(19)30489-x

Bussi, C., and Gutierrez, M. G. (2019). *Mycobacterium tuberculosis* infection of host cells in space and time. *FEMS Microbiol. Rev.* 43, 341–361. doi: 10.1093/femsre/fuz006

Cateni, F., Doljak, B., Zacchigna, M., Anderluh, M., Piltaver, A., Scialino, G., et al. (2007). New biologically active epidioxysterols from Stereum hirsutum. *Bioorg. Med. Chem. Lett.* 17, 6330–6334. doi: 10.1016/j.bmcl.2007.08.072

Duarte, N., Ferreira, M. J., Martins, M., Viveiros, M., and Amaral, L. (2007). Antibacterial activity of ergosterol peroxide against *Mycobacterium tuberculosis*: dependence upon system and medium employed. *Phytother. Res.* 21, 601–604. doi: 10.1002/ptr.2119

Ehrt, S., and Schnappinger, D. (2009). Mycobacterial survival strategies in the phagosome: defence against host stresses. *Cell Microbiol.* 11, 1170–1178. doi: 10.1111/j.1462-5822.2009.01335.x

Farshori, N. N., Banday, M. R., Zahoor, Z., and Rauf, A. (2010). DCC/DMAP mediated esterification of hydroxy and non-hydroxy olefinic fatty acids with beta-sitosterol: in vitro antimicrobial activity. *Chin. Chem. Lett.* 21, 646–650. doi: 10.1016/j.cclet.2010.01.003

Feng, K., Wu, L. Z., Zhang, L. P., and Tung, C. H. (2007). IRA-200 resin-supported platinum(II) complex for photooxidation of olefins. *Tetrahedron* 63, 4907–4911. doi: 10.1016/j.tet.2007.03.148

Fieweger, R. A., Wilburn, K. M., and VanderVen, B. C. (2019). Comparing the metabolic capabilities of bacteria in the *Mycobacterium tuberculosis* complex. *Microorganisms* 7:177. doi: 10.3390/microorganisms7060177

Giampaglia, C. M., Martins, M. C., Chimara, E., Oliveira, R. S., de Oliveira Vieira, G. B., Marsico, A. G., et al. (2007). Differentiation of *Mycobacterium tuberculosis* from other mycobacteria with rho-nitrobenzoic acid using MGIT960. *Int. J. Tuberc. Lung. Dis.* 11, 803–807.

Griffin, J. E., Pandey, A. K., Gilmore, S. A., Mizrahi, V., McKinney, J. D., Bertozzi, C. R., et al. (2012). Cholesterol catabolism by *Mycobacterium tuberculosis* requires transcriptional and metabolic adaptations. *Chem. Biol.* 19, 218–227. doi: 10.1016/j.chembiol.2011.12.016

Gygli, S. M., Borrell, S., Trauner, A., and Gagneux, S. (2017). Antimicrobial resistance in *Mycobacterium tuberculosis*: mechanistic and evolutionary perspectives. *FEMS Microbiol. Rev.* 41, 354–373. doi: 10.1093/femsre/fux011

Hajian, B., Scocchera, E., Shoen, C., Krucinska, J., Viswanathan, K., G-Dayanandan, N., et al. (2019). Drugging the folate pathway in *Mycobacterium tuberculosis*: the role of multi-targeting agents. *Cell Chem. Biol.* 26, 781.e6–791.e6.

Joshi, S. M., Pandey, A. K., Capite, N., Fortune, S. M., Rubin, E. J., Sassetti, C. M., et al. (2006). Characterization of mycobacterial virulence genes through genetic interaction mapping. *Proc. Natl. Acad. Sci. U.S.A.* 103, 11760–11765. doi: 10.1073/pnas.0603179103

Lange, C., Dheda, K., Chesov, D., Mandalakas, A. M., Udwadia, Z., Horsburgh, C. R., et al. (2019). Management of drug-resistant tuberculosis. *Lancet* 394, 953–966.

Larrouy-Maumus, G., Marino, L. B., Madduri, A. V. R., Ragan, T. J., Hunt, D. M., Bassano, L., et al. (2016). Cell-envelope remodeling as a determinant of phenotypic antibacterial tolerance in *Mycobacterium tuberculosis*. *ACS Infect. Dis.* 2, 352–360. doi: 10.1021/acsinfecdis.5b00148

Laws, M., Shaaban, A., and Rahman, K. M. (2019). Antibiotic resistance breakers: current approaches and future directions. *FEMS Microbiol. Rev.* 43, 490–516. doi: 10.1093/femsre/fuz014

Lee, J., Lee, S., Kim, K. K., Lim, Y., Choi, J., Cho, S., et al. (2019). Characterisation of genes differentially expressed in macrophages by virulent and attenuated *Mycobacterium tuberculosis* through RNA-Seq analysis. *Sci. Rep.* 9:4027.

Lopez-Agudelo, V. A., Baena, A., Ramirez-Malule, H., Ochoa, S., Barrera, L. F., Ríos-Estepa, R., et al. (2017). Metabolic adaptation of two in silico mutants of *Mycobacterium tuberculosis* during infection. *BMC Syst. Biol.* 11:107. doi: 10.1186/s12918-017-0496-z

Mashabela, G. T., de Wet, T. J., and Warner, D. F. (2019). *Mycobacterium tuberculosis* metabolism. *Microbiol. Spectr.* 7:a021121.

McShane, H. (2019). Insights and challenges in tuberculosis vaccine development. *Lancet Respir. Med.* 7, 810–819. doi: 10.1016/s2213-2600(19)30274-7

Minato, Y., Thiede, J. M., Kordus, S. L., McKlveen, E. J., Turman, B. J., Baughn, A. D., et al. (2015a). *Mycobacterium tuberculosis* folate metabolism and the mechanistic basis for para-aminosalicylic acid susceptibility and resistance. *Antimicrob. Agents Ch.* 59, 5097–5106. doi: 10.1128/aac.00647-15

Miner, M. D., Chang, J. C., Pandey, A. K., Sassetti, C. M., and Sherman, D. R. (2009). Role of cholesterol in *Mycobacterium tuberculosis* infection. *Indian J. Exp. Biol.* 47, 407–411. doi: 10.1007/978-981-32-9413-4_22

Mshana, R. N., Tadesse, G., Abate, G., and Miorner, H. (1998). Use of 3-(4,5-dimethylthiazol-2-yl)-2,5-diphenyl tetrazolium bromide for rapid detection of rifampin-resistant *Mycobacterium tuberculosis*. *J. Clin. Microbiol.* 36, 1214–1219. doi: 10.1128/jcm.36.5.1214-1219.1998

Nixon, M. R., Saionz, K. W., Koo, M. S., Szymonifka, M. J., Jung, H., Roberts, J. P., et al. (2014). Folate pathway disruption leads to critical disruption of methionine derivatives in *Mycobacterium tuberculosis*. *Chem. Biol.* 21, 819–830. doi: 10.1016/j.chembiol.2014.04.009

Nunn, A. J., Phillips, P. P. J., Meredith, S. K., Chiang, C., Conradie, F., Dalai, D., et al. (2019). A trial of a shorter regimen for rifampin-resistant tuberculosis. *N. Engl. J. Med.* 380, 1201–1213.

Pandey, A. K., and Sassetti, C. M. (2008). Mycobacterial persistence requires the utilization of host cholesterol. *Proc. Natl. Acad. Sci. U.S.A.* 105, 4376–4380. doi: 10.1073/pnas.0711159105

Pontali, E., Raviglione, M. C., Migliori, G. B., and the writing group members of the Global Tb Network Clinical Trials Committee (2019). Regimens to treat multidrug-resistant tuberculosis: past, present and future perspectives. *Eur. Respir. Rev.* 28:190035. doi: 10.1183/16000617.0035-2019

Queval, C. J., Brosch, R., and Simeone, R. (2017). The macrophage: a disputed fortress in the battle against *Mycobacterium tuberculosis*. *Front. Microbiol.* 8:2284. doi: 10.3389/fmicb.2017.02284

Rashid, F., Awan, H. M., Shah, A., Chen, L., and Shan, G. (2017). Induction of miR-3648 Upon ER stress and its regulatory role in cell proliferation. *Int. J. Mol. Sci.* 18:1375. doi: 10.3390/ijms18071375

Russell, D. G. (2011). *Mycobacterium tuberculosis* and the intimate discourse of a chronic infection. *Immunol. Rev.* 240, 252–268. doi: 10.1111/j.1600-065x.2010.00984.x

Saludes, J. P., Garson, M. J., Franzblau, S. G., and Aguinaldo, A. M. (2002). Antitubercular constituents from the hexane fraction of *Morinda citrifolia* Linn. (*Rubiaceae*). *Phytother. Res.* 16, 683–685. doi: 10.1002/ptr.1003

Spellberg, B. (2014). The future of antibiotics. *Crit. Care* 18:228.

VanderVen, B. C., Fahey, R. J., Lee, W., Liu, Y., Abramovitch, R. B., Memmott, C., et al. (2015). Novel inhibitors of cholesterol degradation in *Mycobacterium tuberculosis* reveal how the bacterium's metabolism is constrained by the intracellular environment. *PLoS Pathog.* 11:e1004679. doi: 10.1371/journal.ppat.1004679

World Health Organization [WHO] (2018). *Global Tuberculosis Report*. Geneva: WHO.

Zhou, H., Zhao, L., Li, W., Yang, Y., Xu, L., Ding, Z., et al. (2015). Anti-*Mycobacterium tuberculosis* active metabolites from an endophytic *Streptomyces* sp YIM65484. *Rec. Nat. Prod.* 9, 196–200.

Zimmermann, M., Kogadeeva, M., Gengenbacher, M., McEwen, G., Mollenkopf, H., Zamboni, N., et al. (2017). Integration of Metabolomics and Transcriptomics reveals a complex diet of *Mycobacterium tuberculosis* during early macrophage infection. *mSystems* 2:e00057-17. doi: 10.1128/mSystems.00057-17

Conflict of Interest: The authors declare that the research was conducted in the absence of any commercial or financial relationships that could be construed as a potential conflict of interest.

frontiers in Microbiology

ORIGINAL RESEARCH
published: 17 September 2020
doi: 10.3389/fmicb.2020.559469

In vitro Study of Bedaquiline Resistance in *Mycobacterium tuberculosis* Multi-Drug Resistant Clinical Isolates

Giulia Degiacomi[1], José Camilla Sammartino[1,2], Virginia Sinigiani[1], Paola Marra[1], Alice Urbani[1] and Maria Rosalia Pasca[1]**

[1] *Laboratory of Molecular Microbiology, Department of Biology and Biotechnology Lazzaro Spallanzani, University of Pavia, Pavia, Italy,* [2] *Istituto Universitario di Studi Superiori-IUSS, Pavia, Italy*

Tuberculosis (TB) is one of the major causes of death related to antimicrobial resistance worldwide because of the spread of *Mycobacterium tuberculosis* multi- and extensively drug resistant (multi-drug resistant (MDR) and extensively drug-resistant (XDR), respectively) clinical isolates. To fight MDR and XDR tuberculosis, three new antitubercular drugs, bedaquiline (BDQ), delamanid, and pretomanid were approved for use in clinical setting. Unfortunately, BDQ quickly acquired two main mechanisms of resistance, consisting in mutations in either *atpE* gene, encoding the target, or in *Rv0678*, coding for the repressor of the MmpS5-MmpL5 efflux pump. To better understand the spreading of BDQ resistance in MDR- and XDR-TB, *in vitro* studies could be a valuable tool. To this aim, in this work an *in vitro* generation of *M. tuberculosis* mutants resistant to BDQ was performed starting from two MDR clinical isolates as parental cultures. The two *M. tuberculosis* MDR clinical isolates were firstly characterized by whole genome sequencing, finding the main mutations responsible for their MDR phenotype. Furthermore, several *M. tuberculosis* BDQ resistant mutants were isolated by both MDR strains, harboring mutations in both *atpE* and *Rv0678* genes. These BDQ resistant mutants were further characterized by studying their growth rate that could be related to their spreading in clinical settings. Finally, we also constructed a data sheet including the mutations associated with BDQ resistance that could be useful for the early detection of BDQ-resistance in MDR/XDR patients with the purpose of a better management of antibiotic resistance in clinical settings.

Keywords: *Mycobacterium tuberculosis*, bedaquiline, multi-drug resistance, Rv0678, MmpL5, AtpE

OPEN ACCESS

Edited by:
Marta Martins,
Trinity College Dublin, Ireland

Reviewed by:
Diana Machado,
New University of Lisbon, Portugal
Divakar Sharma,
Indian Institute of Technology Delhi, India

****Correspondence:***
Giulia Degiacomi
giulia.degiacomi@unipv.it
Maria Rosalia Pasca
mariarosalia.pasca@unipv.it

Specialty section:
This article was submitted to Antimicrobials, Resistance and Chemotherapy, a section of the journal Frontiers in Microbiology

Received: *06 May 2020*
Accepted: *26 August 2020*
Published: *17 September 2020*

Citation:
Degiacomi G, Sammartino JC, Sinigiani V, Marra P, Urbani A and Pasca MR (2020) In vitro Study of Bedaquiline Resistance in Mycobacterium tuberculosis Multi-Drug Resistant Clinical Isolates. Front. Microbiol. 11:559469. doi: 10.3389/fmicb.2020.559469

INTRODUCTION

According to the World Health Organization (WHO) report, in 2018, tuberculosis (TB), caused by *Mycobacterium tuberculosis*, was one of the major causes of death related to antimicrobial resistance (World Health Organization [WHO], 2019a). Globally, in 2018 about half a million TB infections were rifampicin-resistant, of which 78% were multi-drug resistant (MDR)-TB (World Health Organization [WHO], 2019a). Among these cases, 6.2% were estimated to have extensively drug-resistant (XDR)-TB (World Health Organization [WHO], 2019a). Even if it is a relatively small percentage of all MDR-TB cases, these infections are more complicated to treat and to manage and are a challenge for the health systems worldwide.

Recently, three new antitubercular drugs, bedaquiline (BDQ) (Janssen, Beerse, Belgium), delamanid (Otsuka, Tokyo, Japan), and pretomanid (TB Alliance) were approved for the treatment of MDR-TB (Li et al., 2019; Nieto Ramirez et al., 2020). Interestingly, several studies demonstrated that patients treated with a BDQ-containing regimen showed a high culture conversion rate (65–100%) (Li et al., 2019; Pontali et al., 2019).

BDQ is a diarylquinoline that targets *atpE* gene, coding for the subunit c of the ATP synthase complex (Andries et al., 2005). Its use reduces the mortality when added to treatment for MDR- and XDR-TB (Li et al., 2019; Conradie et al., 2020). The potential risk of BDQ of prolonging the QT interval has occurred in only 0.6% of treated patients; consequently, the advantage in its use is uncontested, even if it is still under investigation. In fact, many clinical studies are testing the effectiveness of new drug combinations, which include BDQ, to design the next generation regimens (Sharma et al., 2020).

In this context, WHO has recently updated the treatment for MDR-TB, by recommending two possible regimens (the longer regimen and the shorter one), both including BDQ and other drugs (Caminero et al., 2019; World Health Organization [WHO], 2019b). Interestingly, in a recent study, NIX-TB trial, a three-drug regimen including linezolid, BDQ and pretomanid was tested with XDR- and MDR-TB patients; the therapy was successful for 90% of patients (Conradie et al., 2020). As evident, BDQ use is rapidly spreading, and 90 countries reported having imported or started using BDQ by the end of 2018 (World Health Organization [WHO], 2019a).

In spite of its recent use in clinical practice, primary BDQ resistance appeared among *M. tuberculosis* clinical isolates (Veziris et al., 2017; Villellas et al., 2017; Zimenkov et al., 2017; Ismail et al., 2018). BDQ resistance is especially associated with mutations in *atpE* and *Rv0678* genes.

The most common mutations linked to low-level of BDQ resistance are present in *Rv0678* gene coding for the *M. tuberculosis* repressor of MmpS5-MmpL5 efflux system. This transporter pumps out of the cells also clofazimine and azoles (Milano et al., 2009; Hartkoorn et al., 2014; Smith et al., 2017). In some cases, *Rv0678* mutations occurred together with polymorphisms in other genes encoding the uncharacterized transporter Rv1979c and the cytoplasmic peptidase PepQ (Rv2535c), both associated with cross-resistance to clofazimine (CFZ) (Nieto Ramirez et al., 2020). Furthermore, a report demonstrated that mutations in *pepQ* gene confer low-level of BDQ resistance in mice (Almeida et al., 2016).

As expected, high BDQ resistance levels are caused by mutations in *atpE* gene, even if their frequency is extremely low among TB patients (Nieto Ramirez et al., 2020).

The surveillance of drug resistance during clinical management is mandatory in order to prevent the occurrence of BDQ resistance among TB patients. To this aim, *in vitro* studies could be a valuable tool for understanding the reasons linked to the spreading of BDQ resistance in particular amongst *M. tuberculosis* MDR and XDR clinical isolates. While acquiring resistance to first-line drugs such as rifampicin (RIF) and isoniazid (INH) is linked to a perturbance in the *M. tuberculosis* fitness (Kodio et al., 2019), mutations in *Rv0678* and *atpE* have not been yet demonstrated to have this behavior (Andries et al., 2014; Nieto Ramirez et al., 2020). On the other hand, the low frequency of *atpE* mutants in the clinical setting in comparison to *Rv0678* mutations could suggest a possible reduced fitness cost linked to some *atpE* mutations (Nieto Ramirez et al., 2020).

To better understand the spreading of BDQ resistance in MDR- and XDR-TB, we reported an *in vitro* generation of *M. tuberculosis* mutants resistant to BDQ starting from MDR clinical isolates as parental cultures, since BDQ is used to treat patients affected by MDR-TB. Moreover, we performed growth curves of both obtained BDQ resistant mutants and original MDR isolates to detect possible differences in strains harboring either *Rv0678* or *atpE* mutations. Furthermore, we compared these mutations to a compiled data sheet of previously published SNPs, deriving from *in vitro*, *in vivo* and clinically resistant strains, thus providing additional information for rapid and efficient detection of all known BDQ-resistance associated mutations to ensure an optimal treatment monitoring.

MATERIALS AND METHODS

Bacterial Strains, Growth Conditions and Drugs

Mycobacterium tuberculosis H37Rv and clinical isolates as well as their mutants were grown at 37°C in Middlebrook 7H9 broth (Becton Dickinson), supplemented with 0.05% w/v Tween 80 or on Middlebrook 7H11, both supplemented with 0.2% w/v glycerol, and 10% v/v Middlebrook OADC enrichment (oleic acid, albumin, D-glucose, catalase; Becton Dickinson). *M. tuberculosis* MDR clinical isolates were collected and characterized at the Sondalo Division of the Valtellina and Valchiavenna, Italy, hospital authority in 2012 (Menendez et al., 2013). Bedaquiline (D.B.A. Italia s.r.l.) was dissolved in DMSO (Sigma Aldrich).

All the experiments with *M. tuberculosis* were performed in Biosafety level 3 laboratory by authorized and trained researchers.

Genomic DNA Preparation and Whole-Genome Sequencing of *M. tuberculosis* Clinical Isolates

Genomic DNA of *M. tuberculosis* MDR clinical isolates (hereafter named IC1 and IC2) was extracted as previously described (Belisle and Sonnenberg, 1998). Genomic DNA samples were sequenced by using an Illumina HiSeq2000 technology at Fisabio (Valencia, Spain). Illumina reads were aligned to the annotated genome sequence of the wild-type H37Rv (Cole et al., 1998) (NC_000962.3) to identify SNPs. For the bioinformatic analysis of Illumina data, repetitive PE and PPE gene families were discarded as well as SNPs and indels with less than 50% probability. The possible polymorphisms associated to the resistance to the following drugs were investigated: streptomycin (*rrs*, *rpsL*, *gidB*), INH (*katG*, *inhA*, *ndh*, *nat*), RIF (*rpoB*), ethambutol (*embA*, *embB*, *embC*, *embR*), ethionamide (*ethA*, *inhA*, *ethR*), pyrazinamide (*pncA*, *rpsA*, *panD*), capreomycin (*tlyA*, *rrs*), and BDQ (*Rv0678*, *atpE*, *pepQ*).

Determination of Minimal Inhibitory Concentration (MIC)

The drug susceptibility of *M. tuberculosis* strains was determined using the resazurin microtiter assay (REMA), as previously described (Palomino et al., 2002). Briefly, log-phase bacterial cultures were diluted to a theoretical OD_{600} = 0.0005 and grown in a 96-well black plate (Fluoronunc, Thermo Fisher) in the presence of serial compound dilution. A growth control containing no compound and a sterile control without inoculum were also included. After 7 days of incubation at 37°C, 10 μl of resazurin (0.025% w/v) were added and fluorescence was measured after 24 h further incubation using a Fluoroskan™ Microplate Fluorometer (Thermo Fisher Scientific; excitation = 544 nm, emission = 590 nm). Bacterial viability was calculated as a percentage of resazurin turnover in the absence of compound.

Isolation and Characterization of *M. tuberculosis* Spontaneous Mutants Resistant to BDQ

Mycobacterium tuberculosis BDQ resistant mutants were isolated by plating approximately 10^8 and 10^9 CFU from exponential growth phase cultures of IC1 and IC2 clinical isolates onto solid medium containing drug at concentrations exceeding the MIC (5X, 10X, 20X MIC). Following 6–8 weeks of incubation, BDQ resistant colonies were streaked onto 7H11 medium. At the same time, these colonies were streaked also onto 7H11 medium plus the same BDQ concentration used for mutant isolation to confirm the resistant phenotype. BDQ MIC values were also assessed by REMA. Genomic DNA was extracted from each mutant and *Rv0678*, *atpE*, and *pepQ* genes were amplified by PCR (oligonucleotides in **Supplementary Table S1**), purified using Wizard® SV Gel and PCR Clean-Up System (Promega) and analyzed by conventional Sanger sequencing (Eurofins Genomics, Italy).

Growth Curves of *M. tuberculosis* BDQ Resistant Mutants and MDR Clinical Isolates

The cultures of *M. tuberculosis* mutants, as well as their corresponding parental strain, were inoculated in 7H9 medium in round bottom tubes at 37°C to reach an early exponential phase. Then, each strain was reinoculated in new 7H9 medium at final OD_{600} = 0.06. The cultures were incubated in standing at 37°C for 8 days. After 24, 48, 96, 168, 192 h, the optical densities at 600 nm were recorded to plot growth curves. The H37Rv strain was also included as control.

Data Sheet Creation

The Medical Subject Headings vocabulary of biomedical terms (MeSH) search builder was used to construct the query for the terms "Bedaquiline," "*Mycobacterium*," and "Mutation", with which the Pubmed and Pubmed Central databases were skimmed, then all the abstracts were downloaded in a MEDLINE format. The information gathered was then manually filtered in two categories: relevant papers (i.e., original works, case studies, and clinical studies) and papers not pertinent to our purpose. The filtered-as-relevant papers were downloaded as full text, thoroughly analyzed and the type of mutations linked to BDQ resistance were annotated to set-up the data sheet.

RESULTS

Characterization of *M. tuberculosis* MDR Clinical Isolates

IC1 and IC2 strains are two *M. tuberculosis* MDR clinical isolates previously characterized (Menendez et al., 2013). In detail, IC1 is resistant to streptomycin (SM), INH, RIF, ethambutol (EMB), ethionamide (ETH); IC2 is resistant not only to the previously mentioned drugs, but also to pyrazinamide (PYR), and capreomycin (CM) (Menendez et al., 2013).

REMA was used to determine the BDQ MIC values of both isolates (MIC = 0.06 μg/ml, as for the H37Rv wild-type strain). This MIC value (0.06 μg/ml) for *M. tuberculosis* BDQ sensitive strains is in agreement with that proposed in 7H9 medium by both EUCAST and previously (Kaniga et al., 2016; EUCAST, 2020).

In order to pinpoint the SNPs responsible for their drug-resistance profile, the *M. tuberculosis* clinical strains were subjected to whole-genome sequencing (WGS) analysis. Using the obtained Illumina data, the genes involved in the resistance to the following drugs were checked: SM (*rrs*, *rpsL*, *gidB*), INH (*katG*, *inhA*, *ndh*, *nat*), RIF (*rpoB*), EMB (*embA*, *embB*, *embC*, *embR*), ETH (*ethA*, *inhA*, *ethR*), PYR (*pncA*, *rpsA*, *panD*), CAP (*tlyA*, rrs), and BDQ (*Rv0678*, *atpE*, *pepQ*).

For both *M. tuberculosis* isolates, the non-synonymous mutations found to be associated to their drug-resistance phenotype are enlisted in **Table 1**. As expected, no mutation was found in *Rv0678*, *atpE*, and *pepQ* genes according to their BDQ sensitivity.

Mycobacterium tuberculosis IC1 and IC2 clinical strains were used for further experiments because of their drug-resistance phenotype as well as their BDQ sensitivity.

Isolation and Phenotypic Characterization of Spontaneous *M. tuberculosis* Mutants Resistant to BDQ

Once shown their BDQ sensitivity, *M. tuberculosis* IC1 and IC2 clinical isolates were used to select and to isolate BDQ-resistant spontaneous mutants, since patients affected by MDR-TB are likely to receive BDQ as part of their therapy.

Mutants were selected onto solid medium containing high BDQ concentrations (0.3, 0.6, 1.2 μg/ml, corresponding to 5, 10, 20-fold MIC, respectively). *Mycobacterium tuberculosis* BDQ-resistant mutants were isolated at a frequency of about 1.8×10^{-8} for IC1 and 6×10^{-9} for IC2.

All the 12 isolated mutants showed to be BDQ resistant and their MIC value was confirmed by REMA, ranging from 0.25 μg/ml (4X MIC of sensitive strain) to 8 μg/ml (128X MIC of

TABLE 1 | Phenotypic and genotypic characteristics of *M. tuberculosis* IC1 and IC2 clinical isolates.

Resistance	Genome position (bp)	Gene	Mutation	Amino acid substitution
Clinical isolate IC1				
STR	4407880	*gidB*	T323G	L108R
INH	2155168	*katG*	G944C	S315T
RIF	761155	*rpoB*	C1349T	S450L
EMB	4242803	*embC*	G2941C	V981L
EMB	4247429	*embB*	A916G	M306V
ETH	4327058	*ethA*	G416A	G139D
Clinical isolate IC2				
STR	781687	*rpsL*	A128G	K43R
INH	2155168	*katG*	G944C	S315T
RIF	761155	*rpoB*	C1349T	S450L
EMB	4242803	*embC*	G2941C	V981L
EMB	4247429	*embB*	A916G	M306V
PYR	2288807	*pncA*	C435G	D145E
PYR	2289106	*pncA*	G136A	A46T
ETH	4327058	*ethA*	G416A	G139D
CM	1918707	*tlyA*	insAG	Frameshift

sensitive strain) (**Table 2**). The different levels of drug-resistance could be linked to different associated mutations.

In order to investigate this possibility, *Rv0678*, *atpE*, and *pepQ* genes were amplified by PCR from the genomic DNA of *M. tuberculosis* BDQ resistant mutants and sequenced by Sanger method.

None of 12 *M. tuberculosis* resistant mutants had mutation in *pepQ* gene, while polymorphisms were found either in *atpE* or *Rv0678* genes (**Table 2** and **Supplementary Data Sheet S1**).

In particular, seven strains carried a mutation in AtpE, the cellular BDQ target. Among them, five mutants harbored the same replacement of alanine at position 63 by a proline (A63P).

TABLE 2 | Phenotypic and genotypic characteristics of mutants resistant to BDQ obtained from *M. tuberculosis* clinical isolates IC1 and IC2.

M. tuberculosis strains	MIC (μg/ml)	Mutation	Amino acid substitution
H37Rv	0.06		
IC1	0.06		
IC2	0.06		
IC1 B	8	*atpE*: g187c	A63P
IC1 C	4	*atpE*: g187c	A63P
IC1 D	4	*atpE*: g187c	A63P
IC1 F	4	*atpE*: g187c	A63P
IC1 G	4	*atpE*: g187c	A63P
IC1 H	2	*atpE*: a83c	D28A
IC2 Q	0.5	*atpE*: a83g	D28G
IC1 L	0.5	*rv0678*: c400t	R124Stop
IC1 M	0.5	*rv0678*: g120c	L40F
IC1 N	0.5	*rv0678*: a271c	T91P
IC1 O	0.5	*rv0678*: g61t	E21Stop
IC2 P	0.25	*rv0678*: g197a	G66E

IC2Q mutant had a substitution of the aspartic acid at position 28 with a glycine (D28G), while IC1H mutant presented at the same position a substitution with an alanine (D28A), (**Table 2** and **Supplementary Data Sheet S1**). Furthermore, these mutants were characterized by a high level of BDQ resistance (2–8 μg/ml) ranging from 32 to 128X MIC of the wild-type strain.

The other five isolated *M. tuberculosis* mutants harbored mutations in *Rv0678*, encoding the MmpR transcriptional repressor of the efflux pump MmpS5-MmpL5. These mutants were characterized by a low level of BDQ resistance (0.25–0.5 μg/ml) corresponding to 4–8X MIC the wild-type strain. Three mutants, IC1M, IC1N, and IC2P, presented an amino acid change: respectively, the leucine at position 40 was replaced by a phenylalanine, the tyrosine at position 91 by a proline, and, finally, the glycine at position 66 by a glutamate (**Table 2** and **Supplementary Data Sheet S1**). The MmpR of the other two mutants, IC1L and IC1O, was truncated by a stop codon at position 400 and at position 61, respectively. Additional experiments to demonstrate the role of Rv0678 in BDQ resistance were not performed. None of these *Rv0678* polymorphisms was already published, at the best of our knowledge.

Evaluation of the Possible Influence of *atpE* and *Rv0678* Mutations to the Growth Rate of *M. tuberculosis* BDQ Resistant Mutants

The growth curves of BDQ resistant mutants with respect to that of the *M. tuberculosis* H37Rv strain and the two parental MDR isolates were also evaluated (**Figure 1**).

As expected, IC1 and IC2 isolates presented a longer lag phase with respect to that of the wild-type strain. This is also in agreement with their lower growth rate (**Figure 1A**).

Interestingly, the rate of growth of IC2Q (*atpE* mutant) was lower than that of IC2 strain and of IC2P mutant (*Rv0678* mutant); on the other hand, IC2P grew faster than the other two strains (**Figure 1C**).

In the case of IC1-derived mutants, the lag phase length is similar between the mutants and the parental strain, while the rate of growth of IC1L, IC1M, IC1N, and IC1O (*Rv0678* mutants) was faster than that of IC1 (**Figure 1B**). These latter harbor mutations in *Rv0678* which do not perturb *M. tuberculosis* essential functions, whilst IC1C and IC1N (both *atpE* mutants) displayed a rate of growth similar to the parental one.

Overall, our data highlight that the *Rv0678* mutations do not affect growth rate of our parental strains, but could actually give an advantage in the growth rate.

Collection of All Known Polymorphisms Causing BDQ Resistance in *M. tuberculosis* and Other Mycobacteria

The previously published mutations associated with BDQ-resistance as well as the new ones found in this work were included in **Supplementary Data Sheet S1**.

BDQ is also active against non-tuberculous mycobacteria (NTM) belonging to the *Mycobacterium avium-intracellulare* complex (MAC) and the *Mycobacterium abscessus* complex

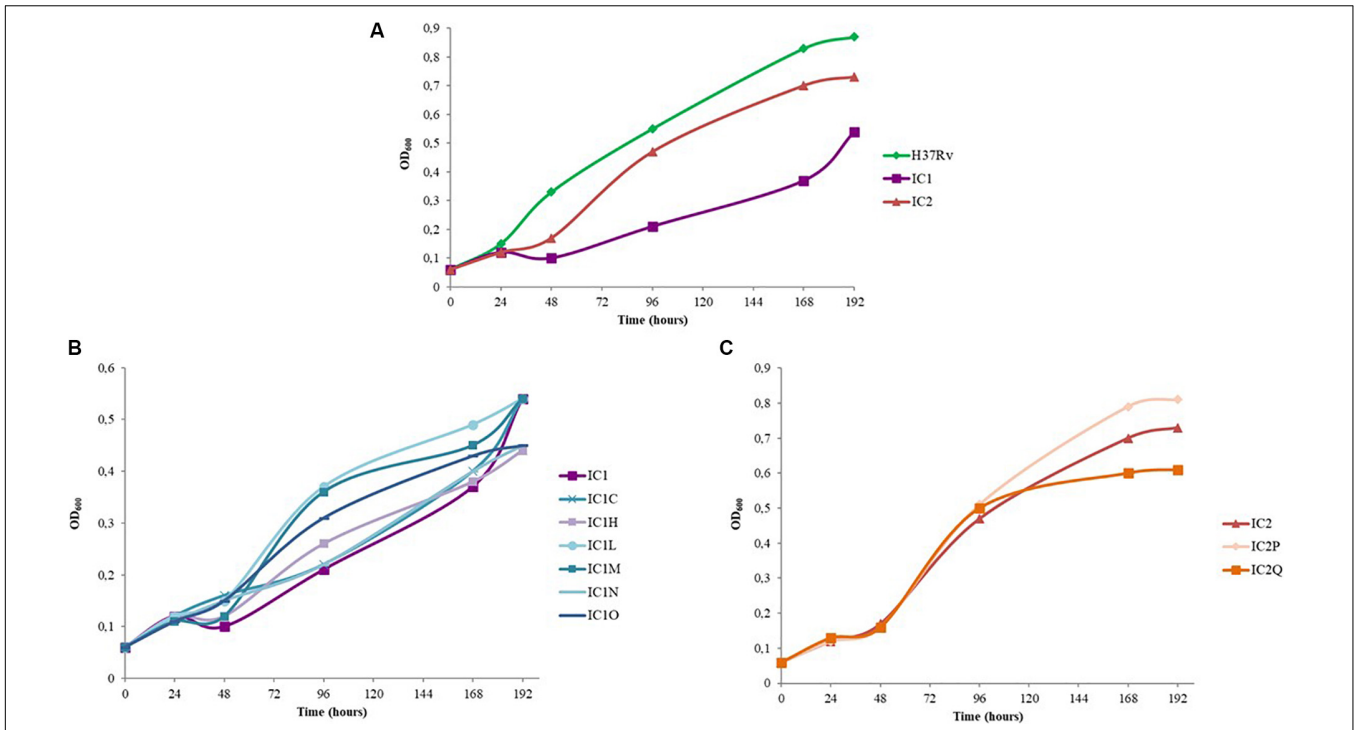

FIGURE 1 | Growth curves of standing cultures of *M. tuberculosis* strains (H37Rv, clinical isolates and mutant strains). The experiment was repeated three times giving comparable results. The figure shows one representative experiment. **(A)** Growth curves of *M. tuberculosis* H37Rv strain and IC1 and IC2 clinical isolates. **(B)** Growth curves of IC1 clinical isolate and the following BDQ resistant mutants: IC1 C (representative mutant strain with A63P mutation in AtpE), IC1 H, IC1 L, IC1 M, IC1 N, IC1 O. **(C)** Growth curves of IC2 clinical isolate and the BDQ resistant mutants IC2 P and IC2 Q.

(MABSC) (Philley et al., 2015). Its possible use against these other mycobacterial species is under investigation. In NTM species BDQ presents the same mechanisms of resistance found in *M. tuberculosis*; consequently, the evaluation of the BDQ resistance associated polymorphisms could be useful also in these species. For this reason, in this collection, all the mycobacterial species in which an actual clinical use or possible use is under evaluation were included. Moreover, both *in vitro* isolated mutants and clinical isolates were added. At the end, all the mutations linked to BDQ resistance in mycobacteria have been considered in this data sheet that could be useful for the better understanding of BDQ resistance.

DISCUSSION

The current use of BDQ in the treatment for MDR- and XDR-TB reduces the mortality and it is highly effective (Ahmad et al., 2018; Conradie et al., 2020).

Nevertheless, the two main mechanisms of BDQ resistance, which are already widespread, are: modification of target (mutations in *atpE*, coding for the target) and over-expression of an efflux pump (mutations in *Rv0678* gene, coding for the repressor of MmpS5-MmpL5 efflux system). Several reports showed that the most spreading mechanism of BDQ resistance in clinical setting is represented by mutations in *Rv0678* gene even if with a low level of BDQ-resistance (Villellas et al., 2017; Nieto Ramirez et al., 2020). To fight BDQ-resistance caused by Rv0678 mutations and to allow its use for the largest possible part of patients, verapamil, an efflux inhibitor, could be the keystone, since it has been demonstrated to increase the efficacy of BDQ against both *M. tuberculosis* and *Mycobacterium abscessus* (Ghajavand et al., 2019; Viljoen et al., 2019).

In this study, an *in vitro* generation of *M. tuberculosis* mutants resistant to BDQ was performed starting from two MDR clinical isolates as parental cultures since patients affected by MDR-TB are eligible to receive BDQ as part of their therapy.

Polymorphisms were identified in both *Rv0678* and *atpE* genes. Our results confirm that these genes represent the main genetic drivers for the onset of BDQ-resistance, as previously pointed out.

Most *in vitro* isolated mutants harbored mutations in the BDQ target, AtpE at positions 28 and 63, according to previous multiple reports (Huitric et al., 2010; Segala et al., 2012; Zimenkov et al., 2017; Ismail et al., 2018). In particular, the mutation A63P was found in the first report regarding BDQ discovery (Andries et al., 2005). The 28 and 63 amino acid positions are considered mutation hotspots, as described in **Supplementary Data Sheet S1**. In fact, the AtpE D28 and A63 are not directly involved in the BDQ binding, but the disruption of the non-covalent bonds they form causes resistance (Preiss et al., 2015). Thanks to the previously published structure of complex crystals obtained by the co-crystallization of the *Mycobacterium phlei* c-ring with BDQ, it is well-known that BDQ forms an extensive amount

of van derWaals interactions with a stretch of nine residues (in *M. phlei*: G62, L63, E65, A66, A67, Y68, F69, I70, and L72) provided by two adjacent *c*-subunits (Preiss et al., 2015). The mutations (D28A/G, A63P) harbored by BDQ-resistant mutants isolated in this study are positioned close to BDQ-binding site causing indirect structural interference with BDQ binding (Preiss et al., 2015), as evident by the higher MIC showed.

Different mutations could be linked to different levels of drug-resistance, as previously shown (Andries et al., 2005; Hartkoorn et al., 2014; Almeida et al., 2016). In general, *atpE* gene associated variants lead to high level of BDQ-resistance, but the most troublesome polymorphisms are linked to *Rv0678* gene, that are also the most represented ones found in clinical isolates even if the *Rv0678* mutations are linked to a lower level of BDQ resistance (Villellas et al., 2017; Nieto Ramirez et al., 2020), as typical for efflux pump mechanism. When over-expressed, MmpS5-MmpL5 efflux system can extrude different classes of drugs, for example CFZ and azoles, further limiting the therapeutic options of patients affected by M/XDR-TB. As well exemplified also in this present study, different mutations were identified in *Rv0678* and were disseminated across the gene (**Table 2** and **Supplementary Data Sheet S1**). Both the missense mutations and the nonsense mutations are reported to abolish the repressor activity of Rv0678, causing an over-expression of the MmpL5 efflux pump leading to drug extrusion (Zhang et al., 2015). It is worth noting that a G66 missense mutation was found not only in this study (G66E), but also in CFZ-resistant *M. tuberculosis* mutant isolated *in vitro* (G66V) (Zhang et al., 2015).

As responsible for BDQ resistance, mutations in the intergenic region between *Rv0678* and *MmpS5* as well as mutations in the genes encoding the efflux pump MmpS5/MmpL5 were also reported (Ghajavand et al., 2019).

Furthermore, several reports showed that *Rv0678* mutations could be present prior the BDQ treatment both *in vitro* and *in vivo* (Pang et al., 2017; Veziris et al., 2017; Villellas et al., 2017; Xu et al., 2017; Chawla et al., 2018; Martinez et al., 2018). Consequently, it could be hypothesized that these mutations are adaptative or could improve the growth rate of the MDR mutants, representing an advantage for them. In this work, we evaluated the growth rate of our *M. tuberculosis* BDQ-resistant mutants in comparison with that of the parental strains (two MDR clinical isolates). The *atpE* mutants presented a growth rate similar or lower than that of the parental strains, since *atpE* is essential for *M. tuberculosis* growth, while *Rv0678* mutants showed either a similar growth rate as parental strains or better. Noteworthy, *Rv0678* gene is not essential for *M. tuberculosis* growth (Radhakrishnan et al., 2014). Finally, from our work the relative fitness of the mutants could be speculated. In fact, fitness cost determines in part the fate of resistance mutations (Melnyk et al., 2015). *In vitro* the *atpE* mutants seem to show a little decrease in fitness relative to that of the respective parental strain. On the opposite hand, *Rv0678* mutants seem to have the same fitness in comparison to the corresponding isolate or even a little advantage.

Previous studies showed that Rv0678 repressor controls the expression of MmpS5-MmpL5 efflux system as well as of other transporters such as IniAB and DrrA (Milano et al., 2009; Andries et al., 2014). Among the regulated proteins, there were also some essential enzymes and proteins important for the virulence (e.g., PimA, an antitoxin VapB1, etc.) (Andries et al., 2014), that could play a role in *M. tuberculosis* growth and/or infection. Apart from a genomic approach, proteomics-based approaches coupled with bioinformatics could be useful for the characterization of novel proteins which might be related to drug resistance, especially when no related mutations could explain it (Sharma et al., 2018).

CONCLUSION

The presented *in vitro* growth rate data could explain the spreading of *Rv0678* naturally occurring mutations in clinical settings also prior BDQ treatment, even if we cannot exclude the presence of other compensatory mutations that alleviate the cost of resistance without altering it. This evidence also suggests a role for fitness in BDQ-resistance spread, even if further investigations are needed to clearly elucidate this mechanism.

Overall, due to an increasing BDQ usage, it is urgent to implement a more extensive surveillance for such resistance in order to prevent the emergence of resistance in clinical settings. Our collection of polymorphisms responsible for BDQ resistance could be used as theranostics targets, such as in the development of a diagnostic kit for the early detection of BDQ resistant isolates to better manage the available therapeutic options.

DATA AVAILABILITY STATEMENT

All datasets presented in this study are included in the article/**Supplementary Material**.

AUTHOR CONTRIBUTIONS

GD and MP designed this study and interpreted the data. GD, JS, and MP wrote the manuscript. GD, JS, VS, PM, and AU performed experiments. All authors approved the final version of the manuscript.

FUNDING

GD is funded by a fellowship from the University of Pavia (FRG – Fondo Ricerca and Giovani: "Assegno di ricerca di tipo A"). This research was supported by the Italian Ministry of Education, University and Research (MIUR): Dipartimenti di Eccellenza Program (2018–2022) – Department of Biology and Biotechnology "Lazzaro Spallanzani", University of Pavia.

SUPPLEMENTARY MATERIAL

The Supplementary Material for this article can be found online at: https://www.frontiersin.org/articles/10.3389/fmicb.2020.559469/full#supplementary-material

REFERENCES

Ahmad, N., Ahuja, S. D., Akkerman, O. W., Alffenaar, J. C., Anderson, L. F., Baghaei, P., et al. (2018). Treatment correlates of successful outcomes in pulmonary multidrug-resistant tuberculosis: an individual patient data meta-analysis. *Lancet* 392, 821–834. doi: 10.1016/S0140-6736(18)31644-1

Almeida, D., Ioerger, T., Tyagi, S., Li, S. Y., Mdluli, K., Andries, K., et al. (2016). Mutations in pepQ Confer Low-level resistance to Bedaquiline and Clofazimine in *Mycobacterium tuberculosis*. *Antimicrob. Agents Chemother.* 60, 4590–4599. doi: 10.1128/AAC.00753-16

Andries, K., Verhasselt, P., Guillemont, J., Göhlmann, H. W., Neefs, J. M., Winkler, H., et al. (2005). A diarylquinoline drug active on the ATP synthase of *Mycobacterium tuberculosis*. *Science* 307, 223–227. doi: 10.1126/science.1106753

Andries, K., Villellas, C., Coeck, N., Thys, K., Gevers, T., Vranckx, L., et al. (2014). Acquired resistance of *Mycobacterium tuberculosis* to bedaquiline. *PLoS One* 9:e102135. doi: 10.1371/journal.pone.0102135

Belisle, J. T., and Sonnenberg, M. G. (1998). Isolation of genomic DNA from *Mycobacteria*. *Methods Mol. Biol.* 101, 31–44. doi: 10.1385/0-89603-471-2:31

Caminero, J. A., García-Basteiro, A. L., Rendon, A., Piubello, A., Pontali, E., and Migliori, G. B. (2019). The future of drug-resistant tuberculosis treatment: learning from the past and the 2019 World Health Organization consolidated guidelines. *Eur. Respir. J.* 54:1901272. doi: 10.1183/13993003.01272-2019

Chawla, K., Martinez, E., Kumar, A., Shenoy, V. P., and Sintchenko, V. (2018). Whole-genome sequencing reveals genetic signature of bedaquiline resistance in a clinical isolate of *Mycobacterium tuberculosis*. *J. Glob. Antimicrob. Resist.* 15, 103–104. doi: 10.1016/j.jgar.2018.09.006

Cole, S. T., Brosch, R., Parkhill, J., Garnier, T., Churcher, C., Harris, D., et al. (1998). Deciphering the biology of *Mycobacterium tuberculosis* from the complete genome sequence. *Nature* 393, 537–544.

Conradie, F., Diacon, A. H., Ngubane, N., Howell, P., Everitt, D., Crook, A. M., et al. (2020). Treatment of highly drug-resistant pulmonary tuberculosis. *N. Engl. J. Med.* 382, 893–902. doi: 10.1056/NEJMoa1901814

EUCAST (2020). *Bedaquiline/Mycobacterium tuberculosis 7H9 International MIC Distribution - Reference Database 2020-08-09*. Available online at: https://mic.eucast.org/Eucast2/regShow.jsp?Id=44655 (accessed August 9, 2020).

Ghajavand, H., Kargarpour Kamakoli, M., Khanipour, S., Pourazar Dizaji, S., Masoumi, M., Rahimi Jamnani, F., et al. (2019). High prevalence of bedaquiline resistance in treatment-naive tuberculosis patients and verapamil effectiveness. *Antimicrob. Agents Chemother.* 63:e02530-18. doi: 10.1128/AAC.02530-18

Hartkoorn, R. C., Uplekar, S., and Cole, S. T. (2014). Cross-resistance between clofazimine and bedaquiline through upregulation of MmpL5 in *Mycobacterium tuberculosis*. *Antimicrob. Agents Chemother.* 58, 2979–2981. doi: 10.1128/AAC.00037-14

Huitric, E., Verhasselt, P., Koul, A., Andries, K., Hoffner, S., and Andersson, D. I. (2010). Rates and mechanisms of resistance development in *Mycobacterium tuberculosis* to a novel diarylquinoline ATP synthase inhibitor. *Antimicrob. Agents Chemother.* 54, 1022–1028. doi: 10.1128/AAC.01611-09

Ismail, N. A., Omar, S. V., Joseph, L., Govender, N., Blows, L., Ismail, F., et al. (2018). Defining Bedaquiline susceptibility, resistance, cross-resistance and associated genetic determinants: a retrospective cohort study. *Ebiomedicine* 28, 136–142. doi: 10.1016/j.ebiom.2018.01.005

Kaniga, K., Cirillo, D. M., Hoffner, S., Ismail, N. A., Kaur, D., Lounis, N., et al. (2016). A multilaboratory, multicountry study to determine bedaquiline MIC quality control ranges for phenotypic drug susceptibility testing. *J. Clin. Microbiol.* 54, 2956–2962. doi: 10.1128/JCM.01123-16

Kodio, O., Georges Togo, A. C., Sadio Sarro, Y. D., Fane, B., Diallo, F., Somboro, A., et al. (2019). Competitive fitness of *Mycobacterium tuberculosis* in vitro. *Int. J. Mycobacteriol.* 8, 287–291. doi: 10.4103/ijmy.ijmy_97_19

Li, Y., Sun, F., and Zhang, W. (2019). Bedaquiline and delamanid in the treatment of multidrug-resistant tuberculosis: Promising but challenging. *Drug Dev Res.* 80, 98–105. doi: 10.1002/ddr.21498

Martinez, E., Hennessy, D., Jelfs, P., Crighton, T., Chen, S. C., and Sintchenko, V. (2018). Mutations associated with in vitro resistance to bedaquiline in *Mycobacterium tuberculosis* isolates in Australia. *Tuberculosis* 111, 31–34. doi: 10.1016/j.tube.2018.04.007

Melnyk, A. H., Wong, A., and Kassen, R. (2015). The fitness costs of antibiotic resistance mutations. *Evol. Appl.* 8, 273–283. doi: 10.1111/eva.12196

Menendez, C., Rodriguez, F., Ribeiro, A. L., Zara, F., Frongia, C., Lobjois, V., et al. (2013). Synthesis and evaluation of α-ketotriazoles and α,β-diketotriazoles as inhibitors of *Mycobacterium tuberculosis*. *Eur. J. Med. Chem.* 69, 167–173. doi: 10.1016/j.ejmech.2013.06.042

Milano, A., Pasca, M. R., Provvedi, R., Lucarelli, A. P., Manina, G., Ribeiro, A. L., et al. (2009). Azole resistance in *Mycobacterium tuberculosis* is mediated by the MmpS5-MmpL5 efflux system. *Tuberculosis* 89, 84–90. doi: 10.1016/j.tube.2008.08.003

Nieto Ramirez, L. M., Quintero Vargas, K., and Diaz, G. (2020). Whole genome sequencing for the analysis of drug resistant strains of *Mycobacterium tuberculosis* : a systematic review for Bedaquiline and Delamanid. *Antibiotics* 9:E133. doi: 10.3390/antibiotics9030133

Palomino, J. C., Martin, A., Camacho, M., Guerra, H., Swings, J., and Portaels, F. (2002). Resazurin microtiter assay plate: simple and inexpensive method for detection of drug resistance in *Mycobacterium tuberculosis*. *Antimicrob. Agents Chemother.* 46:2720.

Pang, Y., Zong, Z., Huo, F., Jing, W., Ma, Y., Dong, L., et al. (2017). In vitro drug susceptibility of bedaquiline, delamanid, linezolid, clofazimine, moxifloxacin, and gatifloxacin against extensively drug-resistant tuberculosis in Beijing, China. *Antimicrob. Agents Chemother.* 61:e0900-17. doi: 10.1128/AAC.00900-17

Philley, J. V., Wallace, R. J. Jr., Benwill, J. L., Taskar, V., Brown-Elliott, B. A., and Thakkar, F. (2015). Preliminary Results of Bedaquiline as salvage therapy for patients with nontuberculous mycobacterial lung disease. *Chest* 148, 499–506. doi: 10.1378/chest.14-2764

Pontali, E., Raviglione, M. C., Migliori, G. B., and The writing group members of the Global TB Network Clinical Trials Committee (2019). Regimens to treat multidrug-resistant tuberculosis: past, present and future perspectives. *Eur. Respir. Rev.* 28:190035. doi: 10.1183/16000617.0035-2019

Preiss, L., Langer, J. D., Yildiz, O., Eckhardt-Strelau, L., Guillemont, J. E., Koul, A., et al. (2015). Structure of the mycobacterial ATP synthase Fo rotor ring in complex with the anti-TB drug bedaquiline. *Sci. Adv.* 1:e1500106. doi: 10.1126/sciadv.1500106

Radhakrishnan, A., Kumar, N., Wright, C. C., Chou, T. H., Tringides, M. L., Bolla, J. R., et al. (2014). Crystal structure of the transcriptional regulator Rv0678 of *Mycobacterium tuberculosis*. *J. Biol. Chem.* 289, 16526–16540. doi: 10.1074/jbc.M113.538959

Segala, E., Sougakoff, W., Nevejans-Chauffour, A., Jarlier, V., and Petrella, S. (2012). New mutations in the mycobacterial ATP synthase: new insights into the binding of the diarylquinoline TMC207 to the ATP synthase C-ring structure. *Antimicrob. Agents Chemother.* 56, 2326–2334. doi: 10.1128/AAC.06154-11

Sharma, D., Bisht, D., and Khan, A. U. (2018). Potential alternative strategy against drug resistant tuberculosis: a proteomics prospect. *Proteomes* 6:26. doi: 10.3390/proteomes6020026

Sharma, D., Sharma, S., and Sharma, J. (2020). Potential strategies for the management of drug-resistant tuberculosis. *J. Glob. Antimicrob. Resist.* 22, 210–214. doi: 10.1016/j.jgar.2020.02.029

Smith, C. S., Aerts, A., Saunderson, P., Kawuma, J., Kita, E., and Virmond, M. (2017). Multidrug therapy for leprosy: a game changer on the path to elimination. *Lancet Infect. Dis.* 17:e00293-97. doi: 10.1016/S1473-3099(17)30418-8

Veziris, N., Bernard, C., Guglielmetti, L., Le Du, D., Marigot-Outtandy, D., Jaspard, M., et al. (2017). Rapid emergence of *Mycobacterium tuberculosis* bedaquiline resistance: lessons to avoid repeating past errors. *Eur. Respir. J.* 49:1601719. doi: 10.1183/13993003.01719-2016

Viljoen, A., Raynaud, C., Johansen, M. D., Roquet-Banères, F., Herrmann, J. L., Daher, W., et al. (2019). Improved activity of bedaquiline by verapamil against Mycobacterium abscessus in vitro and in macrophages. *Antimicrob. Agents Chemother.* 63:e0705-19. doi: 10.1128/AAC.00705-19

Villellas, C., Coeck, N., Meehan, C. J., Lounis, N., de Jong, B., Rigouts, L., et al. (2017). Unexpected high prevalence of resistance-associated Rv0678 variants in MDR-TB patients without documented prior use of clofazimine or bedaquiline. *J. Antimicrob. Chemother.* 72, 684–690. doi: 10.1093/jac/dkw502

World Health Organization [WHO] (2019a). *Global Tuberculosis Report*. Available online at: https://apps.who.int/iris/bitstream/handle/10665/329368/9789241565714-eng.pdf?ua=1 (accessed October 17, 2019).

World Health Organization [WHO] (2019b). *World Health Organization [WHO] Consolidated Guidelines on Drug-Resistant Tuberculosis Treatment*. Available at: https://www.who.int/tb/publications/2019/consolidated-guidelines-drug-resistant-TB-treatment/en/ (accessed October 17, 2019).

Xu, J., Wang, B., Hu, M., Huo, F., Guo, S., Jing, W., et al. (2017). Primary clofazimine and bedaquiline resistance among isolates from patients with multidrug-resistant tuberculosis. *Antimicrob. Agents Chemother.* 61:e0239-17. doi: 10.1128/AAC.00239-17

Zhang, S., Chen, J., Cui, P., Shi, W., Zhang, W., and Zhang, Y. (2015). Identification of novel mutations associated with clofazimine resistance in *Mycobacterium tuberculosis*. *J. Antimicrob. Chemother.* 70, 2507–2510. doi: 10.1093/jac/dkv150

Zimenkov, D. V., Nosova, E. Y., Kulagina, E. V., Antonova, O. V., Arslanbaeva, L. R., Isakova, A. I., et al. (2017). Examination of bedaquiline- and linezolid-resistant *Mycobacterium tuberculosis* isolates from the Moscow region. *J. Antimicrob. Chemother.* 72, 1901–1906. doi: 10.1093/jac/dkx094

Conflict of Interest: The authors declare that the research was conducted in the absence of any commercial or financial relationships that could be construed as a potential conflict of interest.

frontiers in Microbiology

ORIGINAL RESEARCH
published: 18 September 2020
doi: 10.3389/fmicb.2020.553962

High-Content Screening of Eukaryotic Kinase Inhibitors Identify CHK2 Inhibitor Activity Against *Mycobacterium tuberculosis*

*Tirosh Shapira[1], Leah Rankine-Wilson[2], Joseph D. Chao[1], Virginia Pichler[2], Celine Rens[2], Tom Pfeifer[2] and Yossef Av-Gay[1,2]**

[1] Division of Infectious Diseases, Department of Medicine, The University of British Columbia, Vancouver, BC, Canada, [2] Department of Microbiology and Immunology, Life Sciences Institute, The University of British Columbia, Vancouver, BC, Canada

A screen of a eukaryotic kinase inhibitor library in an established intracellular infection model identified a set of drug candidates enabling intracellular killing of *Mycobacterium tuberculosis* (*M.tb*). Screen validity was confirmed internally by a $Z' = 0.5$ and externally by detecting previously reported host-targeting anti-*M.tb* compounds. Inhibitors of the CHK kinase family, specifically checkpoint kinase 2 (CHK2), showed the highest inhibition and lowest toxicity of all kinase families. The screen identified and validated DDUG, a CHK2 inhibitor, as a novel bactericidal anti-*M.tb* compound. CHK2 inhibition by RNAi phenocopied the intracellular inhibitory effect of DDUG. DDUG was active intracellularly against *M.tb*, but not other mycobacteria. DDUG also had extracellular activity against 4 of 12 bacteria tested, including *M.tb*. Combined, these observations suggest DDUG acts in tandem against both host and pathogen. Importantly, DDUG's validation highlights the screening and analysis methodology developed for this screen, which identified novel host-directed anti-*M.tb* compounds.

Keywords: tuberculosis, CHK2, host-directed therapy, kinase inhibitor, screen

OPEN ACCESS

Edited by:
Alessandra Polissi, University of Milan, Italy

Reviewed by:
Priscille Brodin, Institut National de la Santé et de la Recherche Médicale (INSERM), France
Parvinder Kaur, Foundation for Neglected Disease Research, India

****Correspondence:***
Yossef Av-Gay
yossi@mail.ubc.ca

Specialty section:
This article was submitted to Antimicrobials, Resistance and Chemotherapy, a section of the journal Frontiers in Microbiology

Received: *20 April 2020*
Accepted: *21 August 2020*
Published: *18 September 2020*

Citation:
Shapira T, Rankine-Wilson L, Chao JD, Pichler V, Rens C, Pfeifer T and Av-Gay Y (2020) High-Content Screening of Eukaryotic Kinase Inhibitors Identify CHK2 Inhibitor Activity Against Mycobacterium tuberculosis. Front. Microbiol. 11:553962. doi: 10.3389/fmicb.2020.553962

INTRODUCTION

Tuberculosis (TB) caused by *Mycobacterium tuberculosis* (*M.tb*) infects one quarter of the world's population and kills 1.5–2 million people annually, with a global case fatality rate of 16% and a poor treatment success rate of 55% for multidrug resistant TB (WHO, 2018). Current treatment for tuberculosis involves a cocktail of four first-line drugs including rifampicin, isoniazid, ethambutol, and pyrazinamide for 6–9 months (CDC, 2016), often involving patient isolation in treatment facilities specializing in tuberculosis management. To further exacerbate the threat TB places on global health and economy, global rates of multidrug resistant *M.tb* cases has been rising considerably (WHO, 2018). Second-line drugs are intended to be used sparingly due to decreased efficacy and greater toxicity-associated complications, as well as to limit the emergence of extensively drug resistant strains. The development of safer drugs and the use of synergistic drugs to reduce drug concentrations and subsequent toxicity has been in the forefront of the global campaign against TB. Identifying the mechanisms of action of current drugs, as well as understanding the mechanisms of host-pathogen interactions between *M.tb* and alveolar macrophage to generate new targets for drug intervention, is fundamental to this effort (Parish, 2020).

Mycobacterium tuberculosis' pathogenicity is strongly associated with its long co-evolution with its obligate human host, which allowed the development of mechanisms of subverting host defenses to permit its successful infection, persistence, and dissemination (Poirier and Av-Gay, 2012; Hmama et al., 2015). *M.tb* primarily infects, survives, and replicates inside human macrophages, and it evades host phagocytic activity via a series of kinase and phosphatase effectors, among other methods (Poirier and Av-Gay, 2012). The most notable of these is the secreted protein tyrosine phosphatase PtpA, which inhibits both phagosome acidification and phagosome-lysosome fusion (Bach et al., 2008; Wong et al., 2011). By tracing the activity of PtpA, the macrophage's GSK3 was discovered as a prominent host target of PtpA (Poirier et al., 2014). Anti-inflammatory agents such as the non-steroidal anti-inflammatory drugs (Kroesen et al., 2017) and signaling modulation agents such as metformin (Padmapriyadarsini et al., 2019) provide a promising avenue for a new line of adjunctive TB therapeutics termed host-directed therapies (HDTs). HDTs are exciting for their potential to treat drug-resistant *M.tb*, synergistically enhance the activity of current *M.tb* drugs, and may not be susceptible themselves to resistance development (Tobin, 2015).

Current anti-tuberculosis treatments have been developed against extracellular bacteria without the consideration for intracellular infection dynamics or host responses outside general toxicity testing. For example, the most recently FDA-approved TB compound, pretomanid, developed in 1993 (Ashtekar et al., 1993), was initially tested *in vitro* and *in vivo* only, with *ex vivo* (via macrophage infection) analytics being overshadowed. New developments of intracellular screening technologies have made *ex vivo* screening a powerful tool for high throughput drug discovery, taking into consideration the first and arguably most important infection niche (Sorrentino et al., 2016; Parish, 2020). Another historic hurdle to overcome in development of drugs against *M.tb* is the use of non-*M.tb* models for top-down screening due to their simpler upkeep requirements. However, drugs have proven to have significantly different activities against different mycobacteria family members, as in the case of pretomanid, which shows no activity against the closely related *Mycobacterium avium* and *Mycobacterium intracellulare* (Ashtekar et al., 1991). In compound screening campaigns, compromising on screening models that are remote from the pathogen (*M.tb*) and its host (human macrophages) can generate false negatives, i.e., hit compounds that fail "hit-to-lead" development, and false positives, i.e., rejection of compounds that may be active if the screening would have presented a biologically relevant model. One major hurdle in screening campaigns for new therapeutics against *M.tb* is the expensive and labor-intensive requirements of Biological Contamination Level (BCL) 3 facilities. The BCL2-safe MC^2 6206 auxotrophic strain of *M.tb* (ΔleuDΔpanCD), originally developed as a vaccine model (Sampson et al., 2004), was previously used successfully to test anti-*M.tb* compounds (Schaaf et al., 2016; Mouton et al., 2019).

With the pressing need for new drugs to combat the TB pandemic and development of technologies that allow accurate testing of intracellular *M.tb* infection models, HDTs have been increasingly investigated in recent years (Kolloli and Subbian, 2017). A study that investigated RNAi targeting host kinases and their effect on intracellular *M.tb* growth in mouse macrophages uncovered a variety of important host pathways crucial for infection (Jayaswal et al., 2010) including the TGFβR1 and CDC25A signaling networks, and this was corroborated in a human macrophage screen (Kumar et al., 2010). Screening of prospective HDTs has been accelerated by the development of anti-cancer therapeutics libraries, with a multitude of libraries available for academic and commercial use (Babichev et al., 2016). Additionally, high-content screening (HCS) allows for reliable and valid data acquisition from macrophages infected vs. uninfected with *M.tb* (Sahile et al., 2020). Additionally, the development of the THP-1 human macrophage model as a validated model for human primary macrophages has allowed for high throughput advances (Johnson and Abramovitch, 2015; Madhvi et al., 2019). This study aimed to harness all these advancements to identify novel anti-*M.tb* HDTs and characterize the networks of host kinases important for inhibition of intracellular *M.tb*.

MATERIALS AND METHODS

Bacterial and Mammalian Strains and Culturing

Mycobacterium tuberculosis strain H37Rv, *Mycobacterium abscessus* ATCC 19977T, R (rough form), and *Mycobacterium bovis*-BCG were all transformed with the pTEC27 fluorescent reporter plasmid, harboring a tomatoRFP and hygromycin resistance gene (Bernut et al., 2014; Cambier et al., 2014). All the mycobacterial strains were routinely grown in 7H9 broth (Difco Middlebrook) supplemented with 10% (v/v) OADC (5% bovine albumin fraction, 2% dextrose, 0.004% catalase, 0.05% oleic acid, and 0.8% sodium chloride solution), 0.05% (v/v) Tween-80 (Sigma-Aldrich), and 50 μg/mL hygromycin B at 37°C in standing cultures. Other bacteria used are listed in **Table 3** with their strain number and were cultivated according to ATCC recommendations.

The THP-1 cells (ATCC TIB-202^{TM}) used are derived from human monocytes obtained from a patient with acute monocytic leukemia. THP-1 cells were grown in complete RPMI1640 medium (5% FBS, 2% glutamine, 1% non-essential amino acids, and 1% penicillin and streptomycin). Cells were grown in T75 flask with 5% carbon dioxide (CO2) at 37°C. Cell density was kept between 0.25 and 1 × 10^6 cells/mL. Cultures were used for up to three months. For assays, RPMI1640 medium with all supplements but antibiotics (incomplete RPMI1640 medium) was used. Bone marrow derived macrophages (BMDM) were kindly provided by P. Johnson and M. Dosanjh from C57BL/6, produced using 500 UI/mL M-CSF in DMEM.

Compounds

A duplicated OICR Kinase library at 10 μM was the kind contribution of the Centre for Drug Research and Development (now adMare, BC, Canada). Imatinib (G40700), 10-DEBC (D298368), and Tandutinib (T006550) were purchased

from TRC Canada (ON, Canada). DDUG (SML0781) was purchased from Sigma-Aldrich (MO, United States). Bedaquiline (TMC-207) was purchased from AddoQ (CA, United States). All compounds were solubilized in DMSO at a concentration of 10 mM.

Infection

Bacterial culture grown to log phase was centrifuged (4000 rpm, RT for 10 min) and washed once in 7H9 media containing 0.05% Tween 80 (20%). The supernatant was discarded after centrifugation and the pellets were then re-suspended in RPMI1640 medium, de-clumped using a 25G blunt syringe, and OD_{600} was measured (OD_{600} of 1 $\approx$ 3.3 $\times$ 10^8 CFU/mL). Immediately before the infection the bacterial suspension was opsonized by adding non-decomplemented 10% human serum and incubating for 30 min at 37°C. A cell suspension of THP-1 cells (1 $\times$ 10^6 cells/mL) in incomplete RPMI1640 was incubated with the opsonized *M.tb* single cells suspension at a Multiplicity of Infection of 2:1, and phorbol12-myristate13-acetate PMA (40 ng/mL) for 4 h at 37°C under constant agitation, as previously described (Sorrentino et al., 2016). After infection, the THP-1 cell suspension was centrifuged (750 rpm, RT, 10 min) and washed with RPMI1640 3 times. After the final wash, cell suspension was dispensed onto 96-well plates (clear, flat bottom), at a concentration of ∼50,000 THP-1 cells/well. Infected cells plus compounds were incubated for 4 days at a volume of 100 μL/well at 5% CO_2 and 37°C. After incubation, cells were fixed with paraformaldehyde (PFA, 4% in warm PBS buffer) for 60 min (*M.tb*) or 30 min (*M. abscessus*, *M. bovis*-BCG), fixative removed, and stained with 1 μg/mL Hoechst 33342 in RPMI1640 for 10 min. Hoechst stain was removed, and cells kept in 100 μL RPMI1640. Plates were kept covered in aluminum foil until scanning to avoid photobleaching.

Bone marrow derived macrophages (BMDM) were identically used, with the sole difference of using DMEM medium rather than RPMI1640 medium.

Salmonella typhimurium transformed with a luminescent reporter plasmid, pCS26-Pac (Bjarnason et al., 2003), was grown overnight on a Luria-Bertani (LB) agar plate. A broth culture was started several hours prior to the infection. Once the culture reached an OD_{600} of 1, bacteria were pelleted by centrifugation and washed three times with RPMI media. The bacteria were then opsonized for 30 min at 37°C with 10% human serum. The opsonized bacteria were diluted in RPMI up to 1 $\times$ 10^6 CFU/mL and further incubated with THP-1 macrophages seeded at 1 $\times$ 10^5 cells per well in a 96-well plate, differentiated with PMA (40 ng/mL) for a 24 h prior to the infection. After 30 min of incubation, the infected cells were washed three times with fresh RPMI and incubated for an additional hour with 100 μg per mL of gentamicin to kill remaining extracellular bacteria. The infected cells were incubated with the tested compounds in presence of 10 μg/mL of gentamicin. The intracellular growth of the bacteria was assessed after 72 h of infection using luminescence. In order to normalize the bacterial growth to the number of surviving macrophages after 72 h of infection, THP-1 cells were counted using an HCS Platform as detailed below.

High Content Screening Methodology and Parameters

Monitoring of the intracellular bacterial growth and eukaryote nuclei was performed using the CellInsight CX5 High Content platform. First, the THP-1 nuclei are identified and counted using the 350/461 nm wavelength (Hoechst 33342); cell debris and other particles are deducted based on a size filter tool. Following that a Region of Interest (ROI, or "circle") is drawn around each host cell nuclei and validated against the brightfield image to correspond with most cell membranes. The ROI encompass where 533/588 nm wavelength (pTEC27, or "spots") are located. Finally, the software identifies, counts, and measures the pixel intensity of the "spots" within the "circle." The fluorescent spot intensity measured within each cell (circle) is then added and quantified for each well using Thermo Fisher Scientific™ HCS Studio™ Cell Analysis Software. The total circle spot intensity of each well corresponds to the intracellular bacterial load. We (Richter et al., 2019) and others have previously validated these fluorescent measurements closely correspond with CFUs. Nuclei stain (Hoechst 33342) was used to quantify THP-1 cell loss (due to cytotoxicity or loss of adherence).

Screening

A compound screen strategy utilized the Ontario Institute for Cancer Research Kinase Inhibitor library (Babichev et al., 2016) was kindly supplied by the Centre for Drug Research & Development, BC, Canada. Library was screened in duplicate, at a single dose-concentration of 10 μM. Before the screen, a Z′ calibration was performed testing rifampicin and bedaquiline (data not shown), after which bedaquiline at a concentration of 4 μM was chosen as the positive control, while the compound solvent, DMSO was used as a negative control at a concentration of 1%. Z′ were tested for each individual compound plate, with an average Z′ of 0.5 (±0.1) using the "CircSpotTotalInten" readout. The Z′ factor was determined using the formula:

$$Z' = 1 - \frac{3(\mathrm{SD}_{\mathrm{bedaquilin}} + \mathrm{SD}_{\mathrm{DMSO}})}{(\mathrm{M}_{\mathrm{bedaquilin}} - \mathrm{M}_{\mathrm{DMSO}})}$$

where SD is the standard deviation and M is mean.

For compound targets, close family-members were clustered together. For example, checkpoint kinase 1 (CHK1) and CHK2 were clustered under the CHK family, and VEGFR1, 2, and 3 were clustered under the VEGFR family. Target family average activities, average toxicities, filtering, and graphing were preformed using JMP®, version 14 (SAS Institute Inc.).

Intracellular and Broth Dose-Response, Disk Diffusion Test

Intracellular dose-response of bacterial load (pTEC27 intracellular signal) was performed at dilution factors of 1:1, at range 0.2 μM < (C) < 50 μM, with at least three biological replications per concentration ($4 \leq n \leq 8$ technical replication). Bacterial loads were interpolated to negative control (1% DMSO) = 0, and positive

control (4 μM bedaquiline) = 100. GraphPad Prism 6 (GraphPad Software, Inc.) non-linear regression fit modeling variable slope was used to generate a dose-response curve $[Y = \text{Bottom} + (\text{Top} - \text{Bottom})/1 + 10^{(\text{LogIC50}-X)\times\text{HillSlope}}]$, constrained to top = 100, bottom = 0.

Broth dose-response performed at similar concentrations and replications, using 0.02% resazurin sodium salt (B21187.06, Alfa Aesar Chemicals, MA, United States). Bacteria strains listed in **Table 3** and cultivated using strain-appropriate culturing methods. To apply identical controls for all bacteria tested, a cocktail of 10 μM apramycin, vancomycin, and gentamicin was used as a positive control, and water as negative control.

Disk diffusion assay based on the Kirby-Bauer method (Bauer et al., 1966) using 10 μg DDUG, disks of 10 μg apramycin, vancomycin, or gentamicin as positive controls, and water disk as negative control. Sensitivity (%) calculated based on gentamicin, as the active control in all strains who showed a DDUG effect. The experiment was performed in triplicate.

RNAi Interference

THP-1 cells were seeded at 50,000 cells per well in 96-well clear flat bottom plates and differentiated overnight in incomplete RPMI1640 media with 40 ng/mL PMA to ensure RNAi treatment is performed on fully differentiated cells. Cells were transfected using 10 pmole siRNA (IDT) and 2 μL of HiPerFect transfection reagent (Qiagen, Germany) per well, following the supplied protocol. Cells were infected with *M.tb* after 24 h. RNAi inhibition was not verified with qPCR due to COVID-19 efforts, resulting in lack of reagents.

RESULTS

HCS Reveals Established and Novel Active Compounds Against Intracellular *M.tb*

To identify host-targeting anti-*M.tb* compounds, we screened the OICR Kinase library, a small library of kinase inhibitors at various stages of clinical trials, or those used as molecular tools in kinase-inhibitory studies. Our strategy used an established THP-1 human macrophage model (Madhvi et al., 2019), infected with fluorescence-expressing *M.tb*, automatically analyzed and quantified using HCS (**Supplementary Figure 1**). Screening of the OICR Kinase library revealed that 32 out of 400 compounds showed inhibition of *M.tb* intracellular growth >50% compared to that of 4 μM bedaquiline positive control (**Table 1** and **Supplementary Table 1**).

TABLE 1 | Criteria used to filter screen hits.

	Yes (%)	No (%)
Inhibition >50%	32 (8)	368 (92)
Cell loss <30%	169 (42)	231 (58)
Negative *z*-score	56 (14)	344 (86)
Duplicate	365 (91)	35 (9)

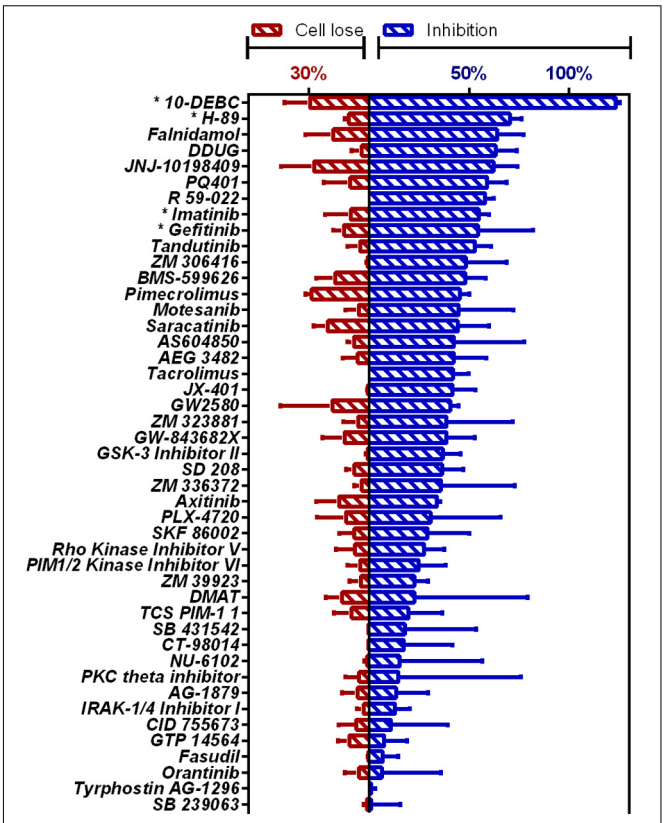

FIGURE 1 | HCS of OICR Kinase Inhibitor library against intracellular *M.tb*. Inhibition of *M.tb* growth (blue), interpolated to the negative control (1% DMSO) set at 0% inhibition and the positive control (4 μM bedaquiline) defined as 100% inhibition. Cell loss (red), normalized to negative control. Previously identified host-targeting *M.tb* inhibitors marked with asterisk (*). Means from compounds with negative *z*-score and cell loss <30% (n = 45) are graphed. Error bars represent the SD from two independent screens. Full list of compounds and *z*-scores are tabled in **Supplementary Table 2**.

Novel compounds highly active against *M.tb* in our assay (**Figure 1** and **Supplementary Table 2**) were Falnidamol, targeting host epidermal growth factor receptor (EGFR); DDUG, targeting host CHK2; JNJ-10198409, targeting host platelet-derived growth factor receptor (PDGF-R); PQ401, targeting host insulin-like growth factor 1 receptor (IGF-1R); R 59-022, targeting diacylglycerol kinase (DAG); and Tandutinib, targeting host fms-like tyrosine kinase 3 (FLT3), KIT, and platelet-derived growth-factor receptor (PDGFR).

Additionally, our assay identified many compounds previously shown to inhibit *M.tb* growth in various other intracellular models of infection. For example, 10-DEBC inhibits *M.tb* in macrophages differentiated from human embryonic stem cells (Han et al., 2019); H-89 inhibits *M.tb* in primary human macrophages (Kuijl et al., 2007); Imatinib in J774A.1 murine macrophage-like cell line (Napier et al., 2011); and Gefitinib also in J774 (Stanley et al., 2014; Sogi et al., 2017).

Our HCS assay enabled us to simultaneously monitor the effect of candidate drugs on bacterial growth and the host cells' viability, measured as intracellular fluorescence and loss of host

cells, respectively (**Supplementary Figure 2**). As such, although the effect of compounds that eradicate host cells also reduce bacterial load, we were able to distinguish between the two.

Kinase Target Families Show Different Inhibition of Intracellular *M.tb*, With Clear Link Between Toxicity and Activity

While allowing identification of specific inhibitory compounds and their host toxicity, using a library with well-defined compounds allows investigation of the compound families as well. Following similar, biologically relevant, filtering parameters for individual compound analysis (**Figure 2A**), we investigated the intracellular *M.tb* growth inhibition (activity) and host cell loss (toxicity).

In the activity and toxicity analysis, we chose library compounds that were characterized as inhibiting only single targets. The average activity across represented kinase families was 27.16% (**Figure 2B**), with the CHK family of inhibitors representing the highest mean activity.

Many of the library compounds were developed to exert toxicity to cancerous cells and are hypothesized to have a similar effect on the leukemia-derived THP-1 cell line. As our assay measures intracellular bacteria, such measurements can be biased by host-cell toxicity. We therefore set to test the relation between target activity and its toxicity (**Figure 2C**). A regression fit of R^2 = 0.36 and RMSE of 9.66% suggests for many compounds' targets, increase in toxicity was correlated with increase in activity and can partially or completely explain the observed activity.

Compound targets residual analysis (**Figure 2D**) exposed targeting the CHK, IGF-1R, and DAG kinases resulted in activity higher than can be expected from toxicity, while targeting casein kinases (CK), PDGF-R, and human epidermal growth factor receptor 2 (HER2) displayed much lower activity relative to the levels of associated toxicity. Of note, from the top 10 active compounds, Tandutinib is the only novel compound targeting multiple kinases, including FLT3 (+5% residual) and PDGF-R (−12% residual), while the rest are single-target inhibitors.

Confirmation of the CHK2 Inhibitor DDUG as a Host-Targeting *M.tb* Inhibitor

To confirm the HCS results, we chose to focus on DDUG, a CHK2 inhibitor displaying low host cell loss but high level of inhibition of *M.tb* intracellular growth. We also examined Tandutinib as multi-target inhibitor, and Imatinib and 10-DEBC as controls. Dose-dependant analysis of the effect of the selected compounds against intracellular *M.tb* (**Figure 3A**) confirmed the HCS results and demonstrated, as previously reported, that host-targeting compounds can also exert their inhibitory effect in a dose-dependant manner like antibiotics (Stanley et al., 2014). DDUG's MIC_{50} values were approximately twice as inhibitory as those of 10-DEBC, indicating the high inhibition by 10-DEBC in the screen might be somewhat biased by high cell loss. DDUG was not active against *M.tb* in mouse primary macrophages (**Figure 3B**).

To validate cell-loss HCS results, we examined cell loss in THP-1 and in mouse bone-marrow derived macrophages (BMDM) (**Figure 3C**). Like inhibition, HCS results were confirmed in dose-dependant analysis. In BMDM, DDUG and 10-DEBC showed low cell loss, corresponding to ∼16- and 10-fold higher, than their respective MIC_{50} values. While DDUG cell loss was comparable between primary and immortalized cells (LD_{50} = 25.1 μM and LD_{50} = 27.2 μM, respectively), 10-DEBC's stark cell loss in THP-1 cells was almost completely nullified (LD_{50} = 6.5 μM and LD_{50} = 33.3 μM, respectively). As 10-DEBC showed no significant toxicity in macrophages differentiated from primary stem cells (Han et al., 2019), it is likely that 10-DEBC is specifically toxic to the THP-1 model.

DDUG is a selective inhibitor of the cell-cycle regulator kinase CHK2. CHK2 suppression using RNAi was able to inhibit intracellular *M.tb* growth with inhibition levels equivalent to those found in the screen (∼10 μM, **Figure 3D**), suggesting host CHK2 inhibition may explain the inhibitory potential of DDUG and providing validation to the small compound approach using a gene-knockdown approach.

DDUG Is Bactericidal and Specific to Intracellular *M.tb*, While 10-DEBC Is Bacteriostatic and Inhibits Other Intracellular Mycobacteria Species

To test whether DDUG is bacteriostatic or bacteriolytic to *M.tb* during intracellular infection, a time-course colony-forming units (CFU) assay of *M.tb* in the presence of 10 μM DDUG was performed, and 10-DEBC was similarly tested, as this fundamental information was not reported. DDUG showed bactericidal properties similar to that of the positive rifampicin bactericidal control, while 10-DEBC seemed to act as a bacteriostatic compound with no significant change in CFU/cell in a span of 4 days, where the untreated control replicated twice (**Figure 4A**).

To test if these compounds are specific to *M.tb* or might be affecting mycobacteria in general, we infected THP-1 with the fast-growing *M. abscessus* and the vaccine strain, *M. bovis*-BCG, harboring the same pTEC27 fluorescent reporter plasmid. DDUG's intracellular activity specifically inhibited *M.tb* and had no inhibitory effect on the growth of the other mycobacteria tested (**Figure 4B**) compared to the untreated control. Conversely, 10-DEBC was found to be a general inhibitor against mycobacteria, inhibiting both *M. abscessus* and *M. bovis*-BCG, each with a MIC_{50} of approximately 10 μM (**Figure 4B**). DDUG was also able to inhibit another intracellular bacteria, luciferase-expressing *S. typhimurium*, at a MIC_{50} = 8.9 μM (**Figure 4C**), ∼5-fold less intracellular inhibition than with *M.tb* (**Figure 4D**).

DDUG and Other Host-Directed Therapies Are Effective Against the *M.tb* Auxotroph

To examine if the BCL2-safe MC^2 6206 auxotrophic strain of *M.tb* may be a plausible model for host-targeted compound screens, we tested if the auxotroph is sensitive to DDUG and the previously characterized HDTs Imatinib and 10-DEBC. The auxotroph was indeed inhibited intracellularly by all three

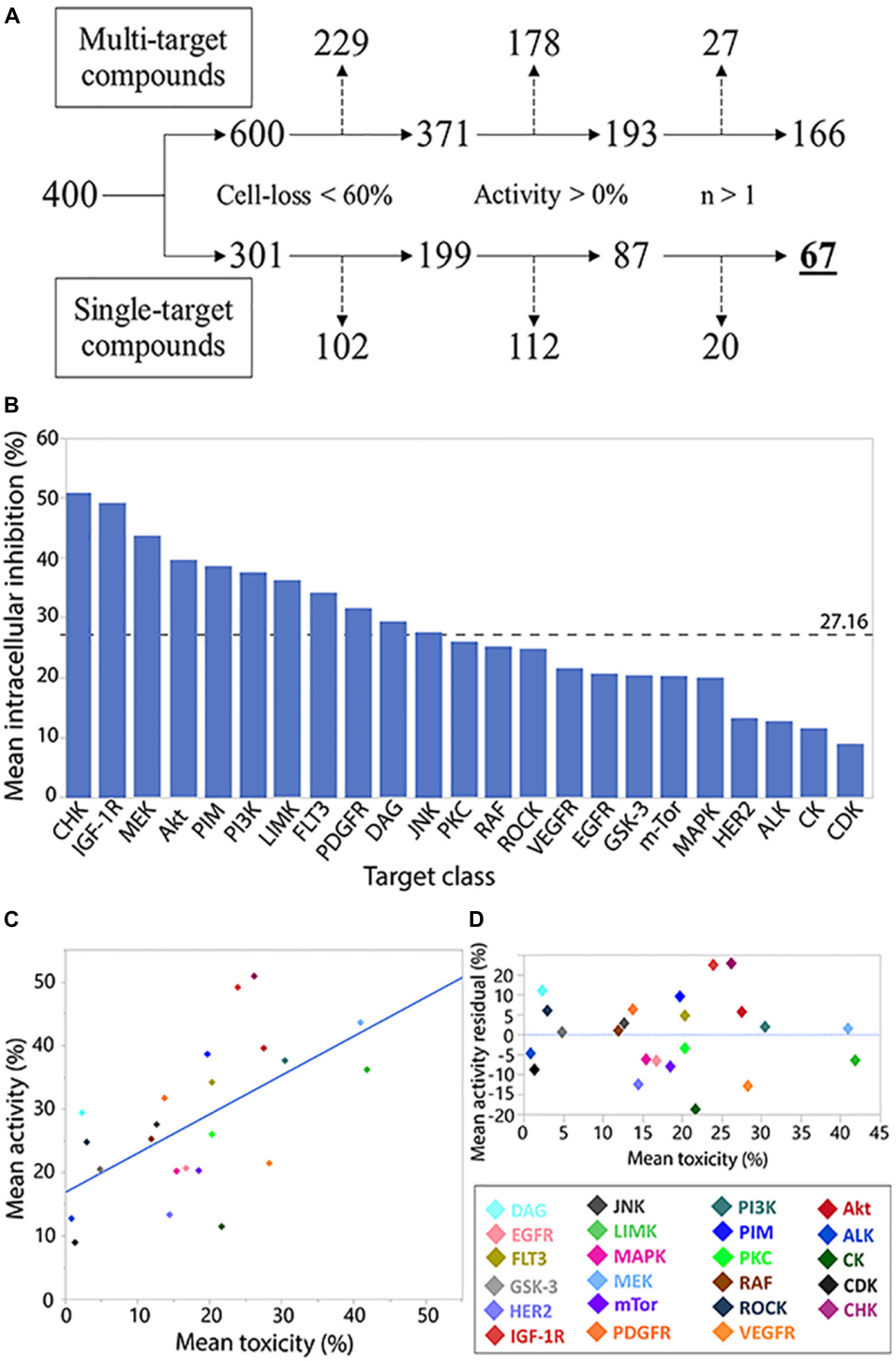

FIGURE 2 | Analysis of compound target class/family. Flowchart analysis of the logic steps taken to ensure activity characterization (measuring normalized intracellular bacterial growth inhibition) of target families was gathered from non-pleiotropic compounds (single-target compounds) and were not skewed by THP-1 cell-loss, exhibit anti-*M.tb* activity, and were represented by more than 1 compound in the library. Branch shifts from compound numbers (400) to compound target numbers (600/301). Excluded targets from each step marked by dashed arrows **(A)**. Compound family charted by mean inhibitory activity. Weighted average marked by dashed line **(B)**. Regression analysis of family toxicity (cell-loss) on activity resulted in linear regression with RMSE = 9.66% (R^2 = 0.36) **(C)**. Analysis of residual activity by target family classes. Positive or negative residual values represent higher or lower activity, respectively, than can be explained by toxicity effects against THP-1 cells **(D)**.

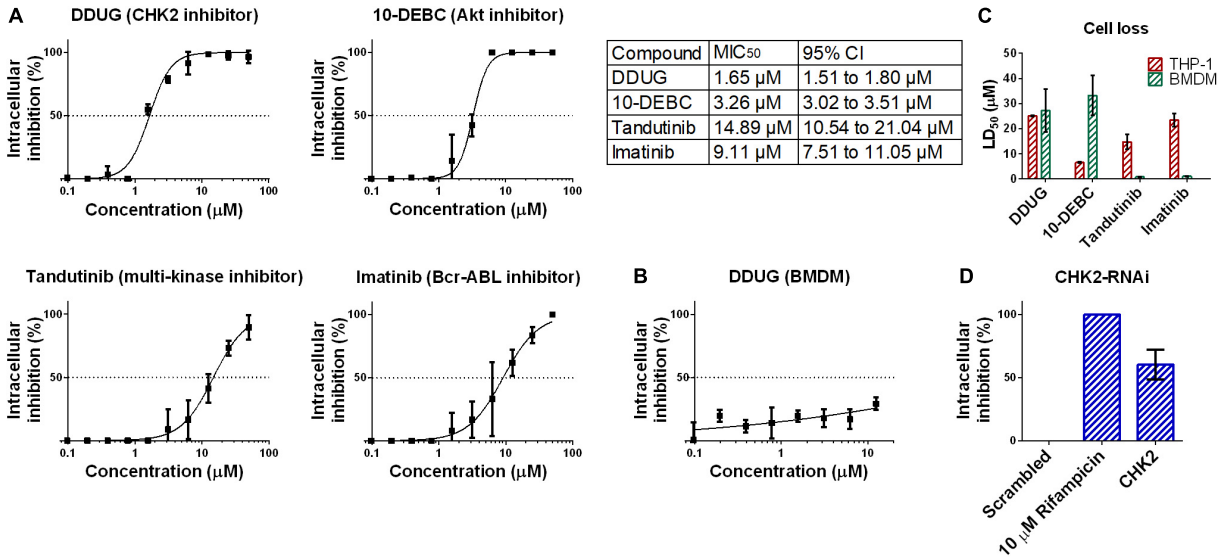

Compound	MIC50	95% CI
DDUG	1.65 μM	1.51 to 1.80 μM
10-DEBC	3.26 μM	3.02 to 3.51 μM
Tandutinib	14.89 μM	10.54 to 21.04 μM
Imatinib	9.11 μM	7.51 to 11.05 μM

FIGURE 3 | Confirmation of DDUG inhibition of *M.tb* growth in infected THP-1 cells. Dose-dependent inhibition of *M.tb*:THP-1 intracellular growth by novel and established compounds, normalized to 1% DMSO negative control (0% inhibition) **(A)**. CI, confidence interval. DDUG inhibition of *M.tb* growth in infected bone marrow derived macrophages (BMDM) cells **(B)**. Dose-dependant cell loss of THP-1 (red) and bone marrow derived macrophages (BMDM) cells (green) **(C)**. *M.tb* intracellular growth inhibition by RNAi suppression of the DDUG target, CHK2, interpolated to the negative control (1% DMSO) set at 0% inhibition and the positive control (4 μM bedaquiline) defined as 100% inhibition **(D)**. Each data point is an average of 4 independent trials, and error bars are the SEM.

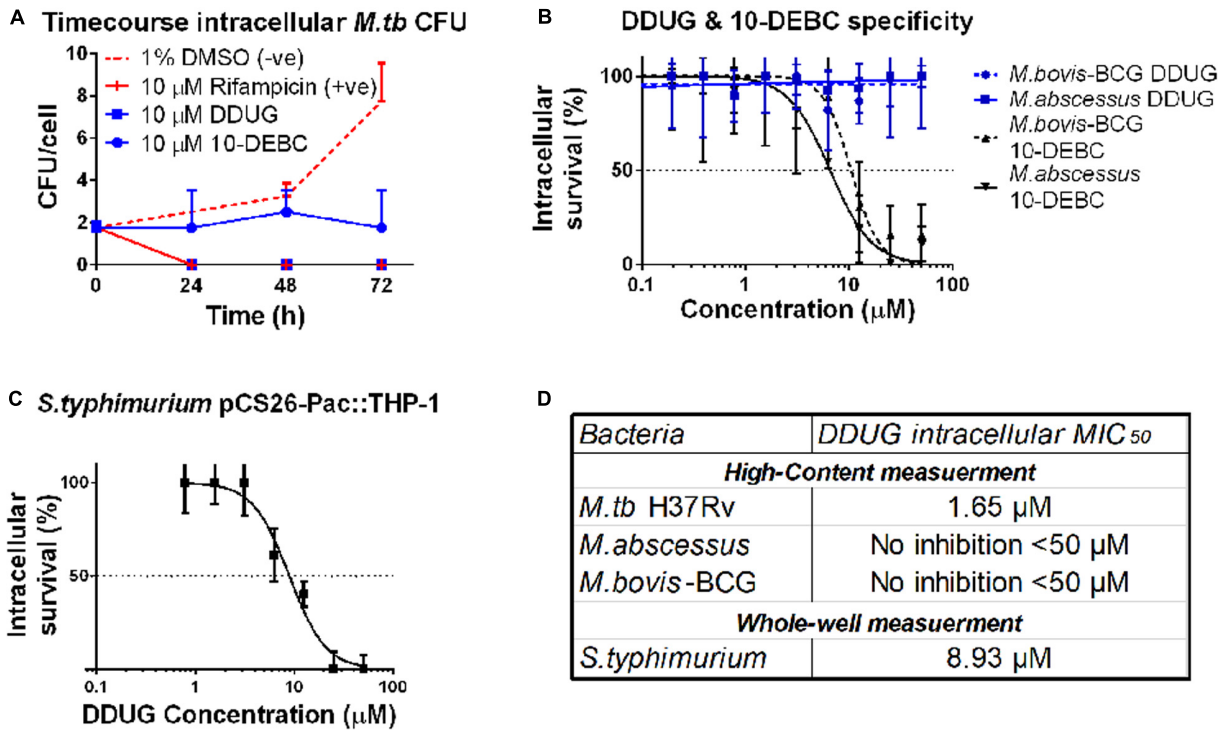

D

Bacteria	*DDUG intracellular MIC 50*
High-Content measuerment	
M.tb H37Rv	1.65 μM
M.abscessus	No inhibition <50 μM
M.bovis-BCG	No inhibition <50 μM
Whole-well measuerment	
S.typhimurium	8.93 μM

FIGURE 4 | DDUG Mode of intracellular inhibition and Mycobacteria specificity. Intracellular CFU calculated by normalizing to number of THP-1 cells, treated with DDUG (blue squares) or 10-DEBC (blue circles) or controls (red) **(A)**. Compound specificity was compared by challenging pathogenic mycobacteria (*M. abscessus*, solid line; *M. bovis*-BCG, dotted line) with DDUG (blue) or 10-DEBC (black) in an intracellular dose-dependency assay, normalized to 1% DMSO (0% inhibition) and 4 μ M bedaquiline (100% inhibition) **(B)**. DDUG inhibition of luciferase-expressing *S. typhimurium* growth in infected THP-1 cells **(C)**. Error bars represent the SEM from four **(A,B)** or six **(C)** independent trials. Comparison of DDUG intracellular effect on different bacteria **(D)**.

compounds, with MIC_{50} absolute difference values relative to those in *M.tb,* ranging between 0.4 and 6.71 μM (**Table 2**).

DDUG Antibacterial Activity *in vitro*

Some host-targeting compounds have been demonstrated to possess activity against bacterial kinases, such as the cyclin-dependent kinase 1 inhibitor NU-6027 (Kidwai et al., 2019) and the CHK1 inhibitor AZD7762 (Kanehiro et al., 2018), which inhibit the *M.tb* kinase, PknG. To examine if DDUG can inhibit bacterial growth in broth, disk diffusion and resazurin assays were conducted, examining a range of pathogenic bacteria and *M.tb* (**Table 3**). DDUG inhibited *M.tb* growth at concentrations similar to those displayed intracellularly (**Tables 2**, **3**). In addition, DDUG showed inhibitory activity against three of the 12 tested bacteria, including both Gram-positive (*Bacillus subtilis* and *Staphylococcus epidermidis*) and Gram-negative (*Moraxella catarrhalis*) members, without obvious unifying characteristics. *M. catarrhalis* was the most sensitive to DDUG with an MIC50 of less than 1.6 μM. Overall, 75% of the tested bacteria were not inhibited by DDUG in broth and 80% were not inhibited on solid media, including *M. abscessus*. Despite the reproducible activity of DDUG against *M.tb* in broth, DDUG activity in agar was inconsistent, with repeated failures to generate a DDUG-resistant mutant on plates for bacterial target identification.

In summary, by screening a kinase inhibitor library with well-characterized targets using a validated and scalable THP-1:*M.tb*-pTEC27 screen, we were able to reproduce findings from previous reports in other infection models, as well as identify both specific targets and target families that highly inhibit *M.tb* intracellular growth. We confirmed and validated one of the novel compounds, DDUG, and characterized its bactericidal activity, its specificity to *M.tb,* and the auxotrophic BCL2-safe MC^2 6206 strain, and we tested its activity in broth against an array of pathogenic bacteria.

DISCUSSION

In this campaign we demonstrated the power of utilizing a combination of validated and reliable tools, namely THP-1 cells, fluorescent *M.tb*, HCS, and a well-characterized library, to identify and validate potential HDTs. Overall ∼3% of screened compounds answered "yes" to all our hit criteria (**Table 1**), showcasing that targeting host kinase signaling is a valid approach for novel HDT discovery in TB. A similar screen conducted on an embryonic cell derived macrophage (iMACs) model also reported a ∼3% hit rate (Han et al., 2019). While similar in outcome, THP-1 screening in comparison to iMACs is well established, highly reproducible, and much simpler and cheaper to carry out. Previous screening campaigns in non-human macrophage models, such as carried out *in vitro* (Pethe et al., 2013) and in infected mouse macrophages (Stanley et al., 2014), both reported a ∼0.08% hit rate. Our ability to identify many previously reported anti-*M.tb* host targeting compounds identified in different screening campaigns and the relatively high hit rate together support the use of THP-1 cells for kinase inhibitor screens.

One limitation of this host-cell model of infection is that THP-1 cells are derived from cancerous leukemia. Kinase inhibitors were developed primarily to target cancerous cells, and may therefore be markedly toxic to THP-1 cells. By simultaneously measuring inhibitory activity and cell loss, which can be caused by compound toxicity or compound modulation of cellular adherence, we are able to partially predict compound toxicity and, more importantly, quality control the main outcome measure to avoid bias by host cell count. The main benefit of screening compounds at various stages of clinical trials, as well as tool compounds, is their potential for quick development compared to unknown compounds, with the added benefit that toxicological data exists for most of these compounds.

A secondary analysis of kinase inhibitor families (**Figure 2**) utilized the well-described compound targets to create a non-biased filter in selecting which compounds to further peruse. With only 400 compounds, the OICR library is relatively small, prohibiting the use of rigorous statistical analysis. However, as a proof-of-concept, we demonstrate that even descriptive statistics can enhance the otherwise arbitrary selection of compounds

TABLE 2 | Activity of host-directed compounds on intracellular *M.tb* strain MC^2 6206.

Compound	MIC_{50}	95% Confidence interval	H37Rv MIC_{50}	Absolute difference
DDUG	3.8 μM	3.4–4.4 μM	1.65 μM	2.15 μM
10-DEBC	2.9 μM	2.3–4.2 μM	3.26 μM	0.36 μM
Imatinib	2.4 μM	2.1–2.8 μM	9.11 μM	6.71 μM

Dose-response regression generated from three independent trials.

TABLE 3 | DDUG broth activity against a range of pathogenic bacteria.

Bacteria	Disk diffusion	Resazurin (MIC)
Acinetobacter baumannii BAA-747	R	R (MIC > 50 μM)
B. subtilis ATCC 6633	R	S (MIC = 9.4 μM ± 2.7 μM)
Escherichia coli ATCC 25922	R	R (MIC > 50 μM)
Enterococcus faecalis ATCC 29212	R	R (MIC > 50 μM)
M. abscessus ATCC 19977T (R)	R	R (MIC > 50 μM)
M. catarrhalis ATCC 25240	S (19% ± 2%)	S (MIC < 1.6 μM)
M. tuberculosis H37Rv	N/A	S (MIC 3.125 μM)
Pseudomonas aeruginosa ATCC 14210	R	R (MIC > 50 μM)
Staphylococcus aureus ATCC 25923	R	R (MIC = 50 μM)
MRSA ATCC 700698	R	R (MIC = 50 μM)
S. epidermidis ATCC 35984	S (7% ± 2%)	S (MIC = 6.25 μM)
Salmonella typhi ATCC 13311	R	R (MIC > 50 μM)

R, resistant; S, sensitive; MIC, minimal inhibitory concentration; N/A, not available. Disk sensitive percent measures the diameter of the zone of inhibition relative to the positive control.

of interest for downstream validation. Upscaling our screen methodology has the potential to provide invaluable data on which target families are good candidates for host-targeting compounds for *M.tb* infection, and can also be generalized to other infection models. Based on our observation, we hypothesize that focused screening using CHK, IGF-1R, and Akt inhibitors is likely to result in discovery of novel, highly active, and non-toxic HDTs. One signaling pathway that is both well-characterized in *M.tb* infections and enriched in our analysis is the PI3K-Akt-GSK3-mTOR pathway. Previous work from our lab (Poirier et al., 2014) and others (Singh and Subbian, 2018; Hu et al., 2020), as well as this work, highlight this pathway's inhibition in controlling intracellular infection via control of cellular apoptosis and autophagy. Since signaling pathways commonly interreact with each other, upscaling our screen and analysis can highlight those sub-paths relevant to *M.tb* inhibition, providing a complimentary and unbiased approach to classical biochemical pathway characterization techniques.

DDUG and its target CHK2 were validated as inhibitory by a dose-dependency test and by using RNAi (**Figure 3**), respectively. Tandutinib, an inhibitor of three different kinases that was also validated, showed MIC_{50} value above 10 μM, making it an unlikely treatment candidate, and 10-DEBC was originally inspected as a novel compound and since reported by Han et al. (2019). For both DDUG and 10-DEBC, we were able to characterize their intracellular mode of inhibition as bactericidal and bacteriostatic, respectively, and demonstrated that while DDUG was not active against other pathogenic mycobacteria, 10-DEBC was non-specific. Of note, 10-DEBC is a member of the chlorpromazine family of compounds, which were demonstrated to inhibit *M.tb* (Raffel et al., 1960; Crowle et al., 1992) without being Akt inhibitors themselves. Rather than being an HDT, 10-DEBC seems to be concentrated by the macrophage, where it is suggested to bind calmodulin to disrupt calcium transport (Amaral et al., 2001).

The characterized role of CHK2 is the arrest of cell-cycle via CDC25A, activation of DNA damage-repair mechanisms, and promotion of apoptosis via p53 in response to double-stranded DNA damage (Cai et al., 2009). Knockdown of CDC25A was also previously reported to decrease intracellular *M.tb* burden in THP-1 cells (Jayaswal et al., 2010). Some human viruses, such as human T-cell leukemia virus 1 (Durkin et al., 2008) and Epstein-Barr virus (Choudhuri et al., 2007), were shown to modify CHK2 for their replicative needs. However currently, other than CDC25A there is little evidence tying these pathways with inhibition of *M.tb* growth intracellularly. The activity of DDUG against *M.tb* in broth at concentrations similar to those achieved intracellularly suggests an alternative, CHK2-independent mode of activity. Similarly, the activity of DDUG against some bacteria further suggest DDUG might have promiscuous activity on bacterial kinases, similar to NU-6027 (Kidwai et al., 2019) and AZD7762 (Kanehiro et al., 2018), or otherwise be toxic due to physical properties such as crystallization if concentrated by the macrophage. Conversely, DDUG is not active against *M.tb*'s close family members, *M. abscessus* and *M. bovis*-BCG, or *Salmonella,* which it did inhibit in macrophages, and is active against a small array of seemingly unrelated bacteria (**Table 3**). Since it is unlikely the compound specifically binds a molecular target shared between a subset of the bacteria tested but not the others, these observations do not support a bacterial kinase target mode of action hypothesis.

We are unable to decisively determine if DDUG is acting via a CHK2-dependant or independent mechanism. Supporting the first are independent inhibition of CHK2 by RNAi, inhibition by other library-screened CHK2 inhibitors (provided validation), specificity of DDUG to *M.tb* vs. *M. bovis*-BCG and *M. abscessus* in THP-1 cells, and the lack of CHK2 activity in BMDM. Supporting the latter are activity against *M.tb* (and 25% of other bacteria tested) in broth at concentrations only twofold higher than observed intracellularly. Of note, a literature-grounded hypothesis can support CHK2-dependant inhibition of *M.tb* intracellular growth. Examining an array of CHK2 inhibitors and further investigating the CHK2-CDC25A pathway can help resolve this challenge, as well as further examination of DDUG's toxicity in *M. catarrhalis* and *S. epidermidis*, yet are beyond the scope of this screening campaign. However, this temporary lack of a definitive mode of inhibition does not take away from DDUG's remarkable intracellular inhibition of *M.tb* with low associated cell loss, and the demonstrated effect CHK2 inhibition has on intracellular *M.tb* growth in macrophages.

Host-targeting compounds were also equally potent against the BCL2-safe auxotroph MC^2 6206 strain. This is particularly promising, as current screens against mycobacterial models (such as *M. bovis*-BCG, *Mycobacterium marinum*, and others) face complications struggles coming up with viable antibiotics for *M.tb*, complications that intensify with HDTs as *Mycobacterium* spp. adopt unique host-pathogen interactions. In demonstrating that the auxotrophic *M.tb* strain is susceptible to current HDTs, the prohibitive barrier of access to and automatization in BCL3 settings can be bypassed, with the auxotroph used for future screening campaigns and in studying compound modes of action. Clearly, findings from any auxotroph study will require corroboration in WT *M.tb* to account for the differences in metabolic activity between the strains, which may certainly have an effect on compound activity.

The exploration of HDT compounds against intracellular *M.tb* is gaining momentum, with this study and others offering promising findings on the ability to treat *M.tb* by targeting the host cell. However, as HDT can have synergistic, additive, or even antagonistic actions with current TB therapeutics, and for clinical relevancy, HDT should be tested in concert with current approved TB drugs.

CONCLUSION

In conclusion, we demonstrated here how intelligible small scale, top-down screens can replicate and improve screening efforts of much larger, more expensive strategies. The key factors contributing to the success of the screen were its anchors in ground-level microbiology: (1) screening a reliable and valid intracellular niche model, (2) testing compounds that are well-characterized or in advanced clinical stages to expedite

potential knowledge translation to meet clinical needs, and (3) investigating kinase signaling—processes quintessential to *M.tb* host-pathogen interactions.

DATA AVAILABILITY STATEMENT

All datasets presented in this study are included in the article/**Supplementary Material**.

AUTHOR CONTRIBUTIONS

TS designed, conducted, managed, and wrote the research. LR-W tested broth activity of DDUG in BCL3 and assisted with design and writing. JC performed RNAi validation and assisted with writing. VP tested broth activity of DDUG in BCL2. CR tested DDUG intracellular activity against *S. typhi* and assisted with design and writing. TP contributed with experimental design and analysis. YA-G proposed, designed, and initiated the study, obtained funding, and participated in writing. All authors contributed to the article and approved the submitted version.

FUNDING

The research reported in this publication was supported by the Canadian Institutes for Health Research (CIHR PJT-148646 and PJT-152931) to YA-G.

ACKNOWLEDGMENTS

We thank Mary Ko for reagent, laboratory, and strain management; the Facility for Infectious Diseases and Epidemiology Research (FINDER) staff for BCL3 support; Paulin Johnson and Manisha Dosanjh for providing BMDM; and Nataliya Shishov from Simon Fraser University for support with statistics.

SUPPLEMENTARY MATERIAL

The Supplementary Material for this article can be found online at: https://www.frontiersin.org/articles/10.3389/fmicb.2020.553962/full#supplementary-material

REFERENCES

Amaral, L., Kristiansen, J. E., Viveiros, M., and Atouguia, J. (2001). Activity of phenothiazines against antibiotic-resistant *Mycobacterium tuberculosis*: a review supporting further studies that may elucidate the potential use of thioridazine as anti-tuberculosis therapy. *J. Antimicrob. Chemother.* 47, 505–511. doi: 10.1093/jac/47.5.505

Ashtekar, D. R., Costa-Periera, R., Shrinivasan, T., Iyyer, R., Vishvanathan, N., and Rittel, W. (1991). Oxazolidinones, a new class of synthetic antituberculosis agent. In vitro and in vivo activities of DuP-721 against *Mycobacterium tuberculosis*. *Diagn. Microbiol. Infect. Dis.* 14, 465–471. doi: 10.1016/0732-8893(91)90002-w

Ashtekar, D. R., Costa-Perira, R., Nagrajan, K., Vishvanathan, N., Bhatt, A. D., and Rittel, W. (1993). In vitro and in vivo activities of the nitroimidazole CGI 17341 against *Mycobacterium tuberculosis*. *Antimicrob. Agents Chemother.* 37, 183–186. doi: 10.1128/aac.37.2.183

Babichev, Y., Kabaroff, L., Datti, A., Uehling, D., Isaac, M., Al-Awar, R., et al. (2016). PI3K/AKT/mTOR inhibition in combination with doxorubicin is an effective therapy for leiomyosarcoma. *J. Transl. Med.* 14:67. doi: 10.1186/s12967-016-0814-z

Bach, H., Papavinasasundaram, K. G., Wong, D., Hmama, Z., and Av-Gay, Y. (2008). *Mycobacterium tuberculosis* virulence is mediated by PtpA dephosphorylation of human vacuolar protein sorting 33B. *Cell Host Microbe* 3, 316–322. doi: 10.1016/j.chom.2008.03.008

Bauer, A. W., Kirby, W. M., Sherris, J. C., and Turck, M. (1966). Antibiotic susceptibility testing by a standardized single disk method. *Am. J. Clin. Pathol.* 45, 493–496.

Bernut, A., Le Moigne, V., Lesne, T., Lutfalla, G., Herrmann, J. L., and Kremer, L. (2014). In vivo assessment of drug efficacy against *Mycobacterium abscessus* using the embryonic zebrafish test system. *Antimicrob. Agents Chemother.* 58, 4054–4063. doi: 10.1128/AAC.00142-14

Bjarnason, J., Southward, C. M., and Surette, M. G. (2003). Genomic profiling of iron-responsive genes in *Salmonella enterica* serovar typhimurium by high-throughput screening of a random promoter library. *J. Bacteriol.* 185, 4973–4982. doi: 10.1128/jb.185.16.4973-4982.2003

Cai, Z., Chehab, N. H., and Pavletich, N. P. (2009). Structure and activation mechanism of the CHK2 DNA damage checkpoint kinase. *Mol. Cell* 35, 818–829. doi: 10.1016/j.molcel.2009.09.007

Cambier, C. J., Falkow, S., and Ramakrishnan, L. (2014). Host evasion and exploitation schemes of *Mycobacterium tuberculosis*. *Cell* 159, 1497–1509. doi: 10.1016/j.cell.2014.11.024

CDC (2016). *Tuberculosis (TB)*. Avaliable at: https://www.cdc.gov/tb/topic/treatment/tbdisease.htm (accessed March 01, 2020).

Choudhuri, T., Verma, S. C., Lan, K., Murakami, M., and Robertson, E. S. (2007). The ATM/ATR signaling effector Chk2 is targeted by epstein-barr virus nuclear antigen 3C to release the G2/M cell cycle block. *J. Virol.* 81, 6718–6730. doi: 10.1128/JVI.00053-07

Crowle, A. J., Douvas, G. S., and May, M. H. (1992). Chlorpromazine: a drug potentially useful for treating mycobacterial infections. *Chemotherapy* 38, 410–419. doi: 10.1159/000239036

Durkin, S. S., Guo, X., Fryrear, K. A., Mihaylova, V. T., Gupta, S. K., Belgnaoui, S. M., et al. (2008). HTLV-1 Tax oncoprotein subverts the cellular DNA damage response via binding to DNA-dependent protein kinase. *J. Biol. Chem.* 283, 36311–36320. doi: 10.1074/jbc.M804931200

Han, H. W., Seo, H. H., Jo, H. Y., Han, H. J., Falcao, V. C. A., Delorme, V., et al. (2019). Drug discovery platform targeting *M. tuberculosis* with human embryonic stem cell-derived macrophages. *Stem Cell Rep.* 13, 980–991. doi: 10.1016/j.stemcr.2019.10.002

Hmama, Z., Pena-Diaz, S., Joseph, S., and Av-Gay, Y. (2015). Immunoevasion and immunosuppression of the macrophage by *Mycobacterium tuberculosis*. *Immunol. Rev.* 264, 220–232. doi: 10.1111/imr.12268

Hu, Y., Wen, Z., Liu, S., Cai, Y., Guo, J., Xu, Y., et al. (2020). Ibrutinib suppresses intracellular *Mycobacterium tuberculosis* growth by inducing macrophage autophagy. *J. Infect.* 80, e19–e26. doi: 10.1016/j.jinf.2020.03.003

Jayaswal, S., Kamal, M. A., Dua, R., Gupta, S., Majumdar, T., Das, G., et al. (2010). Identification of host-dependent survival factors for intracellular *Mycobacterium tuberculosis* through an siRNA screen. *PLoS Pathog.* 6:e1000839. doi: 10.1371/journal.ppat.1000839

Johnson, B. K., and Abramovitch, R. B. (2015). Macrophage infection models for *Mycobacterium tuberculosis*. *Methods Mol. Biol.* 1285, 329–341. doi: 10.1007/978-1-4939-2450-9_20

Kanehiro, Y., Tomioka, H., Pieters, J., Tatano, Y., Kim, H., Iizasa, H., et al. (2018). Identification of novel mycobacterial inhibitors against mycobacterial protein kinase G. *Front. Microbiol.* 9:1517. doi: 10.3389/fmicb.2018.01517

Kidwai, S., Bouzeyen, R., Chakraborti, S., Khare, N., Das, S., Priya Gosain, T., et al. (2019). NU-6027 inhibits growth of *Mycobacterium tuberculosis* by targeting protein kinase D and protein kinase G. *Antimicrob. Agents Chemother.* 63:e00996-19. doi: 10.1128/AAC.00996-19

Kolloli, A., and Subbian, S. (2017). Host-directed therapeutic strategies for tuberculosis. *Front. Med.* 4:171. doi: 10.3389/fmed.2017.00171

Kroesen, V. M., Groschel, M. I., Martinson, N., Zumla, A., Maeurer, M., van der Werf, T. S., et al. (2017). Non-steroidal anti-inflammatory drugs as host-directed therapy for tuberculosis: a systematic review. *Front. Immunol.* 8:772. doi: 10.3389/fimmu.2017.00772

Kuijl, C., Savage, N. D., Marsman, M., Tuin, A. W., Janssen, L., Egan, D. A., et al. (2007). Intracellular bacterial growth is controlled by a kinase network around PKB/AKT1. *Nature* 450, 725–730. doi: 10.1038/nature06345

Kumar, D., Nath, L., Kamal, M. A., Varshney, A., Jain, A., Singh, S., et al. (2010). Genome-wide analysis of the host intracellular network that regulates survival of *Mycobacterium tuberculosis*. *Cell* 140, 731–743. doi: 10.1016/j.cell.2010.02.012

Madhvi, A., Mishra, H., Leisching, G. R., Mahlobo, P. Z., and Baker, B. (2019). Comparison of human monocyte derived macrophages and THP1-like macrophages as in vitro models for *M. tuberculosis* infection. *Comp. Immunol. Microbiol. Infect. Dis.* 67:101355. doi: 10.1016/j.cimid.2019.101355

Mouton, J. M., Heunis, T., Dippenaar, A., Gallant, J. L., Kleynhans, L., and Sampson, S. L. (2019). Comprehensive characterization of the attenuated double auxotroph *Mycobacterium tuberculosis* DeltaleuDDeltapanCD as an alternative to H37Rv. *Front. Microbiol.* 10:1922. doi: 10.3389/fmicb.2019.01922

Napier, R. J., Rafi, W., Cheruvu, M., Powell, K. R., Zaunbrecher, M. A., Bornmann, W., et al. (2011). Imatinib-sensitive tyrosine kinases regulate mycobacterial pathogenesis and represent therapeutic targets against tuberculosis. *Cell Host Microbe* 10, 475–485. doi: 10.1016/j.chom.2011.09.010

Padmapriyadarsini, C., Bhavani, P. K., Natrajan, M., Ponnuraja, C., Kumar, H., Gomathy, S. N., et al. (2019). Evaluation of metformin in combination with rifampicin containing antituberculosis therapy in patients with new, smear-positive pulmonary tuberculosis (METRIF): study protocol for a randomised clinical trial. *BMJ Open* 9:e024363. doi: 10.1136/bmjopen-2018-024363

Parish, T. (2020). In vitro drug discovery models for *Mycobacterium tuberculosis* relevant for host infection. *Expert Opin Drug Discov.* 15, 349–358. doi: 10.1080/17460441.2020.1707801

Pethe, K., Bifani, P., Jang, J., Kang, S., Park, S., Ahn, S., et al. (2013). Discovery of Q203, a potent clinical candidate for the treatment of tuberculosis. *Nat. Med.* 19, 1157–1160. doi: 10.1038/nm.3262

Poirier, V., and Av-Gay, Y. (2012). *Mycobacterium tuberculosis* modulators of the macrophage's cellular events. *Microbes Infect.* 14, 1211–1219. doi: 10.1016/j.micinf.2012.07.001

Poirier, V., Bach, H., and Av-Gay, Y. (2014). *Mycobacterium tuberculosis* promotes anti-apoptotic activity of the macrophage by PtpA protein-dependent dephosphorylation of host GSK3alpha. *J. Biol. Chem.* 289, 29376–29385. doi: 10.1074/jbc.M114.582502

Raffel, S., Kochan, I., Poland, N., and Hollister, L. E. (1960). The action of chlorpromazine upon *Mycobacterium tuberculosis*. *Am. Rev. Respir. Dis.* 81, 555–561. doi: 10.1164/arrd.1960.81.4.555

Richter, A., Shapira, T., and Av-Gay, Y. (2019). THP-1 and dictyostelium infection models for screening and characterization of anti-*Mycobacterium abscessus* hit compounds. *Antimicrob. Agents Chemother.* 64:e01601-19. doi: 10.1128/AAC.01601-19

Sahile, H. A., Rens, C., Shapira, T., Andersen, R. J., and Av-Gay, Y. (2020). DMN-Tre labeling for detection and high-content screening of compounds against intracellular mycobacteria. *ACS Omega* 5, 3661–3669. doi: 10.1021/acsomega.9b04173

Sampson, S. L., Dascher, C. C., Sambandamurthy, V. K., Russell, R. G., Jacobs, W. R. Jr., Bloom, B. R., et al. (2004). Protection elicited by a double leucine and pantothenate auxotroph of *Mycobacterium tuberculosis* in guinea pigs. *Infect. Immun.* 72, 3031–3037. doi: 10.1128/iai.72.5.3031-3037.2004

Schaaf, K., Hayley, V., Speer, A., Wolschendorf, F., Niederweis, M., Kutsch, O., et al. (2016). Macrophage infection model to predict drug efficacy against *Mycobacterium tuberculosis*. *Assay Drug Dev. Technol.* 14, 345–354. doi: 10.1089/adt.2016.717

Singh, P., and Subbian, S. (2018). Harnessing the mTOR pathway for tuberculosis treatment. *Front. Microbiol.* 9:70. doi: 10.3389/fmicb.2018.00070

Sogi, K. M., Lien, K. A., Johnson, J. R., Krogan, N. J., and Stanley, S. A. (2017). The tyrosine kinase inhibitor gefitinib restricts *Mycobacterium tuberculosis* growth through increased lysosomal biogenesis and modulation of cytokine signaling. *ACS Infect. Dis.* 3, 564–574. doi: 10.1021/acsinfecdis.7b00046

Sorrentino, F., Gonzalez del Rio, R., Zheng, X., Presa Matilla, J., Torres Gomez, P., Martinez Hoyos, M., et al. (2016). Development of an intracellular screen for new compounds able to inhibit *Mycobacterium tuberculosis* growth in human macrophages. *Antimicrob. Agents Chemother.* 60, 640–645. doi: 10.1128/AAC.01920-15

Stanley, S. A., Barczak, A. K., Silvis, M. R., Luo, S. S., Sogi, K., Vokes, M., et al. (2014). Identification of host-targeted small molecules that restrict intracellular *Mycobacterium tuberculosis* growth. *PLoS Pathog.* 10:e1003946. doi: 10.1371/journal.ppat.1003946

Tobin, D. M. (2015). Host-directed therapies for tuberculosis. *Cold Spring Harb. Perspect. Med.* 5:a021196. doi: 10.1101/cshperspect.a021196

WHO (2018). *Global Tuberculosis Report*. Avaliable at: https://apps.who.int/iris/bitstream/handle/10665/274453/9789241565646-eng.pdf?ua=1 (accessed March 01, 2020).

Wong, D., Bach, H., Sun, J., Hmama, Z., and Av-Gay, Y. (2011). *Mycobacterium tuberculosis* protein tyrosine phosphatase (PtpA) excludes host vacuolar-H+-ATPase to inhibit phagosome acidification. *Proc. Natl. Acad. Sci. U.S.A.* 108, 19371–19376. doi: 10.1073/pnas.1109201108

Conflict of Interest: The authors declare that the research was conducted in the absence of any commercial or financial relationships that could be construed as a potential conflict of interest.

frontiers in Microbiology

ORIGINAL RESEARCH
published: 19 October 2020
doi: 10.3389/fmicb.2020.583194

A Glutamine Insertion at Codon 432 of RpoB Confers Rifampicin Resistance in *Mycobacterium tuberculosis*

*Li-Yin Lai[1], Li-Yu Hsu[1], Shang-Hui Weng[1], Shuo-En Chung[1], Hui-En Ke[1], Tzu-Lung Lin[1], Pei-Fang Hsieh[1], Wei-Ting Lee[2,3], Hsing-Yuan Tsai[2,3], Wan-Hsuan Lin[2,3], Ruwen Jou[2,3] and Jin-Town Wang[1,4]**

[1] Department of Microbiology, National Taiwan University College of Medicine, Taipei, Taiwan, [2] Tuberculosis Research Center, Centers for Disease Control, Ministry of Health and Welfare of Taiwan, Taipei, Taiwan, [3] Center for Diagnostics and Vaccine Development, Centers for Disease Control, Ministry of Health and Welfare of Taiwan, Taipei, Taiwan, [4] Department of Internal Medicine, National Taiwan University Hospital, Taipei, Taiwan

OPEN ACCESS

Edited by:
Maria Rosalia Pasca, University of Pavia, Italy

Reviewed by:
Divakar Sharma, Indian Institute of Technology Delhi, India
Yu Pang, Beijing Chest Hospital, Capital Medical University, China

***Correspondence:**
Jin-Town Wang
wangjt@ntu.edu.tw

Specialty section:
This article was submitted to Antimicrobials, Resistance and Chemotherapy, a section of the journal Frontiers in Microbiology

Received: *14 July 2020*
Accepted: *23 September 2020*
Published: *19 October 2020*

Citation:
Lai L-Y, Hsu L-Y, Weng S-H, Chung S-E, Ke H-E, Lin T-L, Hsieh P-F, Lee W-T, Tsai H-Y, Lin W-H, Jou R and Wang J-T (2020) A Glutamine Insertion at Codon 432 of RpoB Confers Rifampicin Resistance in Mycobacterium tuberculosis. Front. Microbiol. 11:583194. doi: 10.3389/fmicb.2020.583194

Tuberculosis (TB) is an infectious respiratory disease caused by *Mycobacterium tuberculosis* and one of the top 10 causes of death worldwide. Treating TB is challenging; successful treatment requires a long course of multiple antibiotics. Rifampicin (RIF) is a first-line drug for treating TB, and the development of RIF-resistant *M. tuberculosis* makes treatment even more difficult. To determine the mechanism of RIF resistance in these strains, we searched for novel mutations by sequencing. Four isolates, CDC-1, CDC-2, CDC-3, and CDC-4, had high-level RIF resistance and unique mutations encoding RpoB $G^{158}R$, RpoB $V^{168}A$, RpoB $S^{188}P$, and RpoB Q^{432}insQ, respectively. To evaluate their correlation with RIF resistance, plasmids carrying *rpoB* genes encoding these mutant proteins were transfected into the $H_{37}Rv$ reference strain. The plasmid complementation of RpoB indicated that $G^{158}R$, $V^{168}A$, and $S^{188}P$ did not affect the MIC of RIF. However, the MIC of RIF was increased in $H_{37}Rv$ carrying RpoB Q^{432}insQ. To confirm the correlation between RIF resistance and Q^{432}insQ, we cloned an *rpoB* fragment carrying the insertion (encoding RpoB Q^{432}insQ) into $H_{37}Rv$ by homologous recombination using a suicide vector. All replacement mutants expressing RpoB Q^{432}insQ were resistant to RIF (MIC $>$ 1 mg/L). These results indicate that RpoB Q^{432}insQ causes RIF resistance in *M. tuberculosis*.

Keywords: *Mycobacterium tuberculosis*, drug resistance, rifampicin, *rpoB*, codon 432 of RpoB

INTRODUCTION

Mycobacterium tuberculosis is an important human pathogen that causes tuberculosis (TB). It was first isolated by Robert Koch in 1882, and numerous TB drugs have been developed since the 1930s, although the first effective anti-TB drug was not discovered until 1944 (Vilcheze and Jacobs, 2014; Islam et al., 2017; Long et al., 2019; Mabhula and Singh, 2019). TB is a common, chronic infectious respiratory disease that affects nearly one-third of the world's population (Long et al., 2019; Yong et al., 2019) and is transmitted via aerosol (e.g., cough) from infected persons. According to the World Health Organization, TB is one of the top 10 causes of death worldwide. In 2018, there

were approximately 10 million people with TB and 1.4 million deaths due to TB worldwide (World Health Organization [WHO], 2019). Approximately 500,000 new cases were found to be resistant to the most effective first-line drug, rifampicin (RIF), of which 78% had multidrug-resistant TB (resistant to at least isoniazid and RIF) (World Health Organization [WHO], 2019). According to the Taiwan Centers for Disease Control, there were 9,179 new cases of TB in Taiwan in 2018, and 294 of these were RIF-resistant. Over the period of long-term anti-TB therapy, *M. tuberculosis* is exposed to the appropriate drug concentration, which might lead to the development of drug-resistant TB and increase the risk of transmission (Yong et al., 2019). It takes at least 6 months to successfully treat TB, and the development of drug resistance makes therapy even more difficult and is a threat to public health. The treatment of drug-resistant TB requires the administration of more than five drugs for more than 9 months (Vekemans et al., 2020). In addition, RIF-resistant TB is frequently not adequately treated because of a delay in the diagnosis of drug resistance. Such delayed treatment not only has a poor therapeutic effect on the infected patient but also increases the risk of transmission (Boyd et al., 2017; Yong et al., 2019). First-line RIF acts by binding the β-subunit of RNA polymerase, blocking RNA synthesis, and inducing hydroxyl radical formation, which likely contributes to its killing effect (Piccaro et al., 2014; Lohrasbi et al., 2018). It has been reported that drug resistance develops when mutations in *rpoB* block RIF binding to the β-subunit. Most point mutations causing RIF resistance occur in an 81-nucleotide region (codons 426–452 in *M. tuberculosis* or codons 507–533 in the *Escherichia coli* codon numbering system) of *rpoB* that is called the RIF resistance-determining region (RRDR) (Pang et al., 2013; Chikaonda et al., 2017). According to previous studies, >90% of RIF-resistant TB strains have mutations in the RRDR within codon 435, 445, and 450 (codon 516, 526, and 531 in *E. coli*) (Pang et al., 2013; Swain et al., 2020). Drug resistance is a major challenge for TB control. Due to the slow growth rate of *M. tuberculosis*, conventional drug susceptibility testing takes several weeks. Therefore, sequencing drug resistance-related mutations can be used to quickly detect drug-resistant TB, significantly reducing the duration of therapy, and avoiding treatment delays. Thus, we examined the effects of novel mutations in known target gene regions and mutations outside of the target region on RIF resistance in *M. tuberculosis* with the aim to expand upon known RIF resistance-causing mutations for use in clinical molecular diagnostics.

MATERIALS AND METHODS

Bacteria Strains

Clinical isolates were obtained from the Reference Laboratory of Mycobacteriology of the Taiwan Centers for Disease Control. *M. tuberculosis* $H_{37}Rv$ was used as the reference strain. *M. tuberculosis* $H_{37}Rv$ and clinical isolates were cultured in Difco™ Middlebrook 7H9 medium (BD REF: 271310; MD, NJ, United States) supplemented with 10% oleic acid/albumin/dextrose/catalase (OADC), 0.5% glycerol, and 0.05% tween-80 at 37°C (Tan et al., 2006). *E. coli* DH10B was grown in Luria broth (LBL405.1; BioShop, Burlington, Canada). All experiments involving *M. tuberculosis* strains were conducted at the Biosafety level 3 lab in the National Taiwan University College of Medicine and followed institutional biosafety procedures.

Isolation of Clinical Strains and Drug Susceptibility Testing

Clinical isolates of *M. tuberculosis* were tested in the Reference Laboratory of Mycobacteriology of the Taiwan Centers for Disease Control. Each isolate was initially obtained from a patient and was inoculated in solid and liquid culture. The minimum inhibitory concentration (MIC) of RIF was determined using a Sensititre™ Mycobacterium tuberculosis MIC Plate (MYCOTB; Thermo Fisher Scientific, Cleveland, OH, United States) according to the manufacturer's instructions. The bacterial culture was adjusted to a 0.5 McFarland standard and then added to the Sensititre™ plate, which was covered with an adhesive plastic seal. After incubation at 37°C, the results were recorded with a Sensititre™ Vizion™ Digital MIC Viewing System. The critical concentration of RIF was 1 mg/L.

Microplate Alamar Blue Assays (MABAs)

Microplate alamar blue assays were performed as previously described with minor modifications (Burke et al., 2017). Briefly, *M. tuberculosis* strains were cultured in Middlebrook 7H9 medium, and then the OD_{600nm} was adjusted to 0.1. A 200-μL aliquot of each prepared bacterial suspension was placed in a 96-well sterile plate (LabServ, Singapore) and incubated at 37°C for 14 days with and without RIF (0.03–512 mg/L). After 14 days of incubation, 50 μL of a freshly prepared 1:1 mixture of Alamar blue (alamarBlue®; BioRad, Hercules, CA, United States) and 10% tween 80 was added to each well. Then, the plate was incubated at 37°C for 48 h, and the color was recorded. Blue indicates no growth, and pink indicates growth. During incubation and staining, the plate was sealed with an adhesive plate seal.

RpoB Expression Plasmids

The plasmid pMN437 was used to express RpoB in *M. tuberculosis* (Steinhauer et al., 2010). Derivative plasmids

TABLE 1 | Rifampicin (RIF) resistance levels of clinical strains as measured by Sensititre™ Mycobacterium tuberculosis MIC Plate.

Strains	RpoB substitutions	RpoB Codon change	MIC of RIF (mg/L)
CDC-1	$G^{158}R$ & $V^{170}F$	158 GGC → CGC 170 GTC → TTC	8
CDC-2	$V^{168}A$ & $V^{170}F$	168 GTG → GCG 170 GTC → TTC	>16
CDC-3	$V^{170}F$ & $S^{188}P$	170 GTC → TTC 188 TCC → CCC	>16
CDC-4	$S^{431}G$ & Q^{432}insQ	431 AGC → GGC 432 CAA → CAACAA	>16

RIF resistance: >1mg/L. MIC, minimum inhibitory concentration.

TABLE 2 | Plasmids used in this study.

Plasmids	Amino acid substitutions*	Target strain	Predicted consequence	Obtained phenotypic consequences
pMN437-RpoB $G^{158}R$	RpoB $G^{158}R$	$H_{37}Rv$	S → R	S → S
pMN437-RpoB $V^{168}A$	RpoB $V^{168}A$	$H_{37}Rv$	S → R	S → S
pMN437-RpoB $S^{188}P$	RpoB $S^{188}P$	$H_{37}Rv$	S → R	S → S
pMN437-RpoB-CDC-4	RpoB $S^{431}G$ & Q^{432}insQ	$H_{37}Rv$	S → R	S → R
pMN437-RpoB Q^{432}insQ	RpoB Q^{432}insQ	$H_{37}Rv$	S → R	S → R
pGOAL19-Rv RpoB Q^{432}insQ	RpoB Q^{432}insQ	$H_{37}Rv$	S → R	S → R

*S, sensitive strain; R, resistant strain. *Rifampicin resistance-related amino acid substitutions.*

TABLE 3 | Susceptibility test results of clinical isolates and $H_{37}Rv$ strains carrying RpoB expression plasmids as measured by microplate Alamar blue assays.

Strains	RpoB substitutions	MIC of RIF (mg/L)		
		Exp. 1	Exp. 2	Exp. 3
$H_{37}Rv$	None	0.125	0.03	0.125
$H_{37}Rv$:pMN437	None	0.03	0.03	0.125
CDC-1	$V^{170}F$ & $G^{158}R$	32	4	–
$H_{37}Rv$:pMN437-RpoB $G^{158}R$	$G^{158}R$*	0.06	0.125	–
CDC-2	$V^{170}F$ & $V^{168}A$	256	512	–
$H_{37}Rv$:pMN437-RpoB $V^{168}A$	$V^{168}A$*	0.125	0.25	–
$H_{37}Rv$:pMN437-RpoB $S^{188}P$	$S^{188}P$*	0.06	0.03	–
CDC-4	$S^{431}G$ & Q^{432}insQ	128	128	256
$H_{37}Rv$:pMN437-RpoB Q^{432}insQ	Q^{432}insQ*	128	64	128
$H_{37}Rv$:pMN437-RpoB-CDC-4	$S^{431}G$ & Q^{432}insQ*	256	128	256

*Exp., experiment; MIC, minimum inhibitory concentration. *Amino acid substitutions in RpoB based on pMN437. ⁻Was not included in the experiment. RIF resistance: >1 mg/L.*

carrying resistance-associated *rpoB* mutations were generated using the QuikChange II Site-Directed Mutagenesis Kit (Agilent, Santa Clara, CA, United States). The primers used are shown in **Supplementary Table 1**. *M. tuberculosis* was transformed by electroporation at 2,500 V, 1,000 Ω, and 25 μF and recovered in 10 mL of Middlebrook 7H9 medium supplemented with 10% OADC and 0.5% glycerol for 24 h (Larsen et al., 2007; Lai et al., 2018). Recovered cells were then plated on BBL™ 7H11 solid agar (BD REF: 212203; BD, MD, NJ, United States) containing 50 mg/L hygromycin and incubated at 37°C for 4 weeks.

Site-Directed Mutagenesis

The putative resistance-associated *rpoB* mutations were amplified by PCR from the genomic DNA of the resistant strains as a template and then cloned into the *Sca*I site of the suicide plasmid pGOAL19 (Addgene; MA, United States) (Parish and Stoker, 2000). The primers used are shown in **Supplementary Table 1**. The resulting plasmids were transformed into *M. tuberculosis* $H_{37}Rv$, and point mutants were selected after two rounds of homologous recombination, as previously described (Parish and Stoker, 2000; Larsen et al., 2007).

DNA Sequencing

Mycobacterium tuberculosis isolates were lysed with InstantGet™ DNA Extraction Solution (Catalog Number: 17001; HNG, Taipei, Taiwan) and heat-killed (100°C for 15 min). Then, the supernatants of heat-killed *M. tuberculosis* isolates were added to the PCR reagent containing KOD Xtreme™ Hot Start DNA Polymerase (Catalog Number: 71976; Novagen, CA, United States) and gene-specific primers, rpoB out F1 and rpoB-out-R (**Supplementary Table 1**), to amplify the *rpoB* fragment. The PCR products were sent for sequencing (Mission Biotech, Taipei, Taiwan) and were verified by capillary electrophoresis (ABI 3730xl; Thermo Fisher Scientific, Cleveland, OH, United States). The *rpoB* sequences of clinical strains CDC-1, CDC-2, and CDC-4 were submitted to NCBI (GenBank accession numbers: MT774526, MT774527, and MT774528, respectively).

RESULTS

Identification of Novel *rpoB* Mutations in RIF-Resistant Clinical Isolates

Four clinical isolates, CDC-1, CDC-2, CDC-3, and CDC-4, had high-level RIF resistance and different novel mutations within the *rpoB* gene. The RIF resistance levels of clinical strains were determined using a Sensititre™ Mycobacterium tuberculosis MIC Plate. The MIC of RIF for CDC-1 was 8 mg/L, and the MICs of RIF for CDC-2, CDC-3, and CDC-4 were >16 mg/L (**Table 1**). Sequencing showed that each of these four clinical isolates harbored genes encoding two amino acid changes in RpoB. When compared to the sequence of the reference strain $H_{37}Rv$, in CDC-1, the G at codon 158 was replaced with R ($G^{158}R$) and the V at codon 170 was replaced with F ($V^{170}F$). In CDC-2, the V at codon 168 was replaced with A ($V^{168}A$) and the V at codon 170 was replaced with F ($V^{170}F$). In CDC-3, the V at codon 170 of RpoB was substituted with F ($V^{170}F$), and the S at codon 188 was replaced with P ($S^{188}P$). In CDC-4, the S at codon 431

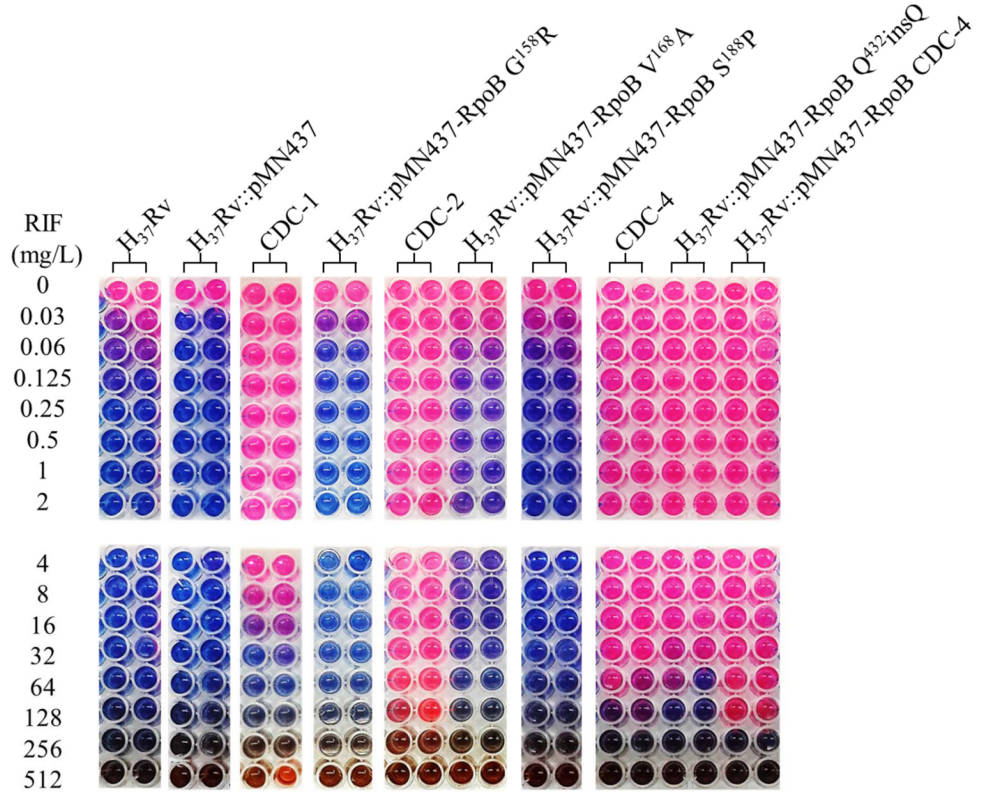

FIGURE 1 | Rifampicin (RIF) susceptibility test for *Mycobacterium tuberculosis* strains expressing wild-type and mutant RpoB as measured by microplate Alamar blue assays (MABAs). The MIC of RIF for *M. tuberculosis* strains carrying RpoB expression plasmids was measured by MABA. *M. tuberculosis* was cultured in 7H9 broth containing different concentrations of RIF for 2 weeks and then stained with Alamar blue for 2 days. CDC-1, CDC-2, and CDC-4 are RIF-resistant clinical strains that harbored RpoB amino acid changes ($G^{158}R$ & $V^{170}F$, $V^{168}A$ & $V^{170}F$, and $S^{431}G$ & Q^{432}insQ, respectively). Red indicates bacterial growth, and blue indicates no growth. The critical concentration for RIF resistance was1.0 mg/L. All experiments were performed in duplicate to confirm reproducibility and repeated at least twice with similar results (**Table 3**).

was replaced with G ($S^{431}G$) and a Q was inserted at codon 432 (Q^{432}insQ). However, $G^{158}R$, $V^{168}A$, $S^{188}P$, and Q^{432}insQ had not previously been confirmed to be related to drug resistance.

An RpoB Q^{432}insQ Expression Plasmid Increases the MIC of RIF in $H_{37}Rv$

Clinical isolates CDC-1, CDC-2, CDC-3, and CDC-4 had high-level RIF resistance and harbored unique RpoB amino acid changes ($G^{158}R$, $V^{168}A$, $S^{188}P$, and Q^{432}insQ, respectively). To evaluate the association between these unique amino acid changes and the RIF resistance of the clinical isolates, plasmids (pMN437-derived) expressing these RpoB proteins were transformed into $H_{37}Rv$ (**Table 2**), and RIF susceptibility was measured in these strains by a MABA. The results showed that the MICs of RIF for the wild-type strains, $H_{37}Rv$ and $H_{37}Rv$:pMN437, were 0.03–0.125 mg/L. The MIC of RIF for clinical strain CDC-1 was 4–32 mg/L, that for clinical strain CDC-2 was 256–512 mg/L, and that for clinical strain CDC-4 was 128–256 mg/L. These results were consistent with the MIC data obtained with the Sensititre™ Mycobacterium tuberculosis MIC Plate. However, the MIC of RIF for clinical strain CDC-3 could not be determined by the MABA because it could not be cultured. The MIC of RIF for $H_{37}Rv$:pMN437-RpoB $G^{158}R$, $H_{37}Rv$:pMN437-RpoB $V^{168}A$, and $H_{37}Rv$:pMN437-RpoB $S^{188}P$ was 0.03–0.25 mg/L, that for $H_{37}Rv$:pMN437-CDC-4 was 128–256 mg/L, and that for $H_{37}Rv$:pMN437-RpoB Q^{432}insQ was 64–128 mg/L (**Tables 2**, **3**, **Figure 1**). These results showed that $H_{37}Rv$:pMN437-RpoB $G^{158}R$, $H_{37}Rv$:pMN437-RpoB $V^{168}A$, and $H_{37}Rv$:pMN437-RpoB $S^{188}P$ were not resistant to RIF (MIC < 1 mg/L). The MIC of RIF for $H_{37}Rv$:pMN437-CDC-4 was the same as that of clinical strain CDC-4, and the MIC of RIF for $H_{37}Rv$:pMN437-RpoB Q^{432}insQ was two-fold lower than that for $H_{37}Rv$:pMN437-CDC-4 and clinical strain CDC-4. This suggests that RpoB $G^{158}R$, RpoB $V^{168}A$, and RpoB $S^{188}P$ likely do not contribute to RIF resistance, whereas RpoB Q^{432}insQ contributes to high-level RIF resistance in *M. tuberculosis*.

RpoB Q^{432}insQ Confers RIF Resistance to *M. tuberculosis* $H_{37}Rv$

Among the tested RpoB expression plasmids, only RpoB Q^{432}insQ increased the MIC of RIF in $H_{37}Rv$. To further confirm that the RpoB Q^{432}insQ was correlated with RIF resistance, unmarked mutants of $H_{37}Rv$ expressing RpoB Q^{432}insQ were generated. The *rpoB* fragment with the CAA insertion was

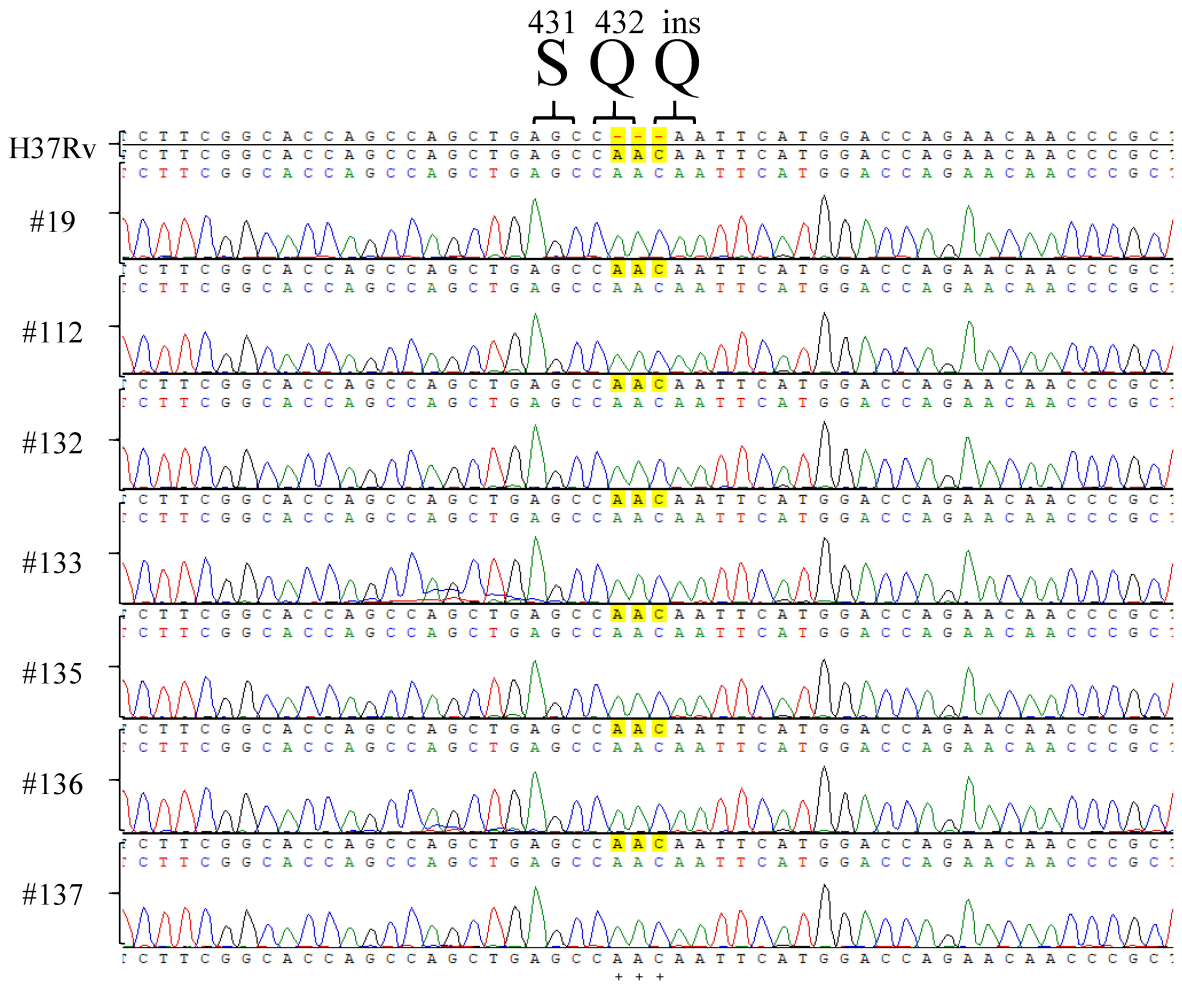

FIGURE 2 | *rpoB* sequencing results of *Mycobacterium tuberculosis* H_{37}Rv RpoB Q^{432}insQ strains generated by site-directed mutagenesis. Sequencing of *rpoB* gene fragments of the strains generated by site-directed mutagenesis, specifically #9, #112, #132, #133, #135, #136, and #137, showed that RpoB was successfully substituted with RpoB Q^{432}insQ in *M. tuberculosis* H_{37}Rv-derived strains. H_{37}Rv: *M. tuberculosis* H_{37}Rv. Green pick: adenine, A. Red pick: thymine, T. Blue pick: cytosine, C. Black pick: guanine, G.

subcloned from pMN437-RpoB Q^{432}insQ into the *Sca*I site of the pGOAL19 plasmid, and the resulting construct, pGOAL19-Rv RpoB Q^{432}insQ (**Table 2**) was checked by sequencing. Then, the plasmid was transformed into *M. tuberculosis* H_{37}Rv, and the unmarked replacement mutant (RpoB Q^{432}insQ) was selected after two rounds of homologous recombination. DNA sequencing confirmed that seven strains (#19, #112, #132, #133, #135, #136, and #137) had the CAA insertion in codon 432 of *rpoB*, which leads to a Q insertion (**Figure 2**). All tested strains were resistant to RIF, with an MIC >1 mg/L.

DISCUSSION

Clinical strains CDC-1, CDC-2, and CDC-3 have high-level RIF resistance and unique *rpoB* gene mutations. All of them also encoded V^{170}F, which is a well-known RIF-resistance associated mutation, as it has been reported that *M. tuberculosis* isolates encoding the V^{170}F mutation have high-level resistance to RIF (8–32 mg/L) (Heep et al., 2000). According to our data, G^{158}R, V^{168}A, and S^{188}P mutations likely did not contribute to RIF resistance in these strains. However, strain CDC-2 had a RIF MIC of 256–512 mg/L, which was 32–64 fold higher than the MIC previously reported for a strain encoding RpoB V^{170}F (Heep et al., 2000), suggesting that strain CDC-2 might have another drug-resistance mechanism not involving RpoB. Because we only sequenced the *rpoB* genes of RIF-resistant strains, resistance mechanisms outside *rpoB* could not be detected. Mutations causing other antibiotic resistance could be missed too. Chromosome mutations comprise the major mechanism causing drug resistance in *M. tuberculosis* (Miotto et al., 2018). Drug resistance in strains could be caused by other resistance mechanisms such as antibiotic modifications or neutralization, augmented efflux pumps, porin alterations, and the downregulation of cell-wall permeability (Mnyambwa et al., 2017; Sharma et al., 2018).

Codons 431 and 432 of *rpoB* are located in the RRDR (Friehs, 2004), and mutations in this region are related to RIF resistance (Sandgren et al., 2009). Mutations at codon 431 ($S^{431}T$, $S^{431}I$, $S^{431}R$, and $S^{431}G$) were previously reported to be associated with RIF resistance (Kapur et al., 1994; Sajduda et al., 2004; Chan et al., 2007). Multiple mutations including codon 431 or 432 of RpoB resulted in higher-level RIF resistance (MIC > 100 mg/L) (Bahrmand et al., 2009). We also demonstrated that plasmid complementation or chromosomal mutagenesis of Q^{432}insQ alone could cause RIF resistance, whereas $S^{431}G$ plus Q^{432}insQ complementation resulted in a two-fold higher MIC of RIF (**Tables 2**, **3**, **Figure 1**).

RIF interacts with the β-subunit of RpoB, and most RIF resistance in *M. tuberculosis* is caused by mutations in the RRDR of RpoB (Tupin et al., 2010). The domain structure of RpoB was previously deduced by analyzing the crystal structure, which showed that RpoB directly interacts with RIF via 12 hydrogen bonds (Nusrath Unissa et al., 2016). Molecular docking experiments showed stronger RIF binding by wild-type RpoB than by mutant RpoB proteins (Nusrath Unissa et al., 2016). Q432 is an energetically favorable binding site and is considered part of the active site that is involved in ligand binding (Campbell et al., 2001; Nusrath Unissa et al., 2016). RpoB Q^{432}insQ might influence the binding enthalpy to weaken the molecular interaction between RpoB and RIF, which could result in RIF resistance.

We observed that CDC-4 grew slower compared to the H_{37}Rv strain. Therefore, mutants survived better only in the presence of RIF. Multiple mutations in *rpoB* have been reported, shown to result in increased drug resistance (Bahrmand et al., 2009). The occurrence of multiple mutations could be accumulated due to continuous RIF usage after a first mutation or they could occur simultaneously in high RIF environments.

Rifampicin is an effective drug used to treat most cases of drug-susceptible TB (Long et al., 2019). However, cases of RIF resistance have been reported since the early 1990s, leading to problems in TB control (Zaw et al., 2018). In *M. tuberculosis*, drug resistance is mostly caused by genetic changes rather than gene transfer from other bacteria (Tupin et al., 2010; Zaw et al., 2018). Thus, sequencing well-known mutation sites is important to detect drug-resistant *M. tuberculosis*. Several molecular diagnostic methods have been developed for the rapid detection of drug resistance in *M. tuberculosis* (Yong et al., 2019). Nevertheless, more comprehensive information on drug resistance-associated mutations must be established to improve the diagnosis and treatment of TB.

CONCLUSION

In summary, we studied four isolates with high-level RIF resistance and unique mutations encoding RpoB $G^{158}R$, RpoB $V^{168}A$, RpoB $S^{188}P$, and RpoB Q^{432}insQ. Results of plasmid complementation of RpoB indicated that $G^{158}R$, $V^{168}A$, and $S^{188}P$ of RpoB do not affect the MIC of RIF. However, the transfer of pMN437-RpoB Q^{432}insQ plasmids to *M. tuberculosis* H_{37}Rv or chromosomal mutagenesis generating RpoB Q^{432}insQ turned sensitive strains into RIF-resistant strains. Therefore, RpoB Q^{432}insQ confers RIF resistance in *M. tuberculosis*.

DATA AVAILABILITY STATEMENT

The datasets presented in this study can be found in online repositories. The names of the repository/repositories and accession number(s) can be found in the article/**Supplementary Material**.

AUTHOR CONTRIBUTIONS

J-TW designed the study. L-YL, P-FH, T-LL, and J-TW discussed the results and revised the manuscript. W-TL, H-YT, W-HL, and RJ provided and analyzed the clinical strains. L-YL, S-HW, S-EC, L-YH, and H-EK prepared materials and performed experiments. L-YL and P-FH analyzed the data. L-YL wrote the manuscript. All authors reviewed and approved the final version of the manuscript.

ACKNOWLEDGMENTS

This study was supported by the Ministry of Science and Technology, the Excellent Translational Medicine Research Projects of National Taiwan University College of Medicine and National Taiwan University Hospital, the Liver Disease Prevention and Treatment Research Foundation of Taiwan, and "Center of Precision Medicine" from the Featured Areas Research Center Program within the framework of the Higher Education Sprout Project by the Ministry of Education (MOE) in Taiwan.

SUPPLEMENTARY MATERIAL

The Supplementary Material for this article can be found online at: https://www.frontiersin.org/articles/10.3389/fmicb.2020.583194/full#supplementary-material

REFERENCES

Bahrmand, A. R., Titov, L. P., Tasbiti, A. H., Yari, S., and Graviss, E. A. (2009). High-level rifampin resistance correlates with multiple mutations in the rpoB gene of pulmonary tuberculosis isolates from the Afghanistan border of Iran. *J. Clin. Microbiol.* 47, 2744–2750. doi: 10.1128/jcm.r00548-09

Boyd, R., Ford, N., Padgen, P., and Cox, H. (2017). Time to treatment for rifampicin-resistant tuberculosis: systematic review and meta-analysis. *Int. J. Tuberc. Lung Dis.* 21, 1173–1180. doi: 10.5588/ijtld.17.0230

Burke, R. M., Coronel, J., and Moore, D. (2017). Minimum inhibitory concentration distributions for first- and second-line antimicrobials against *Mycobacterium tuberculosis*. *J. Med. Microbiol.* 66, 1023–1026. doi: 10.1099/jmm.0.000534

Campbell, E. A., Korzheva, N., Mustaev, A., Murakami, K., Nair, S., Goldfarb, A., et al. (2001). Structural mechanism for rifampicin inhibition of bacterial rna polymerase. *Cell* 104, 901–912. doi: 10.1016/s0092-8674(01)00286-0

Chan, R. C., Hui, M., Chan, E. W., Au, T. K., Chin, M. L., Yip, C. K., et al. (2007). Genetic and phenotypic characterization of drug-resistant *Mycobacterium tuberculosis* isolates in Hong Kong. *J. Antimicrob. Chemother.* 59, 866–873. doi: 10.1093/jac/dkm054

Chikaonda, T., Ketseoglou, I., Nguluwe, N., Krysiak, R., Thengolose, I., Nyakwawa, F., et al. (2017). Molecular characterisation of rifampicin-resistant *Mycobacterium tuberculosis* strains from Malawi. *Afr. J. Lab. Med.* 6:463.

Friehs, K. (2004). Plasmid copy number and plasmid stability. *Adv. Biochem. Eng. Biotechnol.* 86, 47–82.

Heep, M., Rieger, U., Beck, D., and Lehn, N. (2000). Mutations in the beginning of the rpoB gene can induce resistance to rifamycins in both *Helicobacter pylori* and *Mycobacterium tuberculosis*. *Antimicrob. Agents Chemother.* 44, 1075–1077. doi: 10.1128/aac.44.4.1075-1077.2000

Islam, M. M., Hameed, H. M. A., Mugweru, J., Chhotaray, C., Wang, C., Tan, Y., et al. (2017). Drug resistance mechanisms and novel drug targets for tuberculosis therapy. *J. Genet. Genom.* 44, 21–37. doi: 10.1016/j.jgg.2016.10.002

Kapur, V., Li, L. L., Iordanescu, S., Hamrick, M. R., Wanger, A., Kreiswirth, B. N., et al. (1994). Characterization by automated DNA sequencing of mutations in the gene (rpoB) encoding the RNA polymerase beta subunit in rifampin-resistant *Mycobacterium tuberculosis* strains from New York City and Texas. *J. Clin. Microbiol.* 32, 1095–1098. doi: 10.1128/jcm.32.4.1095-1098.1994

Lai, L. Y., Lin, T. L., Chen, Y. Y., Hsieh, P. F., and Wang, J. T. (2018). Role of the *Mycobacterium marinum* ESX-1 secretion system in sliding motility and biofilm formation. *Front. Microbiol.* 9:1160. doi: 10.3389/fmicb.2018.01160

Larsen, M. H., Biermann, K., Tandberg, S., Hsu, T., and Jacobs, W. R. Jr. (2007). Genetic manipulation of *Mycobacterium tuberculosis*. *Curr. Protoc. Microbiol. Chap.* 10:Unit 10A 12.

Lohrasbi, V., Talebi, M., Bialvaei, A. Z., Fattorini, L., Drancourt, M., Heidary, M., et al. (2018). Trends in the discovery of new drugs for *Mycobacterium tuberculosis* therapy with a glance at resistance. *Tuberculosis* 109, 17–27. doi: 10.1016/j.tube.2017.12.002

Long, B., Liang, S. Y., Koyfman, A., and Gottlieb, M. (2019). Tuberculosis: a focused review for the emergency medicine clinician. *Am. J. Emerg. Med.* 38, 1014–1022. doi: 10.1016/j.ajem.2019.12.040

Mabhula, A., and Singh, V. (2019). Drug-resistance in *Mycobacterium tuberculosis*: where we stand. *Med. Chem. Commun.* 10, 1342–1360. doi: 10.1039/c9md00057g

Miotto, P., Zhang, Y., Cirillo, D. M., and Yam, W. C. (2018). Drug resistance mechanisms and drug susceptibility testing for tuberculosis. *Respirology* 23, 1098–1113. doi: 10.1111/resp.13393

Mnyambwa, N. P., Kim, D. J., Ngadaya, E. S., Kazwala, R., Petrucka, P., and Mfinanga, S. G. (2017). Clinical implication of novel drug resistance-conferring mutations in resistant tuberculosis. *Eur. J. Clin. Microbiol. Infect. Dis.* 36, 2021–2028. doi: 10.1007/s10096-017-3027-3

Nusrath Unissa, A., Hassan, S., Indira Kumari, V., Revathy, R., and Hanna, L. E. (2016). Insights into RpoB clinical mutants in mediating rifampicin resistance in *Mycobacterium tuberculosis*. *J. Mol. Graph. Model.* 67, 20–32. doi: 10.1016/j.jmgm.2016.04.005

Pang, Y., Lu, J., Wang, Y., Song, Y., Wang, S., and Zhao, Y. (2013). Study of the rifampin monoresistance mechanism in *Mycobacterium tuberculosis*. *Antimicrob. Agents Chemother.* 57, 893–900. doi: 10.1128/aac.01024-12

Parish, T., and Stoker, N. G. (2000). Use of a flexible cassette method to generate a double unmarked *Mycobacterium tuberculosis* tlyA plcABC mutant by gene replacement. *Microbiology* 146(Pt 8), 1969–1975. doi: 10.1099/00221287-146-8-1969

Piccaro, G., Pietraforte, D., Giannoni, F., Mustazzolu, A., and Fattorini, L. (2014). Rifampin induces hydroxyl radical formation in *Mycobacterium tuberculosis*. *Antimicrob. Agents Chemother.* 58, 7527–7533. doi: 10.1128/aac.03169-14

Sajduda, A., Brzostek, A., Poplawska, M., Augustynowicz-Kopec, E., Zwolska, Z., Niemann, S., et al. (2004). Molecular characterization of rifampin- and isoniazid-resistant *Mycobacterium tuberculosis* strains isolated in Poland. *J. Clin. Microbiol.* 42, 2425–2431. doi: 10.1128/jcm.42.6.2425-2431.2004

Sandgren, A., Strong, M., Muthukrishnan, P., Weiner, B. K., Church, G. M., and Murray, M. B. (2009). Tuberculosis drug resistance mutation database. *PLoS Med.* 6:e1000002. doi: 10.1371/journal.pmed.1000002

Sharma, D., Bisht, D., and Khan, A. U. (2018). Potential alternative strategy against drug resistant tuberculosis: a proteomics prospect. *Proteomes* 6:26. doi: 10.3390/proteomes6020026

Steinhauer, K., Eschenbacher, I., Radischat, N., Detsch, C., Niederweis, M., and Goroncy-Bermes, P. (2010). Rapid evaluation of the mycobactericidal efficacy of disinfectants in the quantitative carrier test EN 14563 by using fluorescent *Mycobacterium terrae*. *Appl. Environ. Microbiol.* 76, 546–554. doi: 10.1128/aem.01660-09

Swain, S. S., Sharma, D., Hussain, T., and Pati, S. (2020). Molecular mechanisms of underlying genetic factors and associated mutations for drug resistance in *Mycobacterium tuberculosis*. *Emerg. Microb. Infect.* 9, 1651–1663. doi: 10.1080/22221751.2020.1785334

Tan, T., Lee, W. L., Alexander, D. C., Grinstein, S., and Liu, J. (2006). The ESAT-6/CFP-10 secretion system of *Mycobacterium marinum* modulates phagosome maturation. *Cell Microbiol.* 8, 1417–1429. doi: 10.1111/j.1462-5822.2006.00721.x

Tupin, A., Gualtieri, M., Roquet-Baneres, F., Morichaud, Z., Brodolin, K., and Leonetti, J. P. (2010). Resistance to rifampicin: at the crossroads between ecological, genomic and medical concerns. *Int. J. Antimicrob. Agents* 35, 519–523. doi: 10.1016/j.ijantimicag.2009.12.017

Vekemans, J., Brennan, M. J., Hatherill, M., Schrager, L., Fritzell, B., Rutkowski, K., et al. (2020). Preferred product characteristics for therapeutic vaccines to improve tuberculosis treatment outcomes: key considerations from World Health Organization consultations. *Vaccine* 38, 135–142. doi: 10.1016/j.vaccine.2019.10.072

Vilcheze, C., and Jacobs, W. R. Jr. (2014). Resistance to isoniazid and ethionamide in *Mycobacterium tuberculosis*: genes, mutations, and causalities. *Microbiol. Spectr.* 2:MGM2-0014-2013. doi: 10.1128/microbiolspec.MGM2-0014-2013

World Health Organization [WHO] (2019). *Global Tuberculosis Report 2019*. Geneva: World Health Organization.

Yong, Y. K., Tan, H. Y., Saeidi, A., Wong, W. F., Vignesh, R., Velu, V., et al. (2019). Immune biomarkers for diagnosis and treatment monitoring of tuberculosis: current developments and future prospects. *Front. Microbiol.* 10:2789. doi: 10.3389/fmicb.2018.02789

Zaw, M. T., Emran, N. A., and Lin, Z. (2018). Mutations inside rifampicin-resistance determining region of rpoB gene associated with rifampicin-resistance in *Mycobacterium tuberculosis*. *J. Infect. Public Health* 11, 605–610. doi: 10.1016/j.jiph.2018.04.005

Conflict of Interest: The authors declare that the research was conducted in the absence of any commercial or financial relationships that could be construed as a potential conflict of interest.

frontiers in Microbiology

ORIGINAL RESEARCH
published: 18 January 2021
doi: 10.3389/fmicb.2020.622629

Search for Antimicrobial Activity Among Fifty-Two Natural and Synthetic Compounds Identifies Anthraquinone and Polyacetylene Classes That Inhibit *Mycobacterium tuberculosis*

Luiz A. E. Pollo[1], Erlon F. Martin[1], Vanessa R. Machado[1], Daire Cantillon[2], Leticia Muraro Wildner[2], Maria Luiza Bazzo[1], Simon J. Waddell[2], Maique W. Biavatti[1] and Louis P. Sandjo[3]**

[1] Programa de Pós-Graduação em Farmácia, CCS, Universidade Federal de Santa Catarina, Florianópolis, Brazil, [2] Department of Global Health and Infection, Brighton and Sussex Medical School, University of Sussex, Brighton, United Kingdom, [3] Programa de Pós-Graduação em Química, CFM, Departamento de Química, Universidade Federal de Santa Catarina, Florianópolis, Brazil

OPEN ACCESS

Edited by:
Maria Rosalia Pasca,
University of Pavia, Italy

Reviewed by:
Divakar Sharma,
Indian Institute of Technology Delhi, India
Diana Machado,
New University of Lisbon, Portugal

***Correspondence:**
Simon J. Waddell
s.waddell@bsms.ac.uk
Louis P. Sandjo
p.l.sandjo@ufsc.br

Specialty section:
This article was submitted to Antimicrobials, Resistance and Chemotherapy, a section of the journal Frontiers in Microbiology

Received: 28 October 2020
Accepted: 29 December 2020
Published: 18 January 2021

Citation:
Pollo LAE, Martin EF, Machado VR, Cantillon D, Wildner LM, Bazzo ML, Waddell SJ, Biavatti MW and Sandjo LP (2021) Search for Antimicrobial Activity Among Fifty-Two Natural and Synthetic Compounds Identifies Anthraquinone and Polyacetylene Classes That Inhibit Mycobacterium tuberculosis. Front. Microbiol. 11:622629. doi: 10.3389/fmicb.2020.622629

Drug-resistant tuberculosis threatens to undermine global control programs by limiting treatment options. New antimicrobial drugs are required, derived from new chemical classes. Natural products offer extensive chemical diversity and inspiration for synthetic chemistry. Here, we isolate, synthesize and test a library of 52 natural and synthetic compounds for activity against *Mycobacterium tuberculosis*. We identify seven compounds as antimycobacterial, including the natural products isobavachalcone and isoneorautenol, and a synthetic chromene. The plant-derived secondary metabolite damnacanthal was the most active compound with the lowest minimum inhibitory concentration of 13.07 μg/mL and a favorable selectivity index value. Three synthetic polyacetylene compounds demonstrated antimycobacterial activity, with the lowest MIC of 17.88 μg/mL. These results suggest new avenues for drug discovery, expanding antimicrobial compound chemistries to novel anthraquinone and polyacetylene scaffolds in the search for new drugs to treat drug-resistant bacterial diseases.

Keywords: *Mycobacterium tuberculosis*, drug discovery, natural product, synthetic polyacetylenes, antimicrobial drug resistance

INTRODUCTION

Tuberculosis (TB) is an infectious disease that is among the top 10 causes of death worldwide, and the leading bacterial cause of death. In 2019, an estimated 10 million people developed TB and 1.4 million people died as result of the disease (World Health Organization, 2020). TB treatment requires the use of multiple drugs for at least 6 months. This lengthy therapy together with adverse drug reactions contribute to patient non-adherence, resulting in treatment failure and the development of drug-resistant *Mycobacterium tuberculosis*. The emergence of multidrug-resistant (MDR) TB and extensively drug resistant (XDR) TB is undermining global control efforts. In 2019,

3.3% of new TB cases and 17.7% of previously treated cases were rifampicin-resistant (RR)/MDR-TB. There were an estimated 465,000 incident cases of RR-TB in the same year, of which 78% were MDR-TB (World Health Organization, 2020). Therefore, there is an urgent need, recognized by the World Health Organization (World Health Organization, 2014), for new drugs to treat drug-resistant TB, and to shorten therapy for drug-sensitive TB. However, despite sustained international efforts, only pretomanid, delamanid and bedaquiline have been marketed as new drugs for TB treatment in the last 40 years (The Working Group for New TB Drugs, 2020). Intensified research and innovation are needed to meet the End TB Strategy targets set for 2030, a key priority of which is to discover new drugs based on new chemical entities (World Health Organization, 2014).

Over the past 60,000 years, plant-derived medicines have been used as decoctions, infusions and tinctures to improve human health (Solecki and Shanidar, 1975). Numerous studies have attempted to correlate ethnological knowledge with the scientific evidence base (De Smet, 1997). Natural products are an essential source of biologically active components (Thomford et al., 2018; Wright, 2019), and naturally occurring secondary metabolites have inspired the development of therapeutic drugs for infectious, cardiovascular, and degenerative diseases (Thomford et al., 2018; Lautié et al., 2020). Natural products are composed of numerous structural diversities, often containing complex hydrocarbon skeletons that have been explored to produce libraries of biologically relevant derivatives (Salomon and Schmidt, 2012; Pascolutti and Quinn, 2014). *Dorstenia* plant species are used in sub-Saharan African and South American countries as herbal medicines to treat cough, pneumonia and other infectious diseases such as malaria, syphilis, and hepatitis (Togola et al., 2008; Teklehaymanot, 2009; Bieski et al., 2012; Adem et al., 2018). Prenylated flavonoids obtained from *Dorstenia* species showed antibacterial activity against a broad-spectrum of bacteria, including *M. tuberculosis* (Mbaveng et al., 2012). Secondary metabolites from *Erythrina senegalensis*, the Senegal coral tree, have been demonstrated to exhibit strong inhibition of methicillin resistant *Staphylococcus aureus*, *Enterococcus faecalis,* and *Bacillus subtilis* (Koné et al., 2004). Damnacanthal, an anthraquinone obtained from *Pentas schimperi*, displayed moderate activity against the *Trypanosoma cruzi* amastigote (Sandjo et al., 2016b). As numerous biologically active molecules have been inspired by the organic constituents of plants, our group prepared a series of pyridine and chromene derivatives (Pollo et al., 2017; Martin et al., 2018). These compounds were evaluated for their antiparasitic activities against *Leishmania amazonensis* and *T. cruzi* amastigotes. Three pyridines and three chromenes inhibited *T. cruzi* with IC_{50} values less than 7 μM. Similarly, a coumarin scaffold was used to generate anti-TB agents, while polyacetylenes from plants and pyridine derivatives have been shown to express antimycobacterial activities (Rogoza et al., 2010; Somagond et al., 2019; Kumar et al., 2020).

Here, we report the extraction, synthesis, and anti-*M. tuberculosis* activity of 52 compounds: six plant secondary metabolites from *Dorstenia kameruniana*, *Dorstenia mannii*, *P. schimperi*, and *E. senegalensis*, and 46 synthetic compounds including 20 dihydropyridines, 12 pyranocoumarins, seven chromenes, one oxazinone, one conjugated ester and five polyacetylenes. This study identifies anthraquinone and polyacetylene compounds as the basis for novel drug discovery toward new therapeutic options for drug-resistant TB.

MATERIALS AND METHODS

Origin of the Natural Products

Isobavachalcone (C1) was isolated from *D. kameruniana*, while 4-hydroxylonchocarpine (C21) and 6,8-diprenyleriodictyol (C24) were obtained from *D. mannii* (Abegaz et al., 1998; Ngadjui et al., 1998). Damnacanthal (C22) and its reduced derivative (C25) were isolated from *P. schimperi* (Kuete et al., 2015a). Isoneorautenol (C23) was extracted from *E. senegalensis* (Kuete et al., 2014). The structures of these natural secondary metabolites are displayed in **Figures 1**, **2**.

Preparation of the Pyranocoumarin Derivatives

Compound 50 (C50) was synthesized by treating phloroglucinol at 60°C for 6 h with one equivalent of ethyl acetoacetate and a catalytic amount of polyphosphoric acid. This coumarin was then used as the starting material to prepare a series of pyranocoumarins. C50, arylaldehydes, malononitrile, and K_2CO_3 were submitted to reflux conditions to generate compounds C2–C7. Compounds C8–C12 were obtained using the same one-pot conditions except that malononitrile was replaced by methyl α-cyanoacetate. C13 was a by-product formed from the Knoevenagel condensation reaction of cinnamaldehyde and α-cyanoacetate in the same reaction conditions. The structures are detailed in **Figures 1**, **2**, **4** (Martin et al., 2018).

Preparation of Chromenes

Chromene derivatives C14–C20 were obtained by a direct reaction of phloroglucinol, arylaldehydes and methyl α-cyanoacetate in alkaline reflux conditions. We have previously described the synthesis and the identification of C2–C20 (Martin et al., 2018), shown in **Figure 2**.

Preparation of Dihydropyridine Derivatives and Analogs

Bismuth chloride was used to promote the reaction, which was carried out in tetrahydrofuran under reflux conditions and was stirred for 6 h to synthesize compounds C29–C33 (Sandjo et al., 2016a). C34–C41 were obtained from the same reaction conditions replacing ethyl benzoylacetate with ethyl acetylacetate in reflux and free catalyst conditions to prepare these dihydropyridine analogs. C42–C49 were also synthesized in reflux conditions without any catalyst, replacing ammonium acetate with aniline. The preparation of these dihydropyridine analogs has been described (Pollo et al., 2017), and their structures are displayed in **Figures 3**, **4**.

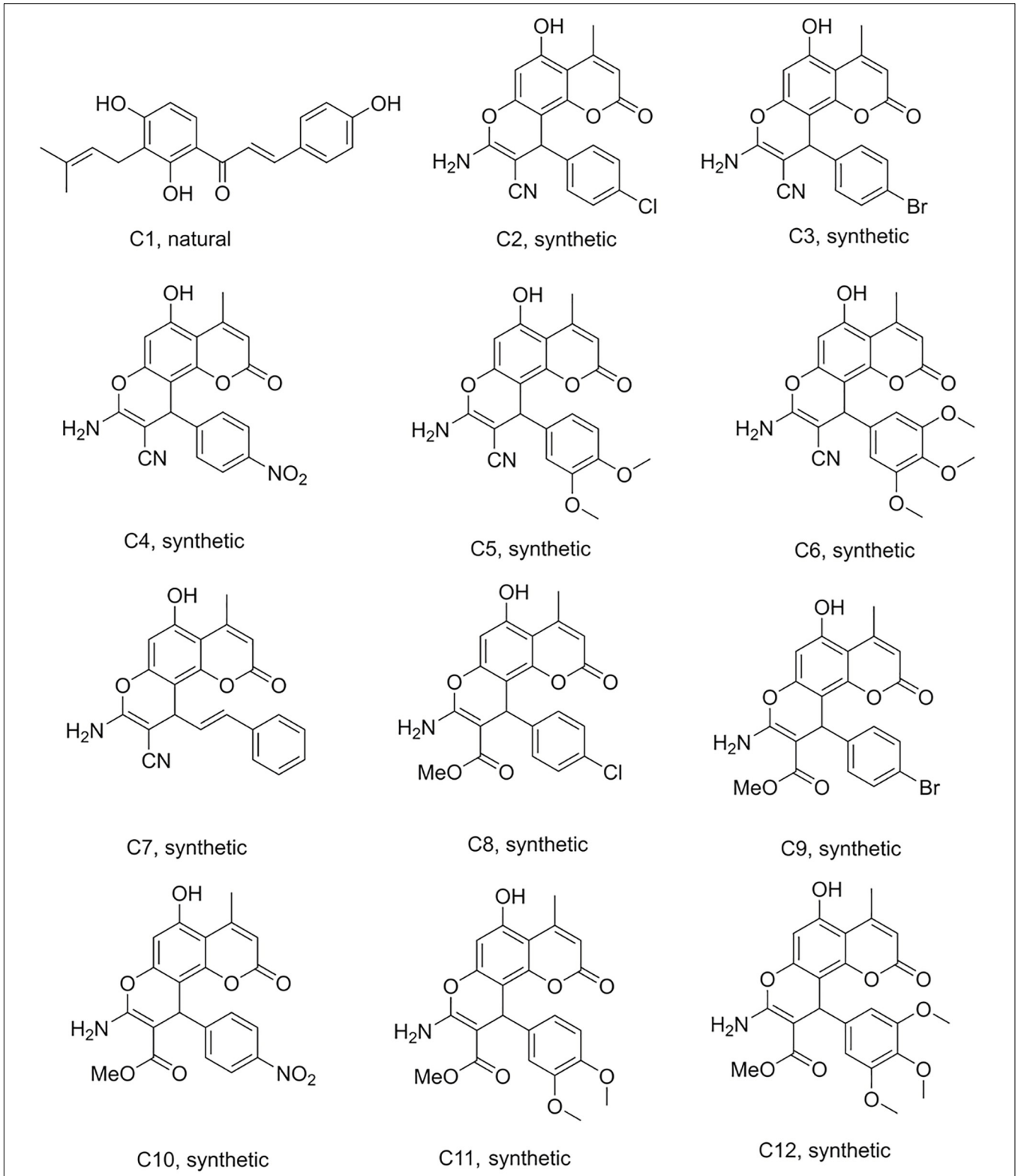

FIGURE 1 | Structures of the compounds tested for anti-*M. tuberculosis* activity: Chalcone C1, and the pyranocoumarins C2–C12 (Abegaz et al., 1998; Martin et al., 2018).

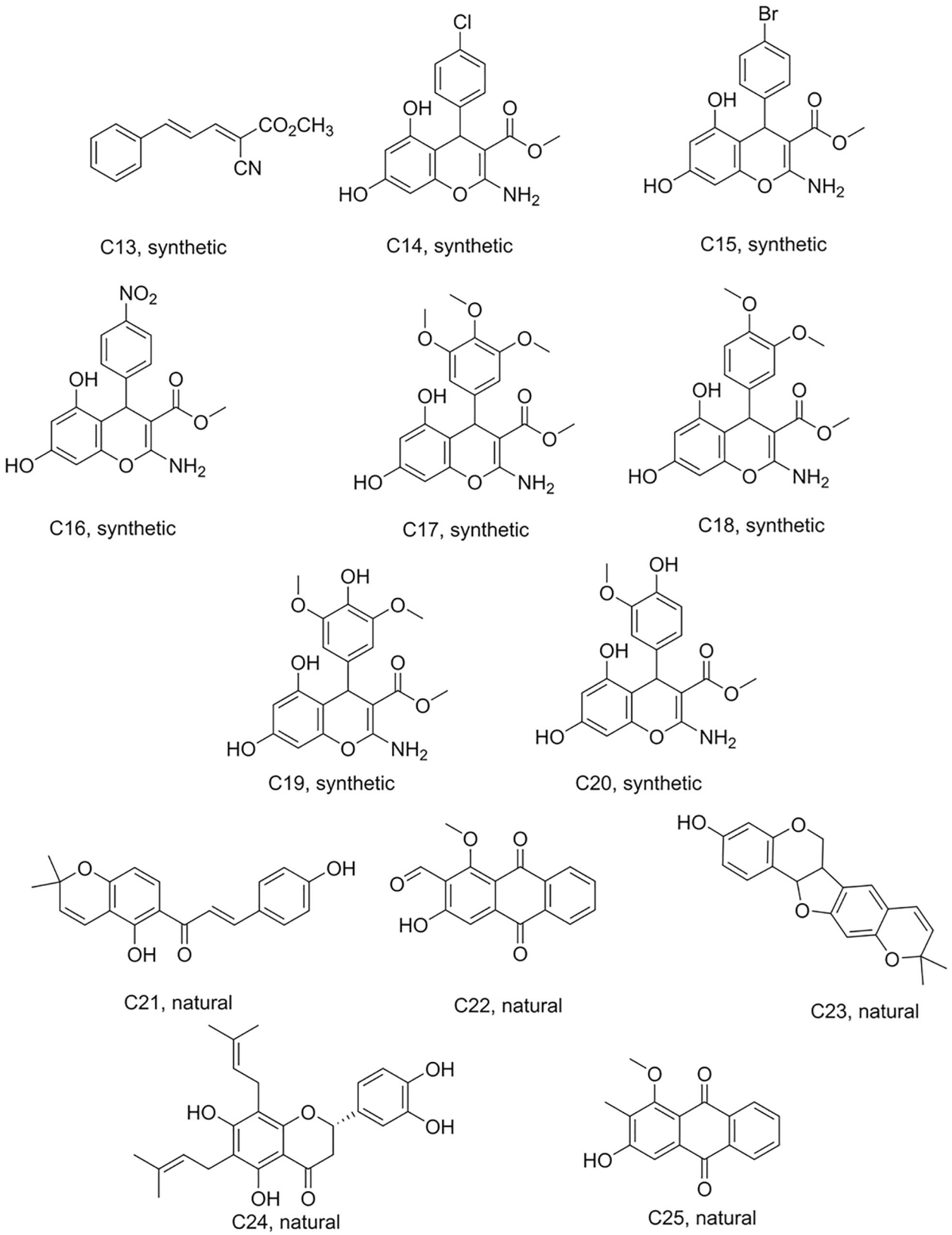

FIGURE 2 | Structures of the compounds tested for anti-*M. tuberculosis* activity: Ester C13, chromenes C14–C20, and natural products C21–C25 (Ngadjui et al., 1998; Kuete et al., 2014, 2015a; Martin et al., 2018).

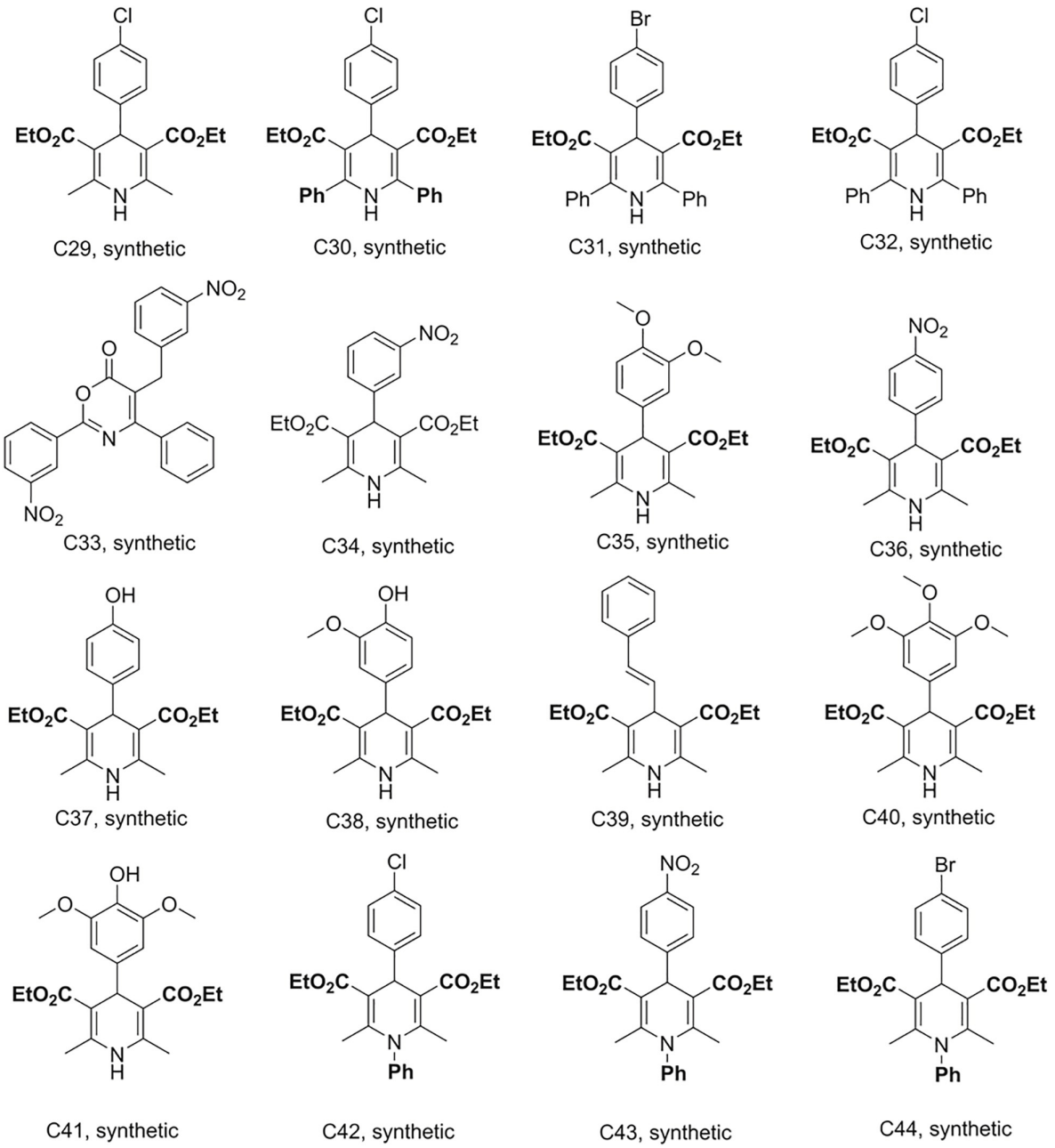

FIGURE 3 | Structures of the compounds tested for anti-*M. tuberculosis* activity: Dihydropyridines C29–C44 (Sandjo et al., 2016a; Pollo et al., 2017).

Preparation of the Polyacetylene Derivatives

Deca-4,6,8-triyn-1-ol (C51), deca-4,6,8-triynal (C52), 7-(triisopropylsilyl)hepta-4,6-diyn-1-ol (C54) and 9-(triisopropylsilyl)nona-4, 6-,8-triyn-1-ol (C55) were previously synthesized, identified and reported by Machado and co-workers (Machado et al., 2018). Tetradeca-4,6,8,10-tetrayne-1,14-diol (C53) was prepared by homodimerization reaction in a 25 mL, two neck, round-bottom flask equipped with rubber septum and a magnetic stir bar, filled with a solution of hepta-4,6-diyn-1-ol (0.1 g; 0.925 mmol; 1 equiv.) in CH_3CN (10 mL). To this solution was added $Cu(OAc)_2$ (0.353 g; 1.94 mmol; 2.1 equiv) and K_2CO_3 (0.153 g; 1.11 mmol; 1.2 equiv. The resulting mixture was stirred vigorously at room temperature overnight (∼18 h). The organic extract was washed with brine (20 mL), dried over $MgSO_4$, filtered, and concentrated under reduced pressure. Purification by column chromatography on silica gel (elution with 40% EtOAc-hexanes) afforded 0.063 g (32 %) of tetradeca-4,6,8,10-tetrayne-1,14-diol as a pale yellow oil. mp 116.5 - 117°C; *R.f*: 0.75 (40% hexane-ethyl acetate; ^{1}H NMR (300 MHz, CD_3OD)

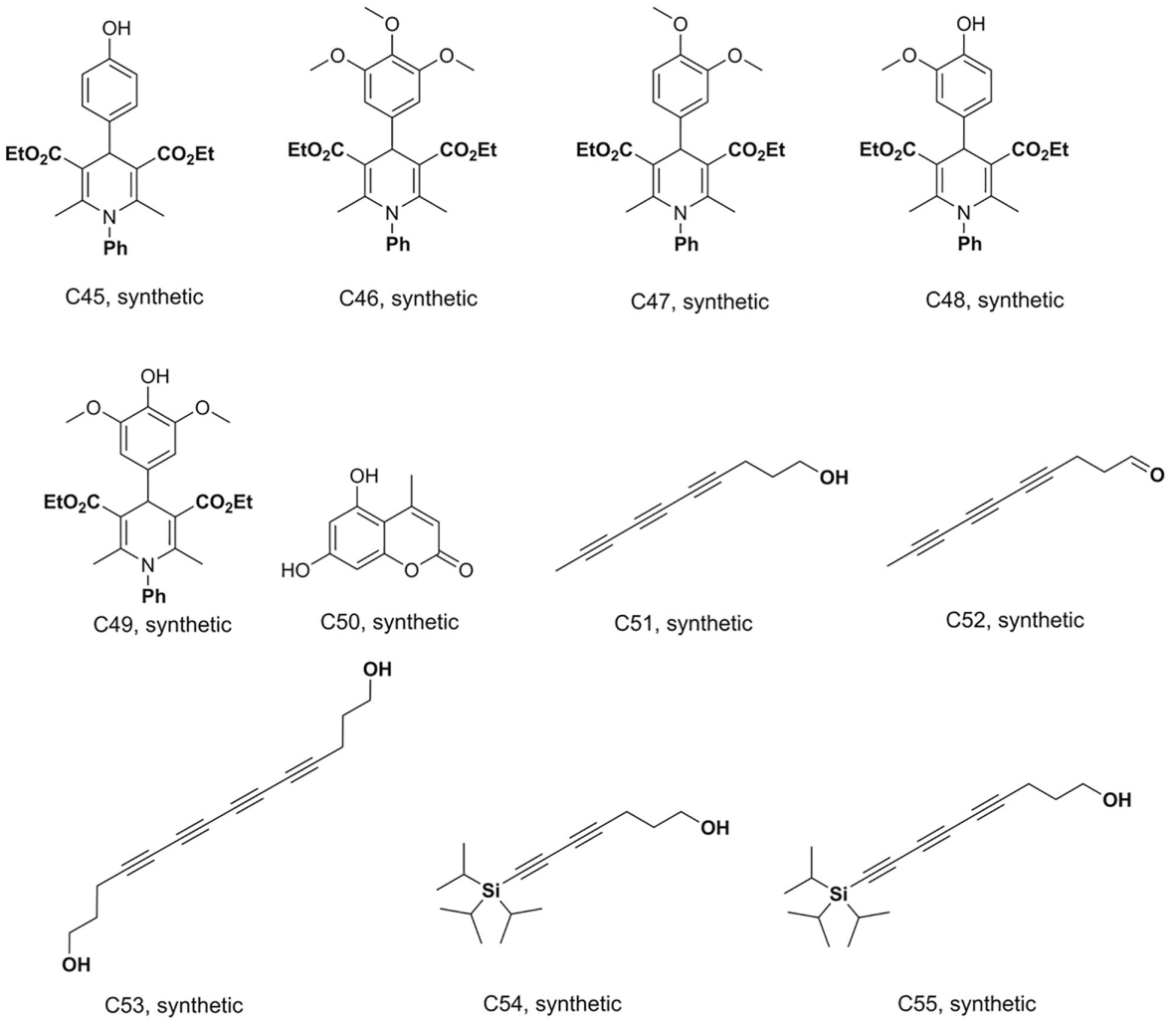

FIGURE 4 | Structures of the compounds tested for anti-*M. tuberculosis* activity: Dihydropyridines C45–C49, coumarin C50, and polyacetylenes C51–C55 (Sandjo et al., 2016a; Pollo et al., 2017; Machado et al., 2018; Martin et al., 2018).

δ in ppm: 3.61(t, 4H), 2.44 (t, J=7.15 Hz, 4H), 1.74 (m, 4H). ^{13}C-NMR (75 MHz, CD_3OD) δ in ppm: 81.4; 66.1; 62.1; 61.2; 60.8; 31.9; 16.5. The structures of these compounds are shown in **Figure 4**.

Bacteria and Culture Conditions

Mycobacterium tuberculosis H37Rv reference strain was cultured in Middlebrook 7H9 broth (Sigma-Aldrich) supplemented with albumin dextrose catalase (ADC, 10% v/v) and Tween 80 (0.05% v/v) at 37°C. Optical density was measured using a spectrophotometer (Promega) at absorbance 600 nm. Colony forming units (CFU) were determined by serially diluting cultures onto Middlebrook 7H10 agar (Sigma-Aldrich) supplemented with 0.5% glycerol and oleic acid albumin dextrose catalase (OADC, 10% v/v) and incubated at 37°C for 4 weeks. All *M. tuberculosis* work was conducted in containment level three laboratories, following institutional biosafety and biosecurity standards for working with hazard group three pathogens.

Antimycobacterial Activity

All compounds were prepared as 10 mg/mL stock solutions in sterile dimethyl sulfoxide (DMSO), except for rifampicin which was prepared with 90% w/v methanol. Single use aliquots of compounds were prepared and stored at −20°C. Log phase *M. tuberculosis* cultures were adjusted from 2×10^5 to 5×10^5 CFU/mL, added to 96 well microtiter plates containing test compounds at a final concentration of 100 μg/mL (1% DMSO final concentration), and incubated for 7 days at 37°C. To determine cell viability, CellTiter-Blue (Promega) was added to the plates at a final concentration of 10% v/v and incubated overnight (Franzblau et al., 1998). Fluorescence was measured at excitation 580–640 nm and emission 520 nm using a Glomax Discover plate reader (Promega). Hits were classified as any compound that inhibited growth by ≥40% compared to drug-free *M. tuberculosis* controls. This cut-off was selected to capture the range of antimicrobial activity of related chemical compounds, rather than highlight individual

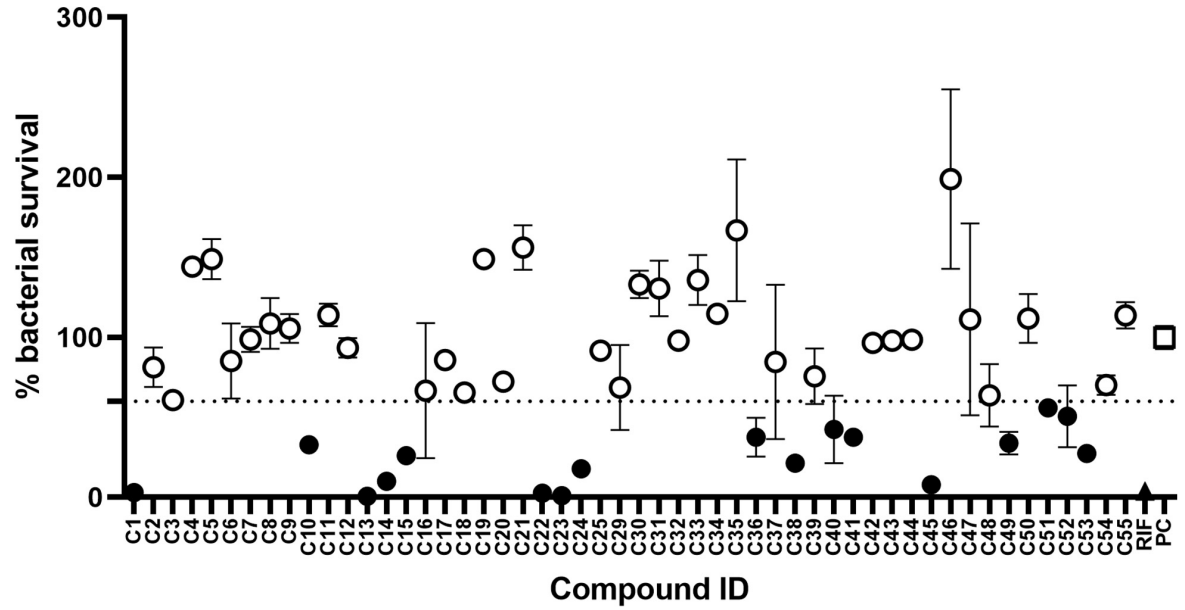

FIGURE 5 | Compound library screen against *Mycobacterium tuberculosis*. Log phase *M. tuberculosis* was treated with compounds at 100 μg/mL for 7 days, bacterial survival was measured after overnight incubation with CellTiter-Blue. Data points are expressed as mean % survival compared to drug-free controls. Error bars represent the standard deviation. Hits were classified as any compound that inhibited growth by ≥40%. Filled circles identify hit compounds. Empty circles indicate compounds not classified as hits. The mean bacterial survival ≤60% shown as a dotted line. Filled triangle (RIF) marks rifampicin-treated bacilli. Empty square (PC) indicates drug-free positive controls.

compounds with superior activity. Minimum inhibitory concentrations (MIC) of hit compounds were determined using a resazurin microtiter plate assay (REMA) with CellTiter-Blue (Promega) as described above, with two-fold serial dilutions from 100 μg/mL to 1.56 μg/mL. The MIC experiments were repeated in triplicate. MICs were calculated by non-linear regression, fitting these data to a modified Gompertz equation for MIC determination, using GraphPad Prism 8. Validation of this assay for established TB drugs (isoniazid and linezolid) is detailed in **Supplementary Figure 1**.

Cytotoxicity Assay

The human monocytic THP-1 cell line was maintained at 37°C, 5% CO_2 in supplemented RPMI 1640 medium (Gibco, Life Technologies) containing 2 mM L-glutamine (Gibco, Life Technologies) and 10% heat inactivated FBS (Pan Biotech). The cells were passaged every 4 days. To measure compound cytotoxicity, 5×10^4 monocytes per well were added to 96 well plates and treated for 24 h with the compounds at concentrations ranging from 200 μg/mL to 1.56 μg/mL. Cell viability was determined by fluorescence quantification after 2 h incubation with CellTiter-Blue (Promega), according to the manufacturer's instructions. Fluorescence was measured at excitation 580–640 nm and emission 520 nm using a Glomax Discover plate reader (Promega). Fluorescence values were adjusted for media fluorescence and the inhibitory concentration 50% (IC_{50}) was calculated using Graphpad Prism 8. The selectivity index (SI) of each compound was calculated by dividing the IC_{50} by the corresponding *M. tuberculosis* MIC value.

RESULTS AND DISCUSSION

The discovery of biologically active new chemical entities is crucial to developing novel chemotherapeutic agents against drug resistant bacterial infections, including TB. Chemistry uses synthetic approaches and analytic techniques to identify and isolate natural products and to produce small molecules bearing diverse hydrocarbon skeletons for preclinical studies (Lombardino and Lowe, 2004; Campbell et al., 2018). To contribute to the search for new anti-tubercular agents, a library of 52 natural and synthetic compounds (**Figures 1–4**) were tested against log phase *M. tuberculosis*. The library contained compounds with diverse chemistries including 11 pyranocoumarins (C2–C12), seven chromenes (C14–C20), one conjugated arylester (C13), two chalcones (C1 and C21), two anthraquinones (C22 and C25), one pterocarpan (C23), one flavanone (C24), 20 dihydropyridines (C29–C32 and C34–C49), one oxazinone (C33), one coumarin (C50), and five polyacetylenes (C51–C55).

Antimycobacterial Activity

The initial screen of the compound library at 100 μg/mL, using the colorimetric CellTiter-Blue assay to measure mycobacterial viability, identified 17 of the 52 compounds that inhibited *M. tuberculosis* survival by at least 40% in comparison to drug-free bacilli (**Figure 5**). Five compounds inhibited *M. tuberculosis* at a level similar to the first line anti-TB drug rifampicin. To verify the results of the initial screen and to establish compound activity, minimum inhibitory concentrations (MICs)

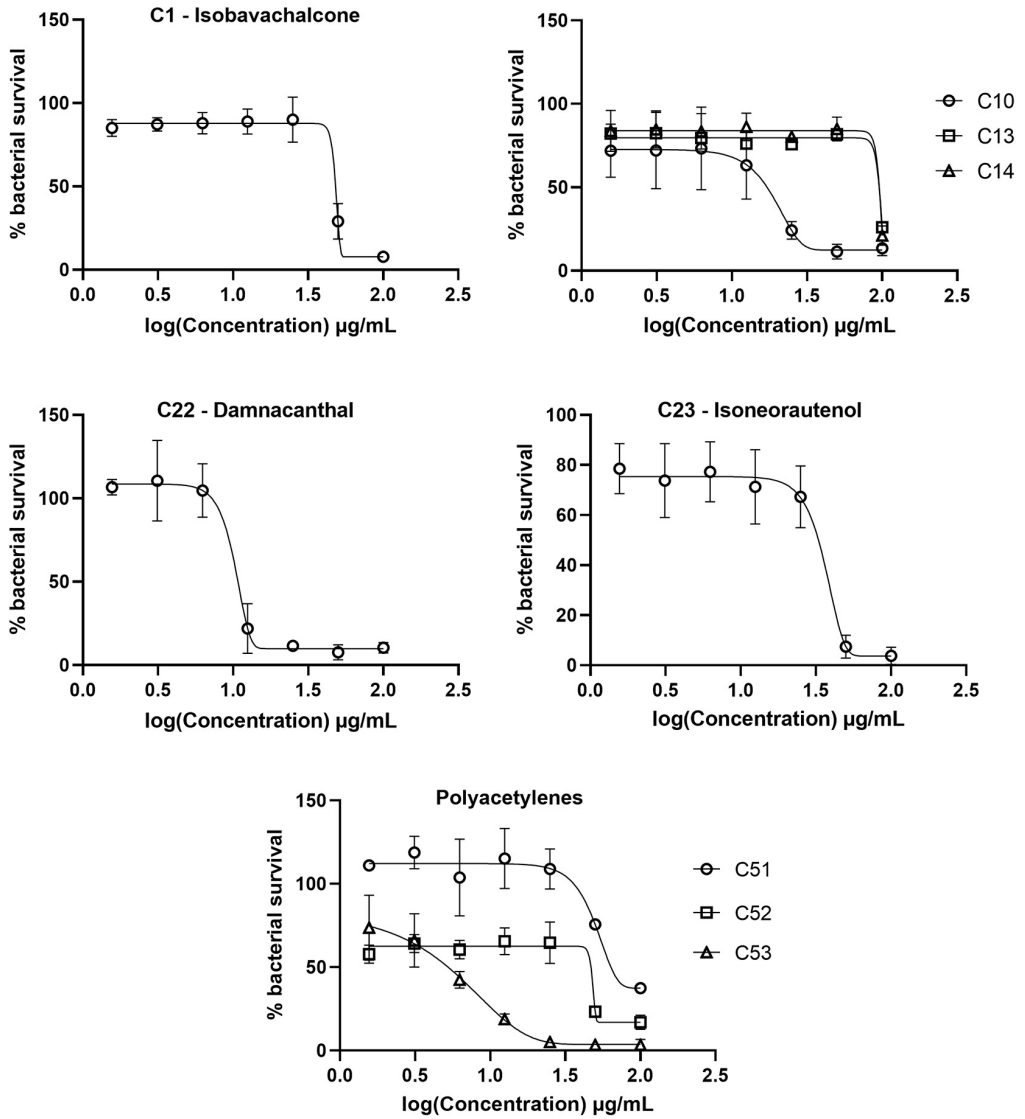

FIGURE 6 | Dose response curves of *Mycobacterium tuberculosis* treated with hit compounds. *M. tuberculosis* was treated for 7 days with compounds ranging in concentration from 100 µg/mL to 1.56 µg/mL. Bacterial survival was measured after overnight incubation with CellTiter-Blue to establish minimum inhibitory concentrations (MICs). Data points are expressed as mean % survival relative to drug-free controls from duplicate biological replicates. Error bars represent the standard deviation.

were determined for all 17 hits using the microbroth dilution method. Compound C22 (the natural product damnacanthal) displayed the greatest activity, with a MIC of 13.07 µg/mL, followed by the polyacetylene C53 with a MIC of 17.88 µg/mL (**Figure 6** and **Table 1**). Compounds C1, C10, C23, C51, and C52 were demonstrated to have MICs against *M. tuberculosis* between 25 and 71 µg/mL (**Figure 6** and **Table 1**). Compounds C13, C14, C15, C24, C36, C38, C40, C41, C45, and C49 resulted in MICs ≥100 µg/mL. Thus, we identified seven chemically diverse compounds that inhibited *M. tuberculosis*.

The top hit against *M. tuberculosis* was damnacanthal (C22 – MIC of 13.07 µg/mL), a naturally occurring secondary metabolite isolated from the tropical plant *P. schimperi* (**Figure 6**), which has previously been demonstrated to have antibacterial activity against *S. aureus* and *Pseudomonas aeruginosa*. Further investigation revealed that its inhibitory effect on *S. aureus* might be related to an increase in toxic reactive oxygen species (Comini et al., 2011). This natural metabolite has also been demonstrated to have prominent antifungal activity against *Aspergillus ochraceus*, *Aspergillus niger* and *Candida lipolytica* (Ali et al., 2000). It also displayed anti-parasitic properties against *T. cruzi* amastigotes (Sandjo et al., 2016b). The antimycobacterial activity of damnacanthal (C22) is likely linked to its aldehyde functional group as compound C25 (rubiadin 1-methyl ether), its reduced form, showed no anti-*M. tuberculosis* activity.

TABLE 1 | Antimycobacterial and cytotoxic activities of hit compounds against *Mycobacterium tuberculosis*.

Compound	MIC (μg/mL)	IC_{50} (μg/mL)	Selectivity index
C1	51.77	45.85	0.89
C10	29.13	64.18	2.20
C13	105.6	95.94	0.91
C14	105.4	47.22	0.45
C15	>100	N/D	N/A
C22	13.07	21.41	1.64
C23	49.22	44.27	0.90
C24	>100	N/D	N/A
C36	>100	N/D	N/A
C38	>100	N/D	N/A
C40	>100	N/D	N/A
C41	>100	N/D	N/A
C45	>100	N/D	N/A
C49	>100	N/D	N/A
C51	70.69	170.5	2.41
C52	50.58	N/D*	N/A
C53	17.88	17.00	0.95

*Detailing MIC, IC_{50}, and selectivity index values. MIC, minimum inhibitory concentration against M. tuberculosis; IC_{50}, inhibitory concentration 50% for human monocyte THP-1 cells; N/D, not done; N/A, not applicable. *IC_{50} for C52 was not conducted due to compound degradation over time.*

The dimeric polyacetylene C53 (tetradeca-4,6,8,10-tetrayne-1,14-diol) was the second most active compound against *M. tuberculosis,* with a MIC of 17.88 μg/mL. Several naturally occurring polyacetylene alcohols with acyclic hydrocarbon backbones have been reported with moderate to significant antimycobacterial activity against *Mycobacterium fortuitum*, *Mycobacterium avium*, *Mycobacterium aurum,* and *M. tuberculosis* H37Ra (Kobaisy et al., 1997; Schinkovitz et al., 2008; Haoxin et al., 2012). These metabolites also showed a wide spectrum of antibacterial action against Gram positive bacteria (*S. aureus* and *B. subtilis*), Gram negative bacteria (*Escherichia coli* and *P. aeruginosa*), *Candida albicans*, *M. tuberculosis,* and isoniazid-resistant *M. avium* (Kobaisy et al., 1997; Christensen, 2011), supporting the antimicrobial activity presented here using a synthetic polyacetylene. Other synthetic polyacetylenes of the series tested (C51 and C52) were active against *M. tuberculosis* (**Figure 6**), while C54 and C55 were not. C52 was more active than C51, with MICs of 50.58 μg/mL and 70.69 μg/mL, respectively, and both compounds differ from each other by the hybridization of atoms in the C-O bond. C53, obtained from the homodimerization of C51, showed the highest anti-*M. tuberculosis* activity among the polyacetylenes, suggesting that the observed bioactivity might be promoted by the high conjugated π-electron system.

The natural product isobavachalcone (C1), isolated from *D. kameruniana*, was moderately inhibitory to *M. tuberculosis* with a MIC of 51.77 μg/mL (**Figure 6**). This compound has been previously determined to be active against *M. tuberculosis* (Chiang et al., 2010), verifying our library screen. Antibacterial activity against both Gram positive and Gram negative bacteria (Mbaveng et al., 2008) has also been observed, alongside antifungal activity, inhibiting *C. albicans* (ElSohly et al., 2001). Prenylated chalcones structurally close to isobavachalcone have also been identified as broad-spectrum antibacterial agents (Sugamoto et al., 2011). Isoneorautenol (C23), a natural secondary metabolite isolated from *E. senegalensis*, had a MIC of 49.22 μg/mL against *M. tuberculosis* (**Figure 6**), and has also been shown to inhibit growth of the fast-growing non-pathogenic *Mycobacterium smegmatis* and Gram negative bacteria (Mitscher et al., 1988; Mbaveng et al., 2015). Of note, the natural product 4-hydroxylonchocarpine (C21), a flavonoid class chalcone isolated from *D. mannii*, was not mycobactericidal despite previous reports of antibacterial activity (Kuete et al., 2013).

The synthetic chromene C10 showed good antimycobacterial activity with a MIC of 29.13 μg/mL against *M. tuberculosis* (**Figure 6**). This compound, prepared for a previous study, demonstrated anti-parasitic action against both *T. cruzi* and *L. amazonensis* (Martin et al., 2018). Chromene derivatives bearing trisubstituted amines were previously reported as antimycobacterial against *M. tuberculosis* H37Rv (Raj and Lee, 2020). C10, the most active compound among the pyranocoumarin derivatives, differs from the others with the substituent group on the aryl moiety and the ester function on the pyran ring. C16, different from C10 by the coumarin ring, was not active against *M. tuberculosis*. However, when the NO_2 group in C16 was replaced by the halogen atom (compound C14), a weak antimycobacterial activity was observed (**Figure 6**). C13 also contains a high conjugated π-electron system, although not as linear as in the C53 structure, which might support the weak activity of this compound against *M. tuberculosis* (**Figure 6**).

Compound Toxicity

Compounds that exhibited significant antimycobacterial activity were assessed for toxicity toward human monocytic (THP-1) cells *in vitro*, and the IC_{50} and selectivity index (SI) values were calculated for each compound. Compounds C1, C13, C14, C23, and C53 exhibited SI values lower than 1, while compounds C10, C22, and C51 exhibited SI values greater than 1, but limited to a maximum of 2.41 (**Table 1**). Therefore, efforts will be required to improve the selectivity of these compounds for mycobacteria.

Several of these compounds have been previously described to have moderate to low cytotoxicity to healthy cells. During evaluation of isobavachalcone (C1) on intracellular parasites, C1 showed some toxicity to THP-1 cells with a cytotoxic concentration 50% (CC_{50}) of 11.65 μg/mL. Compound C22 in the same study inhibited the growth of THP-1 cells with a CC_{50} of 8.87 μg/mL (Sandjo et al., 2016b). Compounds C13 and C14 were also identified to be moderately toxic to human monocyte cells alongside their intracellular antiprotozoal activity (Martin et al., 2018), correlating with our findings here. Isoneorautenol (C23) was reported as antiproliferative without showing cytotoxicity to AML12 hepatocytes at concentrations up to 123.46 μM (Kuete et al., 2014; Kuete et al., 2015b). No cytotoxicity studies have been performed on the polyacetylenes (C51–C53). The intermediate MIC values for these compounds against *M. tuberculosis* (as shown in this study) are close to the IC_{50} values, resulting in greater potential for cytotoxicity. The reduction of this toxicity should be a priority for further compound development.

CONCLUSION

New drugs are required to treat drug-resistant TB and the rising threat of antimicrobial drug resistance (AMR). Natural products, and synthetic compounds derived and inspired by natural products, offer an extensive diversity of bioactive chemical structures for drug discovery. Natural product screens offer the opportunity to identify new chemical entities, with likely novel modes of action to overcome existing bacterial drug resistance mechanisms. Here, we report the anti-TB activity of 52 natural and synthetic compounds selected to have different hydrocarbon scaffolds and reported antimicrobial or antiparasitic activities. We identify two compounds (C22 damnacanthal, and the dimeric polyacetylene C53) with MIC values <20 μg/mL against *M. tuberculosis*, and five with MIC values between 25 and 71 μg/mL. The synthetic chromene C10 and polyacetylene C51 with moderate antimycobacterial activity displayed low toxicity compared to the other active compounds. This study suggests that the anthraquinone damnacanthal (C22) and synthetic polyacetylenes (C53, C52, and C51) deserve further chemical investigation as novel antimycobacterial scaffolds, and biological experimentation to elucidate mechanism of action in the search for new antimicrobial drugs.

DATA AVAILABILITY STATEMENT

The original contributions presented in the study are included in the article/**Supplementary Material**, further inquiries can be directed to the corresponding author/s.

AUTHOR CONTRIBUTIONS

LP, EM, VM, MLB, MWB, and LS conducted the compound isolation, synthesis, and characterization. DC, LW, and SW conducted the antimicrobial activity and cytotoxicity work. DC, LW, SW, and LS wrote the manuscript. All authors contributed to the design of the experiments and reviewed the manuscript.

FUNDING

Brazilian authors would like to thank CNPq and CAPES for their financial support through the post-graduation program. SW, LW, and DC acknowledge funding from the Wellcome Trust Institutional Strategic Support Fund (204833/Z/16/A) and (204538/Z/16/Z), and the University of Brighton Santander Travel Award.

SUPPLEMENTARY MATERIAL

The Supplementary Material for this article can be found online at: https://www.frontiersin.org/articles/10.3389/fmicb.2020.622629/full#supplementary-material

Supplementary Figure 1 | Dose response curves of *M. tuberculosis* treated with isoniazid or linezolid. *M. tuberculosis* was treated for 7 days with drug concentrations ranging from 200 μg/mL to 0.09 μg/mL, in three-fold serial dilutions. Bacterial survival was measured after overnight incubation with CellTiter-Blue to establish minimum inhibitory concentrations (MICs). Data points are expressed as mean % survival relative to drug-free controls from duplicate biological replicates. Error bars represent the standard deviation.

REFERENCES

Abegaz, B. M., Ngadjui, B. T., Dongo, E., and Tamboue, H. (1998). Prenylated chalcones and flavones from the leaves of *Dorstenia kameruniana*. *Phytochemistry* 49, 1147–1150. doi: 10.1016/S0031-9422(98)00061-2

Adem, F. A., Kuete, V., Mbaveng, A. T., Heydenreich, M., Ndakala, A., Inguru, B., et al. (2018). Cytotoxic benzylbenzofuran derivatives from *Dorstenia kameruniana*. *Fitoterapia* 128, 26–30. doi: 10.1016/j.fitote.2018.04.019

Ali, A. M., Ismail, N. H., Mackeen, M. M., Yazan, L. S., Mohamed, S. M., Ho, A. S. H., et al. (2000). Antiviral, cytotoxic and antimicrobial activities of anthraquinones isolated from the roots of *Morinda elliptica*. *Pharm Biol.* 38, 298–301. doi: 10.1076/1388-0209(200009)3841-AFT298

Bieski, I. G. C., Santos, F. R., Oliveira, R. M., Espinosa, M. M., Macedo, M., Albuquerque, U. P., et al. (2012). Ethnopharmacology of medicinal plants of the pantanal region (Mato Grosso, Brazil). *Evid. Based Comp. Altern. Med.* 2012, 1–36. doi: 10.1155/2012/272749

Campbell, I. B., Macdonald, S. J. F., and Procopiou, P. A. (2018). Medicinal chemistry in drug discovery in big pharma: past, present and future. *Drug Discov. Today* 23, 219–234. doi: 10.1016/j.drudis.2017.10.007

Chiang, C. C., Cheng, M. J., Peng, C. F., Huang, H. Y., and Chen, I. S. (2010). A novel dimeric coumarin analog and antimycobacterial constituents from *Fatoua pilosa*. *Chem. Biodiversity.* 7, 1728–1736. doi: 10.1002/cbdv.200900326

Christensen, L. P. (2011). Aliphatic C17-polyacetylenes of the falcarinol type as potential health promoting compounds in food plants of the Apiaceae family. *Recent Pat. Food Nutr. Agric.* 3, 64–77. doi: 10.2174/2212798411103010064

Comini, L. R., Montoya, S. C. N., Páez, P. L., Argüello, G. A., Albesa, I., and Cabrera, J. L. (2011). Antibacterial activity of anthraquinone derivatives from *Heterophyllaea pustulata* (Rubiaceae). *J. PhotochemPhotobiol. B* 102, 108–114. doi: 10.1016/j.jphotobiol.2010.09.009

De Smet, P. A. (1997). Role of plant-derived drugs and herbal medicines in healthcare. *Drugs* 54, 801–840. doi: 10.2165/00003495-199754060-00003

ElSohly, H. N., Joshi, A. S., Nimrod, A. C., Walker, L. A., and Clark, A. M. (2001). Antifungal chalcones from *Maclura tinctoria*. *Planta Med.* 67, 87–89. doi: 10.1055/s-2001-10621

Franzblau, S. G., Witzig, R. S., McLaughlin, J. C., Torres, P., Madico, G., Hernandez, A., et al. (1998). Rapid, low-technology MIC determination with clinical *Mycobacterium tuberculosis* isolates by using the microplate Alamar Blue assay. *J. Clin. Microbiol.* 36, 362–366. doi: 10.1128/JCM.36.2.362-366.1998

Haoxin, L., O'Neill, T., Webster, D., Johnson, J. A., and Gray, C. A. (2012). Antimycobacterial diynes from the Canadian medicinal plant *Aralia nudicaulis*. *J. Ethnopharmacol.* 140, 141–144. doi: 10.1016/j.jep.2011.12.048

Kobaisy, M., Abramowski, Z., Lermer, L., Saxena, G., Hancock, R. E. W., and Towers, G. H. N. (1997). Antimycobacterial polyynes of Devil's Club (*Oplopanax horridus*), a North American native medicinal plant. *J. Nat. Prod.* 60, 1210–1213. doi: 10.1021/np970182j

Koné, W. M., Antindehou, K. K., Terreaux, C., Hostettmann, K., Traoré, D., and Dosso, M. (2004). Traditional medicine in North Cote-d'Ivoire: screening of 50 medicinal plants for antibacterial activity. *J. Ethnopharmacol.* 93, 43–49. doi: 10.1016/j.jep.2004.03.006

Kuete, V., Donfack, A. R. N., Mbaveng, A. T., Zeino, M., Tane, P., and Efferth, T. (2015a). Cytotoxicity of anthraquinones from the roots of *Pentas schimperi* towards multi-factorial drug-resistant cancer cells. *Invest. New Drugs* 33, 861–869. doi: 10.1007/s10637-015-0268-9

Kuete, V., Mbaveng, A. T., Zeino, M., Fozing, C. D., Ngameni, B., Kapche, G. D., et al. (2015b). Cytotoxicity of three naturally occurring flavonoid derived compounds (artocarpesin, cycloartocarpesin and isobavachalcone) towards multi-factorial drug-resistant cancer cells. *Phytomedicine* 22, 1096–1102. doi: 10.1016/j.phymed.2015.07.006

Kuete, V., Noumedem, J. A., and Nana, F. (2013). Chemistry and pharmacology of 4-hydroxylonchocarpin: a review. *Chin. J. Integr. Med.* 19, 475–480. doi: 10.1007/s11655-013-1195-7

Kuete, V., Sandjo, L. P., Kwamou, G. M., Wiench, B., Nkengfack, A. E., and Efferth, T. (2014). Activity of three cytotoxic isoflavonoids from *Erythrina excelsa* and *Erythrina senegalensis* (neobavaisoflavone, sigmoidin H and isoneorautenol) toward multi-factorial drug resistant cancer cells. *Phytomedicine* 21, 682–688. doi: 10.1016/j.phymed.2013.10.017

Kumar, G., Krishna, V. S., Sriram, D., and Jachak, S. M. (2020). Pyrazole–coumarin and pyrazole–quinoline chalcones as potential antitubercular agents. *Arch. Pharm.* 353, 1–14. doi: 10.1002/ardp.202000077

Lautié, E., Russo, O., Ducrot, P., and Boutin, J. A. (2020). Unraveling plant natural chemical diversity for drug discovery purposes. *Front. Pharmacol.* 11:397. doi: 10.3389/fphar.2020.00397

Lombardino, J. G., and Lowe, J. A. III (2004). The role of the medicinal chemist in drug discovery – then and now. *Nat. Rev. Drug Discov.* 3, 853–862. doi: 10.1038/nrd1523

Machado, V. R., Biavatti, M. W., and Danheiser, R. L. (2018). A short and efficient synthesis of the polyacetylene natural product deca-4,6,8-triyn-1-ol. *Tetrahedron Lett.* 59, 3405–3408. doi: 10.1016/j.tetlet.2018.07.059

Martin, E. F., Mbaveng, A. T., Moraes, M. H., Kuete, V., Biavatti, M. W., Steindel, M., et al. (2018). Prospecting for cytotoxic and antiprotozoal 4−aryl−4H−chromenes and 10−aryldihydropyrano[2,3−f] chromenes. *Arch. Pharm. (Weinheim)* 351, 1–11. doi: 10.1002/ardp.201800100

Mbaveng, A. T., Kuete, V., Ngameni, B., Beng, V. P., Ngadjui, B. T., Meyer, J. J. M., et al. (2012). Antimicrobial activities of the methanol extract and compounds from the twigs of *Dorstenia mannii* (Moraceae). *BMC Comp. Altern. Med.* 12:83. doi: 10.1186/1472-6882-12-83

Mbaveng, A. T., Ngameni, B., Kuete, V., Simo, I. K., Ambassa, P., Roy, R., et al. (2008). Antimicrobial activity of the crude extracts and five flavonoids from the twigs of *Dorstenia barteri* (Moraceae). *J. Ethnopharmacol.* 116, 483–489. doi: 10.1016/j.jep.2007.12.017

Mbaveng, A. T., Sandjo, L. P., Tankeo, S. B., Ndifor, A. R., Pantaleon, A., Nagdjui, B. T., et al. (2015). Antibacterial activity of nineteen selected natural products against multi-drug resistant Gram-negative phenotypes. *SpringerPlus.* 4, 823–831. doi: 10.1186/s40064-015-1645-8

Mitscher, L. A., Okwute, S. K., Gollapudi, S. R., Drake, S., and Avona, E. (1988). Antimicrobial pterocarpans of Nigerian *Erythrina mildbraedii*. *Phytochemistry* 27, 3449–3452. doi: 10.1016/0031-9422(88)80746-5

The Working Group for New TB Drugs (2020). *New Drugs for TB Clinical Pipeline*. Available online at: https://www.newtbdrugs.org/pipeline/clinical (accessed October 19, 2020).

Ngadjui, B. T., Abegaz, B. M., Dongo, E., Tamboue, H., and Fogue, S. K. (1998). Geranylated and prenylated flavonoids from the twigs of *Dorstenia mannii*. *Phytochemistry* 48, 349–354. doi: 10.1016/S0031-9422(97)01120-5

Pascolutti, M., and Quinn, R. J. (2014). Natural products as lead structures: chemical transformations to create lead-like libraries. *Drug Discov. Today* 19, 215–221. doi: 10.1016/j.drudis.2013.10.013

Pollo, L. A. E., Moraes, M. H., Cisilotto, J., Creczynski-Pasa, T. B., Biavatti, M. W., Steindel, M., et al. (2017). Synthesis and *in vitro* evaluation of Ca2+ channel blockers 1,4-dihydropyridines analogues against *Trypanosoma cruzi* and *Leishmania amazonensis*: SAR analysis. *Parasitol. Int.* 66, 789–797. doi: 10.1016/j.parint.2017.08.005

Raj, L., and Lee, J. (2020). 2H/4H-Chromenes – A versatile biological attractive scaffold. *Front. Chem.* 8:623. doi: 10.3389/fchem.2020.00623

Rogoza, L. N., Salakhutdinov, N. F., and Tolstikov, G. A. (2010). Antituberculosis activity of natural and synthetic compounds. *Chem. Sustain. Dev.* 10, 343–375.

Salomon, C. E., and Schmidt, L. E. (2012). Natural products as leads for tuberculosis drug development. *Curr. Top. Med. Chem.* 12, 735–765. doi: 10.2174/156802612799984526

Sandjo, L. P., Kuete, V., Nana, F., Kirsch, G., and Efferth, T. (2016a). Synthesis and cytotoxicity of 1,4-Dihydropyridines and an unexpected 1,3-Oxazin-6-one. *HelvChim. Acta* 99, 310–314. doi: 10.1002/hlca.201500265

Sandjo, L. P., Moraes, M. H., Kuete, V., Kamdoum, B. C., Ngadjui, B. T., and Steindel, M. (2016b). Individual and combined antiparasitic effect of six plant metabolites against *Leishmania amazonensis* and *Trypanosoma cruzi*. *Bioorg. Med. Chem. Lett.* 26, 1772–1775. doi: 10.1016/j.bmcl.2016.02.044

Schinkovitz, A., Stavri, M., Gibbons, S., and Bucar, F. (2008). Antimycobacterial polyacetylenes from *Levisticum officinale*. *Phytother. Res.* 22, 681–684. doi: 10.1002/ptr.2408

Solecki, E., and Shanidar, I. V. (1975). A Neanderthal flower burial in northern Iraq. *Science* 190, 880–881. doi: 10.1126/science.190.4217.880

Somagond, S. M., Kamble, R. R., Bayannavar, P. K., Shaikh, S. K. J., Joshi, S. D., Kumbar, V. M., et al. (2019). Click chemistry based regioselective one-pot synthesis of coumarin-3-yl-methyl-1,2,3-triazolyl-1,2,4-triazol-3(4*H*)-ones as newer potent antitubercular agents. *Arch. Pharm. (Weinheim)* 352, 1–13. doi: 10.1002/ardp.201900013

Sugamoto, K., Matsusita, Y. I., Matsui, K., Kurogi, C., and Matsui, T. (2011). Synthesis and antibacterial activity of chalcones bearing prenyl or geranyl groups from *Angelica keiskei*. *Tetrahedron.* 67, 5346–5359. doi: 10.1016/j.tet.2011.04.104

Teklehaymanot, T. (2009). Ethnobotanical study of knowledge and medicinal plants use by the people in Dek Island in Ethiopia. *J. Ethnopharmacol.* 124, 69–78. doi: 10.1016/j.jep.2009.04.005

Thomford, N. E., Senthebane, D. A., Rowe, A., Munro, D., Seele, P., Maroyi, A., et al. (2018). Natural products for drug discovery in the 21st century: innovations for novel drug discovery. *Int. J. Mol. Sci.* 19, 1578–1606. doi: 10.3390/ijms19061578

Togola, A., Austarheim, I., Theis, A., Diallo, D., and Paulse, B. S. (2008). Ethnopharmacological uses of *Erythrina senegalensis*: a comparison of three areas in Mali, and a link between traditional knowledge and modern biological science. *J. Ethobiol. Ethnomed.* 4, 6–14. doi: 10.1186/1746-4269-4-6

World Health Organization (2014). *End TB Strategy*. Geneva: WHO.

World Health Organization (2020). *Global Tuberculosis Report 2020*. Geneva: WHO.

Wright, G. D. (2019). Unlocking the potential of natural products in drug discovery. *Microb. Biotechnol.* 12, 55–57. doi: 10.1111/1751-7915.13351

Conflict of Interest: The authors declare that the research was conducted in the absence of any commercial or financial relationships that could be construed as a potential conflict of interest.

frontiers in Microbiology

ORIGINAL RESEARCH
published: 18 January 2021
doi: 10.3389/fmicb.2020.618278

Unbiased Identification of Angiogenin as an Endogenous Antimicrobial Protein With Activity Against Virulent *Mycobacterium tuberculosis*

*Reiner Noschka[1], Fabian Gerbl[1], Florian Löffler[1], Jan Kubis[1], Armando A. Rodríguez[2,3], Daniel Mayer[1], Mark Grieshober[1], Armin Holch[1], Martina Raasholm[4], Wolf-Georg Forssmann[5], Barbara Spellerberg[1], Sebastian Wiese[2], Gilbert Weidinger[4], Ludger Ständker[3] and Steffen Stenger[1]**

[1]*Institute of Medical Microbiology and Hygiene, University Hospital Ulm, Ulm, Germany,* [2]*Core Unit Mass Spectrometry and Proteomics, Ulm University, Ulm, Germany,* [3]*Core Facility of Functional Peptidomics, Ulm University, Ulm, Germany,* [4]*Institute of Biochemistry and Molecular Biology, Ulm University, Ulm, Germany,* [5]*Pharis Biotec GmbH, Hannover, Germany*

OPEN ACCESS

Edited by:
Maria Rosalia Pasca, University of Pavia, Italy

Reviewed by:
Divakar Sharma, Indian Institute of Technology Delhi, India
Shashank Gupta, National Institutes of Health, United States

***Correspondence:**
Steffen Stenger
steffen.stenger@uniklinik-ulm.de

Specialty section:
This article was submitted to Antimicrobials, Resistance and Chemotherapy, a section of the journal Frontiers in Microbiology

Received: *16 October 2020*
Accepted: *23 December 2020*
Published: *18 January 2021*

Citation:
Noschka R, Gerbl F, Löffler F, Kubis J, Rodríguez AA, Mayer D, Grieshober M, Holch A, Raasholm M, Forssmann W-G, Spellerberg B, Wiese S, Weidinger G, Ständker L and Stenger S (2021) Unbiased Identification of Angiogenin as an Endogenous Antimicrobial Protein With Activity Against Virulent Mycobacterium tuberculosis. Front. Microbiol. 11:618278. doi: 10.3389/fmicb.2020.618278

Tuberculosis is a highly prevalent infectious disease with more than 1.5 million fatalities each year. Antibiotic treatment is available, but intolerable side effects and an increasing rate of drug-resistant strains of *Mycobacterium tuberculosis* (*Mtb*) may hamper successful outcomes. Antimicrobial peptides (AMPs) offer an alternative strategy for treatment of infectious diseases in which conventional antibiotic treatment fails. Human serum is a rich resource for endogenous AMPs. Therefore, we screened a library generated from hemofiltrate for activity against *Mtb*. Taking this unbiased approach, we identified Angiogenin as the single compound in an active fraction. The antimicrobial activity of endogenous Angiogenin against extracellular *Mtb* could be reproduced by synthetic Angiogenin. Using computational analysis, we identified the hypothetical active site and optimized the lytic activity by amino acid exchanges. The resulting peptide-Angie1-limited the growth of extra- and intracellular *Mtb* and the fast-growing pathogens *Escherichia coli*, *Pseudomonas aeruginosa*, and *Klebsiella pneumoniae*. Toward our long-term goal of evaluating Angie1 for therapeutic efficacy *in vivo*, we demonstrate that the peptide can be efficiently delivered into human macrophages *via* liposomes and is not toxic for zebrafish embryos. Taken together, we define Angiogenin as a novel endogenous AMP and derive the small, bioactive fragment Angie1, which is ready to be tested for therapeutic activity in animal models of tuberculosis and infections with fast-growing bacterial pathogens.

Keywords: antimicrobial peptide, *Mycobacterium tuberculosis*, endogenous protein, antibacterial, human

INTRODUCTION

Tuberculosis is among the top 10 causes of death and the leading cause from a single infectious agent (World Health Organization, 2019). Even though tuberculosis is a treatable and curable disease, conventional antibiotic therapy may fail. Major obstacles in the treatment are non-adherence of patients to the 6-months therapy, intolerable side effects, and the

emergence of drug resistant strains of *Mycobacterium tuberculosis* (*Mtb*). WHO estimates that approximately 350 new cases of multidrug-resistant tuberculosis (MDR-TB) occur each year and declared MDR-TB as a public health crisis, which requires global attention by health care authorities. Second-line drugs are available for the treatment of MDR-TB but they are expensive, toxic, and require at least 12 months of therapy with cure rates below 60% (World Health Organization, 2019). Therefore, new therapeutic strategies are desperately needed. Ideally, new compounds would attack the bacteria by mechanisms distinct from conventional antituberculotic drugs, which mostly act by inhibiting bacterial RNA or protein synthesis. An attractive approach is the development of antimicrobial peptides (AMP), which are small peptidic compounds (<10 kDa) that are highly diverse in length, sequence, structure, and activity (Wang, 2014). AMPs are widespread in nature and are also part of the human innate immune system. Endogenous AMPs with activity against virulent *Mtb*, include Granulysin, Cathelicidin (LL-37), ß-Defensins, Cecropin, Lipocalin 2, or Teixobactin (Gutsmann, 2016). Studies on the mechanisms of action of these AMPs are limited since *Mtb* has a notoriously low metabolism, long generation time and is a biosafety level 3 pathogen. Imaging of AMP-treated *Mtb* indicates that Granulysin and LL-37 disrupt the mycobacterial cell wall (Stenger et al., 1998; Deshpande et al., 2020). It is unclear whether this is the lethal hit or only the initial step to allow the entry into the bacterial cytosol to reach its final intracellular target. The advantages of endogenous AMPs for the treatment of infectious diseases include the easy synthesis and the limited propensity to induce toxicity, allergic reactions, or drug resistance (Gutsmann, 2016). Recently, we developed a standardized protocol to generate libraries of highly concentrated endogenous peptides from human bodily fluids (Schulz-Knappe et al., 1997; Bosso et al., 2018). Starting from thousands of liters of hemofiltrate, a waste product of hemodialysis of patients with renal failure, a peptide library was generated. Peptides were separated into 300–500 pools based on charge (cation-exchange separation) and hydrophobicity (reversed-phase liquid chromatography). This hemofiltrate peptide library is a salt free source of highly concentrated peptides and small proteins (<30 kDa), which can be exploited for the unbiased search for antimicrobial peptides (Bosso et al., 2018). Here, we screened the pools of the peptide library for activity against virulent *Mtb*. We identified the 14.1 kDa protein Angiogenin, which activates several signaling transduction pathways in eukaryotic cells thereby affecting physiological and pathological processes (Sheng and Xu, 2016). We chemically modified Angiogenin for size, solubility, and activity, yielding "Angie1." Angie1 is not only active against extracellular *Mtb*, but importantly also enters macrophages, the major host cell of mycobacteria, where it limits mycobacterial proliferation.

Abbreviations: AMP, Antimicrobial peptide; BSA, Bovine serum albumin; CFU, Colony forming units; GM-CSF, Granulocyte-macrophage colony-stimulating factor; MOI, Multiplicity of infection; *Mtb*, *Mycobacterium tuberculosis*; PBMC, Peripheral blood mononuclear cell; PFA, Paraformaldehyde; TFA, Trifluoroacetic acid.

MATERIALS AND METHODS

Generation of a Hemofiltrate Peptide Library and Further Purification of the Active Molecule

A peptide bank (HF040823) prepared from 10 L hemofiltrate was generated by combining stepwise pH (from 3.6 to 9) elution in cation-exchange chromatography with reversed-phase chromatographic fractionation of every pH pool as described (Schulz-Knappe et al., 1997). Further bioassay-guided purification was performed by reversed-phase liquid chromatography on Source 15 (GE Healthcare, Buckinghamshire, United Kingdom) and Aqua C18 (Phenomenex, Aschaffenburg, Germany) columns. Aliquots of these peptide bank fractions were lyophilized and used for testing the antimicrobial activity against extracellular *M. tuberculosis* as mentioned below.

Mass Spectrometry Identification of the Active Molecule

Intact mass measurement was performed on a REFLEX III MALDI-TOF mass spectrometer (Bruker-Daltonics, Billerica, MA, United States) in linear mode (Rodríguez et al., 2018). Sequencing of proteolytic fragments was performed as previously described (Groß et al., 2020). Briefly, reduction with DTT (5 mM), carbamidomethylation with iodoacetamide (50 mM) and trypsin-digestion were performed prior to analysis on an Orbitrap Elite™ Hybrid Ion Trap-Orbitrap Mass Spectrometer coupled to an U3000 RSLCnano uHPLC (Thermo Fisher Scientific, Waltham, MA, United States). Databases were searched using PEAKs X+ studio (Zhang et al., 2012). For peptide identification, MS spectra were correlated with the UniProt human reference proteome set. Theoretical average molecular masses were calculated with ProtParam.

Identification of Antimicrobial Regions in Angiogenin

Antimicrobial regions of Angiogenin were predicted by an automated web server (AMPA; Torrent et al., 2012) followed by determination of antimicrobial sequences using the database CAMPR3 (Waghu et al., 2016).

Synthesis of Angiogenin and Angie1

Angiogenin, Angie1, and Atto647N-labeled Angie1-Atto647N were obtained from PSL Heidelberg (PSL, Heidelberg, Germany) using F-moc chemistry. For selected experiments Angie1 was synthesized on site (CFP, Ulm, Germany) on a Liberty blue peptide synthesizer (CEM, Kamp-Lintfort, Germany). All peptides were purified to >95% homogeneity by reversed-phase HPLC and diluted in aqua ad iniectabilia (Ampuwa, Fresenius Kabi) prior to use. Composition of peptides was confirmed by amino acid analysis and mass spectrometry as described (Ständker et al., 1998). Specifically, the absence of additional peptides in the Angie1 preparation was confirmed by reverse phase HPLC (**Supplementary Figure S1**).

Bacteria

Mycobacterium tuberculosis H37Rv (ATCC 27294) was grown in suspension with constant gentle rotation in roller bottles (Corning, Corning, NY, United States) containing Middlebrook 7H9 broth (BD Biosciences, Franklin Lakes, NK, United States) supplemented with 1% glycerol (Roth, Karlsruhe, Germany), 0.05% Tween 80 (Sigma-Aldrich, Steinheim, Germany), and 10% Middlebrook oleic acid, albumin, dextrose, and catalase enrichment (BD Biosciences, OADC). Aliquots from logarithmically growing cultures were frozen at −80°C in 7H9 broth with 20% glycerol, and representative vials were thawed and enumerated for viable colony forming units (CFU) on Middlebrook 7H11 plates (BD Biosciences). Staining of bacterial suspensions with fluorochromic substrates differentiating between live and dead bacteria (BacLight, Invitrogen, Carlsbad, CA, United States) revealed a viability of the bacteria >90%. Thawed aliquots were sonicated in a water bath for 10 min at 40 kHz and 110 W before use. *Pseudomonas aeruginosa* (ATCC 27853), Extended Spectrum Beta-Lactamase (ESBL) *Klebsiella pneumoniae* (ATCC 7000603), and *Escherichia coli* DH5α (Law and Kelly, 1995) were cultured in liquid THY broth (Oxoid, ThermoFisher Scientific, Schwerte, Germany) supplemented with 0.5% yeast extract (BD Biosciences) at 37°C overnight in a 5% CO_2 atmosphere.

Generation of Human Monocyte Derived Macrophages

Human peripheral blood mononuclear cells (PBMC) were isolated by density gradient centrifugation (Ficoll-Paque™ Plus; GE Healthcare) of buffy coat preparations from anonymous donors (Institute of Transfusion Medicine, Ulm University). Monocytes were isolated from PBMCs by adherence on tissue culture treated plastic flasks (Falcon, Corning, NY, United States). Monocyte-derived macrophages were generated by incubation with granulocyte-macrophage colony-stimulating factor (10 ng/ml; Miltenyi Biotec, Bergisch Gladbach, Germany) in Macrophage-Serum Free Medium (M-SFM; Gibco, ThermoFisher Scientific, Schwerte, Germany) for 6 days. Phenotypic characterization by flow cytometry demonstrated that macrophages expressed CD68 (anti–CD68-FITC, clone Y1/82A; BD Biosciences, Franklin Lakes, NJ, United States) and MHCII (anti–HLA-DR-PerCP, clone L243; BD Biosciences) as described (Bruns et al., 2012).

^{3}H-Uracil Proliferation Assay

As a correlate of mycobacterial metabolism, we measured the rate of RNA synthesis by determining the uptake of radioactively-labeled 5.6-^{3}H-Uracil (ART-0282, Biotrend, Cologne, Germany). About 2×10^6 sonicated *Mtb* were incubated with peptides in a 96-well plate in RPMI 1640 diluted 1:4 in distilled water and supplemented with 2 mM L-glutamine (PAN biotech, Aidenbach, Germany), 10 mM sodium bicarbonate ($NaHCO_3$, Roth), as previously described (Liu et al., 2006). The final volume was 100 µl and all samples were set up in triplicates. After 72 h, ^{3}H-Uracil (0.3 µCi/well) was added and cultures were incubated for additional 18 h. *Mtb* were inactivated by 4% PFA for 20 min, followed by a transfer onto glass fiber filters (Printed Filtermat A, PerkinElmer, Waltham, MA, United States) using a 96-well-cell harvester (Inotech, Nabburg, Germany). Fiber filters were sealed at 75°C with a wax plate containing the scintillation liquid (MeltiLex, Perkin Elmer). Incorporation of ^{3}H-Uracil by the bacilli was measured using a ß-counter (Sense Beta, Hidex, Turku, Finland). Antimicrobial activity (%) was calculated as follows: (cpm of the treated sample)/(cpm of the un-treated sample) × 100.

Activity of Angie1 Against Fast-Growing Bacteria

The activity of Angie1 against fast-growing bacteria was determined by radial diffusion assay. Overnight cultures of bacteria were suspended in 10 mM sodium phosphate buffer (Merck) and optical density was determined spectrophotometrically (UV-1800, Shimadzu Corporation) at 600 nm (OD_{600}). An OD_{600} value of 1.0 equals 8×10^8 cells/ml. After dilution, 2×10^7 bacteria were seeded into a petri dish in 1% agarose (Sigma-Aldrich) dissolved in 10 mM sodium phosphate buffer. Plates were cooled and cavities with a diameter of 2–3 mm were placed into the agar. Angie1 was diluted in 10 µl ddH_2O to its final concentration and added into the cavities. Following incubation at 37°C in ambient air for 3 h, plates were overlaid with 10 ml of a 1% agarose solution containing 3% Tryptone Soy broth (Oxoid) dissolved in 10 mM phosphate buffer. The diameters of the inhibition zones were determined following 16–18 h incubation at 37°C in a 5% CO_2 atmosphere.

Quantification of Intracellular Mycobacterial Growth

Macrophages were infected in six-well plates with single-cell suspensions of *Mtb* [multiplicity of infection (MOI) = 5] in macrophage-serum free medium. After 2 h, macrophages were washed thoroughly to remove extracellular *Mtb* and harvested using EDTA (1 mM). The rate of infection and cellular viability were determined using Auramine-Rhodamine (Merck) and Annexin V staining (BD, Franklin Lakes, NJ, United States) as previously described (Bruns et al., 2012). The rate of infected macrophages was donor-dependent and ranged between 25 and 40%. About 2×10^5 infected macrophages were seeded in 24-well plates and incubated with Angiogenin (10 µM; PSL, Heidelberg, Germany) or Angie1 (27, 54, and 108 µM; CFP, Ulm, Germany) for 4 days. To enumerate the number of viable bacilli, infected macrophages were lysed with 0.3% saponin (Sigma-Aldrich). Cell lysates were vigorously resuspended, transferred in screw cap tubes and sonicated for 10 min. Afterward, serial dilutions (1:10; 1:100; and 1:1000) of the sonicates were plated on 7H11 agar plates (BD) and incubated for 21 days before counting the CFU.

Toxicity of Peptides Against Macrophages

About 1×10^5 macrophages were incubated with peptides for 18 h in a 96-well plate, followed by addition of 10% PrestoBlue™ (Thermo Fisher) for 20 min. The non-fluorescent

resazurin-based PrestoBlue is reduced to fluorescent resorufin by mitochondrial enzymes of viable cells (Xu et al., 2015). The fluorescence intensity (FI) was measured at λ_{ex} 560 nm and λ_{em} 600 nm using Infinite 200 PRO (Tecan, Männedorf, Suisse) plate reader. Cell viability (%) was calculated using the following formula where the ratio of the FIs of the sample and the untreated control is calculated after subtracting the background FI introduced by the same volume of cell culture medium: [FI (sample)-FI (background)]/[FI (untreated control)-FI (background)] × 100.

Toxicity of Angie1 Against Zebrafish Embryos

Wild-type zebrafish embryos were dechorionated at 24 h post fertilization (hpf) using digestion with 1 mg/ml pronase (Sigma) in E3 medium (83 μM NaCl, 2.8 μM KCl, 5.5 μM $CaCl_2$, and 5.5 μM $MgSO_4$). Embryos were exposed for 24 h, in groups of three, to 100 μl of E3 medium containing Angie1 at 1, 10, and 100 μM. Each concentration was tested in two independent assays, each of which was performed on 10 × 3 embryos. The peptide solvent (PBS), diluted in E3, was used as negative control at the same amount as introduced by the highest peptide concentration. As positive control for acute toxicity/cytotoxicity the pleurocidin antimicrobial peptide NRC-03 (GRRKRKWLRRIGK-GVKIIGGAALDHL-NH2) was used at a concentration of 6 μM as described (Morash et al., 2011). Abamectin at a concentration of 3.125 μM was used as positive control for neurotoxicity (Raftery et al., 2014). At 48 hpf (after 24 h of incubation) embryos were scored in a stereomicroscope for signs of acute toxicity/cytotoxicity (lysis and/or necrosis), developmental toxicity (delay and/or malformations), or cardiotoxicity (heart edema and/or reduced or absent circulation). Each embryo was also touched with a needle and reduced or absent touch response (escape movements) was evaluated as signs of neurotoxicity if and only if no signs of acute toxicity were present in the same embryo. Embryos were categorized within each of these toxicity categories into several classes of severity according to the criteria listed in **Supplementary Figure S3A**. Chi-Square test was used to calculate whether the distribution of embryos into toxicity classes differed significantly between the PBS negative control and the test substances.

Half-Life of Angie1 in Human Serum

Human serum (14-490E, Lonza, Basel, Switzerland) was spiked with 10 μM Angie1 and incubated at 37°C for 2 h in triplicates. After 5, 10, 20, 30, 45, 60, 90, and 120 min; aliquots (5 μl) were diluted with 1.5 ml ice cold TFA (0.1%). Around 15 μl of each sample was analyzed using an Orbitrap Elite system (Thermo Fisher Scientific) as described above. XCalibur Qual Browser (Thermo Fisher Scientific) was used for visualization of the total ion chromatograms and spectra, as well as for signal area calculation. The theoretical spectrum of Angie1 and its degradation products were generated and the highest intensity signals were used as reference for detecting Angie1 and its degradation products. Plot graphs (signal area vs. time) and half-lives were calculated with GraphPad Prism 8.0 (GraphPad, La Jolla, CA, United States).

Generation of Angie1 and Angiogenin-Containing Liposomes

Liposomes were generated by lipid film hydration as described (Kallert et al., 2015). Briefly, dimethyldioctadecylammonium (DDA; 0.3 mg/ml; Avanti Polar Lipids), D-(+)-trehalose 6,6′-dibehenate (TDB; 0.25 mg/ml; Avanti Polar Lipids, Sigma Aldrich) and L-α-phosphatidylcholine (PC; 0.9 mg/ml; Avanti Polar Lipids) were mixed in chloroform (VWR): methanol (Sigma-Aldrich; 9:1, v/v). The organic solvents were evaporated under nitrogen flow. Liposomes were formed by hydrating the lipidfilm in 500 μl 10 mM Tris-buffer (pH 7.4; Sigma-Aldrich) for 25 min at 57°C within between vortexing, as previously described (Kennerknecht et al., 2020). Angie1 or Angiogenin were added in a 1:1 mixture to the liposomes at a final concentration of 2.7 mM. The size of liposomes was determined by Nanoparticle Tracking Analysis (NTA) using a ZetaView TWIN (Particle Metrix, Inning, Germany). Samples were diluted in TRIS-buffer and videos of the light-refracting particles were recorded with the following settings: 25°C fixed temperature, 11 positions, 1 cycle, sensitivity 85, shutter 100, 15 fps, 2 s videos/position, and six measurements. The number and size distribution were evaluated by ZetaView Analyze (Version 08.05.05 SP2), as previously described (Conzelmann et al., 2020).

Uptake of Angie1 by Macrophages: Flow Cytometry and Confocal Laser Microscopy

For investigation of Angie1 internalization, 1×10^6 macrophages were incubated with Angie1-Atto647N or Angie1-Atto647N Lip for 18 h. Samples were then analyzed using a FACS Calibur (BD Biosciences) with FlowJo v10.4.1 (BD). For confocal laser microscopy, 0.1×10^6 macrophages were seeded in 200 μl M-SFM in an eight-chamber slide (Thermo Fisher) and incubated with Angie1-Atto 647 N (54 μM) or Angie1-Atto 647 N Lip (54 μM) or Angiogenin-Atto647N Lip. After overnight incubation, cells were fixed (4% PFA, Sigma-Aldrich), followed by blocking in 2% BSA. Subsequently macrophages were labeled with major histocompatibility antigen class II antibodies (HLA-DR; 1:200, clone L243, Leinco, St. Louis, MS, United States) detected by Cy2-conjugated goat anti-mouse antibodies (1:200, Dianova, Hamburg, Germany). Cell nuclei were stained with DAPI (1:200, Sigma-Aldrich) diluted in 1% BSA and 0.1% Triton X-100 in PBS (all Sigma-Aldrich). Images were acquired using the inverted laser scanning confocal microscope LSM 710 (Zeiss, Oberkochen, Germany). Image processing was performed using ImageJ software (v 1.52c). All images displayed in this study are processed for brightness/contrast.

Statistical Analysis

All statistical analyses were performed using GraphPad Prism v8.2.1 (GraphPad Software). A difference in results giving a value of $p < 0.05$ was defined as significant.

Ethical Statement

Zebrafish embryos were used at stages up to 2 days post fertilization (dpf), which is before they start to feed at 6 dpf. Embryos that do not yet require feeding are not covered by EU and German animal experiment and welfare legislation (§14 TierSchVersV). Embryos were euthanized at the end of the test by rapid freezing, which is considered the most humane method for euthanasia for fish embryos. Adult fish housing and care were approved by the state of Baden-Württemberg and are monitored by Ulm University animal welfare executives and veterinaries of the city of Ulm.

RESULTS

In searching for endogenous AMPs with activity against virulent *Mtb* we screened a peptide library obtained from hemofiltrate as described (Schulz-Knappe et al., 1997). Extracellular bacilli were incubated with three dilutions (1:10, 1:100, and 1:1,000) of these fractions. As a correlate for mycobacterial viability, we measured the incorporation of ^{3}H-Uracil after 72 h of incubation. We tested eight pools (separated by charge), each containing 48 fractions (separated for hydrophobicity) from the original hemofiltrate library. Fractions yielding a dose-dependent antimicrobial activity >50%, that were reproducible in at least two experiments, were scored positive (**Figure 1A**, pool seven, fractions 16/17). After two additional rounds of sub-fractionation, we analyzed the most active fraction by mass spectrometry to identify the bioactive peptide(s). Mass spectrometry yielded three distinct peaks all unequivocally assigned to differently charged Angiogenin (mass 14,137 Da; **Figure 1B**) after MS/MS sequencing (**Figure 1C**). To validate the result of the screening, we tested the activity of recombinant Angiogenin against extracellular *Mtb* and found a dose dependent activity peaking at 100 µM (94 ± 2%; **Figure 2**).

Since Angiogenin is an endogenous peptide it should not be toxic for human cells. However, to exclude a diluent-mediated toxic effect, we incubated Angiogenin with primary human macrophages and determined cell viability after 18 h. Angiogenin at concentrations active against extracellular *Mtb* (10 µM) did not affect the viability of macrophages as determined by the ability to metabolize resazurin (**Figure 3A**). After the initial exponential multiplication in the pulmonary parenchyma, *Mtb* infects macrophages where the pathogen can multiply, persist, and cause chronic disease or latent infection. Effective drugs should therefore not only limit the

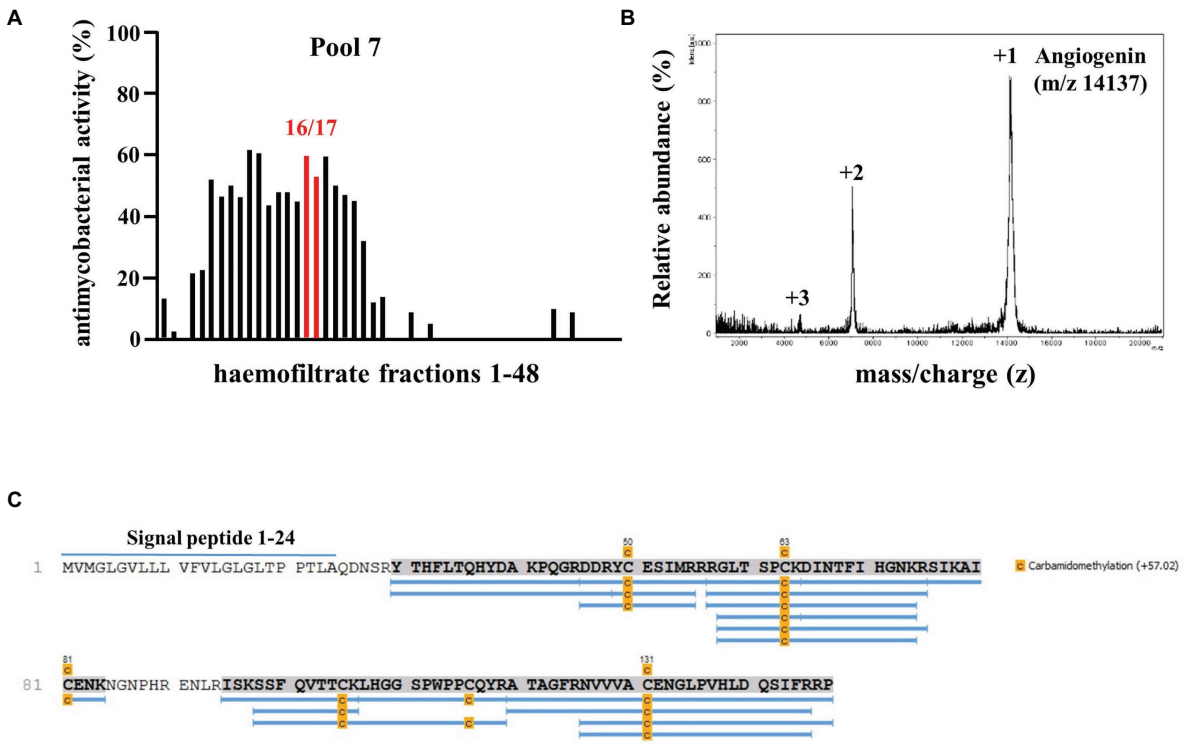

FIGURE 1 | Screening a hemofiltrate library for activity against extracellular *Mycobacterium tuberculosis* (*Mtb*). **(A)** Around 48 fractions (each 10 µl) of pool seven of the hemofiltrate library were incubated for 96 h with extracellular *Mtb*. ^{3}H-Uracil was added for the final 24 h of incubation. The uptake of ^{3}H-Uracil was measured by scintillation counting in a ß-counter. Antimicrobial activity was calculated by comparison to the untreated control. The bars present the average antimycobacterial activity (%) calculated from triplicates of a single experiment. **(B)** Subfractions 7–16/17 were analyzed *via* mass spectrometry. Spectrum analysis yielded three distinct peaks, identifying Angiogenin with a molecular mass of 14,137 Dalton. **(C)** Angiogenin sequence coverage (88%) by MS/MS analysis of the sample after carbamidomethylation and digestion with trypsin. Full sequence (Angiogenin precursor): signal peptide: 1–24 and Angiogenin 25–147.

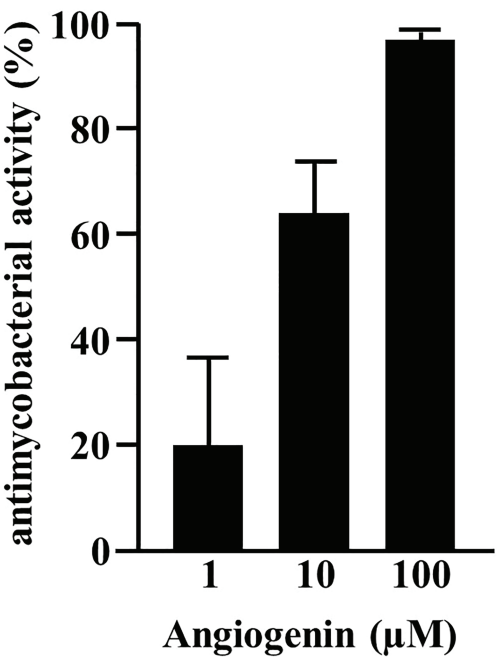

FIGURE 2 | Activity of synthetic Angiogenin against extracellular *Mtb*. About 2×10^6 extracellular *Mtb* were incubated for 96 h with synthetic Angiogenin (PSL Heidelberg). ^{3}H-Uracil was added for the final 24 h, of incubation and ^{3}H-Uracil uptake was measured by scintillation counting. Antimycobacterial activity was calculated as follows: [(counts/sample: count/untreated control) ×100]. Bars represent the mean antibacterial activity (%) ± SD calculated from triplicates of three independent experiments.

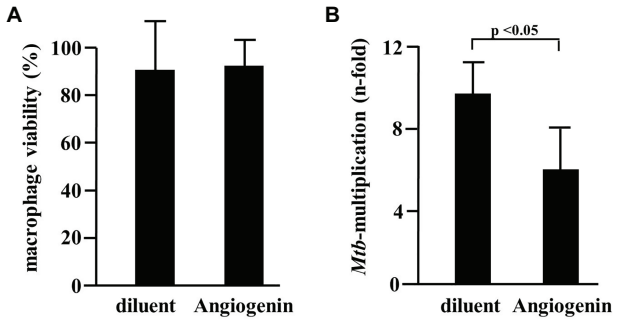

FIGURE 3 | Effect of Angiogenin on macrophage viability and *Mtb* multiplication. **(A)** Macrophages were incubated for 24 h with Angiogenin (10 μM, PSL Heidelberg) or diluent. Macrophage viability was quantified using a PrestoBlue™ assay and is given in % of the un-treated sample. Bars represent the mean viability of macrophages (%) ± SD calculated from triplicates of three independent experiments. **(B)** Macrophages were infected with *Mtb*, followed by incubation with Angiogenin (10 μM) for 4 days. Lysates were plated on 7H11 agar plates and the number of CFU counted after 21 days of incubation. *Mtb*-multiplication was calculated by comparison of the CFU determined at d4 and d0. The graph gives the mean values ± SD of n-fold mycobacterial growth as compared to d0 for six independent donors. Statistical analysis was performed using a paired *t*-test.

growth of extracellular *Mtb*, but also act on the intracellular pathogen. To test the ability of Angiogenin to limit the growth of intracellular *Mtb*, we infected primary human macrophages with virulent *Mtb* in the presence of the peptide or the diluent (water) only. Angiogenin (10 μM) significantly limited the multiplication of intracellular *Mtb* from 9.5 to 5.2-fold ($p < 0.05$; **Figure 3B**). These results demonstrate that screening of a hemofiltrate library is a successful strategy to identify novel AMPs. A major challenge for the clinical application of AMPs is the stability of the compound. One strategy to increase the stability is to identify active sequences within the peptide and generate smaller compounds, while maintaining bioactivity. *In silico* databank analysis predicted that amino acids 64–80 of Angiogenin are responsible for the antimicrobial effect (**Figure 4A**). Since positively charged peptides presumably interact more effectively with the negatively charged mycobacterial cell wall (Gutsmann, 2016), aspartic acid was changed to alanine and arginine was changed to isoleucine to prevent interference of the positively charged arginine and lysine (**Figure 4B**). The novel peptide "Angie1" contains 16 amino acid residues, has a molecular weight of 1.86 kDa (**Figure 4C**) and a net charge of +3 and is soluble in water. The presence of degradation products is highly unlikely, since MS revealed distinct peaks depending on the charge. In addition, the experimental monoisotopic mass is 1867.104 Da and almost identical to the theoretical mass (1867.094 Da).

As predicted, the modified fragment Angie1 maintained the activity against extracellular *Mtb* to a similar extent as the parental Angiogenin (78% at 100 μM; **Figure 5**). Angie1 was not toxic for primary human macrophages at 27, 54, or 108 μM (**Figure 6A**) and showed moderate but reproducible activity against intracellular *Mtb*. The antimicrobial activity did not increase at higher concentrations (108 μM; **Figure 6B**).

One potential advantage of AMPs is the broad spectrum of bacteria on which they act, because they do not target specific metabolic or biochemical pathways like many conventional antibiotics. To determine whether Angie1 also acts on other bacterial species than *Mtb*, we evaluated the activity against three fast-growing bacteria (*E. coli*, *K. pneumoniae*, and *P. aeruginosa*), all of which are relevant pathogens especially in hospital-acquired infections. Angie1 inhibited the growth of all three species in a dose dependent manner at concentrations in the low micromolar range (**Figure 7**). Taken together our results demonstrate that Angie1 is a novel antimicrobial peptide with activity against extracellular and intracellular *Mtb* and a selection of Gram-negative rods.

This prompted us to take initial steps toward developing Angie1 as a therapeutic agent to be evaluated in experimental models of tuberculosis infection. Along these lines, we measured the half-life in human serum, designed Angie1 containing liposomes as delivery vehicles and evaluated toxicity in an *in vivo* model. The half-life of Angie1 in human serum was 3.058 min as determined by mass spectrometry using an Orbitrap Elite System (**Figure 8**).

One strategy to increase the stability of peptides *in vivo* is to deliver the compounds by liposomes, which gradually release the bioactive molecules. To evaluate whether this is an option for the delivery of Angie1, we labeled the peptide with the fluorescent dye Atto647N and incubated it with macrophages.

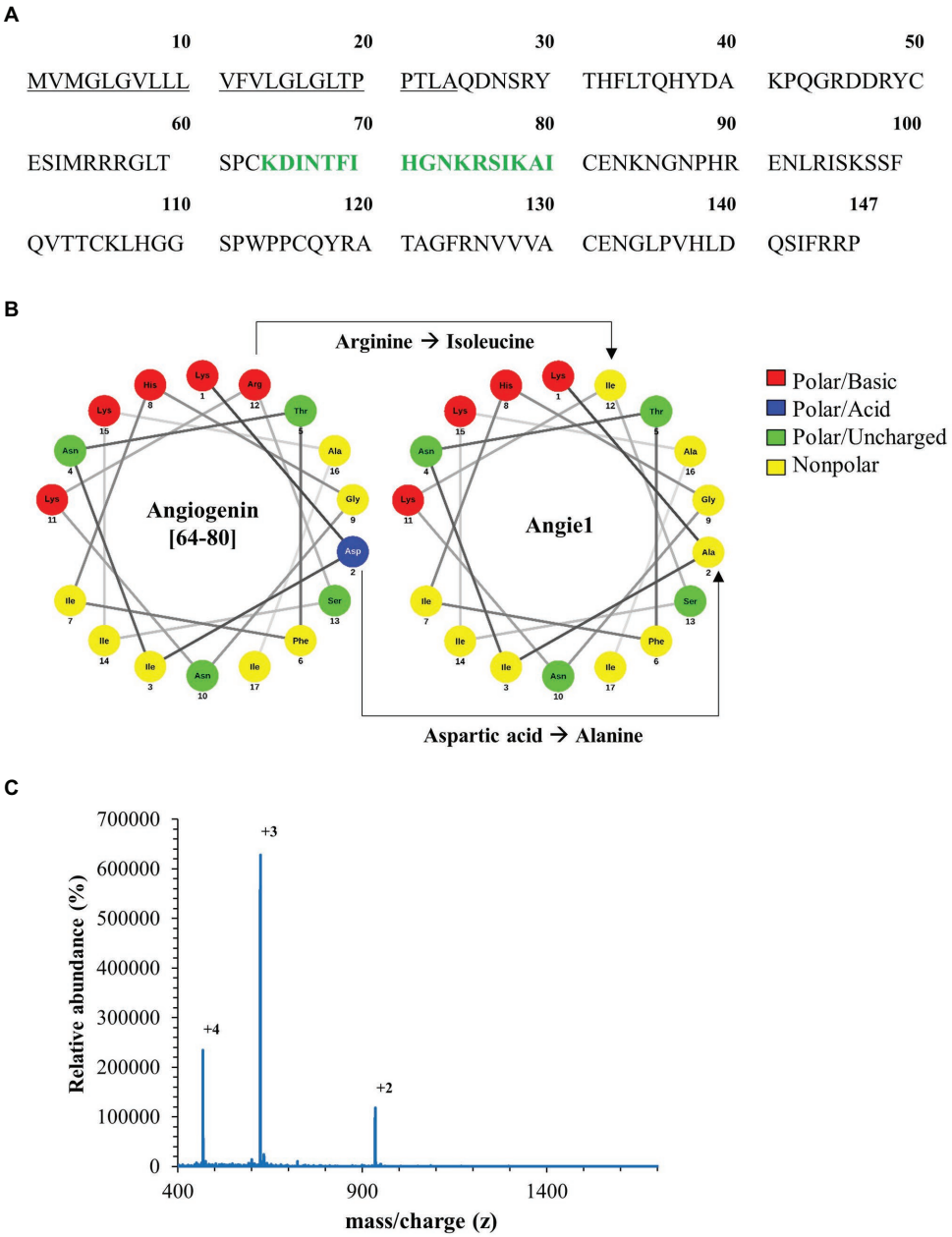

FIGURE 4 | *In silico* design of Angie1 from Angiogenin. **(A)** Sequence of Angiogenin precursor (1–24: signal peptide; 25–147: Angiogenin). The cytolytic active site was determined by AMPA (64–80aa) and is highlighted in green. **(B)** Helical wheel projection of the cytolytic region (left panel) demonstrating the polarity of the amino acids. The right projection shows the modifications of the cytolytic region yielding Angie1. **(C)** Mass spectrometry analysis of Angie1. Angie1 was analyzed by LC-ESI-MSMS (Orbitrap Elite system). The spectrum shows the $[M+2H]^{2+}$, $[M+3H]^{3+}$, and $[M+4H]^{4+}$ multicharged signals with the monoisotopic m/z value.

Uptake of labeled and unlabeled Angie1 was determined by flow cytometry and confocal laser microscopy. Angie1 was readily incorporated into liposomes and yielded particles with a size of 190 nm (**Supplementary Figure S2**, left panel). Uptake of Angie1 by macrophages was equally efficient when delivered alone or incorporated into liposomes (**Figures 9A–C**). The intracellular localization of Angie1 in MHC class II positive macrophages was confirmed by confocal laser microscopy (**Figure 9D**). This demonstrates that liposomes provide an appropriate delivery platform for Angie1 and may be useful for increasing the stability of the peptide *in vivo*. Incorporation of Angiogenin into liposomes (Angiogenin-Lip) yielded particles with a size of 180 nm (**Supplementary Figure S2**, left panel). However, the delivery of Angiogenin-Lip into macrophages was not feasible due to the toxicity of the compound as evidenced by loss of

adherence on plastic and nuclear condensation (**Supplementary Figure S4**).

Zebrafish embryos provide a useful *in vivo* model for evaluating toxicity. We developed an experimental model, in which zebrafish embryos are exposed to a compound for 24 h, starting at 24 hpf, when most organ systems have already developed and are functional. Transparency of the embryos than allows for evaluation not only of mortality, but also for sublethal toxicity causing necrosis or lysis (acute toxicity/cytotoxicity), heart edema or reduced / absent circulation (cardiotoxicity), developmental delay or malformations (developmental toxicity), or reduced/absent touch escape response (neurotoxicity) under a light microscope. A standardized scoring system (**Supplementary Figure S3A**) together with the possibility of investigating embryos on a large scale, yields statistically solid and reproducible results. Angie1 in concentrations that demonstrated antimicrobial activity (1, 10, and 100 μM) showed no toxicity (**Figure 10**; **Supplementary Figures S3B–D**).

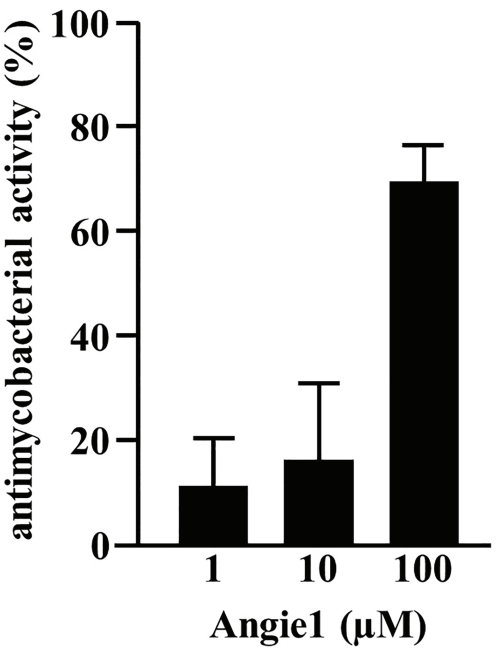

FIGURE 5 | Antimycobacterial activity of Angie1 against extracellular *Mtb*. About 2 × 10^6 extracellular *Mtb* were incubated for 96 h with Angie1 (CFP). Uptake of ^{3}H-Uracil was measured by scintillation counting. Antimicrobial activity was calculated by comparison of treated samples to untreated controls. Bars represent the mean antibacterial activity (%) ± SD calculated from triplicates of three independent experiments.

Taken together, our unbiased screen of a hemofiltrate peptide library identified a novel function of Angiogenin as an antimicrobial peptide with activity against *Mtb*. We designed a smaller derivative (Angie1), which maintains activity against *Mtb* can be efficiently delivered into human macrophages by liposomes and is not toxic for zebrafish embryos *in vivo*. Therefore, Angie1 is a novel AMP with favorable characteristics that is now ready to be tested for therapeutic efficacy in animal models of tuberculosis.

DISCUSSION

The application of antimicrobial peptides provides a novel concept for the treatment of infectious diseases, which fail to respond to conventional antibiotic treatment. By unbiased screening of a peptide library for activity against virulent *M. tuberculosis*, we identified Angiogenin as an antimicrobial compound in hemofiltrate. Activity against extracellular and intracellular *Mtb* was confirmed with synthesized Angiogenin. Using Angiogenin as a template, we generated a smaller peptide "Angie1" which could be delivered into *Mtb*-infected human macrophages by liposomes and limited the growth of the pathogen. These results highlight that (i) functional screening of human peptide libraries is a powerful approach to identify bioactive compounds, (ii) Angiogenin has antimicrobial activity, and (iii) *in silico* predictions can guide the optimization of lead components toward small, bioactive compounds with favorable toxicity and stability.

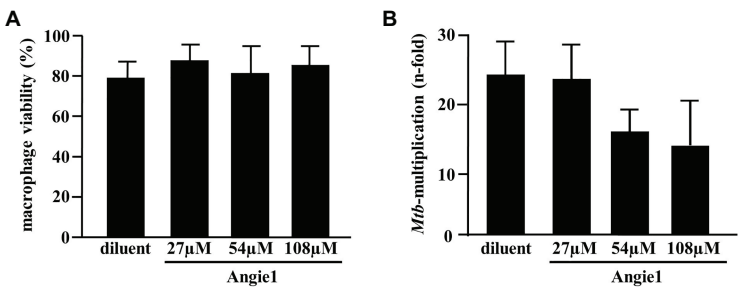

FIGURE 6 | Effect of Angie1 on macrophage viability and multiplication of intracellular *Mtb*. **(A)** Macrophages were incubated with Angie1 (PSL Heidelberg) at indicated concentrations for 24 h and viability was determined by the PrestoBlue™ assay. Bars represent the mean viability of macrophages (%) ± SD calculated from triplicates of three independent experiments. **(B)** Macrophages were infected with *Mtb* followed by incubation with Angie1 for 4 days. *Mtb*-multiplication was determined by plating cell lysates on 7H11 agar plates to determine and counting the number of CFU after 21 days of incubation. The graph gives the mean values ± SD of n-fold mycobacterial growth as compared to d0 for four independent donors.

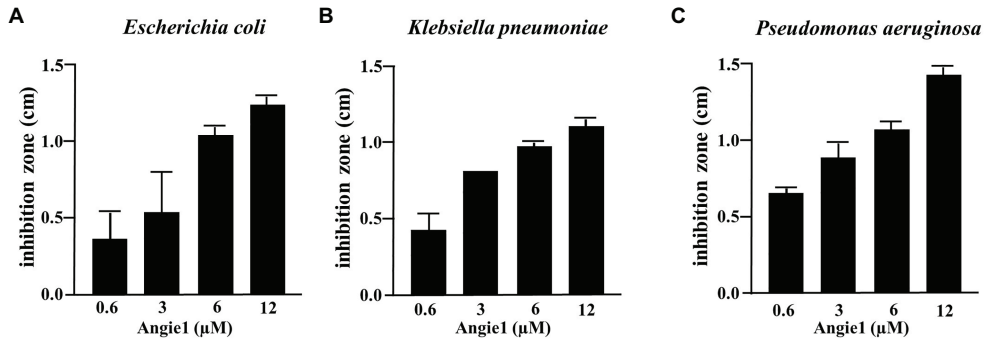

FIGURE 7 | Antimicrobial effect of Angie1 against fast-growing bacteria. About 2 × 10^7 bacteria were seeded into a petri dish containing agarose. Angie1 (Core Facility Peptidomics) was given into cavities in the agarose. After 3 h, plates were overlaid with agarose and after 18 h of incubation, inhibition zones were measured for **(A)** *Escherichia coli*, **(B)** *Klebsiella pneumoniae* and **(C)** *Pseudomonas aeruginosa*. Bars represent the mean values of inhibition zone size (cm) ± SD calculated from three independent experiments.

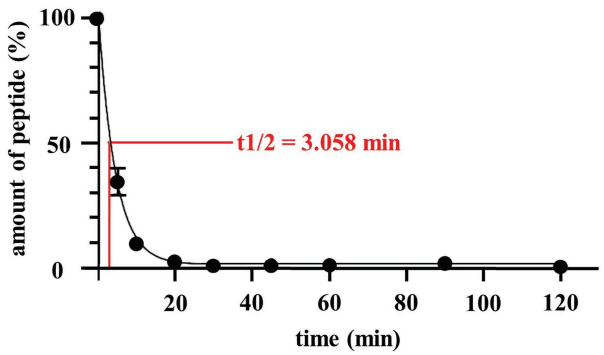

FIGURE 8 | Half-life of Angie1 in human serum. Human serum was spiked with Angie1 (10 µM) and aliquots of the samples were harvested at indicated time points. The amount of peptide was determined by mass spectrometry. The graph shows the amount of peptide (%) of the initial inoculum ± SD of three individual measurements.

Angiogenin, also known as ribonuclease (RNase) 5, was first described as a potent inducer of vasculogenesis (Fett et al., 1985; Strydom et al., 1985). The peptide consists of 123 amino acids resulting in a molecular weight of 14.4 kDa. Mice express four Angiogenin genes, whereas there is only one gene (ANG) in humans (Cho et al., 2005). Angiogenin is secreted by multiple cell types, including macrophages, epithelial cells, and mast cells (Rybak et al., 1987). Release is increased in neurodegenerative diseases, malignancies, and inflammation (Sheng and Xu, 2016). Only one report associated human Angiogenin with antimicrobial activity against microbes, specifically *Enterococcus faecalis*, *Listeria monocytogenes*, *Streptococcus pneumoniae*, and *Candida albicans* (Hooper et al., 2003). The specificity of this finding was challenged because bovine serum albumin in the absence of Angiogenin had very similar effects (Avdeeva et al., 2006). Both studies were performed with recombinant Angiogenin expressed in *E. coli*. Our results strongly favor a specific activity of Angiogenin against *Mtb* as it was unequivocally identified by an unbiased approach from a hemofiltrate library and the activity was confirmed by using highly purified Angiogenin generated by solid-phase synthesis. Our experimental approach was designed to identify AMPs with activity against the major human pathogen *Mtb*, because tuberculosis is notoriously difficult to treat and only few antituberculotic drugs are available. Whether synthetic Angiogenin is also active against other microbial pathogens such as extracellular bacteria or fungi remains to be determined.

The route of delivery for AMPs to the site of infection remains a key challenge. Oral application is hampered by the catalytic cleavage in the acidic environment of the stomach. Intravenous infusion will expose the peptide to an unfavorable environment in the serum with high concentrations of salt and digestive enzymes. In addition, the synthesis of sufficient quantities of peptide required for *in vivo* application is costly. These drawbacks are directly related to the size of the peptide. Restriction of the peptide length to regions directly required for the bioactivity would be highly advantageous. Therefore, we applied *in silico* bioinformatic tools to screen databases of antimicrobial sequences to identify the antimicrobial region. The candidate sequence was further modified to increase the positive charges required for the interactions with the mycobacterial cell wall. The resulting peptide Angie1 (123aa→16aa; molecular weight 14.1 kDa→1.9 kDa) can easily be produced in large quantities, is accessible to further modifications and importantly maintains activity against virulent *Mtb* in the same order of magnitude as the parental Angiogenin. We do not provide experimental evidence that Angie1 is the most active region of Angiogenin. We took an *in silico* approach to identify the potential cytolytic region. The alternative and possibly more definitive approach would have been to synthesize overlapping peptides. As cellular biologists, we preferred to take the hypothesis-driven approach and will now improve uptake and activity by engineering delivery vehicles such as liposomes (**Figure 9**) or mesoporous particles. Even though the activity of Angie1 against extracellular *Mtb* is lower as compared to Angiogenin the abovementioned benefits regarding the potential stability, specificity and availability make Angie1 the superior candidate for further evaluation in *in vivo* models of infectious diseases.

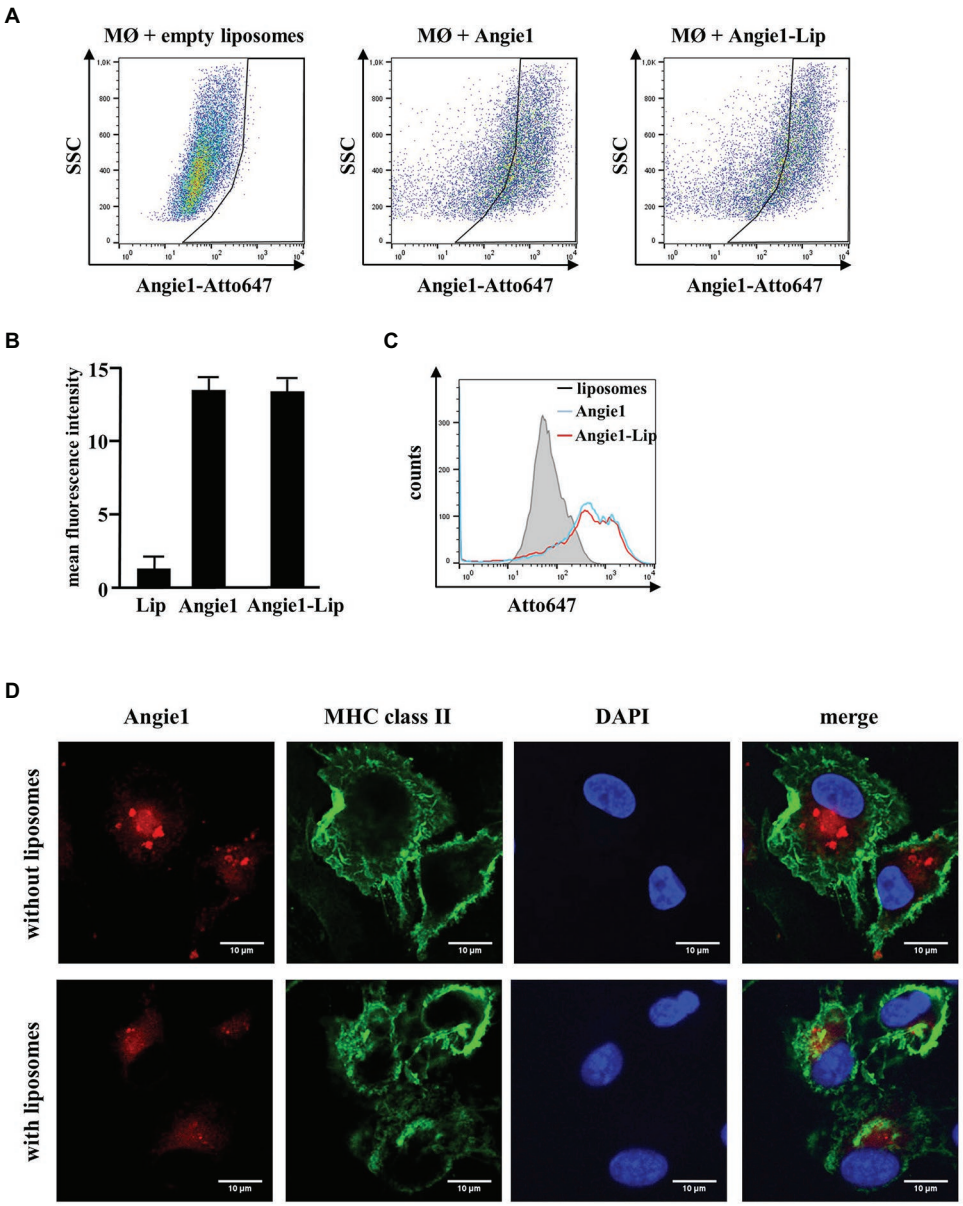

FIGURE 9 | Uptake of Angie1 and Angie1-lip in macrophages. **(A)** Macrophages were incubated overnight with Atto647N-labeled Angie1 or Angie1-lip (both 54 µM, PSL Heidelberg). After 18 h, cells were harvested and analyzed by flow cytometry. Dot plots show one representative donor of three for each group. **(B)** The graph shows the mean fluorescence intensity (FI) ± SD of Atto647-positive cells for empty liposomes, Angie1 and Angie1-Lip of three independent donors. Statistical analysis was performed using a non-parametric Wilcoxon-Rank Test for paired samples. **(C)** The histogram shows the counts of Atto647-positive populations for empty liposomes, Angie1 and Angie1-Lip for one representative donor of three donors. **(D)** Macrophages were incubated with Angie1-Atto647N (upper panels) or Angie1-Atto647N-Lip (lower panels). After 18 h, cells were stained for MHC class II. Cell nuclei were stained with DAPI. Images were acquired using an inverted laser scanning confocal microscope (Zeiss LSM 710). Depicted images show representative area of one out of three donors with similar result.

The application of AMPs in tuberculosis or other systemic infectious diseases would be in combination with-rather than replacing-conventional antibiotic treatment. In principle AMPs could be combined with (i) conventional tuberculosis drugs in accordance with drug susceptibility testing, (ii) adjuvants which promote effector mechanisms of macrophages, or (iii) molecules that optimize the targeting of AMPs to the site of infection. One approach to achieve this goal is the design of multipurpose nanoparticles, which serve as a delivery vehicle for multiple bioactive molecules (Singh, 2019). Toward this goal, we initially generated liposomes containing a DDB backbone, the adjuvant trehalose dibehenat (TDB), and Angie1. TDB is synthetic derivative of the mycobacterial cord factor and binds to Mincle (Ishikawa et al., 2009), thereby supporting the activation of macrophages

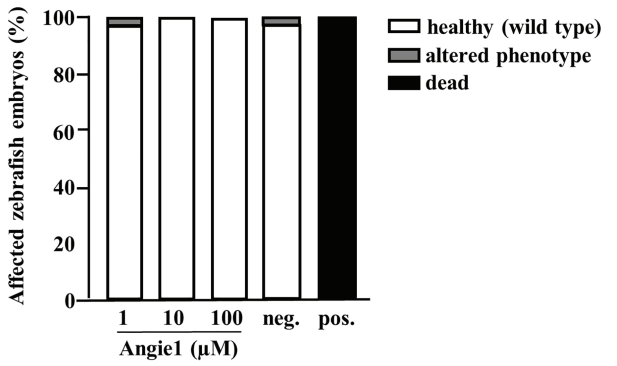

FIGURE 10 | Angie1 is not toxic to zebrafish embryos. Zebrafish embryos were scored for mortality or altered phenotypes at 48 h post fertilization (hpf) after exposure for 24 h to Angie1 at the indicated concentrations or the negative control (PBS) or positive control [NRC-03 antimicrobial peptide, (AMP)]. Altered phenotypes include necrosis and non-lethal lysis (cytotoxicity), heart edema, reduced or absent circulation (cardiotoxicity), delayed development or malformations (developmental toxicity), and reduced or absent touch escape response (neurotoxicity). Note that Angie1 caused no significant toxicity. *n* = 60 embryos each group.

(Ostrop et al., 2015; Huber et al., 2020). These liposomes (CAF01) are well established for the delivery of vaccine antigens and have increased the protective efficacy of subunit vaccines against tuberculosis (Agger et al., 2008; van Dissel et al., 2014). The biochemically related mycobacterial cell wall component muramyl dipeptide packed into liposomes is already a licensed adjuvant treatment for osteosarcoma (Kleinerman et al., 1992). Such liposomes provide a versatile platform and can be loaded with additional adjuvants, for example, to trigger Toll like receptor-mediated antimicrobial pathways (Kennerknecht et al., 2020). Angie1-containing liposomes were efficiently taken up by macrophages (**Figure 9**) and will provide the starting point for designing optimized nanodrug delivery systems, for example, by including SIGLEC-7 to support specific targeting of *Mtb*-infected macrophages (Kawasaki et al., 2014). In addition, liposomes support storage and gradual release of the incorporated compounds in tissue (Simão et al., 2015). Another beneficial effect of a liposomal delivery system is that uptake and clearance of the active compound by macrophages can be reduced or avoided (Li et al., 2019). By inference, we hypothesize that delivery of Angie1 by liposomes will extend the half-life of Angie1 in human serum and tissue beyond the 3 min measured for free Angie1 (**Figure 8**).

Another promising delivery platform are mesoporous nanoparticles, which have been used to deliver antimicrobial peptides, such as NZX and LL-37 (Braun et al., 2016; Tenland et al., 2019) to enhance protection against tuberculosis in mice (Tenland et al., 2019). Nanoparticles also promote stability, bioavailability, and efficacy of conventional antituberculotic drugs (Clemens et al., 2012; Singh, 2019). These studies will guide the development of multipurpose nanoparticles combining Angie1, antibiotics, and adjuvants to achieve optimized antimicrobial activity at the site of infection.

Only few AMPs with activity against virulent *Mtb* have been described, which may be related to the complexity of the lipid-rich mycobacterial cell wall, the slow metabolism/generation time of *Mtb* or simply due to the requirements for a biological safety level 3 laboratory. Granulysin (Stenger et al., 1998), human neutrophil peptides, such as human ß-defensins (Linde et al., 2001), Protegrin 1 (Fattorini et al., 2004), Lipocalin 1 (Martineau et al., 2007), LL-37 (Deshpande et al., 2020), Lassomycin (Gavrish et al., 2014), Teixobactin (Ling et al., 2015), or Hepcidin (Sow et al., 2007) act at fairly high concentrations ranging between 10 and 50 μM, which is within the same range as we observed for Angiogenin and Angie1 (**Figures 2, 5**). Generally, cationic AMPs interact with the negatively charged mycomembrane and plasma membrane of *Mtb* (Gutsmann, 2016). Angiogenin, which has a net charge of +10 is also highly cationic and we hypothesize that it will also interact with the mycomembrane. Accordingly, we modified the predicted cytotoxic region of Angiogenin (aa 64–80) to increase the positive net charge (+3) which resulted in higher antibacterial activity, even though, we do not provide proof that there is an interaction with the mycobacterial cell wall. Whether the disruption of the mycobacterial cell wall by AMPs is already sufficient to kill the bacilli or only represents the first step of an antimicrobial pathway remains to be determined. Since Angiogenin belongs to the ribonuclease A (RNase A) superfamily, the catalytic activity could contribute to the degradation of bacterial RNA and cause lethal damage to the pathogen (Ganz, 2003). Other possible effector mechanisms include the inhibition of cell wall synthesis, the interference with the mycobacterial iron metabolism or the targeting of ATP-dependent proteases (Gutsmann, 2016). In the case of intracellular *Mtb*, the direct effect on the bacteria could be supported by AMP-mediated modulation of macrophage function. LL-37, Defensins (Hancock et al., 2016), and Granulysin (Deng et al., 2005; Tewary et al., 2010) affect chemotaxis and cytokine responses by macrophages. While Angiogenin or Angie1 do not induce chemotaxis or cytokine release by primary human monocytes or macrophages (not shown) it remains to be determined whether there is an immune-modulatory effect on *Mtb*-infected macrophages.

In conclusion, we detected Angiogenin as an endogenous antimycobacterial peptide in human serum. Using Angiogenin as a template, we engineered the small, biologically active derivative Angie1 with activity against virulent *Mtb* and fast-growing bacteria. Angie1 can be efficiently delivered into human macrophages *via* liposomes, providing the intriguing perspective of testing the therapeutic efficacy in small animal models of infection. The combined application of peptidomics, *in silico* prediction of biological function, nanomedicine, and microbiology is a powerful multidisciplinary approach for the discovery of novel antimicrobial compounds.

DATA AVAILABILITY STATEMENT

The raw data supporting the conclusions of this article will be made available by the authors, without undue reservation, to any qualified researcher. Proteomic datasets are available at the following link: http://massive.ucsd.edu/ProteoSAFe/status.jsp?task=b7605ed4d7b74921b49260d202cd0103.

AUTHOR CONTRIBUTIONS

RN and FG performed experiments with *Mtb* and edited the manuscript. RN performed flow cytometry and confocal microscopy. FG helped with flow cytometry and data analysis. JK, DM, and MG helped with *Mtb* assays. FL produced and characterized liposomes. AH performed assays with fast-growing bacteria under supervision of BS. MR and GW investigated cytotoxicity against zebrafish embryos. W-GF provided the hemofiltrate library and AR with LS purified Angiogenin. SW and AR performed mass spectrometry analysis and determined half-life in serum. SS designed all experiments, supervised the study, validated the data, and wrote the manuscript. All authors contributed to the article and approved the submitted version.

FUNDING

This work was funded by the German Research Foundation (CRC 1279 Exploiting the Human Peptidome for Novel Antimicrobial and Anticancer Agents, Project Number 316249678) and the Graduate School of Molecular Medicine at the University Ulm. The Weidinger lab also was funded by the German Research Foundation (CRC 1279).

ACKNOWLEDGMENTS

RN is part of the International Graduate School in Molecular Medicine Ulm (IGradU) and thanks for constant support. We thank Angelika Rück and Sviatlana Kalinina for support with the confocal laser microscopy. AR especially thanks the Alexander von Humboldt Foundation for its support through the postdoctoral fellowship 3.2-KUB/1153731 STP.

SUPPLEMENTARY MATERIAL

The Supplementary Material for this article can be found online at: https://www.frontiersin.org/articles/10.3389/fmicb.2020.618278/full#supplementary-material

REFERENCES

Agger, E. M., Rosenkrands, I., Hansen, J., Brahimi, K., Vandahl, B. S., Aagaard, C., et al. (2008). Cationic liposomes formulated with synthetic mycobacterial cordfactor (CAF01): a versatile adjuvant for vaccines with different immunological requirements. *PLoS One* 3:e3116. doi: 10.1371/journal.pone.0003116

Avdeeva, S. V., Chernukha, M. U., Shaginyan, I. A., Tarantul, V. Z., and Naroditsky, B. S. (2006). Human angiogenin lacks specific antimicrobial activity. *Curr. Microbiol.* 53, 477–478. doi: 10.1007/s00284-006-0033-6

Bosso, M., Ständker, L., Kirchhoff, F., and Münch, J. (2018). Exploiting the human peptidome for novel antimicrobial and anticancer agents. *Bioorg. Med. Chem.* 26, 2719–2726. doi: 10.1016/j.bmc.2017.10.038

Braun, K., Pochert, A., Lindén, M., Davoudi, M., Schmidtchen, A., Nordström, R., et al. (2016). Membrane interactions of mesoporous silica nanoparticles as carriers of antimicrobial peptides. *J. Colloid Interface Sci.* 475, 161–170. doi: 10.1016/j.jcis.2016.05.002

Bruns, H., Stegelmann, F., Fabri, M., Döhner, K., van Zandbergen, G., Wagner, M., et al. (2012). Abelson tyrosine kinase controls phagosomal acidification required for killing of *Mycobacterium tuberculosis* in human macrophages. *J. Immunol.* 189, 4069–4078. doi: 10.4049/jimmunol.1201538

Cho, S., Beintema, J. J., and Zhang, J. (2005). The ribonuclease A superfamily of mammals and birds: identifying new members and tracing evolutionary histories. *Genomics* 85, 208–220. doi: 10.1016/j.ygeno.2004.10.008

Clemens, D. L., Lee, B. Y., Xue, M., Thomas, C. R., Meng, H., Ferris, D., et al. (2012). Targeted intracellular delivery of antituberculosis drugs to *Mycobacterium tuberculosis*-infected macrophages via functionalized mesoporous silica nanoparticles. *Antimicrob. Agents Chemother.* 56, 2535–2545. doi: 10.1128/AAC.06049-11

Conzelmann, C., Groß, R., Zou, M., Krüger, F., Görgens, A., Gustafsson, M. O., et al. (2020). Salivary extracellular vesicles inhibit Zika virus but not SARS-CoV-2 infection. *J. Extracell. Vesicles* 9:1808281. doi: 10.1080/20013078.2020.1808281

Deng, A., Chen, S., Li, Q., Lyu, S., Clayberger, C., and Krensky, A. M. (2005). Granulysin, a cytolytic molecule, is also a chemoattractant and proinflammatory activator. *J. Immunol.* 174, 5243–5248. doi: 10.4049/jimmunol.174.9.5243

Deshpande, D., Grieshober, M., Wondany, F., Gerbl, F., Noschka, R., Michaelis, J., et al. (2020). Super-resolution microscopy reveals a direct interaction of intracellular *Mycobacterium tuberculosis* with the antimicrobial peptide LL-37. *Int. J. Mol. Sci.* 21:6741. doi: 10.3390/ijms21186741

Fattorini, L., Gennaro, R., Zanetti, M., Tan, D., Brunori, L., Giannoni, F., et al. (2004). In vitro activity of protegrin-1 and beta-defensin-1, alone and in combination with isoniazid, against *Mycobacterium tuberculosis*. *Peptides* 25, 1075–1077. doi: 10.1016/j.peptides.2004.04.003

Fett, J. W., Strydom, D. J., Lobb, R. R., Alderman, E. M., Bethune, J. L., Riordan, J. F., et al. (1985). Isolation and characterization of angiogenin, an angiogenic protein from human carcinoma cells. *Biochemistry* 24, 5480–5486. doi: 10.1021/bi00341a030

Ganz, T. (2003). Angiogenin: an antimicrobial ribonuclease. *Nat. Immunol.* 4, 213–214. doi: 10.1038/ni0303-213

Gavrish, E., Sit, C. S., Cao, S., Kandror, O., Spoering, A., Peoples, A., et al. (2014). Lassomycin, a ribosomally synthesized cyclic peptide, kills *Mycobacterium tuberculosis* by targeting the ATP-dependent protease ClpC1P1P2. *Chem. Biol.* 21, 509–518. doi: 10.1016/j.chembiol.2014.01.014

Groß, R., Bauer, R., Krüger, F., Rücker-Braun, E., Olari, L. R., Ständker, L., et al. (2020). A placenta derived c-terminal fragment of β-hemoglobin with combined antibacterial and antiviral activity. *Front. Microbiol.* 11:508. doi: 10.3389/fmicb.2020.00508

Gutsmann, T. (2016). Interaction between antimicrobial peptides and mycobacteria. *Biochim. Biophys. Acta* 1858, 1034–1043. doi: 10.1016/j.bbamem.2016.01.031

Hancock, R. E. W., Haney, E. F., and Gill, E. E. (2016). The immunology of host defence peptides: beyond antimicrobial activity. *Nat. Rev. Immunol.* 16, 321–334. doi: 10.1038/nri.2016.29

Hooper, L. V., Stappenbeck, T. S., Hong, C. V., and Gordon, J. I. (2003). Angiogenins: a new class of microbicidal proteins involved in innate immunity. *Nat. Immunol.* 4, 269–273. doi: 10.1038/ni888

Huber, A., Killy, B., Grummel, N., Bodendorfer, B., Paul, S., Wiesmann, V., et al. (2020). Mycobacterial cord factor reprograms the macrophage response to IFN-γ towards enhanced inflammation yet impaired antigen presentation and expression of GBP1. *J. Immunol.* 205, 1580–1592. doi: 10.4049/jimmunol.2000337

Ishikawa, E., Ishikawa, T., Morita, Y. S., Toyonaga, K., Yamada, H., Takeuchi, O., et al. (2009). Direct recognition of the mycobacterial glycolipid, trehalose dimycolate, by C-type lectin mincle. *J. Exp. Med.* 206, 2879–2888. doi: 10.1084/jem.20091750

Kallert, S., Zenk, S. F., Walther, P., Grieshober, M., Weil, T., and Stenger, S. (2015). Liposomal delivery of lipoarabinomannan triggers *Mycobacterium tuberculosis* specific T-cells. *Tuberculosis* 95, 452–462. doi: 10.1016/j.tube.2015.04.001

Kawasaki, N., Rillahan, C. D., Cheng, T. -Y., Van Rhijn, I., Macauley, M. S., Moody, D. B., et al. (2014). Targeted delivery of mycobacterial antigens to human dendritic cells via Siglec-7 induces robust T cell activation. *J. Immunol.* 193, 1560–1566. doi: 10.4049/jimmunol.1303278

Kennerknecht, K., Noschka, R., Löffler, F., Wehrstedt, S., Pedersen, G. K., Mayer, D., et al. (2020). Toll like-receptor agonist Pam3Cys modulates the immunogenicity of liposomes containing the tuberculosis vaccine candidate H56. *Med. Microbiol. Immunol.* 209, 163–176. doi: 10.1007/s00430-020-00657-3

Kleinerman, E. S., Jia, S. F., Griffin, J., Seibel, N. L., Benjamin, R. S., and Jaffe, N. (1992). Phase II study of liposomal muramyl tripeptide in osteosarcoma: the cytokine cascade and monocyte activation following administration. *J. Clin. Oncol.* 10, 1310–1316. doi: 10.1200/JCO.1992.10.8.1310

Law, D., and Kelly, J. (1995). Use of heme and hemoglobin by *Escherichia coli* O157 and other shiga-like-toxin-producing *E. coli* serogroups. *Infect. Immun.* 63, 700–702. doi: 10.1128/iai.63.2.700-702.1995

Li, M., Du, C., Guo, N., Teng, Y., Meng, X., Sun, H., et al. (2019). Composition design and medical application of liposomes. *Eur. J. Med. Chem.* 164, 640–653. doi: 10.1016/j.ejmech.2019.01.007

Linde, C. M. A., Hoffner, S. E., Refai, E., and Andersson, M. (2001). In vitro activity of PR-39, a proline-arginine-rich peptide, against susceptible and multi-drug-resistant *Mycobacterium tuberculosis*. *J. Antimicrob. Chemother.* 47, 575–580. doi: 10.1093/jac/47.5.575

Ling, L. L., Schneider, T., Peoples, A. J., Spoering, A. L., Engels, I., Conlon, B. P., et al. (2015). A new antibiotic kills pathogens without detectable resistance. *Nature* 517, 455–459. doi: 10.1038/nature14098

Liu, P. T., Stenger, S., Li, H., Wenzel, L., Tan, B. H., Krutzik, S. R., et al. (2006). Toll-like receptor triggering of a vitamin D-mediated human antimicrobial response. *Science* 311, 1770–1773. doi: 10.1126/science.1123933

Martineau, A. R., Newton, S. M., Wilkinson, K. A., Kampmann, B., Hall, B. M., Nawroly, N., et al. (2007). Neutrophil-mediated innate immune resistance to mycobacteria. *J. Clin. Invest.* 117, 1988–1994. doi: 10.1172/JCI31097

Morash, M. G., Douglas, S. E., Robotham, A., Ridley, C. M., Gallant, J. W., and Soanes, K. H. (2011). The zebrafish embryo as a tool for screening and characterizing pleurocidin host-defense peptides as anti-cancer agents. *Dis. Model. Mech.* 4, 622–633. doi: 10.1242/dmm.007310

Ostrop, J., Jozefowski, K., Zimmermann, S., Hofmann, K., Strasser, E., Lepenies, B., et al. (2015). Contribution of MINCLE–SYK signaling to activation of primary human APCs by mycobacterial cord factor and the novel adjuvant TDB. *J. Immunol.* 195, 2417–2428. doi: 10.4049/jimmunol.1500102

Raftery, T. D., Isales, G. M., Yozzo, K. L., and Volz, D. C. (2014). High-content screening assay for identification of chemicals impacting spontaneous activity in zebrafish embryos. *Environ. Sci. Technol.* 48, 804–810. doi: 10.1021/es404322p

Rodríguez, A. A., Garateix, A., Salceda, E., Peigneur, S., Zaharenko, A. J., Pons, T., et al. (2018). PhcrTx2, a new crab-paralyzing peptide toxin from the sea anemone *Phymanthus crucifer*. *Toxins* 10:72. doi: 10.3390/toxins10020072

Rybak, S. M., Fett, J. W., Yao, Q. Z., and Vallee, B. L. (1987). Angiogenin mRNA in human tumor and normal cells. *Biochem. Biophys. Res. Commun.* 146, 1240–1248. doi: 10.1016/0006-291X(87)90781-9

Schulz-Knappe, P., Schrader, M., Ständker, L., Richter, R., Hess, R., Jürgens, M., et al. (1997). Peptide bank generated by large-scale preparation of circulating human peptides. *J. Chromatogr. A* 776, 125–132. doi: 10.1016/S0021-9673(97)00152-0

Sheng, J., and Xu, Z. (2016). Three decades of research on angiogenin: a review and perspective. *Acta Biochim. Biophys. Sin.* 48, 399–410. doi: 10.1093/abbs/gmv131

Simão, A. M. S., Bolean, M., Cury, T. A. C., Stabeli, R. G., Itri, R., and Ciancaglini, P. (2015). Liposomal systems as carriers for bioactive compounds. *Biophys. Rev.* 4, 391–397. doi: 10.1007/s12551-015-0180-8

Singh, R. (2019). Nanotechnology based therapeutic application in cancer diagnosis and therapy. *3 Biotech* 9:415. doi: 10.1007/s13205-019-1940-0

Sow, F. B., Florence, W. C., Satoskar, A. R., Schlesinger, L. S., Zwilling, B. S., and Lafuse, W. P. (2007). Expression and localization of hepcidin in macrophages: a role in host defense against tuberculosis. *J. Leukoc. Biol.* 82, 934–945. doi: 10.1189/jlb.0407216

Ständker, L., Wobst, P., Mark, S., and Forssmann, W. G. (1998). Isolation and characterization of circulating 13-kDa C-terminal fragments of human insulin-like growth factor binding protein-5. *FEBS Lett.* 441, 281–286. doi: 10.1016/S0014-5793(98)01497-5

Stenger, S., Hanson, D. A., Teitelbaum, R., Dewan, P., Niazi, K. R., Froelich, C. J., et al. (1998). An antimicrobial activity of cytolytic T cells mediated by granulysin. *Science* 282, 121–125. doi: 10.1126/science.282.5386.121

Strydom, D. J., Fett, J. W., Lobb, R. R., Alderman, E. M., Bethune, J. L., Riordan, J. F., et al. (1985). Amino acid sequence of human tumor derived angiogenin. *Biochemistry* 24, 5486–5494. doi: 10.1021/bi00341a031

Tenland, E., Pochert, A., Krishnan, N., Rao, K. U., Kalsum, S., Braun, K., et al. (2019). Effective delivery of the anti-mycobacterial peptide NZX in mesoporous silica nanoparticles. *PLoS One* 14:e0212858. doi: 10.1371/journal.pone.0212858

Tewary, P., Yang, D., De La Rosa, G., Li, Y., Finn, M. W., Krensky, A. M., et al. (2010). Granulysin activates antigen-presenting cells through TLR4 and acts as an immune alarmin. *Blood* 116, 3465–3474. doi: 10.1182/blood-2010-03-273953

Torrent, M., Di Tommaso, P., Pulido, D., Nogués, M. V., Notredame, C., Boix, E., et al. (2012). AMPA: an automated web server for prediction of protein antimicrobial regions. *Bioinformatics* 28, 130–131. doi: 10.1093/bioinformatics/btr604

van Dissel, J. T., Joosten, S. A., Hoff, S. T., Soonawala, D., Prins, C., Hokey, D. A., et al. (2014). A novel liposomal adjuvant system, CAF01, promotes long-lived *Mycobacterium tuberculosis*-specific T-cell responses in human. *Vaccine* 32, 7098–7107. doi: 10.1016/j.vaccine.2014.10.036

Waghu, F. H., Barai, R. S., Gurung, P., and Idicula-Thomas, S. (2016). CAMPR3: a database on sequences, structures and signatures of antimicrobial peptides. *Nucleic Acids Res.* 44, D1094–D1097. doi: 10.1093/nar/gkv1051

Wang, G. (2014). Human antimicrobial peptides and proteins. *Pharmaceuticals* 7, 545–594. doi: 10.3390/ph7050545

World Health Organization (2019). Tuberculosis report.

Xu, M., McCanna, D. J., and Sivak, J. G. (2015). Use of the viability reagent PrestoBlue in comparison with alamarBlue and MTT to assess the viability of human corneal epithelial cells. *J. Pharmacol. Toxicol. Methods* 71, 1–7. doi: 10.1016/j.vascn.2014.11.003

Zhang, J., Xin, L., Shan, B., Chen, W., Xie, M., Yuen, D., et al. (2012). PEAKS DB: de novo sequencing assisted database search for sensitive and accurate peptide identification. *Mol. Cell. Proteomics* 11:M111.010587. doi: 10.1074/mcp.M111.010587

Conflict of Interest: W-GF was employed by Pharis Biotec GmbH.

The remaining authors declare that the research was conducted in the absence of any commercial or financial relationships that could be construed as a potential conflict of interest.

frontiers in Microbiology

ORIGINAL RESEARCH
published: 22 January 2021
doi: 10.3389/fmicb.2020.613963

Protein Kinase R Restricts the Intracellular Survival of *Mycobacterium tuberculosis* by Promoting Selective Autophagy

*Robin Smyth[1], Stefania Berton[1], Nusrah Rajabalee[1], Therese Chan[1] and Jim Sun[1,2]**

[1]*Department of Biochemistry, Microbiology and Immunology, University of Ottawa, Ottawa, ON, Canada,* [2]*Centre for Infection, Immunity and Inflammation, University of Ottawa, Ottawa, ON, Canada*

Tuberculosis (TB) is a deadly infectious lung disease caused by the pathogenic bacterium *Mycobacterium tuberculosis* (Mtb). The identification of macrophage signaling proteins exploited by Mtb during infection will enable the development of alternative host-directed therapies (HDT) for TB. HDT strategies will boost host immunity to restrict the intracellular replication of Mtb and therefore hold promise to overcome antimicrobial resistance, a growing crisis in TB therapy. Protein Kinase R (PKR) is a key host sensor that functions in the cellular antiviral response. However, its role in defense against intracellular bacterial pathogens is not clearly defined. Herein, we demonstrate that expression and activation of PKR is upregulated in macrophages infected with Mtb. Immunological profiling of human THP-1 macrophages that overexpress PKR (THP-PKR) showed increased production of IP-10 and reduced production of IL-6, two cytokines that are reported to activate and inhibit IFNγ-dependent autophagy, respectively. Indeed, sustained expression and activation of PKR reduced the intracellular survival of Mtb, an effect that could be enhanced by IFNγ treatment. We further demonstrate that the enhanced anti-mycobacterial activity of THP-PKR macrophages is mediated by a mechanism dependent on selective autophagy, as indicated by increased levels of LC3B-II that colocalize with intracellular Mtb. Consistent with this mechanism, inhibition of autophagolysosome maturation with bafilomycin A1 abrogated the ability of THP-PKR macrophages to limit replication of Mtb, whereas pharmacological activation of autophagy enhanced the anti-mycobacterial effect of PKR overexpression. As such, PKR represents a novel and attractive host target for development of HDT for TB, and our data suggest value in the design of more specific and potent activators of PKR.

Keywords: ***Mycobacterium tuberculosis*, macrophage signaling, autophagy, host-directed therapy, Protein Kinase R**

OPEN ACCESS

Edited by:
Giorgia Mori,
The University of Queensland, Australia

Reviewed by:
Shashank Gupta,
National Institutes of Health, United States
Vikram Saini,
All India Institute of Medical Sciences, India

***Correspondence:**
Jim Sun
jim.sun@uottawa.ca

Specialty section:
This article was submitted to Antimicrobials, Resistance and Chemotherapy, a section of the journal Frontiers in Microbiology

Received: *04 October 2020*
Accepted: *30 December 2020*
Published: *22 January 2021*

Citation:
Smyth R, Berton S, Rajabalee N, Chan T and Sun J (2021) Protein Kinase R Restricts the Intracellular Survival of Mycobacterium tuberculosis by Promoting Selective Autophagy. Front. Microbiol. 11:613963. doi: 10.3389/fmicb.2020.613963

INTRODUCTION

Mycobacterium tuberculosis (Mtb) is responsible for 1.5 million deaths each year and remains the leading cause of infectious disease-related deaths worldwide (WHO, 2020). Due to the emergence of antibiotic-resistant tuberculosis (TB), the development of alternative anti-TB therapeutics is urgently needed. Host-directed therapy (HDT) is a promising treatment

strategy, since it aims to boost the host immune response to Mtb rather than targeting the bacterium itself, thereby possessing the potential to circumvent the development of antibiotic resistance.

It has been observed that nearly half of individuals in close contact with highly active TB patients do not produce antibodies against Mtb (Morrison et al., 2008). This suggests that a strong innate immune response can successfully clear Mtb in certain individuals. Since alveolar macrophages are the first line of defense against inhaled bacteria, the persistence of Mtb is largely determined by the bactericidal capacity of macrophages (Behar et al., 2010). As such, the ability of certain individuals to achieve early clearance of Mtb may be due to an enhanced antibacterial response by their macrophages. Targeting host proteins to boost the antibacterial activity of macrophages could therefore be a promising strategy for HDT.

Double stranded RNA-activated protein kinase R (PKR) is one such host protein that has been suggested as a prime candidate for HDT against TB infection (Wu et al., 2012; Tobin, 2015). PKR is a serine/threonine kinase encoded by the human *EIF2AK2* gene and is well characterized for its role in defense against viral infections (García et al., 2007). Transcription of PKR is stimulated by type I interferons (IFN), and the canonical activator of PKR is double-stranded RNA (dsRNA; Zhang et al., 2001). PKR binds viral dsRNA, triggering dimerization and subsequent autophosphorylation events that lead to the activation of the kinase (Zhang et al., 2001). Activated PKR phosphorylates its substrate, eukaryotic translation initiation factor EIF2α, which inhibits mRNA protein translation to prevent viral replication (Dey et al., 2005). PKR is also reported to induce stress-activated apoptosis during viral infection or serum starvation (García et al., 2006), and it has been shown to regulate pyroptosis and necroptosis (Lu et al., 2012; Thapa et al., 2013). The role of PKR in controlling cell death pathways suggests that it may be a promising target for TB HDT, since the specific mode of cell death that occurs in Mtb-infected macrophages largely influences the progression of infection (Behar et al., 2010).

PKR has also been demonstrated to play a role in autophagy. Autophagy was traditionally described as a homeostatic process that generates nutrients by degrading cytoplasmic constituents. However, there is rapidly accumulating evidence that autophagy also plays an important role in immunity. In addition to organelles and proteins, it is now known that the autophagy process can degrade intracellular pathogens (Gutierrez et al., 2004; Nakagawa et al., 2004). Importantly, PKR is required for autophagic degradation of Herpes Simplex Virus-1 (Tallóczy et al., 2006) and activates autophagy in macrophages during parasitic infection (Ogolla et al., 2013). Autophagy is an important defense mechanism in macrophages infected with Mtb, since it can target and degrade cytosolic Mtb after it escapes the phagosome (Watson et al., 2012). Indeed, autophagy induction in Mtb-infected macrophages allows for progressive elimination of the bacteria (Singh et al., 2006), decreased Mtb burden (Gutierrez et al., 2004), and improved control of inflammation (Zhang et al., 2017). Interestingly, current anti-tuberculosis drugs have been shown to activate autophagy. The first-line antibiotics pyrazinamide and isoniazid activate autophagy in Mtb-infected macrophages, and inhibition of autophagy reduces the effectiveness of these drugs (Kim et al., 2012). Due to the antibacterial role of autophagy in macrophages, therapeutic activation of autophagy is a promising HDT strategy against TB (Tobin, 2015; Paik et al., 2019). However, a potential role for PKR in regulating autophagy during bacterial infections has not been studied.

Given that PKR regulates several key macrophage defense mechanisms that are critical for Mtb clearance, PKR could be a promising target for TB HDT. However, knowledge of the function of PKR in macrophages during bacterial infection is surprisingly limited. The impact of PKR on the antibacterial response of macrophages during Mtb infection must therefore be investigated to assess its suitability as a candidate for HDT against TB infection. Herein, we demonstrate that PKR expression and activation is induced during Mtb infection in THP-1 macrophages and primary human macrophages. Through genetic overexpression of PKR, we determined that PKR enhances the production of antibacterial cytokines and limits the intracellular survival of Mtb in macrophages. Our data reveal that PKR enhances the anti-mycobacterial response of macrophages through a mechanism dependent on activation of selective autophagy, and not by manipulation of cell death pathways. As such, a search for pharmacological activators of PKR as a novel TB therapeutic would be desirable.

MATERIALS AND METHODS

Cell Culture and Reagents

THP-1 monocytes (ATCC TIB-202) and primary human monocytes were maintained in RPMI 1640 medium (Gibco, Gaithersburg, MD). HEK GP-293 cells (Clontech, Mountain View, CA) and HEK293T cells (ATCC CRL-3216) were maintained in DMEM medium (Gibco). RPMI 1640 and DMEM medium were supplemented with 2 mM L-glutamine, Penicillin-Streptomycin (100 I.U./ml penicillin, 100 μg/ml streptomycin), 10 mM HEPES, and 10% heat-inactivated fetal bovine serum purchased from Gibco. Cells were maintained at 37°C in a humidified atmosphere of 5% CO_2. Human peripheral blood mononuclear cells were collected according to approved ethics protocols (Protocol# 2005388-01H) and isolated from buffy coats by the Ficoll-Paque density centrifugation method. Positive selection of monocytes was performed using anti-CD14 coated magnetic particles from StemCell Technologies (Vancouver, BC) according to manufacturer's protocol. Monocytes were then differentiated with 5 ng/ml GM-CSF (Gibco) for 6 days to obtain human monocyte-derived macrophages (MDMs). THP-1 monocytes were differentiated with 100 ng/ml phorbol ester 13-phorbol-12-myristate acetate (PMA, Alfa Aesar, Haverhill, MA) for 72 h. Puromycin and recombinant human IFNγ were purchased from Gibco. Bafilomycin A1 was purchased from Santa Cruz Biotechnology (Dallas, TX). Rapamycin was purchased from Alfa Aesar.

Bacteria and Plasmids

The *Mycobacterium tuberculosis* H37Rv-derived auxotroph strain mc^{2}6206 was grown in Middlebrook 7H9 medium (BD Biosciences, Franklin Lakes, NJ) supplemented with 0.2% glycerol (Fisher Chemical, Waltham, MA), 0.05% Tween-80 (Acros Organics, Fair Lawn, NJ), 10% OADC (BD Biosciences), 24 μg/ml D-pantothenic acid (Alfa Aesar), and 50 μg/ml L-leucine (Alfa Aesar). *M. tuberculosis* mc^{2}6206 expressing green fluorescent protein (GFP; Mtb-GFP) was generated previously (Sun et al., 2016). *M. tuberculosis* mc^{2}6206 expressing luciferase (Mtb-luciferase) was generated by transforming the pSMT3 plasmid encoding for firefly luciferase gene (generous gift from Dr. Zakaria Hmama). GFP-expressing and luciferase-expressing Mtb were maintained in antibiotic selection with 50 μg/ml Hygromycin B (Calbiochem, San Diego, CA). Liquid Mtb cultures were maintained at 37°C with slow shaking (50 rpm). *Salmonella enterica* serovar Typhimurium strain SL1344 and *Listeria monocytogenes* strain 10403s were grown in Luria-Bertani broth (Fisher BioReagents, Waltham, MA) at 37°C. *Escherichia coli* strain NEB Stable (New England Biolabs, Ipswich, MA) was used for plasmid propagation and was grown in Luria-Bertani broth at 37°C. Plasmid pMSCV-PKR was constructed by inserting the PCR amplified *EIF2AK2* gene (Entrez Gene ID 5610, variant 1) from THP-1 cell-derived cDNA using the oligonucleotide pair 5'-gctaCTCGAGatggctgg tgatctttcagcaggtttc and 5'-gctaGTTAACctaacatgtgtgtcgttcatttttct ctg flanked by the XhoI and HpaI restriction sites (capitalized), respectively, into the multiple cloning site of pMSCV-puro (Clontech) for retroviral expression. The CRISPR/Cas9 knock-out plasmid targeting human PKR was generated by inserting the annealed single guide RNA (sgRNA) oligonucleotide pair 5'-agctgttgagatacttaata and 5'-tattaagtatctcaacagct into a modified LentiCRISPR v2 vector (pSL50) linearized by the restriction enzyme BsmBI. The sgRNA was designed to target exon 2 of the human *EIF2AK2* gene and off-target binding was minimized using publicly available online design tools. To optimize the CRISPR/Cas9 system, we performed modifications to the LentiCRISPR v2 vector by creating an A-U base pair flip in the sgRNA stem-loop and by extending the Cas9-binding hairpin structure, as demonstrated by Chen et al. (2013), which resulted in the plasmid pSL50. LentiCRISPR v2 was a gift from Feng Zhang (Addgene plasmid #52961; RRID:Addgene_52961; Sanjana et al., 2014).[1] The generated plasmids were verified by Sanger sequencing.

Generation of THP-PKR, THP-Ø, and THP-ΔPKR Cells

HEK GP-293 or HEK 293T cells were seeded at 60% confluency to produce viral supernatant. Retroviral plasmids (empty pMSCV-puro and pMSCV-PKR) were co-transfected with the pVSVG envelope plasmid into HEK GP-293 cells, whereas the pSL50 containing the sgRNA targeting PKR was co-transfected with the pVSVG envelope plasmid and the psPAX2 packaging plasmid (Gift from Didier Trono, Addgene plasmid # 12260; RRID:Addgene_12260) into HEK 293T cells.[2] FuGENE (Promega, Madison, WI) was used as the transfection reagent at a ratio of 4:1 (FuGENE:DNA). Culture supernatants were harvested after 48 h, aliquoted, and stored at −80°C. The supernatants containing retroviral or lentiviral particles were supplemented with 10 μg/ml DEAE-Dextran (Sigma-Aldrich, St. Louis, MO) and used to transduce THP-1 cells. Cells were selected using 1 μg/ml puromycin and analyzed by western blot to verify overexpression or deletion of PKR protein.

Bacterial Infection

Mycobacterium tuberculosis mc^{2}6206 growing in log-phase was quantified by optical density measurement at 600 nm using the conversion of OD 1 = 3 × 10^8 Mtb bacteria per ml. The amount of bacteria required for various multiplicity of infections (MOIs) was washed and resuspended in RPMI 1640 cell culture media without antibiotics. Bacteria were added to the differentiated THP-1 macrophages or primary human MDMs and the cells were incubated at 37°C for 4 h. Three phosphate buffered saline (PBS) washes were then performed to remove extracellular, non-phagocytosed bacteria and infection was continued at 37°C for the desired time. For infections with *S. Typhimurium* and *L. monocytogenes*, frozen stocks with pre-determined CFU/ml were thawed and the amount of bacteria required for various MOIs was resuspended in RPMI 1640 media without antibiotics. The bacteria were added to THP-1 macrophages and incubated at 37°C for 30 min. After 30 min, the extracellular bacteria were removed by performing three PBS washes and the cells were cultured in RPMI medium containing 50 μg/ml gentamicin for 1.5 h. After 1.5 h incubation, cells were washed three times with PBS and cultured in RPMI medium containing 10 μg/ml gentamicin for the remainder of the experiment.

Macrophage Viability Assay

Serial dilutions of bafilomycin A1 or rapamycin were added to THP-1 macrophages and maintained in the medium for the duration of the experiments. The compounds were replenished every second day. At the indicated time-points, 30 μl of 0.02% resazurin (Sigma-Aldrich) diluted in PBS was added to the wells. After a 4 h incubation at 37°C, fluorescence was measured using the Synergy™ H1 Hybrid Multi-Mode Reader (BioTek, Winooski, VT) with an excitation wavelength of 560 nm and an emission wavelength of 590 nm. Cell cytotoxicity was assessed by comparing the fluorescence of treated cells to untreated cells.

Intracellular Mtb Survival Assay

Cell culture supernatant was removed from the infected wells and the macrophages were lysed in Glo Lysis Buffer (Promega) at the indicated days post-infection to measure the amount of viable Mtb in each well. Luciferase activity, proportional to viable bacteria, was determined using the BrightGlo Luciferase Assay System (Promega) according to the manufacturer's protocol. Resultant luminescence was measured with the Synergy™

[1]http://n2t.net/addgene:52961

[2]http://n2t.net/addgene:12260

H1 Hybrid Multi-Mode Microplate Reader (BioTek) using 96-well solid white plates (Corning, Corning, NY) and an integration time of 1 s per well. The linear relationship between luminescence and viable bacteria [evaluated by colony forming units (CFU)] was experimentally confirmed. Briefly, 10-fold serial dilutions of pre-determined Mtb stocks were made in triplicate. The Mtb dilutions were then in part assayed to measure the luciferase activity and in part inoculated on Middlebrook 7H10 (7H10) medium for the detection of CFU by plating. Luciferase activity was determined using the BrightGlo Luciferase Assay System according to the manufacturer's protocol. Resultant luminescence was measured with the Synergy H1 Hybrid Multi-Mode Microplate Reader using 96-well solid white plates and an integration time of 1 s per well. For CFU detection by plating, bacteria were spread on 7H10 agar plates (with Hygromycin B) and incubated at 37°C for 3 weeks before colony counting was performed.

Real-Time Cell Analysis Assay

Macrophage adhesion was measured in specialized 96-well plates (E-plate 96) with the xCELLigence Real-time Cell Analyzer (RTCA) SP apparatus (ACEA Biosciences, San Diego, CA). Data was quantified by measuring impedance changes between the sensing electrodes located in the well-bottom, which changes as a function of the adhesion of cells to the surface of the plate. The Cell Index (CI) is a dimensionless value that is representative of these impedance changes. Using this system, macrophage adhesion and therefore viability was monitored in real-time. Plates were removed after ~72 h of macrophage differentiation for the addition of Mtb for infection. After addition of Mtb, plates were placed back in the RTCA apparatus for kinetic monitoring. The CI at every time point represents the mean of three biological replicates.

Apoptosis Assay

Supernatant was collected from the sample wells to preserve detached cells. The wells were washed twice with PBS and TrypLE Express Enzyme (Gibco) was added to the wells. The plate was incubated at 37°C for 5 min to allow for detachment of adherent THP-1 macrophages. The floating and harvested cells were combined and washed twice with PBS. Cells were stained with Annexin V conjugated to FITC (eBioscience, San Diego, CA) according to manufacturer's protocol and flow cytometric analysis was used to measure apoptotic cells.

Multiplex Cytokine and Chemokine Analysis

Cytokine and chemokine expression was measured in culture supernatants harvested from Mtb-infected THP-1 macrophages at 24 h after infection. The LEGENDplex™ Human Essential Immune Response bead-based multiplex assay (BioLegend, San Diego, CA) was used according to the manufacturer's protocol to measure expression of the following cytokines: IL-10 (0.77 + 1.18), TGF-β (3.10 + 2.92), IL-1β (0.65 + 0.47), TNFα (0.88 + 0.27), IFNγ (0.76 + 0.53), IP-10 (1.28 + 0.48), IL-6 (0.97 + 1.46), IL-8 (1.90 + 0.65), IL-2 (1.81 + 0.93), IL-4 (0.97 + 0.83), IL-17A (2.02 + 0.04), and MCP-1 (1.45 + 0.27). The minimum detectable concentration (MDC) in pg/ml for each cytokine is reported in brackets as MDC + 2 STDEV. Data analysis was performed using LEGENDplex™ Data Analysis Software Version 7.1 (BioLegend).

Flow Cytometry

Flow cytometric analysis was performed using the CytoFLEX (Beckman Coulter, Indianapolis, IN). Data analysis was performed using CytExpert software (Beckman Coulter) or FlowJo V10 software (BD Life Sciences, Ashland, OR). Flow cytometry was performed to measure cell density and viability using scattering properties. Flow cytometry was also performed to measure cytokine expression, apoptosis, and phagocytosis levels in macrophages.

Quantitative Real-Time PCR

Total RNA was isolated from THP-1 or primary macrophages using the Aurum Total RNA Mini Kit from Bio-Rad (Hercules, CA). 500 ng of total RNA was used in the cDNA synthesis reaction using the iScript Reverse Transcription Supermix (Bio-Rad). About 4 µl of synthesized cDNA (out of 10 µl reaction) was used to analyze gene expression of *EIF2AK2* or the reference genes *ACTB* and *GAPDH* by real-time PCR on a CFX96 Touch Real-Time PCR Detection System (Bio-Rad) using custom primers that were designed according to MIQE guidelines (Bustin et al., 2009) in combination with the SsoAdvanced Universal SYBR Green Supermix (Bio-Rad). Thermocycling parameters were 95°C for 3 min, followed by 40 cycles of 95°C for 10 s, 60°C for 20 s, and 72°C for 20 s. Gene expression was determined using the ΔΔCq method (Livak and Schmittgen, 2001). ΔCq values were obtained by normalizing the Cq values of *EIF2AK2* with the geometric mean of two reference genes (*ACTB* and *GAPDH*). Relative fold expression was estimated as 2^−ΔΔCq when normalizing to uninfected (day 0) macrophages as 1.0. The following primer pairs were used: *EIF2AK2* forward primer 5'GAAGTGGACCTCTACGCTTTGG and reverse primer 5'TGATGCCATCCCGTAGGTCTGT, *ACTB* forward primer 5'ATTGCCGACAGGATGCAGAA and reverse primer 5'GCTGATCCACATCTGCTGGAA, and *GAPDH* forward primer 5'CAACAGCGACACCCACTCCT and reverse primer 5'CACCCTGTTGCTGTAGCCAAA.

Western Blot

Macrophages were washed once with PBS and lysed in the wells using RIPA buffer (Sigma-Aldrich) according to manufacturer's instructions. Protein concentration of the lysates was determined using the RC DC™ Protein Assay Kit (Bio-Rad) according to the manufacturer's protocol. About 20 µg of protein per sample was separated by SDS-PAGE using handcast 10% polyacrylamide gels (SureCast Gel Handcast System, Invitrogen, Carlsbad, CA) or precast 4–15% polyacrylamide gels (Mini-PROTEAN® TGX Gels, Bio-Rad) and subsequently transferred to a polyvinylidene diluoride (PVDF) membrane using the Mini Trans-Blot Transfer Cell system (Bio-Rad).

Primary monoclonal rabbit antibodies to PKR (D7F7), LC3B (D11), and p-S403 p62 (D8D6T) were purchased from Cell Signaling Technology (Danvers, MA). Primary monoclonal rabbit antibody to p-T446 PKR (E120) was purchased from ABCAM (Cambridge, MA). Primary monoclonal mouse antibodies to GAPDH (GA1R) and beta tubulin (BT7R) were purchased from Invitrogen, and primary monoclonal mouse antibody to p62 (D-3) was purchased from Santa Cruz Biotechnology. A horseradish peroxidase-conjugated goat anti-rabbit or anti-mouse polyclonal antibody (Bio-Rad) was used as the secondary antibody. The blot was developed using the Clarity Western Enhanced Chemiluminescence Substrate (Bio-Rad) and detected in an ImageQuant LAS 4000 imaging system (GE Healthcare Life Sciences, Malborough, MA). Densitometry analysis was performed using ImageJ to quantify protein band intensities.

Fluorescence Microscopy

Differentiated THP-1 cells grown on glass coverslips were infected with Mtb-GFP for 4 h and then washed with PBS to remove extracellular bacteria. To label lysosomes, differentiated THP-1 cells were pre-loaded with 5 ng/ml Texas-Red-conjugated dextran (10,000 Molecular Weight, Invitrogen), a non-biodegradable polysaccharide that accumulates in the lysosome, 24 h prior to Mtb infection. At 24 h post-infection, cells were fixed with 4% methanol-free formaldehyde, permeabilized using 0.2% TritonX-100, and then blocked with 1% BSA-PBS. Cells were incubated overnight at 4°C in a humidified chamber with a primary polyclonal rabbit antibody to LC3 (MBL International Corporation, Woburn, MA), followed by incubation with Alexa Fluor 568 goat anti-rabbit secondary antibody (Invitrogen). For cells pre-loaded with Texas-Red-conjugated dextran, Alexa Fluor 647 goat anti-rabbit secondary antibody (Invitrogen) was used instead. Nuclei were stained with Hoechst 33342 according to manufacturer's protocol (NucBlue™ Live ReadyProbes™ Reagent, Invitrogen). Slides were mounted with FluorSave™ reagent (Calbiochem) and imaged using an Axio Imager M2 microscope (Carl Zeiss AG) with 40x objective. Images (z-stacks) were recorded with AxioCam mRm CCD coupled to Zen Blue software and the analyses were performed with Fiji software.

Statistical Analysis

Data are expressed as the mean ± SEM of three independent biological replicates. Statistical analysis was performed using unpaired *t*-tests (Student's *t*-test) when comparing two independent cell-lines and paired *t*-tests when comparing within the same cell-line. Values of $p < 0.05$ were considered to be significant. All statistical analyses were performed using GraphPad Prism version 7 (GraphPad Prism Software, San Diego, CA).

RESULTS

Intracellular Bacteria Trigger Expression and Activation of PKR in Macrophages

Protein Kinase R has been demonstrated to play a role in the antiviral (Tallóczy et al., 2006) and antiparasitic (Ogolla et al., 2013) response of macrophages. However, knowledge of its role during bacterial infection is surprisingly limited. To investigate whether PKR played a role in the innate immune response to bacterial infections, we measured expression levels of the *EIF2AK2* gene that encodes for PKR following Mtb infection using quantitative real-time PCR (qRT-PCR). Human THP-1 macrophages were infected using the Mtb mc^{2}6206 strain, a derivative of Mtb H37Rv (Jain et al., 2014) that has been demonstrated to have similar *in vitro* and intra-macrophage replication rates, similar responses to anti-TB drugs, and induces comparable cytokine production relative to the parent strain (Schaaf et al., 2016; Mouton et al., 2019). By day 3 post-infection, qRT-PCR showed a 3-fold increase in the mRNA expression levels of *EIF2AK2* in THP-1 macrophages (**Figure 1A**). These findings were then confirmed in primary human MDMs, where mRNA expression of *EIF2AK2* at day 3 post-infection was 28-fold higher compared to uninfected macrophages (**Figure 1B**). To examine whether the increase in PKR expression translated to the protein level, we measured levels of total PKR protein and phosphorylated PKR protein at threonine 446 (p-T446) following Mtb infection over 6 days. Following activation, PKR homodimerizes, which triggers autophosphorylation on multiple serine and threonine sites, including threonine 446 and 451 (Zhang et al., 2001). These two threonine residues are consistently phosphorylated during PKR activation, thus increasing the catalytic activity of PKR and further stabilizing its homodimerization (Zhang et al., 2001; Dey et al., 2005). Levels of p-T446 were therefore used as a marker for active PKR. Western blot analysis of cell lysates revealed that total and p-T446 levels of PKR start to increase as early as 24 h post-infection (**Figure 1C**). Total and phosphorylated levels of PKR increased with the length of infection and stabilized at day 4 post-infection, when there was 7-fold and 17-fold higher total and p-T446 PKR expression, respectively, compared to uninfected macrophages (**Figure 1D**). These findings were confirmed in primary human MDMs (**Figure 1E**). By day 6 post-infection, levels of total and p-T446 PKR were 14-fold and 15-fold higher, respectively, when compared to uninfected macrophages (**Figure 1F**). The dramatic increase in PKR expression levels may indicate an innate immune response by macrophages to control bacterial infection. Since PKR expression and activation have not been previously explored in the context of bacterial infections, we sought to further address whether the increase in PKR expression and phosphorylation was a specific response to only Mtb infection. Interestingly, infection by *L. monocytogenes* and *S. Typhimurium* also triggered PKR expression and phosphorylation (**Figure 1G**), suggesting that regulation of PKR may be a general response to intracellular bacterial infections.

Genetic Overexpression of PKR Results in Increased and Stable Production of Active PKR During *Mycobacterium tuberculosis* Infection

Given a report that deletion of PKR does not affect control of Mtb infection (Wu et al., 2018), along with our observation that PKR expression and activation is triggered during bacterial infection

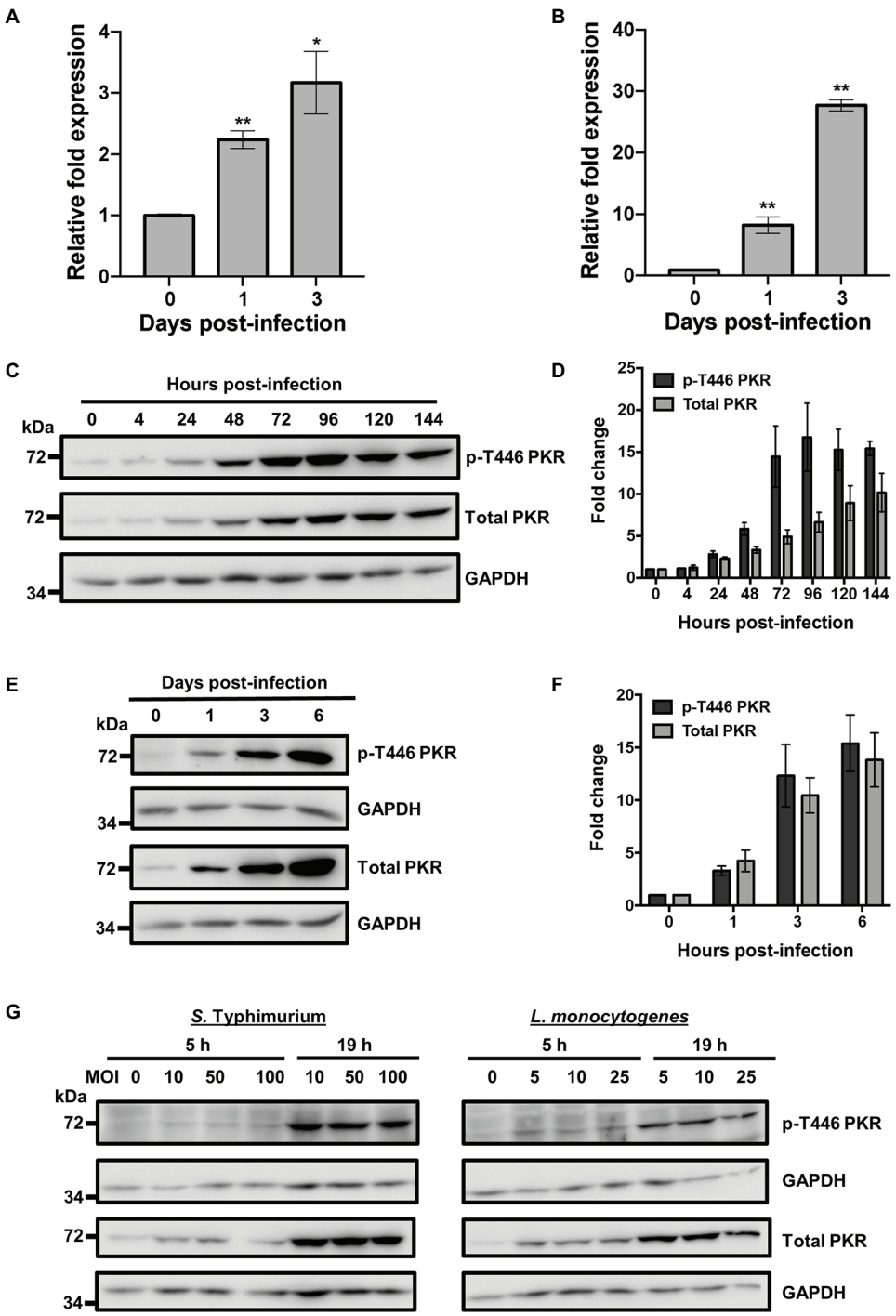

FIGURE 1 | Bacterial infection triggers Protein Kinase R (PKR) expression and activation in macrophages. **(A)** THP-1 macrophages or **(B)** primary human monocyte-derived macrophages (MDMs) were infected with *Mycobacterium tuberculosis* (Mtb) at a multiplicity of infection (MOI) of 5 and quantitative real-time PCR (qRT-PCR) was used to measure the relative expression levels of *EIF2AK2* mRNA at 0, 1, and 3 days post-infection. The ΔΔCT method was used for data analysis by normalizing the Cq values of *EIF2AK2* with two reference genes (*ACTB* and *GAPDH*), and relative fold expression was normalized to uninfected (day 0) macrophages as 1.0. Error bars in **(A,B)** represent the mean ± SEM of three technical replicates. **(C)** THP-1 macrophages were infected with Mtb at an MOI of 5. Cell lysates were prepared at the indicated hours post-infection and total PKR or phosphorylated PKR (p-T446 PKR) protein levels were analyzed by western blotting. The blot shown is representative of three independent experiments. **(D)** Densitometry analysis of the blot in **(C)** was performed by ImageJ to quantify total or p-T446 PKR band intensities as normalized to GAPDH and fold increase of PKR levels is expressed relative to uninfected cells. Error bars represent the mean ± SEM of three independent western blots. **(E)** Primary human MDMs

(Continued)

FIGURE 1 | were infected as in **(C)**. Cell lysates were prepared at the indicated days post-infection and total PKR or p-T446 PKR protein levels were analyzed by western blotting. The blot shown is representative of three independent experiments. **(F)** Densitometry analysis of the blot in **(E)** was performed by ImageJ to quantify total or p-T446 PKR band intensities as normalized to GAPDH and fold increase of PKR levels is expressed relative to uninfected cells. Error bars represent the mean ± SEM of three independent western blots. **(G)** THP-1 macrophages were infected with *Salmonella Typhimurium* or *Listeria monocytogenes* at the indicated MOI. Cell lysates were prepared at 5 and 19 h post-infection and total and p-T446 PKR protein levels were analyzed by western blotting. $^{*}p < 0.05$; $^{**}p < 0.01$ relative to day 0 controls.

(**Figure 1**), we speculated that increased PKR expression and phosphorylation in macrophages would be beneficial to the antibacterial response. To examine the role and function of PKR on the antibacterial functions of macrophages, we genetically overexpressed PKR in THP-1 cells. PKR overexpression cells (THP-PKR) were generated by transducing THP-1 cells with a retroviral expression vector encoding the *EIF2AK2* gene. Western blot analysis confirmed that THP-PKR cells have increased expression of PKR (**Figure 2A**). Indeed, THP-PKR cells produced 4-fold higher PKR protein levels compared to THP-1 cells transduced with an empty vector (THP-Ø), which were used as control cells throughout this study (**Figure 2B**). To ensure that overexpression of PKR does not induce any toxic effects in the cells, we compared the proliferation and viability of wild-type (WT), THP-Ø, and THP-PKR macrophages over 72 h, which showed no significant difference between the cell-lines (**Supplementary Figure S1**). Given that PKR expression is already triggered by Mtb infection in WT THP-1 macrophages (**Figures 1C,D**), it was difficult to predict whether there would be a discernible difference in PKR expression between Mtb-infected THP-Ø and THP-PKR macrophages. To evaluate this, we infected THP-Ø and THP-PKR macrophages with Mtb and compared the levels of total PKR expression over the course of infection. Western blot analysis revealed that THP-PKR macrophages produced elevated PKR protein levels before and early after infection with Mtb (4-fold increase at 4 h post-infection), compared to THP-Ø macrophages (**Figures 2C,D**). The increased expression of PKR was also sustained at 24 and 72 h post-infection, when total PKR protein levels remained 2-fold higher in THP-PKR macrophages compared to THP-Ø macrophages (**Figures 2C,D**). We next questioned whether the increased level of PKR protein observed in THP-PKR macrophages was also phosphorylated. Since PKR expression and activation stabilizes at day 4 post-infection (**Figure 1C**), we chose this time-point to compare protein levels of p-T446 PKR in THP-Ø and THP-PKR macrophages. Western blot data revealed that at day 4 post-infection, THP-PKR macrophages have 2-fold higher levels of phosphorylated PKR compared to THP-Ø macrophages (**Figure 2E**). These data collectively show that the generated THP-PKR cells have higher activation and expression levels of PKR in comparison to control cells during basal conditions as well as during Mtb infection. Thus, the generated THP-PKR macrophages provided a suitable cell-line model to examine whether increased expression of PKR functions to improve the cellular antibacterial response against Mtb infection.

PKR Expression Alters the Immunological Profile of Macrophages During *Mycobacterium tuberculosis* Infection

To determine whether sustained PKR expression and activation impacts the antibacterial response of macrophages, we first examined the effect of PKR expression on the production of cytokines during Mtb infection. Antibody-based bead multiplex assays were performed to compare cytokine and chemokine production by uninfected and Mtb-infected THP-Ø and THP-PKR macrophages using culture supernatants collected at 24 h post-infection. Consistent with previous reports (Dutta et al., 2012; Sun et al., 2016), Mtb infection induced production of IL-6, IP-10, IL-10, TGFβ, IL-1β, and TNFα by THP-Ø control macrophages (**Figures 3A–F**). Importantly, overexpression of PKR significantly altered production of cytokines that are of relevance to Mtb infection. The most striking observation was that Mtb-infected THP-PKR macrophages produced 15-fold lower levels of IL-6 compared to THP-Ø macrophages (**Figure 3A**). Mtb is reported to induce production of IL-6 by infected macrophages to inhibit IFNγ-mediated macrophage activation and autophagy (Nagabhushanam et al., 2003; Dutta et al., 2012). Remarkably, Mtb-infected THP-PKR macrophages produced even less IL-6 than uninfected THP-Ø macrophages (**Figure 3A**). Mtb-infected THP-PKR macrophages also produced increased levels of IP-10 (**Figure 3B**), an IFNγ-inducible chemokine. IP-10 functions as a chemoattractant for activated T cells and monocytes and has also been correlated to autophagy induction (Chu et al., 2017). Importantly, a role for IP-10 in restricting Mtb growth has been reported (Palucci et al., 2019). Consistent with this, Mtb-infected THP-PKR macrophages also produced higher levels of IFNγ compared to THP-Ø macrophages (**Supplementary Figure S2A**). IFNγ is a key cytokine in Mtb immunity due to its critical role in macrophage activation to enhance phagocytosis, apoptosis, autophagy, and the production of reactive nitrogen species (Flynn et al., 1993; Herbst et al., 2011; Dutta et al., 2012). We also observed that THP-PKR macrophages produced decreased levels of IL-10 and TGFβ compared to THP-Ø macrophages (**Figures 3C,D**). IL-10 and TGFβ are reported to be conducive to Mtb survival due to their inhibitory effect on pro-inflammatory cytokine production and T cell activation (Othieno et al., 1999). Furthermore, IL-10 is reported to inhibit autophagy in Mtb-infected macrophages (Upadhyay et al., 2018). Infected THP-PKR macrophages also produced lower levels of IL-1β and TNFα compared to control macrophages (**Figures 3E,F**), two cytokines that are critical for host resistance to Mtb due to their pro-inflammatory effects and their role in activating macrophage cell death (Flynn et al., 1995; Keane et al., 1997; Mayer-Barber et al., 2010; Jayaraman et al., 2013). Levels of IL-2, MCP-1, IL-4, IL-8, and IL-17A were also measured but their production did not differ significantly between THP-Ø and THP-PKR macrophages (**Supplementary Figures S2B–F**). Collectively, our data show that THP-PKR macrophages produced lower levels of cytokines that are permissive for Mtb infection (IL-6, IL-10, and TGFβ) and increased levels of anti-mycobacterial cytokines (IFNγ and IP-10), which supports our hypothesis that sustained PKR expression could enhance the anti-Mtb response in macrophages.

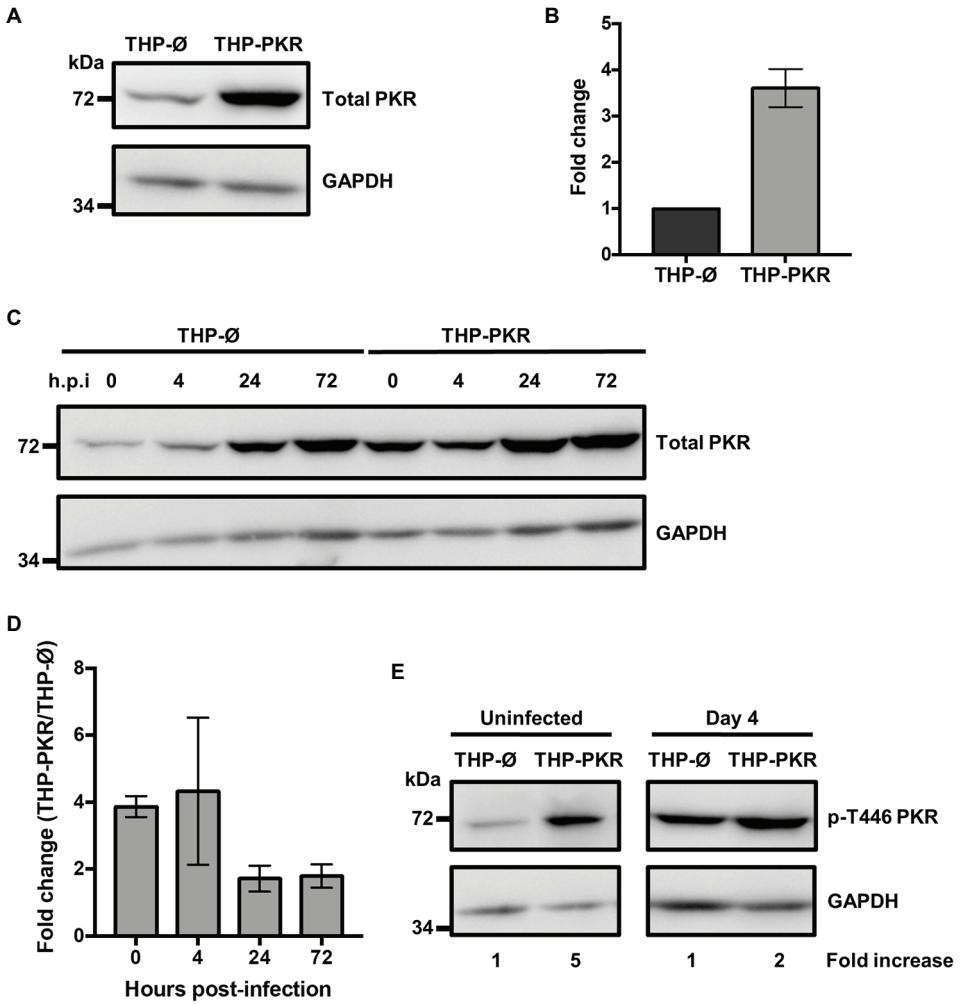

FIGURE 2 | Genetic overexpression of PKR results in increased and stable production of active PKR during *M. tuberculosis* infection. **(A)** PKR protein levels in cell lysates of control THP-1 wild-type (WT) cells transduced with empty vector (THP-Ø) and THP-1 cells transduced with vector overexpressing PKR (THP-PKR) were analyzed by western blotting. **(B)** Densitometry analysis of the blot in **(A)** was performed by ImageJ to quantify PKR band intensities as normalized to GAPDH and fold increase of total PKR levels is expressed relative to THP-Ø cells. **(C)** THP-Ø and THP-PKR macrophages were infected with Mtb at an MOI of 5. Cell lysates were prepared at the indicated hours post-infection (h.p.i) and total PKR protein levels were analyzed by western blotting. **(D)** Densitometry analysis of the blot in **(C)** was performed by ImageJ to quantify PKR band intensities as normalized to GAPDH and fold change of total PKR levels in THP-PKR macrophages relative to THP-Ø macrophages is shown. **(E)** THP-Ø and THP-PKR macrophages were infected as in **(C)**. Cell lysates were prepared at the indicated times post-infection and p-T446 PKR protein levels were analyzed by western blotting. Fold increase of protein expression in THP-PKR macrophages is shown relative to THP-Ø macrophages at the corresponding time-points. The blots in this figure are representative of three independent experiments. Error bars represent the mean ± SEM of three independent western blots.

PKR Is Required to Control *Mycobacterium tuberculosis* Survival in Macrophages

Since the cytokine profiling data suggested that PKR expression could enhance the antibacterial response of Mtb-infected macrophages, we next sought to determine whether PKR is required to limit the intracellular survival of Mtb. To measure the viability of intracellular Mtb, we used a well-characterized luciferase reporter system (Sun et al., 2009; Sorrentino et al., 2016). The luciferase reporter system in mycobacteria is strongly correlative with traditional CFU data obtained by plating serial dilutions of bacteria on solid media. Rigorous studies have demonstrated that the luminescence signal from mycobacteria expressing luciferase maintains a linear relationship with CFU over several orders of magnitude (Andreu et al., 2010; Sharma et al., 2014; Ozeki et al., 2015; Early et al., 2019). To demonstrate that these reports are consistent with our specific firefly luciferase reporter system in Mtb, we compared CFU obtained from plating Mtb-luciferase to luminescence [expressed as relative light units (RLU)] produced by the same sample of Mtb-luciferase. This experiment showed a consistent linear relationship between CFU and RLU within the range of ~100–50,000 RLU, which corresponds to approximately 2,500–1 million CFU (**Figure 4A**). Given that we routinely obtain RLU signals well within this

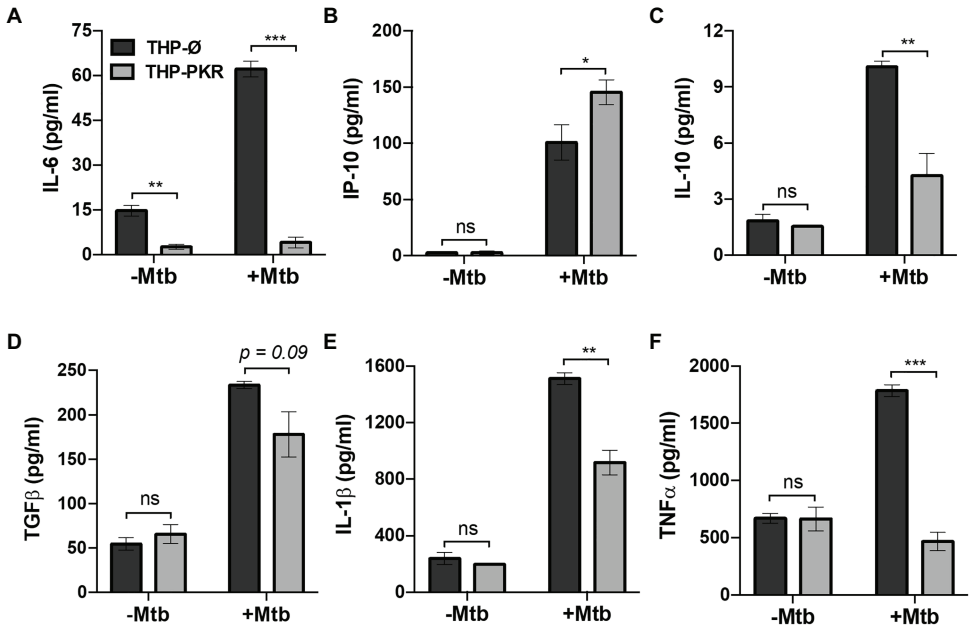

FIGURE 3 | PKR expression alters cytokine production by macrophages during *M. tuberculosis* infection. **(A–F)** THP-Ø and THP-PKR macrophages were infected with Mtb at an MOI of 5 and cell culture supernatant was collected at 24 h post-infection. Production of **(A)** IL-6, **(B)** IP-10, **(C)** IL-10, **(D)** TGFβ, **(E)** IL-1β, and **(F)** TNFα was measured in cell culture supernatant using antibody-based bead multiplex assays. Error bars represent the mean ± SEM of three independent biological replicates. $^{*}p < 0.05$; $^{**}p < 0.01$; and $^{***}p < 0.001$.

linear correlative range, the luciferase reporter system is a suitable method for measuring the intracellular survival of Mtb.

To address whether PKR is required for control of Mtb survival in macrophages, we deleted PKR in THP-1 cells (THP-ΔPKR) using CRISPR/Cas9-mediated genome editing methods. Western blot analysis confirmed that the THP-ΔPKR cells do not express any PKR protein (**Supplementary Figure S3**), and these cells exhibit normal cell proliferation and viability compared to control cells (**Supplementary Figure S1**). Importantly, we observed increased intracellular survival of Mtb in THP-ΔPKR macrophages compared to control macrophages as indicated by an 84% increase in luminescence signal (**Figure 4B**). This observation suggests that PKR expression is required to control Mtb survival in human macrophages, which is consistent but slightly different from the report by Wu et al. (2018), which showed that deletion of PKR does not affect Mtb burden in the mouse model. This data is also consistent with our hypothesis that increased production of PKR could lead to an enhanced anti-mycobacterial effect in macrophages.

We then examined whether THP-1 macrophages overexpressing PKR would be more effective at controlling intracellular Mtb survival. Since Mtb-infected THP-PKR macrophages produced higher levels of IFNγ (**Supplementary Figure S2A**) and IFNγ-stimulated genes (IP-10, **Figure 3B**), we also wanted to investigate whether PKR functions through an IFNγ-dependent mechanism. We thus performed bacterial survival assays in either mock-treated or IFNγ-treated THP-PKR and THP-Ø macrophages. At day 6 post-infection, the luminescence signal in the mock-treated condition was 79% lower in THP-PKR macrophages compared to THP-Ø macrophages (**Figure 4C**). In addition, treatment with IFNγ further reduced the intracellular survival of Mtb in THP-PKR macrophages, resulting in a decrease in luminescence of 89% at day 6 post-infection compared to THP-Ø macrophages (**Figure 4C**). Although IFNγ treatment is reported to reduce Mtb survival in mouse macrophages (Herbst et al., 2011), IFNγ treatment did not reduce Mtb survival in the THP-Ø control macrophages (**Figure 4C**). This may be explained by the fact that IFNγ reduces Mtb survival via nitric oxide (NO)-dependent apoptosis, but PMA-differentiated THP-1 macrophages are reported to have limited NO production (Daigneault et al., 2010; Herbst et al., 2011). Altogether, these findings suggest that the function of PKR to limit the survival of Mtb in macrophages could be enhanced by addition of IFNγ. This finding is consistent with the cytokine data demonstrating that THP-PKR macrophages produced significantly lower levels of IL-6 and IL-10 compared to THP-Ø macrophages (**Figures 3A,C**), which antagonize the macrophage activating effects of IFNγ (Gazzinelli et al., 1992; Nagabhushanam et al., 2003; Upadhyay et al., 2018).

Next, we wanted to determine the specific IFNγ-dependent mechanism responsible for the enhanced ability of PKR overexpressing macrophages to limit Mtb survival. Since IL-6 is reported to inhibit IFNγ-induced autophagy in Mtb-infected macrophages (Dutta et al., 2012), we hypothesized that autophagy could be the mechanism responsible for the reduced Mtb survival in THP-PKR macrophages. This hypothesis is also consistent with our observation that Mtb-infected THP-PKR macrophages

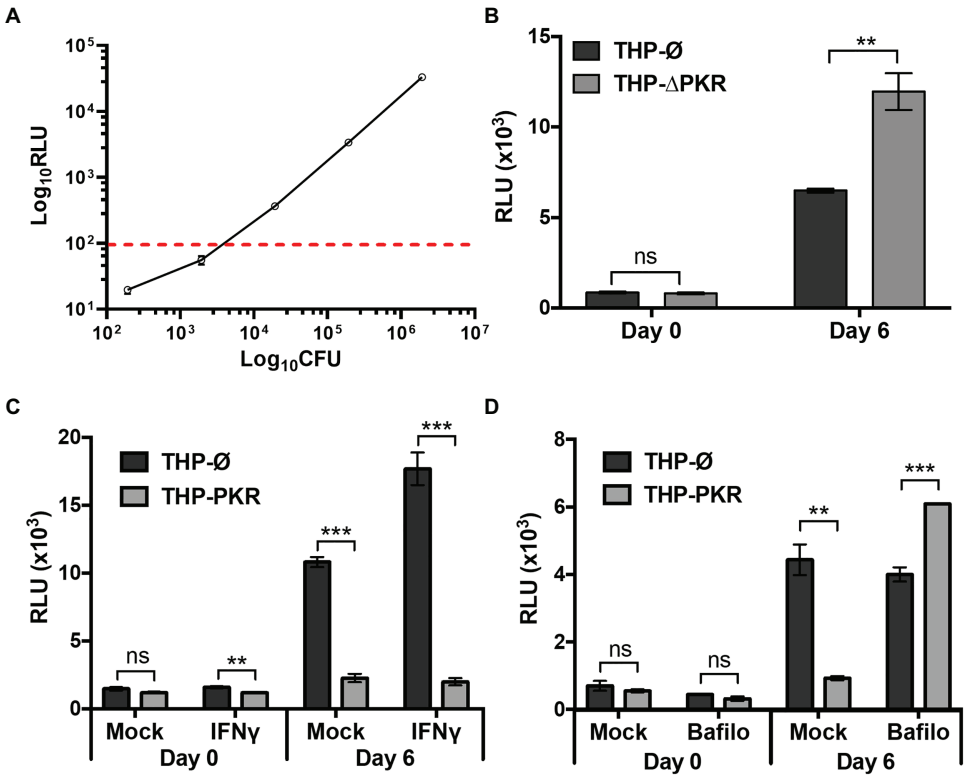

FIGURE 4 | PKR is required to control *M. tuberculosis* survival in macrophages. **(A)** Ten-fold serial dilutions of pre-determined Mtb-luciferase stocks were made in triplicate. The luciferase activity of the Mtb dilutions was measured using a microplate reader to detect luminescence. RLU, relative light units. The Mtb dilutions were also inoculated on agar plates and incubated at 37°C for 3 weeks prior to counting colony forming units (CFU). The dashed line indicates the sensitivity threshold for a linear relationship between CFU and RLU. **(B)** THP-Ø and THP-ΔPKR macrophages were infected with Mtb-luciferase at an MOI of 5. Cells were lysed at the indicated time post-infection and the resultant luminescence signal (RLU) was measured. **(C,D)** THP-Ø and THP-PKR macrophages were **(C)** mock-treated or pre-treated for 24 h with IFNγ (100 ng/ml), or **(D)** mock-treated or pre-treated for 1 h with bafilomycin A1 (12 nM) as indicated. Macrophages were infected as in **(B)** and lysed at the indicated time post-infection to measure RLU. IFNγ and bafilomycin A1 were maintained in the medium for the duration of the experiments and replenished every second day. Error bars represent mean ± SEM of three independent biological replicates. $^{**}p < 0.01$; and $^{***}p < 0.001$.

produced increased levels of IP-10 (**Figure 3B**), a chemokine linked to induction of autophagy (Chu et al., 2017). Furthermore, although the role of PKR in autophagy during bacterial infection has not yet been studied, PKR is reported to induce autophagy during viral (Tallóczy et al., 2006) and parasitic (Ogolla et al., 2013) infections. To investigate whether autophagy is the mechanism responsible for the reduced Mtb survival in THP-PKR macrophages, we examined the impact of bafilomycin A1 treatment on the bacterial survival in Mtb-infected macrophages. Bafilomycin A1 is a vacuolar H^+-ATPase inhibitor that blocks the autophagic flux by inhibiting lysosome acidification (Yamamoto et al., 1998). After determining a non-cytotoxic concentration of bafilomycin A1 (**Supplementary Figure S4**), we measured the intracellular survival of Mtb in mock-treated or bafilomycin A1-treated macrophages. Consistent with our previous bacterial survival assay (**Figure 4C**), mock-treated THP-PKR macrophages showed decreased intracellular Mtb survival, with a 79% decrease in luminescence signal compared to THP-Ø macrophages (**Figure 4D**). Importantly, treatment with bafilomycin A1 completely inhibited the ability of THP-PKR macrophages to limit Mtb survival. Indeed, bafilomycin A1-treated THP-PKR macrophages showed a 52% increase in luminescence signal compared to THP-Ø macrophages (**Figure 4D**) at day 6 post-infection. These data suggest selective autophagy as a potential mechanism responsible for the enhanced ability of THP-PKR macrophages to control intracellular Mtb replication. However, bafilomycin A1 also inhibits acidification of Mtb-containing phagosomes, a molecular pathway distinct from autophagy (Gutierrez et al., 2004). Therefore, we next sought to examine specific markers of autophagy activation to support this hypothesis.

PKR Expression Activates the Selective Autophagy Pathway in *Mycobacterium tuberculosis*-Infected Macrophages

To ascertain that autophagy is indeed the mechanism responsible for reduced Mtb survival in PKR overexpressing macrophages, we examined specific markers of selective autophagy. We compared protein expression levels of p62, phosphorylated p62 (p-S403 p62), and LC3-II in Mtb-infected macrophages treated with bafilomycin A1 (**Figure 5A**). LC3-II and p62 are well-characterized markers for selective autophagy (Klionsky et al., 2012).

LC3-II is extensively used to measure autophagic flux, which is the dynamic process of autophagy that takes into account autophagic degradation activity (Klionsky et al., 2012). It is necessary to use bafilomycin A1 to block the degradation of autophagy markers when performing western blot experiments to enable a true representation of the autophagic flux (Klionsky et al., 2012). An increase in LC3-II expression in bafilomycin A1-treated cells is thus associated with an increase in autophagy. Phosphorylation of serine 403 (p-S403) on p62 regulates selective autophagy through the recognition of ubiquitinated bacteria targeted for autophagic degradation (Matsumoto et al., 2011), and as such, increased levels of p-S403 p62 in bafilomycin A1-treated cells is also an indicator of increased autophagy. Western blot analysis revealed that during Mtb infection, bafilomycin A1-treated THP-PKR macrophages showed 3-fold higher expression levels of LC3-II and 2-fold higher expression of p-S403 p62 compared to THP-Ø macrophages (**Figures 5A,B**). Therefore, our western blot data suggest that THP-PKR macrophages have increased autophagy activation compared to control macrophages. However, since western blot analysis of cell lysates only measures bulk autophagy and not selective autophagy, we then used fluorescence microscopy to quantify the specific colocalization between intracellular Mtb and LC3. Immunofluorescence microscopy showed that PKR expression induced LC3 association with Mtb (**Figure 5C**). A significantly higher percentage of $LC3^+$ Mtb autophagosomes was observed in THP-PKR macrophages (12%) compared to control THP-Ø macrophages (8%; **Figure 5D**). We also performed fluorescence microscopy to quantify Mtb and LC3 colocalization in PKR knockout macrophages (**Supplementary Figure S5A**). A significantly lower percentage of $LC3^+$ Mtb autophagosomes was observed in THP-ΔPKR macrophages (3%) compared to control cells (6%; **Supplementary Figure S5B**), further supporting our conclusion that PKR expression is important for selective autophagy and limiting the survival of intracellular Mtb.

Although THP-PKR macrophages had a higher percentage of $LC3^+$ Mtb autophagosomes, it was important for us to determine the status of the autophagosomes, since Mtb inhibits autophagolysosome formation by blocking autophagosome fusion with lysosomes (Chandra et al., 2015). THP-Ø and THP-PKR macrophages were pre-loaded with dextran, a lysosome marker (Eissenberg and Goldman, 1988), prior to Mtb infection, and then immunofluorescence microscopy was performed. When specifically counting only Mtb autophagosomes, which are denoted as $LC3^+$ Mtb, we found a higher percentage of lysosome colocalization in THP-PKR macrophages (36%) compared to THP-Ø macrophages (12%; **Figures 5E,F**). This supports our hypothesis that sustained PKR expression enhances the activation of autophagy and promotes increased autophagolysosome fusion. Furthermore, the ability of PKR to increase autophagolysosome fusion explains the reduced bacterial survival observed in THP-PKR macrophages (**Figures 4C,D**). Importantly, there was no difference in the percentage of lysosome colocalization with LC3-negative Mtb, which are presumed to be located mostly in phagosomes, when comparing THP-PKR and THP-Ø macrophages (**Figure 5F**). This suggests that the effect of PKR overexpression is specific to the selective autophagy pathway and not the phagosome maturation pathway. Altogether, these findings demonstrate that PKR expression induces selective autophagy in Mtb-infected macrophages, thereby contributing to the reduced intracellular survival of Mtb.

Overexpression of PKR Does Not Alter Macrophage Cell Death Pathways or Phagocytosis

Our data indicate that sustained expression of PKR induces selective autophagy and reduces intracellular survival of Mtb. However, differences in intracellular bacterial survival between cell-lines can also be caused by changes in cell death or phagocytosis efficiency. Our cytokine profile revealed that THP-PKR macrophages had altered IL-1β and TNFα production compared to control macrophages (**Figures 3E,F**), cytokines that are positively correlated to macrophage cell death (Keane et al., 1997; Jayaraman et al., 2013). Furthermore, although the role of PKR in macrophage apoptosis during bacterial infection is unclear, it has been well-established to activate stress-induced apoptosis during viral infection or serum starvation (García et al., 2006). As such, we sought to rule-out any potential differences in cell death and phagocytosis between the cell-lines as the cause of the reduced bacterial survival in THP-PKR macrophages to further support our hypothesis that autophagy is the mechanism responsible for this effect. We first examined the impact of PKR expression on the apoptosis of Mtb-infected macrophages. At day 1 post-infection, there was no significant difference in apoptosis levels between THP-Ø and THP-PKR macrophages, as measured by Annexin V assays (**Figure 6A**). At day 3 post-infection, THP-PKR macrophages showed slightly lower levels of apoptosis (**Figure 6A**). However, uninfected THP-PKR macrophages also showed a minor decrease in baseline apoptosis compared to THP-Ø macrophages (**Figure 6A**). When accounting for this, there was no significant difference in fold-change in apoptosis of infected cells relative to uninfected cells when comparing THP-PKR and THP-Ø macrophages (**Figure 6B**). These results suggest that PKR expression does not induce apoptosis in Mtb-infected macrophages. However, PKR is also reported to induce other forms of cell death, including pyropotosis (Lu et al., 2012) and necroptosis (Thapa et al., 2013). To rule-out all types of cell death caused by modulating PKR, we measured overall cell death using the RTCA assay, a method that quantifies the viability of adherent cells over time (Limame et al., 2012). The RTCA system measures changes in impedance between electrodes at the bottom of E-well plates, which is then translated into a dimensionless value known as the CI. An increase in the CI reflects an increase in macrophage adherence (differentiation), whereas a decrease in the CI reflects the loss of macrophage viability as they detach from the bottom of the well (Schaaf et al., 2017). RTCA data revealed that there was no difference in cell death between Mtb-infected THP-Ø and THP-PKR macrophages over the course of infection (**Figure 6C**). Therefore, we concluded that overexpression of PKR does not affect cell death in Mtb-infected macrophages.

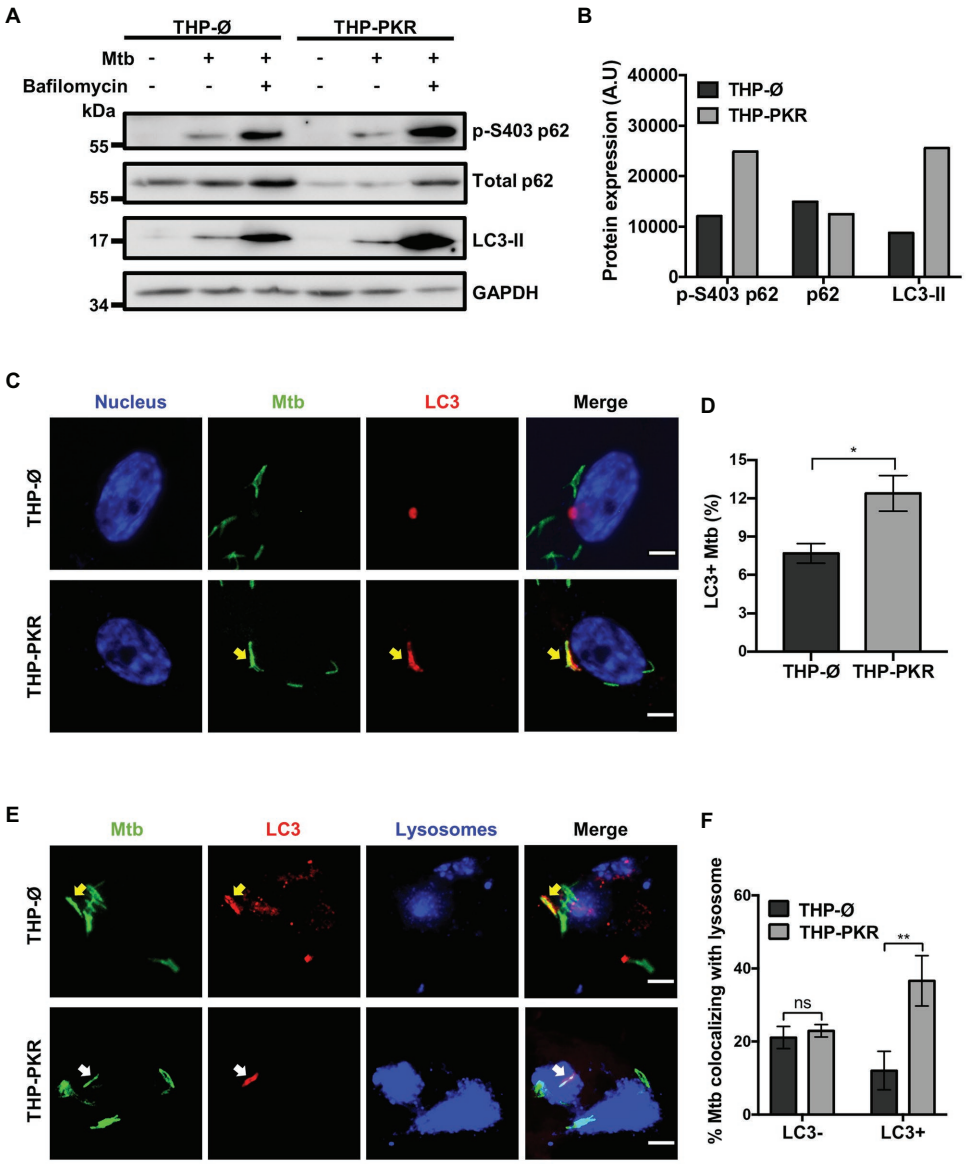

FIGURE 5 | PKR expression activates the autophagy pathway in *M. tuberculosis*-infected macrophages. **(A)** THP-Ø and THP-PKR macrophages were pre-treated with bafilomycin A1 (12 nM) for 1 h where indicated and then infected with Mtb at an MOI of 10. Bafilomycin A1 was maintained in the medium for the duration of the experiment. Cell lysates were prepared at 24 h post-infection and phosphorylated p62 (p-S403 p62), total p62, and LC3-II protein levels were analyzed by western blotting. **(B)** Densitometry analysis of the blot in **(A)** was performed by ImageJ to quantify p-S403 p62, total p62, and LC3-II band intensities in Mtb-infected, bafilomycin A1-treated macrophages as normalized to GAPDH. A.U, arbitrary units. **(C)** THP-Ø and THP-PKR macrophages were infected with Mtb-GFP at an MOI of 10. At 24 h post-infection, cells were fixed, permeabilized, and incubated with an anti-LC3 antibody to visualize autophagosomes. Representative images show nuclei (blue channel), Mtb (green channel), and LC3 (red channel) as detected by fluorescence microscopy. Yellow arrow denotes colocalization between Mtb and LC3. Scale bar, 5 μm. **(D)** Quantification of percent Mtb colocalization with LC3 ($LC3^+$Mtb) per total number of intracellular Mtb. A minimum of 20 visual fields, each with 15–30 infected cells, were counted per cell-line. **(E)** THP-Ø and THP-PKR macrophages were loaded with dextran (lysosome marker) for 24 h and then infected and treated as in **(C)**. Representative images show Mtb (green channel), LC3 (red channel), and lysosomes (blue channel) as detected by fluorescence microscopy. Yellow arrow denotes colocalization between Mtb and LC3, and white arrow denotes colocalization of Mtb with both LC3 and lysosomes. Scale bar, 5 μm. **(F)** Quantification of lysosome colocalization with LC3-negative or LC3-positive Mtb is reported as percentage over the total number of LC3-negative or LC3-positive intracellular Mtb, respectively. A minimum of 20 visual fields, each with 15–30 infected cells, were counted per cell-line. Data in **(D,F)** represent the mean ± SEM of all the analyzed visual fields. $^*p < 0.05$; $^{**}p < 0.01$.

Lastly, we wanted to ensure that the reduced bacterial survival observed in THP-PKR macrophages was not due to an altered ability to phagocytose Mtb. We infected THP-Ø and THP-PKR macrophages with Mtb expressing GFP for 4 h to allow for bacterial uptake. After 4 h, extensive washes were performed to remove extracellular bacteria and the macrophages were analyzed by flow cytometry to compare the level of phagocytosis using GFP as a marker for internalized Mtb. We observed no

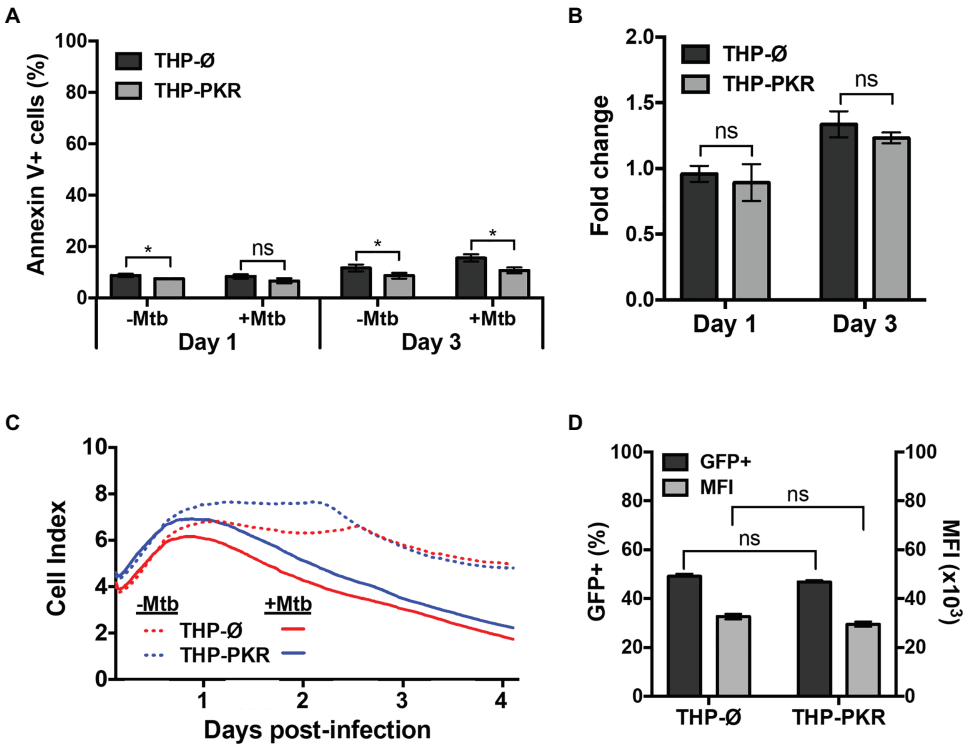

FIGURE 6 | Overexpression of PKR does not affect cell death or phagocytosis. **(A,B)** THP-Ø and THP-PKR macrophages were infected with Mtb at an MOI of 5. At the indicated time post-infection, cells were stained with Annexin V and analyzed by flow cytometry to measure **(A)** the percentage of apoptotic cells, and **(B)** the fold change in apoptosis relative to uninfected cells. **(C)** THP-Ø and THP-PKR macrophages were infected with Mtb at an MOI of 5 and changes in cell adherence were monitored by RTCA as indicated by the Cell Index (CI). CI (viability) was measured continuously for 96 h post-infection. **(D)** THP-Ø and THP-PKR macrophages were infected with Mtb-GFP at an MOI of 10. At 4 h post-infection, PBS washes were performed to remove the extracellular bacteria and the macrophages were analyzed by flow cytometry to quantify the level of phagocytosis using GFP as a marker for internalized Mtb. MFI, mean fluorescent intensity. Error bars indicate mean ± SEM of three independent biological replicates. *$p < 0.05$.

significant differences in the percentage of GFP-positive cells or in the numbers of Mtb per macrophage between the two cell-lines (**Figure 6D**). Therefore, we concluded that the reduced Mtb survival in THP-PKR macrophages is not due to an impact of PKR expression on the phagocytic ability of macrophages. Altogether, these data indicate that the reduced Mtb survival in THP-PKR macrophages is not due to an effect of PKR expression on cell death or phagocytosis, further supporting our hypothesis that autophagy is the predominant mechanism responsible for this effect.

Pharmacological Activation of Autophagy Enhances the Anti-mycobacterial Effect of PKR Overexpression

Since we observed that genetic upregulation of PKR can limit Mtb survival in macrophages by inducing selective autophagy, we then wanted to determine whether pharmacological activation of autophagy in PKR overexpression macrophages could enhance this effect. Rapamycin, an mTOR inhibitor (Kim and Guan, 2015), was used to pharmacologically activate autophagy. After selecting 50 nM as a non-cytotoxic dose of rapamycin (**Supplementary Figure S6**), a western blot was performed to verify that this concentration of rapamycin was sufficient to induce LC3-II expression (**Supplementary Figure S7**). We then measured the intracellular survival of Mtb in mock-treated or rapamycin-treated THP-Ø and THP-PKR macrophages (**Figure 7**). Interestingly, while mock-treated THP-PKR macrophages did not show a decrease in Mtb survival compared to THP-Ø macrophages at day 2 post-infection, rapamycin-treated THP-PKR macrophages showed a 45% reduction in luminescence relative to similarly treated THP-Ø macrophages (**Figure 7**). This result showed that rapamycin treatment accelerated and enhanced the effect of PKR overexpression on reducing intracellular Mtb survival. At day 4 post-infection, this effect was less pronounced, as the decrease in luminescence relative to THP-Ø macrophages was more comparable between rapamycin-treated THP-PKR macrophages (66%) and mock-treated THP-PKR macrophages (59%; **Figure 7**). This suggests that pharmacological activation of autophagy with rapamycin may only limit Mtb survival in the initial phase of infection. Overall, this proof-of-concept experiment supports our hypothesis that PKR functions to decrease Mtb survival through a mechanism dependent on activation of autophagy. Importantly, these findings also suggest that induction of PKR activation/expression in combination with autophagy activation could be a promising strategy for HDT against TB.

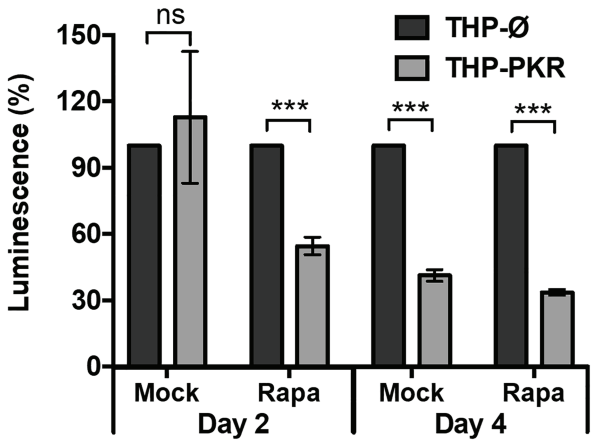

FIGURE 7 | Pharmacological activation of autophagy enhances the anti-mycobacterial effect of PKR overexpression. THP-1 macrophages were mock-treated or pre-treated with rapamycin (50 nM) for 1 h and then infected with Mtb-luciferase at an MOI of 5. Rapamycin was maintained in the medium for the duration of the experiment and replenished every second day. Infected macrophages were lysed at the indicated time post-infection and viable bacteria were determined by measuring the luminescence signal (RLU). RLU signals were normalized to THP-Ø as 100% and reported as % luminescence. Error bars indicate mean ± SEM of three independent biological replicates. ***$p < 0.001$.

DISCUSSION

There is an urgent need for the development of novel TB therapeutics due to the emergence of antibiotic-resistant Mtb strains. While PKR is established to enhance the macrophage response to viral infection (García et al., 2007), knowledge of its role during bacterial infections is surprisingly limited. Since PKR has been suggested as a potential target for HDT against TB infection (Wu et al., 2012; Tobin, 2015), we sought to investigate the role of PKR in the antibacterial response of Mtb-infected macrophages.

Herein, we provide evidence to suggest that PKR is a promising target for HDT. We show for the first time that PKR expression and activation is triggered by Mtb infection (**Figures 1A–F**). Our data reveal that PKR enhances the immunological profile of Mtb-infected macrophages by stimulating or inhibiting the production of autophagy-regulating proteins, IP-10, IL-10, and IL-6 (**Figures 3A–C**). Importantly, we show that PKR expression limits the intracellular survival of Mtb in macrophages through a mechanism dependent on the activation of selective autophagy (**Figures 4, 5**). A screen of differentially expressed genes in macrophages led Wu et al. (2012) to explore PKR as a potential target for HDT against TB. However, this group investigated the effects of PKR deletion rather than activation, since PKR deletion leaves mice in good health and shows limited or no phenotype upon challenge with certain viruses (Nakayama et al., 2010). While Wu et al. (2012) initially reported that PKR deletion in mice decreases Mtb burden in the lungs, there was a discrepancy between the genetic backgrounds of the mutant and control mice used in the study (Wu et al., 2018). Indeed, their follow-up study using mutant and control mice from the same genetic background revealed that deletion of PKR has no effect on Mtb burden (Mundhra et al., 2018; Wu et al., 2018). This could be due to a redundant role of PKR, since three other EIF2α kinases exist. Indeed, one group showed that EIF2α is still phosphorylated after PKR deletion, albeit to a lesser extent (Zhang and Samuel, 2007). Furthermore, while PKR is reported to induce NF-κB activation (Kumar et al., 1994) – a transcription factor that plays a key role in controlling bacterial load in granulomas during Mtb infection (Fallahi-Sichani et al., 2012) – PKR knockdown did not significantly alter NF-κB activation in response to treatment with TNFα or dsRNA (Zhang and Samuel, 2007). Altogether, these findings suggest that one or more of the other known EIF2α kinases may compensate for the loss of PKR, which could explain why Wu and colleagues did not observe an effect of PKR deletion on Mtb burden. In the human THP-1 macrophage model, we observed that PKR deletion increased the intracellular survival of Mtb (**Figure 4B**). Based on these results, we speculated that increased PKR expression and activation could instead produce a pro-host effect to reduce intracellular Mtb survival. Since pharmacological activation of PKR has been shown to be well-tolerated in mice (López-Cara et al., 2011), and given that PKR is reported to play a role in the innate immune response to viral and parasitic infection (Tallóczy et al., 2006; Ogolla et al., 2013), we decided it was worthwhile to investigate PKR overexpression as a strategy for TB HDT. Importantly, our findings show that macrophages overexpressing PKR have significantly lower Mtb burden compared to control cells, suggesting that PKR is indeed a promising target for novel TB therapeutics (**Figures 4C,D**).

Our data showing an antibacterial effect for PKR is consistent with a previous report that PKR is required for the production of anti-mycobacterial cytokines in response to Bacillus Calmette-Guérin (BCG) infection (Cheung et al., 2005), a live attenuated mycobacterium used for tuberculosis vaccination. While Cheung et al. (2005) observed that PKR inhibition by a pharmacological compound or by the transfection of a transdominant negative PKR mutant decreases production of IL-6, IL-10, and TNFα during BCG infection, we report that PKR overexpression decreases the production of these cytokines during Mtb infection. This discrepancy in findings is likely due to the strain of mycobacteria used, since Mtb is capable of escaping to the macrophage cytosol to trigger the cytosolic surveillance and the induction of autophagy (Watson et al., 2012), whereas BCG is known to be incapable of escaping the phagosome (Simeone et al., 2012). In addition, Cheung and colleagues used macrophage precursors, human $CD14^+$ blood monocytes, and promonocytic U937 cells, whereas we used primary human monocyte-derived macrophages and differentiated THP-1 macrophages. Cheung et al. (2005) suggest that the effect of PKR on anti-BCG cytokine production is due to downstream activation of NF-κB, since pharmacological inhibition of NF-κB lowered the production of IL-6, IL-,10, and TNFα in response to BCG infection, and treatment with 2-aminopurine (2-AP), a pharmacological inhibitor of PKR, prevented NF-κB activation. However, it is noteworthy that 2-AP has been shown to inhibit

other kinases (Posti et al., 1999). Importantly, another group reported that genetic knockdown of PKR did not cause a difference in NF-κB activation compared to control cells (Zhang and Samuel, 2007). This suggests that the effect of 2-AP treatment on NF-κB inhibition observed by Cheung and colleagues may be due to PKR-independent effects of the compound. Further investigation is required to identify the mechanisms responsible for the impact of PKR on anti-mycobacterial cytokine production. Our observation that Mtb-infected macrophages overexpressing PKR have reduced IL-1β (**Figure 3E**) and TNFα (**Figure 3F**) production was also unexpected, since these cytokines are reported to assist in Mtb clearance (Flynn et al., 1995; Keane et al., 1997; Mayer-Barber et al., 2010; Jayaraman et al., 2013), yet PKR overexpressing macrophages showed reduced bacterial survival despite lower production of these cytokines. However, Mtb-infected PKR overexpressing macrophages also produced lower amounts of TGFβ and IL-10, two anti-inflammatory cytokines that function to counteract the effects of TNFα and IL-1β (Othieno et al., 1999). As such, it is possible that PKR overexpressing macrophages require a lower threshold of TNFα and IL-1β to prevent hyper-inflammation.

Our data suggest a new role for PKR in regulation of selective autophagy in response to intracellular bacterial infection. Western blot analysis of autophagy markers and immunofluorescence microscopy analysis of LC3 and lysosome colocalization with Mtb revealed that PKR expression induces selective autophagy of Mtb (**Figures 5A–F**). Inhibition of autophagy also reversed the effects of PKR overexpression on intracellular Mtb survival (**Figure 4D**). These findings are consistent with previous reports that PKR induces LC3-associated autophagy of *Toxoplasm gondii* (Ogolla et al., 2013) and is required for autophagic degradation of HSV-1 (Tallóczy et al., 2006). Given the key role that IFNγ plays in induction of macrophage autophagy (Gutierrez et al., 2004), and considering that IL-6 inhibits IFNγ-induced autophagy (Dutta et al., 2012), we speculate that the increased activation of autophagy observed in PKR overexpressing macrophages is due, at least in part, to decreased production of IL-6 and increased production of IP-10 and IFNγ by these cells. Consistent with this, we observed that addition of IFNγ enhanced the ability of THP-PKR macrophages to limit the intracellular survival of Mtb (**Figure 4C**). IFNγ activates autophagy by inducing phosphorylation of mitogen activated protein kinases (MAPK), whereas IL-6 inhibits MAPK phosphorylation to block IFNγ-induced autophagy (Dutta et al., 2012). Interestingly, PKR has been shown to be important for MAPK activation during BCG infection (Cheung et al., 2005) and is also reported to activate MAPK in response to viral infection (Zhang et al., 2009) and stress stimuli (Goh, 2000). As such, it is possible that the induction of autophagy in PKR overexpressing macrophages is dependent on a mechanism involving MAPK activation, whether by a direct effect of PKR on MAPK activation and/or an indirect effect from increased IFNγ production and decreased IL-6 production by PKR overexpressing macrophages.

Collectively, our findings suggest that PKR is a promising target for HDT against TB infection. Since autophagy induction is frequently proposed as an HDT strategy for TB and PKR was observed to induce selective autophagy, we examined whether pharmacological activation of autophagy in combination with PKR overexpression/activation would enhance the antibacterial effect of PKR. Importantly, we observed that rapamycin treatment accelerated and enhanced the decrease in intracellular Mtb survival observed in PKR overexpressing macrophages relative to control cells (**Figure 7**). This suggests that combination therapy with pharmacological activators of both autophagy and PKR could be a successful strategy for HDT against TB. Although DHBDC is a pharmacological activator of PKR currently available for research use, this compound is not specific since it also activates Protein Kinase R Like Protein (PERK; Bai et al., 2013). Therefore, a search for more specific pharmacological activators of PKR would be desirable. The efficacy of such PKR activators should also be assessed in combination with autophagy activators on Mtb survival both *in vitro* and in mouse models. Furthermore, it will be interesting to ascertain whether the findings in this study extend to other pathogenic intracellular bacteria given that PKR was also highly upregulated in *S. Typhimurium*-infected and *L. monocytogenes*-infected macrophages (**Figure 1G**).

DATA AVAILABILITY STATEMENT

The original contributions presented in the study are included in the article/**Supplementary Material**, further inquiries can be directed to the corresponding author.

ETHICS STATEMENT

The studies involving human participants were reviewed and approved by Ottawa Health Science Network Research Ethics Board. The patients/participants provided their written informed consent to participate in this study.

AUTHOR CONTRIBUTIONS

RS and JS conceived and designed experiments, analyzed data, and wrote and edited the manuscript. RS, SB, NR, and TC performed experiments. All authors contributed to the article and approved the submitted version.

FUNDING

This research was supported by the Canadian Institutes for Health Research (CIHR) PJT-162424, the National Sanitarium Association Scholar's Program, the Lung Health Foundation Team Breathe/Pfizer Canada Research Awards (formerly known as an Ontario Lung Association Grant-in-Aid/Pfizer Canada Research Award), and the University of Ottawa Seed Funding Opportunity to JS. RS was supported by the Ontario Graduate Scholarship program. NR was supported by the Canada Graduate Scholarship (NSERC-M and NSERC-PGS-D). TC was supported

by a summer scholarship from the University of Ottawa, Centre for Infection, Immunity and Inflammation.

ACKNOWLEDGMENTS

We thank Dr. William Jacobs for kindly providing *M. tuberculosis* mc^{2}6206, Dr. Subash Sad for providing the *Salmonella Typhimurium* and *Listeria monocytogenes* bacterial strains, and Dr. Zakaria Hmama for the generous gift of the pSMT3 luciferase plasmid. We thank the support staff at the University of Ottawa Common Equipment and Technical Service Core and the Cell Biology and Image Acquisition Core for their technical assistance.

SUPPLEMENTARY MATERIAL

The Supplementary Material for this article can be found online at: https://www.frontiersin.org/articles/10.3389/fmicb.2020.613963/full#supplementary-material

REFERENCES

Andreu, N., Zelmer, A., Fletcher, T., Elkington, P. T., Ward, T. H., Ripoll, J., et al. (2010). Optimisation of bioluminescent reporters for use with mycobacteria. *PLoS One* 5:e10777. doi: 10.1371/journal.pone.0010777

Bai, H., Chen, T., Ming, J., Sun, H., Cao, P., and Fusco, D. N., et al. (2013). Dual activators of protein kinase r (PKR) and protein kinase R-like kinase (PERK) identify common and divergent catalytic targets. *Chembiochem* 14, 1255–1262. doi: 10.1002/cbic.201300177

Behar, S. M., Divangahi, M., and Remold, H. G. (2010). Evasion of innate immunity by *Mycobacterium tuberculosis*: is death an exit strategy? *Nat. Rev. Microbiol.* 8, 668–674. doi: 10.1038/nrmicro2387

Bustin, S. A., Benes, V., Garson, J. A., Hellemans, J., Huggett, J., Kubista, M., et al. (2009). The MIQE guidelines: minimum information for publication of quantitative real-time PCR experiments. *Clin. Chem.* 55, 611–622. doi: 10.1373/clinchem.2008.112797

Chandra, P., Ghanwat, S., Matta, S. K., Yadav, S. S., Mehta, M., Siddiqui, Z., et al. (2015). *Mycobacterium tuberculosis* inhibits RAB7 recruitment to selectively modulate autophagy flux in macrophages. *Sci. Rep.* 5:16320. doi: 10.1038/srep16320

Chen, B., Gilbert, L. A., Cimini, B. A., Schnitzbauer, J., Zhang, W., Li, G. W., et al. (2013). Dynamic imaging of genomic loci in living human cells by an optimized CRISPR/Cas system. *Cell* 155, 1479–1491. doi: 10.1016/j.cell.2013.12.001

Cheung, B. K. W., Lee, D. C. W., Li, J. C. B., Lau, Y. -L., and Lau, A. S. Y. (2005). A role for double-stranded RNA-activated protein kinase PKR in *Mycobacterium*-induced cytokine expression. *J. Immunol.* 175, 7218–7225. doi: 10.4049/jimmunol.175.11.7218

Chu, L. Y., Hsueh, Y. C., Cheng, H. L., and Wu, K. K. (2017). Cytokine-induced autophagy promotes long-term VCAM-1 but not ICAM-1 expression by degrading late-phase IκBα. *Sci. Rep.* 7:12472. doi: 10.1038/s41598-017-12641-8

Daigneault, M., Preston, J. A., Marriott, H. M., Whyte, M. K. B., and Dockrell, D. H. (2010). The identification of markers of macrophage differentiation in PMA-stimulated THP-1 cells and monocyte-derived macrophages. *PLoS One* 5:e8668. doi: 10.1371/journal.pone.0008668

Dey, M., Cao, C., Dar, A. C., Tamura, T., Ozato, K., Sicheri, F., et al. (2005). Mechanistic link between PKR dimerization, autophosphorylation, and eIF2α substrate recognition. *Cell* 122, 901–913. doi: 10.1016/j.cell.2005.06.041

Dutta, R. K., Kathania, M., Raje, M., and Majumdar, S. (2012). IL-6 inhibits IFN-γ induced autophagy in *Mycobacterium tuberculosis* H37Rv infected macrophages. *Int. J. Biochem. Cell Biol.* 44, 942–954. doi: 10.1016/j.biocel.2012.02.021

Early, J. V., Mullen, S., and Parish, T. (2019). A rapid, low pH, nutrient stress, assay to determine the bactericidal activity of compounds against non-replicating *Mycobacterium tuberculosis*. *PLoS One* 14:e0222970. doi: 10.1371/journal.pone.0222970

Eissenberg, L. G., and Goldman, W. E. (1988). Fusion of lysosomes with phagosomes containing *Histoplasma capsulatum*: use of fluoresceinated dextran. *Adv. Exp. Med. Biol.* 239, 53–61. doi: 10.1007/978-1-4757-5421-6_6

Fallahi-Sichani, M., Kirschner, D. E., and Linderman, J. J. (2012). NF-κB signaling dynamics play a key role in infection control in tuberculosis. *Front. Physiol.* 3:170. doi: 10.3389/fphys.2012.00170

Flynn, J. A. L., Chan, J., Triebold, K. J., Dalton, D. K., Stewart, T. A., and Bloom, B. R. (1993). An essential role for interferon γ in resistance to *Mycobacterium tuberculosis* infection. *J. Exp. Med.* 178, 2249–2254. doi: 10.1084/jem.178.6.2249

Flynn, J. A. L., Goldstein, M. M., Chan, J., Triebold, K. J., Pfeffer, K., Lowenstein, C. J., et al. (1995). Tumor necrosis factor-α is required in the protective immune response against *Mycobacterium tuberculosis* in mice. *Immunity* 2, 561–572. doi: 10.1016/1074-7613(95)90001-2

García, M. A., Gil, J., Ventoso, I., Guerra, S., Domingo, E., Rivas, C., et al. (2006). Impact of protein kinase PKR in cell biology: from antiviral to antiproliferative action. *Microbiol. Mol. Biol. Rev.* 70, 1032–1060. doi: 10.1128/MMBR.00027-06

García, M. A., Meurs, E. F., and Esteban, M. (2007). The dsRNA protein kinase PKR: virus and cell control. *Biochimie* 89, 799–811. doi: 10.1016/j.biochi.2007.03.001

Gazzinelli, R. T., Oswald, I. P., James, S. L., and Sher, A. (1992). IL-10 inhibits parasite killing and nitrogen oxide production by IFN-gamma-activated macrophages. *J. Immunol.* 148, 1792–1796.

Goh, K. C. (2000). The protein kinase PKR is required for p38 MAPK activation and the innate immune response to bacterial endotoxin. *EMBO J.* 19, 4292–4297. doi: 10.1093/emboj/19.16.4292

Gutierrez, M. G., Master, S. S., Singh, S. B., Taylor, G. A., Colombo, M. I., and Deretic, V. (2004). Autophagy is a defense mechanism inhibiting BCG and *Mycobacterium tuberculosis* survival in infected macrophages. *Cell* 119, 753–766. doi: 10.1016/j.cell.2004.11.038

Herbst, S., Schaible, U. E., and Schneider, B. E. (2011). Interferon gamma activated macrophages kill mycobacteria by nitric oxide induced apoptosis. *PLoS One* 6:e19105. doi: 10.1371/journal.pone.0019105

Jain, P., Hsu, T., Arai, M., Biermann, K., Thaler, D. S., Nguyen, A., et al. (2014). Specialized transduction designed for precise high-throughput unmarked deletions in *Mycobacterium tuberculosis*. *mBio* 5, e01245–e01214. doi: 10.1128/mBio.01245-14

Jayaraman, P., Sada-Ovalle, I., Nishimura, T., Anderson, A. C., Kuchroo, V. K., Remold, H. G., et al. (2013). IL-1β promotes antimicrobial immunity in macrophages by regulating TNFR signaling and caspase-3 activation. *J. Immunol.* 190, 4196–4204. doi: 10.4049/jimmunol.1202688

Keane, J., Balcewicz-Sablinska, M. K., Remold, H. G., Chupp, G. L., Meek, B. B., Fenton, M. J., et al. (1997). Infection by *Mycobacterium tuberculosis* promotes human alveolar macrophage apoptosis. *Infect. Immun.* 65, 298–304. doi: 10.1128/iai.65.1.298-304.1997

Kim, Y. C., and Guan, K. L. (2015). MTOR: a pharmacologic target for autophagy regulation. *J. Clin. Invest.* 125, 25–32. doi: 10.1172/JCI73939

Kim, J. J., Lee, H. M., Shin, D. M., Kim, W., Yuk, J. M., Jin, H. S., et al. (2012). Host cell autophagy activated by antibiotics is required for their effective antimycobacterial drug action. *Cell Host Microbe* 11, 457–468. doi: 10.1016/j.chom.2012.03.008

Klionsky, D. J., Abdalla, F. C., Abeliovich, H., Abraham, R. T., Acevedo-Arozena, A., Adeli, K., et al. (2012). Guidelines for the use and interpretation of assays for monitoring autophagy. *Autophagy* 8, 445–544. doi: 10.4161/auto.19496

Kumar, A., Haque, J., Lacoste, J., Hiscott, J., and Williams, B. R. G. (1994). Double-stranded RNA-dependent protein kinase activates transcription factor NF-κB by phosphorylating IκB. *Proc. Natl. Acad. Sci. U. S. A.* 91, 6288–6292. doi: 10.1073/pnas.91.14.6288

Limame, R., Wouters, A., Pauwels, B., Fransen, E., Peeters, M., Lardon, F., et al. (2012). Comparative analysis of dynamic ell viability, migration and

invasion assessments by novel real-time technology and classic endpoint sssays. *PLoS One* 7:e46536. doi: 10.1371/journal.pone.0046536

Livak, K. J., and Schmittgen, T. D. (2001). Analysis of relative gene expression data using real-time quantitative PCR and the $2^{-\Delta\Delta CT}$ method. *Methods* 25, 402–408. doi: 10.1006/meth.2001.1262

López-Cara, L. C., Conejo-García, A., Marchal, J. A., MacChione, G., Cruz-López, O., Boulaiz, H., et al. (2011). New (RS)-benzoxazepin-purines with antitumour activity: the chiral switch from (RS)-2,6-dichloro-9-[1-(p-nitrobenzenesulfonyl)-1,2,3,5-tetrahydro-4,1- benzoxazepin-3-yl]-9H-purine. *Eur. J. Med. Chem.* 46, 249–258. doi: 10.1016/j.ejmech.2010.11.011

Lu, B., Nakamura, T., Inouye, K., Li, J., Tang, Y., Lundbäck, P., et al. (2012). Novel role of PKR in inflammasome activation and HMGB1 release. *Nature* 488, 670–674. doi: 10.1038/nature11290

Matsumoto, G., Wada, K., Okuno, M., Kurosawa, M., and Nukina, N. (2011). Serine 403 phosphorylation of p62/SQSTM1 regulates selective autophagic clearance of ubiquitinated proteins. *Mol. Cell* 44, 279–289. doi: 10.1016/j.molcel.2011.07.039

Mayer-Barber, K. D., Barber, D. L., Shenderov, K., White, S. D., Wilson, M. S., Cheever, A., et al. (2010). Cutting edge: Caspase-1 independent IL-1β production is critical for host resistance to *Mycobacterium tuberculosis* and does not require TLR signaling in vivo. *J. Immunol.* 184, 3326–3330. doi: 10.4049/jimmunol.0904189

Morrison, J., Pai, M., and Hopewell, P. C. (2008). Tuberculosis and latent tuberculosis infection in close contacts of people with pulmonary tuberculosis in low-income and middle-income countries: a systematic review and meta-analysis. *Lancet Infect. Dis.* 8, 359–368. doi: 10.1016/S1473-3099(08)70071-9

Mouton, J. M., Heunis, T., Dippenaar, A., Gallant, J. L., Kleynhans, L., and Sampson, S. L. (2019). Comprehensive characterization of the attenuated double auxotroph *Mycobacterium tuberculosisΔleudΔpanCD* as an alternative to h37Rv. *Front. Microbiol.* 10:1922. doi: 10.3389/fmicb.2019.01922

Mundhra, S., Bryk, R., Hawryluk, N., Zhang, T., Jiang, X., and Nathan, C. F. (2018). Evidence for dispensability of protein kinase R in host control of tuberculosis. *Eur. J. Immunol.* 48, 612–620. doi: 10.1002/eji.201747180

Nagabhushanam, V., Solache, A., Ting, L. -M., Escaron, C. J., Zhang, J. Y., and Ernst, J. D. (2003). Innate inhibition of adaptive immunity: *Mycobacterium tuberculosis*-induced IL-6 inhibits macrophage responses to IFN-γ. *J. Immunol.* 171, 4750–4757. doi: 10.4049/jimmunol.171.9.4750

Nakagawa, I., Amano, A., Mizushima, N., Yamamoto, A., Yamaguchi, H., Kamimoto, T., et al. (2004). Autophagy defends cells against invading group A *Streptococcus*. *Science* 306, 1037–1040. doi: 10.1126/science.1103966

Nakayama, Y., Plisch, E. H., Sullivan, J., Thomas, C., Czuprynski, C. J., Williams, B. R. G., et al. (2010). Role of PKR and type I IFNs in viral control during primary and secondary infection. *PLoS Pathog.* 6:1000966. doi: 10.1371/journal.ppat.1000966

Ogolla, P. S., Portillo, J. -A. C., White, C. L., Patel, K., Lamb, B., Sen, G. C., et al. (2013). The protein kinase double-stranded RNA-dependent (PKR) enhances protection against disease caused by a non-viral pathogen. *PLoS Pathog.* 9:e1003557. doi: 10.1371/journal.ppat.1003557

Othieno, C., Hirsch, C. S., Hamilton, B. D., Wilkinson, K., Ellner, J. J., and Toossi, Z. (1999). Interaction of *Mycobacterium tuberculosis*-induced transforming growth factor β1 and interleukin-10. *Infect. Immun.* 67, 5730–5735. doi: 10.1128/IAI.67.11.5730-5735.1999

Ozeki, Y., Igarashi, M., Doe, M., Tamaru, A., Kinoshita, N., Ogura, Y., et al. (2015). A new screen for tuberculosis drug candidates utilizing a luciferase-expressing recombinant *Mycobacterium bovis* Bacillus Calmette-Guéren. *PLoS One* 10:e0141658. doi: 10.1371/journal.pone.0141658

Paik, S., Kim, J. K., Chung, C., and Jo, E. -K. (2019). Autophagy: a new strategy for host-directed therapy of tuberculosis. *Virulence* 10, 448–459. doi: 10.1080/21505594.2018.1536598

Palucci, I., Battah, B., Salustri, A., De Maio, F., Petrone, L., Ciccosanti, F., et al. (2019). IP-10 contributes to the inhibition of mycobacterial growth in an ex vivo whole blood assay. *Int. J. Med. Microbiol.* 309, 299–306. doi: 10.1016/j.ijmm.2019.05.005

Posti, K., Leinonen, S., Tetri, S., Kottari, S., Viitala, P., Pelkonen, O., et al. (1999). Modulation of murine phenobarbital-inducible CYP2A5, CYP2B10 and CYP1A enzymes by inhibitors of protein kinases and phosphatases. *Eur. J. Biochem.* 264, 19–26. doi: 10.1046/j.1432-1327.1999.00539.x

Sanjana, N. E., Shalem, O., and Zhang, F. (2014). Improved vectors and genome-wide libraries for CRISPR screening. *Nat. Methods* 11, 783–784. doi: 10.1038/nmeth.3047

Schaaf, K., Hayley, V., Speer, A., Wolschendorf, F., Niederweis, M., Kutsch, O., et al. (2016). A macrophage infection model to predict drug efficacy against *Mycobacterium tuberculosis*. *Assay Drug Dev. Technol.* 14, 345–354. doi: 10.1089/adt.2016.717

Schaaf, K., Smith, S. R., Duverger, A., Wagner, F., Wolschendorf, F., Westfall, A. O., et al. (2017). *Mycobacterium tuberculosis* exploits the PPM1A signaling pathway to block host macrophage apoptosis. *Sci. Rep.* 7:42101. doi: 10.1038/srep42101

Sharma, S., Gelman, E., Narayan, C., Bhattacharjee, D., Achar, V., Humnabadkar, V., et al. (2014). Simple and rapid method to determine antimycobacterial potency of compounds by using autoluminescent *Mycobacterium tuberculosis*. *Antimicrob. Agents Chemother.* 58, 5801–5808. doi: 10.1128/AAC.03205-14

Simeone, R., Bobard, A., Lippmann, J., Bitter, W., Majlessi, L., Brosch, R., et al. (2012). Phagosomal rupture by *Mycobacterium tuberculosis* results in toxicity and host cell death. *PLoS Pathog.* 8:e1002507. doi: 10.1371/journal.ppat.1002507

Singh, S. B., Davis, A. S., Taylor, G. A., and Deretic, V. (2006). Human IRGM induces autophagy to eliminate intracellular mycobacteria. *Science* 313, 1438–1441. doi: 10.1126/science.1129577

Sorrentino, F., Del Rio, R. G., Zheng, X., Matilla, J. P., Gomez, P. T., Hoyos, M. M., et al. (2016). Development of an intracellular screen for new compounds able to inhibit *Mycobacterium tuberculosis* growth in human macrophages. *Antimicrob. Agents Chemother.* 60, 640–645. doi: 10.1128/AAC.01920-15

Sun, J., Lau, A., Wang, X., Liao, T. Y. A., Zoubeidi, A., and Hmama, Z. (2009). A broad-range of recombination cloning vectors in mycobacteria. *Plasmid* 62, 158–165. doi: 10.1016/j.plasmid.2009.07.003

Sun, J., Schaaf, K., Duverger, A., Wolschendorf, F., Speer, A., Wagner, F., et al. (2016). Protein phosphatase, Mg^{2+}/Mn^{2+}-dependent 1A controls the innate antiviral and antibacterial response of macrophages during HIV-1 and *Mycobacterium tuberculosis* infection. *Oncotarget* 7, 15394–15409. doi: 10.18632/oncotarget.8190

Tallóczy, Z., Virgin, H. W. IV, and Levine, B. (2006). PKR-dependent autophagic degradation of herpes simplex virus type 1. *Autophagy* 2, 24–29. doi: 10.4161/auto.2176

Thapa, R. J., Nogusa, S., Chen, P., Maki, J. L., Lerro, A., and Andrake, M., et al. (2013). Interferon-induced RIP1/RIP3-mediated necrosis requires PKR and is licensed by FADD and caspases. *Proc. Natl. Acad. Sci. U. S. A.* 110:E3109. doi: 10.1073/pnas.1301218110

Tobin, D. M. (2015). Host-directed therapies for tuberculosis. *Cold Spring Harb. Perspect. Med.* 5:a021196. doi: 10.1101/cshperspect.a021196

Upadhyay, R., Sanchez-Hidalgo, A., Wilusz, C. J., Lenaerts, A. J., Arab, J., Yeh, J., et al. (2018). Host directed therapy for chronic tuberculosis via intrapulmonary delivery of aerosolized peptide inhibitors targeting the IL-10-STAT3 pathway. *Sci. Rep.* 8:16610. doi: 10.1038/s41598-018-35023-0

Watson, R. O., Manzanillo, P. S., and Cox, J. S. (2012). Extracellular *M. tuberculosis* DNA targets bacteria for autophagy by activating the host DNA-sensing pathway. *Cell* 150, 803–815. doi: 10.1016/j.cell.2012.06.040

WHO (2020). *Global tuberculosis report 2019*. Geneva: World Health Organization.

Wu, K., Koo, J., Jiang, X., Chen, R., Cohen, S. N., and Nathan, C. (2012). Improved control of tuberculosis and activation of macrophages in mice lacking protein kinase R. *PLoS One* 7:e30512. doi: 10.1371/journal.pone.0030512

Wu, K., Koo, J., Jiang, X., Chen, R., Cohen, S. N., and Nathan, C. (2018). Correction: improved control of tuberculosis and activation of macrophages in mice lacking protein kinase R. *PLoS One* 13:e0205424. doi: 10.1371/journal.pone.0205424

Yamamoto, A., Tagawa, Y., Yoshimori, T., Moriyama, Y., Masaki, R., and Tashiro, Y. (1998). Bafilomycin A1 prevents maturation of autophagic vacuoles by inhibiting fusion between autophagosomes and lysosomes in rat hepatoma cell line, H-4-II-E cells. *Cell Struct. Funct.* 23, 33–42. doi: 10.1247/csf.23.33

Zhang, P., Langland, J. O., Jacobs, B. L., and Samuel, C. E. (2009). Protein kinase PKR-dependent activation of mitogen-activated protein kinases occurs through mitochondrial adapter IPS-1 and is antagonized by vaccinia virus E3L. *J. Virol.* 83, 5718–5725. doi: 10.1128/jvi.00224-09

Zhang, F., Romano, P. R., Nagamura-Inoue, T., Tian, B., Dever, T. E., Mathews, M. B., et al. (2001). Binding of double-stranded RNA to protein kinase PKR is

required for dimerization and promotes critical autophosphorylation events in the activation loop. *J. Biol. Chem.* 276, 24946–24958. doi: 10.1074/jbc.M102108200

Zhang, P., and Samuel, C. E. (2007). Protein kinase PKR plays a stimulus- and virus-dependent role in apoptotic death and virus multiplication in human cells. *J. Virol.* 81, 8192–8200. doi: 10.1128/jvi.00426-07

Zhang, Q., Sun, J., Wang, Y., He, W., Wang, L., Zheng, Y., et al. (2017). Antimycobacterial and anti-inflammatory mechanisms of baicalin via induced autophagy in macrophages infected with *Mycobacterium tuberculosis*. *Front. Microbiol.* 8:2142. doi: 10.3389/fmicb.2017.02142

Conflict of Interest: The authors declare that the research was conducted in the absence of any commercial or financial relationships that could be construed as a potential conflict of interest.

frontiers in Microbiology

MINI REVIEW
published: 26 January 2021
doi: 10.3389/fmicb.2020.634640

The Prospective Synergy of Antitubercular Drugs With NAD Biosynthesis Inhibitors

Kyle H. Rohde[1] *and Leonardo Sorci*[2]*

[1]*Burnett School of Biomedical Sciences, College of Medicine, University of Central Florida, Orlando, FL, United States,* [2]*Division of Bioinformatics and Biochemistry, Department of Materials, Environmental Sciences and Urban Planning, Polytechnic University of Marche, Ancona, Italy*

Given the upsurge of drug-resistant tuberculosis worldwide, there is much focus on developing novel drug combinations allowing shorter treatment duration and a lower toxicity profile. Nicotinamide adenine dinucleotide (NAD) biosynthesis targeting is acknowledged as a promising strategy to combat drug-susceptible, drug-resistant, and latent tuberculosis (TB) infections. In this review, we describe the potential synergy of NAD biosynthesis inhibitors with several TB-drugs in prospective novel combination therapy. Despite not directly targeting the essential NAD cofactor's biosynthesis, several TB prodrugs either require a NAD biosynthesis enzyme to be activated or form a toxic chemical adduct with NAD(H) itself. For example, pyrazinamide requires the action of nicotinamidase (PncA), often referred to as pyrazinamidase, to be converted into its active form. PncA is an essential player in NAD salvage and recycling. Since most pyrazinamide-resistant strains are PncA-defective, a combination with downstream NAD-blocking molecules may enhance pyrazinamide activity and possibly overcome the resistance mechanism. Isoniazid, ethionamide, and delamanid form NAD adducts in their active form, partly perturbing the redox cofactor metabolism. Indeed, NAD depletion has been observed in *Mycobacterium tuberculosis* (Mtb) during isoniazid treatment, and activation of the intracellular NAD phosphorylase MbcT toxin potentiates its effect. Due to the NAD cofactor's crucial role in cellular energy production, additional synergistic correlations of NAD biosynthesis blockade can be envisioned with bedaquiline and other drugs targeting energy-metabolism in mycobacteria. In conclusion, future strategies targeting NAD metabolism in Mtb should consider its potential synergy with current and other forthcoming TB-drugs.

Keywords: isoniazid, pyrazinamide, nicotinamide, ethionamide, delamanid, tuberculosis, toxin-antitoxin system, NAD biosynthesis inhibition

OPEN ACCESS

Edited by:
Maria Rosalia Pasca, University of Pavia, Italy

Reviewed by:
Satoshi Mitarai, Research Institute of Tuberculosis, Japan Anti-tuberculosis Association, Japan
Jun Yoshino, Washington University School of Medicine in St. Louis, United States

***Correspondence:**
Leonardo Sorci
l.sorci@staff.univpm.it

Specialty section:
This article was submitted to Antimicrobials, Resistance and Chemotherapy, a section of the journal Frontiers in Microbiology

Received: *28 November 2020*
Accepted: *23 December 2020*
Published: *26 January 2021*

Citation:
Rohde KH and Sorci L (2021) The Prospective Synergy of Antitubercular Drugs With NAD Biosynthesis Inhibitors. Front. Microbiol. 11:634640. doi: 10.3389/fmicb.2020.634640

INTRODUCTION

Tuberculosis (TB), caused by *Mycobacterium tuberculosis* (Mtb), is the leading infectious cause of mortality, with an estimated 1.2 million deaths and 10 million new cases in 2019, and about a quarter of the world's population latently infected (WHO, 2020). The shortcomings of currently available TB drugs are a major factor underlying the ongoing TB crisis. The current "short course" regimen involves a cocktail of multiple front-line drugs administered

for 6 months. In a sobering finding, Malherbe et al. (2016) reported detection of *Mtb* RNA within nonresolving granulomas in patients who had been declared cured after standard 6-month treatment using PET-CT imaging. This highlights the inability of current drug regimens to effectively eradicate phenotypically tolerant subpopulations of *Mtb* persisters sequestered within granulomas, the hallmark lesions of TB disease. Further, exacerbating the challenge of treating TB is the COVID-19 pandemic which is hampering the TB detection and the increasing emergence of drug resistance. According to the latest report on TB epidemic, in 2019, nearly 400,000 people developed multidrug-resistant TB (MDR-TB), which is caused by strains resistant to the two first-line drugs rifampicin (RIF) and isoniazid (INH) with a treatment success rate of 57% globally (WHO, 2020). Even more concerning are extensively drug resistant TB (XDR-TB), resistant to RIF, INH, fluoroquinolones, and at least one of the three classes of injectables (amikacin, kanamycin, and capreomycin), and totally drug resistant TB (TDR-TB), which are not susceptible to known drugs (Udwadia et al., 2012). Thus, there is an urgent need for new multi-drug regimens with potent bactericidal activity against dormant persisters and drug-resistant mycobacteria. Identifying novel antimicrobials with unique mechanisms of action that can synergize with drugs currently in use or at late stages of development is a promising strategy to address this need. Prompted by our efforts to develop inhibitors of nicotinamide adenine dinucleotide (NAD) biosynthesis, this review seeks to highlight scientific evidence that chemical perturbation of this pathway could be an effective component of new TB drug regimens.

Isoniazid and NAD Metabolism

Discovered back in 1952, isoniazid, also known as isonicotinic acid hydrazide (INH), remains today one of the major first-line antituberculosis drugs. INH only kills actively replicating bacteria, with a minimum inhibitory concentration (MIC) against the slowly growing *M. tuberculosis* of 0.05 μg ml^{-1}. In contrast to the exquisite activity of INH on Mtb, most mycobacteria are only susceptible to INH concentrations over 1 μg/ml (Zhang and Young, 1993). The precise target and mechanism of action of INH have eluded the grasp of science for decades. A combination of biochemical, genetic, and X-ray crystallography studies finally concluded that INH is a prodrug involved in inhibiting the biosynthesis of mycolic acid, an essential cell wall component of Mtb (Winder et al., 1970). This prodrug's most accepted mechanism of action requires its activation into an acyl radical by the catalase-peroxidase KatG enzyme (Lei et al., 2000). The radical reacts with NAD to form an INH-NAD adduct (**Figure 1**), which, in turn, inhibits the FASII enoyl-ACP reductase InhA, leading to mycobacterial cell death (Rawat et al., 2003). The elucidation of the INH action mechanism has been controversial, and alternative target pathways, including DNA and lipid biosynthesis (Russe and Barclay, 1955; Ebina et al., 1961; Gangadharam et al., 1963), cell division (Barclay et al., 1953), or altered NAD metabolism (Bekierkunst, 1966), have been proposed in early reports.

The emergence of NAD enzyme cofactor biosynthesis as a promising antimycobacterial target pathway warrants a reevaluation of the metabolic interplay between INH and NAD. The perturbation of NAD metabolism by isoniazid was an early finding related to isoniazid action and resistance. In 1966, Bekierkunst reported that in *M. tuberculosis* H37Rv, a decrease in NAD content could be observed after only 4 h of exposure to isoniazid, rising to 50% after 6 h (Bekierkunst, 1966). Ten years later, Jackett et al. (1977) established that the NAD content declined with increasing drug concentration and increased exposure. These results, though, did not support a direct causal link between NAD depletion and INH's antibacterial activity, mainly because the NAD drop was marginal at the low bactericidal concentration of INH.

Despite the fact that NAD pool perturbation appears to be an incontrovertible secondary effect of INH action, this link has not been thoroughly elucidated. Several conjectures have been advanced for explaining the mechanism of NAD drop in the presence of INH. These hypotheses have been widely questioned or disproved. For example, it was suggested that NAD loss was as a result of leaks in the cell wall and membrane due to the inhibition of mycolate synthesis, i.e., a post-antibiotic effect (Winder et al., 1971); however, NAD level restored in cells exposed to INH for 24 h, despite the continued inhibition of growth (Jackett et al., 1977). It was also proposed that NAD depletion by INH could be the indirect effect of a NAD glycohydrolase activation (Bekierkunst and Bricker, 1967). Yet, this hypothesis did not explain resistance to isoniazid, as the effects on NAD were equivalent in isoniazid susceptible and resistant strains of *M. tuberculosis* (Sriprakash and Ramakrishnan, 1970).

More clues into the relationship between NAD and INH had to wait for in depth studies of INH resistance. The primary mechanism of resistance to INH results from mutations that either depress its activator (KatG) activity or overexpress/alter InhA, the target of INH-NAD adduct (Vilcheze and Jacobs, 2007). KatG mutants exhibit decreased or complete loss of catalase and peroxidase activity. Because these enzymatic activities are essential for *M. tuberculosis* defense against reactive oxygen species (ROS) and virulence *in vivo* (Pym et al., 2002; Ng et al., 2004), polymorphism in *katG* may result in a loss of fitness to the bacterium. On the other hand, among a set of overexpressed genes during NAD starvation, KatG came up with the highest upregulation (nearly 7-fold; Vilcheze et al., 2010), pointing to NAD depletion as a trigger to ROS production. Hence, INH and prospective NAD inhibitors may potentiate their effects and reduce the emergence of KatG-mediated resistance mechanisms. In support of this assumption, antagonism was reported between isoniazid and nicotinamide (Jordahl et al., 1961), the primary precursor of mycobacterial NAD salvage pathway.

An alternative mechanism of INH resistance in Mtb is based on defects in the *ndh* gene (Rv1854c; Lee et al., 2001), which encodes a type II NADH dehydrogenase. This oxidase transfers electrons from NADH to the respiratory chain without proton translocation. The *ndh*-mediated mechanism of resistance was first described in *Mycobacterium smegmatis* and *M. bovis* (Miesel et al., 1998; Vilcheze et al., 2005). As expected, the

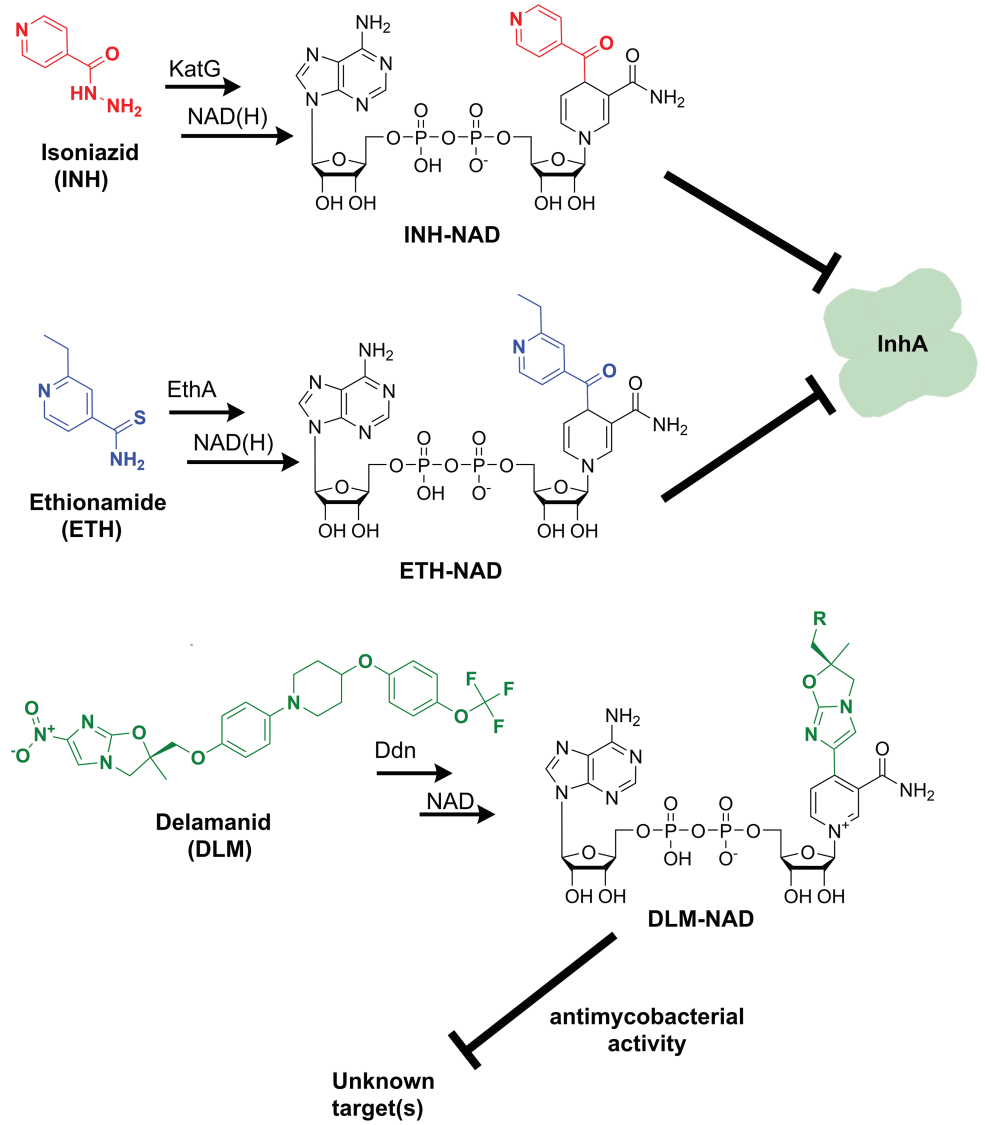

FIGURE 1 | Formation of nicotinamide adenine dinucleotide (NAD) chemical adducts by tuberculosis (TB) drugs. Prothionamide, a close chemical analog of ethionamide, undergoes the same transformation. Pretomanid, belonging to the same class of nitroimidazoles as delamanid, may combine with NAD as well. Their structures have been omitted for clarity.

activity of NdhII mutants was compromised, yielding an increased NADH cellular content and NADH/NAD ratio than wild-type (Vilcheze et al., 2005). In the same study, the authors demonstrated that the accumulation of NADH, the native substrate of InhA, acted as a competitive inhibitor for binding of the INH-NAD adduct to InhA. Despite an impaired NADH to NAD oxidation, the increased NADH/NAD ratio was only achieved by NADH elevation, while NAD remained relatively constant. As a result, the total amount of NAD(H) pyridine nucleotides in *ndh* mutants grew by 10–50% (Vilcheze et al., 2005). This implies that (i) NAD cofactor homeostasis is tightly regulated in tubercle bacilli and (ii) an increased NAD biosynthesis is necessary to avoid a dramatic NAD drop in *ndh* mutants.

Consistently, a gene expression analysis of *M. tuberculosis* exposed to INH showed that *nadC* (Rv1596) and *pntAb* (Rv0156) genes are significantly upregulated (Waddell et al., 2004). The gene *nadC* codes for quinolinate phosphoribosyltransferase (QAPRT), the final enzyme in the *de novo* branch of NAD biosynthesis (Waddell et al., 2004; **Figure 2**), while *pntAB* specifies a component (subunit alpha) of a proton-translocating NAD(P) transhydrogenase transferring reducing equivalents from NADPH to NAD. Supposedly, to counteract INH's bactericidal action, the two enzymes implement a metabolic response whereby the transhydrogenase elevates the NADH content while NadC replenishes the oxidized NAD cofactor. In this perspective, the blocking of NAD biosynthesis with specific inhibitors could represent not only a novel

antimycobacterial strategy but an opportunity to synergize with isoniazid, making the drug more lethal and overcoming some forms of resistance as in *ndh* mutants.

It could be argued that NAD depletion would also impair INH activity as less NAD would be available to form the INH-NAD adduct, thus counteracting this effect. Reasonably, this is not the case as INH-NAD is a tight-binding subnanomolar inhibitor of InhA (K_i = 0.75 nM; Rawat et al., 2003). We have demonstrated that a drop of NAD(H) content of only 3-fold becomes bactericidal for Mtb (Rodionova et al., 2014). Thus, given that typical bacterial NAD(H) pool concentration is around 1 mM, the residual NAD would be large enough to drive the INH-NAD adduct formation.

Recently, Freire et al. (2019) demonstrated that the toxin component MbcT of the Toxin-antitoxin MbcTA system is a novel phosphorylase that degrades NAD (**Figure 2**) and, in the absence of the McbA antidote, reduces mycobacterial survival in macrophages while extending the survival of infected mice. Remarkably, the study revealed a synergistic effect of toxin activity with isoniazid drug in a mouse model of Mtb infection, providing an additional proof-of-concept for INH's foreseen synergy with NAD synthesis blockers (**Figure 2**).

Ethionamide/Prothionamide and Delamanid/Pretomanid: Other NAD Adduct-Forming Prodrugs

Ethionamide (ETH) and its close analog prothionamide (PRO) are interchangeable components of second-line drug regimens used for the treatment of drug-resistant TB. Like its structural analog isoniazid, ETH is a prodrug targeting InhA. However, ETH is activated by a different enzyme, the flavin-dependent monooxygenase EthA (Vannelli et al., 2002). The activated ETH reacts with NAD to yield an ETH-NAD adduct (**Figure 1**), which subsequently inhibits InhA (Wang et al., 2007). Due to the commonalities in the mechanisms of action and

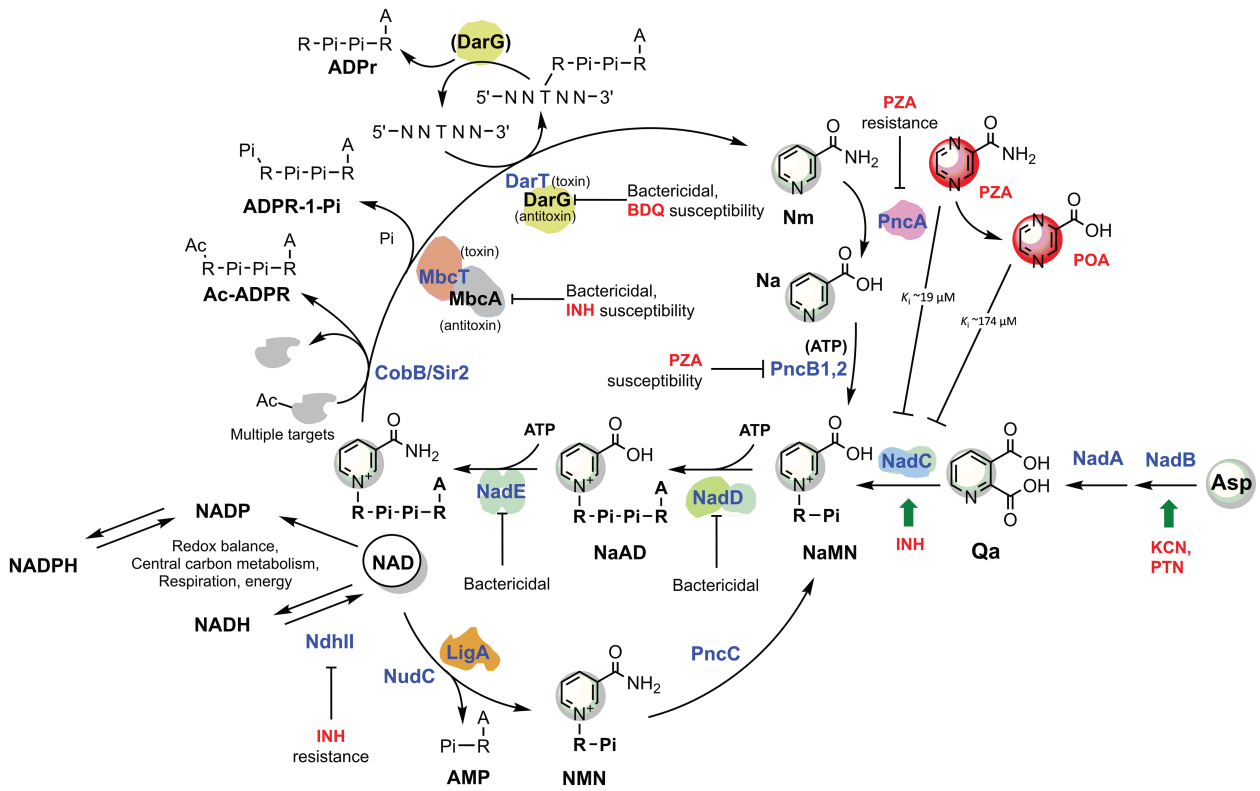

FIGURE 2 | The metabolic interplay between TB drugs and NAD pathways in *Mycobacterium tuberculosis*. Enzymes (blue) are identified with their gene name, metabolites' names are in black, and TB drugs or inhibitors are in red. The effects of targeted enzymes' inhibition/downregulation on bacterial growth or drug efficacy are shown. Green arrows indicate upregulated enzymes upon drug exposure, according to transcriptional analyses. Proteins with available 3D structures are sketched based on their biological quaternary assembly. Enzyme abbreviations: NadB (Rv1595): ASPOX, L-aspartate oxidase; NadA (Rv1594): QSYN, quinolinate synthetase; NadC (Rv1596): QaPRT, quinolinate phosphorybosyltransferase; PncB1 (Rv1330c): NaPRT1, nicotinate phosphoribosyltransferase; PncB2 (Rv0573c): NaPRT1, nicotinate phosphoribosyltransferase; NadD (Rv2421c): NaMNAT, NaMN adenylyltransferase; NadE (Rv2438c): NADS, glutamine-dependent NAD syntetase; PncA (Rv2043c): NMASE, nicotinamide deamidase; PncC (Rv1901): NMND, NMN deamidase; LigA (Rv3014c): NAD-dependent DNA ligase; NudC (Rv3199c): NAD(H) pyrophosphatase; NdhII (Rv1854c); type II NADH:menaquinone oxidoreductase; Sir2/CobB (Rv1151c): NAD-dependent deacetyltransferase. Metabolite abbreviations: NaAD, nicotinic acid adenine dinucleotide; Nam, nicotinamide; Na, nicotinic acid; Qa, quinolinic acid; NaMN, nicotinic acid mononucleotide; NMN, nicotinamide mononucleotide; PRPP, phosphoribosyl diphosphate; PZA, pyrazinamide; POA, pyrazinoic acid; BDQ, bedaquiline; INH, isoniazid; PTN, pretomanid; KCN, potassium cyanide.

cross-resistance of ETH or PRO and isoniazid, similar conclusions regarding the expected interference of ETH or PRO with NAD metabolism can be drawn.

The multi-drug-resistant TB drug delamanid (DLM) is a recently approved drug that also blocks the synthesis of mycolic acids, thereby destabilizing its cell wall (Matsumoto et al., 2006). DLM undergoes activation by the deazaflavin (F_{420})-dependent nitroreductase (*ddn*) to yield a reactive intermediate. This activated metabolite is considered to play a crucial role in the drug's bactericidal effect but whether it represents the final toxic derivative and the exact identification of its molecular target are still unknown (Liu et al., 2018). Strikingly, it has been recently established that after activation, DLM can combine with NAD to form a DLM-NAD adduct (**Figure 1**), which plays an essential role in the antimycobacterial action of DLM (Hayashi et al., 2020). Hence, delamanid is another TB drug that interferes with the pathogen's NAD homeostasis and that can potentially synergize with the NAD biosynthesis blockade. Similar conjectures can be drawn for the drug pretomanid (PTN), belonging to the same class of nitroimidazoles, but no experimental evidence that pretomanid can combine with NAD is currently available in the literature.

Pyrazinamide and NAD Metabolism

Pyrazinamide (PZA) drug partners with isoniazid, rifampicin, and ethambutol in the present-day "short-course" TB drug regimen (Mitchison, 1985). Since the discovery of the *in vivo* sterilizing activity in the animal models and humans (Solotorovsky et al., 1952; Yeager et al., 1952), PZA action mechanism largely remained an enigma. Several modes of action have been proposed in the following decades, though mounting evidence opposing such models was promptly put forward (for in-depth reviews, see Anthony et al., 2018; Lamont et al., 2020). These studies identified a diverse range of potential targets, including fatty acid synthesis (Zimhony et al., 2000), membrane energetics and integrity (Wade and Zhang, 2006), protein translation (Shi et al., 2011), and pantothenate biosynthesis (Zhang et al., 2013a; Dillon et al., 2014). More recently, aspartate decarboxylase PanD, required for Coenzyme A (CoA) biosynthesis, emerged as a convincing target of pyrazinoic acid (PAO), the bioactive form of PZA (Gopal et al., 2019). Remarkably, instead of inhibiting its target protein's function, as most antibacterials do, PAO functions as a target degrader (Gopal et al., 2020).

Hereafter, we will focus on the link between pyrazinamide and NAD metabolism, with the intent of uncovering foreseeable synergies between PZA and NAD pathway inhibitors. PZA is a prodrug hydrolyzed to the bioactive POA in the mycobacterial cytoplasm by the *M. tuberculosis* pyrazinamidase/nicotinamidase (PZAse), encoded by *pncA* (Rv2043c; Scorpio and Zhang, 1996). This amidase hydrolyzes nicotinamide vitamin into nicotinate, subsequently converted by PncB1-2 to nicotinate mononucleotide (NaMN), a shared product with NadABC-mediated *de novo* biosynthesis (**Figure 2**). Due to the redundancy of these pathways, PncA is nonessential for survival and virulence of *M. tuberculosis* (Boshoff et al., 2008; Vilcheze et al., 2010), and loss-of-function mutations represent the predominant mechanism for PZA resistance in clinical isolates (with up to 99.9% frequency; Zhang and Mitchison, 2003). The virulence and fitness of PZA-resistant strains with *pncA* mutations do not seem to be altered (Cheng et al., 2000). However, PncA resistant mutants may be more vulnerable to antibacterials targeting NAD metabolism, and such molecules could help overcome pncA-mediated resistance. Indeed, pncA-mutants would not efficiently salvage the Nm precursor, which is particularly abundant in the human host, nor recycle it out of NAD-consuming reactions (**Figure 2**). Mycobacteria encode Nm-releasing enzymes using NAD as a substrate that play vital roles in the dynamic regulation of metabolic functions (**Figure 2**). For example, in *M. tuberculosis*, the NAD-dependent Sir2-like family protein CobB (Rv1151c) influences the DNA architecture by deacetylating nucleoid-associated protein HU, a protein essential for growth (Anand et al., 2017; Green et al., 2018). Similarly to other Sir2-family proteins, Rv1151c is inhibited by Nm (Gu et al., 2009), which can accumulate in PZAse-defective Mtb strains. As also discussed in the next paragraph, the Mtb DarTG toxin-antitoxin system consumes NAD to mediate the reversible DNA ADP-ribosylation, a process whose biological significance is still poorly understood (Zaveri et al., 2020). If activated intracellularly, two other toxins, like the abovementioned MbcT and the TNT necrotizing toxin (Sun et al., 2015), may challenge intracellular Mtb NAD homeostasis. An uncharacterized NAD glycohydrolase activity, along with its heat-labile inhibitor, have been identified in Mtb crude extracts in the 1960s (Gopinathan et al., 1964, 1966), which likely correspond to the TNT toxin and its inhibitor IFT (Sun et al., 2015).

Thus, even though Nm salvage or recycling does not significantly affect tubercle bacillus survival or pathogenicity, its absence may impair the bacterial capacity to maintain NAD homeostasis under specific stress conditions that yield a sudden drop in NAD content. Such stress conditions may also be induced by PZA drug itself (**Figure 2**), which has been reported being an inhibitor of *de novo* NAD biosynthesis enzyme quinolinate phosphoribosyltransferase (QAPRT; Sharma et al., 1998; Kim et al., 2014). In keeping with this proposition, mutations in NAD pathways and energy production cause increased PZA susceptibility. Of note, mutants in *pncB1*, involved in NAD synthesis, are 5-fold more susceptible to PZA (Zhang et al., 2013b). Other mutants exhibiting higher PZA susceptibility were defective in energy production and include mutations in NADH dehydrogenase subunits H and N (*nuoH* and *nuoN*), nitrate reductase *narH*, and formate dehydrogenase *fdhF* (Zhang et al., 2013b). Given these premises, it seems worthwhile to test whether antimycobacterials that target NAD biosynthesis potentiate the effect of PZA and improve the treatment of TB.

The Metabolic Interplay Between NAD and ATP Metabolism: Bright Prospects for Respiratory and NAD Synthesis Inhibitors

It has been assessed that nearly 17% of the central metabolism enzymatic reactions that are essential for the survival of

M. tuberculosis require the NAD(H) cofactor and its phosphorylated derivative NADP(H) (Beste et al., 2007). Among these are the key pathways required to produce ATP as NAD(H) is the primary entry electron donor in the respiratory chain and the oxidant driving the glycolysis. Thus, a NAD(H) pool decrease induces a glycolytic slowdown and rapid shutdown of the electron transfer chain, ultimately compromising ATP synthesis from both sources.

In turn, NAD(P) biosynthesis is a highly ATP-dependent pathway (**Figure 2**). Each of the three universal enzymatic steps converting NaMN precursor to NADP requires an ATP molecule (Sorci et al., 2010b). Moreover, PncB-driven NaMN synthesis from Na and PRPP is strongly activated by the PncB ATPase activity (Vinitsky and Grubmeyer, 1993), and additional ATP molecules are required for recycling the ADP-ribose moiety into the PRPP precursor. The biogenesis and homeostasis of the NAD pool and ATP are undoubtedly interlinked aspects of energy metabolism, and their simultaneous targeting in innovative drug combinations may hold the promise for potential synergy and overcome resistance mechanisms. In line with this concept, Vilcheze et al. (2010) showed that both *M. tuberculosis* and *M. bovis de novo* NAD synthesis mutants starved for nicotinamide, i.e., in a metabolic status mimicking NAD synthesis inhibition, strongly upregulate ATP synthetase subunits *b*, *d*, and *c*, the latter being targeted by the recently approved bedaquiline drug (Andries et al., 2005). This implies that electron transport is impaired by limiting NAD and the ATP synthetase upregulation represents an attempt to restore electron transport and oxidative phosphorylation efficiency. Consistently, the transcriptional profiles from *M. tuberculosis* during exposure with NadE inhibitors resembled those induced by respiratory inhibitors (Boshoff et al., 2008). Conversely, respiratory poisons such as potassium cyanide and pretomanid positively affected the transcription of Mtb *nadB* (Manjunatha et al., 2009), the first and rate-limiting gene of *de novo* NAD biosynthesis, regulated by classic feedback inhibition of NAD (Seifert et al., 1990; Tedeschi et al., 1999).

Although they require additional supporting evidence, these observations based on transcriptional profiling emphasize the strict interdependence between ATP and NAD biogenesis and homeostasis in Mtb. Thus, we propose that innovative antimycobacterial strategies disrupting energy metabolism should target both of these two pathways for the best outcome. The latest developments on inhibitors interfering with energy-metabolism in *M. tuberculosis* are covered in comprehensive reviews (Thompson and Denny, 2019; Appetecchia et al., 2020). Not surprisingly, partial depletion of Mtb DarG (Rv0060), the hydrolase antitoxin reversing DarT-catalyzed DNA ADP-ribosylation (Jankevicius et al., 2016), sensitizes the mycobacterial cell to drugs targeting respiration (i.e., bedaquiline) and DNA metabolism (Zaveri et al., 2020). DarT (Rv0059) consumes NAD as an ADP-ribose donor and interacts with other proteins involved in DNA replication and repair, whereby additional NAD is drained by the activity of the NAD-dependent DNA ligase LigA (Srivastava et al., 2005). Although the Mtb DarTG toxin-antitoxin system's exact function remains unsolved, the essentiality of DarG and its direct involvement with DNA-repair proteins argues in favor of a significant role in preserving the genome integrity under stress conditions (Ramage et al., 2009). As an obligate human intracellular pathogen, *M. tuberculosis* has evolved complex defenses to endure the stresses experienced during persistent infection. As exemplified by the DarTG Toxin-Antitoxin system, NAD consumption is required to fuel the Mtb resilience under stress conditions, thus reaffirming bacterial NAD replenishment as an attractive target pathway.

CONCLUDING REMARKS AND PERSPECTIVES

In 1945, nicotinamide was serendipitously discovered to have antituberculosis properties (Chlorine, 1945). This prompted the testing of other pyridine derivatives for their antimycobacterial effects and paved the way for discovering isoniazid and pyrazinamide front-line drugs. Since these agents were much more effective than nicotinamide, further efforts were focused on uncovering their mechanism of action, obscuring the interest in nicotinamide. However, the elucidation of how the vitamin nicotinamide exerts its direct antituberculosis action, which must differ from its renowned derivatives, is of paramount importance as it may disclose novel vulnerable targets tied to the mycobacterial NAD metabolism. For example, Mtb CobB is a NAD-dependent deacetylase member of the SIR2 family of proteins that are notoriously inhibited by nicotinamide (Hu et al., 2014). Of relevance, nicotinamide inhibits *Pf*Sir2 activity and intra-erythrocytic growth of *Plasmodium falciparum* (Prusty et al., 2008). An *in vitro* antileishmanial activity is also reported for nicotinamide, partially mediated by direct inhibition of the *Leishmania* Sir2 homolog (Sereno et al., 2005).

Despite the presence of two PncB isozymes, it is well established that Mtb accumulates Na, and its excess is excreted into the culture media, thus allowing it to be detected using the niacin test. Curiously, this metabolic feature may have evolved to respond to high nicotinamide's toxicity rather than resulting from an intrinsic inability to process niacin.

The recent discoveries of DarTG, MbcTA, and TNT-IFT toxin-antitoxin systems uncovered additional NAD-consuming enzymes lethal to mycobacteria in the absence of functional antitoxins. Indeed, small inhibitors aiming at disrupting such complexes or inactivating the essential "antidotes" are promising antimycobacterial strategies (Williams and Hergenrother, 2012) that will surely mark future TB research. On the other hand, host NAD is a crucial molecule for TB immunity (Singhal and Cheng, 2018). Recent studies have shown that Mtb is capable of counteracting host defenses by subverting immune cells NAD metabolism. In detail, this could be achieved by modulation of human NAD-consuming proteins such as Sirtuins (Cheng et al., 2017; Bhaskar et al., 2020) or by direct depletion of host NAD levels through the TNT toxin (Pajuelo et al., 2020). The emerging roles of NAD and Sirtuin biology in host immune cells could be exploited to develop adjunct host-directed therapies against TB.

This review outlined the metabolic interplay between multiple TB drugs and the NAD cofactor, a crucial molecule for the Mtb growth during acute infections and persistence in a dormant state (Boshoff et al., 2008; Vilcheze et al., 2010; Kim et al., 2013; Rodionova et al., 2014, 2015). The perturbation of NAD homeostasis by these TB drugs is not, alone, bactericidal. However, it represents collateral damage that could be exploited to synergize with prospective drugs that specifically deplete NAD. Indeed, NAD biosynthesis is an established antiinfective target pathway not only in mycobacteria, but it has also been validated in other bacterial pathogens (Sorci et al., 2009, 2010a, 2013; Huang et al., 2010; Orsomando et al., 2016), the protozoan Plasmodium (O'Hara et al., 2014) and Leishmania (Mandal et al., 2019), and the flatworm Schistosoma parasite (Schultz et al., 2020). In mycobacteria, a detailed analysis of the NAD salvage vs. *de novo*-synthesis pathway concluded that an inhibitor must target either NadD or NadE, which sequentially catalyze the last two shared steps of NAD synthesis (Boshoff et al., 2008). By combining a target-directed and phenotypic screen, our group successfully developed antimycobacterial benzimidazolium compounds targeting *Mt*NadD (Osterman et al., 2019), while other teams optimized biaryl tethered dimers or urea-sulfonamide analogs directed at *Mt*NadE and inhibiting Mtb cell growth in the medium-micromolar range (Boshoff et al., 2008; Wang et al., 2017). A limitation of these studies is that the inhibitors were initially identified for orthologous enzymes from other bacteria (Rodionova et al., 2015; Wang et al., 2017). Thus, computationally-driven, large-scale high-throughput screening on *Mt*NadD and *Mt*NadE may be necessary for identifying more potent mycobacterial NAD synthesis inhibitors that can advance to a drug status.

AUTHOR CONTRIBUTIONS

LS designed this study and wrote the manuscript. KR critically reviewed the manuscript and contributed to its final writing. Both the authors contributed to the article and approved the submitted version.

FUNDING

This study was funded by the intramural research grant RSA2018-19 from Polytechnic University of Marche to LS.

ACKNOWLEDGMENTS

We want to thank all my lab members for stimulating discussion and Andrei Osterman (SBP Medical Research Institute) for sharing insightful comments.

REFERENCES

Anand, C., Garg, R., Ghosh, S., and Nagaraja, V. (2017). A Sir2 family protein Rv1151c deacetylates HU to alter its DNA binding mode in *Mycobacterium tuberculosis*. *Biochem. Biophys. Res. Commun.* 493, 1204–1209. doi: 10.1016/j.bbrc.2017.09.087

Andries, K., Verhasselt, P., Guillemont, J., Gohlmann, H. W., Neefs, J. M., Winkler, H., et al. (2005). A diarylquinoline drug active on the ATP synthase of *Mycobacterium tuberculosis*. *Science* 307, 223–227. doi: 10.1126/science.1106753

Anthony, R. M., den Hertog, A. L., and van Soolingen, D. (2018). 'Happy the man, who, studying nature's laws, thro' known effects can trace the secret cause.' Do we have enough pieces to solve the pyrazinamide puzzle? *J. Antimicrob. Chemother.* 73, 1750–1754. doi: 10.1093/jac/dky060

Appetecchia, F., Consalvi, S., Scarpecci, C., Biava, M., and Poce, G. (2020). SAR analysis of small molecules interfering with energy-metabolism in *Mycobacterium tuberculosis*. *Pharmaceuticals* 13:227. doi: 10.3390/ph13090227

Barclay, W. R., Ebert, R. H., and Kochweser, D. (1953). Mode of action of isoniazid. *Am. Rev. Tuberc.* 67, 490–496. doi: 10.1164/art.1953.67.4.490

Bekierkunst, A. (1966). Nicotinamide-adenine dinucleotide in tubercle bacilli exposed to isoniazid. *Science* 152, 525–526. doi: 10.1126/science.152.3721.525

Bekierkunst, A., and Bricker, A. (1967). Studies on the mode of action of isoniazid on mycobacteria. *Arch. Biochem. Biophys.* 122, 385–392. doi: 10.1016/0003-9861(67)90209-3

Beste, D. J., Hooper, T., Stewart, G., Bonde, B., Avignone-Rossa, C., Bushell, M. E., et al. (2007). GSMN-TB: a web-based genome-scale network model of *Mycobacterium tuberculosis* metabolism. *Genome Biol.* 8:R89. doi: 10.1186/gb-2007-8-5-r89

Bhaskar, A., Kumar, S., Khan, M. Z., Singh, A., Dwivedi, V. P., and Nandicoori, V. K. (2020). Host sirtuin 2 as an immunotherapeutic target against tuberculosis. *eLife* 9:e55415. doi: 10.7554/eLife.55415

Boshoff, H. I., Xu, X., Tahlan, K., Dowd, C. S., Pethe, K., Camacho, L. R., et al. (2008). Biosynthesis and recycling of nicotinamide cofactors in *Mycobacterium tuberculosis*. An essential role for NAD in nonreplicating bacilli. *J. Biol. Chem.* 283, 19329–19341. doi: 10.1074/jbc.M800694200

Cheng, C. Y., Gutierrez, N. M., Marzuki, M. B., Lu, X., Foreman, T. W., Paleja, B., et al. (2017). Host sirtuin 1 regulates mycobacterial immunopathogenesis and represents a therapeutic target against tuberculosis. *Sci. Immunol.* 2:eaaj1789. doi: 10.1126/sciimmunol.aaj1789

Cheng, S. J., Thibert, L., Sanchez, T., Heifets, L., and Zhang, Y. (2000). pncA mutations as a major mechanism of pyrazinamide resistance in *Mycobacterium tuberculosis*: spread of a monoresistant strain in Quebec, Canada. *Antimicrob. Agents Chemother.* 44, 528–532. doi: 10.1128/AAC.44.3.528-532.2000

Chlorine, V. (1945). Action de l'amide nicotinique sur les bacilles du genre *Mycobacterium*. *C. R. Acad. Sci.* 220, 150–151.

Dillon, N. A., Peterson, N. D., Rosen, B. C., and Baughn, A. D. (2014). Pantothenate and pantetheine antagonize the antitubercular activity of pyrazinamide. *Antimicrob. Agents Chemother.* 58, 7258–7263. doi: 10.1128/AAC.04028-14

Ebina, T., Motomiya, M., Munakata, K., and Kobuya, G. (1961). Effect of isoniazid on fatty acids in Mycobacterium. *C. R. Seances Soc. Biol. Fil.* 155, 1176–1178.

Freire, D. M., Gutierrez, C., Garza-Garcia, A., Grabowska, A. D., Sala, A. J., Ariyachaokun, K., et al. (2019). An NAD(+) phosphorylase toxin triggers *Mycobacterium tuberculosis* cell death. *Mol. Cell* 73, 1282.e1288–1291.e1288. doi: 10.1016/j.molcel.2019.01.028

Gangadharam, P. R., Harold, F. M., and Schaefer, W. B. (1963). Selective inhibition of nucleic acid synthesis in *Mycobacterium tuberculosis* by isoniazid. *Nature* 198, 712–714. doi: 10.1038/198712b0

Gopal, P., Gruber, G., Dartois, V., and Dick, T. (2019). Pharmacological and molecular mechanisms behind the sterilizing activity of pyrazinamide. *Trends Pharmacol. Sci.* 40, 930–940. doi: 10.1016/j.tips.2019.10.005

Gopal, P., Sarathy, J. P., Yee, M., Ragunathan, P., Shin, J., Bhushan, S., et al. (2020). Pyrazinamide triggers degradation of its target aspartate decarboxylase. *Nat. Commun.* 11:1661. doi: 10.1038/s41467-020-15516-1

Gopinathan, K. P., Ramakrishnan, T., and Vaidyanathan, C. S. (1966). Purification and properties of an inhibitor for nicotinamide-adenine dinucleotidase from *Mycobacterium tuberculosis* H37Rv. *Arch. Biochem. Biophys.* 113, 376–382. doi: 10.1016/0003-9861(66)90201-3

Gopinathan, K. P., Sirsi, M., and Vaidyanathan, C. S. (1964). Nicotinamide-adenine dinucleotide glycohydrolase of *Mycobacterium tuberculosis* H37Rv. *Biochem. J.* 91, 277–282. doi: 10.1042/bj0910277

Green, K. D., Biswas, T., Pang, A. H., Willby, M. J., Reed, M. S., Stuchlik, O., et al. (2018). Acetylation by Eis and deacetylation by Rv1151c of *Mycobacterium tuberculosis* HupB: biochemical and structural insight. *Biochemistry* 57, 781–790. doi: 10.1021/acs.biochem.7b01089

Gu, J., Deng, J. Y., Li, R., Wei, H., Zhang, Z., Zhou, Y., et al. (2009). Cloning and characterization of NAD-dependent protein deacetylase (Rv1151c) from *Mycobacterium tuberculosis*. *Biochemistry* 74, 743–748. doi: 10.1134/s0006297909070062

Hayashi, M., Nishiyama, A., Kitamoto, R., Tateishi, Y., Osada-Oka, M., Nishiuchi, Y., et al. (2020). Adduct formation of delamanid with NAD in Mycobacteria. *Antimicrob. Agents Chemother.* 64, e01755–e01819. doi: 10.1128/AAC.01755-19

Hu, J., Jing, H., and Lin, H. (2014). Sirtuin inhibitors as anticancer agents. *Future Med. Chem.* 6, 945–966. doi: 10.4155/fmc.14.44

Huang, N., Kolhatkar, R., Eyobo, Y., Sorci, L., Rodionova, I., Osterman, A. L., et al. (2010). Complexes of bacterial nicotinate mononucleotide adenylyltransferase with inhibitors: implication for structure-based drug design and improvement. *J. Med. Chem.* 53, 5229–5239. doi: 10.1021/jm100377f

Jackett, P. S., Aber, V. R., and Mitchison, D. A. (1977). The relationship between nicotinamide adenine dinucleotide concentration and antibacterial activity of isoniazid in *Mycobacterium tuberculosis*. *Am. Rev. Respir. Dis.* 115, 601–607. doi: 10.1164/arrd.1977.115.4.601

Jankevicius, G., Ariza, A., Ahel, M., and Ahel, I. (2016). The toxin-antitoxin system DarTG catalyzes reversible ADP-ribosylation of DNA. *Mol. Cell* 64, 1109–1116. doi: 10.1016/j.molcel.2016.11.014

Jordahl, C., Prez, R. D., Deuschle, K., Muschenheim, C., and McDermott, W. (1961). Ineffectiveness of nicotinamide and isoniazid in the treatment of pulmonary tuberculosis. *Am. Rev. Respir. Dis.* 83, 899–900. doi: 10.1164/arrd.1961.83.6.899

Kim, J. H., O'Brien, K. M., Sharma, R., Boshoff, H. I., Rehren, G., Chakraborty, S., et al. (2013). A genetic strategy to identify targets for the development of drugs that prevent bacterial persistence. *Proc. Natl. Acad. Sci. U. S. A.* 110, 19095–19100. doi: 10.1073/pnas.1315860110

Kim, H., Shibayama, K., Rimbara, E., and Mori, S. (2014). Biochemical characterization of quinolinic acid phosphoribosyltransferase from *Mycobacterium tuberculosis* H37Rv and inhibition of its activity by pyrazinamide. *PLoS One* 9:e100062. doi: 10.1371/journal.pone.0100062

Lamont, E. A., Dillon, N. A., and Baughn, A. D. (2020). The bewildering antitubercular action of pyrazinamide. *Microbiol. Mol. Biol. Rev.* 84, e00070–e00119. doi: 10.1128/MMBR.00070-19

Lee, A. S., Teo, A. S., and Wong, S. Y. (2001). Novel mutations in ndh in isoniazid-resistant *Mycobacterium tuberculosis* isolates. *Antimicrob. Agents Chemother.* 45, 2157–2159. doi: 10.1128/AAC.45.7.2157-2159.2001

Lei, B., Wei, C. J., and Tu, S. C. (2000). Action mechanism of antitubercular isoniazid. Activation by *Mycobacterium tuberculosis* KatG, isolation, and characterization of inha inhibitor. *J. Biol. Chem.* 275, 2520–2526. doi: 10.1074/jbc.275.4.2520

Liu, Y., Matsumoto, M., Ishida, H., Ohguro, K., Yoshitake, M., Gupta, R., et al. (2018). Delamanid: from discovery to its use for pulmonary multidrug-resistant tuberculosis (MDR-TB). *Tuberculosis* 111, 20–30. doi: 10.1016/j.tube.2018.04.008

Malherbe, S. T., Shenai, S., Ronacher, K., Loxton, A. G., Dolganov, G., Kriel, M., et al. (2016). Persisting positron emission tomography lesion activity and *Mycobacterium tuberculosis* mRNA after tuberculosis cure. *Nat. Med.* 22, 1094–1100. doi: 10.1038/nm.4177

Mandal, H., Vijayakumar, S., Yadav, S., Singh, S. K., and Das, P. (2019). Validation of NAD synthase inhibitors for inhibiting the cell viability of Leishmania donovani: in silico and in vitro approach. *J. Biomol. Struct. Dyn.* 37, 4481–4493. doi: 10.1080/07391102.2018.1552199

Manjunatha, U., Boshoff, H. I., and Barry, C. E. (2009). The mechanism of action of PA-824: novel insights from transcriptional profiling. *Commun. Integr. Biol.* 2, 215–218. doi: 10.4161/cib.2.3.7926

Matsumoto, M., Hashizume, H., Tomishige, T., Kawasaki, M., Tsubouchi, H., Sasaki, H., et al. (2006). OPC-67683, a nitro-dihydro-imidazooxazole derivative with promising action against tuberculosis in vitro and in mice. *PLoS Med.* 3:e466. doi: 10.1371/journal.pmed.0030466

Miesel, L., Weisbrod, T. R., Marcinkeviciene, J. A., Bittman, R., and Jacobs, W. R. Jr. (1998). NADH dehydrogenase defects confer isoniazid resistance and conditional lethality in *Mycobacterium smegmatis*. *J. Bacteriol.* 180, 2459–2467. doi: 10.1128/JB.180.9.2459-2467.1998

Mitchison, D. A. (1985). The action of antituberculosis drugs in short-course chemotherapy. *Tubercle* 66, 219–225. doi: 10.1016/0041-3879(85)90040-6

Ng, V. H., Cox, J. S., Sousa, A. O., MacMicking, J. D., and McKinney, J. D. (2004). Role of KatG catalase-peroxidase in mycobacterial pathogenesis: countering the phagocyte oxidative burst. *Mol. Microbiol.* 52, 1291–1302. doi: 10.1111/j.1365-2958.2004.04078.x

O'Hara, J. K., Kerwin, L. J., Cobbold, S. A., Tai, J., Bedell, T. A., Reider, P. J., et al. (2014). Targeting NAD+ metabolism in the human malaria parasite *Plasmodium falciparum*. *PLoS One* 9:e94061. doi: 10.1371/journal.pone.0094061

Orsomando, G., Agostinelli, S., Bramucci, M., Cappellacci, L., Damiano, S., Lupidi, G., et al. (2016). Mexican sunflower (*Tithonia diversifolia*, Asteraceae) volatile oil as a selective inhibitor of *Staphylococcus aureus* nicotinate mononucleotide adenylyltransferase (NadD). *Ind. Crop. Prod.* 85, 181–189. doi: 10.1016/j.indcrop.2016.03.003

Osterman, A. L., Rodionova, I., Li, X., Sergienko, E., Ma, C. T., Catanzaro, A., et al. (2019). Novel antimycobacterial compounds suppress NAD biogenesis by targeting a unique pocket of NaMN adenylyltransferase. *ACS Chem. Biol.* 14, 949–958. doi: 10.1021/acschembio.9b00124

Pajuelo, D., Gonzalez-Juarbe, N., and Niederweis, M. (2020). NAD hydrolysis by the tuberculosis necrotizing toxin induces lethal oxidative stress in macrophages. *Cell. Microbiol.* 22:e13115. doi: 10.1111/cmi.13115

Prusty, D., Mehra, P., Srivastava, S., Shivange, A. V., Gupta, A., Roy, N., et al. (2008). Nicotinamide inhibits *Plasmodium falciparum* Sir2 activity in vitro and parasite growth. *FEMS Microbiol. Lett.* 282, 266–272. doi: 10.1111/j.1574-6968.2008.01135.x

Pym, A. S., Saint-Joanis, B., and Cole, S. T. (2002). Effect of katG mutations on the virulence of *Mycobacterium tuberculosis* and the implication for transmission in humans. *Infect. Immun.* 70, 4955–4960. doi: 10.1128/IAI.70.9.4955-4960.2002

Ramage, H. R., Connolly, L. E., and Cox, J. S. (2009). Comprehensive functional analysis of *Mycobacterium tuberculosis* toxin-antitoxin systems: implications for pathogenesis, stress responses, and evolution. *PLoS Genet.* 5:e1000767. doi: 10.1371/journal.pgen.1000767

Rawat, R., Whitty, A., and Tonge, P. J. (2003). The isoniazid-NAD adduct is a slow, tight-binding inhibitor of InhA, the *Mycobacterium tuberculosis* enoyl reductase: adduct affinity and drug resistance. *Proc. Natl. Acad. Sci. U. S. A.* 100, 13881–13886. doi: 10.1073/pnas.2235848100

Rodionova, I. A., Schuster, B. M., Guinn, K. M., Sorci, L., Scott, D. A., Li, X., et al. (2014). Metabolic and bactericidal effects of targeted suppression of NadD and NadE enzymes in mycobacteria. *mBio* 5, e00747–e00813. doi: 10.1128/mBio.00747-13

Rodionova, I. A., Zuccola, H. J., Sorci, L., Aleshin, A. E., Kazanov, M. D., Ma, C. T., et al. (2015). Mycobacterial nicotinate mononucleotide adenylyltransferase: structure, mechanism, and implications for drug discovery. *J. Biol. Chem.* 290, 7693–7706. doi: 10.1074/jbc.M114.628016

Russe, H. P., and Barclay, W. R. (1955). The effect of isoniazid on lipids of the tubercle bacillus. *Am. Rev. Tuberc.* 72, 713–717. doi: 10.1164/artpd.1955.72.6.713

Schultz, M. D., Dadali, T., Jacques, S. A., Muller-Steffner, H., Foote, J. B., Sorci, L., et al. (2020). Inhibition of the NAD salvage pathway in schistosomes impairs metabolism, reproduction, and parasite survival. *PLoS Pathog.* 16:e1008539. doi: 10.1371/journal.ppat.1008539

Scorpio, A., and Zhang, Y. (1996). Mutations in pncA, a gene encoding pyrazinamidase/nicotinamidase, cause resistance to the antituberculous drug pyrazinamide in tubercle bacillus. *Nat. Med.* 2, 662–667. doi: 10.1038/nm0696-662

Seifert, J., Kunz, N., Flachmann, R., Laufer, A., Jany, K. D., and Gassen, H. G. (1990). Expression of the *E. coli* nadB gene and characterization of the gene product L-aspartate oxidase. *Biol. Chem. Hoppe Seyler* 371, 239–248.

Sereno, D., Alegre, A. M., Silvestre, R., Vergnes, B., and Ouaissi, A. (2005). In vitro antileishmanial activity of nicotinamide. *Antimicrob. Agents Chemother.* 49, 808–812. doi: 10.1128/AAC.49.2.808-812.2005

Sharma, V., Grubmeyer, C., and Sacchettini, J. C. (1998). Crystal structure of quinolinic acid phosphoribosyltransferase from *Mycobacterium tuberculosis*: a potential TB drug target. *Structure* 6, 1587–1599. doi: 10.1016/S0969-2126(98)00156-7

Shi, W., Zhang, X., Jiang, X., Yuan, H., Lee, J. S., Barry, C. E. 3rd, et al. (2011). Pyrazinamide inhibits trans-translation in *Mycobacterium tuberculosis*. *Science* 333, 1630–1632. doi: 10.1126/science.1208813

Singhal, A., and Cheng, C. Y. (2018). Host NAD+ metabolism and infections: therapeutic implications. *Int. Immunol.* 31, 59–67. doi: 10.1093/intimm/dxy068

Solotorovsky, M., Gregory, F. J., Ironson, E. J., Bugie, E. J., O'Neill, R. C., and Pfister, K. (1952). Pyrazinoic acid amide—an agent active against experimental murine tuberculosis. *Proc. Soc. Exp. Biol. Med.* 79, 563–565. doi: 10.3181/00379727-79-19447

Sorci, L., Blaby, I., De Ingeniis, J., Gerdes, S., Raffaelli, N., de Crecy Lagard, V., et al. (2010a). Genomics-driven reconstruction of acinetobacter NAD metabolism: insights for antibacterial target selection. *J. Biol. Chem.* 285, 39490–39499. doi: 10.1074/jbc.M110.185629

Sorci, L., Blaby, I. K., Rodionova, I. A., De Ingeniis, J., Tkachenko, S., de Crecy-Lagard, V., et al. (2013). Quinolinate salvage and insights for targeting NAD biosynthesis in group A streptococci. *J. Bacteriol.* 195, 726–732. doi: 10.1128/JB.02002-12

Sorci, L., Kurnasov, O., Rodionov, D. A., and Osterman, A. L. (2010b). "Genomics and enzymology of NAD biosynthesis" in *Comprehensive natural products II: Chemistry and biology*. eds. L. Mander and H.-W. Lui (Oxford: Elsevier), 213–257.

Sorci, L., Pan, Y., Eyobo, Y., Rodionova, I., Huang, N., Kurnasov, O., et al. (2009). Targeting NAD biosynthesis in bacterial pathogens: structure-based development of inhibitors of nicotinate mononucleotide adenylyltransferase NadD. *Chem. Biol.* 16, 849–861. doi: 10.1016/j.chembiol.2009.07.006

Sriprakash, K. S., and Ramakrishnan, T. (1970). Isoniazid-resistant mutants of *Mycobacterium tuberculosis* H37RV: uptake of isoniazid and the properties of NADase inhibitor. *J. Gen. Microbiol.* 60, 125–132. doi: 10.1099/00221287-60-1-125

Srivastava, S. K., Tripathi, R. P., and Ramachandran, R. (2005). NAD+-dependent DNA ligase (Rv3014c) from *Mycobacterium tuberculosis*. Crystal structure of the adenylation domain and identification of novel inhibitors. *J. Biol. Chem.* 280, 30273–30281. doi: 10.1074/jbc.M503780200

Sun, J., Siroy, A., Lokareddy, R. K., Speer, A., Doornbos, K. S., Cingolani, G., et al. (2015). The tuberculosis necrotizing toxin kills macrophages by hydrolyzing NAD. *Nat. Struct. Mol. Biol.* 22, 672–678. doi: 10.1038/nsmb.3064

Tedeschi, G., Negri, A., Ceciliani, F., Mattevi, A., and Ronchi, S. (1999). Structural characterization of l-aspartate oxidase and identification of an interdomain loop by limited proteolysis. *Eur. J. Biochem.* 260, 896–903. doi: 10.1046/j.1432-1327.1999.00234.x

Thompson, A. M., and Denny, W. A. (2019). "Inhibitors of enzymes in the electron transport chain of *Mycobacterium tuberculosis*" in *Annual reports in medicinal chemistry*. ed. K. Chibale (Cambridge, MA, USA: Elsevier), 97–130.

Udwadia, Z. F., Amale, R. A., Ajbani, K. K., and Rodrigues, C. (2012). Totally drug-resistant tuberculosis in India. *Clin. Infect. Dis.* 54, 579–581. doi: 10.1093/cid/cir889

Vannelli, T. A., Dykman, A., and Ortiz de Montellano, P. R. (2002). The antituberculosis drug ethionamide is activated by a flavoprotein monooxygenase. *J. Biol. Chem.* 277, 12824–12829. doi: 10.1074/jbc.M110751200

Vilcheze, C., and Jacobs, W. R. Jr. (2007). The mechanism of isoniazid killing: clarity through the scope of genetics. *Annu. Rev. Microbiol.* 61, 35–50. doi: 10.1146/annurev.micro.61.111606.122346

Vilcheze, C., Weinrick, B., Wong, K. W., Chen, B., and Jacobs, W. R. Jr. (2010). NAD+ auxotrophy is bacteriocidal for the tubercle bacilli. *Mol. Microbiol.* 76, 365–377. doi: 10.1111/j.1365-2958.2010.07099.x

Vilcheze, C., Weisbrod, T. R., Chen, B., Kremer, L., Hazbon, M. H., Wang, F., et al. (2005). Altered NADH/NAD+ ratio mediates coresistance to isoniazid and ethionamide in mycobacteria. *Antimicrob. Agents Chemother.* 49, 708–720. doi: 10.1128/AAC.49.2.708-720.2005

Vinitsky, A., and Grubmeyer, C. (1993). A new paradigm for biochemical energy coupling. *Salmonella typhimurium* nicotinate phosphoribosyltransferase. *J. Biol. Chem.* 268, 26004–26010.

Waddell, S. J., Stabler, R. A., Laing, K., Kremer, L., Reynolds, R. C., and Besra, G. S. (2004). The use of microarray analysis to determine the gene expression profiles of *Mycobacterium tuberculosis* in response to anti-bacterial compounds. *Tuberculosis* 84, 263–274. doi: 10.1016/j.tube.2003.12.005

Wade, M. M., and Zhang, Y. (2006). Effects of weak acids, UV and proton motive force inhibitors on pyrazinamide activity against *Mycobacterium tuberculosis* in vitro. *J. Antimicrob. Chemother.* 58, 936–941. doi: 10.1093/jac/dkl358

Wang, X., Ahn, Y. M., Lentscher, A. G., Lister, J. S., Brothers, R. C., Kneen, M. M., et al. (2017). Design, synthesis, and evaluation of substituted nicotinamide adenine dinucleotide (NAD(+)) synthetase inhibitors as potential antitubercular agents. *Bioorg. Med. Chem. Lett.* 27, 4426–4430. doi: 10.1016/j.bmcl.2017.08.012

Wang, F., Langley, R., Gulten, G., Dover, L. G., Besra, G. S., Jacobs, W. R. Jr., et al. (2007). Mechanism of thioamide drug action against tuberculosis and leprosy. *J. Exp. Med.* 204, 73–78. doi: 10.1084/jem.20062100

WHO (2020). Global Tuberculosis Report 2020.

Williams, J. J., and Hergenrother, P. J. (2012). Artificial activation of toxin–antitoxin systems as an antibacterial strategy. *Trends Microbiol.* 20, 291–298. doi: 10.1016/j.tim.2012.02.005

Winder, F. G. A., Collins, P., and Rooney, S. A. (1970). Effects of isoniazid on mycolic acid synthesis in *Mycobacterium tuberculosis* and on its cell envelope. *Biochem. J.* 117:27P. doi: 10.1042/bj1170027Pa

Winder, F. G., Collins, P. B., and Whelan, D. (1971). Effects of ethionamide and isoxyl on mycolic acid synthesis in *Mycobacterium tuberculosis* BCG. *J. Gen. Microbiol.* 66, 379–380. doi: 10.1099/00221287-66-3-379

Yeager, R. L., Munroe, W. G., and Dessau, F. I. (1952). Pyrazinamide (aldinamide*) in the treatment of pulmonary tuberculosis. *Trans. Annu. Meet. Nat. Tuberc. Assoc.* 48, 178–201.

Zaveri, A., Wang, R., Botella, L., Sharma, R., Zhu, L., Wallach, J. B., et al. (2020). Depletion of the DarG antitoxin in *Mycobacterium tuberculosis* triggers the DNA-damage response and leads to cell death. *Mol. Microbiol.* 114, 641–652. doi: 10.1111/mmi.14571

Zhang, S., Chen, J., Shi, W., Liu, W., Zhang, W., and Zhang, Y. (2013a). Mutations in panD encoding aspartate decarboxylase are associated with pyrazinamide resistance in *Mycobacterium tuberculosis*. *Emerg. Microbes Infect.* 2:e34. doi: 10.1038/emi.2013.38

Zhang, Y., and Mitchison, D. (2003). The curious characteristics of pyrazinamide: a review. *Int. J. Tuberc. Lung Dis.* 7, 6–21.

Zhang, Y., Shi, W., Zhang, W., and Mitchison, D. (2013b). Mechanisms of pyrazinamide action and resistance. *Microbiol. Spectr.* 2, 1–12. doi: 10.1128/microbiolspec.MGM2-0023-2013

Zhang, Y., and Young, D. B. (1993). Molecular mechanisms of isoniazid: a drug at the front line of tuberculosis control. *Trends Microbiol.* 1, 109–113. doi: 10.1016/0966-842X(93)90117-A

Zimhony, O., Cox, J. S., Welch, J. T., Vilcheze, C., and Jacobs, W. R. Jr. (2000). Pyrazinamide inhibits the eukaryotic-like fatty acid synthetase I (FASI) of *Mycobacterium tuberculosis*. *Nat. Med.* 6, 1043–1047. doi: 10.1038/79558

Conflict of Interest: The authors declare that the research was conducted in the absence of any commercial or financial relationships that could be construed as a potential conflict of interest.

frontiers in Microbiology

REVIEW
published: 02 February 2021
doi: 10.3389/fmicb.2020.618168

Early Drug Development and Evaluation of Putative Antitubercular Compounds in the -Omics Era

Alina Minias[1], Lidia Żukowska[1,2], Ewelina Lechowicz[1,3], Filip Gąsior[1,2], Agnieszka Knast[1,4], Sabina Podlewska[5,6], Daria Zygała[1,3] and Jarosław Dziadek[1]**

[1]Laboratory of Genetics and Physiology of Mycobacterium, Institute of Medical Biology, Polish Academy of Sciences, Lodz, Poland, [2]BioMedChem Doctoral School of the University of Lodz and the Institutes of the Polish Academy of Sciences in Lodz, Lodz, Poland, [3]Institute of Microbiology, Biotechnology and Immunology, Faculty of Biology and Environmental Protection, University of Lodz, Lodz, Poland, [4]Institute of Molecular and Industrial Biotechnology, Faculty of Biotechnology and Food Sciences, Lodz University of Technology, Lodz, Poland, [5]Department of Technology and Biotechnology of Drugs, Jagiellonian University Medical College, Krakow, Poland, [6]Maj Institute of Pharmacology, Polish Academy of Sciences, Krakow, Poland

OPEN ACCESS

Edited by:
Giorgia Mori, The University of Queensland, Australia

Reviewed by:
Shibali Das, Washington University School of Medicine in St. Louis, United States
Wonsik Lee, Sungkyunkwan University, South Korea

***Correspondence:**
Jarosław Dziadek
jdziadek@cbm.pan.pl
Alina Minias
aminias@cbm.pan.pl;
alinagorna@gmail.com

Specialty section:
This article was submitted to Antimicrobials, Resistance and Chemotherapy, a section of the journal Frontiers in Microbiology

Received: *16 October 2020*
Accepted: *30 December 2020*
Published: *02 February 2021*

Citation:
Minias A, Żukowska L, Lechowicz E, Gąsior F, Knast A, Podlewska S, Zygała D and Dziadek J (2021) Early Drug Development and Evaluation of Putative Antitubercular Compounds in the -Omics Era. Front. Microbiol. 11:618168. doi: 10.3389/fmicb.2020.618168

Tuberculosis (TB) is an infectious disease caused by the bacterium *Mycobacterium tuberculosis*. According to the WHO, the disease is one of the top 10 causes of death of people worldwide. *Mycobacterium tuberculosis* is an intracellular pathogen with an unusually thick, waxy cell wall and a complex life cycle. These factors, combined with *M. tuberculosis* ability to enter prolonged periods of latency, make the bacterium very difficult to eradicate. The standard treatment of TB requires 6–20 months, depending on the drug susceptibility of the infecting strain. The need to take cocktails of antibiotics to treat tuberculosis effectively and the emergence of drug-resistant strains prompts the need to search for new antitubercular compounds. This review provides a perspective on how modern -omic technologies facilitate the drug discovery process for tuberculosis treatment. We discuss how methods of DNA and RNA sequencing, proteomics, and genetic manipulation of organisms increase our understanding of mechanisms of action of antibiotics and allow the evaluation of drugs. We explore the utility of mathematical modeling and modern computational analysis for the drug discovery process. Finally, we summarize how -omic technologies contribute to our understanding of the emergence of drug resistance.

Keywords: *Mycobacterium*, tuberculosis, proteomics, DNA sequencing, transcriptomics, mutagenesis, drug evaluation, drug identification pipeline

INTRODUCTION

Tuberculosis (TB) is an infectious disease caused by *Mycobacterium tuberculosis*. The disease is one of the top 10 causes of death of people, according to the WHO. Each year, about 10 million people fall ill with TB, and 1.5 million people die. WHO estimates that approximately a quarter of the world population is infected with *M. tuberculosis*, and 5–10% of people will develop active TB during their lifetime. Incidence rates are reported in all countries and age groups. The disease affects mostly men (57%). Women account for 32% of cases.

About 11% of cases are children under 15 years of age. People with weakened immune systems are at higher risk of developing the disease, with particular emphasis on people infected with HIV. They are about 19 times more prone to TB. Further factors influencing TB's risk are malnutrition, diabetes, and smoking (World Health Organization, 2019).

Mycobacterium tuberculosis is an intracellular pathogen with an unusually thick, waxy cell wall and a complex life cycle. The bacteria are transmitted by aerosol droplets and most often infect the lungs. Generally, *M. tuberculosis* infects alveolar macrophages, but it can also infect other respiratory system cells. The disease may also be extrapulmonary. *Mycobacterium tuberculosis* can infect cells of bones, genitourinary tract, skin, joints, and meninges (Lee, 2015). Mycobacteria invade macrophages and settle the infection by blocking the maturation of phagosomes. The infection of macrophages results in the host response, where various types of immune cells infiltrate the infection site. The influx of immune cells may result in the eradication of the bacteria. Incomplete eradication of bacteria progresses the disease to the latent stage. *Mycobacterium tuberculosis* becomes enclosed in compact and sometimes calcified cell aggregates. *Mycobacterium tuberculosis* slows down its metabolism due to the restriction of the influx of nutrients and oxygen. The disease becomes latent. *Mycobacterium tuberculosis* can persist in the infected individual's lungs for decades. When the immunity of the person wanes, granulomas liquefy, and bacteria reactivate to the active phase of the disease. The complex life cycle, intracellular life niche, thick cell wall, and the ability to enter prolonged periods of latency make *M. tuberculosis* very difficult to eradicate.

Current Antitubercular Chemotherapy

The standard treatment of tuberculosis requires 6–20 months, depending on the drug susceptibility of the infecting strain. Antibiotics must be taken in combination, as administering a single antibiotic quickly results in pathogen drug resistance. There are four first-line drugs against tuberculosis (isoniazid – INH, rifampicin – RMP, ethambutol – EMB, pyrazinamide – PZA) and nearly 20 s-line drugs, which can be administered during the treatment of drug-resistant tuberculosis. The numbers of multidrug-resistant (MDR-TB) and extensively drug-resistant (XDR-TB) strains of *M. tuberculosis* are a major problem for current antitubercular therapy. MDR-TB is resistant to two first-line drugs, RMP and IHN. XDR-TB is resistant to four core antitubercular drugs, followed by resistance to capreofluoroquinolones and one of the three injectable second-line drugs, e.g., amikacin, capreomycin (CM), or kanamycin (KAN). Nearly 484,000 cases of MDR cases of tuberculosis are estimated to exist worldwide. A total of 13,068 cases of XDR-TB were reported by 81 countries, of which most of them were from the WHO European Region and the South-East Asia Region. Detection of MDR-TB first requires confirmation of TB, followed by testing for drug resistance. In 2018, 51% of people with bacteriologically confirmed TB were tested for RMP resistance (up from 41% in 2017). Even though between 2017 and 2018, there was progress in testing, detection, and treatment of MDR-TB, only 56% of MDR cases were successfully treated globally and only 39% of cases of XDR-TB. As of 2020, WHO recommends that MDR-TB patients are to be treated with fully oral drug regimens. Injectable agents should only be used if other options are not possible. Two such agents, KAN and CM, are no longer recommended (World Health Organization, 2019). High numbers of TB patients, including patients infected with drug-resistant *M. tuberculosis* justify the need to search new antitubercular compounds that could be introduced to antitubercular chemotherapy.

Prospective Antitubercular Chemotherapy

For a long time, the development of XDR-TB left patients without further options for treatment. The principal drugs for the treatment of tuberculosis were discovered between the 1940s and 1970s (streptomycin, para-aminosalicylic acid, INH, cycloserine – CS, KAN, RMP, and others; Murray et al., 2015). The path of drug discovery is long and costly (**Figure 1**). The process starts with the early drug discovery stage. Here, researchers identify potential inhibitors in laboratory conditions and assess their principal biological impact. The next stage is preclinical studies. This time chemicals are tested not only on bacteria but also on cell lines or live animals. The knowledge gained in this phase is helpful in Phase III of the study, which considers the drug doses tested here in later human studies. Several experimental tools are used in the preclinical stage. One is the *in vitro* hollow-fiber system that provides data to improve animal experimentation. The great advantage is the integration of this data with data from many different animal models. Such models are the well-known BALB/c mice and the newer Kramnik mouse model, or the marmoset and rabbit models. The preclinical stage provides valuable information about the activity of the tested drug or sterilization of the pathogen. Unfortunately, it provides limited information on the pharmacokinetics and pharmacodynamics of the drug (Dooley et al., 2019).

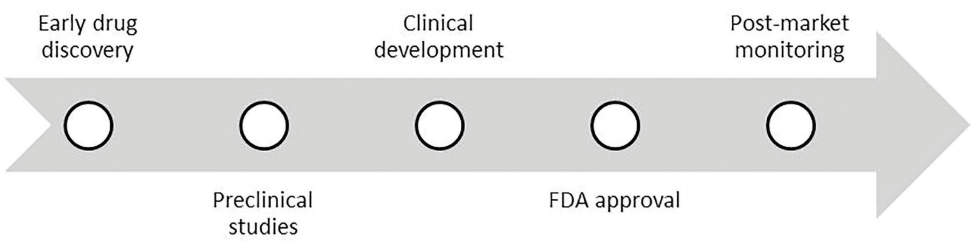

FIGURE 1 | The schematic overview of the drug discovery process.

The main cause of failures in the clinical development of drugs is its insufficient effectiveness, which is associated with an accurate determination of pharmacokinetics (Muliaditan et al., 2017). Before entering clinical trials, it is essential to gather much information about the exposure-response relationship and the relationship between pharmacokinetics and toxicity of the tested substance. Phase I clinical trials provide information on pharmacokinetics and safety, an important element here is to establish drug interactions with food intake or whether the dose depends on the patient's body weight. Phase II studies provide detailed inter-population information. In Phase III, drug efficacy is assessed by collecting post-drug exposure data, timed microbial response, and safety (Dooley et al., 2019). After clinical trials, the development of a new drug requires approval by the Food and Drug Administration (FDA).

In 2012, the United States FDA approved the use of a novel antitubercular drug bedaquiline – BDQ. BDQ was discovered by the pharmaceutical company Johnson and Johnson, under the brand name is Sirturo (Deoghare, 2013). It is the first member of a new class of drugs called diarylquinolines. BDQ is a bactericidal drug. BDQ blocks proton pump of ATP synthase, encoded by gene *atpE*. ATP production is essential for cellular energy turnout (Koul et al., 2008; Deoghare, 2013). BDQ is recommended strictly for the treatment of MDR-TB, and when options to treat this condition using existing drugs have been exhausted. BDQ should not be used to treat latent TB infection. It should not be used alone but as part of combination therapy and never added alone to a failing regimen. By the end of 2018, 90 countries reported having imported or using BDQ (World Health Organization, 2019).

In 2014, European Medicine Agency (EMA) conditionally approved a second novel antitubercular medicine, delamanid (DLM), as a part of combination therapy to treat adults with MDR-TB. The brand name of DLM is Deltyba. DLM exhibits a low minimum inhibitory concentration, distinguishing itself from other clinically approved drugs. This medicine is a pro-drug that requires metabolic activation for its action. It is activated by the deazaflavin F420-dependent nitroreductase. Resistance against DLM includes mutations in genes participating in pro-drug activation or associated with the cofactor Ddn biosynthetic pathway. DLM is known for specifically inhibiting the synthesis of two mycolic acids – keto mycolic acid and methoxy mycolic acid. They are the building components of the mycobacterial cell wall (absent in Gram-positive or Gram-negative bacteria). These components are also making it difficult for medicines to penetrate the cells. The use of DLM allows for more effective treatment through disrupting cell wall and shortening a treatment regimen (Tiberi et al., 2018b; Bahuguna and Rawat, 2020). By the end of 2018, 57 countries reported having imported or started using DLM (World Health Organization, 2019).

Approval of new medicine in Phase III clinical trials is always a risk, but benefits are perceived as more significant. BDQ was the first member of a new class of medicines. The principal study showed that treatment with Situro was effective; the drug worked well and fast. BDQ and DLM are well-working antibiotics, but there is already resistance against BDQ. In particular, they are mutations in *atpE*, gene coding ATP synthase subunit c, the target of BDQ, or gene Rv0678, which plays a role in regulating the expression of the MmpS5-MmpL5 efflux pump (Nguyen et al., 2018; Ghajavand et al., 2019). New antibiotics are most effective in a few first years before resistance is developed and disseminated across the bacterial population. Therefore it is vital to search for new medicines. As of October 2020, a few antitubercular drugs are currently in phase III or II clinical trials (**Table 1**). In addition to new drugs, there are also repurposed drugs like clofazimine (CFM), levofloxacin (LFX), moxifloxacin (MFX), and linezolid (LZD), which are in phase II and phase III trials for TB too. Drugs are also tested for repurposing from the treatment of other diseases, auranofin that is an antirheumatic agent and nitazoxanide that is an antiprotozoal agent. The growing TB epidemic again developed an interest in CFM, which now is an important constituent of newer TB regimens. CFM is a pro-drug, but the exact mechanism of action is not yet known. MFX is investigated in regimens combining BDQ, pretomanid, and PZA, or rifapentine (Bahuguna and Rawat, 2020).

Host-Directed Therapy

Treatment of *M. tuberculosis* infection with currently available antibiotics has several negative features associated with drug toxicity,

TABLE 1 | New drugs in phase III and II clinical trials (Vjecha et al., 2018; Bahuguna and Rawat, 2020).

Drug	Chemical class	Target	Effect	Clinical status
Bedaquiline	Diarylquinoline	ATP synthase	Inhibits energy metabolism of the cell	Phase III*
Delamanid	Nitroimidazole	Exact target not yet known	Inhibits mycolic acid synthesis (keto and methoxy mycolic acids) and cell respiration	Phase III*
Pretomanid	Nitroimidazole	Exact target not yet known	Inhibition of cell wall synthesis and respiratory poisoning	Phase III
Delpazolid	Oxazolidinone	50S subunit of the ribosome	Inhibits protein synthesis	Phase II
Sutezolid	Oxazolidinone	50S subunit of the ribosome	Inhibits protein synthesis	Phase II
SQ109	Diamine	MmpL3	Inhibits cell wall synthesis	Phase II
Macozinone (PBTZ169)	Benzothiazinone	DprE1	Inhibits cell wall synthesis	Phase II
Telacebec (Q203)	Imidazopyridine	Cytochrome *bc1* complex	Inhibits ATP synthesis	Phase II

Recently approved drugs.

and the problem is the increasing presence of drug-resistant *M. tuberculosis* strains. Another approach to supporting the treatment and prevention of tuberculosis is host-directed therapy (HDT). This strategy aims to modify host response related to the development, activity, and pathogenicity of *M. tuberculosis* infection. The HDT agents may have immunomodulatory properties, enhance the host's immune system or influence the host's metabolic pathways, which should aid in fighting the pathogen and protect the lung tissue (Tiberi et al., 2018a). One way is to activate autophagy, which would contribute to the increased intracellular killing of *M. tuberculosis*. In this case, the possibility of using rapamycin, metformin, statins, vitamin D, phenylbutyrate, carbamazepine, or valproic acid is investigated. Rapamycin inhibits the activity of mammalian target of rapamycin (mTOR), which is an inhibitor of autophagy. However, the use of this compound in therapy is limited due to the potential for side effects and its breakdown by the liver enzyme CYP3A4, which is activated by RMP, one of the first-line drugs in the treatment of tuberculosis. In addition, an increase in replication was observed in cells co-infected with HIV and H37Rv in response to rapamycin. Another potential compound is metformin, which can increase AMP-activated protein kinase and reactive oxygen species expression. These abilities contribute to activating autophagy and reducing inflammation. Statins lower lipid levels by inhibiting the enzyme β-hydroxy β-methylglutaryl-CoA, which is involved in lipid metabolism. Statins have a positive effect on the maturation of phagosomes and autophagy processes and reduce the accumulation of lipids inside cells, e.g., in macrophages, limiting the growth of the pathogen. Vitamin D and phenylbutyrate may increase the expression of LL-37, cathelicidin. Moreover, vitamin D regulates the expression of cytokines and immune mediators. Carbamazepine and valpronic acid are responsible for the activation of mTOR-independent autophagy (Dara et al., 2019; Torfs et al., 2019; Ahmed et al., 2020).

Host-directed therapy may also target the disintegration of the granuloma structure. Etanercept, an inhibitor of tumor necrosis factor α (TNF-α) involved in the formation and maintenance of granuloma, may help treat tuberculosis. Another possible drug is bevacizumab targeting vascular endothelial growth factor (VEGF). The drug influences the normalization of the vessels, which in turn causes a change in the morphology of the granuloma and the possibility of interaction with anti-tuberculosis drugs.

An important path of HDT is immunomodulation, increasing the anti-inflammatory response, which would help to reduce tissue damage. Ibuprofen, diclofenac, acetylsalicylic acid, and vitamin D are of interest (Torfs et al., 2019; Ahmed et al., 2020). Nonsteroidal anti-inflammatory drugs such as ibuprofen or diclofenac can reduce the inflammatory response by inhibiting cyclooxygenases. Acetylsalicylic acid activates lipoxin A4, which inhibits neutrophil migration and TNF-α production (Torfs et al., 2019; Ahmed et al., 2020; Young et al., 2020).

Vaccination

Bacillus Calmette-Guérin (BCG) is a vaccine based on attenuated *Mycobacterium bovis*, and it has been available since 1921. The BCG vaccine is currently applied worldwide, mostly in high burden countries of Africa, Asia, and South America. In 2011, among the 180 countries with available data, 157 countries recommended universal BCG vaccination (Zwerling et al., 2011). BCG vaccine efficiency is limited, as reflected by the number of tuberculosis cases worldwide. Therefore there is an ongoing search for novel, more effective vaccines. Several types of novel vaccine candidates are currently in clinical trials. They are composed of recombinant proteins and adjuvants, they are viral vectored, and they are attenuated and whole-cell vaccines (Kaufmann, 2020). The call for new vaccines is supported by the World Health Organization. The principal recommendations are that the new vaccine should be affordable, safe, and more efficient than the current BCG vaccine in the prevention of infection, disease, or recurrence.

One of the most promising vaccine candidates is the M72 subunit vaccine developed by GlaxoSmithKline. The vaccine successfully passed a phase IIb clinical trial. It was 54% effective (Van Der Meeren et al., 2018). The study tested booster vaccination of HIV-positive adults with latent TB infection who had been vaccinated with BCG as infants. This vaccine contains two TB antigens, fused in one protein and combined with AS 01E as an adjuvant. The disadvantage of this adjuvant is its high cost of production and limited availability, which may be an obstacle to the wide scale M72 vaccination (Kaufmann, 2020).

Antitubercular Drug Development Market

It takes a lot of time and cost to bring a new drug to market. The average cost that pharmaceutical companies have to bear is about US$ 2.6 billion during 10 years of research and development. Clinical trials consume most of this funding, about US$ 1–2.5 billion. Clinical trials are also the longest stage during the drug discovery process – they can last up to 6–7 years. Funding for the prevention, diagnosis, and treatment of TB has doubled since 2006, but it is still insufficient. In 2019, 119 low- and middle-income countries funding reached US$ 6.8 billion, up from US$ 3.5 billion in 2006. Most funds (about 87%) are available from domestic sources. Pharmaceutical companies mainly research new antibiotics. Most of them are small and medium-sized institutions (81%). Academia carries out 12% of new antibiotic research. Large pharma companies account for 3% of research. Non-profit institutions and public-private partnerships carry out the rest (Theuretzbacher et al., 2020). In 2019, international donor funding amounted to US$ 0,9 billion, which is far below than what was assumed by the Stop TB Partnership's Global Plan. Most of the international donor funding comes from the Global Fund to Fight AIDS, Tuberculosis, and Malaria. According to data from Treatment Action Group, there was the funding of US$ 772 million for TB research and development in 2017, which is much less than the target of at least US$ 2 billion per year set at the UN high-level meeting on TB (World Health Organization, 2019). High costs born during the drug development process justify the introduction of new technological solutions, including -omic technologies, that can facilitate the introduction of new, effective, and safe drugs to the market.

STRATEGIES TO FIND NEW DRUGS FOR TUBERCULOSIS TREATMENT AND THE DRUG DISCOVERY PROCESS

Designing a new drug and bringing it to market is a very time-consuming process that can take up many years (Hughes et al., 2011). This process is also highly costly, with little prospect of reimbursement from developing countries where tuberculosis is most prevalent. There are several important points to consider when searching for new antitubercular drugs. There is a need to provide shorter, simpler, and affordable multi-drug regimens for drug-sensitive *M. tuberculosis*; shorter, more effective, less toxic, and less expensive regimes for drug-resistant *M. tuberculosis*; and shorter, more straightforward, easily tolerable, and safe regimes for latent tuberculosis. Furthermore, new antitubercular drugs should not antagonize other medications, such as those used during HIV infection treatment. Finally, ideal drugs are those that have restricted the occurrence of drug-resistance.

There are two major paths to discover new antibiotics during the early stage of drug development (**Figure 2**). The first approach involves screening libraries of chemicals to find a "hit" – a molecule that kills a pathogen at the desired concentration. The advantage of this approach is that bacterial cell growth, compound penetration, and target sensitivity are resolved at the time of identification. Once an active chemical is identified, it is vital to establish several issues to evaluate the utility of the compound properly. The first issue is the identification of the drug target protein. Pinpointing the drug target leads to an explanation of the mode of action (MOA) of the novel drug (**Table 2**).

Further, it facilitates the optimization of the chemical structure of the drug. Finally, identifying the drug target protein provides essential information regarding possible causes of potential drug resistance. It is also pertinent to establish if the drug generates adverse effects, like an increase in the pathogen virulence. Finally, the amount of drug resistance variants and drug resistance sources should be determined (**Table 3**). Following the evaluation of the influence of the drug on the bacterium, the chemical toxicity is tested against eukaryotic cells. If the chemical is toxic at low doses for the pathogen but not toxic for eukaryotic cells, the compound may be further tested for its effectiveness in intracellular infection models and animal models before reaching the clinical trial phase.

The second approach for finding new antibiotics begins with identifying a molecular target that is essential or otherwise important for the pathogen virulence. The proteins that make good targets for antibiotics are those for which mutations are often deleterious. Such an approach makes them less susceptible to the random development of resistance. Inhibitors of those

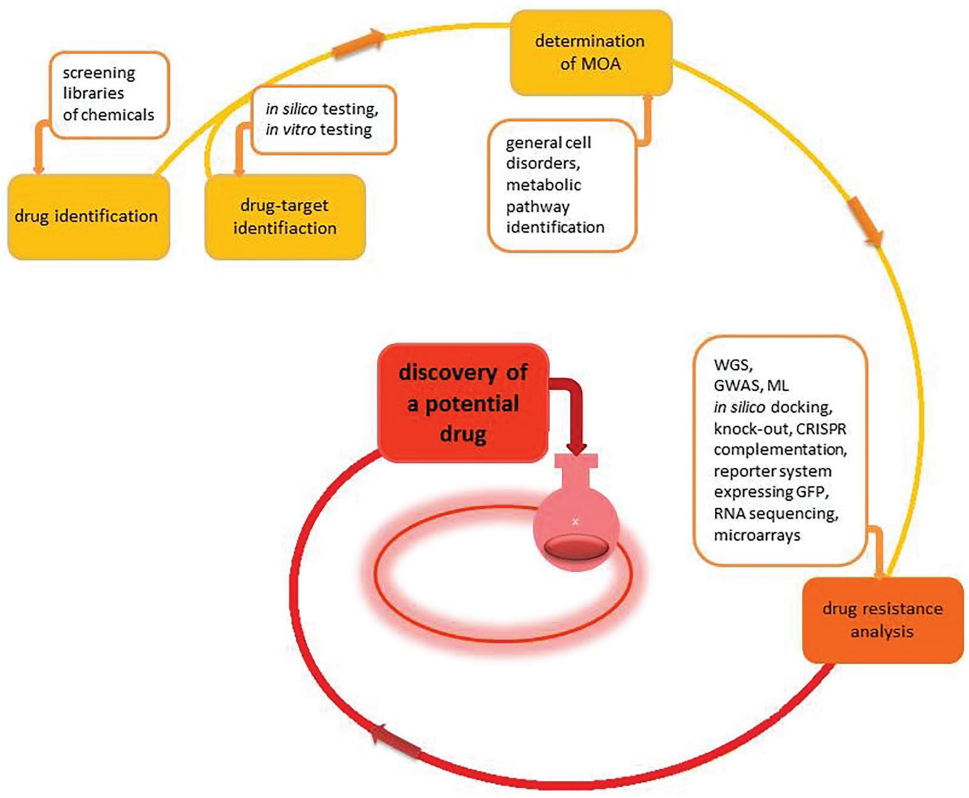

FIGURE 2 | The schematic overview of the early drug discovery process. The process begins with the identification of either a drug target or the drug itself. Next, the determination of the mode of action (MOA) and consideration of drug resistance facilitates an indication of safe and practical potential new drugs.

TABLE 2 | Approaches to establishing MOA of new drugs.

Aim	Methods	Example studies
Identification of general cell disorders and disrupted pathways and linking them to the disrupted metabolic pathway	RNA-Seq	O'Rourke et al., 2020
	Analysis of metabolites by LC-MS	Halouska et al., 2012
	Analysis of lipid content by LC-MS	Pal et al., 2018
Identification and confirmation of the drug target	WGS to identify mutations in the drug target	Andries et al., 2005
	Generation of knock-out strains	Bryk et al., 2008
	Generation of complemented mutants with increased gene expression	Kumar et al., 2015
	Generation of complemented mutants with decreased gene expression	Esposito et al., 2017
	CRISPR system gene expression depletion	McNeil and Cook, 2019

TABLE 3 | Identification of sources of drug resistance.

Aim	Methods	Example studies
Identification of the modification of the drug target	WGS of the resistant strains	Takiff et al., 1994
	GWAS	Farhat et al., 2019
	In silico docking	Nachappa et al., 2020
Identification of the modification of the disrupted metabolite pathway	RNA-Seq	Reviewed in Briffotaux et al. (2019)
	TraSH	Viswanathan et al., 2017
	PIP networks	Raman and Chandra, 2008
	GWAS and ML	Yang et al., 2018; Deelder et al., 2019
Induction of the efflux pumps	Using reporter system expressing fluorescent protein	Jain et al., 2016
	RNA-Seq	Reviewed in Briffotaux et al. (2019)

proteins can be found in two ways: through *in silico* screening using bioinformatic analyses and tested in experimental conditions (Korycka-Machala et al., 2017) or through *in vitro* screening inhibitor trough enzymatic/colorimetric assay (Syre et al., 2003; Grzelak et al., 2019). Potential molecular targets proposed in previous studies are, for example, proteins associated with DNA repair systems (for review, see Minias et al., 2019), DNA replication (for review, see Płocinska et al., 2017), multi-drug efflux pumps (Viveiros et al., 2003; Balganesh et al., 2012), or proteins necessary for cell division (Plocinska et al., 2012; Chatterjee et al., 2018; Gorla et al., 2018).

The ongoing digital revolution introduces novel solutions to old problems. New bioinformatic technologies and the availability of these advanced technologies for research allow for significant advances in the field of drug development. This review provides a perspective on how modern -omic technologies facilitate the drug discovery process for tuberculosis treatment. We discuss how methods of DNA and RNA sequencing, proteomics, and genetic manipulation of organisms increase our understanding of mechanisms of action of antibiotics and allow the evaluation of drugs. We explore the utility of mathematical modeling and modern computational analysis for the drug discovery process. Finally, we summarize how -omic technologies contribute to our understanding of the emergence of drug resistance.

IDENTIFICATION OF ANTIBACTERIAL COMPOUNDS

Screening Trough Libraries of Chemicals

Antibacterial compounds can be identified in high-throughput screens (HTS), which involve searching through a library of chemicals against either bacterial cell culture or chosen bacterial proteins in *in vitro* assay. When there is an observable inhibition of growth or enzyme activity at the desired concentration, the compound is tested further. The key to every HTS endeavor is the compound collection. Libraries of compounds are designed and selected for drug-like properties and structural diversity, critical to identifying unique hits for screening targets (Lushington and Chaguturu, 2014). The main challenge in this approach is the quality of chemical libraries. When creating a library, it is important to pay attention to its composition by excluding compounds that may interfere with screening results. Libraries should not contain unstable, highly reactive, or insoluble compounds. Assessment of the identity of the relationship and validation of purity is also essential. It is important to develop the standard of libraries by engaging library creators in their development, and also scientists dealing with screening research and commercial library managers. There is a forum (Nature Chemical Biology) that brings together this community, where issues in this field are presented and standards are discussed (Screening we can believe in, 2009). Millions of compounds are now commercially available, which allows for the development of research for both academics and the pharmaceutical industry.

Adjusting Culture Conditions

Bacterial culture can be carried out in various environmental conditions. Researchers often try to adapt and resemble culture conditions to those inside the human cells during pathogen infection. Screening of compounds can be done with reporter assays using different types of culture. Grant et al. (2013) screened a library of compounds against both actively replicating and non-replicating bacilli. They constructed fluorescent reporter assays for replicating and non-replicating conditions. Screen of compounds with both assays allowed to characterize the compounds as having effect on only replicating activity, only non-replicating activity, or both replicating and non-replicating activity.

Using Surrogate Models

Working with *M. tuberculosis* brings many difficulties. For example, it is a slow-growing strain, requiring a BSL-3 (biosafety level)

laboratory. Such aspects limit the possibilities of seeking new drug targets. A solution is the use of surrogate strain – *Mycobacterium* (*Mycolicibacterium*) *smegmatis*. It grows faster than *M. tuberculosis*, and working with it is more safe. *Mycobacterium smegmatis* shows good compliance with antitubercular drugs if it is grown in a low nutrient culture medium (Lelovic et al., 2020). The study by Altaf et al. (2010) involving screening of chemical libraries, showed that around 50% of inhibitors active against *M. smegmatis* are also active against *M. tuberculosis*. Another surrogate bacterium, slow-growing *M. bovis* BCG, got much better results with the majority of correlating hits. The less common surrogate models used in the antitubercular drug development process are *Mycobacterium aurum* (Gupta and Bhakta, 2012) and *Mycobacterium marinum* (Boot et al., 2018).

IDENTIFICATION OF THE DRUG TARGET AND DETERMINATION OF ITS MODE OF ACTION

As the mechanism of action of individual antibiotics was discovered, it was understood that each of these drugs had a specific target. In addition to inhibiting their primary target, many drugs affect cell metabolism by generating toxic intermediates and triggering a cascade of molecular events, resulting in significant cell changes. Therefore, it is vital to consider the overall cellular metabolism when the cell is under the influence of the antibiotic (Kana et al., 2014).

Whole-Genome Sequencing

One of the principal paths to identify the drug target is to look for drug resistance mutations, as they often occur in the target. This can be done by whole-genome sequencing (WGS) of the resistant strain. Once the mutation is identified, it should be confirmed by the generation of drug resistant mutant after the introduction of the mutation into a drug-susceptible strain. This approach was used for target identification of BDQ. The authors generated drug-resistant variants of *M. smegmatis* and *M. tuberculosis* and sequenced their genomes. They found that the mutations in *atp*E gene are responsible for resistance to the compound. The *M. smegmatis* wild-type (WT) strain was transformed with a construct expressing the ATP synthetase subunit of the *M. smegmatis* mutant. The complementation with the mutant allele caused drug resistance (Andries et al., 2005). Recently, using a similar strategy, we identified a drug target for 1H-benzoimidazole derivatives. WGS identified mutations in the *mmpl3* gene encoding the integral membrane protein. Strains with trans-complementation of the wild-type mutated target gene were prepared. The resulting 1H-benzoimidazole resistance confirmed the role of the gene in the resistant phenotype (Korycka-Machała et al., 2019).

Genetic Modification of Mycobacteria

The information regarding the genomic DNA sequence provides a base for genetic manipulations. Several genetic modification approaches are currently available, including the construction of knock-out mutants, complemented mutants, and the use of reporter systems and interference systems, including the CRISPR/dCas system. Gene replacement by homologous recombination allows obtaining unmarked genetic mutants carrying large deletions within the genes of interest. These mutants can be complemented with genes of interest under native or inducible promoter (Parish and Stoker, 2000). One can also silence the gene using CRISPR/dCas (Choudhary et al., 2015). Obtaining a mutant with regulated target depletion allows performing several experiments. The use of such strain allows assessing the impact of the depletion of the studied gene in various conditions (anaerobic, acid pH, and antibiotics). Previously, CRISPR/dCas mutants were used to analyze the MmpL3 as a therapeutic target. GoldenGate cloning was used to develop the CRISPR/dCas plJT965 plasmid. As a result, a 6-fold decrease in expression of the *mmpL3* gene was obtained. The mutation led to a 5-fold increase in strain sensitivity to Mmpl3 inhibitor (McNeil and Cook, 2019).

Complementation of mutants with possible drug-target genes allows control of gene expression, which can be used for the evaluation of chemical compounds against specific targets. An example of this approach is evaluating the available library of GlaxoSmith Kline compounds as CTP inhibitors of PyrG synthetase. This essential enzyme is involved in several biochemical pathways affecting several aspects of *Mycobacterium* physiology. Compounds were tested against *M. tuberculosis* conditional knockdown strain using a Pip-ON inducible system. A mutant carrying the *pyrG* gene under promoter induced by pristinamycin I was designed. The dependence of the action of two compounds from the analyzed library on the PyrG level confirmed that the enzyme is an intracellular target (Esposito et al., 2017). Similarly, the antitubercular activity of known compounds was confirmed by constructing conditional mutants of the tetracycline-induced *panC* gene, identifying the inhibitory activity of flavonoid derivatives (Abrahams et al., 2012).

To further study the drug target, it is also useful to overexpress the gene of interest. For the analysis of antifolates, an *M. tuberculosis* strain carrying the plasmid pMRN1 containing a wild copy of the *dfrA* gene under the control of the strong promoter was constructed. A 4-fold increase in the MIC 90 strain overexpressing the gene encoding dihydrofolate reductase was observed for 17 compounds, which indicates the targeted nature of these compounds (Kumar et al., 2015). Similarly, *M. smegmatis* strain overexpressing MtNadD was prepared using the non-interfering plasmid pVV16 and the deletion mutant. The strains were tested in the presence of benzimidazolium (N2) derivatives. The overexpressed strain consistently showed a larger MIC compared to the mutant strain (Osterman et al., 2019).

Transcriptomics

When identifying an antibiotic's mode of action, one can look for changes in the metabolism, growth, and morphology of bacteria. These observations allow the assessment of bacterial target inhibition through comparison with known

mechanisms (Silver, 2012). So an alternative route to identify potential drug targets is through transcriptomic data obtained either through microarrays or RNA-Seq (Fields et al., 2017). O'Rourke et al. (2020) investigated transcriptomic profiles of 37 antibiotics within six different mechanisms of action, which allowed blind predictions of the antibiotic class based on transcriptomic response with an accuracy of <80%. A similar model was developed for *M. marinum* (Boot et al., 2018). Betts et al. (2003) examined *M. tuberculosis* gene expression after treatment with INH, triclosan, and thiolactomycin. Based on gene expression changes, a transcription profile model was proposed that enabled the determination of differences between *M. tuberculosis* treated with each of the three drugs. This model can be used to determine the MOA of uncharacterized mycolic acid biosynthesis inhibitors (Briffotaux et al., 2019). Differentially expressed genes were also evaluated in a whole blood model under the influence of RMP, INH, PZA, and EMB (Kwan et al., 2020). Currently, there are over a hundred reports of differential expression of mycobacterial genes. The results from these reports were recently combined into model INDIGO-MTB. The goal of the model was to identify antibiotic combinations that are most promising for TB drug development. The authors identified the transcription factor Rv1353c as a regulator of multiple drug interaction outcomes. They concluded that this factor could be targeted for rationally enhancing drug synergy (Ma et al., 2019).

Metabolomics

Metabolomics is a useful approach for finding new targets for antituberculosis drugs and understanding compounds' mode of action (Tuyiringire et al., 2018). By analyzing the network of metabolites and the interactions between them, it is possible to obtain knowledge about the cell processes (Goff et al., 2020). de Carvalho et al. (2010) supplemented *M. tuberculosis* cultures with 13C-labeled carbon substrates and then analyzed the metabolites by LC-MS, proving that *Mycobacteria* can catabolize multiple carbon sources simultaneously. In the following study, Prosser and Carvahlo used LC-MS to interrogate the antibiotic action mechanism of d-cycloserine (Prosser and de Carvalho, 2013). Halouska et al. (2012) described metabolomics changes in model *M. smegmatis* under the influence of 12 known drugs and three chemical leads. Nuclear magnetic resonance (NMR) analysis of the *M. smegmatis* metabolome clustered drug-induced patterns, correlating them with *in vivo* drug activity. Zampieri et al. (2018) analyzed the metabolomic response of *M. smegmatis* to 62 reference compounds. They used that information to predict the MOA of a library of 212 new anti-mycobacterial compounds from the pharmaceutical company GlaxoSmithKline.

A separate part of metabolomics is lipidomics, which studies the interactions between currently known lipid species and other lipids, proteins, and metabolites in the cell (Wu et al., 2014). It is based on the use of mass spectrometry (MS), a technique by which the mass-to-charge ratio and the number of ions are measured, gas chromatography (GC-MS), and liquid chromatography (LC-MS; Griffiths and Wang, 2009). Analysis of cell lipid content changes in response to changing environmental conditions may lead to the identification of key pathways in lipid biosynthesis. Pal et al. (2018) used lipidomics to show that INH treatment of *M. tuberculosis* can alter the composition of glycerolipids and glycerophospholipids.

CHOOSING THE DRUG TARGET AND FINDING ITS INHIBITORS

Because of a significant understanding of the processes taking place in bacterial cells, the number of potential molecular targets for inhibition is very long. Proteins taking action in DNA metabolism and cell wall synthesis are of particular interest. Other attractive targets for new drugs are proteins from the RND family (resistance, nodulation, and cell division), especially Mmpl3, for which analogs of EMB displayed inhibiting activity (Campaniço et al., 2018).

Genetic Modification of Mycobacteria

The alternative approach used to identify new drugs is first identifying the target and then looking for its inhibitors. It is usually done by creating knock-out mutants, complemented mutants, and/or CRISPR/dCas mutants with specific gene changes. An important aspect to bear in mind is those target proteins identified as essential may be significant for bacterial survival only under laboratory conditions and not in the infection process (Zuniga et al., 2015). Similarly, part of the mutants obtained in laboratory conditions, during growth in laboratory media, is not viable during animal infection. To test the essentiality of individual genes, the researchers infect animals with knock-out mutants. In an exemplary study, guinea pigs were inhaled with a knock-out mutant of *dlaT*, which product is involved in the restriction of nitric oxide-derived reactive nitrogen intermediates. The authors confirmed a vital role of *dlaT* in establishing infection and searched for *dlaT* inhibitors trough screening a library of chemicals (Bryk et al., 2008). A desirable targeting strategy for drugs is to find a target that will shorten treatment duration and reduce the incidence of tuberculosis relapses. Hu et al. analyzed the *M. tuberculosis* HspX protein, which they previously linked to inhibiting this organism's growth. The BALB/c mice were infected with *hspX* deleted mutant and the WT strain. The animals were treated with popular antibiotics. Treatment of mice infected with the *hspX* mutant resulted in faster clearance of bacteria from internal organs (Hu et al., 2015).

Transposon Mutagenesis

A high-throughput method of obtaining mutants is transposon site hybridization (TraSH) developed by Sassetti et al. (2003) and DeJesus et al. (2017). The knowledge about gene function comes from inserting transposons at AT sites randomly distributed across the genome into the gene and disrupting its functions. Transposon mutagenesis allowed for a search of novel molecular targets such as virulence factors, enzymes of crucial metabolic pathways, and other essential proteins (Alksne and Dunman, 2008). Transposon mutants can be used

to simultaneously analyze a large number of mutants for survival in animal models. Transposon mutants were tested in mice, guinea pigs, and macaques (Sassetti and Rubin, 2003; Hernandez-Abanto et al., 2007; Dutta et al., 2010). In a study by Carey et al. (2018) transposon mutagenesis was used to investigate genetic requirements for the *in vitro* growth of clinical strains of *M. tuberculosis* and the reference *M. tuberculosis* strain H37Rv. The authors identified different requirements for genes in a panel of clinical strains. One of them turned out to be *katG*, encoding the first-line activator of INH.

Originally TraSH was performed using microarrays. Currently, a frequent variant of TraSH is the sequencing of the transposon insertion (Tn-seq). The method is sensitive, and it does not rely on a pre-existing array. It is important to note that transposon mutagenesis is a high-throughput method, and as such, it is affected by a certain level of inaccuracy. The analysis of constructed mutants should confirm results obtained for individual genes.

Lipidomics

In the studies conducted by Raghunandanan et al. (2019) the authors analyzed the changes in the lipid content of *M. tuberculosis* undergoing hypoxia and subsequent re-oxygenation. It turned out that the dormant bacteria's lipid content was drastically low and increased during oxygenation. Despite the drastic reduction in lipid synthesis pathways during hypoxia, some of them were still acting. These pathways are potential targets for antituberculosis drugs.

Bioinformatic Predictions of Drug Targets

Potential drug targets can be identified in protein-protein interaction networks (PIP) studies. Two staples of this method are the identification of the unique non-homologous proteins through the Kyoto Encyclopedia of Gene and Genome (KEGG) database or UniProt and identification of essential genes through the Database of Essential Genes (DEG; Amir et al., 2014; Melak and Gakkhar, 2014, 2015). Search of Amir et al. (2014) for unique proteins of *M. tuberculosis* in metabolic pathways with the KEGG database brought up five pathways consisting of 55 proteins. Selected proteins were analyzed with DEG and UniProt to choose the best candidates for new molecular targets. In another study with a similar approach done by Melak and Gakkhar, out of 1,091 essential genes, 572 were absent in the human genome. The interactome analysis with the STRING database allowed to limiting the number of possible targets. The authors then chose 131 proteins within the close neighborhood of the center of gravity of the proteome network, seeing that they function as important communicators between different metabolic pathways. Most of them were associated with cell wall metabolism. To validate this method, researchers compared their results to known and potential drug targets. Forty-three proteins were already known targets, and some were already reported as candidates (Melak and Gakkhar, 2015). One of the obstacles in this research type is that many *M. tuberculosis* proteins do not have a known function or a 3D structure available. Protein structure is important to conclude the function. However, there are attempts to use proteins with unknown functions (hypothetical proteins) as molecular targets through homology modeling (Uddin et al., 2019). To solve this issue, researchers use their 3D models (Kushwaha and Shakya, 2010) or use The Protein Data Bank (PDB; Melak and Gakkhar, 2015).

Bioinformatic Predictions of Target Inhibitors

The number of chemicals that are required for screening in order to find an appropriate inhibitor can be overwhelming. Therefore HTS is often facilitated by virtual screening (VS; **Figure 3**). VS utilizes computational methods to screen through ligands libraries to find new hits (Kar and Roy, 2013). Molecular docking and pharmacophore modeling are the most commonly used tools (Macalino et al., 2020), being the basis for the distinction of VS approaches into the structure- and ligand-based path. When information about the arrangement of the target atoms is available (e.g., thanks to the presence of the respective crystal structures), it is usually used for docking. Otherwise, the target structure needs to be modeled using homology or *de novo* (restricted to small proteins) modeling (Schmidt et al., 2014). Docking enables rough estimation of compound affinity to the target and making compound comparisons based on the quality of fitting to the binding pocket. Ligand-based VS also uses a quantitative structure-activity relationship (QSAR) analysis for predicting the activity and physicochemical properties of new potential drugs (Nowosielski et al., 2013; Adeniji et al., 2018). Similarity search approaches look for compounds with similar structures to already known ligands, according to the assumption that compounds with similar chemical structures should induce similar biological effects (Martin et al., 2002).

Virtual screening is an useful tool to identify new inhibitors for the key cellular components. For example, VS identified potential inhibitors of MraY, which is necessary for peptidoglycan synthesis (Mallavarapu et al., 2019). Other important cellular components are proteins containing the most frequently occurring drug-resistance mutations like InhA, FabD, and AhpC, which are INH targets. Through the use of VS, researchers can identify new potential drug candidates and limit the number of compounds that need testing in experimental conditions (Jagadeb et al., 2019).

Alternatively, molecular docking aids in finding more effective antitubercular drugs, which structure is based on already existing compounds with proven abilities to inhibit or completely stop *M. tuberculosis* growth. An example of such a study regarding the antitubercular drugs is the search for new inhibitors of arabinosyltransferase C enzyme (EmbC). EmbC participates in the formation of the cell wall, and it is probably the target of EMB. Researchers performed molecular docking of five new derivatives of the EMB. Based on bioinformatic results, the authors indicated two of them that should bind to the EmbC with higher affinity (Das et al., 2020).

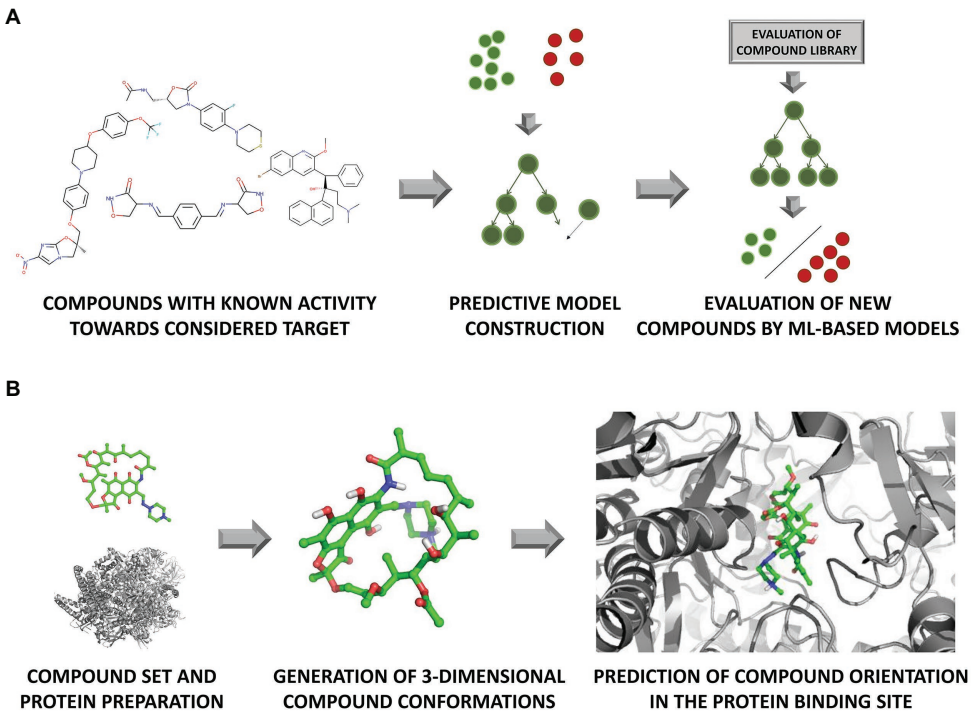

FIGURE 3 | *In silico* evaluation of compound activity with the use of **(A)** machine learning (ML) algorithms representing ligand-based approach, and **(B)** docking (element of the structure-based path).

Intensive growth of computational power on the one hand, and the increasing amount of data both in the ligand- and structure-based field, has made simple statistical methods to be replaced with more complex models to analyze such data, with machine learning (ML) being on the top of the used methodologies (**Figure 3**). The main task of ML is to analyze existing data, and on their basis, construct a predictive model, which is then used for the evaluation of new examples (Mitchell, 2014).

Machine learning tools can be categorized into unsupervised (clustering methods) and supervised (regression, classifier analysis) learning. Both of these types are used in the search for new drugs, depending on the wanted outcome. ML is useful in all steps of the new drug discovery pipeline, especially in tasks where vast amounts of data need to be analyzed. It helps in the identification of new potential ligands in the VS procedure, generation sets of new potentially active compounds [deep learning, (DL)], optimization of compound physicochemical and ADMET properties, and detection of compound interactions with off-targets (Carpenter et al., 2018; Chen et al., 2018). ML is also useful in pre- and clinical development for cell response classification after drug intake (Vamathevan et al., 2019), as well as after the introduction of the drug to the market, e.g., for analyzing and monitoring the drug efficiency and possible side effects (Dimitri and Lió, 2017; Gao et al., 2017).

In an exemplary ML-based study to search for new anti-mycobacterial compounds, Prakash and colleagues built a database of compounds with known antitubercular effect, divided into three activity classes. Then, the compounds were clustered according to their chemical structure and four clusters acting on different targets were selected for further analysis. Cluster numbered 10 consisted of compounds, e.g., aminohydrazones, iso-nicotinoyl hydrazones, and iso-nicotinohydrazides that inhibit KatG and 2-trans-enoyl-acyl carrier protein reductase (InhA). Cluster 57 included pyrrole derivatives and azole antifungals, which interact with CYP51 isozymes. The next cluster contained oxazolidinones, which bind DNA gyrase, and 2-benzylthiopydidine-4-carbithioamide derivatives, which targets are not known. The last cluster contained pyridobenzoxaine derivatives of LFX and nitroquinolones. Hologram QSAR (HQSAR) allowed the search for fragments of molecules contributing to particular compound activity and to detect moieties that discriminated against active and inactive compounds. Individual active motifs found *via* this procedure were fused, and new bioactive motifs were proposed. Furthermore, they verified the effectiveness of new motifs by comparing them to compounds in the previously constructed dataset. One of the created motifs was found in already existing drugs: RMP, rifabutin, cirpofloxacin (COX), and ofloxacin (OX; Prakash and Ghosh, 2006).

Another similar approach used in drug design is searching for molecular patterns in other known drugs. In one of the early studies, researchers built their computational model by combining four linear equations and then apply it to screen the compounds found in Merck and Sigma-Aldrich catalogs. They selected 18 new compounds for microbial tests, which

have not worked in their favor despite careful preparation of the model. ML models at that time were far from ideal. However, the study was able to pick four compounds that already have been experimentally checked for inhibiting *M. tuberculosis* growth, e.g., LZD, paromomycin, reserpine, and trifluoperazine from 5,000 compounds in the database, as well as compounds with new structures not found in currently used drugs treating TB (García-García et al., 2005). Some researchers are leaning toward Bayesian models since they are better suited for global QSAR analysis, can manage more data, and the results are easier to interpret and reproduce. The good performance of this model was proven by a study in which out of 44 antituberculars only six (13,6%) were assigned to the wrong group based on chemical structure (Prathipati et al., 2008). In a similar study, Ekins and colleagues found through Bayesian modeling drugs that have not been yet experimentally verified against *M. tuberculosis* but scored high, e.g., sertaconazole, clofarabine, tioconazole, amodiaquine, quinaldine blue, atorvastatin, montelukast, daunorubicin, 4'-methoxychalcone, inosine, hieracin, iridin, harmane, and irigenol (Ekins and Freundlich, 2011).

Some researchers guided by the principles of polypharmacology are moving away from the "one target-one hit" model and looking into drugs that can potentially inhibit multiple targets (Zhang et al., 2016). The reasoning of this approach lies in the fact that treatment for TB already consists of multiple antimicrobials administered for a very long time (over 6 months for drug-susceptible *M. tuberculosis*; Tiberi et al., 2018a). Therefore drugs inhibiting multiple targets would significantly simplify treatment. There is also the possibility that adequate multi-target compounds will be more effective against drug-resistant TB and will not lead to the emergence of resistance as fast as one-target drugs do. Following this reasoning, Speck-Planche et al. (2012) created a model for mt-QSAR (multiple target QSAR). The difference between this method and QSAR was in the training dataset, which was constructed based on compounds active against all six proteins GyrA, GyrB, InhA, Ag85C, PS, and PD. Through combined VS, QSAR, and structure-based pharmacophore models, researchers found initial hits against InhA, GlmU, and DapB. Next, they added other known drug targets to create possible multi-target drugs (Janardhan et al., 2017). In another study focusing on phytochemicals through VS, researchers found four compounds amentoflavone, carpaine, 13-bromo-tiliacorinine and 2-nortiliacorinine, that bind with high affinity to many *M. tuberculosis* proteins, like Ask, DdIA, PanC, TrpB, AroF, NadE, AtpE, RibH, RpIE, and RpsE (Kumar et al., 2019). All results described above need yet to be confirmed by *in vitro* studies.

Since ML is used as a tool for finding new compounds through the mining of chemical databases, a number of databases gathering information on compound structure and bioactivity have been constructed. An example of such a database is a Collaborative Drug Discovery (CDD, Burlingame, CA), which now consists of more than 200,000 molecules (Hohman et al., 2009; Ekins et al., 2010). Since its construction, CDD was used in many important TB projects like the EU-funded New Medicines 4 Tuberculosis (NM4TB) initiative (Ekins et al., 2011). Other popular databases of bioactive molecules are ChEMBL (which now contains almost 2 million distinct compounds, with over 16 million biological activities annotated) and PDSP with ~10,000 compound affinities toward different targets gathered (Besnard et al., 2012; Gaulton et al., 2012).

CONSIDERATION OF DRUG RESISTANCE

The principal molecular basis for mycobacterial diversity and drug resistance are single-nucleotide polymorphisms (SNPs). SNPs occur in the genome as a result of replication errors or erroneous DNA repair. *M. tuberculosis* lacks horizontal gene transfer trough mobile genetic elements such as plasmids or transposons. The comparison of the genomes of various *M. tuberculosis* strains revealed their similarity at over 99% (Namouchi et al., 2012).

Many mutations encoding drug resistance are located in the direct drug targets of the proteins, e.g., *rpo*B (RMP; Telenti et al., 1993), *emb*CAB operon (EMB; Mikusová et al., 1995; Telenti et al., 1997), *rrs* (KAN; Georghiou et al., 2012), *gyr*A, *gyr*B (fluoroquinolones, FQ; Takiff et al., 1994). However, drug resistance mutations are also associated with other *loci*. For example, in the case of INH, mutations occur in a seemingly unrelated *ahp*C gene encoding alkyl hydroperoxidase It turns out that AhpC takes over the role of KatG, which is a catalase-peroxidase responsible for the transformation of INH from pro-drug to effective drug, in protecting the genome from oxygen-induced damage. The overexpression of AhpC significantly slows down the production of KatG. Thus, less INH is activated, and cells can survive (Sherman et al., 1999).

Mutations occurring in drug targets can negatively affect proteins metabolic activity, resulting in a deficit of cell fitness. Bacterial cells compensate through compensatory mutations. Mutants carrying compensatory mutations are characterized by lower fitness costs associated with drug resistance. The best-known example of drug-resistant mutations causing fitness cost is RpoB (RMP resistance; Gagneux et al., 2006). Compensatory mutations were found in RpoB and other proteins of RNA polymerase complex, RpoA, and RpoC (Gagneux et al., 2006; Comas et al., 2012; de Vos et al., 2013).

DNA Sequencing

The principal identification of drug resistance sources is based on the cultivation of bacteria with antibiotics until drug-resistant variants appear (Takiff et al., 1994; Telenti et al., 1997). The genome sequences of drug-resistant clones are sequenced and screened for mutations (Telenti et al., 1997). This approach was used to identify drug-resistant mutations for major antitubercular drugs like EMB (Telenti et al., 1997) and FQ (Takiff et al., 1994). Notably, the amount of drug-resistant variants that can be detected in such studies is limited. As a high-throughput method, TraSH can be used to identify genes that do not sustain insertion among the pool of mutants

(Sassetti et al., 2003; van Opijnen et al., 2009). Researchers tested the sensitivity of 69 morphotype mutants of *M. smegmatis* to one of the commonly used antibiotics – ampicillin to identify cell envelope genes associated with B-lactam resistance. After receiving four sensitive mutants, the transposon insertion sites were mapped (Viswanathan et al., 2017).

Transcriptomics and Genetic Modification of Bacteria

Changes in gene expression profiles studied through RNA-seq allow understanding of antibiotics' effect on *M. tuberculosis* physiology regarding tolerance mechanisms and drug resistance (Jain et al., 2016; Briffotaux et al., 2019). For example, increased the expression of the *efpA* gene encoding the efflux pump from the MFS family (major facilitator superfamily) and the *iniA* gene encoding one of the putative components of the efflux pump, after treatment with INH, may indicate that microorganisms are acquiring resistance (Briffotaux et al., 2019). Exposition of *M. tuberculosis* to antibiotics results in the overexpression of genes encoding DNA repair proteins (Gorna et al., 2010), e.g., *dinX* after RMP treatment (Boshoff et al., 2004), *ssb* after CM treatment (Fu and Shinnick, 2007), *ada*, *alkA* after treatment LFX (Boshoff et al., 2004) or *xthA* after treatment with OX (Boshoff et al., 2004) and many others.

The induction of efflux pumps can be visualized with reporter systems. Jain et al. (2016) investigated the gene expression profile in the presence of a subinhibitory concentration of INH. The addition of INH to *M. tuberculosis* during the logarithmic growth phase caused a CFU decrease of 2–3 logs. Mycobacterial cells that survived the treatment were characterized by an increased expression of specific genes, which indicate the formation of persister cells. These gene promoters were fused to a gene encoding the red fluorescent protein to create a reporter system for persisters.

Bioinformatic Predictions

Genome-wide association studies (GWAS) identify drug resistance sources after the drugs are already on the market. GWAS utilize genomic DNA sequencing data and statistics to study the association between gene variants across the population and the phenotypic traits, for example, variants of genes giving rise to drug-resistant strains (Power et al., 2017). Importantly, GWAS studies allow the identification of rare drug resistance variants or low-level drug resistance variants. GWAS of Farhat et al. (2013) study showed that potentially noncoding regions of the genome, like promoters of genes, contribute to drug resistance. The same team has confirmed noncoding regions associated with drug resistance for INH, EMB, and PZA. However, their effect on drug MIC was smaller than the effect of coding region mutations (Farhat et al., 2019). In subsequent studies, Coll et al. (2018) used GWAS to identify drug-resistance associated mutations in 6465 clinical strains. Most of the mutations and loci they found were well-known, but some of them were new, including *loci* in *foli*C, *ubi*A, *thy*X-*hsd*S.1, *thy*A, *alr*, *ald*, and *dfr*A-*thy*A. They also found mutations in *eth*A and *thy*X promoters that may contribute to resistance emergence. GWAS is also used for studying characteristics of populations of *M. tuberculosis*. Oppong et al. (2019) through GWAS analysis, examined whether phylogenetic lineage background impacts drug resistance and found that particular drug resistance specific *loci* occur only in selected lineages.

The development of -omic technologies and computational power allowed the development of biological network models. These models are based on systemic biology, which combines knowledge about organisms on all organizational levels. The models take into account all the complex interactions and mechanisms occurring in the cells. There are different types of such networks, e.g., transcription factors-binding, PIP networks, metabolic interaction networks, genetic interaction networks, and others (Zhu et al., 2007; Chandra et al., 2011; Chung et al., 2013).

In silico analyses like PIP are applicable in predicting drug resistance patterns through building networks based on the STRING database and defining proteins that are drug targets and possible components of resistance emergence. Through this research, the concept of "co-target" was created. Co-target is a protein used simultaneously as a primary bacterial growth inhibitor to stop the emergence of resistance by affecting proteins in the resistance emergence pathway. These co-targets can be proteins associated with SOS response (RecA, RuvA, and LexA), involved in HGT (SecA1 and SecA2) or metabolism of drugs inside the cell like cytochromes and degrading enzymes (Cyp135, Erm37), but also proteins involved in the transportation of drugs out of the cell through efflux pumps (PstB; Raman and Chandra, 2008). Besides, PIP networks allow for learning more about the effects of antibiotics on the cells by finding what pathways are set in motion when antibiotics kill bacteria (Kohanski et al., 2010).

Identification of rare drug resistance mutations can also be made through ML. Based on 1983 *M. tuberculosis* isolates, Yang et al. (2018) developed ML models for four first-line drugs – INH, RMP, EMB, PZA, and several second-line drugs that analyze WGS data. The models increased the sensitivity of the detection of drug resistance when compared with previous studies. For EMB and RMP, the sensitivity increased to 97% ($p < 0.01$), and for COX and multi-drug resistant TB, it increased to 96%. The INH had the lowest results, with only a 2–4% increase. In another study, Deelder et al. (2019) utilized WGS data to compare GWAS and their ML model. Both methods reached similar results, but GWAS was slightly more accurate for CM, CS, and KAN.

In the best scenario, mutations associated with drug-resistance are confirmed through obtaining genetic mutants and observing the resulting drug-resistant phenotype. Another approach to confirm that a mutation is linked to drug resistance is through *in silico* docking. *In silico* docking is a useful tool for predicting the roles of mutations causing drug resistance. It can be done by analyzing interactions between the selected drug and protein, the wild-type, and the mutated variant (Nachappa et al., 2020).

ENTERING THE PRECLINICAL STAGE

Researchers thoroughly check compounds with the potential to become drugs during the early discovery stage. Regardless of their usefulness from a biological point of view, novel compounds should have form facilitating administration. They have to go through tests of solubility, stability, and reactivity (Strovel et al., 2004; Hughes et al., 2011). If they fail to obtain satisfactory parameters, they are discarded. If they reach a satisfactory biological safety level and are practical, they proceed to the preclinical drug discovery stage. Preclinical studies are a checkpoint before human administration, and thus they are vital and carried with much caution.

Most of the compounds going through a hit to lead, and lead optimization, do not enter the preclinical stage. If we count all of the structures considered in chemical databases for screening, millions of compounds do not make it to the preclinical stage. Therefore the preclinical stage is often less costly than the early discovery stage. Up to our knowledge, there are no recent estimates on how many compounds go from the preclinical stage to the clinical phase. A common statement found in the articles is that out of 5,000 compounds entering the preclinical stage, five make it to the clinical stage, and then one makes it to the market (Kraljevic et al., 2004). Taken how many compounds undergo tests, the models for early drug discovery need to efficiently investigate broad biological consequences in a short time and at a low-cost.

CONCLUSION

The growing demand for discovering new antibiotics stimulates the constant development of research methods that broaden the knowledge about biological processes occurring in bacterial cells undergoing chemotherapy. Understanding these processes enables more effective identification of antitubercular compounds. Thanks to the -omics technologies, these compounds can now be safer and less prone to the generation of drug resistance. When combined, the -omics technologies allow us to gain a more holistic view of drug utility.

AUTHOR CONTRIBUTIONS

AM and JD designed the manuscript. AM, LŻ, EL, FG, AK, SP, DZ, and JD wrote the manuscript. All authors contributed to the article and approved the submitted version.

FUNDING

This work is part of the research project financed by the National Science Center of Poland, grant number 2019/34/E/NZ6/00221.

REFERENCES

(2009). Screening we can believe in. *Nat. Chem. Biol.* 5:127. doi: 10.1038/nchembio0309-127

Abrahams, G. L., Kumar, A., Savvi, S., Hung, A. W., Wen, S., Abell, C., et al. (2012). Pathway-selective sensitization of *Mycobacterium tuberculosis* for target-based whole-cell screening. *Chem. Biol.* 19, 844–854. doi: 10.1016/j.chembiol.2012.05.020

Adeniji, S. E., Uba, S., and Uzairu, A. (2018). QSAR modeling and molecular docking analysis of some active compounds against *Mycobacterium tuberculosis* receptor (Mtb CYP121). *J. Pathog.* 2018:e1018694. doi: 10.1155/2018/1018694

Ahmed, S., Raqib, R., Guðmundsson, G. H., Bergman, P., Agerberth, B., and Rekha, R. S. (2020). Host-directed therapy as a novel treatment strategy to overcome tuberculosis: targeting immune modulation. *Antibiotics* 9:21. doi: 10.3390/antibiotics9010021

Alksne, L. E., and Dunman, P. M. (2008). "Target-based antimicrobial drug discovery" in *Bacterial pathogenesis*. eds. F. R. DeLeo and M. Otto (Totowa, NJ: Humana Press), 271–283.

Altaf, M., Miller, C. H., Bellows, D. S., and O'Toole, R. (2010). Evaluation of the *Mycobacterium smegmatis* and BCG models for the discovery of *Mycobacterium tuberculosis* inhibitors. *Tuberculosis* 90, 333–337. doi: 10.1016/j.tube.2010.09.002

Amir, A., Rana, K., Arya, A., Kapoor, N., Kumar, H., and Siddiqui, M. A. (2014). *Mycobacterium tuberculosis* H37Rv: in silico drug targets identification by metabolic pathways analysis. *Int. J. Evol. Biol.* 2014:284170. doi: 10.1155/2014/284170

Andries, K., Verhasselt, P., Guillemont, J., Göhlmann, H. W. H., Neefs, J. -M., Winkler, H., et al. (2005). A diarylquinoline drug active on the ATP synthase of *Mycobacterium tuberculosis*. *Science* 307, 223–227. doi: 10.1126/science.1106753

Bahuguna, A., and Rawat, D. S. (2020). An overview of new antitubercular drugs, drug candidates, and their targets. *Med. Res. Rev.* 40, 263–292. doi: 10.1002/med.21602

Balganesh, M., Dinesh, N., Sharma, S., Kuruppath, S., Nair, A. V., and Sharma, U. (2012). Efflux pumps of *Mycobacterium tuberculosis* play a significant role in antituberculosis activity of potential drug candidates. *Antimicrob. Agents Chemother.* 56, 2643–2651. doi: 10.1128/AAC.06003-11

Besnard, J., Ruda, G. F., Setola, V., Abecassis, K., Rodriguiz, R. M., Huang, X. -P., et al. (2012). Automated design of ligands to polypharmacological profiles. *Nature* 492, 215–220. doi: 10.1038/nature11691

Betts, J. C., McLaren, A., Lennon, M. G., Kelly, F. M., Lukey, P. T., Blakemore, S. J., et al. (2003). Signature gene expression profiles discriminate between isoniazid-, thiolactomycin-, and triclosan-treated *Mycobacterium tuberculosis*. *Antimicrob. Agents Chemother.* 47, 2903–2913. doi: 10.1128/AAC.47.9.2903-2913.2003

Boot, M., Commandeur, S., Subudhi, A. K., Bahira, M., Smith, T. C., Abdallah, A. M., et al. (2018). Accelerating early antituberculosis drug discovery by creating mycobacterial indicator strains that predict mode of action. *Antimicrob. Agents Chemother.* 62:e00083–18. doi: 10.1128/AAC.00083-18

Boshoff, H. I. M., Myers, T. G., Copp, B. R., McNeil, M. R., Wilson, M. A., and Barry, C. E. (2004). The transcriptional responses of *Mycobacterium tuberculosis* to inhibitors of metabolism: novel insights into drug mechanisms of action. *J. Biol. Chem.* 279, 40174–40184. doi: 10.1074/jbc.M406796200

Briffotaux, J., Liu, S., and Gicquel, B. (2019). Genome-wide transcriptional responses of *Mycobacterium* to antibiotics. *Front. Microbiol.* 10:249. doi: 10.3389/fmicb.2019.00249

Bryk, R., Gold, B., Venugopal, A., Singh, J., Samy, R., Pupek, K., et al. (2008). Selective killing of nonreplicating mycobacteria. *Cell Host Microbe* 3, 137–145. doi: 10.1016/j.chom.2008.02.003

Campaniço, A., Moreira, R., and Lopes, F. (2018). Drug discovery in tuberculosis. New drug targets and antimycobacterial agents. *Eur. J. Med. Chem.* 150, 525–545. doi: 10.1016/j.ejmech.2018.03.020

Carey, A. F., Rock, J. M., Krieger, I. V., Chase, M. R., Fernandez-Suarez, M., Gagneux, S., et al. (2018). TnSeq of *Mycobacterium tuberculosis* clinical isolates reveals strain-specific antibiotic liabilities. *PLoS Pathog.* 14:e1006939. doi: 10.1371/journal.ppat.1006939

Carpenter, K. A., Cohen, D. S., Jarrell, J. T., and Huang, X. (2018). Deep learning and virtual drug screening. *Future Med. Chem.* 10, 2557–2567. doi: 10.4155/fmc-2018-0314

Chandra, N., Kumar, D., and Rao, K. (2011). Systems biology of tuberculosis. *Tuberculosis* 91, 487–496. doi: 10.1016/j.tube.2011.02.008

Chatterjee, A., Sharma, A. K., Mahatha, A. C., Banerjee, S. K., Kumar, M., Saha, S., et al. (2018). Global mapping of MtrA-binding sites links MtrA to regulation of its targets in *Mycobacterium tuberculosis*. *Microbiology* 164, 99–110. doi: 10.1099/mic.0.000585

Chen, H., Engkvist, O., Wang, Y., Olivecrona, M., and Blaschke, T. (2018). The rise of deep learning in drug discovery. *Drug Discov. Today* 23, 1241–1250. doi: 10.1016/j.drudis.2018.01.039

Choudhary, E., Thakur, P., Pareek, M., and Agarwal, N. (2015). Gene silencing by CRISPR interference in mycobacteria. *Nat. Commun.* 6:6267. doi: 10.1038/ncomms7267

Chung, B. K. -S., Dick, T., and Lee, D. -Y. (2013). In silico analyses for the discovery of tuberculosis drug targets. *J. Antimicrob. Chemother.* 68, 2701–2709. doi: 10.1093/jac/dkt273

Coll, F., Phelan, J., Hill-Cawthorne, G. A., Nair, M. B., Mallard, K., Ali, S., et al. (2018). Genome-wide analysis of multi- and extensively drug-resistant *Mycobacterium tuberculosis*. *Nat. Genet.* 50, 307–316. doi: 10.1038/s41588-017-0029-0

Comas, I., Borrell, S., Roetzer, A., Rose, G., Malla, B., Kato-Maeda, M., et al. (2012). Whole-genome sequencing of rifampicin-resistant *Mycobacterium tuberculosis* strains identifies compensatory mutations in RNA polymerase genes. *Nat. Genet.* 44, 106–110. doi: 10.1038/ng.1038

Dara, Y., Volcani, D., Shah, K., Shin, K., and Venketaraman, V. (2019). Potentials of host-directed therapies in tuberculosis management. *J. Clin. Med.* 8:1166. doi: 10.3390/jcm8081166

Das, N., Jena, P. K., and Pradhan, S. K. (2020). Arabinosyltransferase C enzyme of *Mycobacterium tuberculosis*, a potential drug target: an insight from molecular docking study. *Heliyon* 6:e02693. doi: 10.1016/j.heliyon.2019.e02693

de Carvalho, L. P. S., Fischer, S. M., Marrero, J., Nathan, C., Ehrt, S., and Rhee, K. Y. (2010). Metabolomics of *Mycobacterium tuberculosis* reveals compartmentalized co-catabolism of carbon substrates. *Chem. Biol.* 17, 1122–1131. doi: 10.1016/j.chembiol.2010.08.009

de Vos, M., Müller, B., Borrell, S., Black, P. A., van Helden, P. D., Warren, R. M., et al. (2013). Putative compensatory mutations in the rpoC gene of rifampin-resistant *Mycobacterium tuberculosis* are associated with ongoing transmission. *Antimicrob. Agents Chemother.* 57, 827–832. doi: 10.1128/AAC.01541-12

Deelder, W., Christakoudi, S., Phelan, J., Benavente, E. D., Campino, S., McNerney, R., et al. (2019). Machine learning predicts accurately *Mycobacterium tuberculosis* drug resistance from whole genome sequencing data. *Front. Genet.* 10:922. doi: 10.3389/fgene.2019.00922

DeJesus, M. A., Gerrick, E. R., Xu, W., Park, S. W., Long, J. E., Boutte, C. C., et al. (2017). Comprehensive essentiality analysis of the *Mycobacterium tuberculosis* genome via saturating transposon mutagenesis. *MBio* 8:e02133–16. doi: 10.1128/mBio.02133-16

Deoghare, S. (2013). Bedaquiline: a new drug approved for treatment of multidrug-resistant tuberculosis. *Indian J. Pharm.* 45, 536–537. doi: 10.4103/0253-7613.117765

Dimitri, G. M., and Lió, P. (2017). DrugClust: a machine learning approach for drugs side effects prediction. *Comput. Biol. Chem.* 68, 204–210. doi: 10.1016/j.compbiolchem.2017.03.008

Dooley, K. E., Hanna, D., Mave, V., Eisenach, K., and Savic, R. M. (2019). Advancing the development of new tuberculosis treatment regimens: the essential role of translational and clinical pharmacology and microbiology. *PLoS Med.* 16:e1002842. doi: 10.1371/journal.pmed.1002842

Dutta, N. K., Mehra, S., Didier, P. J., Roy, C. J., Doyle, L. A., Alvarez, X., et al. (2010). Genetic requirements for the survival of tubercle bacilli in primates. *J. Infect. Dis.* 201, 1743–1752. doi: 10.1086/652497

Ekins, S., Bradford, J., Dole, K., Spektor, A., Gregory, K., Blondeau, D., et al. (2010). A collaborative database and computational models for tuberculosis drug discovery. *Mol. BioSyst.* 6, 840–851. doi: 10.1039/B917766C

Ekins, S., and Freundlich, J. S. (2011). Validating new tuberculosis computational models with public whole cell screening aerobic activity datasets. *Pharm. Res.* 28, 1859–1869. doi: 10.1007/s11095-011-0413-x

Ekins, S., Freundlich, J. S., Choi, I., Sarker, M., and Talcott, C. (2011). Computational databases, pathway and cheminformatics tools for tuberculosis drug discovery. *Trends Microbiol.* 19, 65–74. doi: 10.1016/j.tim.2010.10.005

Esposito, M., Szadocka, S., Degiacomi, G., Orena, B. S., Mori, G., Piano, V., et al. (2017). A phenotypic based target screening approach delivers new antitubercular CTP synthetase inhibitors. *ACS Infect. Dis.* 3, 428–437. doi: 10.1021/acsinfecdis.7b00006

Farhat, M. R., Freschi, L., Calderon, R., Ioerger, T., Snyder, M., Meehan, C. J., et al. (2019). GWAS for quantitative resistance phenotypes in *Mycobacterium tuberculosis* reveals resistance genes and regulatory regions. *Nat. Commun.* 10:2128. doi: 10.1038/s41467-019-10110-6

Farhat, M. R., Shapiro, B. J., Kieser, K. J., Sultana, R., Jacobson, K. R., Victor, T. C., et al. (2013). Genomic analysis identifies targets of convergent positive selection in drug-resistant *Mycobacterium tuberculosis*. *Nat. Genet.* 45, 1183–1189. doi: 10.1038/ng.2747

Fields, F. R., Lee, S. W., and McConnell, M. J. (2017). Using bacterial genomes and essential genes for the development of new antibiotics. *Biochem. Pharmacol.* 134, 74–86. doi: 10.1016/j.bcp.2016.12.002

Fu, L. M., and Shinnick, T. M. (2007). Genome-wide exploration of the drug action of capreomycin on *Mycobacterium tuberculosis* using Affymetrix oligonucleotide GeneChips. *J. Inf. Secur.* 54, 277–284. doi: 10.1016/j.jinf.2006.05.012

Gagneux, S., Long, C. D., Small, P. M., Van, T., Schoolnik, G. K., and Bohannan, B. J. M. (2006). The competitive cost of antibiotic resistance in *Mycobacterium tuberculosis*. *Science* 312, 1944–1946. doi: 10.1126/science.1124410

Gao, M., Igata, H., Takeuchi, A., Sato, K., and Ikegaya, Y. (2017). Machine learning-based prediction of adverse drug effects: an example of seizure-inducing compounds. *J. Pharmacol. Sci.* 133, 70–78. doi: 10.1016/j.jphs.2017.01.003

García-García, A., Gálvez, J., de Julián-Ortiz, J. V., García-Domenech, R., Muñoz, C., Guna, R., et al. (2005). Search of chemical scaffolds for novel antituberculosis agents. *J. Biomol. Screen.* 10, 206–214. doi: 10.1177/1087057104273486

Gaulton, A., Bellis, L. J., Bento, A. P., Chambers, J., Davies, M., Hersey, A., et al. (2012). ChEMBL: a large-scale bioactivity database for drug discovery. *Nucleic Acids Res.* 40, D1100–D1107. doi: 10.1093/nar/gkr777

Georghiou, S. B., Magana, M., Garfein, R. S., Catanzaro, D. G., Catanzaro, A., and Rodwell, T. C. (2012). Evaluation of genetic mutations associated with *Mycobacterium tuberculosis* resistance to amikacin, kanamycin and capreomycin: a systematic review. *PLoS One* 7:e33275. doi: 10.1371/journal.pone.0033275

Ghajavand, H., Kamakoli, M. K., Khanipour, S., Dizaji, S. P., Masoumi, M., Jamnani, F. R., et al. (2019). High prevalence of bedaquiline resistance in treatment-naive tuberculosis patients and verapamil effectiveness. *Antimicrob. Agents Chemother.* 63, e02530–e02618. doi: 10.1128/AAC.02530-18

Goff, A., Cantillon, D., Muraro Wildner, L., and Waddell, S. J. (2020). Multi-omics technologies applied to tuberculosis drug discovery. *Appl. Sci.* 10:4629. doi: 10.3390/app10134629

Gorla, P., Plocinska, R., Sarva, K., Satsangi, A. T., Pandeeti, E., Donnelly, R., et al. (2018). MtrA response regulator controls cell division and cell wall metabolism and affects susceptibility of mycobacteria to the first line antituberculosis drugs. *Front. Microbiol.* 9:2839. doi: 10.3389/fmicb.2018.02839

Gorna, A. E., Bowater, R. P., and Dziadek, J. (2010). DNA repair systems and the pathogenesis of *Mycobacterium tuberculosis*: varying activities at different stages of infection. *Clin. Sci.* 119, 187–202. doi: 10.1042/CS20100041

Grant, S. S., Kawate, T., Nag, P. P., Silvis, M. R., Gordon, K., Stanley, S. A., et al. (2013). Identification of novel inhibitors of nonreplicating *Mycobacterium tuberculosis* using a carbon starvation model. *ACS Chem. Biol.* 8, 2224–2234. doi: 10.1021/cb4004817

Griffiths, W. J., and Wang, Y. (2009). Mass spectrometry: from proteomics to metabolomics and lipidomics. *Chem. Soc. Rev.* 38, 1882–1896. doi: 10.1039/b618553n

Grzelak, E. M., Choules, M. P., Gao, W., Cai, G., Wan, B., Wang, Y., et al. (2019). Strategies in anti-*Mycobacterium tuberculosis* drug discovery based on phenotypic screening. *J. Antibiot.* 72, 719–728. doi: 10.1038/s41429-019-0205-9

Gupta, A., and Bhakta, S. (2012). An integrated surrogate model for screening of drugs against *Mycobacterium tuberculosis*. *J. Antimicrob. Chemother.* 67, 1380–1391. doi: 10.1093/jac/dks056

Halouska, S., Fenton, R. J., Barletta, R. G., and Powers, R. (2012). Predicting the in vivo mechanism of action for drug leads using NMR metabolomics. *ACS Chem. Biol.* 7, 166–171. doi: 10.1021/cb200348m

Hernandez-Abanto, S. M., Cheng, Q. -J., Singh, P., Ly, L. H., Klinkenberg, L. G., Morrison, N. E., et al. (2007). Accelerated detection of *Mycobacterium tuberculosis* genes essential for bacterial survival in Guinea pigs, compared with mice. *J. Infect. Dis.* 195, 1634–1642. doi: 10.1086/517526

Hohman, M., Gregory, K., Chibale, K., Smith, P. J., Ekins, S., and Bunin, B. (2009). Novel web-based tools combining chemistry informatics, biology and social networks for drug discovery. *Drug Discov. Today* 14, 261–270. doi: 10.1016/j.drudis.2008.11.015

Hu, Y., Liu, A., Menendez, M. C., Garcia, M. J., Oravcova, K., Gillespie, S. H., et al. (2015). HspX knock-out in *Mycobacterium tuberculosis* leads to shorter antibiotic treatment and lower relapse rate in a mouse model—a potential novel therapeutic target. *Tuberculosis* 95, 31–36. doi: 10.1016/j.tube.2014.11.002

Hughes, J. P., Rees, S., Kalindjian, S. B., and Philpott, K. L. (2011). Principles of early drug discovery. *Br. J. Pharmacol.* 162, 1239–1249. doi: 10.1111/j.1476-5381.2010.01127.x

Jagadeb, M., Rath, S. N., and Sonawane, A. (2019). In silico discovery of potential drug molecules to improve the treatment of isoniazid-resistant *Mycobacterium tuberculosis*. *J. Biomol. Struct. Dyn.* 37, 3388–3398. doi: 10.1080/07391102.2018.1515116

Jain, P., Weinrick, B. C., Kalivoda, E. J., Yang, H., Munsamy, V., Vilcheze, C., et al. (2016). Dual-reporter mycobacteriophages (Φ2DRMs) reveal preexisting *Mycobacterium tuberculosis* persistent cells in human sputum. *MBio* 7:e01023–16. doi: 10.1128/mBio.01023-16

Janardhan, S., John, L., Prasanthi, M., Poroikov, V., and Narahari Sastry, G. (2017). A QSAR and molecular modelling study towards new lead finding: polypharmacological approach to *Mycobacterium tuberculosis*. *SAR QSAR Environ. Res.* 28, 815–832. doi: 10.1080/1062936X.2017.1398782

Kana, B. D., Karakousis, P. C., Parish, T., and Dick, T. (2014). Future target-based drug discovery for tuberculosis? *Tuberculosis* 94, 551–556. doi: 10.1016/j.tube.2014.10.003

Kar, S., and Roy, K. (2013). How far can virtual screening take us in drug discovery? *Expert Opin. Drug Discovery* 8, 245–261. doi: 10.1517/17460441.2013.761204

Kaufmann, S. H. E. (2020). Vaccination against tuberculosis: revamping BCG by molecular genetics guided by immunology. *Front. Immunol.* 11:316. doi: 10.3389/fimmu.2020.00316

Kohanski, M. A., Dwyer, D. J., and Collins, J. J. (2010). How antibiotics kill bacteria: from targets to networks. *Nat. Rev. Microbiol.* 8, 423–435. doi: 10.1038/nrmicro2333

Korycka-Machala, M., Nowosielski, M., Kuron, A., Rykowski, S., Olejniczak, A., Hoffmann, M., et al. (2017). Naphthalimides selectively inhibit the activity of bacterial, replicative DNA ligases and display bactericidal effects against tubercle bacilli. *Molecules* 22:154. doi: 10.3390/molecules22010154

Korycka-Machała, M., Viljoen, A., Pawełczyk, J., Borówka, P., Dziadek, B., Gobis, K., et al. (2019). 1H-Benzo[d]imidazole derivatives affect MmpL3 in *Mycobacterium tuberculosis*. *Antimicrob. Agents Chemother.* 63, e00441–e00519. doi: 10.1128/AAC.00441-19

Koul, A., Vranckx, L., Dendouga, N., Balemans, W., Van den Wyngaert, I., Vergauwen, K., et al. (2008). Diarylquinolines are bactericidal for dormant mycobacteria as a result of disturbed ATP homeostasis. *J. Biol. Chem.* 283, 25273–25280. doi: 10.1074/jbc.M803899200

Kraljevic, S., Stambrook, P. J., and Pavelic, K. (2004). Accelerating drug discovery. *EMBO Rep.* 5, 837–842. doi: 10.1038/sj.embor.7400236

Kumar, A., Guardia, A., Colmenarejo, G., Pérez, E., Gonzalez, R. R., Torres, P., et al. (2015). A focused screen identifies antifolates with activity on *Mycobacterium tuberculosis*. *ACS Infect. Dis.* 1, 604–614. doi: 10.1021/acsinfecdis.5b00063

Kumar, S., Sahu, P., and Jena, L. (2019). An in silico approach to identify potential inhibitors against multiple drug targets of *Mycobacterium tuberculosis*. *Int. J. Mycobacteriol.* 8, 252–261. doi: 10.4103/ijmy.ijmy_109_19

Kushwaha, S. K., and Shakya, M. (2010). Protein interaction network analysis—approach for potential drug target identification in *Mycobacterium tuberculosis*. *J. Theor. Biol.* 262, 284–294. doi: 10.1016/j.jtbi.2009.09.029

Kwan, P. K. W., Lin, W., Naim, A. N. M., Periaswamy, B., De Sessions, P. F., Hibberd, M. L., et al. (2020). Gene expression responses to anti-tuberculous drugs in a whole blood model. *BMC Microbiol.* 20:81. doi: 10.1186/s12866-020-01766-y

Lee, J. Y. (2015). Diagnosis and treatment of extrapulmonary tuberculosis. *Tuberc. Respir. Dis.* 78, 47–55. doi: 10.4046/trd.2015.78.2.47

Lelovic, N., Mitachi, K., Yang, J., Lemieux, M. R., Ji, Y., and Kurosu, M. (2020). Application of *Mycobacterium smegmatis* as a surrogate to evaluate drug leads against *Mycobacterium tuberculosis*. *J. Antibiot.* 73, 780–789. doi: 10.1038/s41429-020-0320-7

Lushington, G., and Chaguturu, R. (2014). To screen or not to screen: an impassioned plea for smarter chemical libraries to improve drug lead finding. *Future Med. Chem.* 6, 497–502. doi: 10.4155/fmc.14.21

Ma, S., Jaipalli, S., Larkins-Ford, J., Lohmiller, J., Aldridge, B. B., Sherman, D. R., et al. (2019). Transcriptomic signatures predict regulators of drug synergy and clinical regimen efficacy against tuberculosis. *MBio* 10:e02627–19. doi: 10.1128/mBio.02627-19

Macalino, S. J. Y., Billones, J. B., Organo, V. G., and Carrillo, M. C. O. (2020). In silico strategies in tuberculosis drug discovery. *Molecules* 25:665. doi: 10.3390/molecules25030665

Mallavarapu, B. D., Abdullah, M., Saxena, S., and Guruprasad, L. (2019). Inhibitor binding studies of *Mycobacterium tuberculosis* MraY (Rv2156c): insights from molecular modeling, docking, and simulation studies. *J. Biomol. Struct. Dyn.* 37, 3751–3763. doi: 10.1080/07391102.2018.1526715

Martin, Y. C., Kofron, J. L., and Traphagen, L. M. (2002). Do structurally similar molecules have similar biological activity? *J. Med. Chem.* 45, 4350–4358. doi: 10.1021/jm020155c

McNeil, M. B., and Cook, G. M. (2019). Utilization of CRISPR interference to validate MmpL3 as a drug target in *Mycobacterium tuberculosis*. *Antimicrob. Agents Chemother.* 63, e00629–e00719. doi: 10.1128/AAC.00629-19

Melak, T., and Gakkhar, S. (2014). Potential non homologous protein targets of *Mycobacterium tuberculosis* H37Rv identified from protein–protein interaction network. *J. Theor. Biol.* 361, 152–158. doi: 10.1016/j.jtbi.2014.07.031

Melak, T., and Gakkhar, S. (2015). Comparative genome and network centrality analysis to identify drug targets of *Mycobacterium tuberculosis* H37Rv. *Biomed. Res. Int.* 2015:212061. doi: 10.1155/2015/212061

Mikusová, K., Slayden, R. A., Besra, G. S., and Brennan, P. J. (1995). Biogenesis of the mycobacterial cell wall and the site of action of ethambutol. *Antimicrob. Agents Chemother.* 39, 2484–2489. doi: 10.1128/aac.39.11.2484

Minias, A., Brzostek, A., and Dziadek, J. (2019). Targeting DNA repair systems in antitubercular drug development. *Curr. Med. Chem.* 26, 1494–1505. doi: 10.2174/0929867325666180129093546

Mitchell, J. B. O. (2014). Machine learning methods in chemoinformatics. *Wiley Interdiscip. Rev. Comput. Mol. Sci.* 4, 468–481. doi: 10.1002/wcms.1183

Muliaditan, M., Davies, G. R., Simonsson, U. S. H., Gillespie, S. H., and Della Pasqua, O. (2017). The implications of model-informed drug discovery and development for tuberculosis. *Drug Discov. Today* 22, 481–486. doi: 10.1016/j.drudis.2016.09.004

Murray, J. F., Schraufnagel, D. E., and Hopewell, P. C. (2015). Treatment of tuberculosis. A historical perspective. *Ann. Am. Thorac. Soc.* 12, 1749–1759. doi: 10.1513/AnnalsATS.201509-632PS

Nachappa, S., Neelambike, S., Sarikhani, A., and Ramachandra, N. (2020). Simultaneous detection of drug-resistant mutations in *Mycobacterium tuberculosis* and determining their role through in silico docking. *Infect. Disord. Drug Targets*. doi: 10.2174/1871526520666200318111140 [Epub ahead of print]

Namouchi, A., Didelot, X., Schöck, U., Gicquel, B., and Rocha, E. P. C. (2012). After the bottleneck: genome-wide diversification of the *Mycobacterium tuberculosis* complex by mutation, recombination, and natural selection. *Genome Res.* 22, 721–734. doi: 10.1101/gr.129544.111

Nguyen, Q. H., Contamin, L., Nguyen, T. V. A., and Bañuls, A. (2018). Insights into the processes that drive the evolution of drug resistance in *Mycobacterium tuberculosis*. *Evol. Appl.* 11, 1498–1511. doi: 10.1111/eva.12654

Nowosielski, M., Hoffmann, M., Kuron, A., Korycka-Machala, M., and Dziadek, J. (2013). The MM2QM tool for combining docking, molecular dynamics, molecular mechanics, and quantum mechanics. *J. Comput. Chem.* 34, 750–756. doi: 10.1002/jcc.23192

O'Rourke, A., Beyhan, S., Choi, Y., Morales, P., Chan, A. P., Espinoza, J. L., et al. (2020). Mechanism-of-action classification of antibiotics by global transcriptome profiling. *Antimicrob. Agents Chemother.* 64, e01207–e01319. doi: 10.1128/AAC.01207-19

Oppong, Y. E. A., Phelan, J., Perdigão, J., Machado, D., Miranda, A., Portugal, I., et al. (2019). Genome-wide analysis of *Mycobacterium tuberculosis* polymorphisms reveals lineage-specific associations with drug resistance. *BMC Genomics* 20:252. doi: 10.1186/s12864-019-5615-3

Osterman, A. L., Rodionova, I., Li, X., Sergienko, E., Ma, C. -T., Catanzaro, A., et al. (2019). Novel antimycobacterial compounds suppress NAD biogenesis

by targeting a unique pocket of NaMN adenylyltransferase. *ACS Chem. Biol.* 14, 949–958. doi: 10.1021/acschembio.9b00124

Pal, R., Hameed, S., Sabareesh, V., Kumar, P., Singh, S., and Fatima, Z. (2018). Investigations into isoniazid treated *Mycobacterium tuberculosis* by electrospray mass spectrometry reveals new insights into its lipid composition. *J. Pathog.* 2018:e1454316. doi: 10.1155/2018/1454316

Parish, T., and Stoker, N. G. (2000). Use of a flexible cassette method to generate a double unmarked *Mycobacterium tuberculosis* tlyA plcABC mutant by gene replacement. *Microbiology* 146, 1969–1975. doi: 10.1099/00221287-146-8-1969

Płocinska, R., Korycka-Machala, M., Plocinski, P., and Dziadek, J. (2017). Mycobacterial DNA replication as a target for antituberculosis drug discovery. *Curr. Top. Med. Chem.* 17, 2129–2142. doi: 10.2174/1568026617666170130114342

Plocinska, R., Purushotham, G., Sarva, K., Vadrevu, I. S., Pandeeti, E. V. P., Arora, N., et al. (2012). Septal localization of the *Mycobacterium tuberculosis* MtrB sensor kinase promotes MtrA regulon expression. *J. Biol. Chem.* 287, 23887–23899. doi: 10.1074/jbc.M112.346544

Power, R. A., Parkhill, J., and de Oliveira, T. (2017). Microbial genome-wide association studies: lessons from human GWAS. *Nat. Rev. Genet.* 18, 41–50. doi: 10.1038/nrg.2016.132

Prakash, O., and Ghosh, I. (2006). Developing an antituberculosis compounds database and data mining in the search of a motif responsible for the activity of a diverse class of antituberculosis agents. *J. Chem. Inf. Model.* 46, 17–23. doi: 10.1021/ci050115s

Prathipati, P., Ma, N. L., and Keller, T. H. (2008). Global Bayesian models for the prioritization of antitubercular agents. *J. Chem. Inf. Model.* 48, 2362–2370. doi: 10.1021/ci800143n

Prosser, G. A., and de Carvalho, L. P. S. (2013). Metabolomics reveal d-alanine:d-alanine ligase as the target of d-cycloserine in *Mycobacterium tuberculosis*. *ACS Med. Chem. Lett.* 4, 1233–1237. doi: 10.1021/ml400349n

Raghunandanan, S., Jose, L., Gopinath, V., and Kumar, R. A. (2019). Comparative label-free lipidomic analysis of *Mycobacterium tuberculosis* during dormancy and reactivation. *Sci. Rep.* 9:3660. doi: 10.1038/s41598-019-40051-5

Raman, K., and Chandra, N. (2008). *Mycobacterium tuberculosis* interactome analysis unravels potential pathways to drug resistance. *BMC Microbiol.* 8:234. doi: 10.1186/1471-2180-8-234

Sassetti, C. M., Boyd, D. H., and Rubin, E. J. (2003). Genes required for mycobacterial growth defined by high density mutagenesis. *Mol. Microbiol.* 48, 77–84. doi: 10.1046/j.1365-2958.2003.03425.x

Sassetti, C. M., and Rubin, E. J. (2003). Genetic requirements for mycobacterial survival during infection. *Proc. Natl. Acad. Sci. U. S. A.* 100, 12989–12994. doi: 10.1073/pnas.2134250100

Schmidt, T., Bergner, A., and Schwede, T. (2014). Modelling three-dimensional protein structures for applications in drug design. *Drug Discov. Today* 19, 890–897. doi: 10.1016/j.drudis.2013.10.027

Sherman, D. R., Mdluli, K., Hickey, M. J., Barry, C. E., and Stover, C. K. (1999). AhpC, oxidative stress and drug resistance in *Mycobacterium tuberculosis*. *Biofactors* 10, 211–217. doi: 10.1002/biof.5520100219

Silver, L. L. (2012). "Rational approaches to antibacterial discovery: pre-genomic directed and phenotypic screening" in *Antibiotic discovery and development*. eds. T. J. Dougherty and M. J. Pucci (Boston, MA: Springer US), 33–75.

Speck-Planche, A., Kleandrova, V. V., Luan, F., Natalia, D. S., and Cordeiro, M. (2012). In silico discovery and virtual screening of multi-target inhibitors for proteins in *Mycobacterium tuberculosis*. *Comb. Chem. High Throughput Screen* 15, 666–673. doi: 10.2174/138620712802650487.

Strovel, J., Sittampalam, S., Coussens, N. P., Hughes, M., Inglese, J., Kurtz, A., et al. (2004). "Early drug discovery and development guidelines: for academic researchers, collaborators, and start-up companies" in *Assay guidance manual*. eds. S. Markossian, G. S. Sittampalam, A. Grossman, K. Brimacombe, M. Arkin and D. Auld et al. (Bethesda (MD): Eli Lilly & Company and the National Center for Advancing Translational Sciences).

Syre, H., Phyu, S., Sandven, P., Bjorvatn, B., and Grewal, H. M. S. (2003). Rapid colorimetric method for testing susceptibility of *Mycobacterium tuberculosis* to isoniazid and rifampin in liquid cultures. *J. Clin. Microbiol.* 41, 5173–5177. doi: 10.1128/JCM.41.11.5173-5177.2003

Takiff, H. E., Salazar, L., Guerrero, C., Philipp, W., Huang, W. M., Kreiswirth, B., et al. (1994). Cloning and nucleotide sequence of *Mycobacterium tuberculosis* gyrA and gyrB genes and detection of quinolone resistance mutations. *Antimicrob. Agents Chemother.* 38, 773–780. doi: 10.1128/aac.38.4.773

Telenti, A., Marchesi, F., Balz, M., Bally, F., Böttger, E. C., and Bodmer, T. (1993). Rapid identification of mycobacteria to the species level by polymerase chain reaction and restriction enzyme analysis. *J. Clin. Microbiol.* 31, 175–178. doi: 10.1128/JCM.31.2.175-178.1993

Telenti, A., Philipp, W. J., Sreevatsan, S., Bernasconi, C., Stockbauer, K. E., Wieles, B., et al. (1997). The emb operon, a gene cluster of *Mycobacterium tuberculosis* involved in resistance to ethambutol. *Nat. Med.* 3, 567–570. doi: 10.1038/nm0597-567

Theuretzbacher, U., Outterson, K., Engel, A., and Karlén, A. (2020). The global preclinical antibacterial pipeline. *Nat. Rev. Microbiol.* 18, 275–285. doi: 10.1038/s41579-019-0288-0

Tiberi, S., du Plessis, N., Walzl, G., Vjecha, M. J., Rao, M., Ntoumi, F., et al. (2018a). Tuberculosis: progress and advances in development of new drugs, treatment regimens, and host-directed therapies. *Lancet Infect. Dis.* 18, e183–e198. doi: 10.1016/S1473-3099(18)30110-5

Tiberi, S., Muñoz-Torrico, M., Duarte, R., Dalcolmo, M., D'Ambrosio, L., and Migliori, G. -B. (2018b). New drugs and perspectives for new anti-tuberculosis regimens. *Pulmonology* 24, 86–98. doi: 10.1016/j.rppnen.2017.10.009

Torfs, E., Piller, T., Cos, P., and Cappoen, D. (2019). Opportunities for overcoming *Mycobacterium tuberculosis* drug resistance: emerging mycobacterial targets and host-directed therapy. *Int. J. Mol. Sci.* 20:2868. doi: 10.3390/ijms20122868

Tuyiringire, N., Tusubira, D., Munyampundu, J. -P., Tolo, C. U., Muvunyi, C. M., and Ogwang, P. E. (2018). Application of metabolomics to drug discovery and understanding the mechanisms of action of medicinal plants with anti-tuberculosis activity. *Clin. Transl. Med.* 7:29. doi: 10.1186/s40169-018-0208-3

Uddin, R., Siddiqui, Q. N., Sufian, M., Azam, S. S., and Wadood, A. (2019). Proteome-wide subtractive approach to prioritize a hypothetical protein of XDR-*Mycobacterium tuberculosis* as potential drug target. *Genes Genomics* 41, 1281–1292. doi: 10.1007/s13258-019-00857-z

Vamathevan, J., Clark, D., Czodrowski, P., Dunham, I., Ferran, E., Lee, G., et al. (2019). Applications of machine learning in drug discovery and development. *Nat. Rev. Drug Discov.* 18, 463–477. doi: 10.1038/s41573-019-0024-5

Van Der Meeren, O., Hatherill, M., Nduba, V., Wilkinson, R. J., Muyoyeta, M., Van Brakel, E., et al. (2018). Phase 2b controlled trial of M72/AS01E vaccine to prevent tuberculosis. *N. Engl. J. Med.* 379, 1621–1634. doi: 10.1056/NEJMoa1803484

van Opijnen, T., Bodi, K. L., and Camilli, A. (2009). Tn-seq: high-throughput parallel sequencing for fitness and genetic interaction studies in microorganisms. *Nat. Methods* 6, 767–772. doi: 10.1038/nmeth.1377

Viswanathan, G., Yadav, S., and Raghunand, T. R. (2017). Identification of mycobacterial genes involved in antibiotic sensitivity: implications for the treatment of tuberculosis with β-lactam-containing regimens. *Antimicrob. Agents Chemother.* 61, e00425–e00517. doi: 10.1128/AAC.00425-17

Viveiros, M., Leandro, C., and Amaral, L. (2003). Mycobacterial efflux pumps and chemotherapeutic implications. *Int. J. Antimicrob. Agents* 22, 274–278. doi: 10.1016/s0924-8579(03)00208-5

Vjecha, M. J., Tiberi, S., and Zumla, A. (2018). Accelerating the development of therapeutic strategies for drug-resistant tuberculosis. *Nat. Rev. Drug Discov.* 17, 607–608. doi: 10.1038/nrd.2018.28

World Health Organization (2019). Global tuberculosis report 2019.

Wu, Z., Shon, J. C., and Liu, K.-H. (2014). Mass spectrometry-based lipidomics and its application to biomedical research. *J. Lifestyle Med.* 4, 17–33. doi: 10.15280/jlm.2014.4.1.17

Yang, Y., Niehaus, K. E., Walker, T. M., Iqbal, Z., Walker, A. S., Wilson, D. J., et al. (2018). Machine learning for classifying tuberculosis drug-resistance from DNA sequencing data. *Bioinformatics* 34, 1666–1671. doi: 10.1093/bioinformatics/btx801

Young, C., Walzl, G., and Du Plessis, N. (2020). Therapeutic host-directed strategies to improve outcome in tuberculosis. *Mucosal Immunol.* 13, 190–204. doi: 10.1038/s41385-019-0226-5

Zampieri, M., Szappanos, B., Buchieri, M. V., Trauner, A., Piazza, I., Picotti, P., et al. (2018). High-throughput metabolomic analysis predicts mode of action of uncharacterized antimicrobial compounds. *Sci. Transl. Med.* 10:eaal3973. doi: 10.1126/scitranslmed.aal3973

Zhang, W., Bai, Y., Wang, Y., and Xiao, W. (2016). Polypharmacology in drug discovery: a review from systems pharmacology perspective. *Curr. Pharm. Des.* 22, 3171–3181. doi: 10.2174/1381612822666160224142812

Zhu, X., Gerstein, M., and Snyder, M. (2007). Getting connected: analysis and principles of biological networks. *Genes Dev.* 21, 1010–1024. doi: 10.1101/gad.1528707

Zuniga, E. S., Early, J., and Parish, T. (2015). The future for early-stage tuberculosis drug discovery. *Future Microbiol.* 10, 217–229. doi: 10.2217/fmb.14.125

Zwerling, A., Behr, M. A., Verma, A., Brewer, T. F., Menzies, D., and Pai, M. (2011). The BCG world atlas: a database of global BCG vaccination policies and practices. *PLoS Med.* 8:e1001012. doi: 10.1371/journal.pmed.1001012

Conflict of Interest: The authors declare that the research was conducted in the absence of any commercial or financial relationships that could be construed as a potential conflict of interest.

Advantages of publishing in Frontiers

OPEN ACCESS
Articles are free to read for greatest visibility and readership

FAST PUBLICATION
Around 90 days from submission to decision

HIGH QUALITY PEER-REVIEW
Rigorous, collaborative, and constructive peer-review

TRANSPARENT PEER-REVIEW
Editors and reviewers acknowledged by name on published articles

Frontiers
Avenue du Tribunal-Fédéral 34
1005 Lausanne | Switzerland

Visit us: www.frontiersin.org
Contact us: frontiersin.org/about/contact

REPRODUCIBILITY OF RESEARCH
Support open data and methods to enhance research reproducibility

DIGITAL PUBLISHING
Articles designed for optimal readership across devices

FOLLOW US
@frontiersin

IMPACT METRICS
Advanced article metrics track visibility across digital media

EXTENSIVE PROMOTION
Marketing and promotion of impactful research

LOOP RESEARCH NETWORK
Our network increases your article's readership